

DIRECTORIO DE PROFESORES DEL CURSO: ANALISIS DE RIESGO

SISMICO 1985.

1. DR. GUSTAVO AYALA MILIAN  
INVESTIGADOR  
INSTITUTO DE INGENIERIA  
U N A M  
MEXICO, D.F.  
550 52 15 EXT. 3628
2. DR. MARIO CHAVEZ  
INVESTIGADOR  
INSTITUTO DE INGENIERIA  
U N A M  
MEXICO, D.F.  
550 52 15 EXT. 3628
3. DR. FRANCISCO SANCHEZ SESMA  
INVESTIGADOR  
INSTITUTO DE INGENIERIA  
U N A M  
MEXICO, D.F.  
550 52 15 EXT. 3625
4. DRA. SONIA RUIZ GOMEZ  
INVESTIGADORA  
INSTITUTO DE INGENIERIA  
U N A M  
MEXICO, D.F.  
550 52 15 EXT. 3629
5. DR. JUAN MANUEL ESPINDOLA  
INVESTIGADOR  
INSITUTO DE GEOFISICA  
U N A M  
MEXICO, D.F.
6. DR. LUIS ESTEVA MARABOTO (COORDINADOR)  
DIRECTOR  
INSTITUTO DE INGENIERIA  
U N A M  
MEXICO, D.F.  
548 30 44

## ANALISIS DE RIESGO SISMICO

### XI CURSO INTERNACIONAL DE INGENIERIA SISMICA 1985

	Día y hora	Expositor
Introducción	Julio 30, Martes 17:00 - 17:30	Dr. Luis Esteva
Sismología, tectónica de placas constitución de la tierra, mecanismos sísmicos. Predicción	Julio 30, Martes 17:30 - 19:15	Dr. Juan Manuel Espíndola
Fundamentos de la teoría de probabilidades para riesgo sísmico	Julio 30, Martes 19:30 - 21:00	Dra. Sonia E. Ruiz
Relaciones entre magnitud, intensidad y distancia, y entre amplitud del movimiento del terreno y ordenadas espectrales	Agosto 1º, Jueves 17:00 - 19:00	Dr. Mario Chávez
Influencia de las condiciones locales en las características del movimiento sísmico	Agosto 1º, Jueves 19:00 - 21:00	Dr. Gustavo Ayala
a) Propagación de ondas		
b) Modelo unidimensional		
c) Comparación de modelo teóricos con observaciones de campo		
d) Espectros de diseño modificados por la influencia de cond. locales		
Influencia de condiciones locales en las características del movimiento sísmico	Agosto 6, Martes 17:00 - 18:30	Dr. Francisco J. Sánchez-Sesma
a) Efectos de la topografía		
b) Modelos bi y tridimensionales		
c) Modelos y observaciones	Agosto 6, Martes 18:30 - 20:00	Dr. Luis Esteva
Análisis de riesgo sísmico:	Agosto 6, Martes	Dr. Mario Chávez
a) Sismicidad local y regional	20:00 - 21:00	
b) Estimación bayesiana		
c) Aplicaciones	Agosto 8, Jueves 17:00 - 19:00	Dr. Mario Chávez
d) Modelos refinados y avances recientes	Agosto 8, Jueves 19:15 - 21:00	Dr. Luis Esteva



**DIVISION DE EDUCACION CONTINUA  
FACULTAD DE INGENIERIA U.N.A.M.**

ANALISIS DE RIESGO SISMICO

SISMOLOGIA Y TECTONICA DE PLACAS  
ONDAS SISMICAS  
SISMOMETROS Y SISMOGRAMAS  
DETERMINACION DEL EPICENTRO  
ESCALAS DE MAGNITUD E INTENSIDAD  
CONSTITUCION DE LA TIERRA  
SISMICIDAD  
SISMICIDAD EN MEXICO  
PREMONITORES Y REPLICAS  
PREDICCION  
QUE HACER EN CASO DE SISMO

DR. JUAN M. ESPINDOLA C.

JULIO, 1985

## INDICE

1. Sismología y Tectónica de placas  
(Teoría del rebote elástico)
2. Ondas sísmicas
3. Sismómetros y sismogramas
4. Determinación del epicentro
5. Escalas de magnitud e intensidad
6. Constitución de la tierra
7. Sismicidad  
Número de temblores por año
8. Sismicidad de México
9. Premonitores y réplicas
10. Predicción
11. Qué hacer en caso de un sismo

## APENDICES

- A. Historia de la Sismología en México
- B. Red Sismológica Mexicana
- C. Sismos importantes
- D. Escala de intensidades

1. Sismología y Tectónica de Placas  
(Teoría del rebote elástico)

## SISMOLOGIA Y TECTONICA DE PLACAS

La ciencia que estudia los aspectos relacionados con la ocurrencia de temblores de tierra o sismos es llamada Sismología. Esta es una ciencia joven ya que gran parte de sus métodos e instrumental fueron desarrollados durante este siglo.

A pesar de esto, la Sismología ha logrado avances notables. Quizá una de sus más valiosas contribuciones al entendimiento de nuestro planeta lo constituya su aportación a la llamada TECTONICA DE PLACAS.

Para esbozar esta teoría consideremos en primer lugar la estructura interna de la tierra. En la figura 1 podemos ver esquemáticamente su constitución. El núcleo terrestre está probablemente compuesto de fierro y níquel. El manto terrestre tiene una composición a base de silicatos ferromagnesianos mientras que la corteza está compuesta por silicatos abundantes en potasio, sodio y calcio. El cascarón más externo de la tierra, el cual comprende la corteza y parte del manto, con un espesor de aproximadamente 100 km parece comportarse como un cuerpo rígido "flotando" en el resto del manto en den-

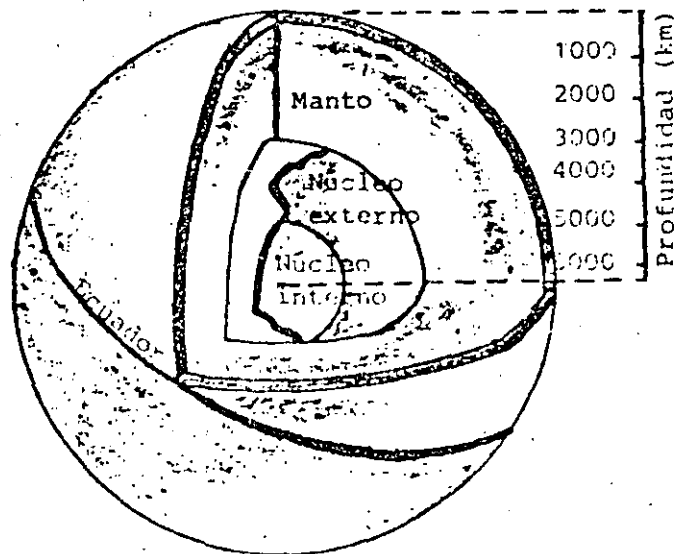


Fig. 1

de pueden presentarse movimientos como si se tratara de un fluido. Esta conducta semejante a la de un fluido tiene sentido solamente en tiempos geológicos, es decir en tiempos del orden de millones de años.

El cascarón exterior llamado litósfera no es continuo sobre la superficie de la tierra sino que está formado por diferentes "placas" en contacto una con otra.

Las placas sufren movimientos relativos debidos a fuerzas de origen aún no completamente conocidos, aplicadas a lo largo de las mismas. Estos mismos esfuerzos producen en algunos de sus márgenes la subducción de una placa bajo la otra y en otras la creación de nueva litósfera (Figura 2). Debido a estos movimientos los continentes han variado su posición relativa a través del tiempo geológico y se cree que en un tiempo estuvieron todos reunidos en un gran continente llamado Pangea. Esto nos explica el ajuste que existe entre, por ejemplo, las costas de Sudamérica y Africa. ¿Cuál es la distribución geográfica de estas placas? La Figura 3 nos la muestra. Las zonas de creación de nueva litósfera se presentan como cordilleras submarinas y las zonas de subducción forman a menudo trincheras submarinas de

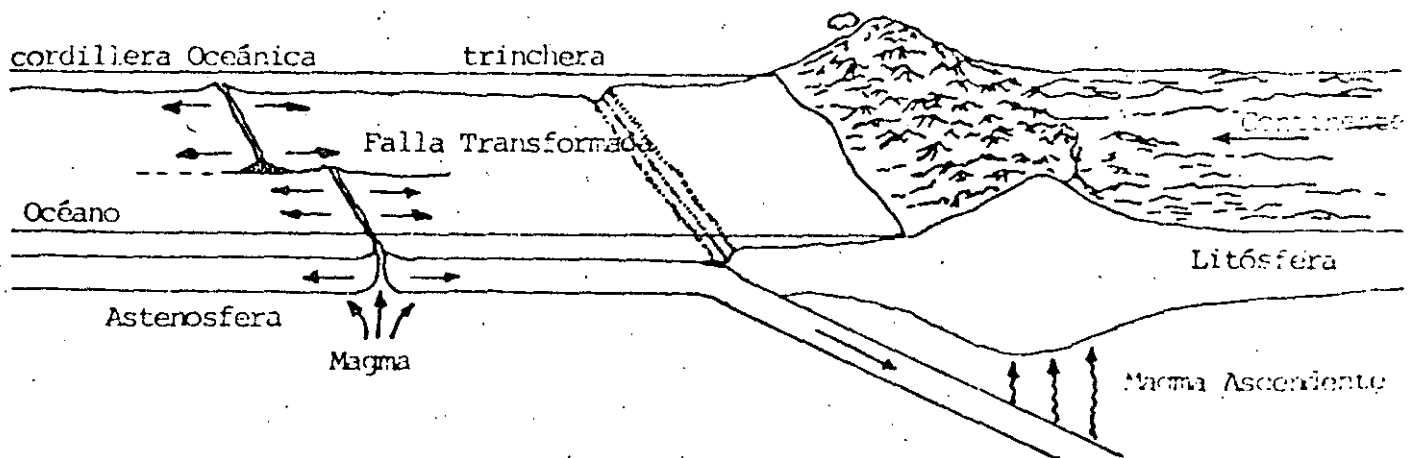
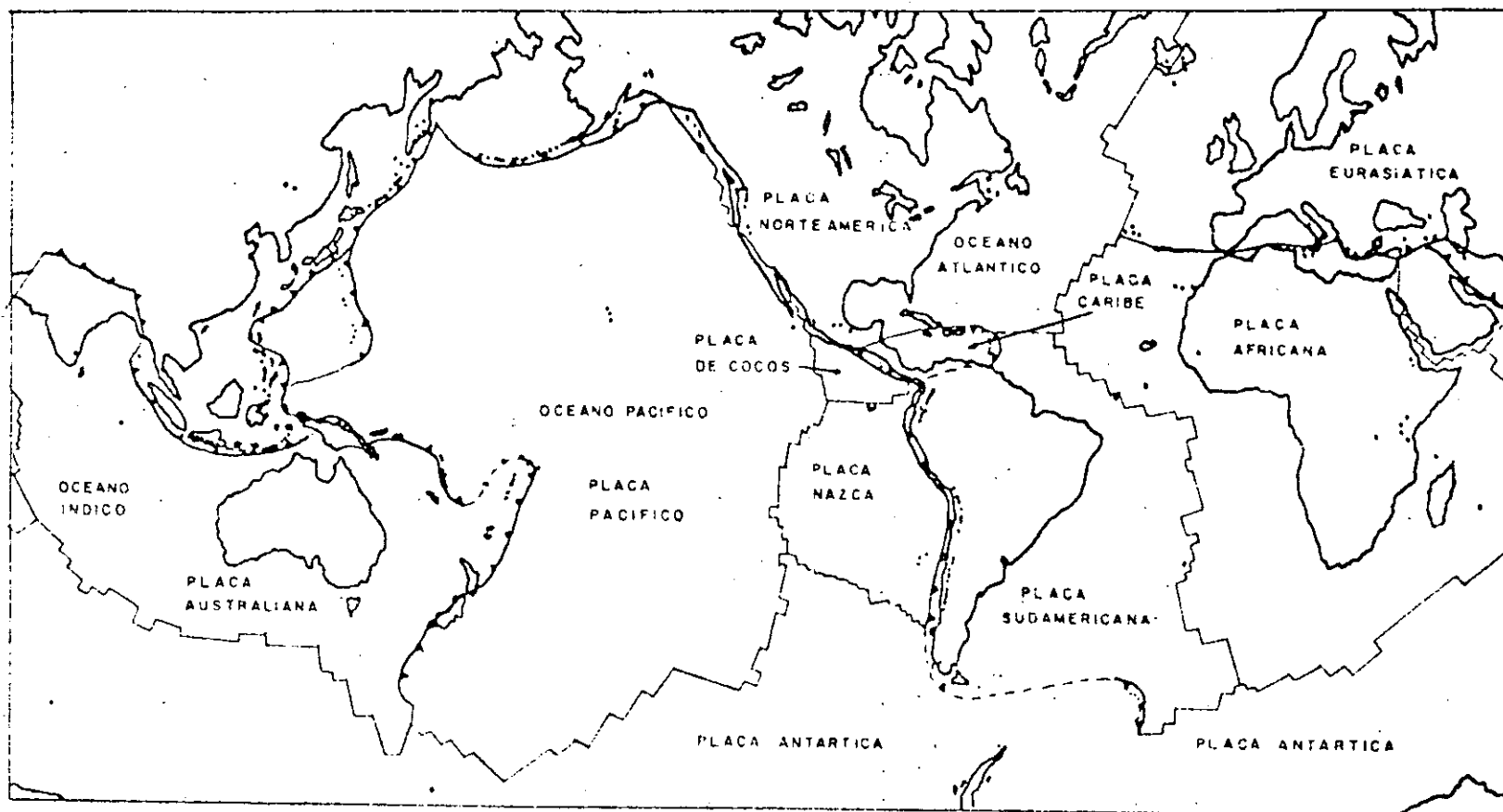


Fig. 2



- ZONA DE SUBDUCCION
- - - EJE DE CORDILLERA
- TRANSFORMACION
- VOLCAN

Fig. 5

3

gran profundidad. Podemos también notar que las diferentes placas no coinciden con los continentes y los océanos, sino que pueden tener corteza continental y oceánica.

No se sabe con certeza que causa los esfuerzos que producen los movimientos de las placas pero se cree que éstos son producidos por transferencia convectiva de calor, de la misma manera como ocurre cuando se hierve agua o cualquier otro líquido. El fluido más cercano a la fuente de calor se expande, se vuelve de esta manera menos denso y tiende por lo tanto a subir a la superficie donde es enfriado y desplazado hacia el fondo por nuevas parcelas ascendentes (Figura 4).

Este tipo de corrientes de convección pueden existir en el manto terrestre aunque no debe por esto suponerse que el mismo se encuentra en estado de fusión como las lavas. Ya se ha mencionado que esto sólo tiene sentido en tiempos muy largos. Una manera de visualizar esto es considerar un cierto

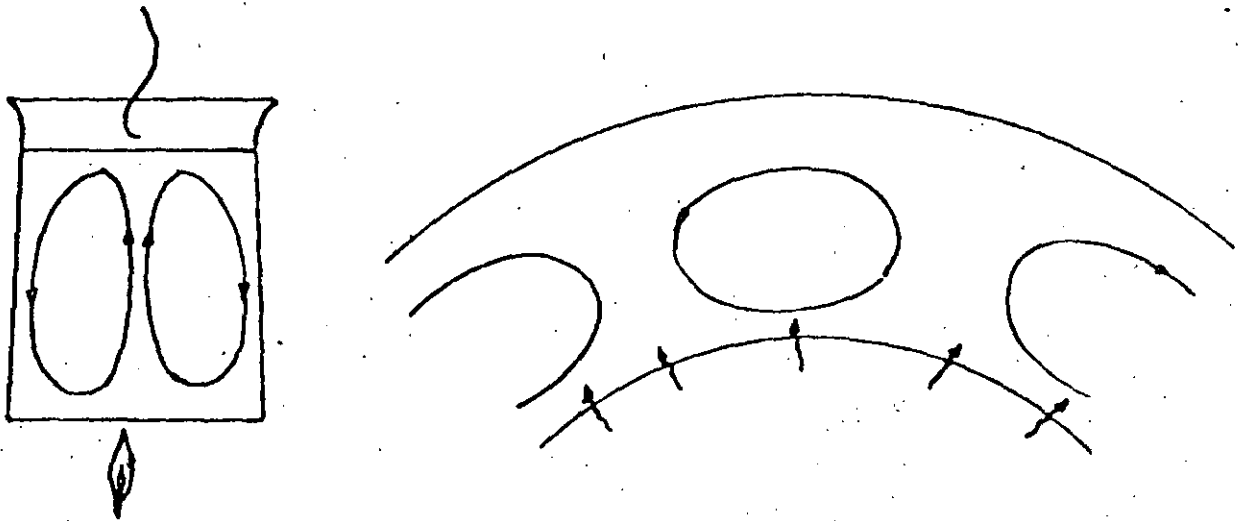


Fig. 4

volumen de roca. Si aplicamos a ésta un esfuerzo tensional por un tiempo corto la roca vuelve a su posición inicial. Si por el contrario aplicamos el esfuerzo por un período prolongado de tiempo la roca quedará deformada permanentemente (Fig. 5). En este último caso la roca "fluye" y se parece, en este sentido, a un fluido, ya que en éstos las deformaciones son permanentes. Esto nos explica también los plegamientos que observamos muchas veces en las cortaduras hechas en las carreteras.

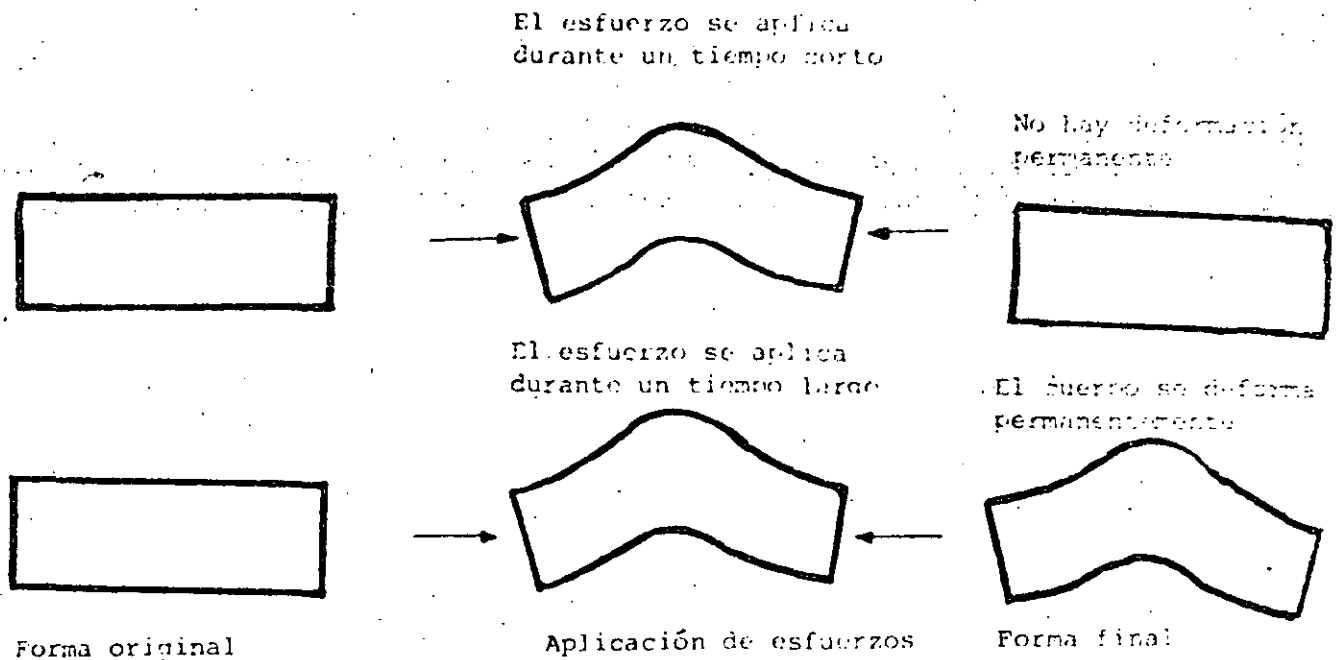


Figura 5

¿Cuál es la relación de esto con los temblores? En primer lugar notaremos que en una zona de subducción el movimiento de una placa bajo la otra se realiza venciendo las fuerzas de fricción generadas en el contacto entre ambas. A lo largo de este contacto, llamado zona de Wadati-Benioff (WB), el movimiento de una placa contra la otra tiene lugar discontinuamente, por "brincos". Es esto precisamente lo que genera los temblores en esas regioes

nes. Para visualizar estos procesos pensemos en un bloque de cemento sobre una mesa como se muestra en la Figura 6.

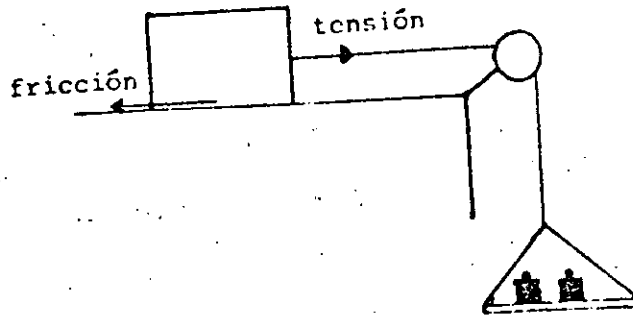


Fig. 6

Si colocamos un peso pequeño en la canastilla el bloque no se moverá debido a la fuerza de fricción entre el bloque y la mesa. Conforme aumentamos el peso la tensión en el cable continúa acumulándose hasta que iguala a la fuerza de fricción, a partir de ese momento el bloque empezará a moverse.

Análogamente en la zona W-B se acumula gradualmente hasta que rebasa un límite, en ese momento comienza a presentarse un fallamiento en algún punto llamado foco desde donde se propaga a toda una superficie (Fig. 7).

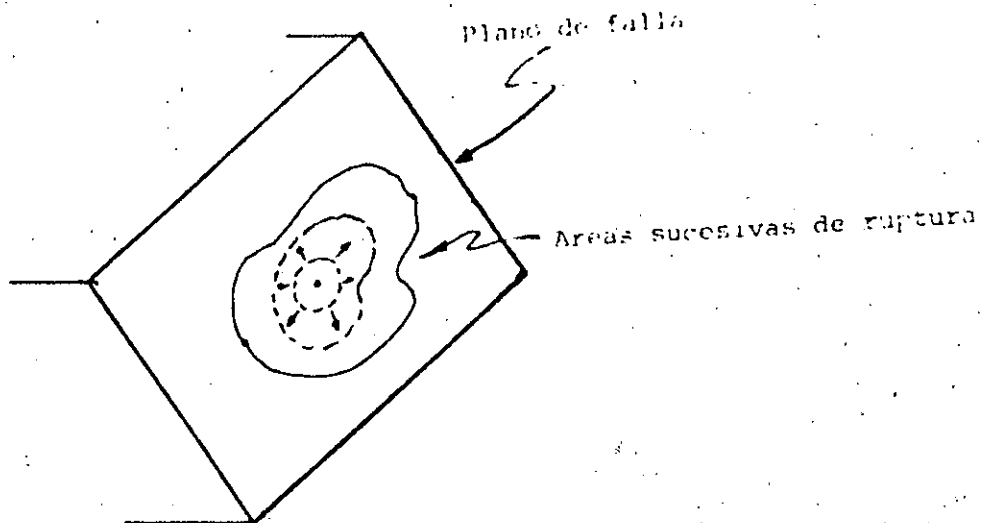


Fig. 7

Este comportamiento puede ser observado cuando el contacto entre placas aflora en la superficie de la tierra como en la famosa Falla de San Andrés en California. De hecho, fue en observaciones hechas en esta falla que pudo deducirse este mecanismo que es conocido como la TEORIA DEL REBOTE ELASTICO. Esto ocurrió durante el sismo de San Francisco en 1906. La Figura 8a muestra las dos placas durante el movimiento lateral que produce la acumulación de esfuerzos. En la Figura 8b los esfuerzos rebasan cierto límite y el fallamiento se produce en un punto y se propaga en ambas direcciones. La Figura 8c muestra la situación después del temblor; existe ahora

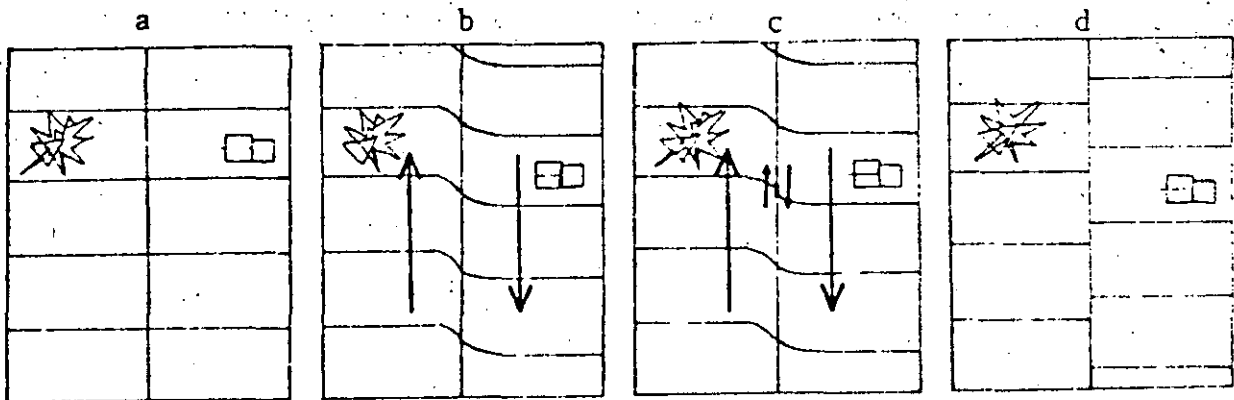


Fig. 8

un desplazamiento permanente entre ambas caras de la falla.

Aunque este proceso puede parecer intuitivamente obvio, en realidad no lo es. Durante mucho tiempo se pensó que el fallamiento de la corteza era un efecto de los temblores y no su origen. Como fuentes de éstos se pensaba en intrusiones de magma o colapso de volúmenes por cambios de densidad de las rocas que componen la corteza. Aunque estos mecanismos pueden ocurrir, se piensa en la actualidad que la mayoría de los temblores en las regiones de subducción se originan por el mecanismo expuesto y son llamados "tectó-

nicos". Otros tipos de sismos están asociados a fenómenos locales como son los volcánicos o algunos otros debido p. ej. al colapso del subsuelo por pérdida de agua, etcétera.

## ONDAS SISMICAS

Si desplazamos un diapazón de su posición de equilibrio y lo soltamos repentinamente percibimos su sonido característico (Fig. 9). Lo mismo sucede

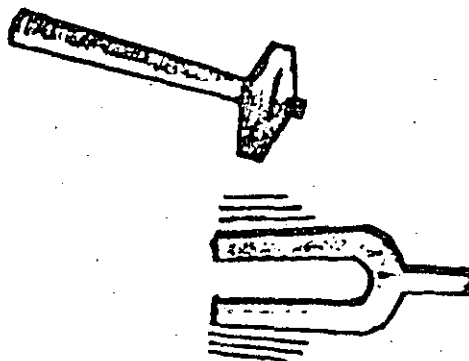


Fig. 9

en la tierra, hemos visto que el fallamiento de la roca consiste precisamente en la liberación repentina de los esfuerzos impuestos al terreno. De esta manera, la tierra es puesta en vibración. Esta vibración es debida a la propagación de ondas como en el caso del diapazón.

Ahora bien, en un sólido pueden transmitirse dos tipos de ondas. El primer tipo de ondas es conocido como compresional porque consiste en la transmisión de compresiones y rarefacciones como en el caso de la transmisión del sonido, en este caso las partículas del medio se mueven en el mismo sentido en que se propaga la onda. El segundo tipo es conocido como ondas transversales o de cizallamiento; las partículas se mueven ahora en dirección perpendicular a la dirección de propagación de la onda.

La figura 10 muestra esquemáticamente la propagación de estas ondas en un bloque sólido.

Las ondas compresionales y transversales han sido llamadas P y S respectivamente por razones que se verán más adelante. Son también conocidas como ondas internas porque pueden viajar en el interior de un sólido elástico.

Además de estas dos clases de ondas pueden existir otros dos tipos más llamadas superficiales. Estas ondas viajan en la superficie de la tierra y su

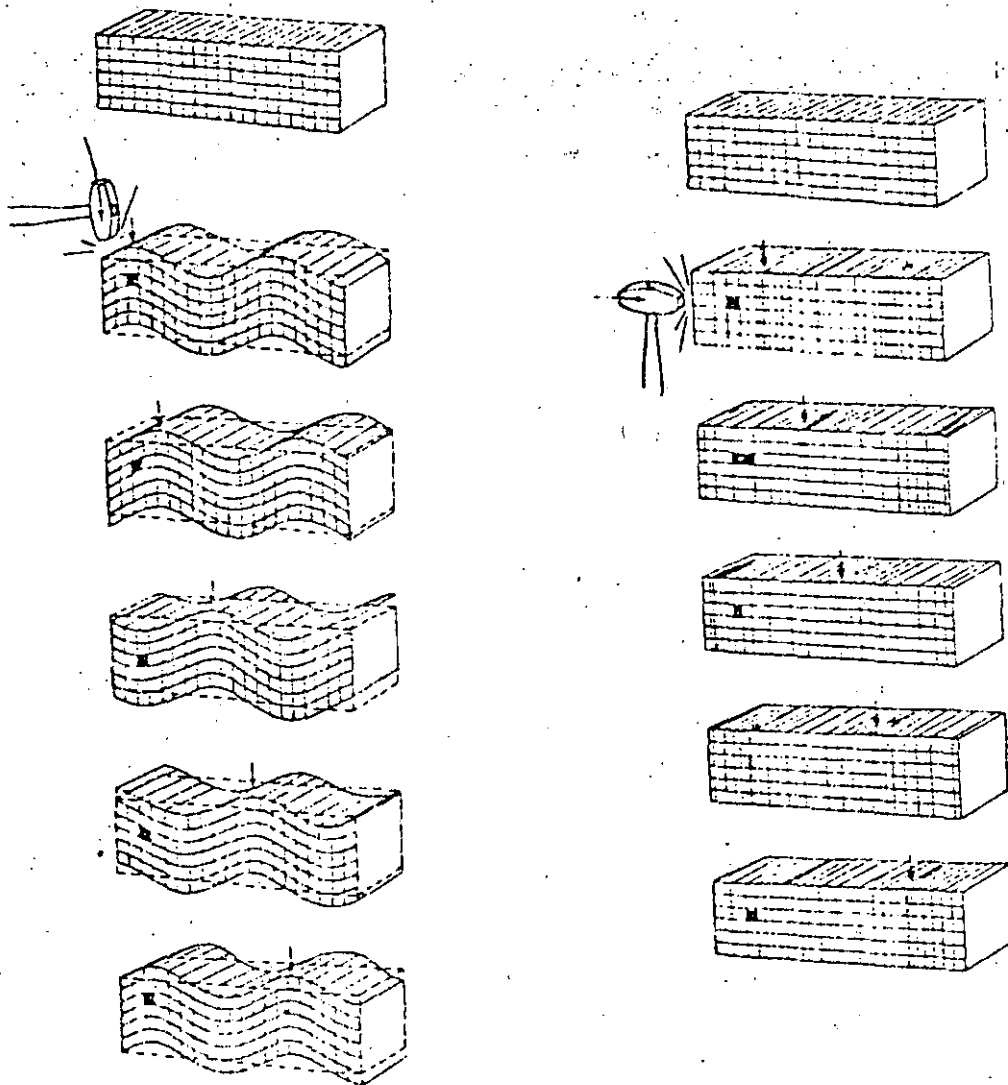


Fig. 10

amplitud decrece con la profundidad. Se les ha denominado con el nombre de los científicos que demostraron teóricamente su existencia: Rayleigh y Love.

Las ondas de Rayleigh se originan en la superficie de un sólido elástico, es decir, estas ondas no podrían generarse en un medio infinito y se caracterizan por la trayectoria elíptica retrógrada que describen las partículas al propagarse la onda. Esta trayectoria ocurre en el plano de propagación de la onda (Fig. 11).

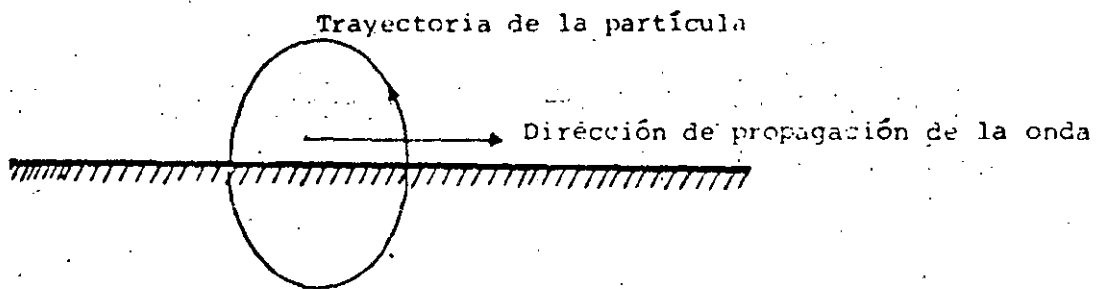


Fig. 11

Por otro lado, las ondas de Love ocurren cuando existe una interfase entre dos medios elásticos de distintas propiedades. Como las ondas S, las ondas de Love ocurren con un movimiento de las partículas perpendicular a la dirección de propagación, sólo que, polarizado en el plano de la superficie terrestre (Fig. 12).

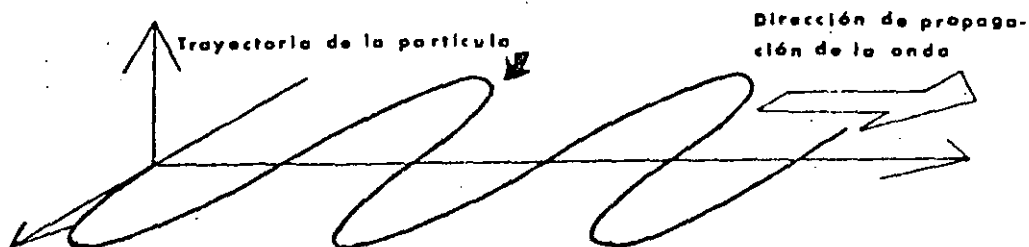


Fig. 12

¿Cuál es la velocidad de estas ondas? Se puede demostrar teóricamente y se observa experimentalmente que la velocidad de las ondas es tal que:

$$V_L < V_S < V_P$$

donde  $V_P$ ,  $V_S$  y  $V_L$  son las velocidades de la onda P, S y superficiales respectivamente.

Las velocidades de las diferentes ondas dependen de las características del medio; por ejemplo, en rocas ígneas la velocidad de las ondas P es del orden de 6 km/seg mientras que en rocas poco consolidadas es de aproximadamente 2 km/seg o menor. Así, las ondas P de un terremoto originado en la Costa de Acapulco serían sentidas en la ciudad de México en menos de 2 minutos.

#### SISMOGRAFOS Y SISMOGRAMAS.

Los mecanismos para detectar los temblores fueron ideados a fines del siglo pasado y perfeccionados a principios de éste. Actualmente estos instrumentos han alcanzado un alto grado de sofisticación, pero al principio básico empleado no ha cambiado. Si tomamos en cuenta que al ocurrir un temblor el suelo se mueve, entonces para poder observar este movimiento tendríamos que estar en un punto fijo fuera de la tierra para no sufrir nosotros mismos ese movimiento y poder detectarlo; ésto obviamente es imposible. Sin embargo, es posible construir un mecanismo que pueda medir este movimiento relativo.

El mecanismo consiste de una masa suspendida de un resorte atado a un soporte acoplado al suelo (Fig. 13), cuando el soporte se sacude al paso de las

ondas sísmicas, la inercia de la masa hace que ésta permanezca un instante

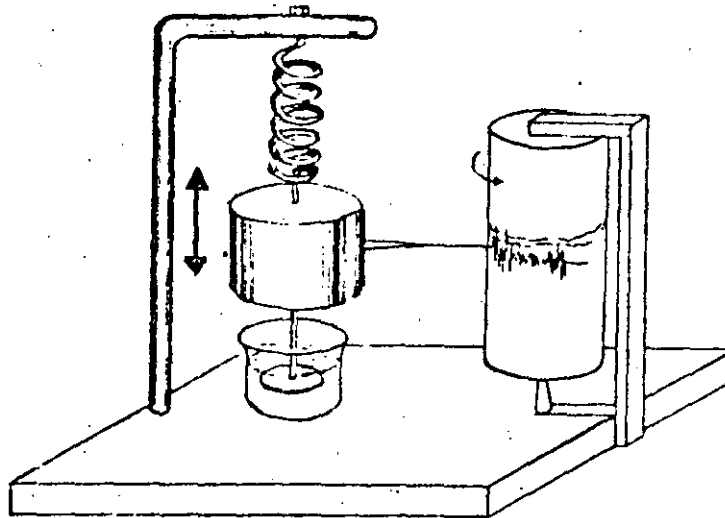
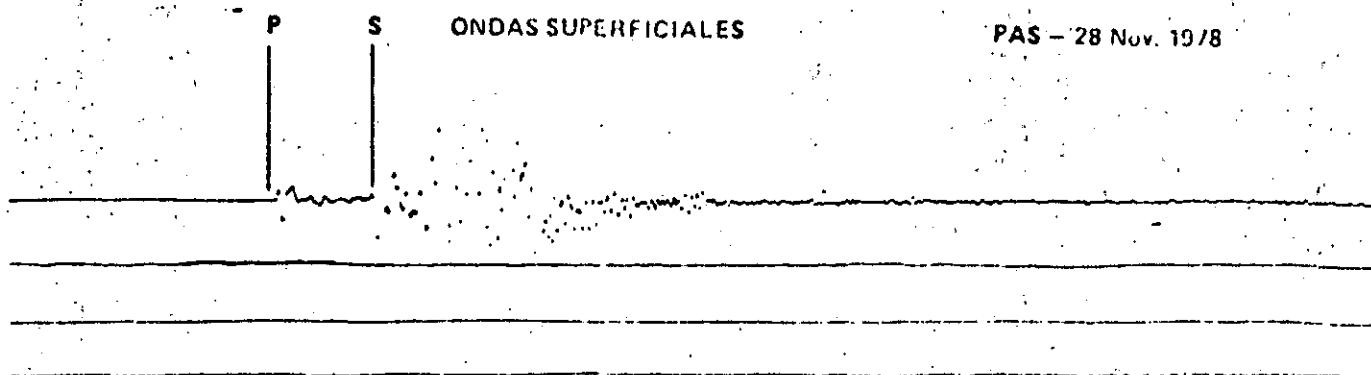


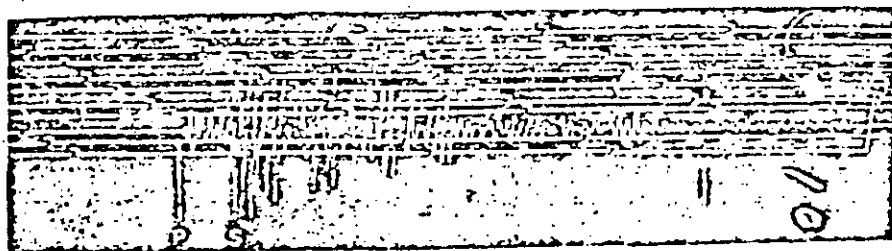
Fig. 13

en el mismo sitio de reposo. Posteriormente cuando la masa sale del reposo, oscila. El movimiento posterior del péndulo no refleja el movimiento del suelo, por lo cual se ha ideado un método para volver a la masa a su sitio original, ésto es lo que se conoce como amortiguamiento del aparato. En la Figura 13 se representa el amortiguamiento como una lámina sumergida en un líquido (comúnmente aceite).

Si se sujeta un lápiz de la masa suspendida para que pueda inscribir sobre un papel pegado sobre un cilindro que gira a velocidad constante, se podrá registrar sucesivamente el movimiento del suelo. El instrumento, hasta aquí descrito, para detectar la componente vertical del movimiento del suelo, se conoce como sismógrafo vertical y el papel donde se inscribe se llama registro o SISMOGRAMA. Sismogramas típicos se muestran en la Figura 14. Los movimientos del suelo también tienen componente horizontal y para me-



Sismograma de la estación sísmológica de Pasadena (EE.UU.) correspondiente al temblor de Oaxaca del 28 de noviembre de 1978  $\Delta \approx 3060$  km.



Sismograma de la estación sísmológica de Tacubaya correspondiente al temblor del día 22 de febrero de 1979, registrado a las 03h 16' 55" y localizado en el "Eje Volcánico Central". Distancia ( $\Delta$ ) de la estación de Tacubaya 120 km

Fig. 14

dir este movimiento se requiere de péndulos horizontales que oscilan como una puerta que tiene su eje inclinado (Fig. 15a). El sísmógrafo horizontal se representa en la (Fig. 15b).

Los sísmógrafos que se emplean actualmente, en general tienen masas que pueden ser de unos gramos hasta 100 kg, mientras que los sísmógrafos antiguos de amplificación mecánica solían tener grandes masas con el fin de vencer las fuerzas de rozamiento, tal es el caso del sísmógrafo horizontal Wiechert de 17000 kg de la estación sísmológica de Tacubaya (apéndice A); el amortiguamiento se hace por corrientes parásitas o imanes, etcétera, la amplificación por medio de palancas y galvanómetros y la inscripción en papel ahumado, papel fotográfico o cinta magnética.

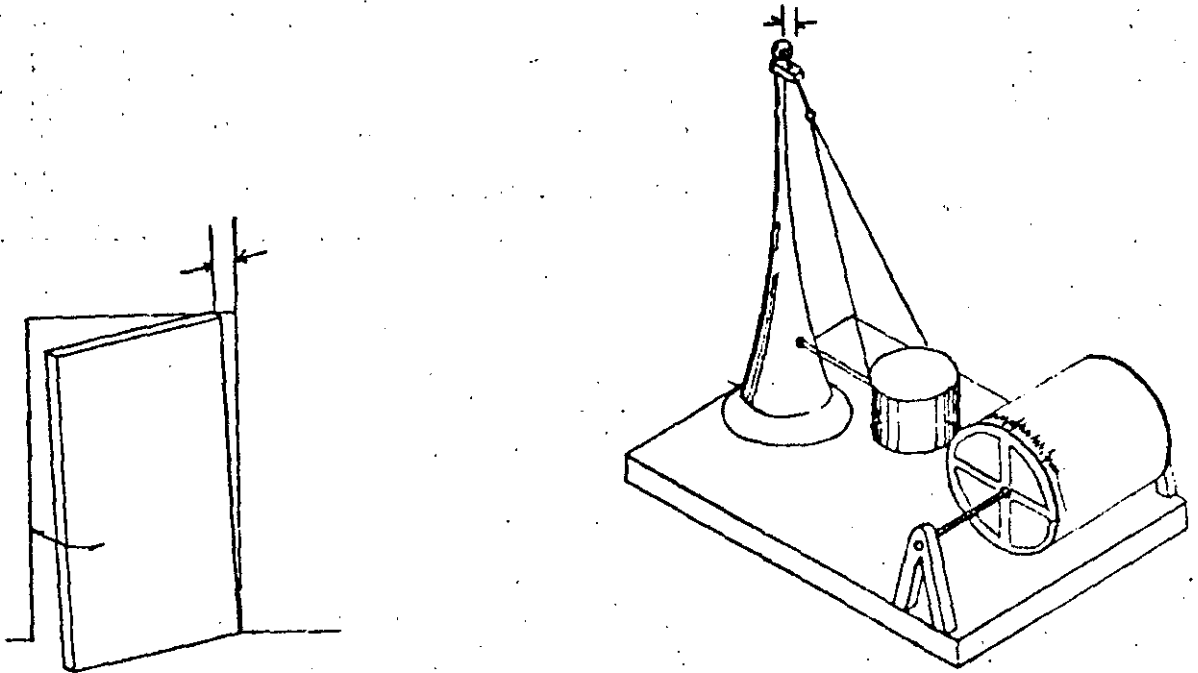


Fig. 15

Los Sismómetros son los sismógrafos cuyas constantes físicas son conocidas de tal manera que se puede conocer el movimiento real del suelo calculado directamente de los sismogramas.

Para determinar con precisión el epicentro de un temblor se requiere del auxilio de varias estaciones sismológicas, por lo cual los observatorios sismológicos requieren por lo menos de tres estaciones sismológicas o formando redes de éstas. Tal como la Red Sismológica Mexicana (ver apéndice B) que controla el Servicio Sismológico Nacional, organismo encargado de la generación de datos e información sismológica. En México existen otras redes de proyectos específicos como RESMAC\*, RESNOR\*\*, y SISMEX\*\*\*. A ni-

\* "RED SISMICA MEXICANA DE APERTURA CONTINENTAL" operada por el Instituto de Matemáticas Aplicadas y Sistemas de la UNAM.

\*\* "RED SISMOLOGICA DEL NOROESTE" operada por el Centro de Investigación y Enseñanza Superior de Ensenada, B.C.

\*\*\* "SISTEMA DE INFORMACION SISMOTECTONICA DE MEXICO" operada por el Instituto de Ingeniería de la UNAM.

vel mundial existen convenios para el intercambio de datos entre los diferentes observatorios, formando así todas las estaciones la red mundial.

#### DETERMINACION DEL EPICENTRO

Hemos mencionado que el lugar en que comienza el fallamiento que produce los temblores es llamado foco. A grandes distancias el plano completo de ruptura aparece como un punto y lo llamamos foco; la proyección de éste sobre la superficie terrestre recibe el nombre de epicentro (Figura 16).

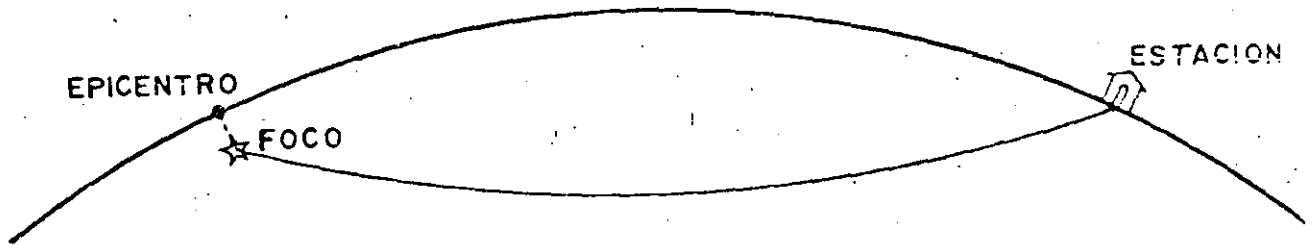


Fig. 16

¿Cómo determinan los sismólogos la ubicación del epicentro?. Ya se dijo que los sismógrafos amplifican e inscriben el movimiento del suelo en una tira de papel (o cualquier otro tipo de material similar) que se llama registro o sismograma. En el sismograma se registran en orden sucesivo de tiempo los diferentes tipos de ondas generadas por un temblor y que arriban a la estación sismológica, como se puede apreciar en la Figura 14. La ubicación del epicentro de un temblor se hace analizando sus registros e identificando los diferentes tipos de ondas como se muestra en la Figura

20. Se ha mencionado ya que la velocidad de las ondas P es mayor que la de las ondas S. Este hecho es utilizado en una de las técnicas más comunes de la Sismología para determinar el epicentro. En efecto, supongamos que la persona A es más veloz que la persona B (Fig. 17). Si ambas empiezan a correr desde el punto 0 en el momento que están juntas a medida que se alejan de 0 la distancia entre ellas será mayor. Puede utilizarse la separación entre ellas en un punto dado para calcular la posición del origen a partir de ese punto.

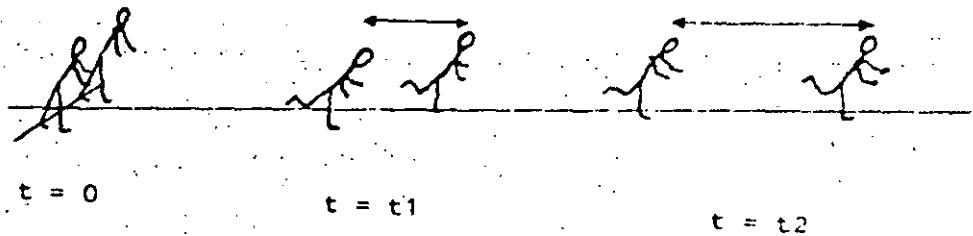


Fig. 17

Sobre la superficie de la tierra, una estación puede proporcionar la distancia al epicentro pero no su dirección de manera que son necesarias al menos tres estaciones para determinarlo sin ambigüedad (Fig. 18).

En la práctica, la intersección de los círculos correspondientes a las tres estaciones no coincide en un solo punto sino comprende una región más o menos grande dependiendo de la calidad de los datos utilizados. La información obtenida de estaciones adicionales es tratada estadísticamente en otras técnicas sismológicas para refinar la posición.

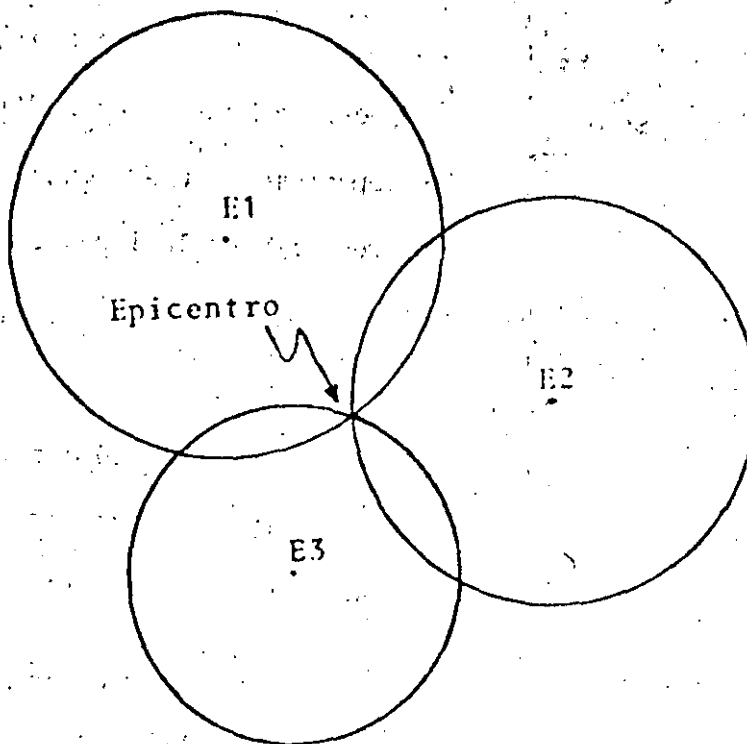


Fig. 18

#### ESCALA DE MAGNITUD E INTENSIDAD.

Las escalas de magnitud e intensidad son utilizadas para cuantizar o medir los temblores. La escala de magnitud está relacionada con la energía liberada como ondas sísmicas; la de intensidad con los daños producidos por el sismo. Ambas escalas son necesarias puesto que miden aspectos diferentes de la ocurrencia de un temblor. Así la escala de magnitud está relacionada con el proceso físico mismo mientras que la de intensidad lo está con el impacto del evento en la población, las construcciones y la naturaleza.

Como es natural, una clasificación de los temblores por medio de sus efectos, que son observables, fue el primer intento de catalogarlos. Escalas

de intensidad fueron propuestas desde los últimos años del siglo pasado. En 1902 Mercalli propuso una tabla, que fue posteriormente modificada en 1931 y desde entonces se le ha llamado escala Modificada de Mercalli (MM). Esta no es la única; pero sí la más frecuentemente usada en nuestro continente. Consta de 12 grados como puede apreciarse en la Tabla I donde se muestran también las características de cada grado.

Podemos ver que la escala de intensidad es en gran medida subjetiva. No nos da información sobre la energía liberada en el temblor puesto que por ejemplo un sismo pequeño puede causar más daños a una población, si ésta está cercana al epicentro, que uno grande pero a mayor distancia.

Así pues es necesario catalogar temblores de acuerdo con los procesos físicos de la fuente; pero también de manera tal que puedan ser medidos. Desde el punto de vista físico sería conveniente clasificar los temblores de acuerdo con la energía que disipan y aunque podríamos hacerlo, no tenemos instrumentos que puedan medirla directamente.

Resulta entonces necesario encontrar una metodología para poder precisar no sólo el epicentro del sismo sino la magnitud y fecha del mismo.

Poseemos sin embargo sismogramas y éstos pueden ser utilizados para catalogar temblores de una manera racional como se verá a continuación.

De dos temblores ocurridos en el mismo epicentro y registrados en el mismo lugar, el más débil producirá un trazo pequeño en el papel y el más fuerte un trazo grande. Para un mismo sismo y estaciones que se alejan gradualmente del epicentro la traza se hace igualmente menor (Fig. 19).

TABLA I

ESCALA MODIFICADA DE MERCALLI

- I. Microsismo.  
Detectado por instrumentos.
- II. Sentido por algunas personas  
(generalmente en reposo).
- III. Sentido por algunas personas dentro de edificios.
- IV. Sentido por algunas personas fuera de edificios.
- V. Sentido casi por todos.
- VI. Sentido por todos.
- VII. Las construcciones sufren daño moderado.
- VIII. Daños considerables en estructuras.
- IX. Daños graves y pánico general.
- X. Destrucción en edificios bien contruidos.
- XI. Casi nada queda en pie
- XII. Destrucción total.

\* Una escala más detallada aparece en el Apéndice D.

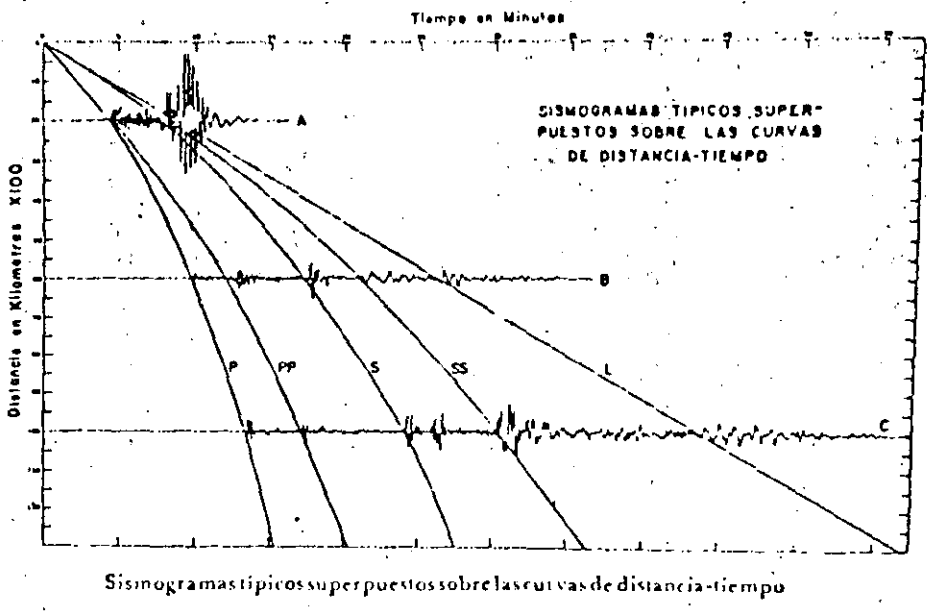


Fig. 19

Si se grafican los valores del logaritmo de la amplitud de la traza contra la distancia, se obtienen gráficas como las mostradas en la Fig. 20. En esa misma figura, la curva más baja representa un temblor más pequeño. Resulta entonces lógico tomar cualquiera de estos sismos como el sismo patrón

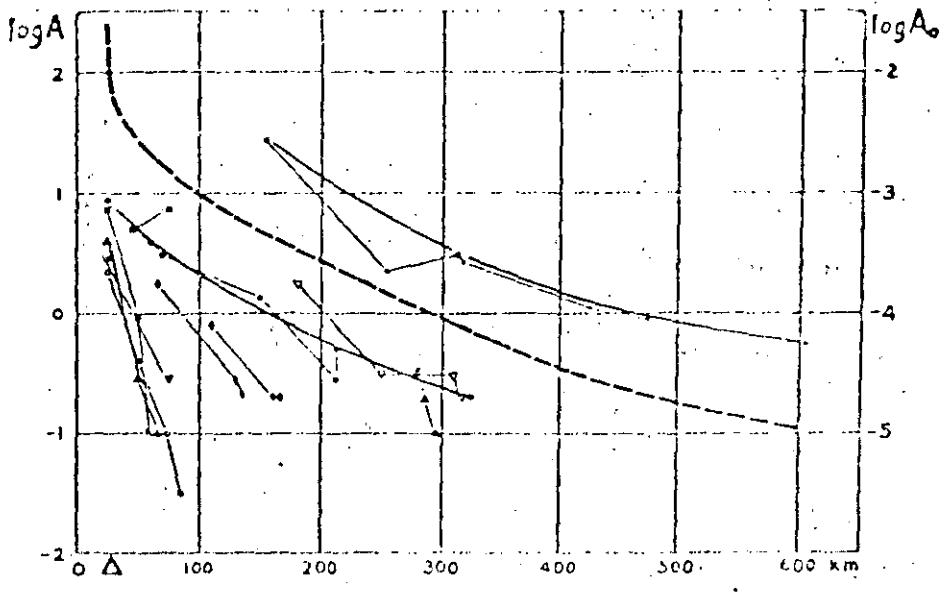


Fig. 20

y asignarle la magnitud cero, los demás pueden ser medidos a partir de éste midiendo la separación entre ellos para cualquier distancia del epicentro.

Se tiene entonces que:

$$M = \log a - \log A_0$$

El temblor patrón, de magnitud cero se define como aquel que teniendo su epicentro a 100 km de distancia deja una traza de una micra en un sismógrafo Wood-Anderson elegido también como sismógrafo patrón.

Se tiene ahora una fórmula que nos proporciona un valor relacionado con el "tamaño" del sismo e independiente de los daños que pueda ocasionar. Este mismo valor ha sido relacionado por los sismólogos con la energía liberada por el sismo. Existen diferentes fórmulas que relacionan la energía con la magnitud de un sismo, éstas varían porque la amplitud medida en el sismograma puede ser la de cualquiera de las distancias fases (P, S, superficiales) que son registradas.

Un temblor de magnitud 5.5 libera una energía del orden de magnitud de la de una explosión atómica\*, es decir unos  $10^{20}$  ergs. Sin embargo, la energía de un sismo de magnitud 8.5 no es tres veces esa energía sino la equivalente a la de unas 27,000 de estas bombas atómicas, esto es, la energía aumenta aproximadamente 30 veces por cada grado. Esto puede verse más claramente en las fórmulas que relacionan magnitud y energía; éstas son de la forma:

$$\log E = a + bM$$

donde a y b dependen de la forma en que es calculada M.

Notemos que la escala de magnitud no tiene límites; sin embargo, no se han

\* como la de Hiroshima (20 Ktn de TNT).

encontrado temblores mayores de 8.6. Esto está relacionado con el hecho de que la corteza tiene un límite de ruptura más allá del cual ya no pueden acumularse más esfuerzos. Un ejemplo de un temblor de esta magnitud es el de Alaska del 28 de marzo de 1964.

Notemos también que pueden existir temblores de magnitud negativa, puesto que el sismo patrón (de magnitud cero), es elegido, hasta cierto punto arbitrariamente.

La determinación de magnitudes ha sido mejorada en las últimas décadas utilizando la disponibilidad de más información y modelos teóricos. Sin embargo el principio básico es el mismo.

En el Apéndice C se detallan algunos de los sismos mexicanos más destructivos.

#### LA CONSTITUCION DE LA TIERRA.

En el primer apartado de este artículo se consideró la estructura de la tierra. ¿Cómo fue posible conocerla si las perforaciones más profundas no alcanzan sino unos pocos kilómetros?. La respuesta está nuevamente en la Sismología.

De igual manera que un médico puede saber si existe fractura en los huesos de un accidentado por medio de rayos X, el sismólogo ha deducido la estructura de la tierra por medio de las ondas sísmicas que viajan a través de ella como los rayos X a través del cuerpo humano.

Supongamos que ocurre un sismo en un punto dado si la tierra fuera completamente homogénea los rayos viajarían en líneas rectas del foco al observador

(Fig. 21a).

Los sismogramas observados serían relativamente simples. Los científicos han hallado que los rayos no viajan en línea recta sino que van curvándose hacia la superficie debido a que la velocidad de las ondas aumenta con la profundidad. (Ver Fig. 21b). Además de esto se encuentra que éstas sufren refracciones y reflexiones que sólo pueden explicarse si la tierra está compuesta por las diferentes regiones de que se habló en el primer apartado. Los temblores resultan entonces, tener un aspecto positivo y es éste el de darnos a conocer el interior de nuestro planeta.

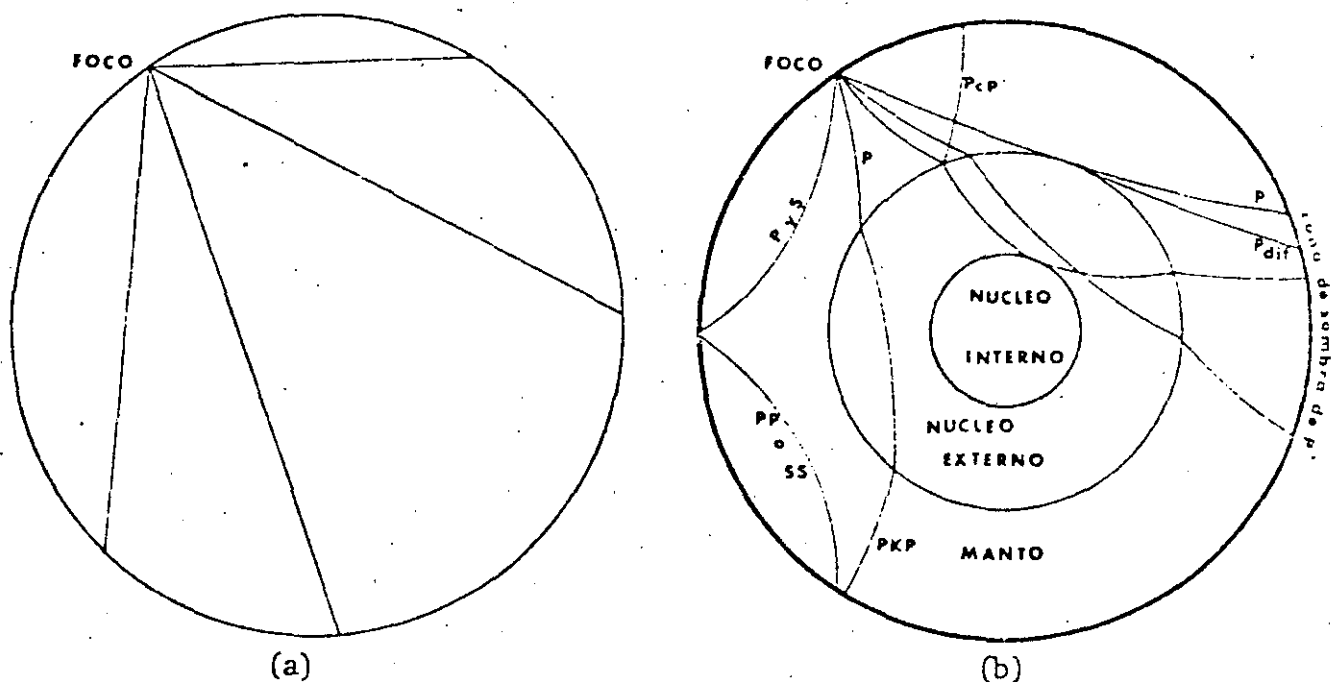


Fig. 21

## SISMICIDAD

En los últimos 80 años se han podido registrar todos los temblores más importantes (en cuanto a energía) de manera que se han podido hacer estudios cualitativos de la sismicidad de la tierra, así se ha obtenido un esquema

global de la sismicidad mundial. El mapa de la Figura 22 muestra la distribución geográfica de sismos. Se puede observar que la mayor parte de energía sísmica se libera en las costas del Océano Pacífico región que se conoce como cinturón de fuego debido a que en esta zona ocurre también gran actividad volcánica. Hay otras regiones, como el Atlántico medio y el cintu-

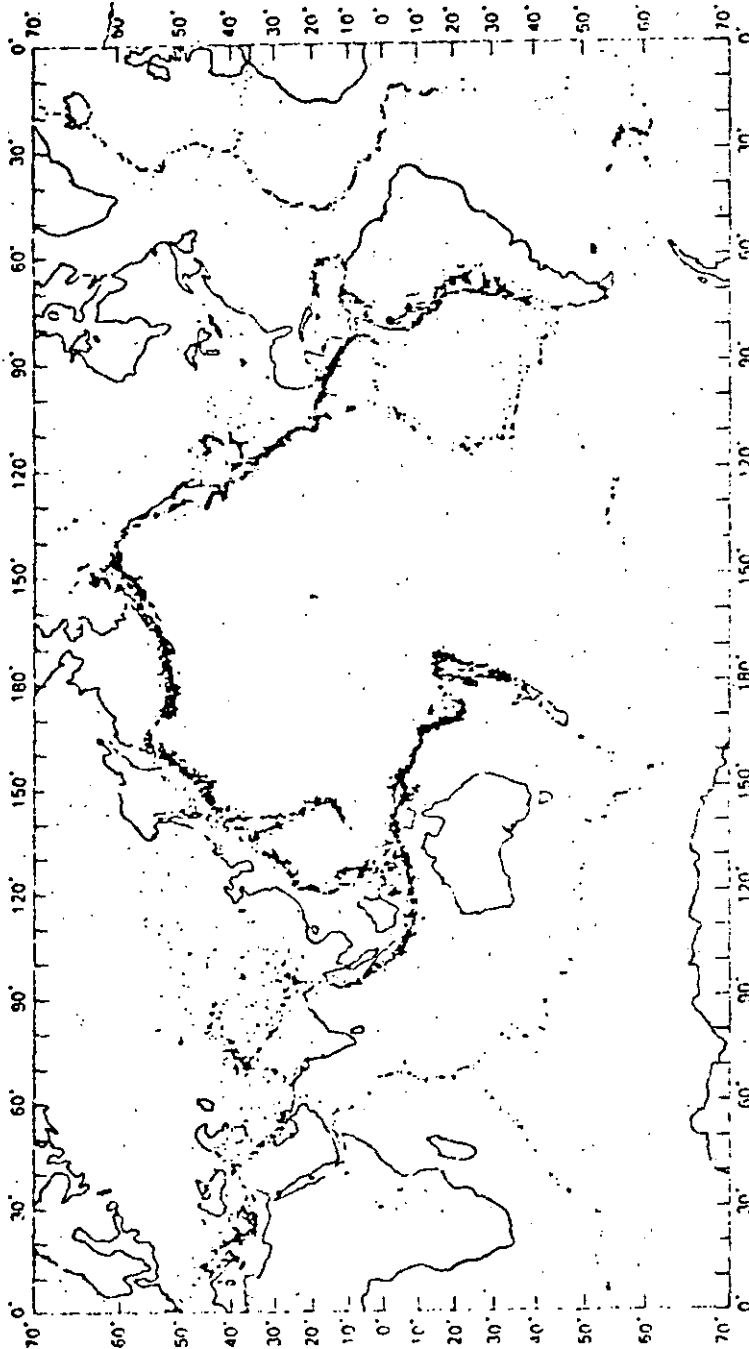


Fig. 22

rón Eurásico pero con una actividad sísmica menor. Nótese que estas franjas coinciden con los límites de placas de la Figura 3. Existen también regiones donde la actividad sísmica es casi nula o desconocida. A estas regiones se les suele llamar escudos. Desde luego que los países que se sitúan en zonas sísmicas serán más afectados por los sismos.

#### SISMICIDAD GLOBAL.

Observando la actividad sísmica mundial se puede estimar el número de temblores de cierta magnitud que ocurren en un año. Se ha visto que por lo menos ocurren dos grandes terremotos actualmente (ver Tabla II). Por otra parte están ocurriendo varios cientos de miles de temblores de magnitud inferior a 3 que pasan desapercibidos.

TABLA II  
PROMEDIO ANUAL DE TEMBLORES

MAGNITUD	NÚMERO PROMEDIO
8	2
7	20
6	100
5	3000
4	15000
3	150000

#### SISMICIDAD DE MEXICO

A fines del siglo pasado se conocía la historia acerca de la actividad sísmica de México desde 1400. Posteriormente con el desarrollo técnico sismológico hacia 1910 se inauguró la red sismológica mexicana (ver apéndice A). De esa fecha a la actualidad se han generado sismogramas que se conservan

en el Servicio Sismológico, en la estación Sismológica de Tacubaya.

Durante los últimos 70 años se han registrado y localizado, utilizando los datos de la red sismológica mexicana, sismos ocurridos en la República Mexicana hecho por el cual actualmente se conoce bastante bien la sismicidad de México (Fig. 23).

#### PREMONITORES Y REPLICAS

Los sismólogos han observado que inmediatamente después de que ocurre un gran temblor, éste es seguido por temblores de menor magnitud llamados réplicas y que ocurren en las vecindades del foco del temblor principal. Se piensa que la ocurrencia de éstos se debe probablemente al reajuste mecánico de la región afectada. Inicialmente la frecuencia de ocurrencia es grande pero decae gradualmente con el tiempo dependiendo de la magnitud del Temblor principal. Por ejemplo para el temblor de Oaxaca del 29 de noviembre de 1978 de magnitud 6.8 inicialmente se observaron hasta 200 réplicas de magnitud mayor que 2.0 diariamente y fue decayendo esta actividad durante 5 meses aproximadamente. El estudio de las réplicas de un gran temblor se ha aprovechado para estimar las dimensiones de la región focal.

Frecuentemente algunos temblores grandes son precedidos por temblores de menor magnitud llamados temblores premonitores que comienzan a fracturar la región focal del gran temblor. No es fácil determinar cuando un temblor queño es un premonitor de un gran temblor ya que se suele confundir con cualquier otro no relacionado. En la generalidad de los casos se sabe que un temblor es premonitor sólo en el contexto de la actividad posterior.

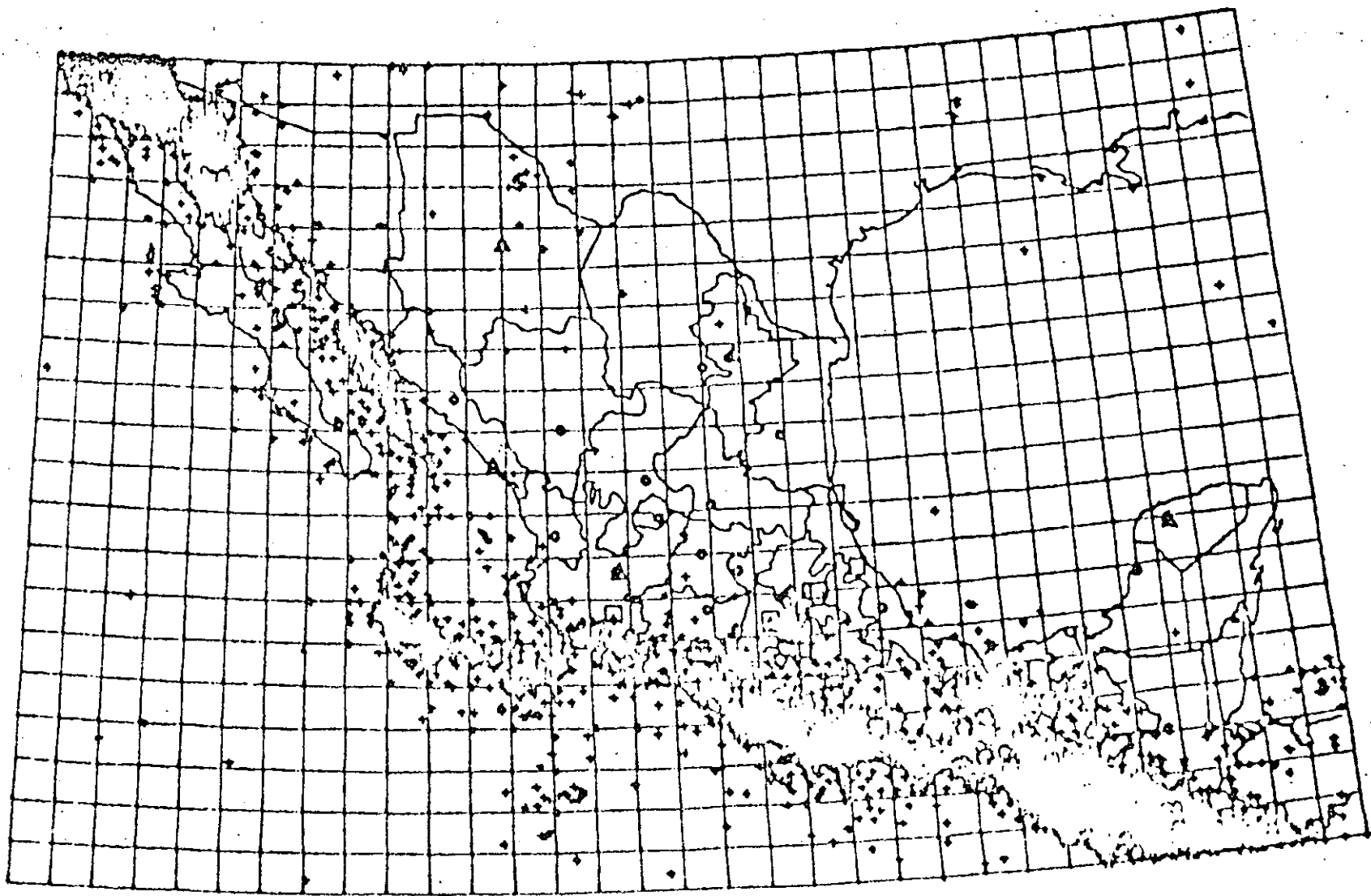


Fig. 23 Sismicidad de México, de 1900 a 1974.

## PREDICCIÓN

¿Se pueden predecir los temblores? La respuesta a esta pregunta depende de lo que se entienda por predicción. Año tras año podemos leer en los periódicos las declaraciones hechas por adivinadores, mediums y otras gentes por el estilo, sobre la futura ocurrencia de temblores en algún lugar del planeta. Estas declaraciones distan mucho de ser predicciones. Se ha visto (Tabla II) que en promedio ocurren cerca de 120 temblores de magnitud mayor a 6 anualmente. Se conocen también las zonas sísmicas del planeta, de manera que por ejemplo el afirmar que durante el año de 1981 ocurrirá un temblor en la costa occidental de México no contiene información novedosa ni útil.

En la última década el desarrollo de la sismología ha llevado a los sismólogos a la convicción de que éstos pueden ser predichos. La investigación en este aspecto es relativamente nueva a pesar de la cual se han logrado resultados prometedores.

Existen esencialmente dos maneras de atacar el problema. En una de ellas se estudia la variación de ciertos parámetros físicos debido a la acumulación de los esfuerzos cuya relajación ocasiona el temblor. Así por ejemplo, se ha observado que la región focal sufre una dilatación que altera la velocidad de las ondas que se propagan en ella. Otros de los parámetros que se alteran son por ejemplo resistencia del terreno al paso de corriente eléctrica y el nivel freático. Todos estos factores pueden ser medidos y correlacionados con la ocurrencia final del temblor.

En otra de las formas de enfrentar el problema se ha estudiado la sistematicidad en la ocurrencia de los temblores. Se ha observado que los epicentros a lo largo de una zona de subducción no se distribuyen al azar sino siguiendo un patrón geográfico y temporal. Puede entonces estudiarse la his-

toria sísmica de una región, estimar los períodos de recurrencia de temblores de cierta magnitud y evaluar de esta manera la posibilidad de ocurrencia de un temblor.

Este breve bosquejo trata solamente de poner de manifiesto que los sismólogos actuales se encuentran trabajando sobre bases científicas para la futura predicción de temblores. Cuanto tiempo tomará el desarrollar un sistema eficiente para predecir temblores es difícil de precisar pero seguramente será de algunas décadas. Indudablemente ésto requerirá del desarrollo de nuevas metodologías tanto teóricas como instrumentales.

#### ¿QUE HACER CUANDO OCURRE UN TEMBLOR?

Existen varias medidas que deben tomarse en caso de ocurrir un temblor, pero ante la eminencia de un suceso de esta naturaleza, en regiones sísmicamente activas es mejor prepararse mentalmente para una eventualidad. Por otra parte conviene buscar las condiciones adecuadas de seguridad de los si tios donde se permanece más tiempo como son: la casa, el trabajo, la escue la, etcétera.

La seguridad de las casas en caso de temblores se garantiza construyendo a éstas según los códigos de construcción antisísmica de la región, si en los centros de trabajo se observa poca seguridad en las instalaciones pedir que sean reforzadas. En México las escuelas, y en general, obras civiles son construidas tomando en cuenta el código de construcción pero si se observa alguna anomalía conviene reportarlo a las autoridades competentes. Debe evitarse el colocar objetos pesados o peligrosos como lámparas, etcétera en repisas y lugares elevados a no ser que estén bien sujetos.

Cuando ocurra el temblor, es conveniente tomar en cuenta lo siguiente:

1. Conservar la calma y tratar de serenar a las personas que nos rodean. Evitar dar gritos ya que éstos infunden pánico, y éste es el origen, en muchos casos, de más fatalidades que el temblor mismo.
2. No desplazarse precipitadamente en interiores, es mejor buscar sitios que ofrezcan seguridad (debajo del dintel de puertas, debajo de mesas robustas, lugares con techumbres livianas, etcétera).
3. Tener cuidado de no permanecer debajo de objetos colgantes u objetos mal colocados. Alejarse de las ventanas ya que los vidrios se rompen con las sacudidas, tampoco permanecer cerca de objetos que se puedan desplazar o derribar (como armarios altos, vitrinas, muebles con ruedas, etcétera).
4. En las escuelas, los maestros deben conservar la serenidad y tratar de dar confianza a los alumnos, pedir a éstos que se alejen de las ventanas y, de ser posible, protegerse debajo de las mesas o los dinteles de las puertas. Si están en los patios de recreo pedir que permanezcan lejos de los edificios. Estas explicaciones y un simulacro deberían constituir práctica ordinaria al inicio de clases en todas las escuelas.
5. En otros centros de mucha concentración se aconseja no salir precipitadamente ya que ésta es la respuesta de la mayor parte de personas y se ha visto que causa muchos accidentes personales. Lo mejor es buscar sitios seguros debajo de estructuras reforzadas.
6. Se debe tomar en cuenta que los temblores no duran mucho tiempo, pero a veces ocurren otros. De manera que debe obrarse con cautela al final de uno.

## QUE HACER DESPUES DE OCURRIR UN TEMBLOR

Después de ocurrir el temblor se debe revisar si hubo daños y accidentados y proveer ayuda si es necesario. Posteriormente revisar si las diferentes instalaciones eléctricas, gas, agua, etcétera no sufrieron daños. Si es de noche no prender fósforos para alumbrarse hasta no estar seguro que no existen fugas de gas. No use el teléfono si no es para transmitir un mensaje de mucha prioridad.

En las escuelas antes de movilizar a los alumnos conviene inspeccionar el estado de los lugares de acceso: puertas, escaleras, barandales, etcétera. Posteriormente evacuar la escuela para una revisión detallada de sus instalaciones. Esto mismo se debe hacer en caso de edificios altos.

A P E N D I C E S

## BIBLIOGRAFIA

- Z. Jiménez (1979). Algunos aspectos relevantes de la interpretación de sismogramas. Ciencia y Desarrollo, No. 26.
- I.P.G.H. (1979). Temblores de Tierra. Cartilla Popular publicación No. 363.
- B. Bolt (19 ). Earthquakes. A primer. Freeman Publishing Co. San Fco. Calif.
- M. Muñoz L. (1918). La Sismología en México hasta 1917. Instituto Geológico de México, Boletín No. 36.
- J. Yamamoto (1980). Cronología de Terremotos: Historia del miedo. Comunidad CONACYT, No. 111, 1980.

## APENDICE A.

## HISTORIA DE LA SISMOLOGIA EN MEXICO.

La República Mexicana está situada en una de las regiones sísmicamente más activas del mundo como se puede apreciar en la Figura 24. El estudio de la actividad sísmica en México es relativamente reciente, sin embargo su observación tiene antecedentes remotos. Sabemos que los primeros pobladores de México se percataron de la actividad sísmica y volcánica en estas regiones y posiblemente hasta existieron personas dedicadas a estudiar estos fenómenos.

En la época de la colonia la descripción de los temblores la hicieron principalmente los monjes en algunos conventos y se encuentran anotadas en algunas obras de Clavijero y Sahagún. Con el uso generalizado de la imprenta se reportaban datos sismológicos en los periódicos de la época con descripciones a veces pintorescas y exageradas. Posteriormente los temblores eran observados por naturalistas, publicistas y por el público en general, pues en todos los folletos antiguos se encuentran notas sobre temblores, cuyas áreas se empezaban a delimitar a medida que las comunicaciones se establecían entre pueblos.

Cuando se instaló la red telegráfica en la República Mexicana los telegrafistas suministraban datos referentes a temblores y se publicaban mensualmente en boletines.

La medición de los temblores por medio de instrumentos se inició a fines del siglo pasado, en la época de Mariano Bárcena, se instaló en el Observatorio Meteorológico Central un sismógrafo del Padre Sechi. Por ese tiempo Juan Orozco y Berra se dedicó a observar estos fenómenos y formar estadísti

cas, reuniendo importantes datos de temblores desde tiempos precolombianos, coleccionados con cuidado y publicados en la sociedad científica Antonio Alzate. Sin embargo es hasta el 5 de septiembre de 1910 que por Decreto Presidencial se crea e inaugura el Servicio Sismológico Nacional. Este evento se enmarcó dentro de los festejos conmemorativos del primer centenario de la iniciación de la Independencia Nacional. Dicho servicio dependía del Instituto Geológico Nacional.

La red inicial consistió del Observatorio Central de Tacubaya y estaciones ubicadas en Oaxaca, Mérida, Zacatecas, Mazatlán, Guadalajara y Monterrey. Se eligieron como sensores los sismógrafos Wiechert de período corto. Básicamente, estos sismógrafos con algunas modificaciones y mejoras continúan operando.

Hacia 1929, el Instituto Geológico Nacional pasó a ser el Instituto de Geología de la UNAM y el Servicio Sismológico formó parte de este nuevo Instituto. En 1949 con la creación del Instituto de Geofísica, el Servicio Sismológico pasó a formar parte de este Instituto.

El Servicio Sismológico vuelve a cobrar vida hacia 1965-1967 cuando se instalaron estaciones de mayor sensibilidad en Tehuantepec (PBJ), Vista Hermosa (VHO), Comitán (COM), Toluca (OXM), León (LCG), Presa Infiernillo (PIM), Presa Mal Paso (PMM), Ciudad Universitaria (UNM), Tepostlán (TPM) y Popocatépetl (PPM). También se instaló por 1970 una red de estaciones en el Noroeste, con el fin de observar la actividad sísmica del Golfo de California. Este conjunto de estaciones ahora es controlado por el Centro de Investigaciones y de Educación Superior de Ensenada, Baja California (CICESE).

Actualmente el Servicio Sismológico cuenta con una red de 14 estaciones

(Apéndice B) siendo el Observatorio Central de Tacubaya la estación más completa y donde se recibe la información sismológica de toda la red.

Desde 1910 el Servicio Sismológico ha generado ininterrumpidamente datos que hoy forman el archivo sismológico del país. Ellos constituyen por sí mismos un valioso acervo formando una fuente de información muy importante.

El Servicio Sismológico ha jugado un papel importante en el desarrollo de la Sismología en México, pero además tiene una función social y económica palpable.

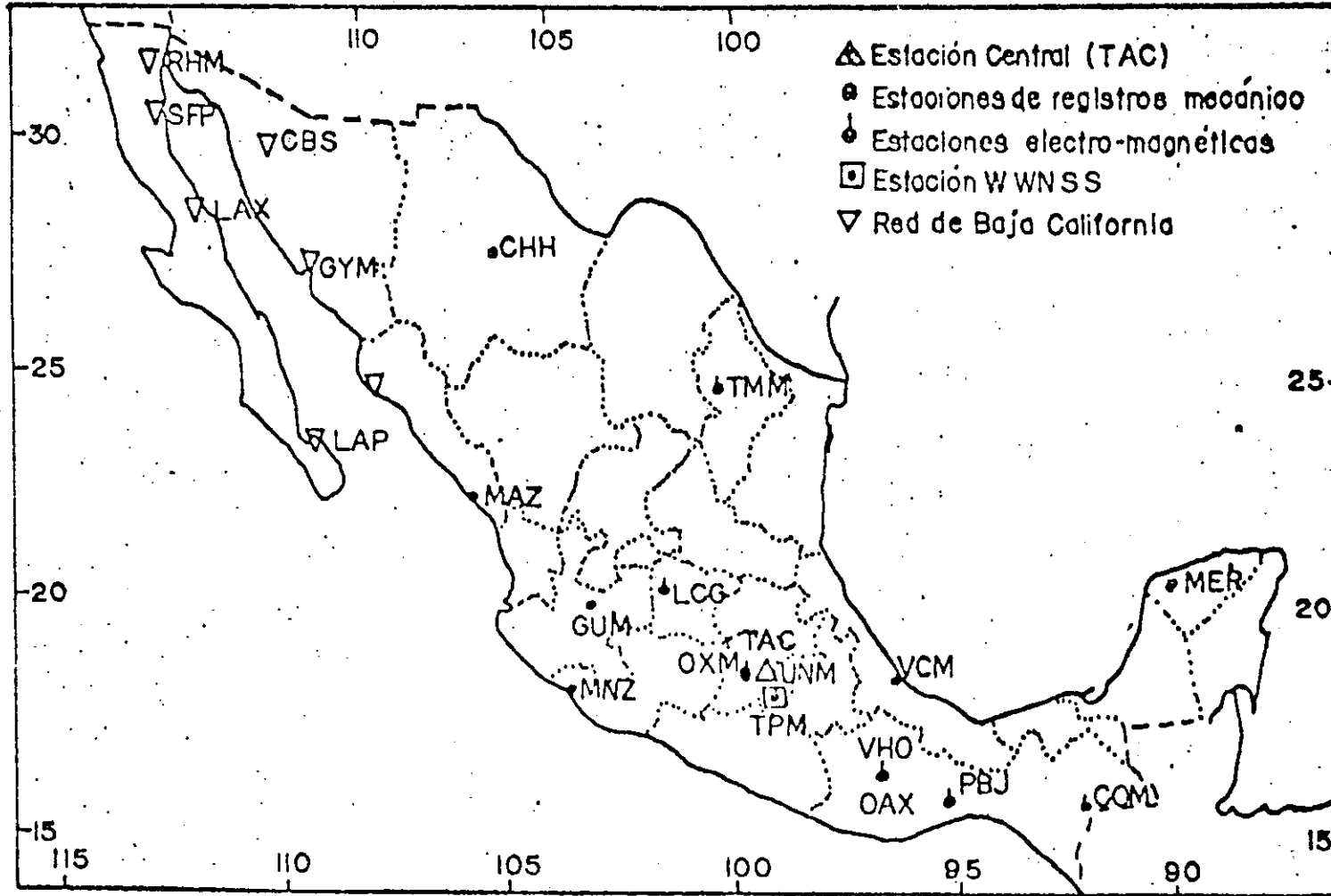
#### DESARROLLO SISMOLOGICO.

En la última década han progresado los estudios de Sismología en México y se han venido formando distintos grupos de trabajo que afrontan los diferentes problemas de Sismología. Existen en la Universidad Nacional Autónoma de México tres de estos grupos de trabajo. El grupo del Instituto de Geofísica, que además de realizar labores de investigación tiene a su cargo el Servicio Sismológico que es el vocero oficial de la UNAM en la divulgación de los parámetros de los temblores. El Instituto de Ingeniería enfoca su trabajo principalmente a problemas de riesgo sísmico y maneja una red de estaciones telemétricas (SISMEX) y el Instituto de Investigaciones Matemáticas Aplicadas y Sistemas, que tiene a su cargo el desarrollo del proyecto de la Red Sísmica de Apertura Continental (RESMAC). Existe otro grupo de trabajo en el Centro de Investigaciones y de Educación Superior de Ensenada, B.C. (CICESE) que enfoca su estudio a la actividad sísmica asociada tanto al Golfo de California como a la falla de San Andrés, igualmente operan la Red Sismológica del Noroeste (RESNOR). Los diferentes grupos tienen comunicación y frecuentemente se realizan simposia donde se dan a conocer los avan-

ces en el estudio de la Sismología.

Existe interés en algunas instituciones de enseñanza superior en el interior de la República por el estudio de la Sismología y, recientemente, están enfocando sus esfuerzos por consolidar grupos de trabajo propios para el desarrollo de esta disciplina en sus localidades.

SERVICIO SISMOLOGICO NACIONAL



33

## ESCALA DE INTENSIDADES SISMICAS

Escala de Mercalli modificada en 1931 por Harry O. Wood y Frank Neuman.

- I. Sacudida sentida por muy pocas personas en condiciones especialmente favorables.
- II. Sacudida sentida sólo por pocas personas en reposo, especialmente en los pisos altos de los edificios. Los objetos suspendidos delicadamente pueden oscilar.
- III. Sacudida sentida claramente en los interiores, especialmente en los pisos altos de los edificios, muchas personas no la estiman como un temblor. Los carros de motor estacionados pueden moverse ligeramente. Vibración como originada por el paso de un carro pesado. Duración estimable.
- IV. Sacudida sentida durante el día por muchas personas en los interiores, por pocas en el exterior. Por la noche algunas despiertan. Estremecimiento de vajillas, vidrieras y puertas; crujimiento de muros. Sensación como de un carro pesado chocando contra un edificio, los carros de motor no en movimiento se balancean claramente.
- V. Sacudida sentida casi por todo mundo; muchos despiertan. Algunas piezas de vajillas, vidrieras, etc. se rompen; pocos casos de agrietamiento de aplanados; objetos inestables caen algunas veces. Se observan perturbaciones en los árboles, postes y otros objetos altos. Detención de relojes de péndulo.
- VI. Sacudida sentida por todo mundo; muchas personas atemorizadas huyen hacia afuera. Algunos muebles pesados cambian de sitio; pocos ejemplos de caída de aplanados o daño en chimeneas. Daños ligeros.
- VII. Todo mundo huye afuera. Daños sin importancia en edificios bien planeados de buena construcción. Daños ligeros en estructuras ordinarias bien construídas; daños considerables en las débiles o mal planeadas; ruptura de algunas chimeneas. Estimado por las personas conduciendo carros de motor.
- VIII. Daños ligeros en estructuras de diseño especialmente bueno; considerable en edificios ordinarios con derrumbe parcial; grande en estructuras débilmente construídas. Los muros salen de sus armaduras. Caída de chimeneas, pilas de productos en los almacenes de las fábricas, columnas, monumentos y muros. Los muebles pesados se vuelcan. Arena y lodo proyectados en pequeñas cantidades. Cambio en el nivel del agua de los pozos. Pérdida de control en las personas que guían carros de motor.

## APENDICE C

## SISMOS IMPORTANTES.

Quizá uno de los fenómenos naturales que más ha impresionado al hombre ha sido los terremotos. Su inquietud ha hecho que desde la antigüedad tratara de explicarse las causas que los originan, pero no fue sino hasta los últimos 100 años que ha ido entendiendo la naturaleza de las fuerzas que ocasionan estos movimientos, como ya se ha explicado.

Los efectos de los temblores a la comunidad y sus edificaciones ha sido la causa del temor a éstos. Esta es la razón por la cual la mayor o menor liberación de energía de los temblores no ha tenido impacto social. Así el temblor de Alaska del 28 de marzo de 1964 de magnitud 8.5, siendo uno de los pocos temblores que han liberado más energía en los últimos 100 años apenas es considerado socialmente, sin embargo el temblor de Tanshan del 27 de julio de 1976, de menor magnitud 6.3  $m_b$  y 7.9  $M_s$  se ha considerado como el terremoto más mortífero de los últimos cuatro siglos y ha tenido un gran impacto social.

Se pueden hacer listas de los temblores más fuertes, pero no nos daría una idea del riesgo a que están sometidos los pueblos asentados en zonas sísmicamente activas. A continuación se mencionan algunos de los temblores que han ocurrido en el mundo (Tabla I) y en la República Mexicana (Tabla II) y que más impacto social han tenido.

- IX. Daño considerable en las estructuras de diseño bueno; las armaduras de las estructuras bien planeadas se desploman; grandes daños en los edificios sólidos, con derrumbe parcial. Los edificios salen de sus cimientos. El terreno se agrieta notablemente. Las tuberías subterráneas se rompen.
- X. Destrucción de algunas estructuras de madera bien construídas; la mayor parte de las estructuras de mampostería y armaduras se destruyen con todo y cimientos; agrietamiento considerable del terreno. Los rieles se tuercen. Considerables deslizamientos de tierra en las fuertes pendientes. Eyecciones de lodo y arena. Invasión del agua de los ríos sobre las márgenes.
- XI. Casi ninguna estructura de mampostería queda en pié. Puentes destruídos. Anchas grietas en el terreno. Las tuberías y subterráneas quedan fuera de servicio. Hundimientos y derrumbes en terreno suave. Bran torsión de vías férreas.
- XII. Destrucción total. Ondas visibles sobre el terreno. Perturbaciones de las cotas de nivel. Objetos lanzados en el aire hacia arriba.

TABLA I

Fecha	Magnitud Richter		Región	No. de Muertos	Datos generales
	Mb	Ms			
1780, agosto 16	8.6		Chile: Valparaíso Santiago	20 000	
1800, diciembre 28	7.5		Italia: Reggio	29 980	
1812, diciembre 16	8.6		China: Kansu y Stransi	100 000	
1868, septiembre 1	8.3		Japón: Tokio, Yokohawa	99 330	Conocido como el terremoto de Kwantó. Tuvo desplazamientos de 4.5 m y grandes incendios le precedieron.
1877, mayo 22	8.3		China: Nan Shan	200 000	Grandes fallas, se sintió hasta Pekín
1887, diciembre 23	5.6	6.2	Nicaragua: Managua	4 000 - 6 000	Miles de heridos. La ciudad de Managua fue casi totalmente destruida.
1888, mayo 30	7.5		Paquistán: Quetta	30 000	Quetta fue totalmente destruida.
1899, junio 25	8.3		Chile	28 000	
1909, diciembre 26	7.9		Turquía: Erzincan	30 000	Se detectaron movimientos oscilatorios de 3.7 m de desplazamiento con movimientos trepidatorios menores.
1904, febrero 29	5.8		Morocco: Agadir	10 000 - 15 000	Es uno de los temblores que más muertos ha ocasionado a pesar de ser poca su magnitud.
1917, febrero 4	6.2	7.5	Guatemala: Guatemala	23 000	Se calcula en 76 000 el número de heridos. La mayor intensidad se ubicó en el área de Mixco.
1920, agosto 27	6.3	7.9	China: Noreste	655 237	Cerca de 800 000 heridos y daños en el área de Janshan. Este terremoto es probablemente el más mortífero de los últimos 4 siglos y el 2o. más fuerte que registra la historia moderna.

Cont. Tabla I

Fecha	Magnitud Richter		Región	No. de muertos	Datos generales
	Mb	Ms			
1970, mayo 31	-	7.7	Perú: Ihuaras Chimbote, Yungay	50 000 - 70 000	Derrumbes, inundaciones. La peor catástrofe registrada en Perú por un terremoto en este siglo.
1978, septiembre 16	-	7.7	Irán	11 000 - 15 000	Muchos heridos y daños considerables en Bozonabad y áreas circunvecinas.

TABLA II

Fecha	Magnitud Richter		Región	No. de Muertos	Datos generales
	Md	Ms			
1951, junio 7	7		Jalisco-Colima	45	Destructor en Cd. Guzmán Jal., ha sido uno de los temblores más fuertes que han ocurrido los últimos 100 años. Se reportaron 45 muertos en el D.F.
1952, julio 16	7		Oaxaca-Puebla	?	Grandes daños en Esperanza, Puebla
1957, julio 29	7.8		Guerrero: San Marcos	55	Miles de heridos y daños materiales en varios estados. La población más dañada fue San Marcos, Gro.
1958, agosto 2	6.3	7.1	Oaxaca: Pinotepa	?	Se estima que hubo varios muertos y miles de heridos. Grandes daños materiales en Pinotepa.
1959, enero 30	6.2	7.5	Colima	50	300 heridos y 30 poblaciones afectadas severamente.
1959, agosto 28	6.8		Oaxaca-Puebla	600	Miles de heridos y damnificados. Cd. Serdán destruida: daños considerables en las ciudades de Puebla, Orizaba, Oaxaca y México. 77 pueblos dañados seriamente.
1961, noviembre 28	6.8		Oaxaca	?	Daños en Lonicha, Oaxaca. Es quizá el temblor que más se ha estudiado en México.
1962, octubre 24	6.5		Oaxaca: Huajuapam	50	Puertes daños en la región fronteriza de los estados de Puebla, Oaxaca y Guerrero. Principalmente en Huajuapam de León, Oax.

LOS SIGUIENTES ANEXOS DAN INFORMACION ADICIONAL  
SOBRE LOS TEMAS TRATADOS

## Deriva Continental. Esparcimiento del Fondo Marino.

## Tectónica de Placas

A principios de siglo el geofísico alemán Alfredo Wegener propuso la teoría conocida como Deriva Continental, en la que se supone que las masas continentales han sufrido largos desplazamientos horizontales que determinaron la posición y distribución actual de tierras y mares.

Wegener se basó fundamentalmente en la concordancia de algunas líneas de costa, como las de América del Sur y África (figura 1); en datos paleoclimáticos y paleontológicos y en la distribución de las cadenas montañosas. Propuso la existencia de un gran continente primario al cual llamó Pangea que en el transcurso de las edades geológicas se fracturó y sus partes navegaron sobre la capa basáltica del piso marino, hasta ocupar diferentes posiciones.

Otros investigadores anteriores ya habían avanzado en la idea de movimientos continentales; sin embargo Wegener en 1912 presentó una considerable cantidad de evidencias y una descripción de las posiciones de los continentes en las diferentes épocas.

La teoría pronto encontró un gran número de objeciones, principalmente por el mecanismo propuesto para explicar el desplazamiento de los continentes así como por la similitud de edades de los océanos, y la existencia de los cratones continentales y de regiones de lentos levantamientos y sub-

sidencias entre otras. Pronto la teoría cayó en desuso.

Con el advenimiento de la Segunda Guerra Mundial las técnicas e instrumentos para la exploración marina experimentaron un fuerte avance, principalmente en los sistemas de navegación así como de registro del fondo, lo que fomentó la investigación de los océanos.

En la década de los cincuenta, las investigaciones oceanográficas se incrementaron enormemente. Se hicieron mediciones de gravimetría, de magnetometría, de flujo de calor de sismología de refracción y reflexión y se tomaron muestras de sedimentos del fondo oceánico. Todos estos estudios aportaron información novedosa cuya interpretación hizo necesaria la revisión cuidadosa de la hipótesis de Wegener.

Dietz en 1961 y Hess en 1962 propusieron la teoría llamada de Esparcimiento del Fondo Oceánico, para explicar sus observaciones sobre el lecho marino. En esta teoría se considera a las dorsales oceánicas como centros generadores de material nuevo proveniente del manto y trasladado a la superficie por corrientes de convección.

La idea general asume que el valle medio de una dorsal oceánica representa una fisura, la cual se rellena por material del manto, probablemente peridotita, que al enfriarse bajo los 500 °C sufre un proceso de serpentización. Esto hace que disminuya la densidad de 3.3 a 2.6 gr/cm<sup>3</sup> y aumente su volumen, lo que provoca la elevación de las montañas que rodean al valle. Este proceso también justifica el espesor

casi uniforme de la corteza oceánica reportado por los estudios sísmicos (Figura 2).

La teoría explica además, la falta de sedimentos antiguos anteriores al Cretácico, los espesores inferiores a 1.3 Km, la distribución de edades (mayores al aproximarse a los continentes) la forma y localización de los guyots (mesetas submarinas, algunas de ellas situadas a gran profundidad), la ausencia de la discontinuidad de Mohorovicic bajo las dorsales y el elevado flujo térmico sobre ellas, y explica la presencia de las fosas profundas en algunas márgenes continentales como zonas en donde el piso oceánico retorna al manto.

La interpretación de las anomalías magnéticas de Campo Total tomadas sobre las cordilleras submarinas empleando las inversiones de polaridad del Campo Geomagnético hecha por Vine y Mattews en 1963, proporcionó un fuerte apoyo a la teoría.

Los años siguientes fueron de intensa actividad y descubrimientos. En 1968 Isacks Oliver y Sykes publicaron un artículo ahora clásico, "Seismology and the New Global Tectonics", en el que se sintetizan la mayoría de las ideas que integran lo que es conocido como Tectónica de Placas o Nueva Tectónica Global.

Brevemente, la teoría considera que la tierra posee un casquete externo rígido de unos 100 Km de espesor. Este casquete no es continuo sino que está dividido en varios segmentos (Figura 3) con movimientos relativos entre sí.

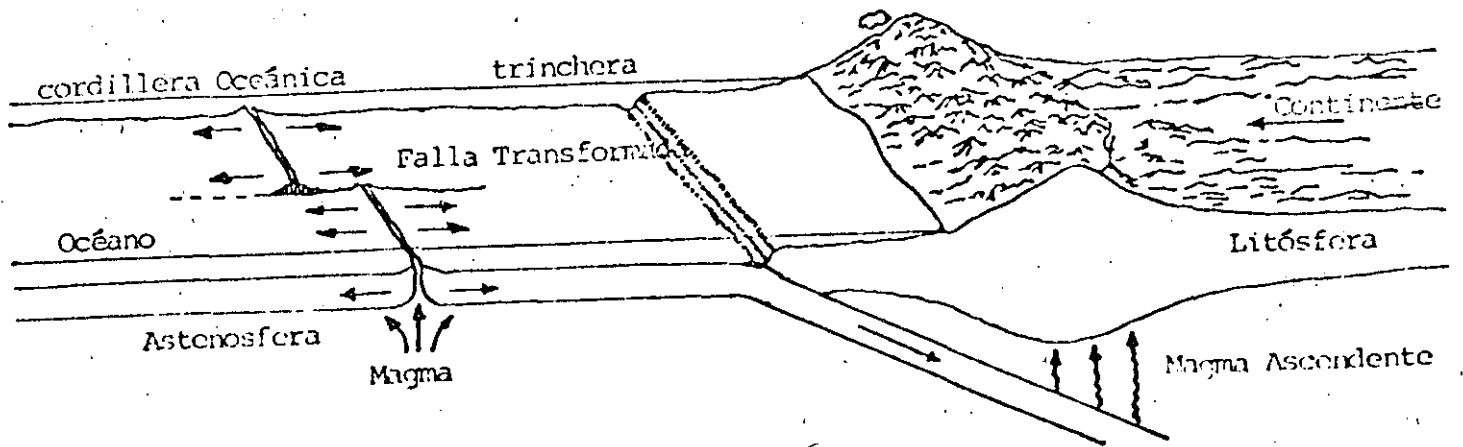
Los movimientos a que están sometidas las placas producen en algunos de sus márgenes la subducción de una de ellas bajo la otra, mientras que en otros márgenes se produce la creación de nueva corteza. (Figura 2).

Aunque el origen de los esfuerzos que producen estos movimientos no es bien comprendido es muy posible que sean debido a la transferencia convectiva de calor hacia la superficie. Cualquiera que sea el mecanismo que produce el desplazamiento, el contacto entre las placas es zona de acumulación de esfuerzos y el lugar donde se libera la mayoría de la energía de la superficie terrestre. En la figura 4 puede verse que las zonas sísmica y volcánicamente activas definen los márgenes de las placas. Nótese también que los límites de las placas no necesariamente coinciden con las fronteras océano-continente.

La distribución de hipocentros en un corte transversal a través de una zona de subducción puede verse en la figura 5. La región definida por los focos es llamada zona de Wadati Bennioff en honor a los investigadores que describieron esta relación geométrica en los años 40.



Figura 1.



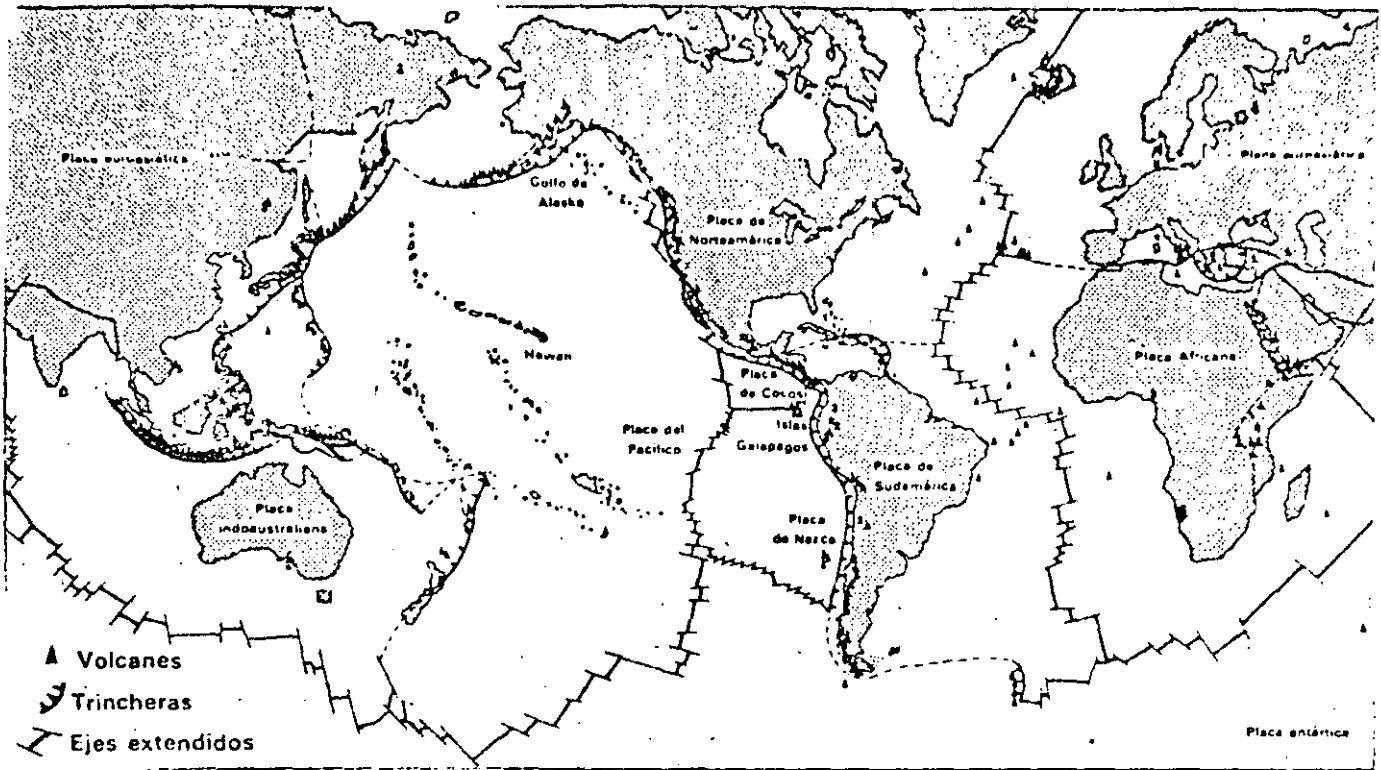
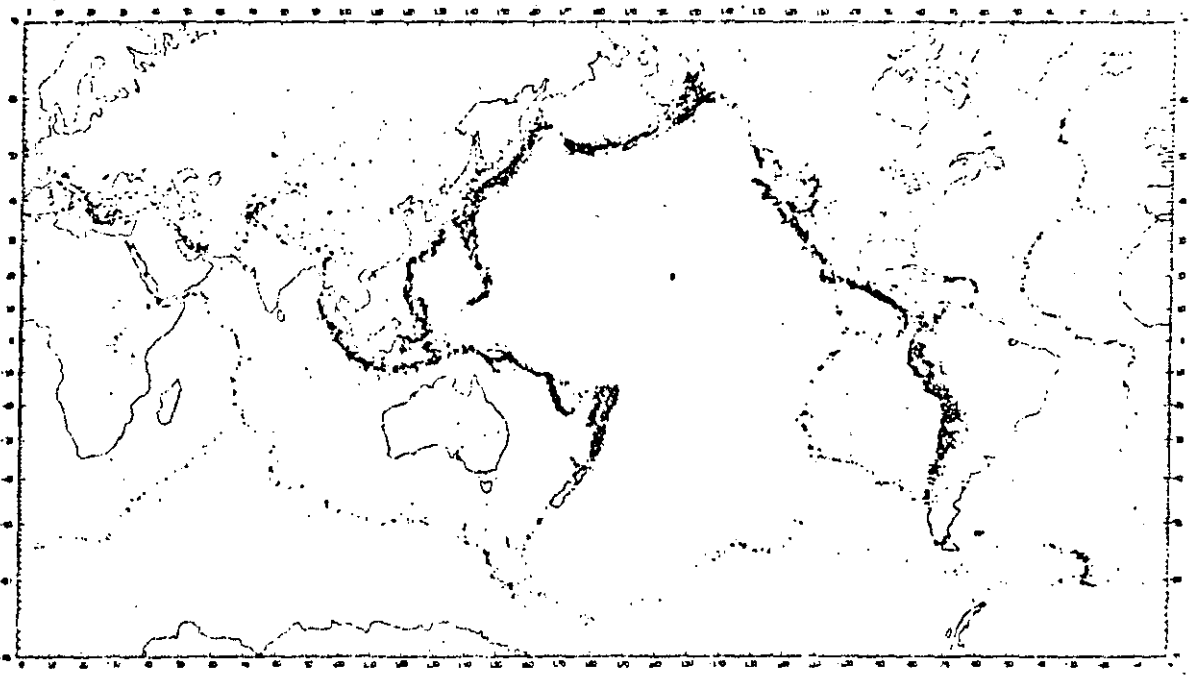


Figura 3.



- 1620 Se notó la concordancia entre las líneas de costa de Africa y América del Sur. (Hacon)
- 1839 Ideas de convección térmica en el manto (Hopkins).
- 1855 Teoría isostática (Airy).
- 1858 Mapa mostrando el movimiento de los continentes (Snider).
- 1859 Teoría isostática (Pratt).
- 1889 Concepto de la astenósfera (Fisher).
- 1906 Primeras evidencias de inversiones del Campo Magnético terrestre (Brunhes).
- 1910 Teoría de movimientos continentales (Taylor).
- 1912 Teoría de Deriva Continental (Wegener).
- 1914 Concepto de la astenósfera (Barrel).
- 1923 Nuevo método de análisis de temblores, llamado de mecanismos focales o plano de falla (Nakano y Byerly).
- 26-28
- 1926 Concepto de la astenósfera (Gutenberg).
- 1929 Establecimiento de una época de polaridad inversa magnética en el Pleistoceno (Matuyama).
- 1939 Celdas de Convección en el manto (Griggs).
- 1940 Determinaciones de edades radiométricas K-Ar (Evans).
- 1944 Mecanismos de deriva continental (Holmes).
- 1946 Descubrimiento de los guyots en el Océano Pacífico. (Hess).
- 1949 Descubrimiento de las zonas de Benioff (Benioff).
- 1950 Estudios de las cordilleras submarinas (Instituto Scripps).  
Comienzo de las mediciones de flujo térmico en el mar (Bullard).  
  
Empleo de los magnetómetros de Campo total en estudios marinos (Instituto Scripps).
- 1952 Descubrimiento de las zonas de fractura en el Océano Pacífico (Menard y Dietz).
- 1955 Investigaciones teóricas del origen del Campo Magnético (Bullard y Elsasser).  
Ideas de fuentes térmicas "Hot spots" (Wilson).
- 1956 Descubrimiento del valle medio de las dorsales y reconocimiento de los temblores que en ellos ocurren (Ewing y Haxen).  
Demostración de la Deriva Continental con datos Paleomagnéticos (Irwing y Runcorn).
- 1957 Levantamiento marino con gravímetro de superficie.
- 1957 Año Geofísico Internacional
- 1958 Reconocimiento de lineamientos magnéticos sobre las dorsales (Mason). Confirmado por Vacquier, 1961 y Mason y aff 1961.

- 1960 Primeras perforaciones del proyecto Mohole.
- 1961-1962 Hipótesis de esparcimiento de los fondos marinos (Hess).
- 1965 Interpretación de los lineamientos magnéticos empleando las ideas de inversiones del Campo Geomagnético y de esparcimiento de los fondos marinos (Vine y Matthews; Morley).  
Primera escala de tiempo cuantitativa de inversiones del Campo Geomagnético usando edades de K.Ar (Cox).
- 1960-70 Proyecto Internacional del Manto Superior bajo la dirección del profesor V.V. Belousov.
- 1965 Concepto de fallas transformadas (Wilson).
- 1967-69 Modelo de una litósfera capaz de soportar tensiones como mecanismo de hundimiento en las trincheras (Elsasser).
- 1967 Conceptos e implicaciones geométricas de las placas (Mc Kenzie y Parker).
- 1968 Estudios sobre las placas y sus límites (Morgan).  
Nueva Tectónica global (Isacks).
- 1969 Concepto de juntas triples (Mc Kenzie y Morgan).  
Relaciones entre la edad, la elevación topográfica y el flujo térmico en los fondos oceánicos (Sclater y Franchetau).
- 1964 Programas del JOIDES (Muestreo de la tierra profunda)  
Información del proyecto de perforación en mar profundo (Deep sea drilling Project) dentro de los programas del JOIDES (from Oceanographic Institutions Deep Earth Sampling).
- 1970 Proyecto Internacional Geodinámica. Con la participación del Grupo de Trabajo No. 2, Grupo de Estudio No. 2, Placa de Cocos, Comité Mexicano de Geodinámica.
- 1970 Proyecto CICAR (Cooperative Investigations of the Caribbean and Adjacent Regions). Participación de México.
- 1971 Proyecto IDOE (International Decade Oceanographic Exploration). Participación de México.

Predicción de Temblores

Como hemos visto, la mayoría de los temblores ocurren en los márgenes de las placas como respuesta a la acumulación de esfuerzos en esas áreas. Los esfuerzos son debidos al movimiento relativo entre placas. Este movimiento, que es del orden de algunos centímetros por año no cambia en plazos cortos de tiempo (geológicamente hablando) por consiguiente es posible estudiar los márgenes sísmicamente activos en términos estadísticos.

Los períodos de recurrencia de los temblores grandes ( $M > 7.0$ ) son altamente variables (30 - 100 años) por lo tanto es necesario contar con un record histórico tan completo como sea posible.

Si el período de recurrencia es conocido, la probabilidad de ocurrencia de un temblor es proporcional al tiempo transcurrido desde el último. Este último aspecto nos lleva a lo que se ha definido como tramo de quietud sísmica a falta de una mejor traducción del inglés "seismic gap".

El concepto anterior fue originalmente desarrollado por Fedotov y Mogi y posteriormente por Sykes y Kelleher y colaboradores\*. Estos últimos autores\* publicaron un mapa de "gaps sísmicos" para el cinturón del Pacífico.

\* Kelleher et al. (1973). Journal of Geophysical research.

El mapa ha sido revisado recientemente por Mc Cann y colaboradores\*. Las siguientes figuras son mapas de "gaps sísmicos" para Mesoamérica, Sudamérica y el Caribe.

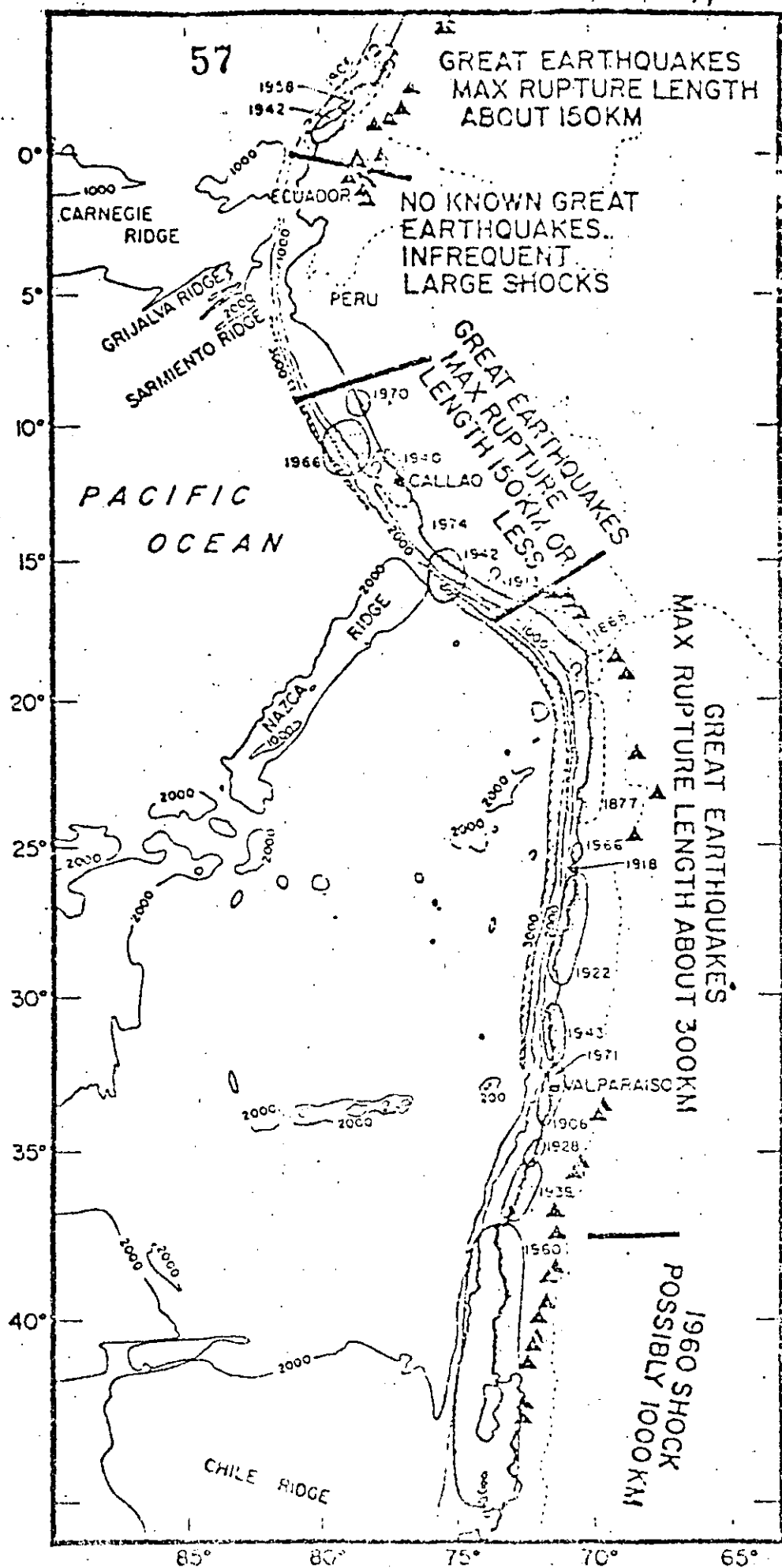
Este tipo de mapas es muy útil no sólo para evaluar el riesgo sísmico sino también como parte de un programa de predicción a largo plazo. Una vez que una región es reconocida como "gap", pueden utilizarse técnicas para determinar cambios físicos asociados con la acumulación de esfuerzos.

Los cambios físicos observados se relacionan al aumento de volumen, previo al temblor, llamado dilatancia. Asociado a la dilatancia se encuentran el cambio en la velocidad de las ondas P y S, el aumento de la resistividad eléctrica, el cambio en el campo magnético y el aumento de gas radón en pozos cercanos así como cambios en temperatura y nivel de los fluidos en los mismos.

Para explicar la dilatancia se desarrollaron dos modelos que han sido llamados el modelo americano y el modelo ruso. Ambos coinciden en las fases iniciales pero divergen en la descripción del episodio final. Quizá la situación real sea una combinación de ambos.

\* Mc Cann et al. (1979). JGR Pageoph Vol 117, pp 1082





57

GREAT EARTHQUAKES  
MAX RUPTURE LENGTH  
ABOUT 150KM

NO KNOWN GREAT  
EARTHQUAKES...  
INFREQUENT  
LARGE SHOCKS

GREAT EARTHQUAKES  
MAX RUPTURE  
LENGTH 150 KM OR  
LESS

GREAT EARTHQUAKES  
MAX RUPTURE LENGTH ABOUT 300KM

1960 SHOCK  
POSSIBLY 1000 KM

PACIFIC  
OCEAN

CHILE RIDGE

CARNEGIE RIDGE

GRIJALVA RIDGE

SARMIENTO RIDGE

ECUADOR

PERU

CALLAO

VALPARAISO

0°

5°

10°

15°

20°

25°

30°

35°

40°

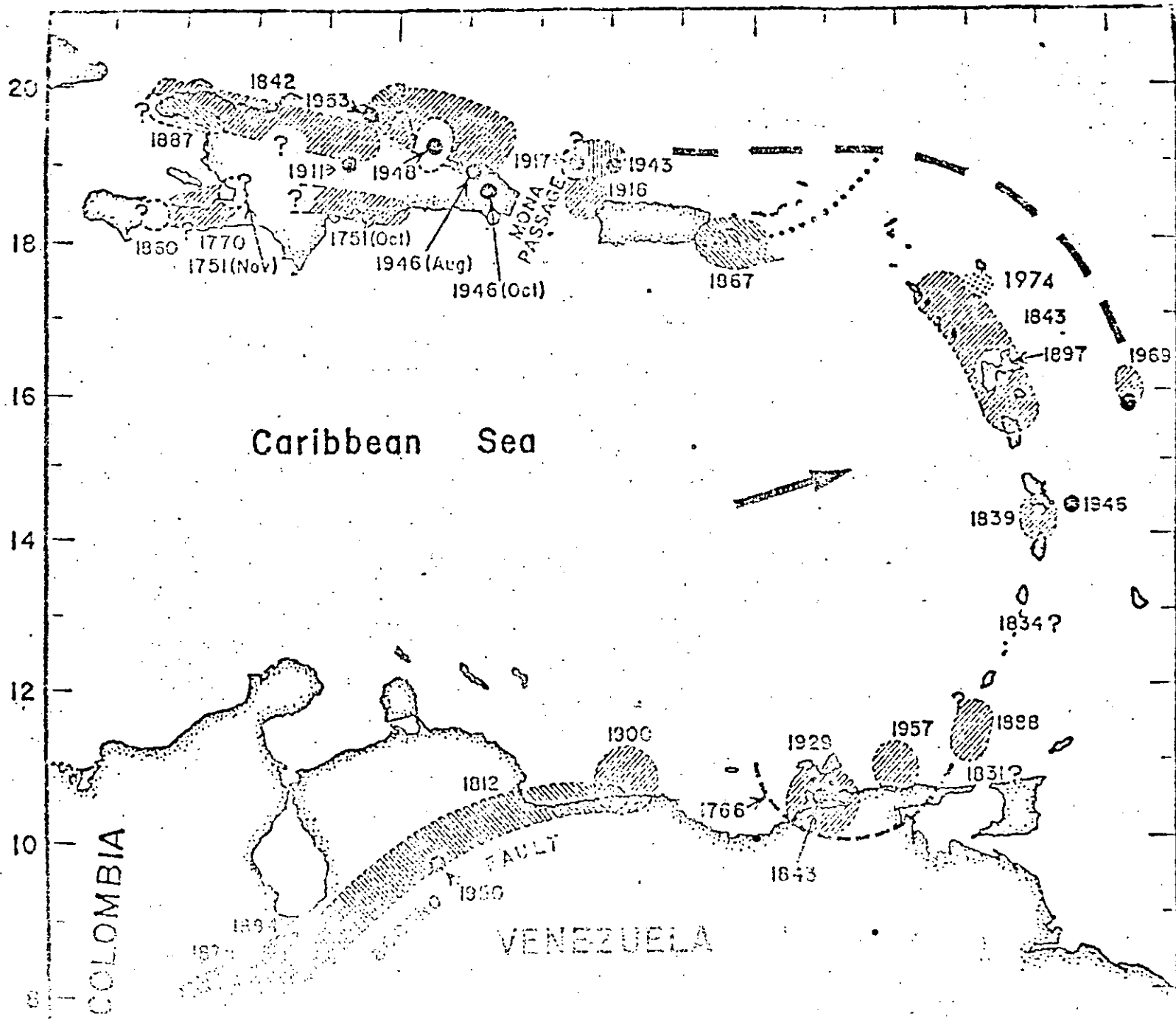
85°

80°

75°

70°

65°



58

1/2

Ondas Sísmicas

Dentro de un cuerpo con constantes elásticas  $\lambda$  y  $\mu$  y densidad  $\rho$  pueden viajar dos tipos de ondas llamadas "de cuerpo" o internas:

Longitudinales  $v_p = \sqrt{\frac{\lambda + 2\mu}{\rho}}$  onda (de primus)

Transversales  $v_s = \sqrt{\frac{\mu}{\rho}}$  onda s (de secundus pues arriba después de  $\rho$ )

En muchos casos  $\lambda = \mu$  y  $v_p = \sqrt{3} v_s$  (Salido de Poisson)

En un sólido elástico estratificado con una superficie libre se generan además dos tipos de ondas superficiales:

Ondas de Rayleigh con velocidad  $C_R$  y ondas de Love con velocidad  $C_L$ ; puede demostrarse que

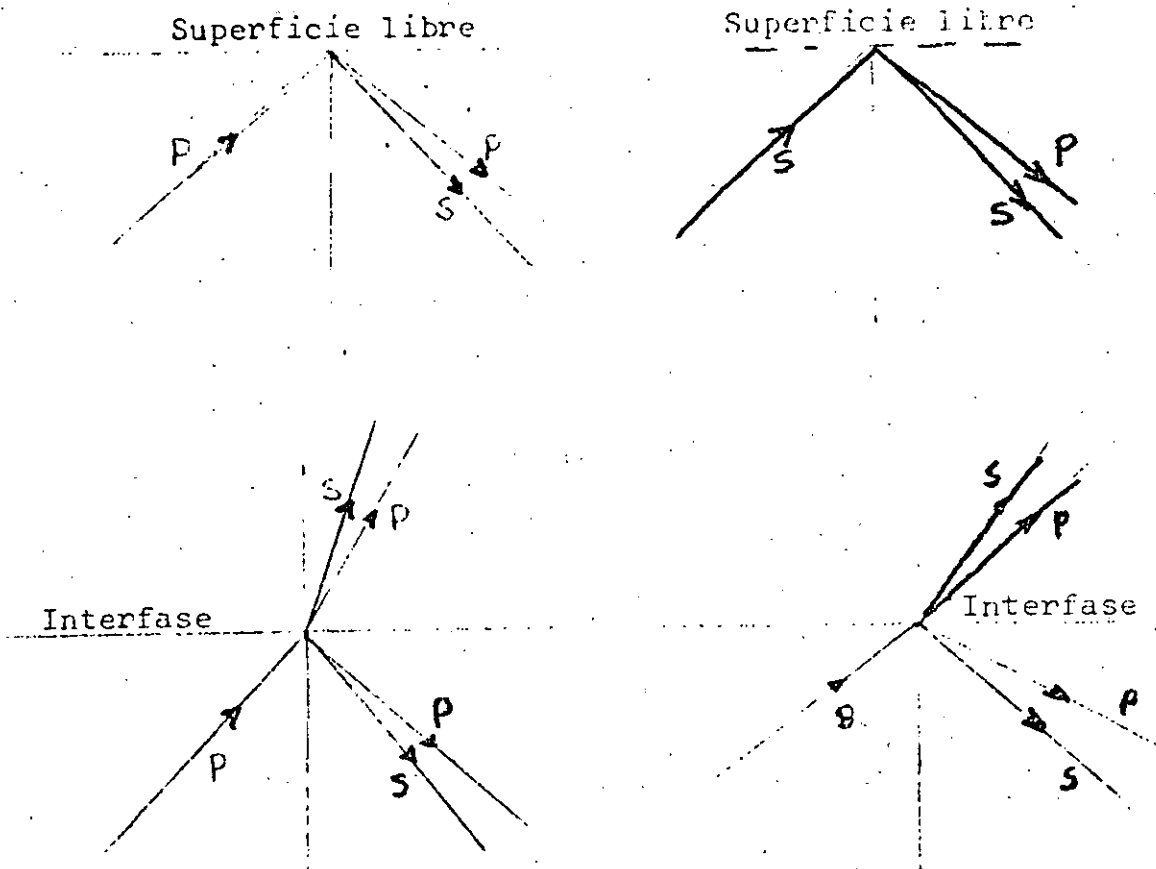
$$C_R < 0.92 v_s$$

$$v_{s_1} < C_L < v_{s_2}$$

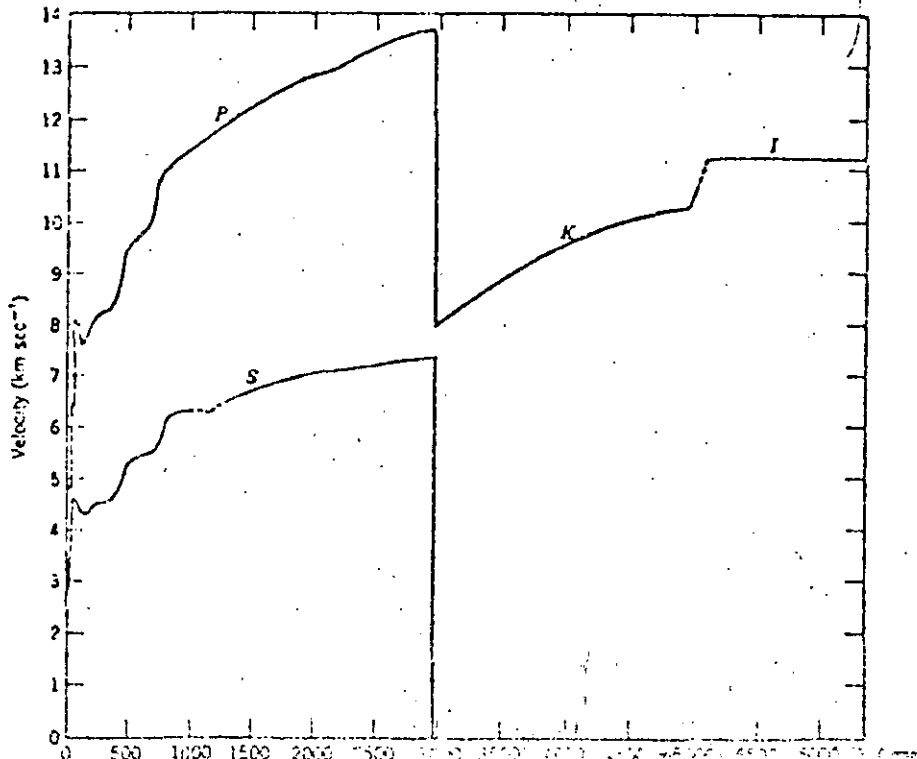
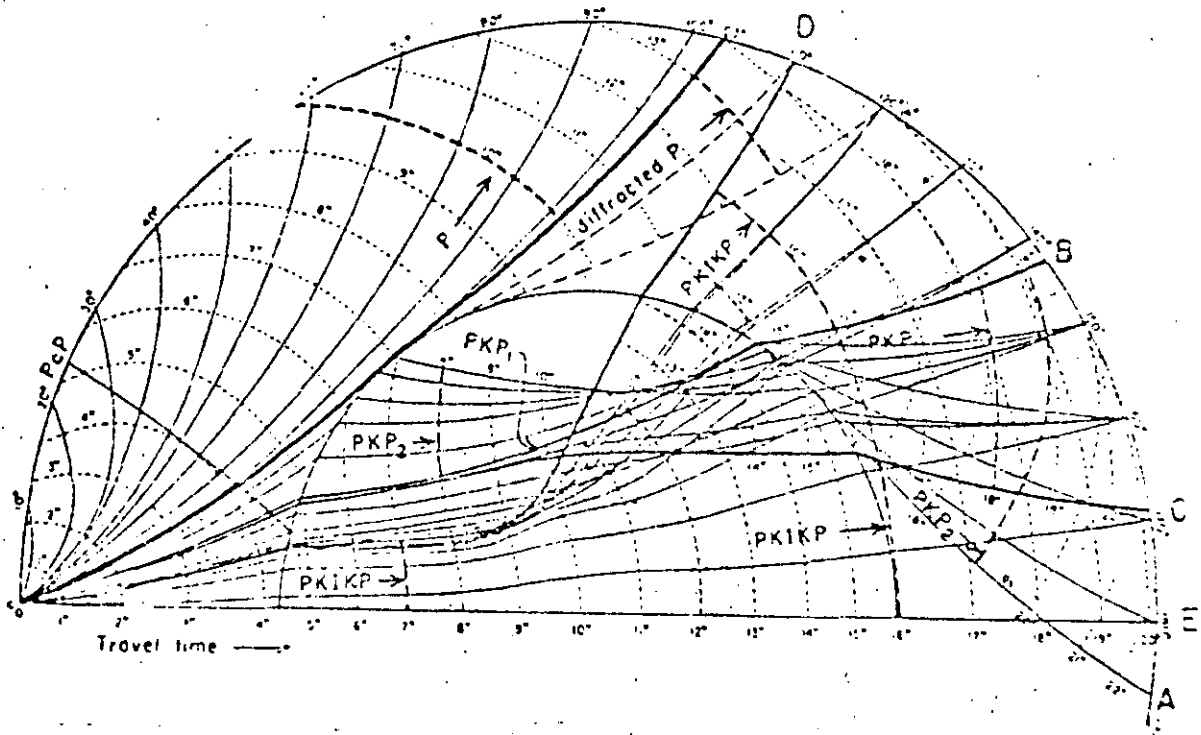
donde  $v_{s_1}$  y  $v_{s_2}$  son las velocidades transversales de los dos estratos.

La velocidad de las ondas superficiales depende de la frecuencia y sufren por lo tanto dispersión. La dispersión i.e. la velocidad de grupo depende de la estructura interna del medio y por lo tanto su estudio puede utilizarse para inferir esta estructura.

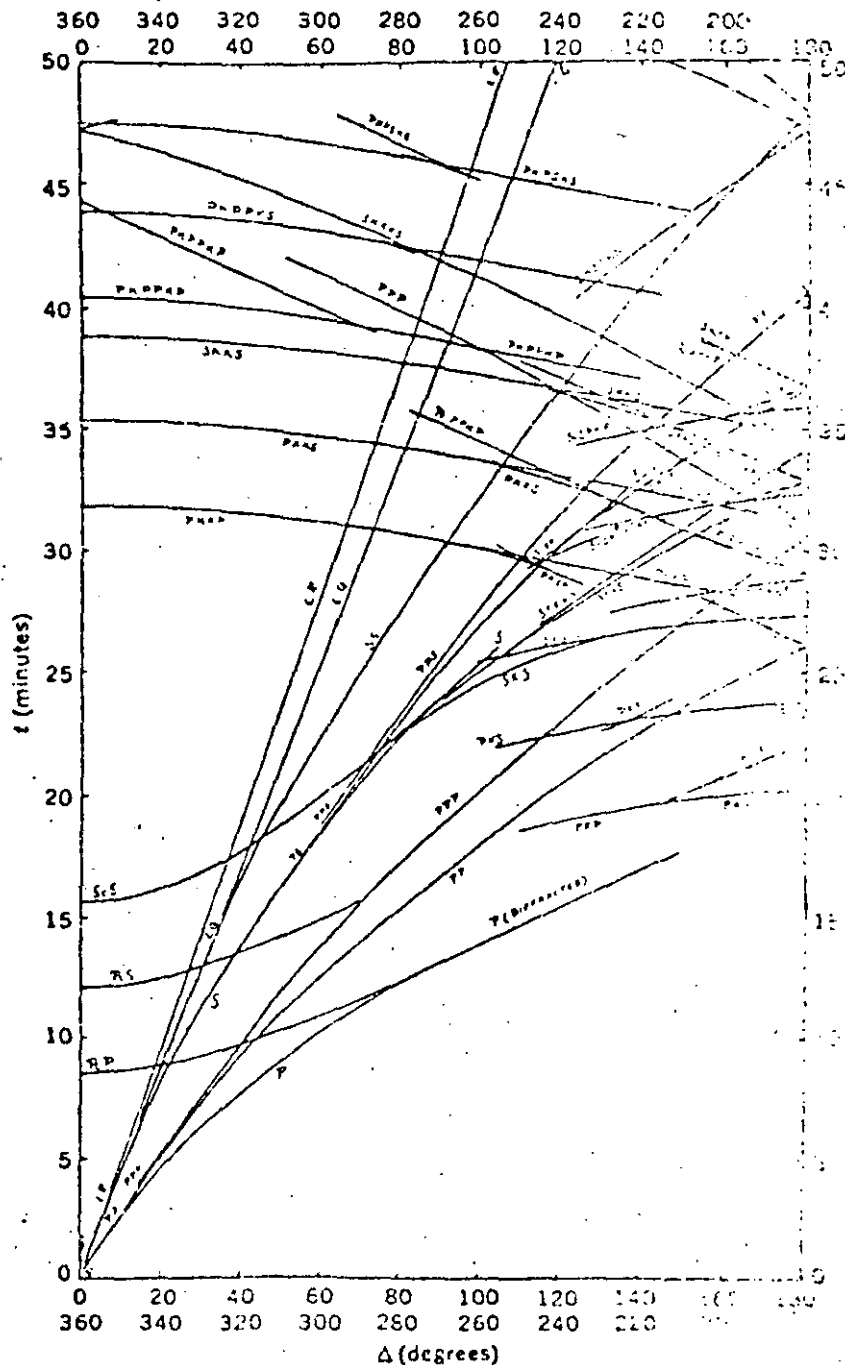
Las fases arriba descritas quedan registradas en los sismogramas (dependiendo de la posición del instrumento con respecto a la fuente) sin embargo su estructura se complica pues también aparecen fases de ondas reflejadas y refractadas:



A escala global muchas de estas fases correspondientes a reflexiones y refracciones en el interior del planeta pueden ser identificadas; a continuación pueden verse las trayectorias de algunas de estas ondas y su nomenclatura, así como su distribución de velocidades con la profundidad.



Las diferentes fases pueden identificarse en el registro con ayuda de las curvas de viaje de Jeffreys y Bullen que nos dan el tiempo de arribo en términos de la distancia al foco. Estas curvas fueron dadas por Jeffreys y Bullen en los años 40 y a pesar de la introducción de los computadores modernos han adquirido poca modificación.



El tipo de onda para determinar  $M_L$  no está especificado es simplemente la máxima amplitud y puede ser de onda P, S o de superficie.

Otras magnitudes en uso comun además de las  $M_L$  (magnitud local) son la mb y la magnitud de ondas superficiales  $M_S$ .

La  $M_S$  fue definida por Gutenberg en 1945 para temblores superficiales como

$$M_S = \log A_H + 1.656 \log \Delta + 1.818 + C \quad (15^\circ < \Delta < 13^\circ)$$

donde

$A_H$  - componente horizontal del máximo movimiento del suelo (de 0 a pico en micrones) para onda superficial de período 20 seg.

$$A_H = (A_N^2 + A_E^2)^{1/2}$$

$A_N$  - Max. amplitud N-S

$A_E$  - Max. amplitud E-W

Una fórmula adoptada por la Asociación Internacional de Sismología y Física del Interior de la Tierra (IASPEI) es

$$M_S = \log (A/T)_{\max} + 1.66 \log \Delta + 3.3$$

para  $T = 20$  seg la fórmula se reduce a

$$M_S = \log A_{20} + 1.66 \log \Delta + 2.0$$

y  $mb = \log (A/T) + Q$

donde  $Q$  es un término que depende de  $\Delta$  y la profundidad.  $A$  es la máxima amplitud de la onda  $P$ . En la práctica  $T$  es en general 1 segundo. También pueden usarse  $PP$  y  $SII$ .

En general  $M_L$ ,  $m_b$  y  $M_S$  son diferentes pues se derivan de diferentes fases.  $M_S$  y  $m_b$  están relacionadas aproximadamente por

$$m_b = 2.5 + 0.63 M_S$$

La energía sísmica se relaciona empíricamente a  $M_S$  por

$$\log E_S = 1.5 M_S + 11.8$$

Se ha demostrado, por otra parte, que para temblores grandes (dimensiones de ruptura de aprox 100 km) la escala  $M_S$  comienza a saturarse es decir que aunque aumenta la energía no aumenta la magnitud ( $M_S$ ). Para evitar este problema se ha introducido la magnitud  $M_w$ .

Esta magnitud, llamada magnitud de mínima energía de deformación ( $M_w$ ), fue introducida por Kanamori\*. La energía total liberado en un temblor puede ser escrita como:

$$\begin{aligned} E_f &= \bar{\sigma} \bar{u} A \\ \text{donde } \bar{\sigma} &= (\sigma_1 + \sigma_2)/2 \text{ caida promedio de esfuerzos} \\ \sigma_1 &= \text{esfuerzo inicial} \\ \sigma_2 &= \text{" final} \\ \bar{u} &= \text{dislocacion promedio} \\ A &= \text{area de ruptura} \end{aligned}$$

\* Journal of Geophysical Research. 82, 1977, 1981-1987

La energía total  $E_t$  es la suma de la energía perdida en fricción,  $E_f$ , y la liberada como ondas sísmicas. Entonces,

$$\begin{aligned} E_t &= E_f + E_s \\ E_s &= -E_f + E_t \\ &= -\sigma_f \bar{u} A + \bar{\sigma} \bar{u} A \\ &= \bar{u} A \left( \frac{\sigma_1 + \sigma_2}{2} - \sigma_f \right) \end{aligned}$$

Si  $\sigma_f = \sigma_2$  (Modelo de Orowan). Entonces,

$$\begin{aligned} E_s &= \bar{u} A \left( \frac{\sigma_1 - \sigma_2}{2} \right) \\ &= \frac{\bar{u} A \Delta \sigma}{2} \end{aligned}$$

$\Delta \sigma \rightarrow$  Caida de esfuerzos  
 $M_0 = \mu A \bar{u}$  momento sísmico

$$= \frac{\bar{u} A \Delta \sigma}{2} = \frac{\Delta \sigma M_0}{2 \mu}$$

La experiencia demuestra que el modelo es razonable.

Ya que  $\frac{\Delta \sigma}{\mu} = 1 \times 10^{-4}$  para temblores de intraplaca entonces

$$\log E_s = \log M_0 - 4.3$$

Así, si podemos estimar  $M_0$  (lo cual es posible si se conoce el área de ruptura etc) entonces podemos estimar  $E_s$  ya que la relación magnitud-energía de Gutenberg-Richter, válida para longitudes de ruptura máxima de 100 km es

$$\begin{aligned} \log E_s &= 1.5 M_s + 11.8 \\ \log E_s &= \log M_0 - 4.3 \end{aligned}$$

para todos los temblores puede definirse una magnitud  $M_w$  tal que

$$\begin{aligned} 1.5 M_w + 11.8 &= \log M_0 - 4.3 \\ \text{o' } M_w &= \frac{2}{3} \log M_0 - 10.73 \end{aligned}$$

Mw es aproximadamente igual a Ms para longitudes máximas de 100 km pero para temblores mayores no sufrirá saturación.

Ejemplo: Temblor de Chile del 22 de mayo de 1960.  $M_s = 8.3$  pero  $M_w = 9.5$ . En la escala Mw éste es el temblor más grande del siglo.

ARTICULOS RELACIONADOS CON EL TEMA

# el mecanismo sísmico

Poco a poco se ha ido comprendiendo cómo ocurren los sismos hasta llegar a formular modelos matemáticos de ellos.

La explicación racional del origen de los temblores y, aun más, su descripción por medio de modelos matemáticos que permitan su caracterización, es una de las áreas más activas de la sismología moderna. Si bien es cierto que quedan aún muchos problemas por resolver, no lo es menos que en esta área se han dado ya algunos de los resultados más notables en la historia de esta ciencia.

## La teoría del rebote elástico

La mayoría de las discusiones sobre el tema comienzan por hacer referencia a la teoría del rebote elástico, propuesta por H F Reid en 1910 a raíz del sismo de California de 1906. Después de este violento terremoto, se encontró que a lo largo de unos

400 kilómetros sobre la falla de San Andrés se habían producido desplazamientos relativos del orden de 3 metros, predominantemente horizontales. Años antes, entre 1851 y 1866, y luego entre 1874 y 1892, se habían llevado a cabo levantamientos geodésicos en el área. Un tercero fue hecho inmediatamente después de la ocurrencia del temblor. Del análisis de estos datos se pudo establecer que entre el primero y segundo levantamientos había ocurrido un desplazamiento de uno a dos metros entre puntos similares a ambos lados de la falla y a una distancia de unos 30 km de ella. Otro movimiento similar ocurrió entre los dos últimos levantamientos. Sin embargo, un resultado singular fue que a lo largo de la falla misma no ocurrió desplazamiento alguno, sino al tiempo de ocurrencia del terremoto. Reid razonó que si el área de falla se comporta elásticamente, el lento movimiento relativo a ambos lados causa un aumento en la energía almacenada y en la componente tangencial de la fuerza de fricción sobre el plano de falla. Cuando se alcanza un punto crítico, el fracturamiento ocurre con un movimiento de restauración hacia una nueva posición de equilibrio al que se llama *rebote elástico*. Ya que es improbable que esto ocurra simultáneamente en toda la falla, la ruptura debe comenzar en algún punto de ella y de allí desplazarse con una velocidad finita. La figura 1 muestra esquemáticamente estas ideas.

Aunque los detalles de este mecanismo no fueron claramente expuestos por Reid, lo esencial de la teoría quedó establecido de esa manera y es ge-

\*El Dr. Juan Manuel Espindola es investigador del Instituto de Geofísica y profesor de la Facultad de Ciencias, ambas instituciones de la UNAM.

neralmente aceptada en la actualidad, al menos para la gran mayoría de los temblores.

Cabe hacer notar que las ideas de Reid no son intuitivas. Durante los primeros días de la sismología, el fallamiento del terreno se consideraba como un efecto de los sismos más que como una causa de los mismos. Si bien durante la segunda mitad del siglo XIX se tenía ya la idea de una fuente sísmica localizada, todavía se suponía que la energía provenía de explosiones subterráneas, colapso de cavernas o, posteriormente, intrusiones de magma en zonas de debilidad. Por ello, la teoría de Reid no fue aceptada inmediatamente por la generalidad de los sismólogos sino después de considerables debates y cuando hubo resistido el peso de las pruebas observacionales.

### Las soluciones de plano focal

Para los años en que se propuso la hipótesis del rebote elástico, el instrumental sismológico se había desarrollado hasta el punto de ser operacional, con lo cual las observaciones eran ya sistemáticas. En 1900, Wiechert había construido su péndulo invertido y la Asociación Sismológica Internacional había sido fundada en 1903.

Durante la década de los años 20, Perry Byerlee de la Universidad de California había notado que la dirección (o polaridad) de las ondas P en los sismogramas de las diferentes estaciones para un sismo en particular, mostraban una distribución en cuadrantes (fig 2). Las líneas que separan los diferen-

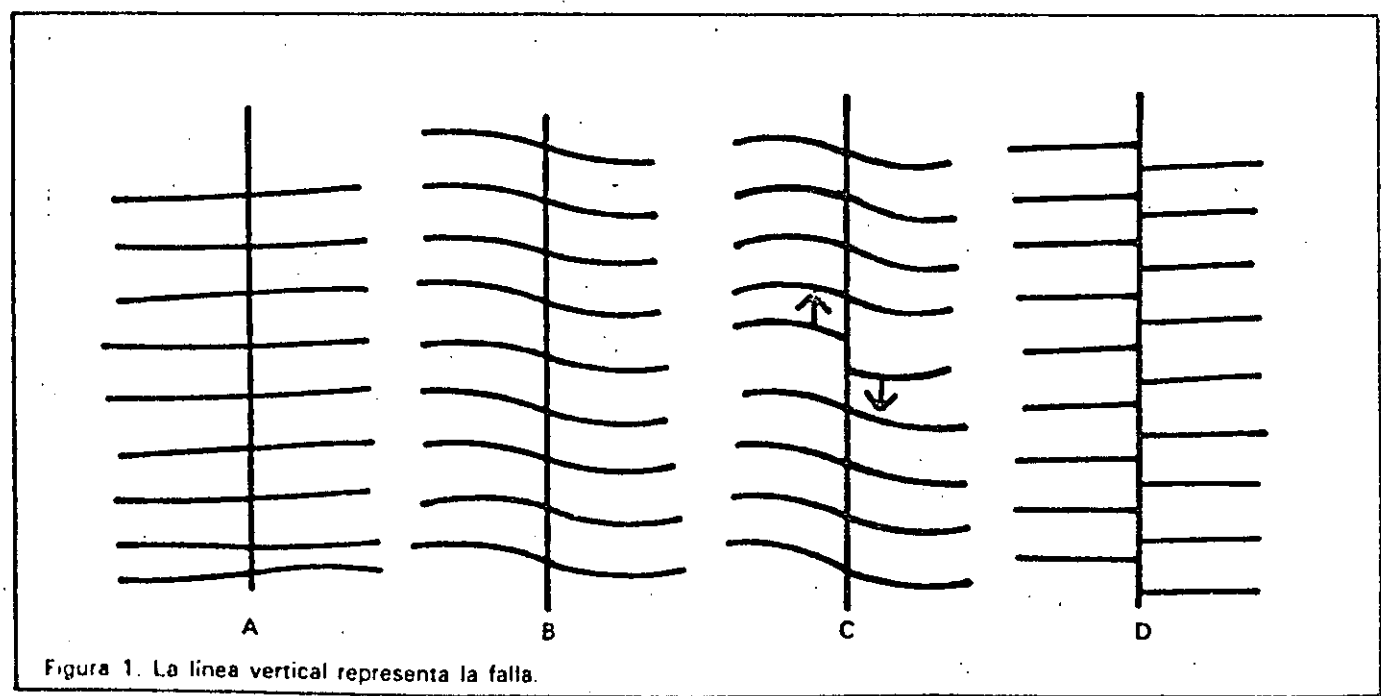


Figura 1. La línea vertical representa la falla.

tes cuadrantes son llamadas líneas nodales y constituyen la intersección con la superficie de los planos nodales. Byerlee desarrolló una técnica para encontrar estos planos y es considerado como el padre de este tipo de análisis. El significado de estos planos se verá enseguida.

La polaridad de un registro indica si el primer arribo de una onda fue una compresión o una rarefacción, y ella cambia a través de las líneas nodales: esto puede interpretarse en términos de la teoría de Reid como el efecto del desplazamiento relativo a lo largo de una falla alineada con uno de estos planos.

\* En un medio elástico pueden propagarse dos tipos de ondas: las compresionales (P) y las ondas transversales (S). Las ondas P se propagan a mayor velocidad y constituyen el primer arribo en un sismograma.

La falla puede modelarse matemáticamente por un par de fuerzas actuando en sentidos opuestos (fig 3a). Este problema de elasticidad había sido resuelto por Nakano en 1923, solución aplicada por Byerlee al problema de los planos nodales en 1926. La figura 3 (b, c) muestra los patrones de radiación para las ondas P y S: éstos dan la intensidad de las ondas: por ejemplo, para ondas P la máxima intensidad ocurre a 45°. Como puede observarse, el patrón de radiación de las ondas P concuerda con los datos observacionales.

El problema, sin embargo, no quedó resuelto allí. En los años subsiguientes se encontró que el patrón de radiación para las ondas S no siempre correspondía al de la figura 3c, sino que en algunos casos se parecía al de la figura 4c. Pronto se de-

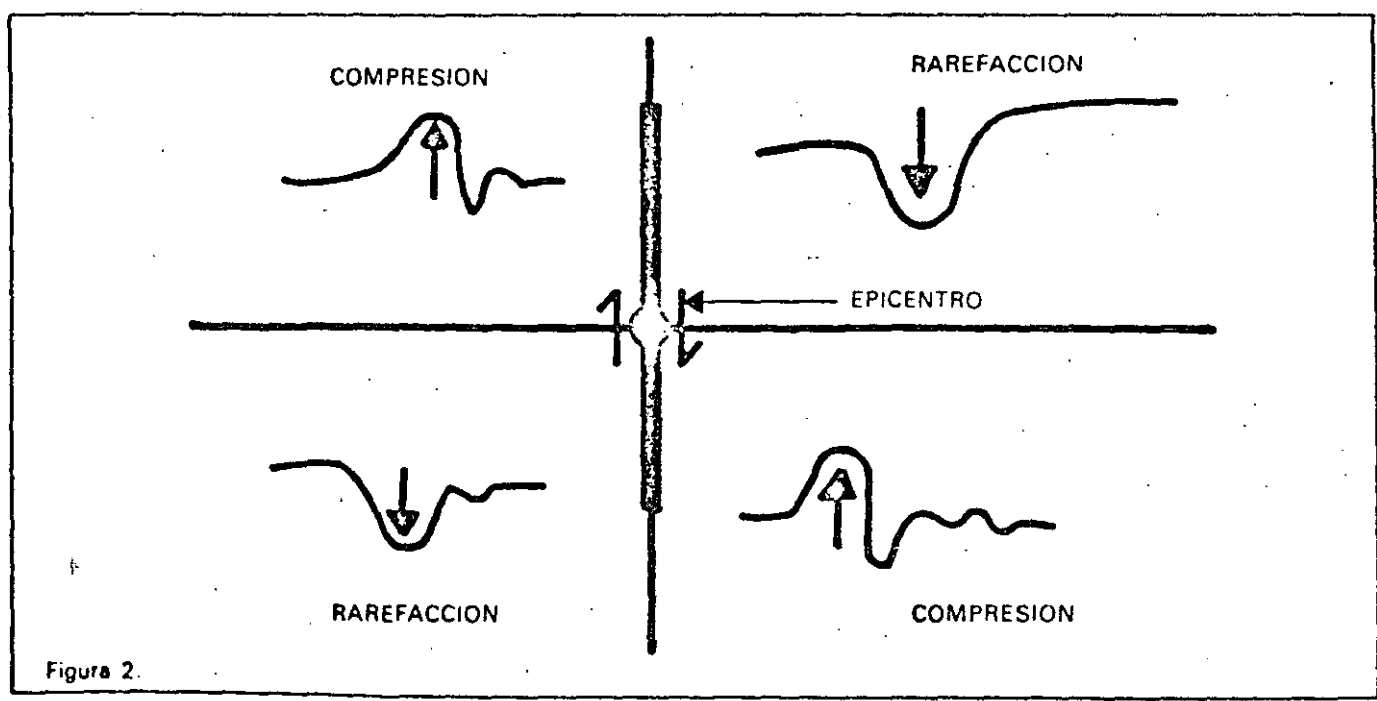


Figura 2.

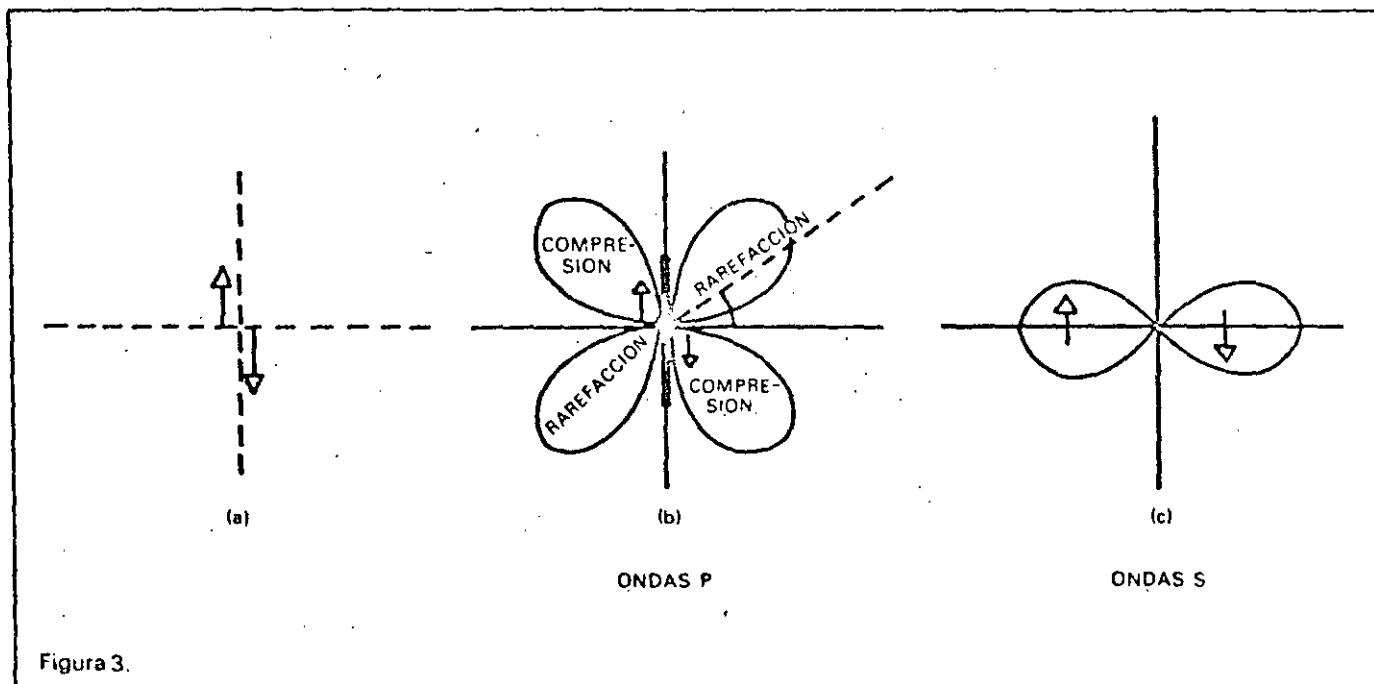
mostró que era necesario considerar un doble par de fuerzas (fig 4a) cuyo patrón de radiación de ondas P es similar al del sistema anterior (fig 4b) pero diferente para las ondas S (fig 4c). La controversia sobre el sistema de fuerzas apropiado para describir el mecanismo focal duró muchos años.

No obstante, el sistema del doble par de fuerzas no es incompatible con la teoría de Reid y puede considerarse como el resultado de un colapso a lo largo de la falla, como consecuencia de una pérdida de rigidez. Considérese, por ejemplo, la fig 5, donde un elemento de volumen está sometido a esfuerzos de cizallamiento; durante el sismo, el elemento cambia a la nueva posición mostrada con líneas punteadas: entonces la línea AD ha su-

frido una tracción y la línea BC una contracción. Si se toman las fuerzas en ambos lados de la falla el resultado es un doble par.

Por otro lado, el par simple no es dinámicamente posible ya que representa un momento no balanceado de fuerzas. Además, la solución al problema de una dislocación en un medio elástico conduce al par doble y no al simple.

Así, después de este período de prueba de la teoría de Reid conservó su validez y se reforzó al correr del tiempo con las nuevas teorías de la deriva continental y de la tectónica de placas. El método de las soluciones de plano focal constituye actualmente una de las herramientas estándar de la investigación sísmica y se aplica incluso a temblores profundos donde no hay fallas visibles.



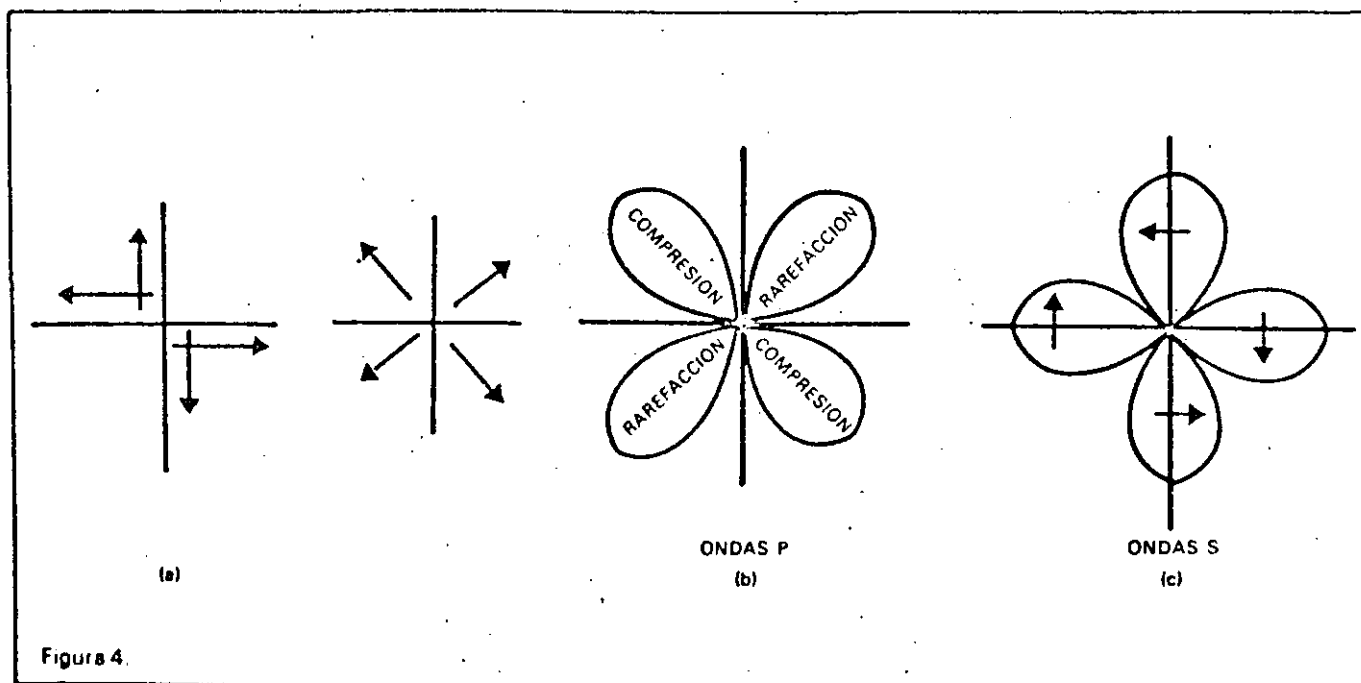
### El mecanismo físico de un sismo

Hemos dicho que Reid no expuso detalladamente cómo ocurre la pérdida de esfuerzos de cizallamiento en el plano de falla, lo cual es indispensable para elaborar un mecanismo. Suponer un par o un doble par de fuerzas es una primera aproximación al problema, ya que es sólo un sistema equivalente en términos de radiación. En la realidad, no existe ningún proceso que pueda crear estas fuerzas; lo que realmente existe es una acumulación de esfuerzos que se relajan catastróficamente.

Por otro lado, quedan problemas que no fueron resueltos por la teoría de Reid. Uno de ellos es que

las caídas de esfuerzos observadas son menores que las que cabría esperar de fracturamiento. Todavía más difícil es explicar lo que ocurre en los sismos más profundos (hasta aproximadamente 700 km), ya que a esas profundidades la fricción en las caras de una falla sería tan alta que sobrepasaría en mucho el límite elástico de las rocas, de manera que habría flujo y no desplazamiento. La respuesta a estas preguntas se ha buscado en la observación experimental.

En los últimos 15 años se han investigado los efectos que sobre la fricción en rocas tienen la temperatura; la presión del fluido presente en los poros y la deshidratación de algunos minerales como la serpentinita. En general, se ha encontrado que todos estos factores facilitan el desplazamiento.



to entre los bloques de una falla. Es entonces posible que un mecanismo de deslizamiento opere a mayor profundidad de lo que se pensaba anteriormente.

Para sismos profundos, se han propuesto mecanismos como fusión parcial o inestabilidad viscosa.\* Estos mecanismos podrían causar la caída de esfuerzos a través de un plano y, por lo tanto, el deslizamiento a lo largo del mismo.

Algunos investigadores proponen el cambio de algunos minerales a fases más densas con una consecuente reducción de volumen. Esto, sin em-

bargo, daría lugar a radiación del tipo de colapso gravitacional. De hecho, este tipo de radiación ha sido encontrado en algunos sismos muy profundos para frecuencias muy bajas, pero "sobrepuesto" a la radiación de tipo de deslizamiento que hemos venido discutiendo.

Existen pues una serie de procesos físicos que pueden intervenir en los fenómenos dinámicos que llamamos temblores. En los párrafos siguientes veremos cómo algunos de ellos pueden ser tratados matemáticamente.

### Modelos teóricos

Como ha sido evidente en los párrafos anteriores, la complejidad del problema requiere que en su

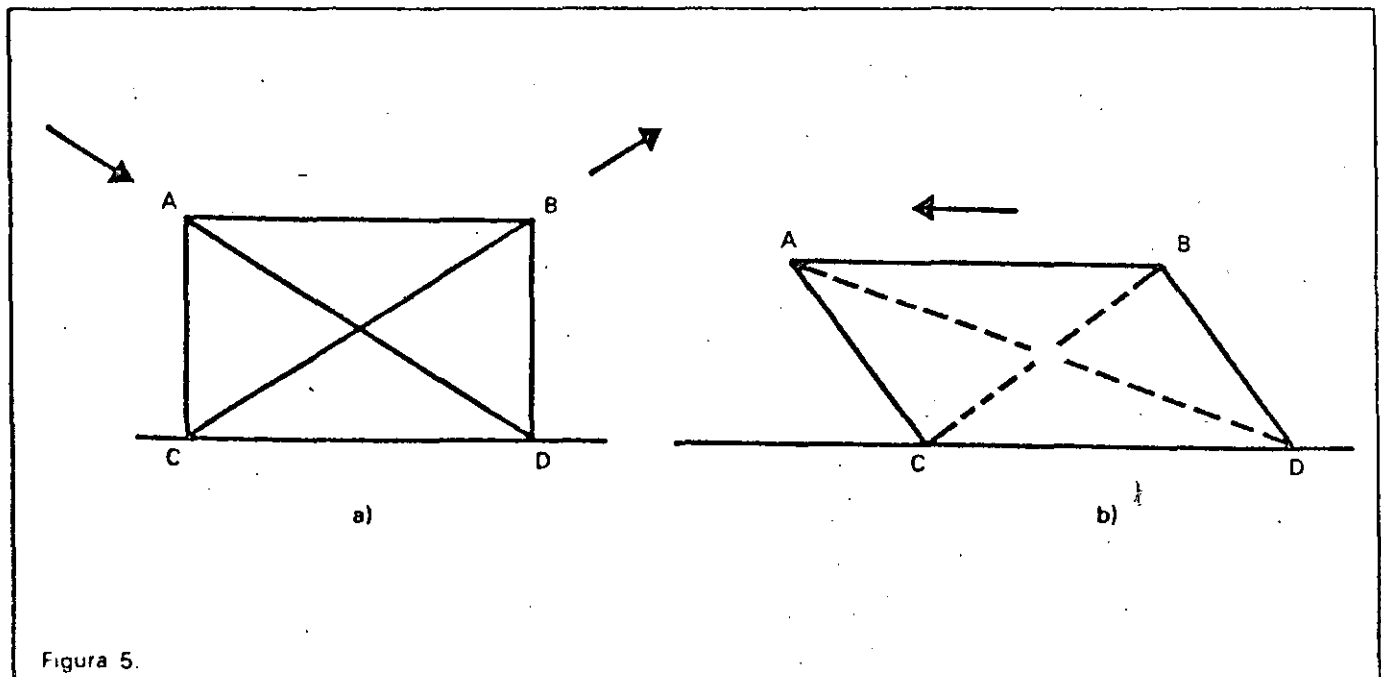


Figura 5.

formulación matemática se hagan una serie de suposiciones que lo simplifiquen. La consideración de un medio elástico y de un sistema de fuerzas constituye una primera aproximación al mismo. Este modelo permite obtener cierta información de los datos observacionales, pero ciertamente no toda ella, y por otra parte, es válido sólo para distancias muy grandes del foco.

A distancias pequeñas, las dimensiones finitas de la falla, la velocidad de ruptura y otros parámetros, influyen sobre la apariencia de las ondas que se registran en el sismograma. El modelo del sistema de fuerzas es incompetente para proporcionar información en esta región.

Un modelo todavía simple que incorpora estas variables es el de dislocación. En este caso se con-

sidera una superficie en un cuerpo elástico sobre la cual se presenta un desplazamiento relativo entre sus lados. Este problema fue resuelto a principios del siglo por Volterra. Maruyama y Knopoff resolvieron el caso en el que la dislocación crece con el tiempo y lo aplicaron específicamente a la sismología. Los resultados han sido aplicados a muchos temblores; la figura 6 muestra la comparación entre un sismograma real y el sismograma teórico obtenido por Boore y Zoback para el sismo del 28 de junio de 1966 en Parkfield, California.

Incidentalmente, esta última es una técnica usual en sismología: generar sismogramas teóricos que luego son comparados con los reales, para estimar así la validez de los parámetros con que fueron generados los sismogramas sintéticos.

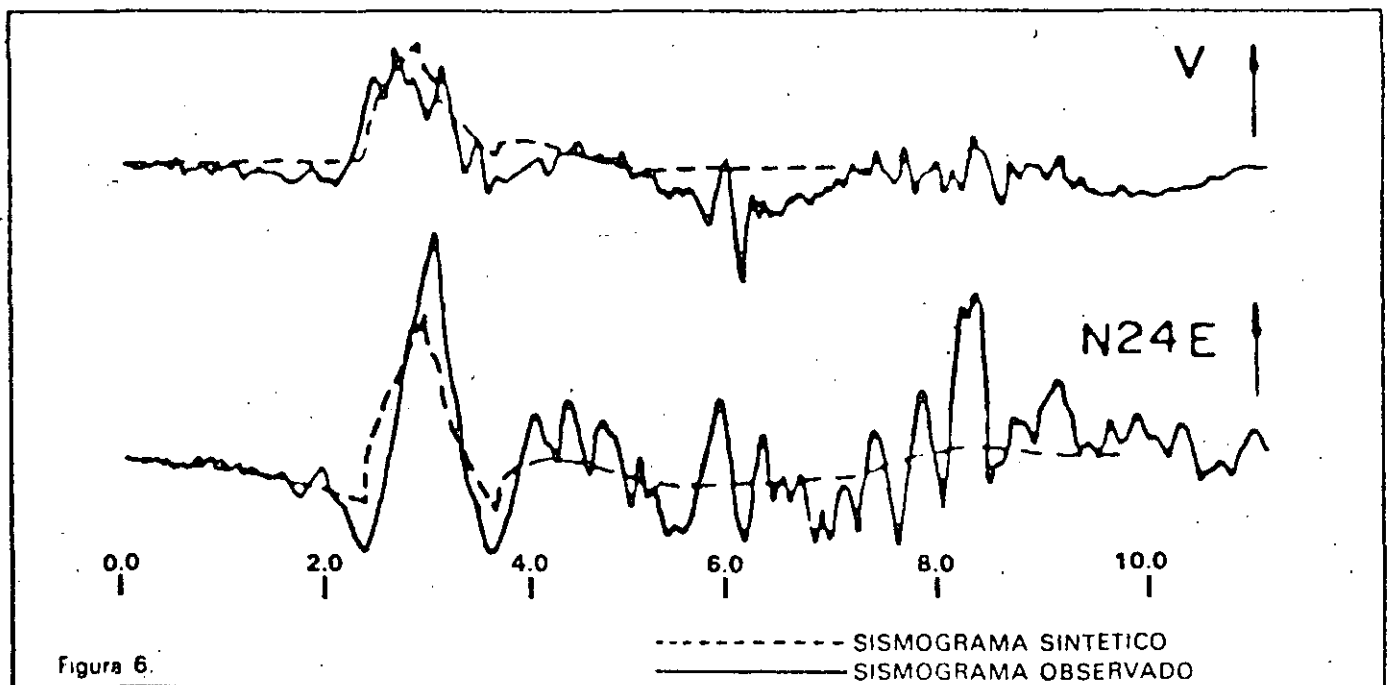


Figura 6.

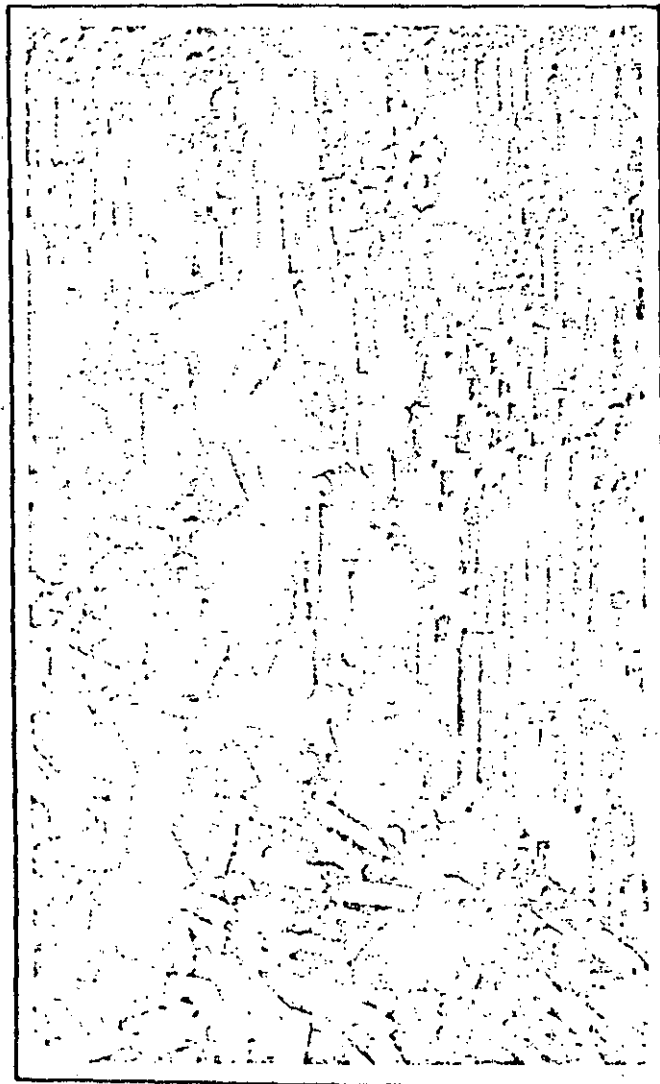
En el modelo de dislocación se suponen conocidos la longitud de la falla, su velocidad de ruptura, los desplazamientos relativos a lo largo de la falla y su evolución en el tiempo. Estos datos son en realidad otras de las incógnitas que se quisieran deter-

minar a partir de datos más elementales. Por este motivo, a los modelos de dislocación se les ha llamado cinemáticos.

Para modelar en detalle lo que sucede en la falla, es necesario en la actualidad suponer un mecanismo para la pérdida de esfuerzos. Ya fueron señalados algunos de los procesos probables, algunos de ellos no son en la práctica, tratables matemáticamente. En la actualidad se ha dado mucha atención a la teoría de fractura, originada inicialmente en problemas de metalurgia y resistencia de materiales, donde se estudia la estabilidad de una fractura en presencia de esfuerzos. Desde luego, también se hacen diferentes simplificaciones, pero se evitan muchas de las que se hacen en los modelos de dislocación. Año con año se resuelven problemas cada vez más complicados. En esta tarea las computadoras electrónicas han resultado de gran ayuda.

Por otra parte, la colocación de instrumental capaz de registrar movimientos fuertes en las zonas sísmicas, también ha crecido últimamente.

Con estos dos factores quizá tendremos en los próximos años una mejor comprensión de los procesos dinámicos que constituyen el mecanismo focal.



**Bibliografía**

- C F. Richter. *Elementary Sismology*. Freeman, San Francisco, 1958.
- W S J Stauder. "The focal mechanism of earthquakes"; en *Advances in Geophysics*. Academic Press, Nueva York, 1962.
- J Z Jiménez. *Mecanismo focal de siete temblores ocurridos en la región de Orizaba*, México. Tesis profesional, Facultad de Ciencias, UNAM, 1977.

4

Temporary networks are often established after a strong earthquake to accurately monitor aftershock activity for periods ranging from days to months. Portable seismographs (durable, lightweight, battery-operated) which can be rapidly installed are used. Because of these advantages, portable systems can also be packed into remote areas. The instruments are characteristically laid out in some type of geometric cluster. 76

## IX. EARTHQUAKE DESCRIPTORS

Earthquakes are described in terms of *magnitude* and *intensity*. Magnitude is a quantitative or absolute measurement, determined instrumentally, while intensity describes an earthquake in qualitative or relative terms, based upon personal observations. (Attempts have been made to quantify intensity parameters; these are reviewed later in this chapter.) Magnitude is expressed in Arabic numbers and intensity most often in Roman numerals. Quite understandably, their meanings have been confused and misunderstood by the public, essentially since the time magnitude ratings were assigned to earthquakes along with the longer established intensity ratings.

### A. Magnitude

The development of a magnitude scale in the U.S. had its beginning in the early 1930s when Charles F. Richter and Beno Gutenberg, both of the California Institute of Technology (CIT), were preparing an earthquake catalog, which indicated that more than 200 shocks per year were centered in southern California.<sup>27</sup> To lend greater credibility to the raw frequency data, Richter decided to attempt a ranking of earthquakes (e.g., small, moderate, and large) "based directly on instrumental indications, and . . . freed from the variations of personal estimates or the accidental circumstances of reported effects."<sup>28</sup> The procedure was patterned after that used earlier by K. Wadati in Japan.<sup>28</sup>

Richter started with two sets of assumptions. First, of two different sized earthquakes, originating at the same depth and recorded by the same seismograph, the larger event will generate the larger ground motion. However, if the epicenters differ, the smaller quake could conceivably produce the larger ground motion if it is located closer to the station. Second, several seismometers, at varying distances, record the same two earthquakes. If a graph is employed, with the maximum ground motion plotted on the Y-axis vs. the epicenter distances on the X-axis for each station, two curves (one for each quake) can be constructed by connecting X-Y station coordinates. The highest curve represents the largest earthquake.

These parameters then enabled Richter to analyze observed earthquakes occurring in southern California. Fortunately the CIT seismic network (seven stations at the time) was equipped with standard Wood-Anderson torsion seismographs. These seismographs<sup>29</sup> were designed specifically for the network. They record the horizontal components of ground motion but not the vertical. All of the seismographs were calibrated to the same constants: time = 0.8 sec, static magnification = 2800, damping = 0.8). This enabled horizontal ground motion to be recorded with system consistency and trace amplitudes to be plotted rather than computed ground motions.

Figure 40 illustrates the type of graph devised by Richter for establishing the magnitude scale. For several observed shocks, Richter plotted maximum trace amplitudes on a logarithmic scale\* (ordinate) vs. the epicenter distances to each station (abscissa). A series of similar curves evolved, approximately parallel to each other but at different amplitude levels (the higher the level, the larger the event). The parallelism meant that

\* A logarithmic scale was used because trace amplitudes ranged from 0.1 mm to 12 cm and because such a scale produced numerical results. All logarithms in this book refer to the base 10.

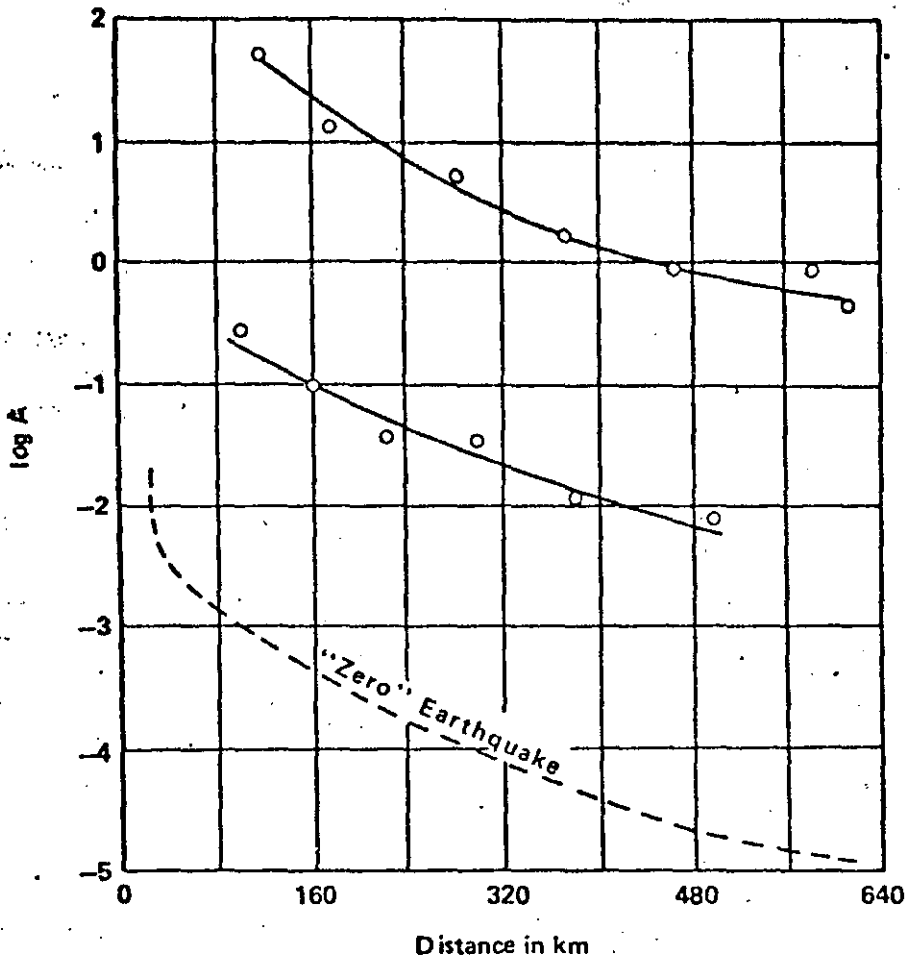


FIGURE 40. Illustration showing the procedure used by Charles F. Richter to establish the magnitude scale for local earthquakes. (From Hodgson, J. D., *Earthquakes and Earth Structure*, Prentice-Hall, Englewood Cliffs, N.J., 1964, 99. By permission of Prentice-Hall, Inc., Englewood Cliffs, N.J.)

the differences between amplitude logs for any two earthquakes was essentially independent of distance (amplitudes stay at a constant ratio).

Richter then plotted a standard or zero earthquake, giving all observed-event plots a base or standard for comparison (Figure 40). This standard shock can be envisioned as the smallest earthquake that could be expected to occur in a given area. Its placement was arbitrary, but its slope was approximately parallel to the others. This shock was assigned a trace amplitude of 0.001 mm on a Wood-Anderson seismograph located 100 km from the epicenter and a magnitude of 0. If the distances were measured from the standard quake curve to the other curves, the differences would be a measure of their respective sizes.

A zero magnitude does not imply the absence of an earthquake. A very small shock might conceivably be recorded with a trace amplitude smaller than 0.001 mm. In this case, the magnitude number would be negative. However, because of the limited magnification function (2800) of Wood-Anderson seismographs, negative-magnitude events were not encountered.

Based upon the previously described factors, magnitude assumed the relation

$$M_L = \log A - \log A_0$$

(5)

78

where  $M_L^*$  = magnitude for a local earthquake;  $A$  = maximum recorded trace amplitude at a given distance written on a Wood-Anderson seismograph in mm;  $A_0$  = predicted trace amplitude of the standard earthquake in mm at the same epicenter distance. In written form, Richter defined earthquake magnitude as "the logarithm of the maximum trace amplitude . . . with which the standard short-period torsion seismometer . . . would register that shock at an epicentral distance of 100 kilometers."<sup>18</sup>

Richter established empirical values for  $\log A_0$  for epicenters ranging from 25 to 600 km. With these data available, it was necessary to know only the epicentral distance and the maximum trace amplitude recorded at a station to solve for  $M_L$ . For greater accuracy, a correction factor was applied to each station in the CIT group to account for local ground and instrument variations.

If an earthquake produced a maximum trace amplitude of 45 mm at an epicenter distance of 100 km,

$$M_L = \log 45 - \log 0.001 = 1.66 - (-3.0)$$

(6)

the earthquake magnitude would equal 4.66. For an actual event, a final magnitude was an average determined from the  $M_L$ s of as many stations as possible. A mean  $M_L$  was determined for a single station if north-south and east-west ground motions were recorded.

Since the  $M_L$  scale is logarithmic, for every increase of one in magnitude, the trace amplitude increases tenfold. Therefore, the wave amplitude for a magnitude 6 event would be 10,000 times larger than that for a magnitude 2 event.

Richter originally believed that the magnitude scale might make it possible to separate the earthquakes of southern California, at best, into only a few magnitude classes (e.g., small, moderate, large). However, magnitudes were easily categorized to the nearest half unit, and for most occurrences, magnitudes could be assigned to the nearest tenth, with the uncertainty not exceeding approximately one tenth. During this period (mid-1930s), the seismic events in southern California generally had magnitudes ranging from 2 to 5; this equated to 15 discrete  $M_L$  values.

Richter's technique was a tremendous breakthrough in quantitative seismology. It became possible to rank earthquake size by a numerical scale and to obtain a detailed seismic history for a region. However, Richter<sup>19</sup> acknowledged several shortcomings of his magnitude scale. The most important of these included:

1. The Wood-Anderson seismographs had to be used.
2. The scale was accurate for only shallow earthquakes (hypocenters of about 16 km).
3. The scale could be used only for earthquakes occurring within 600 km of a seismograph station.

Although the scale was intended to be applicable to southern California, it was used successfully in New Zealand.<sup>19</sup>

In 1936, Beno Gutenberg and Richter,<sup>20</sup> using horizontal surface waves with periods near 20 sec, expanded the  $M_L$  scale to be applicable to shallow earthquakes originating at distances over 1000 km (*teleseisms*) and recorded by different types of seismographs. The equation assumed the form

\* Originally designated as  $M$ , but  $M_L$  (for *local magnitude*) is now in common usage.

$$M_s = \log A - \log B + C + D$$

(7)

79

where  $M_s^*$  = magnitude of teleseismic earthquakes; A = total horizontal component\*\* of maximum ground amplitude\*\*\* in microns (0.001 mm) when surface waves have periods of approximately 20 sec; B = total horizontal component of maximum ground amplitude in microns predicted for an event of zero magnitude at the same epicentral distance; C = constant for each seismic station, correcting for local ground and instrument conditions; D = constant incorporating depth, distribution of energy in azimuth, wave absorption, and wave-path irregularities. Regarding the Term B, Wood-Anderson seismogram trace amplitudes (b) in mm of surface waves (periods approximately 20 sec) could be used according to

$$\log b = \log B - 2.5$$

(8)

if epicentral distances were greater than  $20^\circ$ ; if less than  $20^\circ$ , surface waves have incorrect periods and Equation 8 is not valid. Values of  $-\log B$  (equaled positive numbers) were determined empirically and included in tabular form for various epicenter distances in degrees.

Surface wave magnitude refinements and additions were made by Gutenberg and Richter in 1942,<sup>121</sup> including a nomogram for determining  $M_s$  for "normal" depth earthquakes (16 to 20 km) from either trace or ground amplitudes (epicenter distance greater than  $10^\circ$  for the latter). In 1945, Gutenberg<sup>122</sup> further improved the accuracy of  $M_s$  by revising the values of  $-\log B$  and adding new worldwide station corrections and revised corrections for California stations.

Bath<sup>123</sup> proposed a magnitude equation ( $M_s$ ) based on the vertical component of surface waves (Rayleigh) as opposed to the horizontal component (Rayleigh and Love waves) used by Gutenberg and Richter.<sup>120</sup> Data from only the CIT-Pasadena station were used, and the limited accuracy of several equation constants hampered its implementation.

To determine magnitude for deep-focus earthquakes, body waves were used (e.g., P, PP, S),† since surface waves from such events usually do not have 20-sec periods and surface wave amplitudes are usually too small to be measured.<sup>22</sup> The initial step for determining this type of magnitude was made by Gutenberg in 1945;<sup>124</sup> he determined the empirical relation between magnitude, body wave amplitudes for shallow-focus events, and distance. This relation was

$$m_b = A + 0.1 (M - 7) - \log T + \log u \text{ (or } \log w \text{ with different A)}^{\dagger\dagger}$$

(9)

where  $m_b^{\dagger\dagger\dagger}$  = body wave magnitude; A = maximum ground amplitude in microns; M = surface wave magnitude; T = wave period in seconds; u = horizontal ground amplitude in microns; w = vertical ground amplitude in microns.

Data from two tables, one displaying station corrections to be added to either u or

- \* Originally designated as M, but  $M_s$  (for surface wave magnitude) is now in common usage.
- \*\* The total horizontal component equals the sum of north-south and east-west seismogram components. If only one component was available, the total was determined by multiplying the given by 1.4.
- \*\*\* Because various types of seismographs could be used, computed ground amplitudes had to be used, rather than trace amplitudes as was the case with  $M_s$ .
- † P = direct longitudinal waves, PP = reflected longitudinal waves; S = direct transverse wave.
- †† Additional correction of + 0.1 (M - 7) for all longitudinal waves in "great" ( $\geq 8$ ) earthquakes or events of magnitude less than 6.5.
- ††† Originally designated as M, but  $m_b$  (for body wave magnitude) is now in common usage.

w and the other containing values of A as a function of distance in degrees for P (horizontal, vertical), PP (horizontal, vertical), and S (horizontal only) waves, enabled  $m_b$  to be solved at worldwide stations.

Gutenberg<sup>134</sup> concluded that P, PP, and S wave amplitudes were more accurate than surface wave amplitudes for determining magnitude when focal depths ranged from 30 to 70 km and for calculating the magnitude of "great" ( $\geq 8$ ) earthquakes. The reason for the latter is that surface wave amplitudes may be too large to be completely "written" on the width of seismogram recording paper. The historical seismogram readings for the 1906 San Francisco earthquake produced the following magnitudes:  $m_b$  from P waves =  $8.3 \pm 0.1$ ;  $m_b$  from PP waves =  $8.4 \pm 0.1$ ;  $m_b$  from S waves =  $8.2 \pm 0.1$ ; and  $M_L = 8.25$ .

Gutenberg<sup>135</sup> then proceeded to use body waves for determining the magnitude of deep-focus earthquakes. When moving from shallow- to deep-focus shocks, Gutenberg defined magnitude to incorporate the thesis that two earthquakes of identical size possess the same amount of elastic wave energy regardless of their depth. This made it possible to use the maximum ground amplitudes of body waves as employed for shallow shocks. Gutenberg<sup>135</sup> demonstrated the applicability of  $m_b$  for deep-focus events by the use of Equation 9 and several empirical graphs.

By 1956, Gutenberg<sup>136</sup> had modified body wave magnitude to the form

$$m_b = \log (A/T) + B + C \quad (10)$$

where A = maximum ground amplitude of body waves (vertical or horizontal components for P and PP, and horizontal component for S); T = wave period in seconds; B = value given in tables and graphs, dependent upon wave phase and component, epicentral distance, and focal depth to a lesser degree;\* C = empirically determined station constant which is usually less than 0.2.

Gutenberg<sup>136</sup> believed that the most accurate procedure for assigning magnitudes to earthquakes was by the use of body waves ( $m_b$ ), as opposed to surface waves ( $M_L$  and  $M_S$ ). His reasons were (1) surface wave amplitudes may be smaller than predicted if wave trains traverse boundaries of horizontal structure (energy attenuation) and (2) focal depths may be deeper than the average predicted for determining magnitude by surface waves (if deeper than average,  $M_L$  and  $M_S$  are too small). Because of the advantages of body waves, Gutenberg elevated  $m_b$  to be what he termed the *unified magnitude*. Consequently, in his publications, earthquake magnitudes were given in  $m_b$  units.

Richter, by contrast, believed that there were inadequacies with  $m_b$ , and he reported surface wave magnitudes (either  $M_L$  or  $M_S$ ) in his publications. Richter<sup>137</sup> stated his views in a 1971 interview:

Magnitudes should not be based on body waves alone when surface wave data are available; nor should they be based on P amplitudes alone. Still worse is the practice of assigning magnitudes on the first few waves of the P group . . . . In many instances it has been shown that the initial waves are those of a small foreshock, to which alone the magnitude supposedly determined for the following shock will then apply.

Many seismological stations determine both surface and body wave magnitudes whenever possible. The U.S. Geological Survey and many other organizations currently use the following magnitude equations.<sup>138,139</sup> Surface wave magnitude is determined by

\* For epicentral distances less than  $16^\circ$ , B values change rapidly, and up to  $20^\circ$ , B is largely dependent upon the local geology.

$$M_S = \log (A/T) + 1.66 \log D + 3.3 \quad (11)$$

where  $A$  = maximum horizontal surface wave amplitude in microns;  $T$  = wave period in seconds ( $18 < T < 22$ );  $D$  = distance from the epicenter to a station in geocentric degrees\* ( $20^\circ < D < 160^\circ$ ); no correction is made for focal depths under 50 km.

Body wave magnitude is determined by

$$m_b = \log (A/T) + Q (D,h) \quad (12)$$

where  $A$  = ground amplitude in microns extracted from the P wave group (not necessarily the maximum of this group);  $T$  = wave period in seconds, restricted to  $0.1 \leq T \leq 3.0$ ;  $Q$  = correction factor, a function of distance ( $D$ ) and focal depth ( $h$ ), where  $D = 5^\circ$ . Equations 11 and 12 were recommended for worldwide use by the International Association of Seismology and Physics of the Earth's Interior and the 1967 International Geophysical Assembly.<sup>139,140</sup> Some organizations have varied the ranges of  $T$  and  $D$  to account for the regional geologic structure more closely.

It is often desirable to relate body and surface wave magnitudes for statistical comparisons. Richter and Gutenberg pioneered efforts to formulate an approximate relationship between the two. The latest equations are<sup>27</sup>

$$m_b = 2.5 + 0.63M_S \quad (13)$$

$$M_S = 1.59m_b - 3.97 \quad (14)$$

Magnitudes agree at 6.75 to about 6.8; if higher,  $M_S$  is larger than  $m_b$ ; if lower than 6.75,  $m_b$  is larger than  $M_S$ .

An empirical relationship (less accurate than equations 13 and 14) between  $m_b$  and  $M_L$  was formulated by Gutenberg in the form<sup>136,141</sup>

$$m_b = 1.7 + 0.8M_L - 0.01M_L^2 \quad (15)$$

Richter<sup>27</sup> stresses, however, that this relation is only an approximation that will undoubtedly change as more data become available.

Modifications of Equations 11 and 12 have been proposed by several researchers for earthquakes occurring in the eastern U.S.<sup>142-146</sup> The modifications incorporate observational and theoretical data that account for surface and body waves being attenuated (anelastic) less east of the Rocky Mountains. Magnitude can be overestimated by as much as 1.5 units if the standard equations are used.<sup>142</sup> As reported by Nuttli,<sup>146</sup> body and surface wave magnitude equations are of the general form

$$M = B + C(\log \Delta) + \log (A/T) \quad (16)$$

where  $A$  = ground motion for body or surface waves;  $B$  = constant dependent upon wave excitation of the wave period  $T$  in the source region;  $C$  = constant dependent upon the wave attenuation coefficient, which is a function of  $T$ ;  $\Delta$  = epicentral distance.

As an example, Nuttli<sup>146</sup> has proposed the following equation for calculating surface wave magnitude in the eastern U.S.:

\* Surface distances measured by angles subtended at the earth's center.

$$M_S = 2.60 + 1.66 (\log \Delta) + \log (A/T)_{\max} \quad (17)$$

where  $(A/T)_{\max}$  = maximum value of  $A/T$  in microns per second for the vertical component of Rayleigh waves having 3- to 12-sec periods;  $\Delta$  = epicentral distance in degrees ( $2^\circ < \Delta < 20^\circ$ ).

Nuttli<sup>148</sup> also proposed two local magnitude scales using the vertical component of Love waves ( $L_v$ ) for use in the eastern U.S.  $L_v$  represents guided short-period ( $0.5 \leq T < 5.0$  sec) surface waves that propagate through continental crusts.<sup>149</sup> Although a surface wave, its small amplitude more closely matches short-period P waves than the long-period surface waves.  $L_v$  is, therefore, more closely aligned with  $m_s$  than with  $M_s$ . The equations are

$$m_{bL_v} = 3.75 + 0.90 (\log \Delta) + \log (A/T) \quad (18)$$

$$0.5^\circ < \Delta < 4.0^\circ$$

$$m_{bL_v} = 3.30 + 1.66 (\log \Delta) + \log (A/T) \quad (19)$$

$$4.0^\circ < \Delta < 30.0^\circ$$

where  $\Delta$  = epicentral distance in degrees;  $A$  = maximum ground amplitude in microns;  $T$  = wave period in seconds. These equations are used by seismologists at St. Louis University and the Virginia Polytechnic Institute and State University; resulting magnitudes are reported to and published by the U.S. Geological Survey.

Because short-period, high-gain, vertical seismometers are now available, it is possible to record *microearthquakes* or *microseisms*, and new empirical relations have been introduced for determining local magnitude. Only two techniques are presented here, but many more are found in the literature.

To fully analyze the aftershocks of the 1966 Parkfield-Cholame, California earthquake, Eaton et al.<sup>148</sup> established empirical relationships for assigning magnitudes to more than 600 aftershocks. Magnitudes were calculated on a U.S. Geological Survey IBM 360/65 computer with the program HYPOLAYR.<sup>148</sup> The Richter equation (5) was not applicable because, among other reasons, the portable seismometers recorded only vertical ground motion. The equation was

$$M = \log \left( 1.03 \frac{X \times T}{C10} D^{1.7} \right) - 1.60 \quad (20)$$

where  $X$  = maximum trace amplitude from the vertical component seismogram;  $T$  = period in seconds of the wave with amplitude  $X$ ;  $C10$  = trace amplitude in mm, resulting from a  $10 \mu v$  (microvolt) signal introduced into the instrument amplifier in place of the seismometer output;  $D$  = hypocenter distance.

Magnitudes for 49 events (2.0 to 2.5) were compared to  $M_L$  values derived from the University of California, Berkeley seismic network. The latter magnitudes were approximately 0.1 unit larger.

The coda length or the time of signal duration has been used successfully for determining local magnitude. This method was first demonstrated in eastern Europe by Bisztricsany in 1958,<sup>149</sup> and later by Sole'vev<sup>150</sup> in the Soviet Union, and in Japan by Tsumura.<sup>151</sup> In the U.S., the method has been used by Lee et al.,<sup>152</sup> Crosson,<sup>153</sup> Teng et al.,<sup>154</sup> Real and Teng,<sup>155</sup> and Herrmann.<sup>156</sup> Bisztricsany made use of surface waves, but the other investigators used the total wave train (body and surface waves).

Various methods have been used to define the termination of an earthquake as it is "written" on a seismogram (of vital importance to this technique). Lee et al.<sup>133</sup> defined termination on the basis of the minimum amplitude threshold; once the amplitude fell below this arbitrary level, the earthquake was said to have been terminated. Teng et al.<sup>134</sup> plus Real and Teng<sup>135</sup> defined earthquake termination as that point where the signal-to-noise ratio was 1:1.

Excluding Herrmann's work,<sup>136</sup> the relation between magnitude and signal duration assumed the linear form

$$M_t = C_0 + C_1 \log(t) + C_2 \Delta \tag{21}$$

where  $M_t$  = duration magnitude;  $C_0$ ,  $C_1$ ,  $C_2$  = coefficients determined by stepwise multiple linear regression as described by Draper and Smith;<sup>137</sup>  $t$  = total duration of the seismic wave train in seconds;  $\Delta$  = epicentral distance in km.

Teng et al.<sup>134</sup> established an empirical relation between the duration of more than 100 events in the Los Angeles area and epicenter distance. A stepwise linear regression yielded the following relation, which had a 91% multiple correlation coefficient:

$$M_t = 0.10 + 1.591 \log(t) + 0.001 \Delta \tag{22}$$

Duration magnitudes compared favorably with those based upon trace amplitudes from Wood-Anderson seismographs ( $M_L$ ).

Real and Teng<sup>135</sup> plotted local magnitudes vs. duration logarithms (in seconds) for approximately 400 events in southern California. A nonlinear pattern (slight curvature) was noted in the mean slope of residuals as the magnitude or  $\log(t)$  increased. The slope inflection occurred at  $M_L = 3.8$ . To remove the curvature, the variable  $(\log t)^2$ , called the "quadratic term," was added to the linear regression model. Hence, the relations became

$$M_t = C_0 + C_1 \log(t) + C_2 \Delta \text{ if } M_t < 3.8 \tag{23}$$

$$M_t = C_0 + C_1 (\log t)^2 + C_2 \Delta \text{ if } M_t > 3.8 \tag{24}$$

Their results indicate that  $M_t$  was more accurate than  $M_L$ . For  $M_t$ , the mean standard deviation from the mean was 0.1 magnitude units as compared to 0.27 for  $M_L$ . Signal duration was not significantly affected by variations in wave azimuth or source effects, a major contributing factor for the magnitude accuracy. Much of the variation in  $M_L$  values resulted from horizontal shear waves being amplified by topographic effects. Real and Teng point out, however, that any duration technique cannot be used to determine magnitude for multiple shocks or large earthquakes if there are immediate aftershocks.

From the previous discussion it is apparent that many empirical equations have been developed for determining earthquake magnitude and that their interrelationships are not precisely defined at this time. However, it is now often possible to assign accurate values ( $\pm 0.25$  magnitude units) to large earthquakes occurring anywhere on the earth.

### 1. Magnitude Misunderstandings

Because Charles F. Richter devised the first procedure for determining magnitude, his name is often used erroneously in various media earthquake reports. For example, "Richter scale" and "Richter magnitude" can be used synonymously with local magnitude or  $M_L$ , but they should not be attached to other magnitude types. Magnitudes are designated by appropriate symbols or word descriptors throughout this book.

84  
Earthquake magnitude scales are open-ended, but many believe magnitude units range from 0 to 10 or 0 to 12. This notion is most likely a carryover from intensity scales, which are closed. Theoretically, there is no maximum magnitude number. However, there is an upper limit to the amount of strain that can be stored in rocks before they rupture. To date, the largest magnitude ( $M_L$ ) has been 8.9 ( $m_s = 8.1$ ). This value was assigned to two earthquakes: one off the west coast of South America (January 31, 1906) and the other off the east coast of Honshu, Japan (March 2, 1933). The latter is often referred to as the Sanriku earthquake.

Similarly, the bottom end of the scale is open, making it possible to have negative-magnitude earthquakes. Local shocks of about magnitude  $-3$  can now be detected with modern, high-magnification seismometers. According to Bolt,<sup>90</sup> a quake of magnitude  $-2$  releases the same amount of energy as a brick hitting the ground from a height of about 1 m.

Correlations between magnitude and casualties or property damage are not meaningful. Magnitude is only one descriptor of a seismic event and other factors, including population density, location of the epicenter, focal depth, building types, and soil conditions, must be evaluated. For example, the highest magnitude earthquake in North America for which there are seismograms was the March 27, 1964 Alaska event ( $M_s = 8.5$ ); the death toll, excluding those killed by a *tsunami* or *seismic sea wave*, was 15. Compare this to the January 29, 1960 Agadir, Morocco earthquake ( $M_s = 5.5$  to 6.0), where more than one third (12,000) of the city's inhabitants were killed and the death rate in two districts was 95%;<sup>138</sup> or the  $M_s = 6.2$  West Pakistan earthquake of December 28, 1974 where deaths reached 5300 and injuries totaled 17,000.<sup>139</sup>

It also has been assumed by some that the largest historical earthquake for a given area will not be surpassed by a larger magnitude event in the future. As noted by Allen et al.,<sup>140</sup> the fallacy of this belief was dramatically emphasized by the February 9, 1971 San Fernando, California earthquake. Up until 1971, the April 4, 1893 Pico Canyon event was probably the largest ( $M_L$  estimated to be about 6);<sup>141</sup> the 1971 earthquake registered  $M_L = 6.4$ . Although this may not appear to be a significant difference, 4.4 times more energy was released by the San Fernando earthquake.

## 2. Magnitude and Energy

Earthquakes release varying amounts of *elastic wave energy* ( $E$ ).  $E$  is essentially that portion of the total energy strain, stored in lithospheric rock, that is not consumed as mechanical work (e.g., through faulting) during an earthquake. The elastic wave energy is expressed in *ergs*.\*

Not only does magnitude enable seismic events to be ranked according to size on a unitless numerical scale, but it also makes it possible to estimate the amount of wave energy released. Gutenberg and Richter established a relationship between surface wave magnitude and total seismic wave energy through a series of empirical linear equations.<sup>130, 131, 142-144</sup> The equations and the years in which they were introduced are presented in Table I.

Revisions, especially to the earlier forms, were made because the calculated seismic energies were much too large, in some cases 100 times too large.<sup>141</sup> A large part of the problem was attributable to the geologic setting of participating seismograph stations. Station sites varied from bedrock to loosely consolidated sediments; no instrument corrections were made for the increased ground amplitudes at the latter stations. This had a pronounced effect on  $E$  because the amplitudes were squared in deriving the equation parameters.<sup>134</sup>

\* Erg = unit of work equal to a force of 1 dyne acting through a distance of 1 cm; 1 dyne is the force needed to accelerate a freestanding gram mass 1 cm/sec.

TABLE I

Relation Between Historical Equations and Energy Release for One Unit of Magnitude Change

85

Energy equation (log E) and year of introduction	Energy increase for one unit of magnitude change
8.0 + 2.0 $M_s$ (1936)	100.00 ×
11.3 + 1.8 $M_s$ (1942)	63.12 ×
12.0 + 1.8 $M_s$ (1949)	63.11 ×
11.0 + 1.6 $M_s$ (1954)	39.94 ×
11.8 + 1.5 $M_s$ (1956)	31.62 ×

The effects of energy overassignment can be seen in Table I. Note that the energy increase per one unit of magnitude change shows considerable variation between the 1936 and 1956 equations. The latter equation

$$\log E = 11.8 + 1.5M_s \quad (25)$$

is thought to be the most accurate of the Gutenberg-Richter equations, and it is used widely.

Båth<sup>65</sup> also established a relationship between surface wave magnitude and total seismic wave energy by using records from earthquakes not used by Gutenberg and Richter. His equation assumed the form

$$\log E = 12.24 + 1.44M_s \quad (26)$$

Results obtained by Equations 25 and 26 are very similar, but Equation 26 is not intended for use with magnitudes less than 5.

Two notes of caution should be observed by the reader. First, in Richter's 1958 book,<sup>27</sup> *Elementary Seismology*, the energy equation was printed as

$$\log E = 11.4 + 1.5M_s \quad (27)$$

The 11.4 is a misprint and should be corrected to read 11.8 (Equation 10, page 366). Unfortunately, some writers have used Equation 27 in several recently published textbooks. Second, the reader of historical documents should be aware of the modifications that have been made to the log E equations because the reported energies may be grossly inaccurate.

Using the 1956 Gutenberg-Richter equation (25) and solving for  $M_s = 2$ ,  $M_s = 3$ ,  $M_s = 4$ , etc., one finds that the seismic wave energy released increases approximately 31.6 times for every single unit change in magnitude. Therefore, a magnitude 8 earthquake releases one billion times more energy than a magnitude 2 event (31.6<sup>6</sup>). Table 2 lists a hierarchy of seismic events ( $M_s = 2.5$  to 8.9) with energy comparisons, and Table 3 compares energy differences for several well-known earthquakes.

Gutenberg also devised log E equations for  $m_b$  and  $M_L$ :

$$\log E = 5.8 + 2.4m_b \quad (28)$$

$$\log E = 9.9 + 1.9M_L - 0.024M_L^2 \quad (29)$$

Richter<sup>27</sup> notes that because the parameters describing  $M_L$ <sup>2</sup> are empirical, the relations

TABLE 2

## Energy Relations for Earthquakes with Surface Wave Magnitudes 8.9 to 2.5

Seismic event	Surface wave magnitude	Log E	Energy in ergs	No. of times smaller than 8.9 event
1933, Sanriku, Japan	8.9	25.15	$1.41 \times 10^{28}$	—
1964, Alaska	8.5	24.55	$3.55 \times 10^{27}$	4
1906, San Francisco, Ca.	8.3	24.25	$1.78 \times 10^{27}$	8
1930, Kern County, Ca.	7.7	23.35	$2.24 \times 10^{26}$	63
1971, San Fernando, Ca.	6.5	21.55	$3.55 \times 10^{21}$	3,972
1972, Managua, Nicaragua	6.2	21.10	$1.26 \times 10^{21}$	11,190
1960, Agadir, Morocco	5.8	20.50	$3.16 \times 10^{20}$	44,620
1975, Oregon, Off coast	4.7	18.85	$7.08 \times 10^{18}$	1,991,525
1975, Helena, Montana	3.9	17.65	$4.47 \times 10^{17}$	31,543,624
1974, Northern California	2.5	15.55	$3.55 \times 10^{16}$	3,971,830,986

TABLE 3

## Energy Differences for Several Well-Known Earthquakes

Seismic Events and Magnitudes ( $M_s$ )				$\frac{E(1)^*}{E(2)}$
(1) 1964, Alaska	8.5	(2) 1906, San Francisco	8.3	2
(1) 1971, San Fernando	6.5	(2) 1960, Agadir	5.8	11
(1) 1964, Alaska	8.5	(2) 1971, San Fernando	6.5	999
(1) 1964, Alaska	8.5	(2) 1960, Agadir	5.8	11,220

\* From  $\log E = 11.8 + 1.5 M_s$ .

in Equation 29 will probably be revised in the future. Båth has also expressed  $m_s$  and  $M_s$  in log E equations.<sup>49, 140</sup>

It is perhaps easier to visualize earthquake energy by the use of more familiar units. Båth<sup>49</sup> provides a comparison between E and electrical consumption equivalency for Uppsala, Sweden (population about 100,000 in 1966): (1) a shock of  $M_s = 1.6$  would equal the electrical energy consumed in one second; (2) a 6.8 event would equate to 290,000,000 kilowatt hours (kWh) or the electrical needs of the city for one year; and (3) an 8.75 earthquake would supply the city (assuming a constant population) with electrical energy for 670 years!

A second analogy is between magnitude and atomic bombs or TNT. According to Richter,<sup>27</sup> the World War II type of atomic weapon released about  $8 \times 10^{20}$  ergs of energy (20,000 tons of TNT). When this figure is compared to the magnitudes of several large earthquakes, the results are staggering: (1) 1971 San Fernando, California,  $6.5 M_s = 4.4$  bombs; (2) 1906 San Francisco, California,  $8.3 M_s = 2225$  bombs; (3) 1964 Alaska,  $8.5 M_s = 4438$  bombs; and (4) 1933 Sanriku, Japan,  $8.9 M_s = 17,625$  bombs. Table 4 relates earthquake magnitude to the approximate energy of TNT.

### 3. Magnitude and Faulting

Two general statements can be made in reference to faults and magnitude. First, as the length of a fault trace increases, the potential for larger magnitude earthquakes also increases. The San Andreas fault, therefore, would be more likely to have a great earthquake than the Garlock fault (Figure 5). Second, if the depth is held constant for shocks of shallow foci, the length of surface rupturing and crustal offset increases with magnitude.

TABLE 4

## Earthquake Energy (Magnitudes 1.0--9.0)

Magnitude ( $M_L$ )	Approximate TNT energy	
	English	Metric
1.0	6oz	171g
1.5	2lb	909g
2.0	13lb	6kg
2.5	63lb	29kg
3.0	397lb	180kg
3.5	1,990lb	905kg
4.0	6ton	5t*
4.5	32ton	29t
5.0	199ton	181t
5.5	1,000ton	909t
6.0	6,270ton	5,700t
6.5	31,550ton	28,682t
7.0	199,000ton	180,909t
7.5	1,000,000ton	909,091t
8.0	6,270,000ton	5,700,000t
8.5	31,550,000ton	28,681,818t
9.0	199,000,000ton	180,909,091t

\* t = tonne (metric ton), 1.1 short ton.

From California Division of Mines and Geology,  
*Min. Inf. Ser.*, 22, 77, 1969.

Tocher,<sup>166</sup> Iida,<sup>167</sup> Albee and Smith,<sup>168</sup> Bonilla,<sup>61</sup> and Bolt<sup>169</sup> derived empirical equations between magnitude and rupture lengths. For example, Tocher<sup>166</sup> analyzed all earthquakes in northern California and Nevada from 1906 to 1958 with  $M_L$ s larger than 0.5 and discovered that each event was associated with surface breaks; one event showed a surface rupture at  $M_L = 5.75$ . Upon plotting  $M_L$  vs. the common log of the surface fault rupture length ( $l$ ) in km, Tocher derived the equation for  $M_L$  larger than 6.5:

$$M_L = 5.65 + 0.98 \log l \quad (30)$$

Using the same seismic data, Tocher<sup>166</sup> then related local magnitude with surface rupture length and the maximum displacement ( $D$ ) of rock units on either side of a fault in centimeters. The empirical equation assumed the form

$$M_L = 5.22 + 0.53 \log lD \quad (31)$$

Wesson et al.<sup>69</sup> have estimated surface fault displacements for future earthquakes in the San Francisco Bay region by analyzing offset-magnitude data from past events and maximum estimates predicted for a particular strike-slip fault. Their data suggest that the maximum offsets would be 10 m for a  $M_L = 8$  event, 6 m for  $M_L = 7$ , 2 m for  $M_L = 6$ , and 0.5 m for  $M_L = 5$ .

Until very recently, it was believed that when faulting occurred, rupturing and offsets were confined to a single fault or perhaps to several faults within the epicentral region. However, Wyss et al.<sup>170</sup> and Allen et al.<sup>171</sup> documented breaks not only along the source region segment of the Coyote Creek fault but also on three distant active

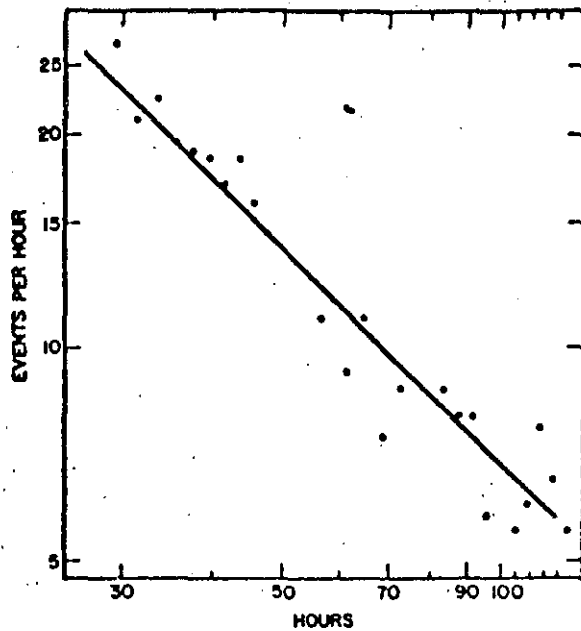


FIGURE 41. Decay plot for aftershocks recorded at the Warm Springs seismograph station, 35 km from the February 9, 1971 San Fernando, California earthquake epicenter. (From Scholz, C. H., Microearthquakes on the San Andreas fault and aftershocks of the San Fernando earthquake, in The San Fernando, California, Earthquake of February 9, 1971, Geological Survey Professional Paper 733, U.S. Government Printing Office, Washington, D.C., 1971, 35.)

faults (showing evidence of repeated Quaternary movement) associated with the moderate 1968 Borrego Mountain, California earthquake ( $M_s = 6.4$ ). The three faults included Superstition Hills, Imperial, and Banning-Mission Creek, all located in the Imperial Valley. These faults ruptured along 23, 20, and 30 km segments at 45, 70, and 50 km epicenter distances, respectively. The rupturing was most likely caused by seismic shaking. Max Wyss of the California Institute of Technology has commented on the engineering implications of this phenomenon:<sup>173</sup> "It implies . . . that damage to structures on or near earthquake faults may even occur even though the earthquake is centered on some other distant fault."

#### 4. Foreshocks, Aftershocks, and Swarms

A primary earthquake can be preceded by *foreshocks* and followed by *aftershocks*, the latter being the more common of the two. Both groups have magnitudes smaller than the main shock. A *swarm* is a series of earthquakes all of about the same size, in which no one event can be identified as the main shock.

K. Mogi, of the University of Tokyo's Earthquake Research Institute, proposed a classification scheme for the above types of earthquakes.<sup>172, 174</sup> Sequences can be one of three classes: (1) a large earthquake with no foreshocks, but followed by aftershocks; (2) a sequence of foreshocks-main shock-aftershocks; and (3) a swarm.

Aftershock frequency and magnitude values are usually higher for large than for moderate earthquakes. However, regardless of the size of the main shock, the aftershock sequence most often follows an exponential decay rate for the first few days because of the rapid stress drop. Figure 41 is a decay plot, as determined by Scholz,<sup>175</sup>

for the aftershocks associated with the February 9, 1971 San Fernando, California earthquake. It is noted that the decay rate closely approximates a  $-1$  regression line. In all, thousands of aftershocks were recorded, and 55 events had  $M_L \geq 4$ .<sup>176</sup> On the first day, 36 (65.5%) of these events were recorded, but only 8 (14.6%) were recorded on the second day.<sup>176</sup>

The largest aftershock often occurs shortly after the main earthquake. Two examples of this occurred in Nevada in 1954. The  $M_L = 6.6$  Rainbow Mountain quake was followed by a 6.4 aftershock about 11 hr later, and the  $M_L = 7.1$  Fairview Peak earthquake was followed by a 6.8 aftershock only 4 min later.<sup>44</sup>

Without question, one of the most intense (in frequency and magnitude) aftershock sequences was associated with the 1964 Alaska earthquake. During the first 24 hr, 28 aftershocks with  $M_L$ s greater than 4 were recorded; 10 of these exceeded  $M_L = 6$ . By the end of the second day, the sequence for  $M_L > 4$  totaled 55, one of which registered 6.7, and the total reached 75 ( $M_L > 4$ ) by the end of the first week.<sup>2</sup> Press and Jackson<sup>177</sup> estimate that 12,000 aftershocks ( $M_L \geq 3.5$ ) occurred in the first 69 days.

As would be expected, aftershocks have a pronounced psychological impact upon a population. Arvidson<sup>109</sup> relates this personal account for the aftershocks associated with the 1964 Alaska earthquake:

We came to anticipate them, and not without apprehension. Both the frequency and magnitude varied. We began to expect a severe shock once a number of minor shocks had occurred, and to this end some type of earthquake detector or warning device could be found in almost every home. In our house, for example, when a ceiling lamp started to sway past a predetermined point, it was time to evacuate the house.

As previously stated, foreshocks, especially those that are perceptible, are less common than aftershocks. However, when felt by a populace they have a strong psychological impact; a feeling of uncertainty prevails as to whether they represent a warning of a larger event yet to arrive.

Two examples of foreshock activity occurred in the United States during 1975. The Pocatello Valley, Idaho-Utah border,  $m_s = 6.1$  earthquake was preceded (22 hr) by a  $M_L = 4.2$  foreshock.<sup>178</sup> Some 21 foreshocks, with the largest  $M_L = 4.7$ , preceded the  $M_L = 5.7$  Oroville, California earthquake.<sup>179</sup> Foreshocks are being investigated as possible prediction signals in several countries, and the prospects are discussed in Volume II, Chapter 1, "Earthquake Prediction."

In January 1975, the Brawley area (Imperial Valley) of California was the locale for a swarm which had a dense sequence for three days. Some 75 events had  $M_L$ s ranging from 3 to 4.7; the total exceeded 260 shocks ( $M_L > 1.5$ ). The swarm activity commenced on a point of the right-lateral Brawley fault and proceeded north and south at a speed of 1 km/hr.<sup>180</sup> Human reaction varied from people sleeping in their cars to the Brawley Fire Department parking all vehicles out of doors until the activity subsided.

The most famous swarm was the August 1965 to January 1967 Matsushiro, Japan sequence. Almost 700,000 shocks were recorded, 60,000 were strong enough to be felt, and 400 were damaging.<sup>181-183</sup> During the period of peak activity, more than 6000 felt and unfelt quakes were detected each day at the Matsushiro Seismological Observatory.<sup>183</sup>

### 5. Earthquake Frequency

Estimates vary as to the number of natural earthquakes that occur every year. Most seismologists are in agreement that the frequency certainly exceeds 1 million (1 every 30 sec), and if the smallest shocks are included, the number undoubtedly reaches several million. Tufty<sup>184</sup> puts the number at about 5 million.

Earthquake frequency varies at an essentially exponential rate with magnitude; small

earthquakes are much more common than large events. Therefore, if one accepts the frequency as being several million per year, the vast majority of events are too small to be detected by human sensors. As a general rule, the smallest magnitude ( $M_L$  or  $M_s$ ) shallow-focus quake that a person can perceive, if near the epicenter, is about 2.

If earthquake frequency and magnitude data are available for a specific region (or the entire planet), and if the number of events per specified magnitude range is plotted on a log scale vs. magnitude on a linear scale, the coordinates will fall on an approximate straight line.<sup>109</sup> This line can be represented by the Gutenberg-Richter equation:<sup>110</sup>

$$\log N = a - bM \quad (32)$$

where  $N$  = number of earthquakes per unit of time;  $M$  = shocks of a certain magnitude (any one type);  $a$  and  $b$  = constants to be determined from the earthquake group under investigation. As noted by Båth,<sup>111</sup> the value of  $b$  varies with the region in question plus the range of focal depths; the variance is usually from 0.5 to 1.5 with most  $b$  values very close to 1.0.<sup>109</sup> The  $b$  value is a reflection of the line slope of the semilog plot of earthquake frequency vs. magnitude.

For the period from 1918 to 1964, Båth<sup>111</sup> analyzed global earthquake frequency for events greater than  $M_s = 6$ , and found  $a$  to be 8.73 and  $b$  to be 1.5. Therefore,

$$\log N = 8.73 - 1.15M_s \quad (33)$$

He then proceeded to equate energy release per magnitude class for a single year. Combining his energy-magnitude equation

$$\log E = 12.24 + 1.44M_s \quad (26)$$

with Equation 33 yielded

$$\log EN = 20.97 + 0.29M_s \quad (34)$$

where  $EN$  = energy release in ergs per year per magnitude class. Based upon this relation, an increase of one in magnitude equates to roughly a doubling ( $1.95 \times$ ) of the energy released. Using Equation 34, Båth<sup>111</sup> concluded that magnitude  $\geq 8$  earthquakes release approximately 50% of the total seismic energy in a single year,  $M_s \geq 7$  about 75%, and  $M_s \geq 6$  almost 90%.

Utsu<sup>106,107</sup> has used a three-parameter equation for determining the frequency of shallow shocks in Japan plus shallow and deep events for the world:

$$\log N = a - bM + \log(c - M) \quad (35)$$

where the additional symbol  $c$  = upper limit of magnitude recognizable in certain earthquake groups. The  $c$  factor accounts for the sharp drop-off in frequency near the maximum limit of magnitude. When this drop-off occurs, the  $\log N$  vs.  $M$  line assumes a convex curve. Other types of three-parameter equations have been formulated by Ryznichenko,<sup>108</sup> Okada,<sup>109</sup> Otsuka,<sup>109</sup> Sacuiu and Zorilescu,<sup>109</sup> and Purcaru and Zorilescu.<sup>109</sup>

Bolt<sup>109</sup> has plotted an average line which can be used to extrapolate the approximate

\* There is less agreement with the plotted line for magnitudes less than 4.

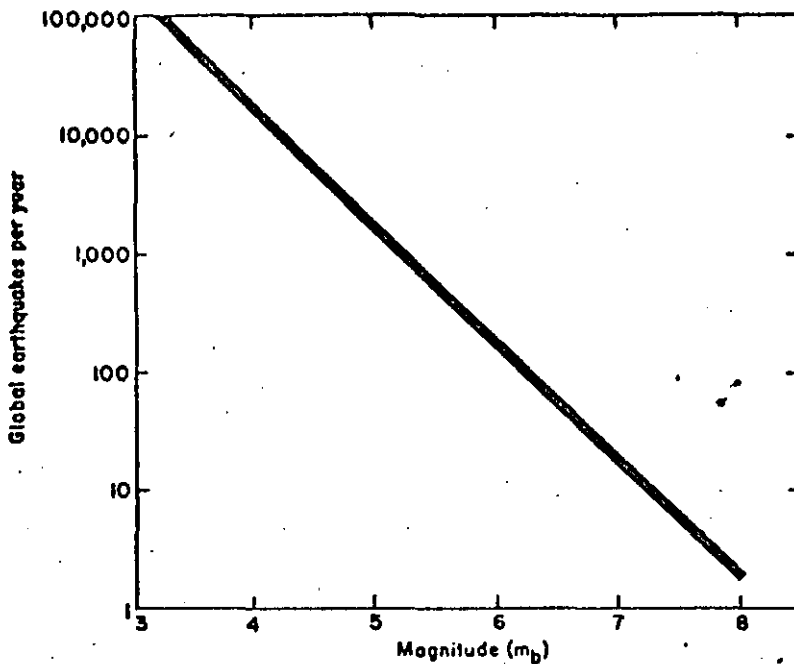


FIGURE 42. Average number of earthquakes above a given body wave magnitude ( $m_b$ ) for the world. (From *Nuclear Explosions and Earthquakes: The Parted Veil*, by Bruce A. Bolt. W. H. Freeman and Company. Copyright © 1976.)

TABLE 5

Earthquake Magnitude ( $M_s$ ) and Annual Frequency

Description	$M_s$	Annual frequency
Great earthquakes	$\geq 8.0$	1
Major earthquakes	7.0—7.9	10
Destructive shocks	6.0—6.9	100
Damaging shocks	5.0—5.9	1,000
Minor strong shocks	4.0—4.9	10,000
Generally felt	3.0—3.9	100,000

From Gutenberg, B., and Richter, C. F., *Seismicity of the Earth*, GSA Special Papers No. 34, Geological Society of America, New York, 1941, 105. With permission.

earthquake frequency per year for body wave magnitudes larger than about 3.5 (Figure 42). Observed frequency plots fall off the line for smaller shocks.

In the first version of *Seismicity of the Earth*,<sup>162</sup> Gutenberg and Richter related magnitude to annual frequency (Table 5); these yearly frequencies were modified in the later two editions of *Seismicity of the Earth*.<sup>162,163</sup> Revised and expanded magnitude/frequency data were published by the National Oceanic and Atmospheric Admin-

\* This mention of *Seismicity of the Earth* affords the author the opportunity to acknowledge one of the monumental efforts in seismology. A few of the accomplishments of the three editions include: (1) the assignment of magnitudes to historical earthquakes for which seismograms were available, (2) magnitude and focal depth correlations, and (3) the determination of the spatial distribution of quakes associated with volcanism, mountain structures, ocean trenches, and gravity anomalies.

TABLE 6

Earthquake Magnitude ( $M_L$ ) and Annual Frequency

Description	$M_L$	Annual frequency
Great	>8.0	1.1
Major	7.0—7.9	18.0
Large (destructive)	6.0—6.9	120.0
Moderate (damaging)	5.0—5.9	1,000.0
Minor (damage slight)	4.0—4.9	6,000.0
Generally felt	3.0—3.9	49,000.0
Potentially perceptible	2.0—2.9	300,000.0
Microearthquake (imperceptible)	<2.0	600,000.0+

From National Earthquake Information Center, Magnitude — determining the "size" of an earthquake, *Earthquake Inf. Bull.*, 2, 26, 1970.

istration in 1970 (Table 6).<sup>194</sup> The word descriptors used in this table are widely used today to describe earthquake classes.

### B. Intensity

Intensity represents the direct or macroseismic effects of an earthquake on humans, their products, and the features of the earth's surface at some locale as determined by direct observation. Intensity is, therefore, an attempt to assess the severity of a seismic event. Earthquake intensity is highly variable due to many factors including magnitude, epicentral distance, focal depth, geologic/soil conditions, type of construction (including age and workmanship), and the expertise of the observer. Intensity varies over a geographic region, whereas the magnitude for the same earthquake would ideally be the same, regardless of locale.

#### 1. Intensity Scales

As with magnitude, scales have been introduced to measure degrees of intensity. The following U.S. Geological Survey description succinctly states the philosophy behind intensity scales:<sup>195</sup>

Early efforts to determine the size of an earthquake were necessarily based upon personal observations of the severity of the earthquake's effects. Investigators found that characteristic effects of damage and human reactions were very similar for most earthquakes and could be categorized to make comparative studies of shocks occurring at different times in the same or different locations. To facilitate their investigations, early seismologists developed intensity scales that grouped earthquake effects characteristic of each scale value.

A number of scales have been introduced in countries with a high seismic risk. Gorshkov and Shenkarev<sup>195</sup> describe 44 such scales.

In the 1880s, De Rossi<sup>196</sup> of Italy and Forel<sup>197</sup> of Switzerland introduced the first scale to gain widespread acceptance; it is still used in parts of Europe. (Both men had devised their own intensity scales earlier; the 1883 scale resulted from their joint effort.) The *Rossi-Forel (RF) scale* is comprised of 10 effect descriptions, each designated by a Roman numeral, with I indicating the least amount of seismic effect (Table 7). The procedure was to compare observation assessments to those of the standard scale descriptions. The number representing the closest match was the numerical intensity assigned to that location. If a tie resulted, the higher intensity number was selected.

It became apparent, especially with rapid advances in technology, that the Rossi-Forel scale had several shortcomings. Some objections included: (1) the effects on tall buildings, motorized vehicles, and underground pipelines could not be included in the

TABLE 7

## Rossi-Forel Intensity Scale of 1883

93

Intensity	Description
I	<i>Microseismic shock.</i> Recorded by a single seismograph or by seismographs of the same model, but not by several seismographs of different kinds; the shock felt by an experienced observer.
II	<i>Extremely feeble shock.</i> Recorded by several seismographs of different kinds; felt by small number of persons at rest.
III	<i>Very feeble shock.</i> Felt by several persons at rest; strong enough for the direction or duration to be appreciable.
IV	<i>Feeble shock.</i> Felt by persons in motion; disturbance of movable objects, doors, windows, cracking of ceilings.
V	<i>Shock of moderate intensity.</i> Felt generally by everyone; disturbance of furniture, beds, etc.; ringing of some bells.
VI	<i>Fairly strong shock.</i> General awakening of those asleep; general ringing of bells; oscillation of chandeliers; stopping of pendulum clocks; visible agitation of trees and shrubs; some startled persons leaving their dwellings.
VII	<i>Strong shock.</i> Overthrow of movable objects; fall of plaster; ringing of church bells; general panic, without damage to buildings.
VIII	<i>Very strong shock.</i> Fall of chimneys; cracks in the walls or ceilings.
IX	<i>Extremely strong shock.</i> Partial or total destruction of some buildings.
X	<i>Shock of extreme intensity.</i> Great disaster; ruins; disturbances of the strata; fissures in the ground; rock falls from mountains.

From Wood, F. J., Ed., *The Prince William Sound, Alaska, Earthquake of 1964 and Aftershocks*, Vol. 1, U. S. Government Printing Office, Washington, D.C., 1966, 18.

assessment procedure; (2) a wide range of intensity effects was grouped at the highest level; (3) the scale did not take construction quality into account; and (4) effect descriptors for buildings and physical features were "too subjective, unmeasurable, and specifically European."<sup>199</sup>

Mercalli<sup>199</sup> updated and expanded RF scale descriptors in 1902, but the 10 levels of intensity were maintained in the *Mercalli scale*. Cancani<sup>200</sup> later expanded the Mercalli scale to 12 levels and made an attempt to correlate intensity and ground acceleration (known as the *Mercalli-Cancani scale*). Sieberg<sup>201</sup> published an expanded version of the Mercalli-Cancani scale in 1923.

In 1931, American seismologists Wood and Neumann<sup>202</sup> made significant modifications to Sieberg's Mercalli-Cancani scale to more closely approximate California conditions. Detailed and abridged versions were constructed. This form became known as the *Modified Mercalli (MM) scale* of 1931; the abridged version is presented in Table 8 with Rossi-Forel equivalents. Endorsements and adoptions from the seismological community were immediate. The U.S. Coast and Geodetic Survey began using the scale the same year that it was introduced.

Richter<sup>27</sup> made the only significant modification to the MM scale in the U.S. He requested that the version be called the *Modified Mercalli scale, 1956 version*, and not bear his name because of probable confusion with the "Richter magnitude". This version is currently used by the U.S. Geological Survey (Table 9).

TABLE 8

## Modified Mercalli Intensity Scale of 1931 (Abridged)

Intensity	Description
I	Not felt except by a very few under specially favorable circumstances. (I Rossi-Forel Scale.)
II	Felt only by a few persons at rest, especially on upper floors of buildings. Delicately suspended objects may swing. (I to II Rossi-Forel Scale.)
III	Felt quite noticeably indoors, especially on upper floors of buildings, but many people do not recognize it as an earthquake. Standing motorcars may rock slightly. Vibration like passing of truck. Duration estimated. (III Rossi-Forel Scale.)
IV	During the day felt indoors by many, outdoors by few. At night some awakened. Dishes, windows, doors disturbed; walls make creaking sound. Sensation like heavy truck striking building. Standing motorcars rocked noticeably. (IV to V Rossi-Forel Scale.)
V	Felt by nearly everyone, many awakened, some dishes, windows, etc., broken; a few instances of cracked plaster; unstable objects overturned. Disturbances of trees, poles, and other tall objects sometimes noticed. Pendulum clocks may stop. (V to VI Rossi-Forel Scale.)
VI	Felt by all, many frightened and run outdoors. Some heavy furniture moved; a few instances of fallen plaster or damaged chimneys. Damage slight. (VI to VII Rossi-Forel Scale.)
VII	Everybody runs outdoors. Damage negligible in buildings of good design and construction; slight to moderate in well-built ordinary structures; considerable in poorly built or badly designed structures; some chimneys broken. Noticed by persons driving motorcars. (VIII Rossi-Forel Scale.)
VIII	Damage slight in specially designed structures; considerable in ordinary substantial buildings with partial collapse; great in poorly built structures. Panel walls thrown out of frame structures. Fall of chimneys, factory stacks, columns, monuments, walls. Heavy furniture overturned. Sand and mud ejected in small amounts. Changes in well water. Persons driving motorcars disturbed. (VIII + to IX - Rossi-Forel Scale.)
IX	Damage considerable in specially designed structures; well-designed frame structures thrown out of plumb; great in substantial buildings, with partial collapse. Buildings shifted off foundations. Ground cracked conspicuously. (IX + Rossi-Forel Scale.)
X	Some well-built wooden structures destroyed; most masonry and frame structures destroyed with foundations; ground badly cracked. Rails bent. Landslides considerable from riverbanks and steep slopes. Shifted sand and mud. Water splashed (slopped) over banks. (X Rossi-Forel Scale.)
XI	Few, if any, (masonry) structures remain standing. Bridges destroyed. Broad fissures in ground. Underground pipelines completely out of service. Earth slumps and land slips in soft ground. Rails bent greatly.
XII	Damage total. Waves seen on ground surfaces. Lines of sight and level distorted. Objects thrown upward into air.

From Wood, H. O. and Neumann, F., Modified Mercalli intensity scale of 1931, *Bull. Seismol. Soc. Am.*, 21, 277, 1931. With permission. Rossi-Forel intensity scale equivalents determined by the U.S. Coast and Geodetic Survey.

The 1956 version incorporates effects on four types of masonry buildings. Specific differences are noted when the 1931 and 1956 scales are closely compared. Simon<sup>203</sup> believes that the scale should be further refined, making it possible to evaluate (1) the effects on a person sleeping on a waterbed (usually awakened by 6- to 60-sec period

TABLE 9

Modified Mercalli Intensity Scale of 1931 (1956 Version Abridged and Rewritten)

95

Intensity	Description
I	Not felt. Marginal and long-period effects of large earthquakes.
II	Felt by persons at rest, on upper floors, or favorably placed.
III	Felt indoors. Hanging objects swing. Vibration like passing of light trucks. Duration estimated. May not be recognized as an earthquake.
IV	Hanging objects swing. Vibration like passing of heavy trucks; or sensation of a jolt like a heavy ball striking the walls. Standing motor cars rock. Windows, dishes, doors rattle. Glasses clink. Crockery clashes. In the upper range of IV, wooden walls and frame creak.
V	Felt outdoors; direction estimated. Sleepers wakened. Liquids disturbed, some spilled. Small unstable objects displaced or upset. Doors swing, close, open. Shutters, pictures move. Pendulum clocks stop, start, change rate.
VI	Felt by all. Many frightened and run outdoors. Persons walk unsteadily. Windows, dishes, glassware broken. Knickknacks, books, etc., off shelves. Pictures off walls. Furniture moved or overturned. Weak plaster and masonry D cracked. Small bells ring (church, school). Trees, bushes shaken (visibly, or heard to rustle).
VII	Difficult to stand. Noticed by drivers of motor cars. Hanging objects quiver. Furniture broken. Damage to masonry D, including cracks. Weak chimneys broken at roof line. Fall of plaster, loose bricks, stones, tiles, cornices (also unbraced parapets and architectural ornaments — CFR). Some cracks in masonry C. Waves on ponds; water turbid with mud. Small slides and caving in along sand or gravel banks. Large bells ring. Concrete irrigation ditches damaged.
VIII	Steering of motor cars affected. Damage to masonry C; partial collapse. Some damage to masonry B; none to masonry A. Fall of stucco and some masonry walls. Twisting, fall of chimneys, factory stacks, monuments, towers, elevated tanks. Frame houses moved on foundations if not bolted down; loose panel walls thrown out. Decayed piling broken off. Branches broken from trees. Changes in flow or temperature of springs and wells. Cracks in wet ground and on steep slopes.
IX	General panic. Masonry D destroyed; masonry C heavily damaged, sometimes with complete collapse; masonry B seriously damaged. (General damage to foundations—CFR.) Frame structures, if not bolted, shifted off foundations. Frames cracked. Serious damage to reservoirs. Underground pipes broken. Conspicuous cracks in ground. In alluviated areas sand and mud ejected, earthquake fountains, sand craters.
X	Most masonry and frame structures destroyed with their foundations. Some well-built wooden structures and bridges destroyed. Serious damage to dams, dikes, embankments. Large landslides. Water thrown on banks of canals, rivers, lakes, etc. Sand and mud shifted horizontally on beaches and flat land. Rails bent slightly.
XI	Rails bent greatly. Underground pipelines completely out of service.
XII	Damage nearly total. Large rock masses displaced. Lines of sight and level distorted. Objects thrown into the air.

**Note:** CFR, Charles F. Richter additions to the 1931 scale. Masonry A, good workmanship, mortar, and design; reinforced, especially laterally, and bound together by using steel, concrete, etc.; designed to resist lateral forces; masonry B, good workmanship and mortar; reinforced, but not designed in detail to resist lateral forces; masonry C, ordinary workmanship and mortar; no extreme weaknesses like failing to tie in at corners, but neither reinforced nor designed against horizontal forces; masonry D, weak materials, such as adobe; poor mortar; low standards of workmanship; weak horizontally.

From *Elementary Seismology* by Charles F. Richter, W. H. Freeman and Company. Copyright © 1958. With permission.

XI CURSO INTERNACIONAL DE INGENIERIA SISMICA

ANALISIS DE RIESGO SISMICO

TEMA

CONCEPTOS FUNDAMENTALES DE LA TEORIA DE PROBABILIDADES PARA  
ANALISIS DE RIESGO SISMICO

Dra. Sonia E. Ruiz

## TEOREMA DE PROBABILIDADES TOTALES

Dado un conjunto de eventos mutuamente exclusivos y colectivamente exhaustivos,  $B_1, B_2, \dots, B_n$ , es posible siempre expresar la probabilidad  $P(A)$  de otro evento  $A$  como sigue

$$P(A) = P(A \cap B_1) + P(A \cap B_2) + \dots = \sum_{i=1}^n P(A \cap B_i)$$

Entonces

$$P(A) = \sum_{i=1}^n P(A|B_i) P(B_i) \quad (2)$$

## TEOREMA DE BAYES

La probabilidad condicional de  $A_j$  dado que ha ocurrido el evento  $B$  es

$$P(A_j|B) = \frac{P(A_j \cap B)}{P(B)} = \frac{P(B \cap A_j)}{P(B)} \quad (3)$$

Por lo visto en las definiciones anteriores es posible llegar a lo siguiente

$$P(A_j|B) = \frac{P(B|A_j) P(A_j)}{\sum_{i=1}^n P(B|A_i) P(A_i)}, \quad j=1, 2, \dots, n \quad (4)$$

Generalmente a la probabilidad resultante se le llama "a posteriori" y a la probabilidad  $P(A_j)$  se le llama "a priori"

## DISTRIBUCION DE PROBABILIDAD DE LAS VARIABLES ALEATORIAS

El comportamiento de una variable aleatoria se describe a través de leyes probabilísticas representadas mediante funciones de distribución de probabilidad.

En el caso de variables aleatorias discretas estas leyes se repre

sentan mediante FUNCIONES DE MASA DE PROBABILIDAD, en el caso de variables continuas se utilizan las FUNCIONES DE DENSIDAD DE PROBABILIDAD. Cuando se tratan varias variables a la vez el comportamiento lo determinan leyes de probabilidad CONJUNTAS.

#### DISTRIBUCION DE PROBABILIDAD MARGINAL

El comportamiento de una (o varias) variable (s) aleatoria(s) se puede obtener a partir de una distribución conjunta, integrando sobre todos los valores de las variables cuyo comportamiento no interesa. La función que representa a este comportamiento es la distribución de probabilidad MARGINAL. Por ejemplo sean X y Y variables aleatorias continuas, con densidad de probabilidades  $f_{x,y}(x, y)$ ; entonces la función de probabilidad marginal de x es igual a

$$f_x(x) = \int_{-\infty}^{\infty} f_{x,y}(x, y) dy \quad (r)$$

Generalizando

$$f_{x_1, x_2}(x_1, x_2) = \int \int \int \dots \int_D f_{x_1, x_2, x_3, \dots, x_n}(x_1, x_2, x_3, \dots, x_n) dx_3 dx_4 \dots dx_n$$

#### DISTRIBUCION DE PROBABILIDAD CONDICIONAL

Si en una función de distribución de probabilidad conjunta algunas variables adquieren valores fijos la función de distribución de probabilidad normalizada resultante representa a la distribución CONDICIONAL. Sean X y Y variables aleatorias continuas y  $f_{x,y}(x, y)$  su función de distribución; si Y adquiere el valor  $y_0$ , entonces la función de probabilidad condicional de X es igual a

$$f_{x|y}(x, y_0) = \frac{f_{x,y}(x, y_0)}{f_y(y_0)} \quad (6)$$

En donde

$$f_y(y_0) = \int_{-\infty}^{\infty} f_{x,y}(x, y_0) dx$$

## FUNCIÓN DE DISTRIBUCION ACUMULADA

Una forma alternativa de representar el comportamiento de una variable aleatoria es mediante la función de distribución acumulada. El valor de dicha función,  $F_X(x)$ , es igual a la probabilidad de que la variable aleatoria sea menor o igual que el argumento, es decir

$$F_X(x) = P(X \leq x) = \int_{-\infty}^x f_X(u) du$$

La función de distribución  $f_X(x)$  se puede encontrar a partir de la función acumulada, a través de

$$\frac{dF_X(x)}{dx} = \frac{d}{dx} \left[ \int_{-\infty}^x f_X(u) du \right] = f_X(x)$$

Sus propiedades son las siguientes

$$0 \leq F_X(x) \leq 1$$

$$F_X(-\infty) = 0$$

$$F_X(\infty) = 1.$$

$$F_X(x_2) - F_X(x_1) = P[x_1 < X \leq x_2]$$

## MOMENTOS DE UNA VARIABLE ALEATORIA

Media ó valor esperado de una variable continua X

$$m_x = E(x) = \int_{-\infty}^{\infty} x f_X(x) dx$$

Variancia de una variable continua X

$$\sigma_x^2 = \text{var}(x) = \int_{-\infty}^{\infty} (x - m_x)^2 f_X(x) dx = E[x^2] - E^2[x]$$

Desviación estándar de una variable continua X;

$$\sigma_x = \sqrt{\sigma_x^2}$$

## FUNCIONES DE MASA DE PROBABILIDAD: BINOMINAL Y DE POISSON

Enseguida se tratan dos distribuciones de variables aleatorias discretas; discontinua de orden finito la BINOMIAL y de orden infinito la de POISSON

### DISTRIBUCION BINOMINAL

Se aplica a experimentos de Bernoulli (acepta únicamente dos posibles resultados: éxito y fracaso).

Sea

$p$  = probabilidad de obtener éxito

$q = 1 - p$  = probabilidad de obtener fracaso

La probabilidad de obtener  $x$  éxito al realizar  $n$  veces el experimento de Bernoulli es

$$\underbrace{p \cdot p \cdot p \cdot p \cdot \dots \cdot p}_x \cdot \underbrace{q \cdot q \cdot q \cdot \dots \cdot q}_{n-x} = p^x q^{n-x}$$

Aquí se supuso que los  $x$  éxitos ocurren al principio. El número total de formas en que pueden presentarse los  $x$  éxitos es igual a las permutaciones de  $n$  objetos formados por dos grupos: uno de  $x$  objetos iguales y otro de  $n-x$  objetos iguales o sea igual a

$$\frac{n!}{x!(n-x)!}$$

o sea que la probabilidad buscada es la siguiente

$$P(x) = \frac{n!}{x!(n-x)!} p^x q^{n-x} \quad (10)$$

La variable aleatoria  $x$  es un número entero entre cero y  $n$

Su media es igual a

$$m_x = \sum_{x=0}^n x P(x) = np$$

Su variancia es

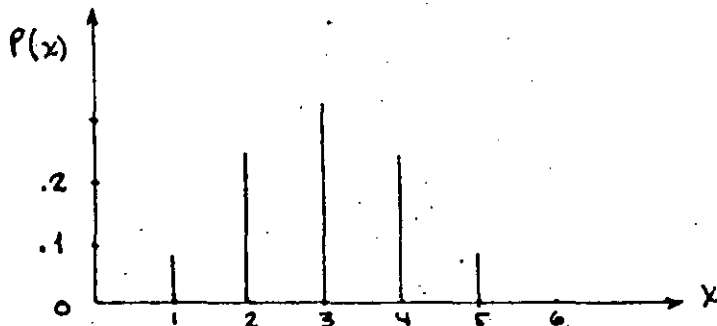
8

$$\sigma_x^2 = \sum_{x=0}^n x^2 P(x) = npq$$

Su desviación estándar

$$\sigma_x = \sqrt{npq}$$

La representación gráfica de  $P(x)$  para  $n = 6$  y  $p = 0.5$  es como sigue



DISTRIBUCION DE POISSON

Si se considera que en la distribución binomial  $n$  tiende a infinito mientras que la probabilidad  $p$  de éxito tiende a cero, entonces la ec. (10) se convierte en

$$P(x) = \frac{\nu^x}{x!} e^{-\nu}, \quad x=0,1,2,3,\dots,\infty \quad (11)$$

Esta distribución de probabilidad se llama de POISSON de parámetro  $\nu$

Su media está dada por

$$m_x = \sum_{x=0}^{\infty} x P(x) = \nu$$

Su variancia es igual a

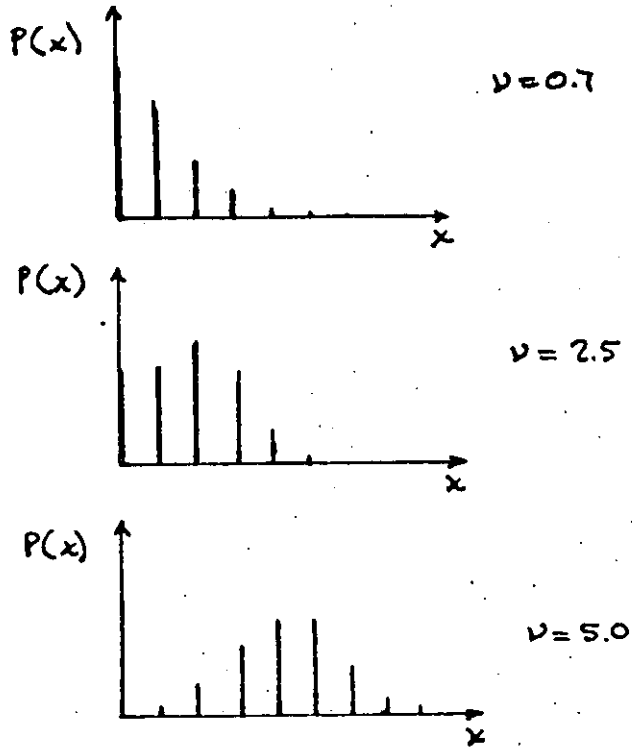
$$\sigma_x^2 = \sum_{x=0}^{\infty} x^2 P(x) = \nu$$

Su desviación estándar

$$\sigma_x = \sqrt{\nu}$$

(La distribución de Poisson de parámetros  $\nu = np$  se aproxima a la binomial siempre que  $n > 50$  y  $np < 5$ ).

En las siguientes figuras se ilustra la variación de la forma de las distribuciones con el parámetro  $\nu$ :

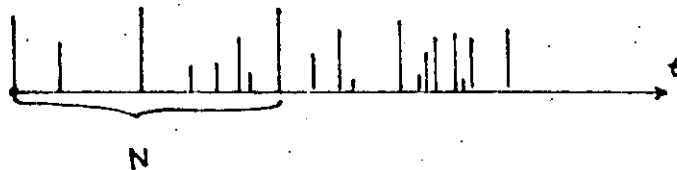


PROCESO DE POISSON

Este proceso representa el número de eventos que ocurre en un tiempo  $t$  cuando dichos eventos tienen distribución de Poisson; es decir,

$$P(n) = \frac{(\lambda t)^n e^{-\lambda t}}{n!}$$

Ilustrando esto gráficamente:



En un proceso de Poisson, la media de su distribución (de Poisson) es  $m_n = \lambda t$ . Al parámetro  $\lambda$  se le llama tasa media de ocurrencia del proceso.

Un proceso de Poisson debe satisfacer las siguientes hipótesis:

## 1. ESTACIONARIEDAD

La probabilidad de un evento en un intervalo *corto* de tiempo  $(t, t + \Delta t)$  es aproximadamente  $\lambda(\Delta t)$  para cualquier  $t$ . Es decir que no importa qué tiempo  $t$  se elige para hacer la estimación.

## 2. NO MULTIPLICIDAD

La probabilidad de 2 o más eventos en un intervalo corto de tiempo es despreciable comparado con  $\lambda(\Delta t)$

## 3. INDEPENDENCIA

El número de eventos en cualquier intervalo de tiempo es independiente de el número en cualquier otro intervalo de tiempo. O sea que la ocurrencia de unos es independiente de los que ocurren en otro intervalo de tiempo.

Varios investigadores han propuesto modelos probabilísticos para describir la ocurrencia de temblores. Algunos de ellos se basan en la construcción de histogramas de tiempos de espera entre eventos sísmicos. Por simplicidad matemática frecuentemente se adopta la hipótesis que la distribución probabilística de tales tiempos de espera es de Poisson. Es decir, para una determinada región, la probabilidad de que ocurran  $n$  temblores con magnitud mayor que  $M$  en el intervalo de tiempo  $(0, t)$  es

$$p(n) = (\lambda_M t)^n e^{-\lambda_M t} / n!$$

en que  $\lambda_M$  es el número medio de temblores con magnitud mayor que  $M$  que ocurran en dicha región por unidad de tiempo. Si se considera  $n$  nulo se obtiene

$$p(0) = e^{-\lambda_M t}$$

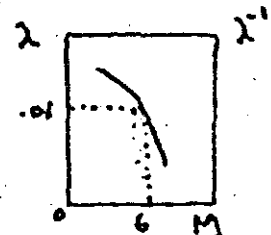
que representa la probabilidad de que no ocurran temblores con magnitud mayor que  $M$  en el intervalo de tiempo  $t$  (aún cuando no empiece en cero) es decir la probabilidad de la intensidad máxima en el intervalo  $t$

## EJEMPLO

Mediante un estudio estadístico sobre la ocurrencia de sismos en cierta región se estimó que un temblor con una magnitud igual a 6 o mayor tiene un periodo de recurrencia de 100 años. Calcular las probabilidades de que en los próximos 10, 50 y 100 años no ocurra ningún sismo en dicha región cuya magnitud exceda a 6, suponiendo que la ocurrencia de los sismos se puede modelar mediante un proceso estocástico de Poisson.

$$\lambda_M = \frac{1}{100} = .01$$

$$P(n) = \frac{(.01t)^n e^{-.01t}}{n!}$$



Para  $t = 10$  años

$$P(0) = \frac{(.01 \times 10)^0 e^{-.01 \times 10}}{0!} = .905$$

Para  $t = 50$  años

$$P(0) = \frac{(.01 \times 50)^0 e^{-.01 \times 50}}{0!} = .607$$

Para  $t = 100$  años

$$P(0) = \frac{(.01 \times 100)^0 e^{-.01 \times 100}}{0!} = .368$$

Las probabilidades de que ocurra por lo menos un sismo con magnitud mayor que 6 son

$$P_{\text{a}}(n \geq 1) = 1 - .905 = .095$$

$$P_{\text{b}}(n \geq 1) = 1 - .607 = .393$$

$$P_{\text{c}}(n \geq 1) = 1 - .368 = .632$$

## FUNCIONES DE DENSIDAD DE PROBABILIDAD:

### EXPONENCIAL, NORMAL Y LOGNORMAL

#### DISTRIBUCION EXPONENCIAL

En la sección anterior se trató el proceso de Poisson. En lo que sigue se describirá la distribución de tiempo de espera entre eventos si ellos se describen mediante un proceso de Poisson.

Si denotamos la variable aleatoria  $T$  como el tiempo de la primera ocurrencia de un evento, entonces la probabilidad de que  $T$  exceda algún valor de  $t$  es igual a la que no ocurran eventos en el intervalo de tiempo  $t$ , o sea igual a  $1 - F_T(t) = p(0)$ , o sea

$$1 - F_T(t) = e^{-\lambda t}, \quad t \geq 0$$

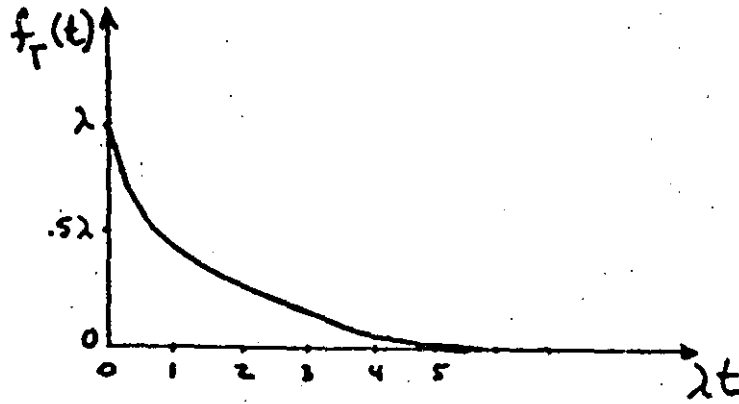
Entonces

$$F_T(t) = 1 - e^{-\lambda t}$$

$$f_T(t) = \frac{dF_T(t)}{dt} = \lambda e^{-\lambda t}, \quad t \geq 0$$

Que es la distribución exponencial. Esta describe el tiempo de la primera ocurrencia de un evento de Poisson. Pero recordando las propiedades de independencia y estacionariedad del proceso de Poisson  $e^{-\lambda t}$  es la probabilidad de que no se presenten eventos en ningún intervalo de tiempo  $t$ , aunque este no empiece en  $t = 0$ . Si utilizamos el tiempo de arribo del  $n$ -ésimo evento como el principio del intervalo de tiempo, entonces  $e^{-\lambda t}$  es la probabilidad de que el tiempo de ocurrencia del  $(n+1)$ -ésimo evento sea mayor  $t$ . Es decir, los tiempos de arribo intermedios de un Proceso de Poisson son independientes y

están distribuidos exponencialmente. Su valor esperado, conocido como período de recurrencia, es igual a  $(\lambda_M)^{-1}$ , su varianza es igual a  $(\lambda_M^2)^{-1}$



Distribución exponencial

## DISTRIBUCION NORMAL

Una de las más importantes funciones dentro de la teoría de Probabilidades es la NORMAL O GAUSSIANA. Esta es aplicable a variables aleatorias continuas dentro del dominio de los números reales.

La función de densidad de probabilidad está dada por

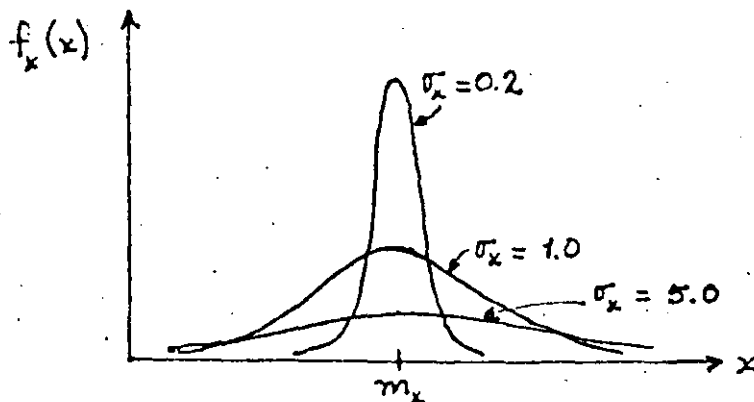
$$f_x(x) = \frac{1}{\sqrt{2\pi} \sigma_x} e^{-\frac{(x-m_x)^2}{2\sigma_x^2}}, \quad -\infty < x < \infty \quad (13)$$

en donde

$m_x$  = media

$\sigma_x^2$  = variancia

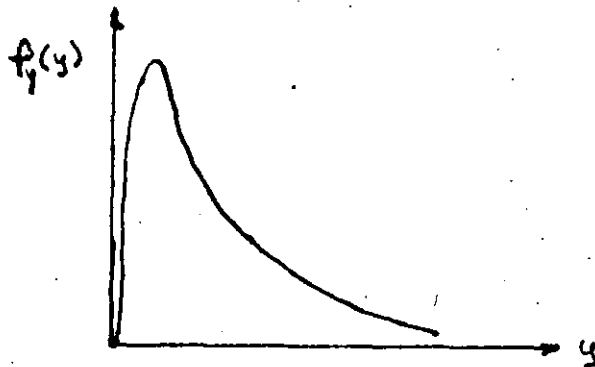
Al examinar esta expresión se deduce que es una función simétrica con respecto a un eje vertical que pasa por  $m_x$ , que es asintótica al eje de las abscisas para valores que tiendan a  $\pm \infty$ , y, que su valor máximo corresponde a  $m_x$ . En la siguiente figura se presenta su representación cuando su media permanece constante igual a  $m_x$  y su desviación estándar ( $\sigma_x$ ) varía



La distribución LOGARITMICO-NORMAL O LOGNORMAL se presenta en el caso de que el logaritmo natural de una variable aleatoria tenga distribución normal. Es decir, si la variable  $X$  tiene una función de densidad dada por la ec 13, y si  $X = \ln Y$ , entonces la función de densidad de  $Y$  resulta lognormal y está dada por

$$f_y(y) = \frac{1}{y \sigma_x \sqrt{2\pi}} \exp \left[ -\frac{1}{2} \left( \frac{\ln y - m_x}{\sigma_x} \right)^2 \right], \quad y \geq 0 \quad (14)$$

La siguiente figura muestra la gráfica de una distribución logaritmico-normal con  $m_x = 0$  y  $\sigma_x = 1$ . Esta es de forma asimétrica positiva



Su media está dada por

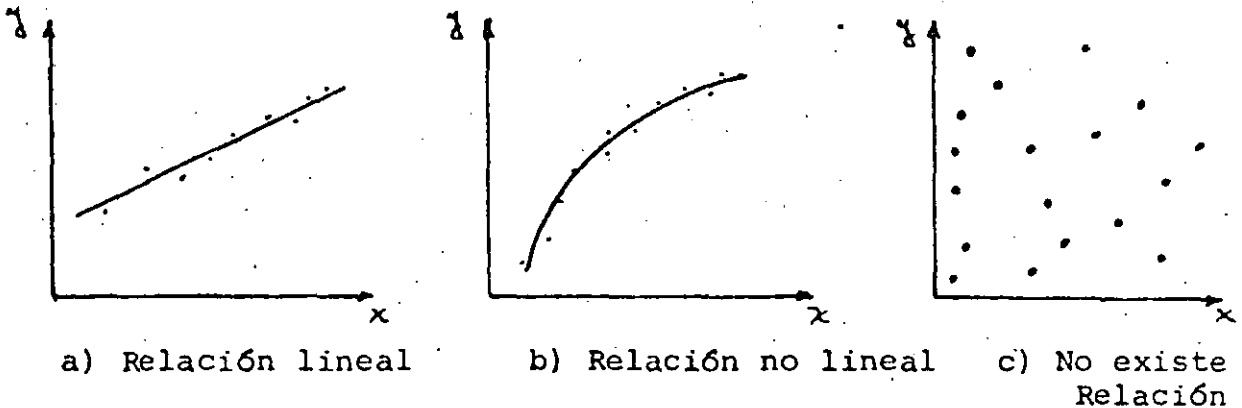
$$m_y = \int_0^{\infty} y f(y) dy = \exp(m_x + \sigma_x^2/2)$$

Su varianza es igual a

$$\sigma_y^2 = \exp(2m_x + \sigma_x^2) \cdot (\exp \sigma_x^2 - 1)$$

## ANALISIS DE REGRESION

Una incógnita importante que debe despejarse en el análisis de regresión es la FORMA GENERAL DE LA EXPRESION MATEMATICA que se piensa puede explicar el comportamiento de cierto fenómeno. Un procedimiento gráfico puede resolver este problema. Dibujando los valores observados de la variable independiente X con los correspondientes valores observados de la variable dependiente y en un sistema de coordenadas rectangulares, se obtiene un conjunto de puntos conocidos como DIAGRAMA DE DISPERSION



La CURVA DE REGRESION es aquella a la cual tienden a aproximarse los puntos del diagrama de dispersión. La ecuación de la curva de regresión es la ECUACION DE REGRESION.

En el caso de regresión lineal se tiene una ecuación de regresión de la forma

$$y = a_0 + a_1 x$$

con dos parámetros por determinar:  $a_0$  y  $a_1$

Existen diferentes métodos para determinar estos parámetros aquí se estudiará el método de MINIMOS CUADRADOS

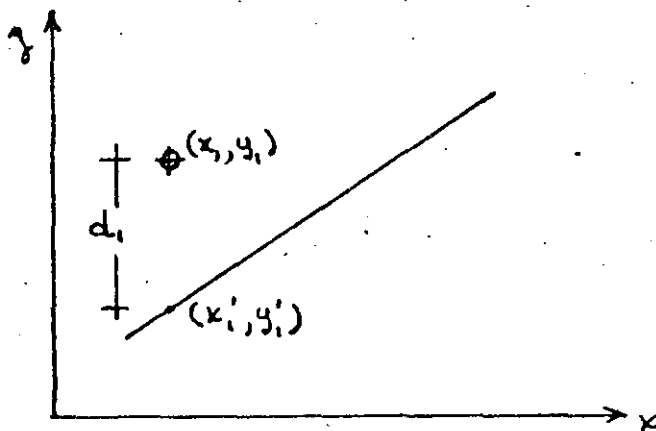
## METODO DE MINIMOS CUADRADOS

Se llama DESVIACION, ERROR O RESIDUO a la diferencia de ordenadas

de un punto muestral y de la curva de regresión correspondiente a una misma abscisa

$$d_i = y_i - y'_i$$

$$y'_i = a_0 + a_1 x'_i$$



El método de los mínimos cuadrados establece que de todas las curvas de regresión que se pueden ajustar al conjunto de puntos muestrales dados la MEJOR es aquella que tenga la propiedad de que la suma de los cuadrados de sus residuos sea mínima

$$\min \sum_{i=1}^n d_i^2$$

Aplicando este criterio para el caso de una recta

$$\min \sum d_i^2 = \min \sum [y_i - (a_0 + a_1 x_i)]^2$$

Para encontrar el mínimo se aplica la condición necesaria conocida para que una función tenga un punto extremo, es decir, se iguala a cero las primeras derivadas parciales de la función con respecto a cada una de sus variables.

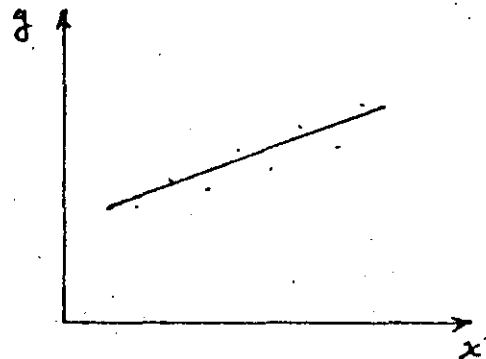
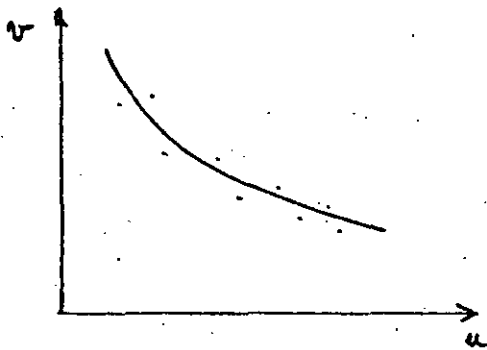
El resultado de esto conduce a un sistema de ecuaciones simultáneas cuya solución es el valor de los parámetros  $a_0$  y  $a_1$ .

## REGRESION NO LINEAL

Para resolver el caso de regresión no lineal, generalmente conviene MAPEAR los puntos muestrales a un sistema de referencia en donde sí se aproximen a una recta, mediante ecuaciones de TRANSFORMACION

$$x = x(u, v)$$

$$y = y(u, v)$$



Los sistemas de transformación que se usan con mayor frecuencia con los SEMILOGARITMICOS Y LOS LOGARITMICOS

Por ejemplo una transformación SEMILOGARITMICA es como sigue:

$$x = u$$

$$y = \log v$$

En el sistema x-y el diagrama de dispersión de los puntos mapeados  $(x_i, y_i)$  corresponde a una recta cuya ecuación es  $y = a_0 + a_1 x$ , en el sistema uv la ecuación correspondiente es

$$\log v = a_0 + a_1 u$$

$$v = 10^{a_0 + a_1 u}$$

$$= (10^{a_0}) (10^{a_1})^u$$

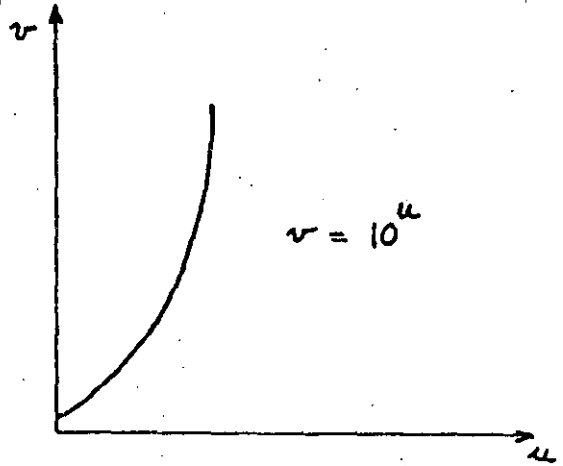
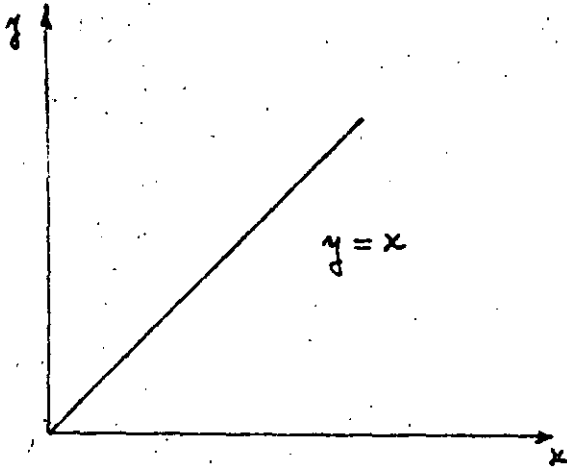
$$= a b^u$$

En donde

$$a = 10^{a_0}$$

$$b = 10^{a_1}$$

Ejemplo. Sea  $a_0 = 0$  ,  $a_1 = 1$





**DIVISION DE EDUCACION CONTINUA  
FACULTAD DE INGENIERIA U.N.A.M.**

ANALISIS DE RIESGO SISMICO

MODELOS DE RIESGO SISMICO

PARTE 1. ESTIMACION BAYESIANA Y EJEMPLO DE APLICACION

DR. MARIO CHAVEZ

JULIO, 1985

X CURSO INTERNACIONAL DE INGENIERIA SISMICA

MODELOS DE RIESGO SISMICO

PARTE I.- ESTIMACION BAYESIANA Y EJEMPLO DE  
APLICACION

Mario Chávez\*

\*Investigador, Instituto de Ingeniería, UNAM

1.	Introducción	1
2.	Temblores y la respuesta de las construcciones a los mismos	4
2.1	Origen de los temblores	4
2.2	Intensidad de Mercalli y magnitud de un temblor	4
2.3	Acelerogramas e intensidad máximas del terreno	6
2.4	Espectros de respuesta	7
3.	Tectónica y sismicidad en el occidente de México	9
3.1	Tectónica	9
3.2	Sismicidad	10
3.3	Conclusiones sobre la tectónica y sismicidad del occidente de México	10
4.	Modelos de riesgo sísmico	11
4.1	Modelos de riesgo sísmico	11
4.2	Modelo de riesgo sísmico con parámetros bayesianos	12
4.2.1	Sismicidad regional y local	12
4.2.2	Modelo de sismicidad local	13
4.2.3	Ecuaciones de atenuación	14
4.2.4	Modelo de sismicidad regional	15
4.2.5	Estimación bayesiana de la sismicidad regional $v(y)$	18
4.2.6	Corrección por incertidumbre en las ecuaciones de atenuación	21
5.	Riesgo sísmico en un sitio en el estado de Jalisco	23
5.1	Información para el sitio	23
5.2	Riesgo sísmico en el sitio de interés	25
6.	Conclusiones	28
7.	Referencias	29
	Tablas	
	Figuras	
	Apéndices	

## 1. INTRODUCCION

Los criterios de diseño modernos tienen como objetivo optimizar las estructuras, es decir, conducir a sistemas estructurales en los cuales la utilidad obtenida de su ejecución sea máxima. La determinación de la estructura óptima se puede lograr a través de estudios costo-beneficio que incluyan explícitamente los siguientes parámetros: los beneficios esperados de su construcción, los costos esperados de las posibles fallas, los costos iniciales de diseño y construcción, así como las probabilidades de ocurrencia y las intensidades máximas de las solicitaciones de diseño. En este trabajo se tratará lo relativo a la determinación de las solicitaciones sísmicas en un sitio dado con base en modelos de riesgo sísmico. Los otros parámetros serán discutidos en otras contribuciones de esta reunión.

Las cargas sísmicas producidas en construcciones durante la ocurrencia de un temblor son generadas por el movimiento errático del suelo que rodea la cimentación de una construcción. Dicho movimiento es transmitido a la estructura como fuerzas de inercia que actúan en los diferentes elementos de la misma. La amplitud de esas fuerzas depende principalmente de las propiedades dinámicas del sistema estructural y de las características del temblor.

Sin embargo, es ampliamente reconocido que se tienen grandes incertidumbres respecto a la intensidad, localización y el número de temblores futuros, por lo cual el diseño de estructuras en una región de actividad sísmica potencial debe incorporar dichas incertidumbres. Una forma racional de hacer esto último es evaluando los niveles de las intensidades máximas esperadas del terreno en un sitio dado para diferentes lapsos de tiempo. Lo anterior puede lograrse haciendo uso de los llamados modelos de riesgo sísmico, los cuales

son modelos matemáticos que en una situación ideal deben sintetizar toda la información sísmica existente sobre la región de interés, así como el estado del arte sobre el proceso de generación de temblores. Los resultados de dichos modelos son generalmente presentados por medio de gráficas o tablas que relacionan los valores de los parámetros del movimiento del suelo (aceleración, velocidad y desplazamiento máximos) en un sitio de interés con lapsos de tiempo llamados periodos de recurrencia.

Una vez que el riesgo sísmico para un sitio ha sido determinado, el calculista estará en posibilidad de analizar el comportamiento de las implicaciones económicas de diferentes diseños bajo varios niveles de la intensidad del movimiento del terreno.

La información sísmica que se mencionó en el párrafo anterior puede dividirse en los siguientes tipos: tectónica, estadística (sismicidad), geofísica y geológica. Como se verá más adelante, con los modelos de riesgo sísmico actuales es muy frecuente utilizar las dos primeras fuentes de información (en particular la relacionada con la sismicidad), mientras que las dos últimas son utilizadas en una forma complementaria e indirecta. Debido a lo anterior en este trabajo se le dará énfasis a la información tectónica y sobre la sismicidad de la región de interés, que es el occidente de México. En el capítulo 2 se presentan brevemente aspectos relacionados con los temblores y la respuesta de las construcciones a los mismos. Una síntesis de los aspectos más importantes sobre la tectónica la sismicidad de esta región se presenta en el capítulo 3.

En el Cap 4 se presenta un modelo de riesgo sísmico cuyos parámetros son estimados aplicando estadística bayesiana. Dicho modelo se ha utilizado recientemente en el Instituto de Ingeniería, UNAM, para determinar las intensidades máximas del terreno (para diferentes lapsos de tiempo) en algunos sitios de México. En el mismo capítulo 5 se presentan los resultados obtenidos de aplicar el modelo mencionado para determinar el riesgo sísmico en un sitio en el estado de Jalisco. Finalmente en el Cap 6 se presentan algunas conclusiones y recomendaciones sobre el riesgo sísmico del occidente de México.

## 2. TEMBLORES Y LA RESPUESTA DE CONSTRUCCIONES A LOS MISMOS

### 2.1 Origen de los temblores

Los temblores de interés en ingeniería se consideran de origen tectónico. Esta clase de temblores se generan cuando la corteza terrestre libera energía elástica al desplazarse las superficies laterales de fallas geológicas. Dicha energía se propaga en la forma de ondas sísmicas a través de la corteza terrestre, las cuales se manifiestan por el movimiento caótico de la superficie de la tierra. Este movimiento errático es el que daña las estructuras localizadas en sitios alcanzados por temblores, cuando éstas estructuras no han sido diseñadas para soportarlos.

Se llama foco de un temblor al punto bajo la superficie de la tierra donde se supone que se inicia la ruptura de una falla geológica. La profundidad de ese punto se conoce como profundidad focal y la distancia del foco a un sitio de interés se denomina distancia focal o hipocentro. La proyección vertical del foco sobre la superficie de la tierra se llama epicentro y la distancia de éste a un sitio se le conoce como distancia epicentral. La longitud de ruptura de una falla se denomina longitud de la falla.

### 2.2 Intensidad de Mercalli y magnitud de un temblor

La intensidad de Mercalli modificada,  $I(MM)$ , es una medida subjetiva del nivel de daño que sufren las estructuras hechas por el hombre, así como de modificaciones a la geología superficial producidas por un temblor en un sitio o una región dada (ref 1). Dependiendo del nivel de daño causado por un temblor en un sitio, se asigna un número romano que varía del I al XII (de la escala de Mercalli modificada) a un temblor en ése sitio. Se llaman isosistas de un temblor las líneas que

unen puntos (sitios) en los cuales ese temblor se manifiesta con una misma intensidad, en la escala de Mercalli modificada. Las isosistas forman parte de los llamados mapas de isosistas de una región para un temblor determinado.

La magnitud,  $M$ , de un temblor es una medida objetiva de la energía liberada durante un temblor; en su forma original se definió como

$$M = \log_{10} \frac{A}{A_0} \quad (1.1)$$

donde  $M$  es la magnitud del temblor,  $A$  es la amplitud máxima (en milímetros) registrados por un sismógrafo Wood-Anderson a una distancia de 100 Km del epicentro y  $A_0$  es una amplitud igual a  $10^{-3}$  milímetros (ref 1). En la actualidad la magnitud de un temblor se obtiene como el promedio de las magnitudes obtenidas por diferentes estaciones sismológicas. Existen algunas variantes de la escala original de magnitudes de los temblores.

La energía sísmica (en ergs) liberada durante un temblor puede calcularse en forma aproximada mediante la expresión semiempírica (ref 1):

$$\log_{10} E = 11.8 + 1.5M \quad (1.2)$$

Dado que la escala de Mercalli modificada no requiere de instrumentos para asignar la intensidad de un temblor en un sitio, los catálogos de  $I(MM)$  constituyen la única fuente de información sísmica disponible para algunos sitios o regiones, especialmente para temblores ocurridos antes de principios de siglo. Los catálogos de magnitudes de temblores se iniciaron en la tercera década de este siglo, principalmente en el área de California, Estados Unidos. Para otras regiones del mundo dichos catálogos se iniciaron hace unos pocos

años. Como se verá en el capítulo 5, la información contenida en esos catálogos constituye una parte esencial de los procedimientos utilizados para predecir las intensidades futuras en algún sitio de interés; por lo cual se han propuesto expresiones semiempíricas que relacionan la magnitud  $M$  de un temblor y su correspondiente  $I(M)$ , así como algunas características geométricas del temblor (como su profundidad focal etc.). Dichas expresiones se utilizan para generar o complementar catálogos de  $M$  en algunos sitios o regiones de interés.

### 2.3 Acelerogramas e intensidades máximas del terreno

Desde el punto de vista de la ingeniería, la información fundamental para estimar las fuerzas sísmicas que actúan sobre una estructura la proporcionan los acelerogramas, los cuales son gráficas que representan la variación en el tiempo de las aceleraciones del terreno. Un acelerograma, el cual se puede idealizar como una secuencia aleatoria de pulsos de aceleraciones generados por el movimiento del terreno durante un temblor, se obtiene por medio de un acelerógrafo. Los acelerogramas también se pueden simular por medio de computadoras analógicas o digitales. Las variaciones en el tiempo de las velocidades y los desplazamientos del terreno obtienen al integrar el acelerograma correspondiente uno y dos veces respectivamente (ref. 2).

De observaciones de campo y de laboratorio, se ha concluido que las respuestas máximas de las construcciones a temblores (aceleraciones, velocidades, desplazamientos) dependen de la intensidad\*, el contenido de frecuencias, la distribución en el tiempo de dicha intensidad y la duración del temblor (ref 1). La intensidad y el contenido de frecuencias de un

---

\* En lo que sigue se entiende por intensidad de un temblor a cualquier parámetro del movimiento del terreno relacionado con la respuesta de una estructura a dicho temblor.

temblor pueden estimarse (en forma aproximada) a partir de su aceleración, velocidad y desplazamiento máximos.

#### 2.4 Espectros de respuesta

Las respuestas máximas de un sistema de un grado de libertad\* sujeto a un temblor se pueden obtener resolviendo la ecuación de equilibrio dinámico (expresión matemática que relaciona las fuerzas de inercia, amortiguamiento y elásticas del sistema con la fuerza sísmica correspondiente, ref 1). Otra forma de obtener dichas respuestas es a partir del registro de las aceleraciones de la masa del sistema, en caso que el sistema estructural esté instrumentado.

Se conoce como espectro de respuesta a la curva que resulta de unir los puntos correspondientes a las respuestas máximas a un acelerograma dado de sistemas de un grado de libertad con el mismo amortiguamiento y diferentes periodos naturales de vibración.

De estudios estadísticos efectuados en diferentes lugares (ref 1 y 2) se ha llegado a la conclusión de que las intensidades máximas del terreno están correlacionadas con los espectros de respuesta. En particular, la aceleración máxima del terreno se relaciona satisfactoriamente con las respuestas máximas de sistemas de periodo corto (estructuras rígidas), mientras que la velocidad máxima y el desplazamiento máximos correlacionan adecuadamente con sistemas de periodo intermedio y largo (estructuras flexibles) respectivamente. De aquí se sigue que los espectros de respuesta pueden calcularse a partir de las intensidades máximas del terreno y factores espectrales de amplificación como los propuestos en la ref 1.

---

\* Un sistema en el cual una sola coordenada define la localización geométrica de su masa, como por ejemplo un pórtico de una cruzija, cuya trabe tiene una rigidez infinita.

Con el procedimiento mencionado en el párrafo anterior es posible obtener los espectros de diseño. Los cuales son gráficas que relacionan las envolventes de las respuestas máximas esperadas de sistemas de un grado de libertad sujetos a diferentes temblores con los periodos naturales (o frecuencias naturales) de vibración de dichos sistemas. A partir de los espectros de diseño se pueden calcular las cargas sísmicas que en un instante dado actuarían sobre un sistema estructural.

### 3. TECTÓNICA Y SISMICIDAD EN EL OCCIDENTE DE MEXICO

#### 3.1 Tectónica

La estructura tectónica de la región comprendida por los estados de Michoacán, Colima, Jalisco, Nayarit y Sinaloa esta relacionada con el movimiento de subducción de las placas de Cocos y de Rivera bajo la placa Americana, así como con los movimientos de las fallas transformadas y centros de dispersión del Golfo de California refs (3, 4, 5, 6).

Los estudios efectuados en dichas refs permiten concluir que la estructura tectónica de la región es muy compleja, en particular en lo que se refiere al comportamiento tectónico de la triple junta de las mencionadas placas. Lo anterior se debe a que tanto las velocidades de subducción, como los rum bos de las placas de Cocos y de Rivera son muy diferentes, ya que la primera se desplaza con una velocidad de 5 cm/año en la dirección noreste ref (4) mientras la segunda lo hace con una velocidad de 2.1 cm/año en la dirección noroeste ref (3). De lo anterior se sigue que los mecanismos de los temblores en la zona sean muy diferentes, dependiendo de cual sea la placa a que se asocien ref (3).

Así, de los temblores localizados fuera de la costa, algunos se asocian a la zona de la Fractura de Tamayo frente a las costas de Sinaloa y Nayarit, otros a la zona de la fractura de Rivera y la mayoría a la trinchera mesoamericana refs (3, 4, 5, 6). En cuanto a los temblores localizados tierra adentro en la ref (7) se sugiere que se les puede asociar a los movimientos en las fallas Zacamboxo, del Pacífico y Clarión Fig 1; debe mencionarse que no se tiene evidencia concluyente sobre la existencia y por tanto de las características específicas de estas fallas.

### 3.2 Sismicidad

La sismicidad de la región ha sido motivo de estudios recientes como los de las refs (3, 6, 7, 8). De dichos estudios se puede concluir que se tiene evidencia estadística de la ocurrencia de temblores destructivos en la región de interés, mas no se cuenta con los correspondientes registros del movimiento del terreno.

Entre los temblores con magnitudes mayores o iguales a 7 ocurridos en la región se puede mencionar tres en el siglo pasado (1845, 1858 y 1875) y cuatro en el presente (1911, 1932, 1941 y 1973) refs (7 y 8) Figs 2 a 7.

En la ref (3) se estudia el problema de la localización del temblor de junio de 1932 con magnitud igual a 8.2 y se concluye que dependiendo de si este temblor fue causado por el movimiento de la placa de Cocos o por la placa de Rivera se espera que un temblor con características similares ocurriría (o sea tendría un periodo de recurrencia) en 56 o 140 años a partir de 1932. En la ref (8) se menciona que la región de Jalisco tiene un potencial sísmico muy alto y que el lapso para que ocurran temblores fuertes (magnitud mayor o igual a 7) varía entre 32 y 56 años.

### 3.3 Conclusiones sobre la tectónica y sismicidad del occidente de México

De lo discutido en los incisos 3.1 y 3.2 se puede concluir lo siguiente:

- a) La información actual sobre la geotectónica y la sismicidad del occidente de México solo permite afirmar que la región es sísmicamente activa.
- b) Que en la región pueden ocurrir temblores destructivos cuyo periodo de recurrencia varía en un rango de decenas a cientos de años.

- c) Se tiene información de tipo estadístico sobre las magnitudes y la localización de temblores ocurridos en la región en el presente siglo y algunos del pasado.
- d) No se cuenta con registros del movimiento del terreno en la región; que sean de interés ingenieril.

#### 4. MODELOS DE RIESGO SISMICO

##### 4.1 Modelos de riesgo sísmico

Los modelos de riesgo sísmico son modelos matemáticos que en una situación ideal sintetizan el conocimiento actual sobre el proceso de generación de temblores y que se combinan con la información sismotectónica disponible en una región, para estimar los valores esperados de las intensidades máximas del movimiento del terreno en un sitio dado durante ciertos lapsos (periodos de recurrencia).

Los modelos de riesgo sísmico que se han utilizado en los últimos años en el Instituto de Ingeniería, UNAM, tienen como hipótesis fundamental que las intensidades máximas del terreno en un sitio determinado resultan de las contribuciones de la actividad sísmica de volúmenes de la corteza terrestre vecinos al sitio. Sin embargo, los modelos mencionados difieren en la forma en que consideran las incertidumbres inherentes a los diferentes tipos de información sísmica disponible y sobre los modelos conceptuales del proceso de generación de temblores.

Se tiene un tipo de modelos que aquí se denomina bayesianos en los cuales las incertidumbres sobre la información y los modelos mencionados son explícitamente considerados por medio del teorema de Bayes (Apéndice A). Los otros modelos, que llamaremos no bayesianos, manejan las incertidumbres men

cionadas apoyandose exclusivamente en la información estadística con que se cuente (generalmente escasa) o en la opinión (generalmente conservadora) de los especialistas para modificar alguna hipótesis sobre el proceso de generación de temblores.

En la Parte II se presenta un modelo de riesgo sísmico no-bayesiano utilizado recientemente. En 4.2 se propone un modelo de riesgo sísmico bayesiano y en el cap 5 un ejemplo de su aplicación a la determinación de las intensidades máximas esperadas del terreno para un sitio en el estado de Jalisco.

#### 4.2 Modelo de riesgo sísmico con parámetros bayesianos

##### 4.2.1 Sismicidad regional y local

La sismicidad regional,  $v$ , en un sitio determinado, o sea el efecto que producen los temblores que ocurren en la región vecina al sitio, depende principalmente de la contribución que a la misma hacen los volúmenes de la corteza terrestre alrededor de dicho sitio. Dada la atenuación de la intensidad con la distancia, solamente los temblores localizados a algunos cientos de kilómetros del sitio contribuyen en forma importante a esta sismicidad.

Los volúmenes citados se designan como fuentes sísmicas y se caracterizan por las incertidumbres asociadas a la frecuencia de ocurrencia y las magnitudes de los temblores que generan. Se denomina sismicidad local,  $\lambda$ , al proceso de ocurrencia de temblores de diversas magnitudes en una fuente sísmica. De lo anterior se puede concluir que la sismicidad regional para un sitio puede estimarse a partir de las sismicidades locales de las fuentes sísmicas correspondientes.

Por ejemplo si  $\lambda(M)$  representa el número de temblores de magnitud igual o mayor que  $M$  generados en promedio por unidad de volumen y por año en fuentes sísmicas vecinas a un sitio específico, el efecto de estos temblores en dicho sitio se puede evaluar con la expresión (ref 10)

$$v_c(y) = \int_v \lambda \{M(y, R)\} dv \quad (4.1)$$

donde  $v_c(y)$  es el número medio anual de temblores con intensidad mayores que "y" registrados en el sitio de interés y generados por las fuentes sísmicas,  $M\{y, R\}$  es la magnitud  $M$  que produce una intensidad "y" a la distancia  $R$  y  $dv$  es un volumen elemental de la corteza terrestre distante  $R$  del sitio de interés. El subíndice  $c$  de  $v$  significa que las intensidades "y" son calculadas a partir de las magnitudes, profundidades y distancias epicentrales provenientes de catálogos de temblores y de leyes de atenuación que relacionan magnitud-distancia-intensidad como se comenta más adelante.

#### 4.2.2 Modelo de sismicidad local

La sismicidad local,  $\lambda(M)$ , asociada a una fuente sísmica determinada puede estimarse utilizando un modelo del proceso estocástico (aleatorio) de la ocurrencia de temblores de diversas magnitudes en dicha fuente. Si se adopta una forma para el proceso, la sismicidad local podría calcularse una vez que se estimen los parámetros que definen a dicho proceso.

En este trabajo se supone que la ocurrencia de eventos se puede idealizar mediante un proceso homogéneo de Poisson. Lo anterior implica que la distribución de los tiempos de ocurrencia de temblores es independiente de la historia previa. Esta independencia se supone también por lo que respecta a la distribución espacial de los focos de los eventos sísmicos. De acuerdo con la referencia (11),  $\lambda(M)$  se expre

sa como

$$\lambda(M) = \alpha e^{-\beta M} (1 - e^{-\gamma(M_u - M)}) \quad M \leq M_u$$

$$= 0 \quad M > M_u$$
(4.2)

donde  $\alpha$ ,  $\beta$ ,  $\gamma$  y  $M_u$  son parámetros del proceso, los cuales deben estimarse a partir de los datos estadísticos, y de las características sismotectónicas de las fuentes vecinas al sitio o de zonas similares de la tierra.  $M_u$  es la magnitud máxima que dichas fuentes pueden generar.

#### 4.2.3 Ecuaciones de atenuación

Las ecuaciones de atenuación son expresiones semiempíricas que relacionan magnitud-distancia-intensidad (aceleraciones, velocidades y desplazamientos máximos) de temblores en terreno firme. Dichas expresiones pueden obtenerse a partir de los datos que existen sobre los parámetros mencionados. En general, los procedimientos utilizados para obtener las leyes de atenuación consisten en ajustar curvas a los datos de eventos ocurridos en diferentes regiones, por lo cual las expresiones así obtenidas reflejan las características geotectónicas de la región para la cual fueran obtenidas (ref 12).

En este estudio se utilizarán leyes de atenuación de la forma siguiente

$$y = b_1 e^{b_2 M} (R + R_0)^{-b_3}$$
(4.3)

donde  $b_1$ ,  $b_2$ ,  $b_3$  y  $R_0$  son los parámetros estimados del ajuste y  $R$  fue definido previamente.

En este trabajo se usarán las leyes de atenuación propuestas en la ref 12 las cuales fueron obtenidas a partir de la in-

formación correspondiente a temblores ocurridos en terreno firme de la costa oeste de los Estados Unidos y de la República Mexicana. Las expresiones propuestas en dicha ref para estimar la aceleración,  $a$ , y la velocidad,  $v$ , máxima del terreno asociadas a un temblor son:

$$a = 5600 e^{0.8M} (R + 40)^{-2} \text{ en (cm/seg}^2\text{)} \quad (4.4a)$$

$$v = 32 e^M (R + 25)^{-1.7} \text{ en (cm/s}^2\text{)} \quad (4.4b)$$

donde  $M$  y  $R$ , la magnitud y la distancia del sitio de interés al foco del temblor se obtienen de la información del catálogo de eventos para la región de interés.

En la ref 12 se efectuó un análisis estadístico de los errores de predicción asociados a las expresiones 4.4a y 4.4b. De este estudio se determinó que los logaritmos naturales de los cocientes de las intensidades ( $a$  o  $v$ ) predichas a las registradas instrumentalmente tienen distribución lognormal. Los parámetros de las mencionadas distribuciones fueron: para la aceleración máxima del terreno, media igual a 0.04 y desviación estándar igual a 0.64; para la velocidad máxima del terreno, media igual a 0.124 y desviación estándar igual a 0.74.

#### 4.2.4 Modelo de sismicidad regional

La contribución de una fuente sísmica de volumen elemental  $\Delta v$  a la sismicidad regional  $v_c$  en un sitio, distante  $R$  de la fuente, se puede obtener combinando las ecs (4.2) y (4.3), de lo cual resulta la siguiente expresión, (ref 11).

$$\Delta v_c(y) = \alpha b_1^r (R+R_0)^{-q} y^{-r} (1-(y/y_1)^e) \Delta v, \quad y \leq y_1 \quad (4.5)$$

$$= 0, \quad y > y_1$$

En (4.5),  $r = \beta/b_2$ ,  $\epsilon = \gamma/b_2$ ,  $q = b_3$ ,  $r$ ,  $y_1$  es la intensidad obtenida con la ec 3 para  $M = M_u$ ;  $\alpha$ ,  $\beta$  y  $\gamma$  son parámetros de la ec (4.2).

Para obtener la contribución de varias fuentes sísmicas a  $v_c$  en un sitio basta con integrar la ec 4.5 con respecto al diferencial de volumen. El resultado de dicha integración no variará en "y" como la ec 4.5; sin embargo, para fines prácticos dicho resultado se puede representar por una expresión similar a su segundo miembro, es decir (ref 11):

$$v_c(y) = k y^{-r} (1 - (y/y_1)^\epsilon), \quad y \leq y_1$$

$$= 0, \quad y > y_1 \quad (4.6)$$

donde  $k$ ,  $r$ ,  $\epsilon$  y  $y_1$  son parámetros que se pueden estimar a partir de información estadística de los temblores y de las características sismotectónicas de las fuentes vecinas al sitio de interés o de zonas similares de la tierra. El parámetro  $y_1$  es el valor máximo esperado, que resulta de aplicar la ec 4.3, a la combinación mas desfavorable de  $M_u$  y  $R$ , para las diferentes fuentes sísmicas vecinas al sitio.

Los valores de  $v$  obtenidos en terminos de los datos estadísticos sobre intensidades calculadas (a partir de magnitudes y distancias) con las ecuaciones de atenuación de 4.2.3 deben corregirse para tomar en cuenta las incertidumbres derivadas de la utilización de dichas leyes. La corrección mencionada se trata en 4.2.6.

Generalmente los catálogos de temblores que contienen la información mencionada en el párrafo anterior están incompletos; es decir, no incluyen todos los eventos que pudieran generar intensidades máximas del terreno capaces de producir daños en las estructuras que se construyan en el sitio de

interés. Esto proviene de que sólo contienen información completa para magnitudes por encima de un cierto límite inferior y por lo tanto emplear estos catálogos sin corrección equivale a ignorar la contribución al riesgo de los temblores muy pequeños, pero frecuentes, que pueden ocurrir a distancias muy cortas. Debido a lo anterior resulta necesario introducir una función correctiva  $f(y)$ , por la cual deberá multiplicarse la sismicidad  $v_c$  obtenida a partir del catálogo; al valor corregido de  $v$  se le designará por  $v_{co}$ ;  $f(y)$  depende de los parámetros de las leyes de atenuación y de las intensidades máximas calculadas con esas leyes. En forma aproximada  $f(y)$  puede representarse así (ref 11)

$$f(y) = 1/(1-b(1-y/y_1)^s); y \leq y_1 \quad (4.7)$$

donde  $b$ ,  $s$ , y  $y_1$  son definidos como sigue  $s > 0$ ,  $0 \leq b \leq 1$  y  $y_1$  es el valor máximo de  $y_1$  que puede esperarse de las fuentes sísmicas vecinas al sitio de interés. Los valores específicos que adoptan  $s$ ,  $b$  y  $y_1$  dependen de los parámetros de  $\lambda(M)$ , de las leyes de atenuación utilizadas y de la distribución espacial de la sismicidad en la zona vecina al sitio.

De la ec 4.7 se puede ver que  $f(y)$  es igual a  $1/(1-b)$ , para  $y = 0$  e igual a 1 para  $y = y_1$ . Los valores límites manifiestan el hecho de que en general los catálogos de temblores están completos para magnitudes grandes y siendo lo contrario para magnitudes pequeñas.

De lo anterior se sigue que la  $v(y)$  corregida por incompletez del catálogo se expresa como

$$v_{co}(y) = f(y) v_c(y) \quad (4.8)$$

donde  $f(y)$  y  $v_c(y)$  están dados por las ecs (4.7) y (4.6) respectivamente.

#### 4.2.5 Estimación bayesiana de la sismicidad regional $v(y)$

En este trabajo la estimación de  $v(y)$  consistirá en obtener la esperanza de esta variable a partir de la distribución conjunta de probabilidades de los parámetros  $k$ ,  $r$ ,  $\epsilon$  y  $y_1$ , que son los que definen a  $v_c(y)$  de acuerdo a la ec 4.6. Para determinar esta distribución se efectuará el análisis bayesiano de dichos parámetros, que esencialmente consiste en aplicar el teorema de Bayes (Apéndice A) a toda la información geotectónica y sismológica significativa de que se disponga en la región donde se localiza el sitio de interés. Si se representa por  $Z$  el vector formado por los parámetros  $k$ ,  $r$ ,  $\epsilon$ ,  $y_1$ ; por  $Y_N$  el vector constituido por los  $N$  valores de las intensidades  $y_i$  observadas durante un lapso  $t$ , por  $f'$  y  $f''$  a las distribuciones bayesianas inicial y posterior de  $Z$  respectivamente; por  $L$  la función de verosimilitud del vector  $Y_N$  para un  $Z$  dado. Se tiene la siguiente expresión (Apéndice A):

$$f''_Z(z|Y_N; t) \propto f'_Z(z) L(Y_N; t|z) \quad (4.9)$$

La distribución  $f'_Z(z)$  depende de las distribuciones marginales iniciales de los parámetros de  $\lambda(M)$ , es decir de  $\alpha$ ,  $\beta$ ,  $\gamma$  y  $M_u$  (ver ecs 4.2 y 4.5). En relación a  $\alpha$  se puede partir de estimaciones de los valores esperados de  $\lambda(M)$  para magnitudes pequeñas en zonas sísmicas que involucren volúmenes considerables de la corteza terrestre. También se puede utilizar la información geofísica sobre la liberación de energía sísmica en regiones de dimensiones intermedias (ref 11). En cuanto a  $\beta$  se puede utilizar valores que provienen de regiones sísmicas semejantes a la de interés, además de que su rango de valores posibles tiene una cota superior (ref 11).

Como no se tiene información sobre los posibles valores de  $\gamma$ , para este parámetro se requiere utilizar distribuciones difusas. Finalmente la distribución inicial de  $M_u$  se puede formu

lar con base en la información geotectónica de la región vecina al sitio, o si dicha información es escasa o inexistente para las máximas magnitudes observadas en la mencionada región.

Cuando se carece de información significativa en la región sísmica de interés, la distribución  $f'_2(z)$  se puede determinar asignando a los parámetros  $k, r, \epsilon, y_1$  distribuciones marginales uniformes en intervalos que se consideren apropiados; además se supone que dichos parámetros son estadísticamente independientes. De lo anterior se puede obtener que

$$f'(z) = f(k) f(r) f(\epsilon) f(y_1) \quad (4.10)$$

donde  $f(i)$ ,  $i = k, r, \epsilon, y_1$  representan las distribuciones marginales de los parámetros  $k, r, \epsilon, y_1$ .

Para obtener la función  $L(\cdot)$  se supone lo siguiente: que las intensidades observadas (es decir las intensidades calculadas para valores observados de magnitud y distancia)  $Y_N$  son variables aleatorias independientes con idéntica distribución, que dichas intensidades tienen un límite inferior  $y_0$ , así como la hipótesis mencionada anteriormente de que la ocurrencia de los temblores constituye un proceso de Poisson (sección 4.2.2). De acuerdo con las hipótesis anteriores se pueden escribir que la función  $L(\cdot)$  satisface la siguiente relación de proporcionalidad

$$L(Y_N; t|Z) \propto v_{co}(y_0) + \sum_{i=1}^N \text{Ln} v'_{co}(y_i) \quad (4.11)$$

En esta relación,  $v_{co}(y_0)$  es la tasa de excedencia correspondiente a  $y_0$  calculada con la ec 4.8,  $t$  es el lapso de observación de  $Y_N$  y  $v'_{co}(y_i)$  es la derivada de  $v_{co}(y)$  con respecto a  $y$  y valuada para  $y = y_i$ . En el apéndice B se muestra la obtención de la ec (4.11) así como la forma explícita de

sus términos.

Sustituyendo las ecs 4.10 y 4.11 en la ec (4.9) es posible obtener la distribución de probabilidades a posteriori de los parámetros  $k, r, \varepsilon, y_1$ , de lo cual se sigue que la esperanza a posteriori,  $E''(\cdot)$ , y la variancia a posteriori,  $\sigma^{2''}(\cdot)$  de  $v_{co}$  para  $y = y_i$  se pueden estimar con las siguientes expresiones:

$$E''(v_{co}(y_i)) = \int_{\xi} v_{co}(y_i) f_Z''(z|Y_N; t) dz \quad (4.12)$$

$$\sigma^{2''}(v_{co}(y_i)) = \int_{\xi} (v_{co}(y_i) - E''(v_{co}(y_i)))^2 f_Z''(z|Y_N; t) dz \quad (4.13)$$

en estas ecs  $dz = dk dr d\varepsilon dy_1$  y  $\xi$  es el dominio de  $Z$ . La integración de las ecs (4.12, 4.13) se efectuará discretizando  $\xi$  por medio de la concentración de las probabilidades bayesianas de  $Z$  en los puntos del dominio definidos por valores preseleccionados de los parámetros  $k, r, \varepsilon, y_1$ ; es decir:

$$E''(v_{co}(y_i)) = \sum_{m=1}^{n_1} \sum_{n=1}^{n_2} \sum_{s=1}^{n_3} \sum_{\mu=1}^{n_4} v_{co}(y_i) f_Z''(z_{m n s \mu} | Y_N; t) \quad (4.14)$$

$$\sigma^{2''}(v_{co}(y_i)) = \sum_{m=1}^{n_1} \sum_{n=1}^{n_2} \sum_{s=1}^{n_3} \sum_{\mu=1}^{n_4} (v_{co}(y_i) - E''(v_{co}(y_i)))^2 f_Z''(z_{m n s \mu} | Y_N; t) \quad (4.15)$$

En las ecs (4.14, 4.15)  $n_1, n_2, n_3$  y  $n_4$  representan el número de valores seleccionados de  $k, r, \varepsilon$  y  $y_1$  respectivamente,  $f''(\cdot)$  es la distribución de probabilidades a posteriori de  $Z$  valuada en  $k_m, r_n, \varepsilon_s, y_{1\mu}$ . En las ecs 4.14 y 4.15 esta

implícito que  $v_{CO}(y_1)$  también debe ser valuada en los mismos puntos que  $f^*(.)$ . El coeficiente de variación a posteriori de  $v_{CO}(y_1)$ ,  $V^*(v_{CO}(y_1))$  se puede obtener directamente con la ec 4.16

$$V^*(v_{CO}(y_1)) = \sigma^*(v_{CO}(y_1)) / E^*(v_{CO}(y_1)) \quad (4.16)$$

donde  $\sigma^*(.)$  es la desviación estandar a posteriori.

#### 4.2.6 Corrección por incertidumbre en las leyes de atenuación

En 4.2.3 se mencionó que los cocientes de las intensidades reales entre las predichas con las leyes de atenuación que se utilizan en este trabajo (ecs 4.4a y 4.4b) tienen una distribución de probabilidades lognormal con medias y desviaciones estándar indicadas en esa sección. Para tomar en cuenta el efecto de las incertidumbres implícitas en las leyes de atenuación en la sismicidad calculada a partir de dichas leyes, en la ref 13 se propuso la siguiente expresión

$$v(y) = \int_{\alpha_u}^{\infty} v_{CO}(y/u) f_e(u) du \quad (4.17)$$

donde  $v(y)$  es la sismicidad en el sitio asociada a la intensidad y corregida por incertidumbre en las leyes de atenuación,  $v_{CO}(y/u)$  es la sismicidad en el sitio sin incluir dicha corrección,  $\alpha_u = y/y_1$ , y  $f_e$  es la función de densidad de probabilidades del cociente de las intensidades reales entre las predichas con las leyes de atenuación.

En el caso que nos ocupa  $v_{CO}(y/u)$  esta dada por la ec 4.8,  $f_e(u)$  es la función de densidad de probabilidades de la distribución lognormal y  $y_1$  se definió anteriormente. Combinando las ecs 4.8 y 4.17 se obtiene (ref 13):

$$v(y) = C_1 K y^{-r} \left(1 - \frac{C_2}{C_1} \left(\frac{y}{y_1}\right)^\epsilon\right) \quad (4.18)$$

$$C_i = e^{Q_i} \left(1 - \phi\left(\frac{\ln(y/y_1) - m - \sigma^2 r_i}{\sigma}\right)\right)$$

$$i = 1, 2$$

$$Q_i = \frac{1}{2} \sigma^2 r_i^2 + m r_i$$

$$r_1 = r$$

$$r_2 = r - \epsilon$$

$K$ ,  $r$ ,  $\epsilon$  y  $y_1$  son los parámetros de  $E'' (v_{co}(y_i))$ ,  $m$  y  $\sigma$  son respectivamente la media y la desviación estándar del error de predicción de las leyes de atenuación (ecs 4.4a y 4.4b) y  $\phi$  es la función normal de distribución de probabilidades con media nula y variancia unitaria.

## 5. RIESGO SISMICO EN UN SITIO EN EL ESTADO DE JALISCO

En este cap se presenta una aplicación del modelo descrito en el cap 4 para la determinación de las intensidades maximas del terreno para diferentes periodos de recurrencia, de un si tio que tiene como coordenadas 21.3°N, 104.4°W, localizado en el estado de Jalisco.

### 5.1 Información para el sitio

Con base en la información tectónica y sobre la sismicidad de la región (la cual fue discutida en el cap 3) se decidió adoptar como fuente sísmica un prisma de 14 x 14 grados de latitud y longitud con centro en el sitio y 300 kilómetros de profundidad. La información de tipo estadístico sobre los temblores ocurridos en dicha fuente provino de las refs (8, 14).

De las refs (8, 14) se generó un catálogo de temblores con magnitudes mayores o iguales a 4.5 para el lapso 1900 a 1981. Como las magnitudes reportadas en dichas refs (10, 18) inclu<sup>yen</sup> magnitudes asociadas a la transmisión de ondas de cuerpo ( $m_b$ ) y de superficie ( $m_s$ ) para los eventos ocurridos en diversas épocas, fue necesario uniformizar el catálogo a una sólo magnitud.

Para lograr lo anterior se utilizaron eventos registrados de 1900 a 1981 y de los cuales se tenían ambas magnitudes; se efectuó un ajuste de mínimos cuadrados a dichos datos, lo cual condujo a las siguientes ecuaciones:

$$m_s = 1.12 m_b - 0.705$$

$$m_b < 5.6$$

(5.1)

$$m_s = 1.312m_b - 1.565 \quad (5.2)$$

$$m_s \geq 5.6$$

Estas expresiones fueron utilizadas para uniformizar los temblores del catálogo inicial a la magnitud  $m_s$  únicamente.

Por otro lado la profundidad de un número importante de eventos del catálogo no fue reportado y dado que se requiere dicha información para poder convertir el catálogo de magnitudes a uno de intensidades (a través de las ecuaciones de atenuación) se utilizaron las siguientes ecuaciones ref (15)

$$(\bar{H} + 40)^{-2} = \frac{1}{n} \sum_{i=1}^n (H_i + 40)^2 \quad (5.3)$$

$$(\bar{H} + 25)^{-2} = \frac{1}{n} \sum_{i=1}^n (H_i + 25)^{-2} \quad (5.4)$$

para calcular una profundidad promedio  $\bar{H}$  de los temblores ocurridos en la fuente sísmica seleccionada.

En las ecs 5.3 y 5.4  $H_i$  es la profundidad reportada para el  $i$ -ésimo temblor y  $n$  es el número de eventos cuya profundidad sí fue reportada. Las ecs 5.3 y 5.4 son utilizadas para calcular la profundidad de un temblor al cual se le determinará su aceleración o velocidad del terreno en el sitio de interés respectivamente.

De la aplicación de las ecs 5.1 - 5.4 se obtuvieron dos catálogos con magnitudes  $m_s$  y con sus profundidades correspondientes para determinar la aceleración y la velocidad del terreno en diferentes sitios de interés.

## 5.2 Riesgo sísmico en el sitio de interés

El modelo de riesgo sísmico descrito en 4.2 fue aplicado utilizando la información mencionada en 5.1.

A partir de las magnitudes, las coordenadas epicentrales y las profundidades focales de los temblores de los catálogos mencionados al final de 5.1 y haciendo uso de las leyes de atenuación para aceleraciones y velocidades máximas ecs 4.4a, 4.4b, se calcularon las intensidades del terreno correspondientes a los 81 años de observaciones.

A continuación se procedió a calcular la tasa media de excedencia de las intensidades observadas,  $v_c(y)$  (donde  $y$  representa las aceleraciones o las velocidades máximas del terreno). Para ello se ordenaron en forma ascendente las  $y$ 's y para calcular las  $v_c(y)$  correspondientes se divide el número de intensidades mayores o iguales a la intensidad de interés entre el lapso de observación, que en este caso es de 81 años.

En la fig 8 se presentan los valores obtenidos de  $v_c$  (o su recíproco el periodo de recurrencia  $T_r$ ) para la aceleración máxima del terreno para el sitio de interés. En la fig 9 se muestran los correspondientes valores para las velocidades máximas del terreno.

De la localización de los epicentros de los temblores del catálogo con relación a los sitios de interés se decidió proponer que  $f(y)$  en la ec 4.7 tendría un valor igual a la unidad. Con esto se supone que el catálogo esta completo en todo el rango de magnitudes utilizadas.

De acuerdo a lo mencionado en el cap 4, para el cálculo de la tasa media de excedencia  $E''(v_{co})$  se requieren los valores

iniciales (a priori) de los parámetros  $k$ ,  $r$ ,  $\epsilon$  y  $y_1$ . Los valores utilizados son los mostrados en la tabla 1. De la inspección de los datos de la muestra para el sitio se decidió que  $k$ ,  $r$  y  $\epsilon$  estarían comprendidos en los rangos indicados en dicha tabla. Los límites de  $y_1$  se obtuvieron a través de las ecs 4.4 y se consideran con base en lo discutido en el cap 2 una magnitud máxima esperada de 8.2 (refs 3), y dos valores de  $R$ , 24.5 y 40 km, los cuales conducen a un rango de aceleraciones y de velocidades máximas del terreno de 617 a 950  $\text{cm/s}^2$  y de 96 a 150  $\text{cm/s}$  respectivamente. De estudios sobre el efecto de  $y_1$  en la estimación de  $E''(v_{co})$  para los datos del sitio se observó que no era necesario que  $y_1$  fluctuará en los rangos indicados, sino que bastaba con tomar sus límites superiores, por lo cual se decidió utilizar los  $y_1$  indicados en la tabla 1.

En este trabajo se supone que a priori los parámetros  $k$ ,  $r$ ,  $\epsilon$  y  $y_1$  son estadísticamente independientes por lo cual la probabilidad a priori de cada una de las combinaciones de los diferentes parámetros es igual a  $1/1024$ , donde el denominador se obtiene de multiplicar el número de valores utilizados de cada parámetro es decir,  $8 \times 8 \times 8 \times 2$ , correspondientes a  $k$ ,  $r$ ,  $\epsilon$  y  $y_1$  respectivamente.

Finalmente los valores de  $m$  y  $\sigma$  en la ec son los mencionados en 4.2.3. es decir,  $m = 0.04$  y  $\sigma = 0.64$  para la aceleración máxima del terreno y  $m = 0.124$  y  $\sigma = 0.74$  para la velocidad máxima del terreno.

Los resultados obtenidos se presentan en las figs 8 y 9, la primera corresponde a las aceleraciones y la segunda a las velocidades máximas del terreno en el sitio de interés, respectivamente. En esas figs se tienen las curvas de la esperanza de posteriori y el coeficiente de variación de  $v_{co}$ .

$E''(v_{CO})$  y  $V''(v_{CO})$  correspondientes. Las curvas de  $E''(v_{CO})$  tienen la forma de la ec 4.6 con los parámetros  $k$ ,  $r$ ,  $\epsilon$  y  $y_1$  de la tabla 2. También se muestran en dichas figs las curvas  $E''(v)$  que representan las esperanzas a posteriori de  $v$  obtenidas después de aplicar las correcciones por incertidumbre en las leyes de atenuación de acuerdo a lo mencionado en 4.2.6. Estas curvas proporcionan los valores finales de las aceleraciones y velocidades máximas del terreno  $a_r$  y  $v_r$  para el sitio de interés para diferentes  $v$  o  $T_r$ . En la tabla 3 se presentan los valores de  $a_r$  y  $v_r$  para varios periodos de recurrencia obtenidos de las mencionadas curvas.

Comparando los valores de las aceleraciones y velocidades máximas del terreno para periodos de recurrencia de 50, 100 y 500 años obtenidos en este trabajo con los proporcionados en la ref 16 se puede concluir lo siguiente:

- a) Las aceleraciones de la ref 16 son 2.42, 2.7 y 3.66 veces menores que las obtenidas en este estudio para los  $T_r$  mencionados;
- b) Las velocidades de la ref 16 son 1.87, 1.9 y 2.64 veces menores que las obtenidas en el presente trabajo.

Lo anterior quizá se deba a que la información utilizada en este trabajo es mas completa, así como a que las ecuaciones de atenuación utilizadas en la ref 16 eran menos precisas que las usadas en este trabajo.

## 6. CONCLUSIONES

Con base en lo descrito en los capitulos anteriores, se concluye lo siguiente:

1. Existe evidencia del alto potencial sísmico del occidente de México en particular en los estados de Colima, Jalisco y Michoacán.
2. Debido a lo anterior y a las posibles consecuencias de los efectos de los temblores en las construcciones, seria muy conveniente que a la brevedad posible se realicen estudios de riesgo sísmico detallados para las ciudades más importantes de la región.
3. Sería muy conveniente que a la brevedad posible se propongan reglamentos de diseño sísmico para las ciudades más importantes de la región.
4. Sería muy recomendable que a la brevedad posible se instalen acelerógrafos para registrar los movimientos sísmicos que ocurran en las ciudades importantes y otros sitios del occidente de México.

## 7. REFERENCIAS

1. Newmark N. M., Rosenblueth E. "Fundamentals of Earthquake Engineering", Prentice Hall, New Jersey (1971).
2. Rascón Ch., Chávez M., Alonso L. y Palencia V., "Registros y espectros de temblores en las ciudades de México y Acapulco, 1961-1968", Informe 385, Instituto de Ingeniería, UNAM. (1977)
3. Eissler H.K., McNally K. C., "Seismicity of the Rivera Fracture Zone and the Great Jalisco Earthquake of 1932", Seismological Lab., CALTECH (1980).
4. Molnar P., Sykes L.R., "Tectonics of the Caribbean and Middle American Regions from Focal Mechanisms and Seismicity", Geological Society of America Bulletin, V 80 (1969).
5. Lomnitz C. et al., "Sismicidad y tectónica de la región norte del Golfo de California", Geofísica Internacional, Vol. 10, No. 2 (1970).
6. McNally K.C., Minster J.B., "Non Uniform Seismic Split Rate Along the Middle America Trench", Journal of Geophysical Research, Vol. 86 No. B6 (1981).
7. Figueroa A.J., "Sismicidad en el estado de Jalisco", Memorias del V Congreso Nacional de Ingeniería Sísmica", SMIS, Guadalajara, (1979).
8. Singh S.K., Astiz L. and Haskov J., "Seismic Gaps and Recurrence Periods of Large Earthquakes Along the Mexican Subduction Zone: A Reexamination", Bull. of the Seism. Soc. of America, Vol. 71, (1981)..

9. Chávez M., Esteva L., De León D., "Estudios de sismicidad y riesgo sísmico para la planta geotérmica de Cerro Prieto, B.C." elaborado para CFE-CECP, Instituto de Ingeniería, UNAM, 21 pp Septiembre (1981).
10. Esteva L., "Bases para la formulación de decisiones de diseño sísmico", Informe 182, Instituto de Ingeniería, UNAM, (1968).
11. Esteva L., Chávez M., "Analysis of Uncertainty on Seismic Risk Estimates", 3rd Int. Earthquake Microzonation Conf., Vol. III, pp 1273-1284, Seattle, U.S.A., (1982).
12. Esteva L., Villaverde R., "Seismic Risk, Design Spectra and Structural Reliability", Proc. 5th World Conf. Earthquake Eng. (1973).
13. Esteva L., "Seismicity", Chap 6, "Seismic Risk and Engineering Decisions", Ed. C. Lomnitz, E. Rosenblueth, Elsevier, Amsterdam (1976).
14. NOAA, U.S. Department of Commerce "Earthquake data file Summary", Boulder, Colorado (1977).
15. Guerra R., Esteva L., "Seismic Design Spectra at the proposed Site for San Roque, Dam, Luzon, Philippine Islands", Instituto de Ingeniería, UNAM, (1979).
16. Esteva, L., "Regionalización sísmica de México para fines de ingeniería", Informe 246, Instituto de Ingeniería, UNAM (1970)

PARAMETRO	$k_{ini}$	$k_{fin}$	$\Delta k$	$r_{ini}$	$r_{fin}$	$\Delta r$	$\epsilon_{ini}$	$\epsilon_{fin}$	$\Delta \epsilon$	$y_{i,ini}$	$y_{i,fin}$	$\Delta y_i$
a	20	27	1	1.50	2.06	0,08	0.10	8.15	1.15	949	951	2
v	0.59	0.73	0.02	1.77	1.84	0.01	0.10	8.15	1.15	149	151	2

TABLA 1 VALORES A PRIORI DE LOS PARAMETROS  $k$ ,  $r$ ,  $\epsilon$ ,  $y_i$  PARA ACELERACIONES (a) Y VELOCIDADES (v) PARA UN SITIO EN EL ESTADO DE JALISCO

PARAMETRO	$k''$	$r''$	$\epsilon''$	$y_i''$
a	22.2053	1.7922	4.6756	950.00
v	0.6449	1.8033	4.6891	149.99

TABLA 2 VALORES ESPERADOS A POSTERIOR DE LOS PARAMETROS  $k$ ,  $r$ ,  $\epsilon$ ,  $y_i$  PARA ACELERACIONES (a) Y VELOCIDADES (v) PARA UN SITIO EN EL ESTADO DE JALISCO

PARAMETRO	PERIODO DE RECURRENCIA $T_r$ (años)						
	50	100	200	300	400	500	1000
a. (cm/s <sup>2</sup> )	92	135	202	250	292	330	495
v (cm/s)	10.3	15.2	22.2	28	33	37	54

TABLA 3 ACELERACIONES (a) Y VELOCIDADES (v) MAXIMAS DEL TERRENO PARA VARIOS PERIODOS DE RECURRENCIA ( $T_r$ ) PARA UN SITIO EN EL ESTADO DE JALISCO

ZONA 3

Prof. focal		Ew. Richter	Mercalli
40 km	60 km		
●	●	7.0 - 8.5	XI - XII
●	●	7.1 - 7.7	IX - X
●	●	6.1 - 7.0	VIII
●	●	5.1 - 6.0	VII
○	○	Menor 5.0	V y VI

Fallas

ZONA 2

ZONA 1

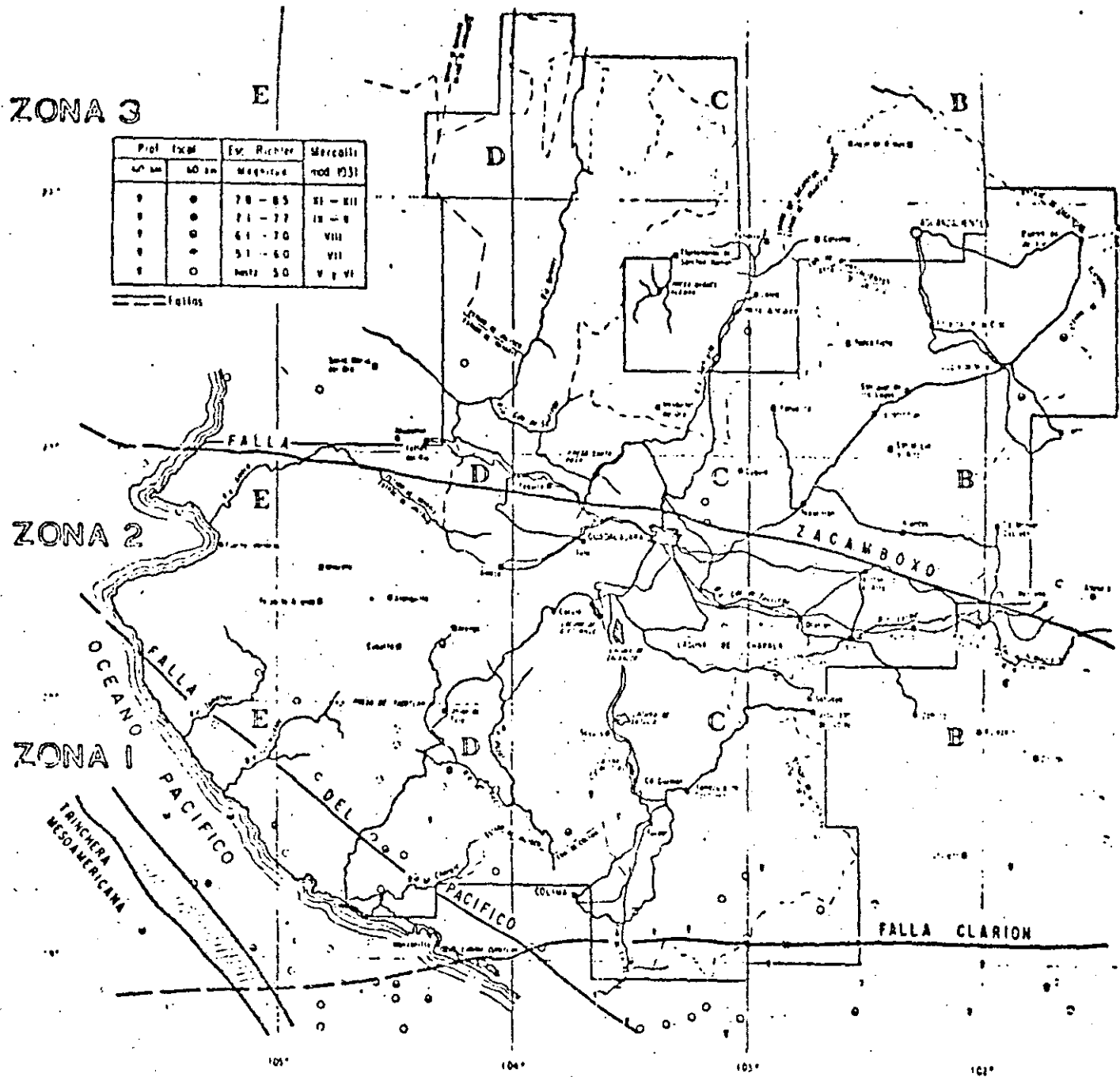


FIG 1 FALLAS DE ZACAMBOYO, CLARION Y DEL PACIFICO (REF 7)



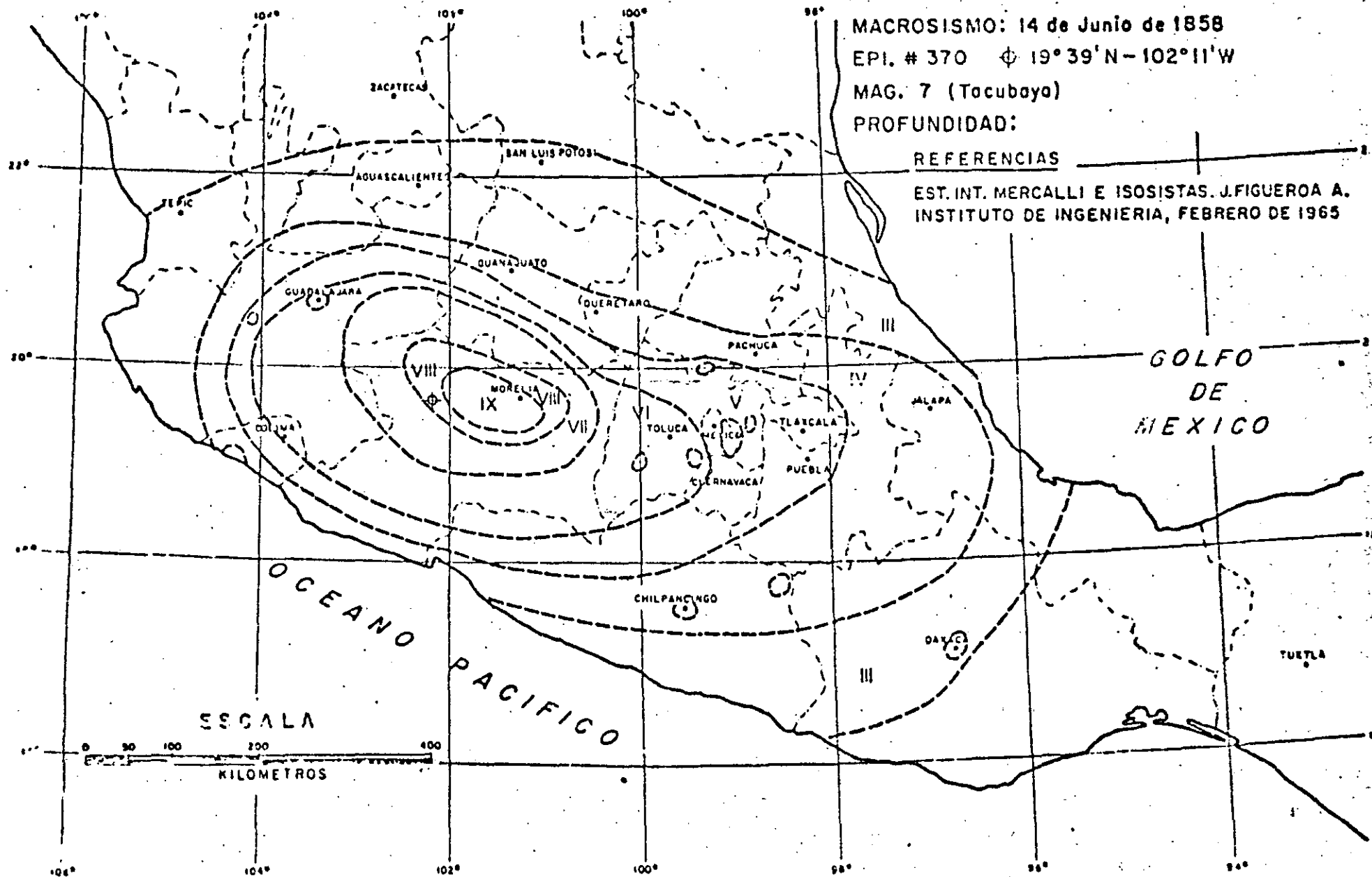


FIG 3 ISOSISTAS DEL TENBLOR DEL 14 DE JUNIO DE 1858 (REF 7)

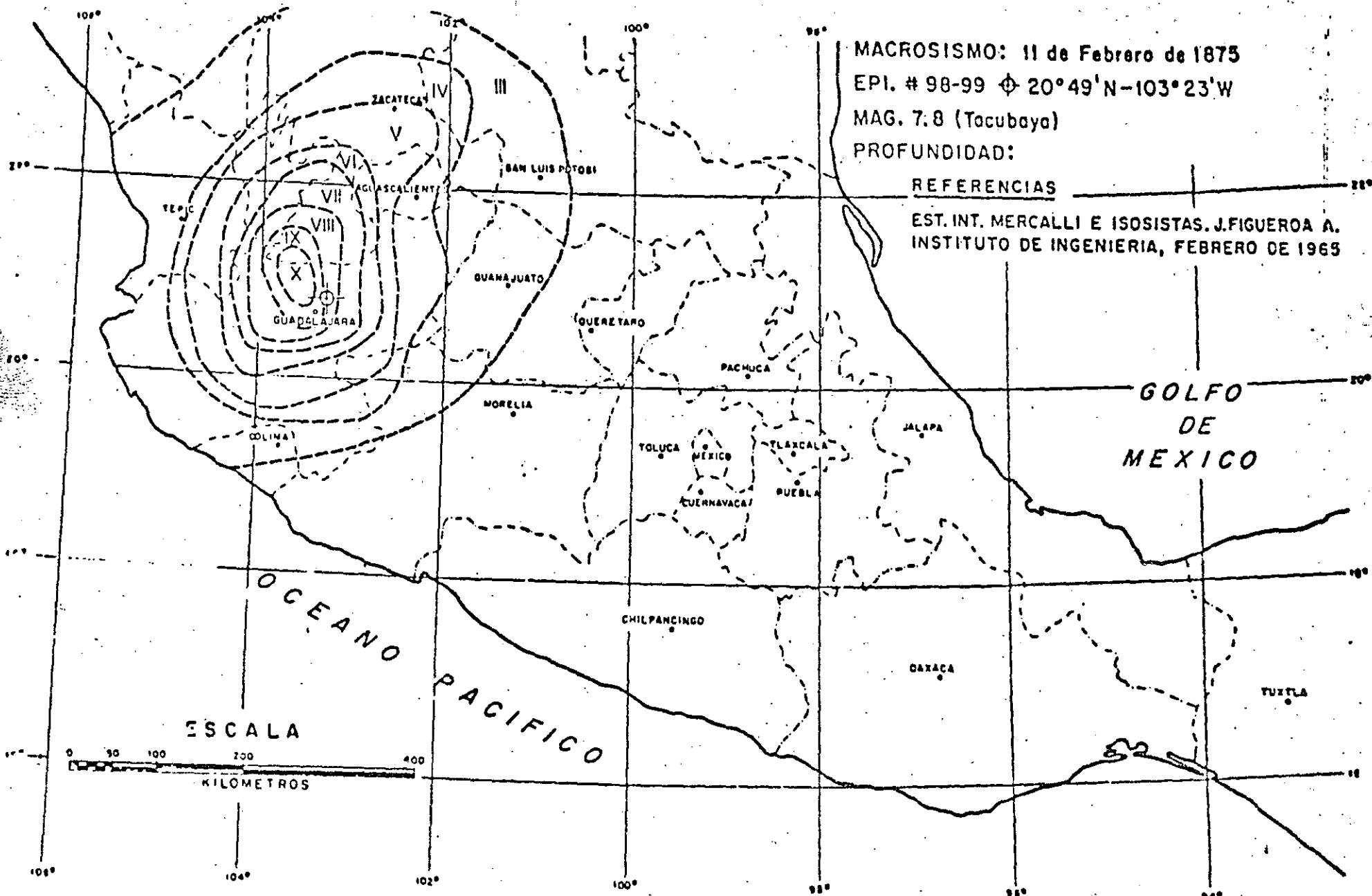


FIG 4 ISOSISTAS DEL TEMBLOR DEL 11 DE FEBRERO DE 1875 (REF 7)

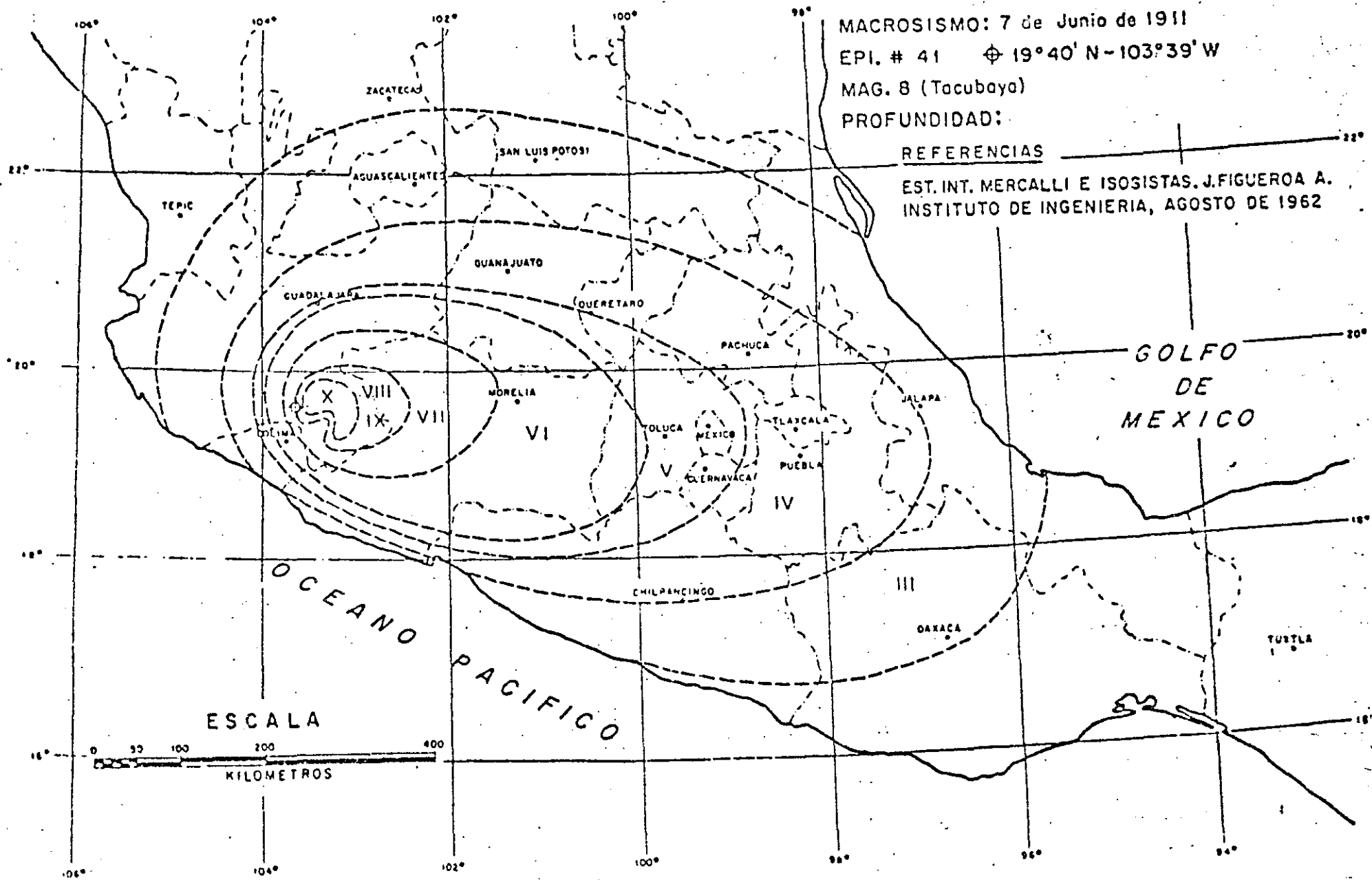


FIG 5 ISOSISTAS DEL TEMBLOR DEL 7 DE JUNIO DE 1911 (REF 7)

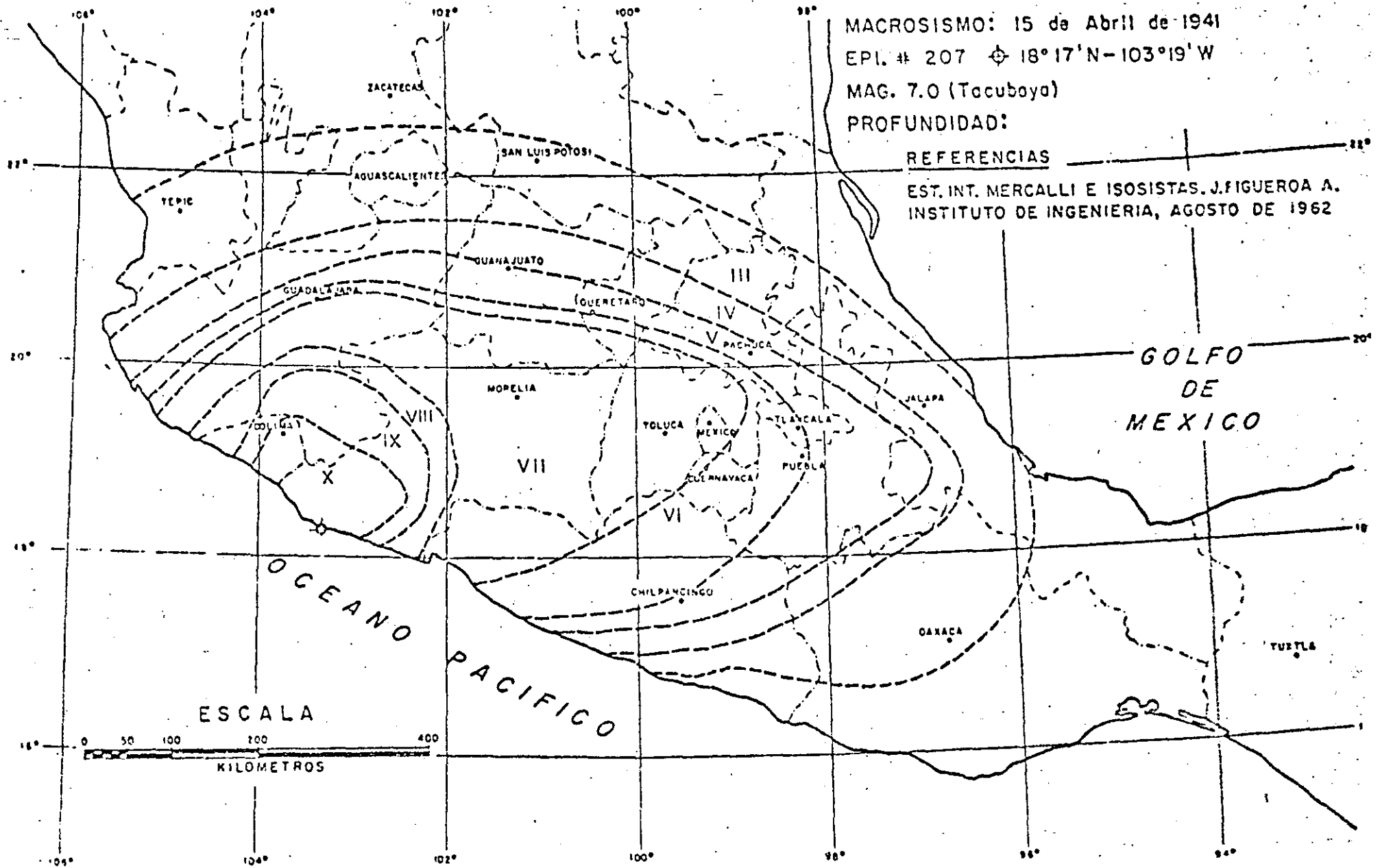


FIG 6 ISOSISTAS DEL TEMBLOR DEL 15 DE ABRIL DE 1941 (REF 7)

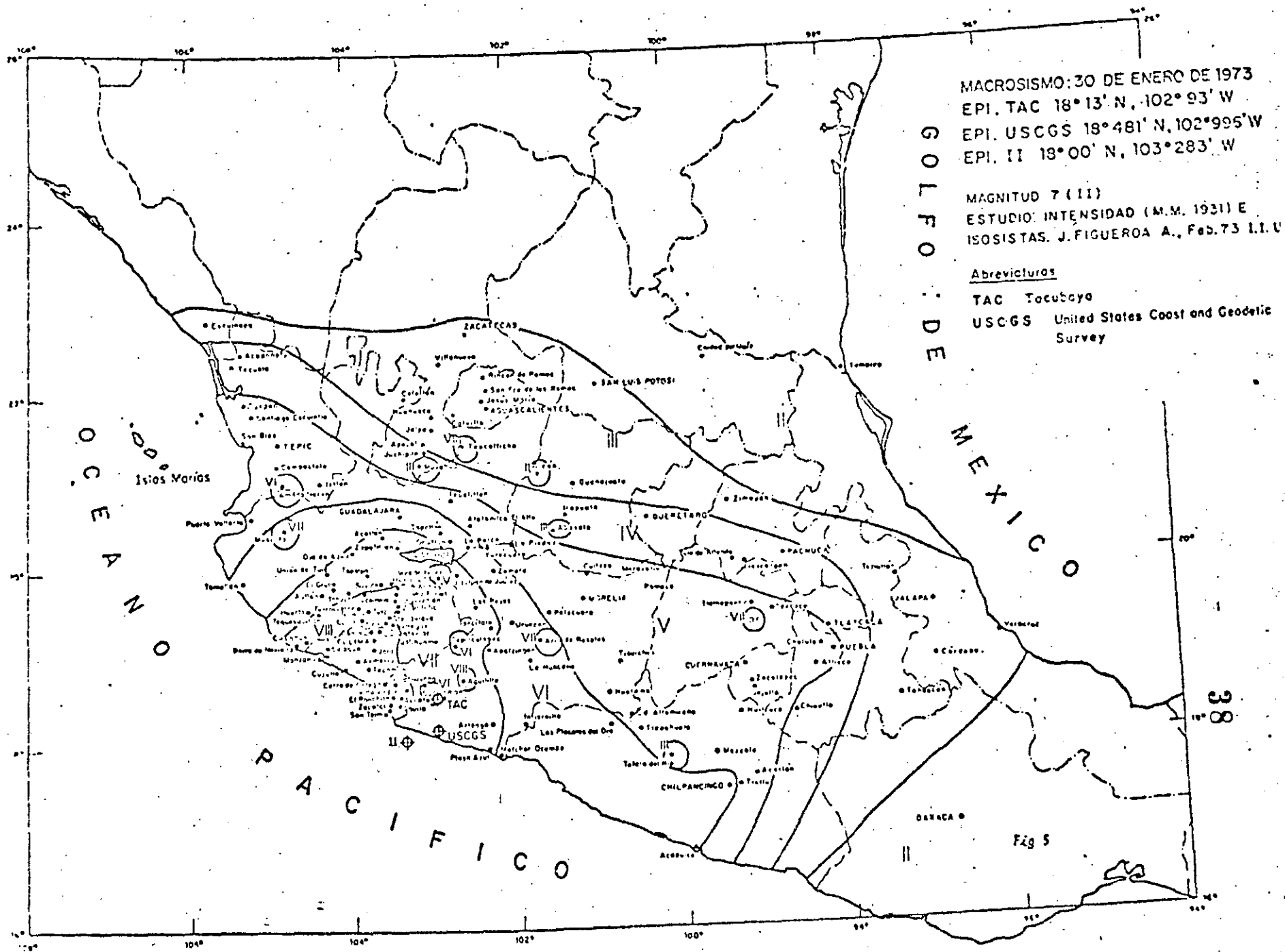


FIG 7 ISOSISTAS DEL TEMPLOR DEL 30 DE ENERO DE 1973 (REF 7)

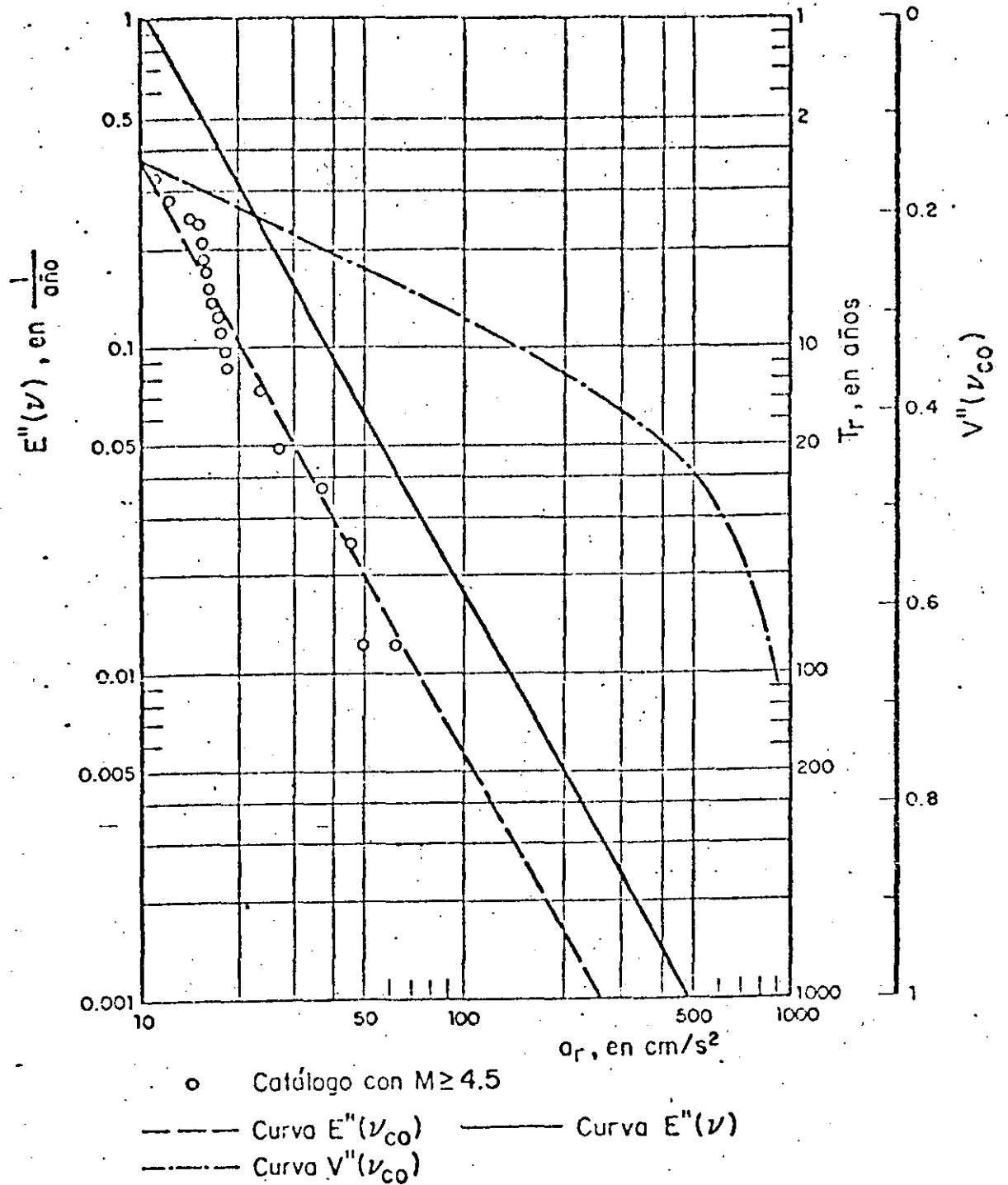


FIG 8 VALORES ESPERADOS A POSTERIOR DE LA TASA MEDIA DE EXCEDENCIA  $E''(\nu)$   
 (Y PERIODO DE RECURRENCIA,  $T_r$ ) VS ACELERACION MAXIMA DEL TERRENO  $a_r$   
 PARA UN SITIO EN EL ESTADO DE JALISCO

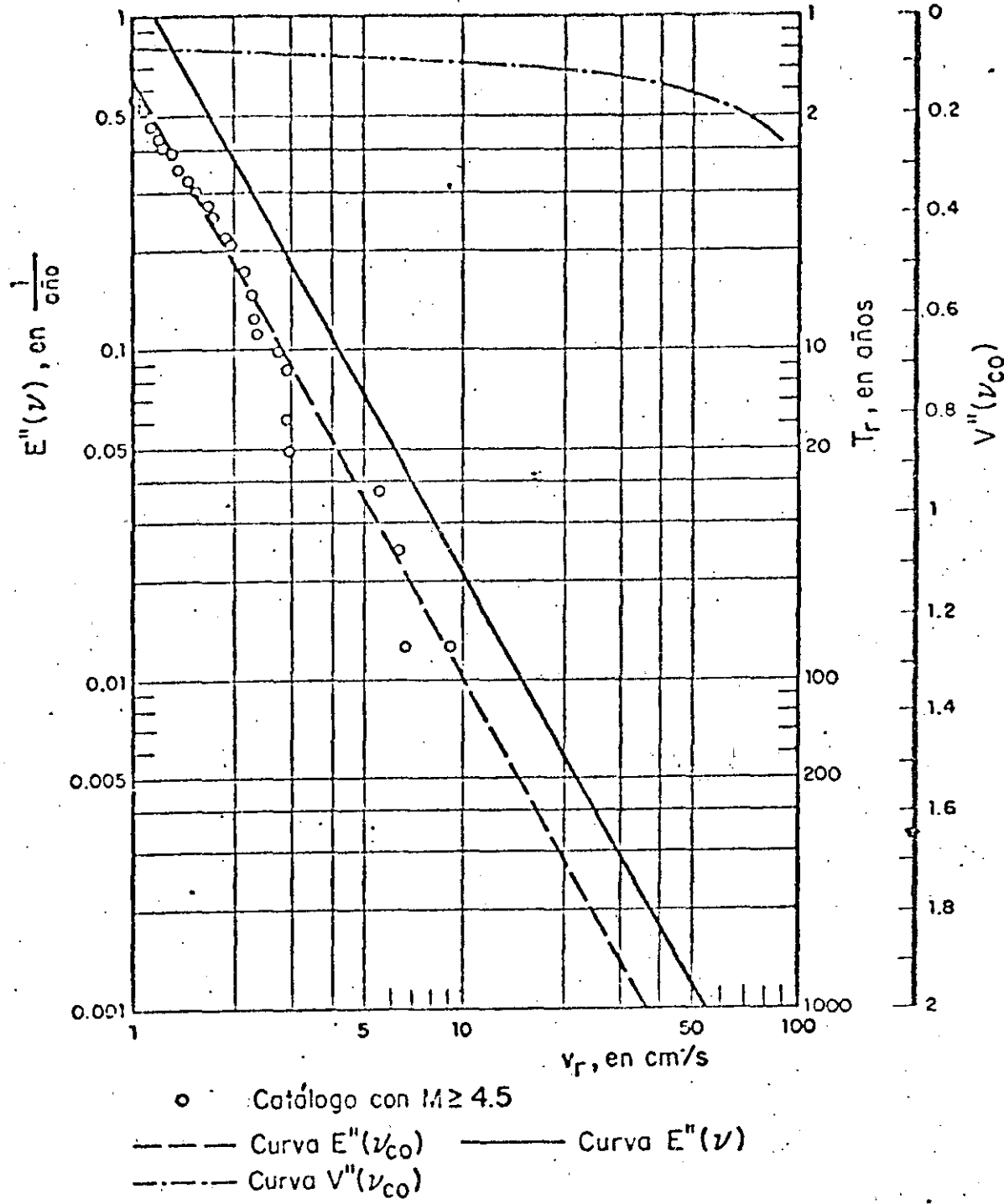


FIG 9 VALORES ESPERADOS A POSTERIOR DE LA TASA MEDIA DE EXCEDENCIA  $E''(v)$  (Y PERIODO DE RECURRENCIA,  $T_r$ ) VS VELOCIDAD MAXIMA DEL TERRENO  $v_r$  PARA UN SITIO EN EL ESTADO DE JALISCO

#### APENDICE A Teorema de Bayes

Si  $H_i$  ( $i = 1, n$ ) representa un conjunto de hipótesis mutuamente excluyentes y colectivamente exhaustivas sobre un fenómeno parcialmente conocido y  $A$  es una observación del fenómeno, el teorema de Bayes se puede expresar como (ref-A1)

$$P(H_i/A) = P(H_i) P(A/H_i) / \sum_{j=1}^n P(H_j) P(A/H_j) \quad (A1)$$

donde  $P(a/b)$  significa la probabilidad de  $a$  dado  $b$ ;  $P(H_i/A)$  es la probabilidad a posteriori de que  $H_i$  es verdadero dado que se observa  $A$ ;  $P(H_i)$  es la probabilidad inicial de  $H_i$  asignada antes de observar  $A$  y  $P(A/H_i)$  es la probabilidad de  $A$  si  $H_i$  es verdadera. El término en el denominador del segundo miembro de la ec (A1) proporciona la constante normalizadora para que el primer miembro sea una probabilidad.

Para el caso que se tiene en el cap 3, se desea aplicar el teorema de Bayes para obtener la densidad de probabilidades a posteriori de  $Z$  (donde  $Z$  es el vector formado por los parámetros de la sismicidad regional  $v_{CO}(y)$ ) dado que se han observado  $N$  temblores con intensidades  $Y_N$  durante el lapso  $t$ ,

A1. Raiffa, H. and Schlaifer R., "Applied Statistical Decision Theory" MIT Press (1968)

A2. Benjamin, J R and Cornell, C A., "Probability, Statistics and Decisions for Civil Engineers", McGraw Hill (1970)

es decir el primer miembro de la ec A1 se asocia a  $f_Z''(Z/Y_N;t)$  de la ec 9.

El término  $P(H_i)$  de la ec (A1) corresponde a la densidad de probabilidades inicial (supuesta) de  $Z_i$  representado por  $f_Z'(Z)$  en la ec (9).

El término  $P(A/H_i)$  de la ec (A1) es la probabilidad de que ocurran las intensidades  $Y_N$ , en caso de que los parámetros que definen la sismicidad regional,  $(v_{20}(y))$ , sean precisamente los que se asignaron inicialmente a  $Z$ . Se puede demostrar (ref A2) que esta probabilidad es proporcional a la función  $L(Y_N;t/Z)$  de la ec (9).

El término en el denominador del segundo miembro de la ec (A1) se omitió en la expresión 9, por lo cual en lugar del símbolo de igualdad de la ec A1 se tiene el de proporcionalidad.

#### APENDICE B Deducción de la ec 4.11

La función de verosimilitud que se requiere es la probabilidad de que en una región específica durante un lapso  $t$  ocurran  $N$  temblores con intensidades  $y_i$  mayores o iguales a una intensidad  $y_0$ , tales que  $n_1$  temblores corresponden al intervalo  $\Delta y_1$  de intensidades,  $n_2$  al intervalo  $\Delta y_2$ , ...,  $n_k$  al intervalo  $\Delta y_k$ . Lo anterior puede escribirse como  $P(Y_N; t|N)$ .

$$P(Y_N; t|N) = P(n_1, n_2, \dots, n_k | N) P(N, t) \quad (B1)$$

De acuerdo a la hipótesis de que la ocurrencia de temblores en la región de interés constituye un proceso de Poisson, se sigue que la intensidad  $y_i$  asociada a cada temblor es independiente de la historia previa, por lo cual la distribución conjunta de  $n_1, n_2, \dots, n_k$  dado  $n$  es multinomial (ref B1)

$$P(n_1, n_2, \dots, n_k | N) = N! \prod_{i=1}^k \frac{P_i^{n_i}}{n_i!} \quad (B2)$$

en la ec (B2)  $P_i$  es la probabilidad de que cada vez que ocurre un temblor en la región de interés su intensidad  $y_i$  se encuentre en el intervalo  $\Delta y_i$ . Si los  $\Delta y_i$  son muy pequeños, los  $n_i$  adoptarán valores cero o uno, por lo cual  $n_i! = 1$ . Sustituyendo este último valor en la ec (B2) conduce a

$$P(n_1, n_2, \dots, n_N | N) = N! \prod_{i=1}^N P_i \quad (B3)$$

en la cual

$$P_i = f_Y(y_i) dy_i \quad (B4)$$

el término  $f_Y(y_i)$  de la ec (B4) es la ordenada de la función de densidad de probabilidad de las intensidades para un temblor cualquiera valuada en  $y_i$  y  $dy_i$  es el intervalo infinitesimal en que se encuentra  $y_i$ . La función de densidad mencionada puede obtenerse a partir de la tasa de excedencia de las intensidades observadas  $v_{co}(y_i)$ , de acuerdo a la expresión siguiente.

$$f_Y(y_i) = \frac{1}{v_{co}(y_0)} \left. \frac{\partial v_{co}(y)}{\partial y} \right|_{y=y_i} \quad (B5)$$

$$= v'_{co}(y_i) / v_{co}(y_0)$$

sustituyendo la ec (B5) en la ec (B4) y esta última en la ec (B3)

$$P(n_1, n_2, \dots, n_N | N) = N! \prod_{i=1}^N (v'_{co}(y_i) / v_{co}(y_0)) \quad (B6)$$

donde  $y_0$  es la intensidad mínima del catálogo de intensidades observadas,  $v_{co}(y_0)$  es la  $v_{co}$  (ec 8) correspondiente a  $y_0$ , el término  $v'_{co}(y_i)$  es la derivada de  $v_{co}$  con respecto a  $y$  valuada para la intensidad  $y_i$ .

Utilizando de nueva cuenta la hipótesis de Poisson sobre la ocurrencia de temblores en la región de interés, la probabilidad,  $P(N, t)$ , de que durante un lapso  $t$  ocurran  $N$  temblores con tasa media de excedencia  $v_{co}(y_0)$  se puede valuar con la expresión siguiente (ref B1)

$$P(N, t) = e^{-v_{co}(y_0)t} (v_{co}(y_0)t)^N / N! \quad (B7)$$

Sustituyendo las ecs B6 y B7 en la ec B1 se obtiene la ec B8

$$P(Y_N; t | N) = t^N e^{-v_{co}(y_0) t} \prod_{i=1}^N v_{co}(y_i) \quad 45 \quad (B8)$$

Se puede demostrar (ref 6) que

$$L(Y_N; t | Z) \propto P(Y_N; t | N) \quad (B9)$$

y si se obtiene el Ln de ambos miembros de (B9)

$$L(Y_N; t | Z) \propto -v_{co}(y_0) t + \sum_{i=1}^N \ln v_{co}(y_i)$$



**DIVISION DE EDUCACION CONTINUA  
FACULTAD DE INGENIERIA U.N.A.M.**

ANALISIS DE RIESGO SISMICO

MODELOS DE RIESGO SISMICO

PARTE 2. ESTIMACION NO BAYESIANA Y EJEMPLO DE APLICACION  
ESTUDIOS COSTO - BENEFICIO

DR. MARIO CHAVEZ

JULIO, 1985

X CURSO INTERNACIONAL DE INGENIERIA SISMICA

MODELOS DE RIESGO SISMICO

PARTE II.- ESTIMACION NO BAYESIANA Y EJEMPLO  
DE APLICACION - ESTUDIOS COSTO -  
BENEFICIO

Mario Chávez\*

\* Investigador, Instituto de Ingeniería, UNAM

1.	INTRODUCCION	2
2.	GEOLOGIA, TECTONICA Y SISMICIDAD DE LA REGION	5
	2.1 Geología	5
	2.2 Tectónica	5
	2.3 Sismicidad	6
3.	MODELO DE RIESGO SISMICO	8
	3.1 Sismicidad regional y local	8
	3.2 Leyes de atenuación	10
	3.3 Corrección por incompletéz del catálogo	11
	3.4 Corrección por incertidumbre en las leyes de atenuación	15
4.	RIESGO SISMICO EN LA PLANTA GEOTERMICA DE CERRO PRIETO	17
	4.1 Información para el sitio	17
	4.2 Riesgo sísmico en el sitio de interés	18
5.	ESPECTROS DE DISEÑO	20
	5.1 Espectros de diseño para terreno firme	21
	5.2 Espectros de diseño para terrenos intermedio y blando	25
6.	REFERENCIAS	28

TABLAS  
FIGURAS

## 1. INTRODUCCION

El objeto de este trabajo es la determinación de *espectros de diseño sísmico* para diversos tipos de terreno en la Planta Geotérmica de Cerro Prieto, B.C. Este sitio se localiza en la vecindad de la ciudad de Mexicali, B.C., y sus coordenadas geográficas son  $32^{\circ}24'$  de latitud norte y  $115^{\circ}14'$  de longitud oeste, fig 1.

Los espectros de diseño sísmico son gráficas que relacionan las envolventes de las respuestas máximas esperadas de sistemas estructurales sencillos (idealizados como de un grado de libertad) sujetos a diferentes temblores con los periodos naturales de vibración de dichos sistemas. A partir de los mencionados espectros es posible estimar las sollicitaciones sísmicas para las cuales se debe diseñar una estructura localizada en una zona sísmica, tal como el sitio donde se localiza la Planta Geotérmica de Cerro Prieto (PGCP).

Los criterios de diseño que se propongan deben tener por objetivo optimizar las estructuras, es decir, conducir a sistemas estructurales en los cuales la utilidad obtenida de su ejecución sea máxima. La determinación de la estructura óptima se puede lograr a través de estudios costo-beneficio que incluyan explícitamente los siguientes parámetros: los beneficios esperados de su construcción, los costos esperados de las posibles fallas, los costos

iniciales de diseñar y construir, así como las probabilidades de ocurrencia (e intensidades máximas) de las sollicitaciones.

Aunque se cuenta con las herramientas necesarias para efectuar los estudios costo-beneficio citados arriba (ref 1) su aplicación práctica se ve a veces limitada por las dificultades asociadas con la estimación de las consecuencias de falla o utilidades de la operación de las estructuras proyectadas. Por ello la determinación de la estructura óptima ante sollicitación sísmica se llevará a cabo siguiendo el criterio propuesto en la ref 1, el cual se basa en la comparación de las intensidades esperadas de diseño (aceleraciones, velocidades, etc)., en dos sitios diferentes, para un mismo periodo de recurrencia. Este parámetro se define como el recíproco de la tasa media de excedencia de una intensidad dada durante un lapso previamente definido.

Como no se cuenta con un número suficiente de registros del movimiento del terreno en el sitio de interés, ni de información suficiente sobre las características sismotectónicas de las fallas cercanas al sitio, la determinación de los espectros de diseño se efectuará a partir de la información estadística (catálogo) sobre las magnitudes y las coordenadas focales de temblores generados cerca del sitio de interés durante este siglo.

Con la información anterior y utilizando leyes de atenuación (relaciones magnitud-distancia-intensidad) previamente propuestas en la ref 2 se obtienen expresiones que relacionan aceleraciones y velocidades máximas del terreno con tasas de excedencia (periodos de recurrencia).

Las expresiones mencionadas se corrigen para tomar en cuenta las incertidumbres asociadas con las intensidades reales en comparación con las calculadas a través de las leyes de atenuación, así como las incertidumbres relacionadas con el uso de un catálogo que no incluye todos los eventos que pudieran producir intensidades importantes en el sitio de interés. Lo descrito en los párrafos anteriores se tratará con detalle en el cap 3.

Los espectros de diseño para diversos periodos de recurrencia se obtienen a partir de las intensidades máximas del terreno. El espectro de diseño propuesto se selecciona siguiendo las recomendaciones de la ref 1, tal como se indica en el cap 5.

## 2. GEOLOGIA, TECTONICA Y SISMICIDAD DE LA REGION

### 2.1 Geología

La PGCP se localiza en el Valle de Mexicali (fig 1) el cual forma parte de la provincia geológica llamada del Golfo de California o depresión de Salton (ref 3). Estructuralmente está formado por grabens (depresiones) llenados por aluviones y horsts (levantamientos) de rocas paleozoicas formadas antes de la actividad tectónica (ref 3).

La litología de la región de interés corresponde a la del delta del Río Colorado (refs 3 y 4) y está formada por arenisca, arcillas y lutitas depositadas cíclicamente. Dichos sedimentos se encuentran cubiertos por aluvión de la Sierra Cucapa y áreas adyacentes (ref 3). La distribución horizontal de los sedimentos deltaicos es desconocida debido a la irregularidad horizontal en que se han depositado los sedimentos mencionados.

### 2.2 Tectónica

La estructura tectónica de la región ha sido descrita por un arreglo simple

de fallas transformadas y centros de dispersión que se caracterizan por generar enjambres de temblores, actividad volcánica reciente, áreas geotérmicas y depresiones topográficas submarinas (ref 5, 6).

Entre las fallas principales que se localizan en el Valle de Mexicali se pueden mencionar a las siguientes: Imperial, Cerro Prieto, Elsinore (también llamada Laguna Salada). Otras fallas en la zona son las de Agua Blanca, San Miguel, de Sierra Juárez (refs 5, 6). Recientemente se ha localizado un sistema de fallas secundario denominado Volcano en la zona donde se encuentra la PGCP (ref 4). Estas últimas fallas se asocian al movimiento lateral derecho de las fallas Imperial y Cerro Prieto (ref 7).

Una característica de la mayoría de las fallas mencionadas en los párrafos anteriores es que solo se conocen parcialmente sus dimensiones (ref 8, 9).

### 2.3 Sismicidad

En la ref 5 se reportó que la actividad sísmica de la región de interés se concentró en las fallas Imperial, Cerro Prieto, Sierra Juárez y San Miguel.

En particular se observaron temblores cuyos epicentros se alinearon con las fallas Imperial y Cerro Prieto. Estudios posteriores realizados entre 1974 y 1975 mencionados en la ref 10 mostraron actividad sísmica asociada a la falla Cerro Prieto únicamente.

Otros estudios de la sismicidad en la región donde se localiza la PGCP (ref 10) mostraron que la mayoría de los eventos identificados se concentraron en el extremo noroeste de la falla Cerro Prieto y el sureste de la falla Imperial.

Desde el punto de vista ingenieril recientemente ocurrieron temblores que causaron daños a estructuras; estos temblores fueron los de octubre 15 de 1979 y junio 9 de 1980. El primero tuvo una magnitud de 5.6 (magnitud de ondas de cuerpo) y aceleraciones máximas de hasta  $500 \text{ cm/seg}^2$  (ref 11). Su

epicentro se localizó cerca de la ciudad de Mexicali (ref 12).

El segundo temblor ocurrió el 8 de junio de 1980 con una magnitud local de 6.7 y aceleraciones máximas del terreno de hasta 663 (cm/seg<sup>2</sup>). Su epicentro se localizó cerca de la falla de Cerro Prieto; las coordenadas fueron 32.213° N y 115.028°W (refs 13 y 14). En la ref 13 se describen los daños observados en diversas estructuras en la región afectada. También se describen en la ref (14) los efectos de los mencionados temblores en el terreno, entre los que destaca la formación de pequeños "volcanes" de arena muy fina y agua con elevaciones de hasta 40 cm sobre el nivel original del terreno, lo cual indica que las capas de suelo superficiales en la región de interés son susceptibles de licuarse. Este efecto de licuación puede ser peligroso para estructuras que se desplanten en terrenos susceptibles a tal fenómeno, dado que al fallar el suelo existe el peligro de colapso total o parcial de las estructuras. Por lo anterior se recomienda identificar las formaciones para las que haya sospechas sobre potencial de licuación y efectuar estudios detallados específicos para decidir sobre uso del suelo, es decir, sobre sitios en donde pueden desplantarse estructuras y en donde debe impedirse la construcción.

### 3. MODELO DE RIESGO SISMICO

#### 3.1 *Sismicidad regional y local*

La sismicidad regional,  $v$ , en un sitio determinado, o sea el efecto que producen los temblores que ocurren en la región vecina al sitio, depende principalmente de la contribución que a la misma hacen los volúmenes de la corteza terrestre alrededor de dicho sitio. Dada la atenuación de la intensidad con la distancia, solamente los volúmenes localizados a algunos cientos de kilómetros del sitio contribuyen en forma importante a esa sismicidad.

Los volúmenes citados se designan como fuentes sísmicas y se caracterizan por las incertidumbres asociadas a la frecuencia de ocurrencia y las magnitudes de los temblores que generan. Se denomina sismicidad local al proceso de ocurrencia de temblores de diversas magnitudes en una fuente sísmica.

De los párrafos anteriores se puede concluir que la sismicidad regional para un sitio puede estimarse a partir de las sismicidades locales de las fuentes sísmicas correspondientes.

La sismicidad local asociada a una fuente sísmica determinada puede estimarse utilizando un modelo del proceso estocástico (aleatorio) de la ocurrencia de temblores de diversas magnitudes en dicha fuente. Si se adopta una forma para el proceso, la sismicidad local podría calcularse una vez que se estimen los parámetros que definen a dicho proceso.

Como se mencionó en el cap 2, la información sobre las características sismotectónicas de la zona vecina al sitio no es suficiente como para definir varias fuentes sísmicas, por lo cual se calculará la sismicidad en el sitio de interés a partir de las intensidades calculadas de los temblores con focos contenidos en un prisma de  $12 \times 12$  grados de longitud y latitud, con centro en el sitio y profundidad de varias decenas de kilómetros. Para estos fines, la sismicidad se definirá en términos de la tasa media de excedencia de cada intensidad por unidad de tiempo. En forma aproximada la sismicidad de un sitio puede expresarse mediante una expresión de la forma

$$v_j(y) = \alpha_j (y^{-r_j} - y_{j \text{ máx}}^{-r_j}) \quad y \leq y_{j \text{ máx}} \quad (1)$$

$$v_j = 0 \quad y > y_{j \text{ máx}}$$

$$j = a, v$$

En la ec 1  $v_j(y)$  es el número medio anual de temblores con intensidades mayores que  $y$  registrados en el sitio de interés y generados por las fuentes sísmicas vecinas al sitio,  $\alpha_j$ ,  $r_j$  y  $y_{j \text{ máx}}$  son los parámetros del proceso, los cuales deben estimarse a partir de los datos estadísticos, y de las características sismotectónicas de las fuentes vecinas; y son las intensidades máximas del terreno (aceleración,  $a$ , y velocidad,  $v$ ) que pueden calcularse a partir de las leyes de atenuación que se presentan en 3.2

Los valores de  $v$  obtenidos en términos de los datos estadísticos sobre intensidades calculadas (a partir de magnitudes y distancias) con las leyes de atenuación de 3.2 deben corregirse para tomar en cuenta las incertidumbres derivadas de la utilización de dichas leyes, así como las incertidumbres relacionadas con el catálogo de temblores empleado. Este no incluye todos

los eventos que pudieran generar intensidades del terreno importantes (desde el punto de vista de diseño) en el sitio. Las correcciones mencionadas se tratan en 3.4 y 3.3 respectivamente.

### 3.2 Leyes de atenuación

Las leyes de atenuación son expresiones semiempíricas que relacionan magnitud-distancia-intensidad (aceleraciones, velocidades y desplazamientos máximos) de temblores en terreno firme. Dichas expresiones pueden obtenerse a partir de los datos que existen sobre los parámetros mencionados. En general, los procedimientos utilizados para obtener las leyes de atenuación consisten en ajustar curvas a los datos de eventos ocurridos en diferentes regiones, por lo cual las expresiones así obtenidas reflejan las características geotectónicas de la región para la cual fueran obtenidas (ref 15).

En este trabajo se usarán las leyes de atenuación propuestas en la ref 2, las cuales fueron obtenidas a partir de la información correspondiente a temblores ocurridos en terreno firme de la costa oeste de los Estados Unidos y de la República Mexicana. La elección de dichas leyes de atenuación se justifica dado que la región de interés (ver cap 2) se localiza cerca de la zona de los Estados Unidos mencionada arriba. Las expresiones propuestas en la ref 2 para estimar la aceleración  $a$ , y la velocidad,  $v$ , máximas del terreno asociadas a un temblor son:

$$a = 5600 e^{0.8 M} (R + 40)^{-2} \quad \text{en (cm/seg}^2\text{)} \quad (2)$$

$$v = 32 e^M (R + 25)^{-1.7} \quad \text{en (cm/seg)} \quad (3)$$

donde  $M$  y  $R$ , la magnitud y la distancia del sitio de interés al foco del temblor se obtienen del catálogo de eventos para la región de interés.

En la ref 2 se efectuó un análisis estadístico de los errores de predicción asociados a las expresiones 2 y 3. De ese estudio se determinó que los logaritmos naturales de los cocientes de las intensidades ( $a$  o  $v$ ) predichas

a las registradas instrumentalmente tienen distribución normal.

Los parámetros de las mencionadas distribuciones fueron: para la aceleración máxima del terreno, media igual a 0.04 y desviación estándar igual a 0.64; para la velocidad máxima del terreno, media igual a 0.124 y desviación estándar igual a 0.74.

### 3.3 Corrección por incompletez del catalogo

Como se mencionó en 3.2 la sismicidad en un sitio puede estimarse a partir de la información estadística sobre las magnitudes, coordenadas y profundidades focales de los temblores ocurridos en las fuentes sísmicas vecinas. Esta información se utiliza en combinación con las leyes de atenuación (ecs 2 y 3) para evaluar las intensidades máximas del terreno en el sitio de interés. Sustituyendo estas intensidades en la ec 1 es posible evaluar la sismicidad en el sitio,  $v_e$ , asociada a la información estadística utilizada.

Generalmente los catálogos de temblores que contienen la información mencionada en el parrafo anterior están incompletos; es decir, no incluyen todos los eventos que pudieran generar intensidades máximas del terreno capaces de producir daños en las estructuras que se construyan en el sitio de interés. Esto proviene de que sólo contienen información completa para magnitudes por encima de un cierto límite inferior y por lo tanto emplear estos catálogos sin corrección equivale a ignorar la contribución al riesgo de los temblores muy pequeños pero frecuentes, que pueden ocurrir a distancias muy cortas. Debido a lo anterior resulta necesario introducir un factor de corrección,  $f_c$ , por el cual deberá multiplicarse la sismicidad  $v_e$  obtenida a partir del catálogo; al valor corregido de  $v$  se le designará por  $v_i$ .

Como se verá más adelante,  $f_c$  depende de los parámetros de la sismicidad local, de los parámetros de las leyes de atenuación y de las intensidades máximas calculadas con esas leyes.

Para fines de obtener el factor correctivo  $f_c$ , la sismicidad local  $\lambda$  aso-

ciada a una fuente sísmica se estimará con la expresión siguiente (ref 15):

$$\lambda(M) = \alpha e^{-\beta M} \quad (4)$$

donde  $\lambda(M)$  es la tasa de excedencia de la magnitud  $M$  por unidad de volumen y por unidad de tiempo, y  $\alpha$  y  $\beta$  son parámetros que dependen de las características sismotectónicas de la fuente sísmica considerada.

Dado que interesa evaluar la sismicidad en términos de las intensidades máximas en el sitio, se deberá expresar la ec.4 en términos de esas intensidades, para lo cual se utilizarán las ecs. 2 y 3. Estas últimas pueden representarse por

$$y = b_1 e^{b_2 M} (R + R_0)^{-b_3} \quad (5)$$

donde  $y$  es la intensidad calculada (aceleración o velocidad) asociada a  $M$ ,  $R_0$  y  $b_i$  ( $i = 1,2,3$ ) son los parámetros de las ecs mencionadas y  $R$  fue previamente definido. Despejando  $M$  en la ec (5) y sustituyendo en la ec 4 se obtiene

$$\lambda(M(y,R)) = \alpha \gamma y^{-r} (R + R_0)^{-s} \quad (6)$$

donde  $\gamma = b_1^r$ ,  $r = \beta/b_2$ ,  $s = \beta b_3/b_2$ .

La sismicidad regional  $v$  puede evaluarse con la expresión siguiente (ref 15)

$$v(y) = \int_V \lambda(M(y,R)) dv \quad (7)$$

donde la integral con respecto al volumen incluye todas las fuentes sísmicas que contribuyen a la sismicidad en el sitio de interés.

Para calcular el factor  $f_c$  partiremos de lo siguiente: supongamos que para una región se tiene un catálogo (para un lapso dado) que se considera confiable para temblores con magnitudes mayores a una magnitud seleccionada, digamos  $M_0$ . La sismicidad total en el sitio de interés,  $v_t(y)$ , o sea la

correspondiente a todos los eventos ocurridos en la región, puede obtenerse como la suma de las sismicidades producidas por los temblores con magnitudes menores o iguales que  $M_0$  y los mayores que dicho valor; a estas dos componentes las llamaremos  $v_1(y)$  y  $v_2(y)$  respectivamente; es decir,

$$v_t(y) = v_1(y) + v_2(y) \quad (8)$$

El factor  $f_c$  es función de la intensidad  $y$ , y se obtiene como el cociente de la sismicidad total que resulta de integrar la ec 7 para un volumen ilimitado, con  $\lambda$  dado por la ec 6, entre la que se obtiene cuando al integrar la ec 7 para un volumen ilimitado se toma  $\lambda$  dado por la ec 6 para  $M > M_0$  e igual a  $\lambda(M_0)$  para  $M \leq M_0$ ; es decir,

$$f_c(y) = \frac{v(y)}{v_2(y)} \quad (9)$$

en donde  $v(y)$  está dada por la ec 7 y  $v_2(y)$  se obtiene como sigue:

$$v_2(y) = \int_{R \leq R^*} \lambda(M_0) dV + \int_{R > R^*} \alpha e^{-\beta M(y,R)} dV \quad (10)$$

En esta ecuación,  $R^*$  es la distancia a la que un temblor con magnitud  $M_0$  produce una intensidad calculada igual a  $y$ , de acuerdo con la ec 5.

Para calcular  $v_t(y)$  se supondrá que la sismicidad es uniforme en un semi-espacio limitado por la superficie del terreno\*, por lo cual al combinar las expresiones (6) y (7) se obtiene

$$v_t(y) = \frac{-4 \alpha \gamma y^{-r} R_0^{(3-s)}}{(1-s)(2-s)(3-s)} \quad (11)$$

$$s > 3$$

\* Aunque esta hipótesis no sería la adecuada para evaluar  $v_t$ , se considera aceptable para la estimación de  $f_c$ .

La expresión para  $R^*$  se puede deducir de la ec 5,

$$R^* = (b_1 e^{b_2 M_0 / y})^{1/b_3} - R_0 \quad (12)$$

donde todos los parámetros han sido previamente definidos.

Una vez que se tiene el valor de  $R^*$  se obtienen las integrales que aparecen en la ec 10:

$$v_2(y) = v_{21}(y) + v_{22}(y) \quad (13)$$

en donde

$$v_{21}(y) = \frac{2 \pi \alpha R^{*3} e^{-\beta M_0}}{3} \quad (14)$$

$$v_{22}(y) = -2 \pi \alpha \gamma y^{-r} \left\{ \frac{R^{*2} R_1 (1-s)}{(1-s)} - \frac{2R^* R_1 (2-s)}{(1-s)(2-s)} + \frac{2 R_1 (3-s)}{(1-s)(2-s)(3-s)} \right\} \quad (15)$$

$$s > 3$$

En la última ecuación,

$$R_1 = (R^* + R_0) \quad (16)$$

Al sustituir las ecs 11, 13, 14 y 15 en la ec 9 se obtiene:

$$f_c(y) = - \frac{2 \gamma y^{-r} R_0 (3-s)}{(1-s)(2-s)(3-s)}$$

$$\left\{ \frac{R^{*3} e^{-\beta M_0}}{3} - \gamma y^{-r} \left( \frac{R^{*2} R_1 (1-s)}{(1-s)} - \frac{2R^* R_1 (2-s)}{(1-s)(2-s)} + \frac{2R_1 (3-s)}{(1-s)(2-s)(3-s)} \right) \right\}^{-1} \quad (17)$$

$$s > 3$$

Finalmente, la sismicidad corregida por incompletez  $v_i(y)$ , asociada a la intensidad  $y$ , se obtiene como

$$v_i(y) = f_c(y) v_e(y) \quad (18)$$

### 3.4 Corrección por incertidumbre en las leyes de atenuación

En 3.2 se mencionó que los cocientes de las intensidades reales entre las predichas con las leyes de atenuación que se utilizan en este trabajo (ecs 2 y 3) tienen una distribución de probabilidades lognormal con medias y desviaciones estándar indicadas en esa sección. Para tomar en cuenta el efecto de las incertidumbres implícitas en las leyes de atenuación en la sismicidad calculada a partir de dichas leyes, en la ref 15 se propuso la siguiente expresión

$$v_c(y) = \int_{\alpha_u}^{\infty} v_p(y/u) f_e(u) du \quad (19)$$

donde  $v_c(y)$  es la sismicidad en el sitio asociada a la intensidad  $y$  corregida por incertidumbre en las leyes de atenuación,  $v_p(y/u)$  es la sismicidad en el sitio sin incluir dicha corrección,  $\alpha_u = y/y_{\text{máx}}$ , y  $f_e$  es la función de densidad de probabilidades del cociente de las intensidades reales entre las predichas con las leyes de atenuación.

En el caso que nos ocupa  $v_p(y/u)$  esta dada por la ec 18,  $f_e(u)$  es la función de densidad de probabilidades de la distribución lognormal y  $y_{\text{máx}}$  se definió en la sección 3.1. Combinando las ecs 18 y 19 se obtiene (ref 15):

$$v_c(y) = c_0 K_0 + c_1 K_1 y^{-r} \quad (20)$$

donde

$$c_0 = 1 - \Phi\left(\frac{\ln(y/y_{\text{máx}}) - m}{\sigma}\right)$$

$$K_0 = -\alpha y_{\text{máx}}^{-r}$$

$$c_1 = \exp(Q) \left\{ \frac{\ln(y/y_{\max}) - m - \sigma^2 r}{\sigma} \right\}$$

$$K_1 = \alpha$$

$$Q = \frac{1}{2} \sigma^2 r^2 + m r$$

$\alpha$ ,  $r$ ,  $y_{\max}$  son los parámetros de la ec 18

$m$ ,  $\sigma$  son la media y la desviación estandar de las leyes de atenuación (ecs 2 y 3)

$\Phi$  es la distribución de probabilidades normal éstandarizada acumulada

#### 4. RIESGO SISMICO EN LA PLANTA GEOTERMICA DE CERRO PRIETO

17

##### 4.1 *Información para el sitio*

La información de tipo estadístico sobre los temblores ocurridos en la fuente sísmica adoptada, que es un prisma de 12 x 12 grados de latitud y longitud con centro en el sitio de interés y algunas decenas de kilómetros de profundidad, provino de las refs 16, 17, 18, 19. De las refs 16 y 17 se generó un catálogo de temblores con magnitudes mayores o iguales a 4.5 para el periodo 1932 a 1980. De las refs 18 y 19 se obtuvieron dos catálogos, ambos para el lapso 1932 a 1974 y para magnitudes mayores o iguales a 5 y 6 respectivamente. En la fig 1 se muestran los epicentros y profundidades de los eventos con magnitudes mayores o iguales a 4.5.

Las intensidades  $y_j$  máx ( $j$  = aceleración, velocidad) es decir, las cotas superiores a las intensidades máximas esperadas del terreno en la región de interés, se estimaron a partir de las ecs 2 y 3 adoptando una magnitud de ondas de cuerpo máxima esperada  $M = 7.4$  y una distancia  $R = 15$  km. El valor de  $M$  fue seleccionado con base en las refs 20 y 21 y el valor de  $R$  se tomó como un valor característico de la región en cuestión (fig 1). Con

los valores de M y R mencionados se obtuvo;

$$a_{\text{m}\acute{\text{a}}\text{x}} = 690 \text{ (cm/seg}^2\text{)}$$

$$v_{\text{m}\acute{\text{a}}\text{x}} = 100 \text{ (cm/seg)}$$

El valor del parámetro  $\beta$  en la ec. 4 fue calculado a partir de la siguiente expresión (ref 22)

$$\beta = 2.3 b \quad (21)$$

donde  $b$  es un parámetro que depende de las características sismotectónicas de la región de interés (ref. 23). En este trabajo se tomó un valor de  $b = 0.87$  con base en las refs. 18 y 24, con lo cual se obtuvo un  $\beta = 2$ .

Finalmente los valores de  $m$  y  $\sigma$  utilizados en la ec. 20 son los mencionados en 3.2, es decir,  $m = 0.04$  y  $\sigma = 0.64$  para la aceleración máxima del terreno y  $m = 0.124$  y  $\sigma = 0.74$  para la velocidad máxima del terreno.

#### 4.2 Riesgo sísmico en el sitio de interés

El modelo de riesgo sísmico descrito en el cap. 3 fue aplicado utilizando la información sobre el sitio mencionado en 4.1. Los resultados obtenidos fueron los siguientes:

En las figs 2 y 3 se presentan los valores calculados de la tasa media de excedencia  $\nu$  (o su recíproco el periodo de recurrencia,  $T_r$ ) para las aceleraciones y velocidades máximas del terreno respectivamente. En ambas figs. se tienen los resultados para cada uno de los catálogos, así como las curvas de ajuste correspondientes. Dichas curvas tienen la forma de la ec. 1 con parámetros  $\alpha = 3600$ ,  $r = 2.23$  para aceleraciones máximas (fig 2) y  $\alpha = 150$ ,  $r = 2.82$  para velocidades máximas (fig 3). Los valores de  $\alpha$  y  $r$  se calcularon aplicando un criterio de mínimos cuadrados dándole mayor peso a las  $\nu$  asociadas a las intensidades medias,

En las figs 4 y 5 se presentan las curvas  $v$  versus aceleración y velocidad máxima del terreno obtenidas después de aplicar las correcciones por incompletez del catálogo y por incertidumbre en las leyes de atenuación respectivamente. Las curvas resultantes de la corrección por incompletez (llamadas la corrección en las figuras) tienen como parámetros  $\alpha = 75\,000$ ,  $r = 2.74$  para aceleraciones (fig 4) y  $\alpha = 200$ ,  $r = 2.9$  para velocidades (fig 5). Las curvas obtenidas de la corrección por incertidumbre en las leyes de atenuación (denominadas curvas finales en ambas figuras), proporcionan los valores esperados de las aceleraciones y velocidades máximas del terreno  $a_r$  y  $v_r$  para el sitio de interés para diferentes  $v$  y  $T_r$ . Por ejemplo, se tiene

$T_r$ (años)	$a_r$ (cm/seg <sup>2</sup> )	$v_r$ (cm/seg)
30	270	29
50	331	38
100	410	53

## 5. ESPECTROS DE DISEÑO

En el capítulo 1 se mencionó que los espectros de diseño para un sitio, es decir, las envolventes de las respuestas máximas esperadas de sistemas estructurales sencillos sujetos a diferentes temblores pueden obtenerse a partir de las intensidades máximas del terreno en el sitio. Dado que estas últimas dependen, entre otros factores, de las propiedades mecánicas de los materiales que forman los estratos superficiales (ref 25), en este trabajo se consideran tres tipos de terreno atendiendo a su rigidez. La clasificación propuesta es la siguiente: terreno firme, tal como tepetate, arenisca medianamente cementada, arcilla compacta; terreno intermedio, tal como arenas no cementadas, limos de mediana o alta compacidad, arcillas de mediana compacidad; terrenos compresibles, como arcillas blandas muy compresibles.

Para definir que tipo de terreno se tiene en un sitio específico se puede aplicar el siguiente criterio (ref 26):

- a) Se localizará el nivel del terreno firme, bajo el cual todos los suelos tengan módulos de rigidez mayores que  $5 \times 10^4$  ton/m<sup>2</sup>, o requieren mas de 50 golpes por cada 30 cm, en la prueba de penetración estándar.

b) Para estratos comprendidos entre el nivel del terreno firme y el nivel en que las aceleraciones horizontales del terreno se transmiten a la construcción se calculará la suma  $\sum H_i \sqrt{\gamma_i / G_i}$  donde

$H_i$  = espesor del  $i$ -ésimo estrato, en m

$\gamma_i$  = su peso volumétrico en  $\text{ton/m}^3$

$G_i$  = módulo de rigidez en  $\text{ton/m}^2$

Si la suma  $\sum H_i \sqrt{\gamma_i / G_i}$  es menor que 0.20, el terreno se considerará firme.

Si la suma  $\sum H_i \sqrt{\gamma_i / G_i}$  es mayor que 0.20, y menor que 0.45 el terreno se considerará intermedio.

A falta de información precisa, para la aplicación del criterio anterior puede tomarse para  $\gamma_i$  el valor de  $1.5 \text{ ton/m}^3$  y los valores de  $G_i$  pueden estimarse como  $G_i = 0.35 E_i$ , en que  $E_i$  es la pendiente inicial de la curva esfuerzo-deformación de una prueba de compresión simple.

Los terrenos cuyas propiedades se desconozcan se supondrán como terrenos compresibles.

Para la clasificación del tipo de terreno anterior se tomarán en cuenta todos los suelos que se encuentren debajo del nivel en que las aceleraciones horizontales se transmiten a la construcción; por ejemplo, en el caso de un cajón de cimentación este nivel correspondría al desplante de la losa inferior.

### 5.1 Espectros de diseño para terreno firme

El criterio que se seguirá en este trabajo para calcular espectros de diseño para terreno firme se apoya en las ref 1 y 27. Dicho criterio consiste en multiplicar la aceleración y la velocidad máxima del terreno en un sitio para un periodo de recurrencia dado,  $a_r$  y  $v_r$ , por los factores de amplificación  $f_a$  y  $f_v$  (que dependen del amortiguamiento) respectivamente (ref 1). Los valores resultantes, que se denominaran  $a^*$  y  $v^*$ , son respec-

tivamente las envolvente de los espectros de diseño de aceleraciones y velocidades para sistemas de un grado de libertad sujetos a diferentes temblores. Estos últimos son congruentes con la sismicidad del sitio de interés.

Dado que las leyes de atenuación utilizadas en este trabajo (cap 3) corresponden a terreno firme, los espectros de diseño obtenidos serán aplicables para estructuras que se apoyen en suelos de esas características.

Las ordenadas  $A_f$ , del espectro de diseño de aceleraciones para un periodo de recurrencia  $T_r$  se obtienen a partir de  $a_r$ ,  $a^*$  y  $v^*$  que ya se definieron, y  $T$ , que son los periodos naturales de los sistemas de un grado de libertad. De acuerdo con estos parámetros, las ordenadas  $A_f(T)$  se calculan así:

• Para  $T = 0$ ,  $A_f = a_r$

• Para  $0 < T < T^*$  (en donde  $T^* = 2\pi v^*/a^*$ ), se tienen dos casos:

a) Si  $a^*/Q > a_r$ ,  $A_f$  varía linealmente con  $T$  desde  $T = 0$  hasta  $T = 0.12$  en que adquiere el valor máximo  $a^*/Q$ , que se mantiene constante para  $0.12 < T \leq T^*$ .

b) Si  $a^*/Q < a_r$ ,  $A_f$  varía linealmente con  $T$  desde  $T = 0$  hasta  $T = T^*$ , en que adquiere el valor  $a^*/Q$ .

• Para  $T > T^*$ ,  $A_f = (a^*/Q)(T^*/T)^{1/2}$ .

En las expresiones anteriores,  $Q$  es el factor de ductilidad, definido para una sección, un miembro o una porción de una estructura con comportamiento elastoplástico, como el cociente de su deformación máxima entre su deformación de fluencia.  $Q$  caracteriza la capacidad de absorción de energía por comportamiento inelástico de una estructura. En diseño sísmico los valores de  $Q$  usados comúnmente son los siguientes: 1 para sistemas frágiles, 1.5 para mamposterías huccas reforzadas, 2 para mamposterías macizas confinadas y 4 para estructuras de marcos de concreto y acero. En la ref (28) se

proponen valores de  $Q$  para diversas condiciones de la estructuración y de los materiales utilizados.

Las figs 6 a 9 contienen espectros elásticos para amortiguamientos viscosos con valores 0.02 y 0.05 del crítico, respectivamente, para distintos tipos de terreno así como los correspondientes espectros reducidos por ductilidad de acuerdo con los criterios propuestos arriba para obtener  $A(T)$ . En las estructuras reales, la parte del amortiguamiento que se presenta para deformaciones pequeñas es muy inferior a los números que suelen citarse como representativos del amortiguamiento "viscoso" para distinto tipo de estructuras; es decir, la mayor parte del amortiguamiento que convencionalmente se asigna a cada tipo de estructura proviene en realidad de disipación de energía mediante comportamiento no lineal histerético. En las páginas que siguen se adopta el criterio de determinar los espectros de diseño sísmico en el sitio de interés mediante calibración con los que la experiencia ha considerado adecuados en otros sitios. En dichos espectros se adopta la convención de separar el amortiguamiento en una parte "viscosa" que no depende del tipo de estructura y en otra que se representa mediante la reducción por ductilidad; la parte viscosa se hace corresponder a 0.05 del crítico. Esta misma convención se adopta aquí; por lo tanto, en lo que sigue los espectros que se proponen para diseño deberán corresponder al amortiguamiento de 0.05 del crítico y al factor  $Q$  reductivo por ductilidad que se recomienda para cada tipo de estructura.

En las figs 6 a 8 se presentan los espectros de diseño aceleraciones para terreno firme en la PGCP. Dichos espectros resultaron de aplicar el criterio descrito en los párrafos anteriores a los datos del sitio de interés. Los valores de  $a_r$  y  $v_r$  utilizados corresponden a períodos de recurrencia  $T_r$  de 30, 50 y 100 años y aparecen tabulados al final del cap 4. Los valores de  $f_a$  y  $f_v$  empleados tomados de la ref 1 son, respectivamente 4.3 y 2.8 para amortiguamiento de 0.02, y 2.6 y 1.9 para amortiguamiento igual a 0.05 (ver tabla 1).

Como se mencionó en el cap 1, los criterios de diseño deben conducir a sistemas estructurales en los cuales la utilidad obtenida de su ejecución sea

máxima. También se comentó que la determinación de la estructura óptima requiere de estudios costo-beneficio. Dichos estudios permiten seleccionar de entre un conjunto de posibles soluciones, aquel proyecto que conduce al equilibrio óptimo entre la seguridad y el costo de la estructura. Dado que los parámetros necesarios para la aplicación directa de los estudios costo-beneficio y optimización son muy difíciles de evaluar, en la práctica suele acudir a criterios de calibración de diseño y seguridad. En este trabajo se utilizará el criterio de calibración propuesto en la ref 1, que consiste en determinar la intensidad de diseño en un sitio a partir de expresiones que relacionan los valores óptimos de diseño para estructuras de características similares en dos sitios con diferentes niveles de riesgo sísmico. Es decir, el criterio supone que se toman como base de comparación las intensidades de diseño en un sitio en donde dichas intensidades hayan sido establecidas a partir de estudios teóricos, experiencia y juicio ingenieril.

El criterio mencionado en el párrafo anterior se traduce en lo siguiente: para definir la intensidad de diseño  $Y_{D1}$  (o el periodo de recurrencia respectivo,  $T_{D1}$ ) de una estructura que se construirá en el sitio 1 se utiliza la expresión

$$Y_{D1}/Y_{D2} = T_{D1}/T_{D2} = \{a_{r1}/a_{r2}\}^{r/(r+1)} \quad (22)$$

la cual relaciona  $Y_{D1}$  con la intensidad de diseño  $Y_{D2}$  (o el periodo de recurrencia respectivo  $T_{D2}$ ) que se juzgue satisfactoria para construir una estructura análoga en el sitio 2.

En la ec 22  $a_{r1}$  y  $a_{r2}$  son las aceleraciones máximas del terreno en los sitios 1 y 2, asociadas a la misma tasa de excedencia (o periodo de recurrencia) y  $r$  es uno de los parámetros de la ec 1.

El criterio de optimización descrito en el párrafo anterior se aplicó con objeto de definir la intensidad de diseño utilizando los datos del sitio de interés, denominado sitio 1. Como sitio 2 se eligió el Distrito Federal para el cual se tiene toda la información que requiere la ec 22.

La tasa de excedencia seleccionada fue de 0.01 (o sea un periodo de recurren-

cia de 100 años); el valor de  $r$  para ambos sitios fue de 2.7, el cual es congruente en los resultados de esta investigación y la ref 1. Los valores  $a_{r1} = 410$  (cm/seg<sup>2</sup>) y  $a_{r2} = 100$  (cm/seg<sup>2</sup>) se obtuvieron de la tabla incluida al final del cap 4, y de la ref 1 respectivamente.

Sustituyendo los valores de  $a_{r1}$ ,  $a_{r2}$  y  $r$  en la ec 22 se obtiene  $Y_{D1} = 2.79 Y_{D2}$ . Si las intensidades de diseño  $Y_{D1}$  y  $Y_{D2}$  son las ordenadas máximas del espectro de aceleraciones para  $Q = 1$  y  $\xi = 0.05$ , el valor de  $Y_{D2}$  obtenido de la ref 28 es 210 cm/seg<sup>2</sup> y por tanto  $Y_{D1} = 587$  cm/seg<sup>2</sup>. Esta última intensidad corresponde aproximadamente a la ordenada máxima del espectro de diseño para un periodo de recurrencia de 17 años.

Dicho periodo de recurrencia es excesivamente corto de acuerdo con la práctica ordinaria teniendo en cuenta los factores de seguridad y métodos de análisis y diseño usuales (ref 28), por lo que se propone adoptar los espectros de diseño de la fig 6 que corresponden a un periodo de recurrencia de 30 años. Estos espectros deberán aplicarse en combinación con los factores de seguridad y criterios de análisis y diseño de la ref 28, que se acaba de mencionar.

## 5.2 *Espectros de diseño para terrenos intermedio y blando*

La determinación de los espectros de diseño para terrenos de baja rigidez se puede efectuar a partir de los espectros para terreno firme. El criterio que se seguirá para este propósito se basa en las ref 26 y 28. Dicho criterio consiste en multiplicar las ordenadas del espectro de diseño para terreno firme por factores de amplificación. Los valores de estos factores dependen de los periodos,  $T$ , de los sistemas estructurales considerados, como se verá más adelante.

El criterio mencionado se apoya en estudios analíticos sobre amplificación dinámica del movimiento del terreno debida a la presencia de mantos blandos, así como en los espectros de respuesta obtenidos a partir de acelerogramas registrados en México, D.F., durante sismos ocurridos en los últimos años. También incluye dicho criterio las incertidumbres asociadas con la determinación de los periodos naturales de vibración de las estructuras, las cuales provienen de la estimación de rigideces tangentes iniciales, así como de la influencia del com

portamiento no lineal y de la interacción suelo-estructura (ref 28 ).

El criterio de construcción de espectros de diseño para terrenos de baja rigidez en un sitio determinado a partir de los espectros para terreno firme se traduce en lo siguiente:

En terrenos de tipo intermedio las ordenadas del espectro correspondiente,  $A_i$ , se obtienen partiendo de las ordenadas  $A_f$  del espectro para terreno firme como sigue:

. Para  $T = 0$ ,  $A_i(T) = 1.6 A_f(T)$

. Para  $0 < T \leq 1.6$ , se tienen dos casos:

- a) si  $a_i^*/Q$  es mayor que  $A_i(0)$ , en donde  $a_i^* = 1.25 A_f(0.12)$ ,  $A_i$  varía linealmente con  $T$  desde  $T = 0$  hasta  $T = 0.20$ , en que adquiere el valor máximo  $a_i^*/Q$ , que se mantiene constante para  $0.20 < T \leq 1.6$ .
- b) si  $a_i^*/Q < A_i(0)$ ,  $A_i$  varía linealmente con  $T$  desde  $T = 0$  hasta  $T = 1.6$ , en que adquiere el valor  $a_i^*/Q$ .

. Para  $T > 1.6$ ,  $A_i = (a_i^*/Q) (1.6/T)^{2/3}$

En terrenos compresibles, las ordenadas de su espectro,  $A_c$ , se evalúan como sigue:

. Para  $T = 0$ ,  $A_c(T) = 2 A_f(T)$

. Para  $0 < T \leq 2.9$ , se tienen dos casos:

- a) si  $a_c^*/Q$  es mayor que  $A_c(0)$ , en donde  $a_c^* = 1.5 A_f(0.12)$ ,  $A_c$  varía linealmente con  $T$  desde  $T = 0$  hasta  $T = 0.30$ , en que adquiere el valor máximo  $a_c^*/Q$ , que se mantiene constante para  $0.30 < T \leq 2.9$ .
- b) si  $a_c^*/Q$  es menor o igual que  $A_c(0)$ ,  $A_c$  varía linealmente con  $T$  desde  $T = 0$

hasta  $T = 2.9$ , en que adquiere el valor  $a_c^*/Q$ .

Para  $T > 2.9$ ,  $A_c = (a_c^*/Q) (2.9/T)$

En la fig 9 se presentan los espectros de diseño de aceleraciones para terrenos intermedios y compresible en la PGCP. Dichos espectros resultaron de aplicar el criterio descrito en los párrafos anteriores al espectro de diseño propuesto para terreno firme que es para un periodo de recurrencia de 30 años, (que también se incluye en la fig 9) con un factor de ductilidad  $Q = 1$  y un porcentaje de amortiguamiento crítico  $\xi = 0.05$ . Los espectros de diseño para otros valores de  $Q$  y  $\xi$  se pueden calcular siguiendo los pasos señalados en los párrafos anteriores.

Los espectros de la fig 9 deberán aplicarse en combinación con los factores de seguridad y criterios de análisis y diseño de la ref 28.

## 6. REFERENCIAS

28

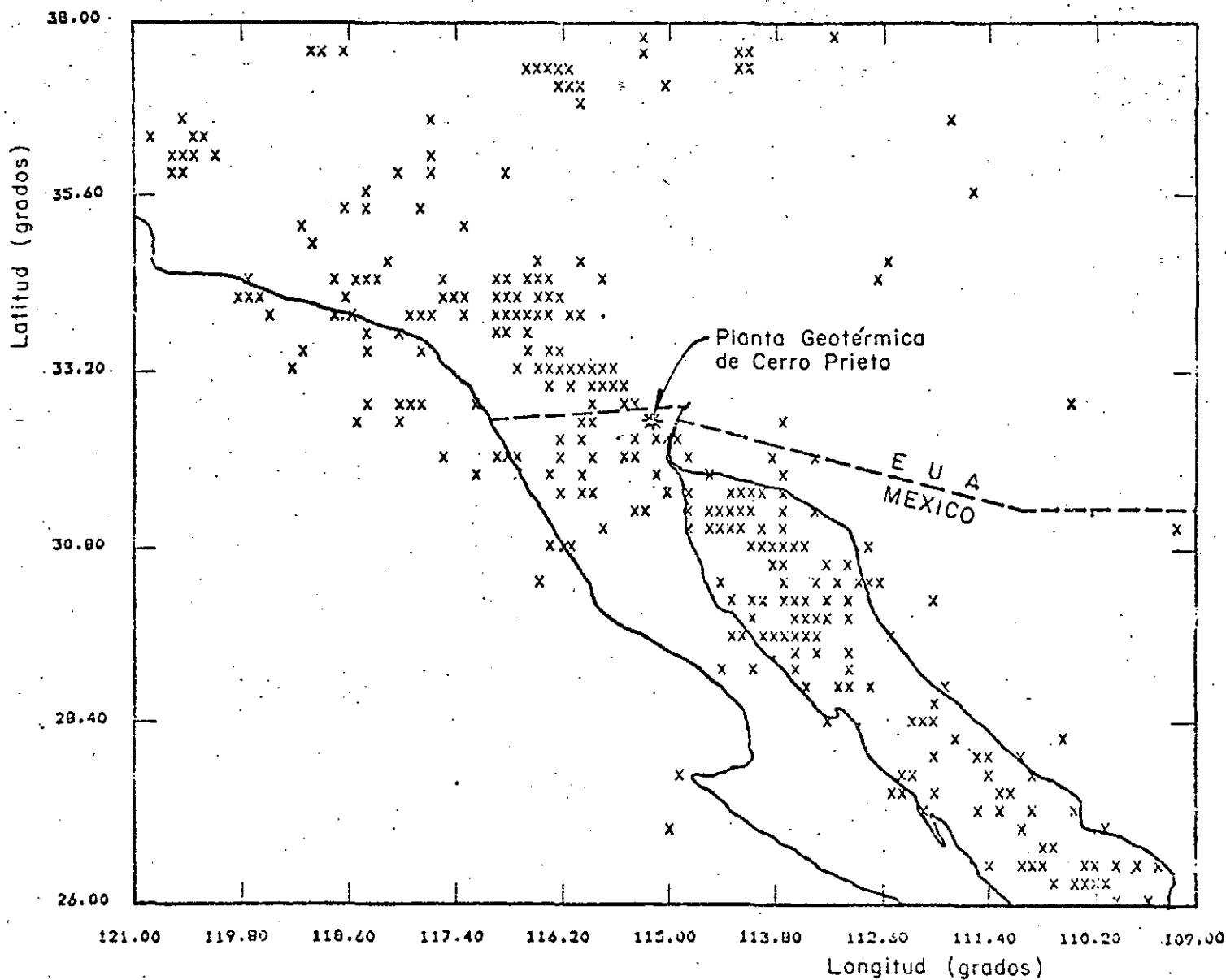
1. Esteva, L., "Regionalización sísmica de México para fines de ingeniería", Instituto de Ingeniería, UNAM, 246 (1970).
2. Esteva, L. y Villaverde R., "Seismic risk, design spectra and structural reliability". Proc. 5th World Conf. Earthquake Eng., Rome pp 2586-2597 (1973).
3. Suárez, Fco., "Sismicidad en el Golfo de California", Discusiones internas sobre labores de investigación y docencia, CICESE (1978).
4. De la Peña, A., Puente, I. y Díaz, F., "Modelo geológico del campo geotérmico de Cerro Prieto (1979).
5. Lomnitz, C. et al., "Sismicidad y tectónica de la región norte del Golfo de California", Geofísica Internacional, Vol 10, No 2 (1970)
6. Elders, W. A. et al., "Crustal spreading in Southern California", Science, Vol 178, No 4056 (1972).
7. Reyes, A., "Estudios sísmicos y su correlación con anomalías de potencial", First symposium on the Cerro Prieto Geothermal Field, Sn. Diego (1978).

8. Moore, D.G., Curray, J.R., Lawver L.A., "Tectonic and geologic history of the Gulf of California", CIBCASIO transactions, Vol III, La Jolla, Cal. (1977).
9. Suárez, Fco. y Reyes A., Comunicación personal (1981).
10. Albores A. et al., "Estudios de sismicidad en la región del campo geotérmico de Cerro Prieto", First symposium on the Cerro Prieto geothermal field, Sn. Diego (1978).
11. Mattiesen, R.B. and Porcella, R.L., "strong-motion data summary Imperial Valley earthquake of October 15, 1979 and aftershocks". Geological Survey Circular 818-C, Seismic Engineering Program Report, September-December (1979).
12. Bazán, E. y Muría, E., "El temblor de Mexicali, Octubre 15 de 1979. Daños en estructuras", Informe interno, Instituto de Ingeniería, UNAM (1980).
13. Reyes, A., "reporte preliminar del sismo Victoria, BCN del 8 de junio de 1980 ( $M_L = 6.7$ )", Informe Técnico GE080-02. Depto. de Geofísica CICESE (1980).
14. Mena, S.E. et al., "Sismo del Valle de Mexicali del 9 de junio de 1980. Primera parte: Daños observados y análisis preliminar de registros en acelerógrafos analógicos", Informe interno, Instituto de Ingeniería, UNAM (1980).
15. Esteva, L., "Seismicity", Capítulo 6 del libro Seismic Risk and Engineering Decisions, editado por Lomnitz C. y Rosenblueth E., Elsevier, Amsterdam (1976).
16. NOAA, U.S. Department of Commerce, "Earthquake data file summary", Boulder, Colorado (1977).
17. NOAA, U.S. Department of Commerce, "Preliminary Determination of Epicenters", Boulder, Colorado (1980).

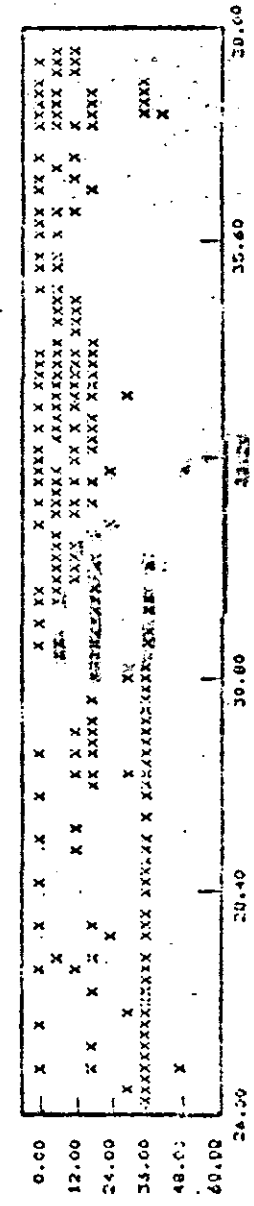
18. Hileman, J.A., Allen, C.R. and Nordquist, J.M., "Seismicity of the Southern California Region 7 January 1932 to 31 December 1972", Seismological Laboratory, California Institute of Technology (1973).
19. Friedman, M.E. et al., "Seismicity of the Southern California Region 1 January 1972 to 31 December 1974", Seismological Laboratory, California Institute of Technology (1976)
20. Brune, J. , Comunicación personal (1981)
21. Kanamori H., Comunicación personal (1981)
22. Cornell, C.A., "Engineering Seismic Risk Analysis", Bull. Seismol. Soc. Am. 58 (1968)
23. Gutenberg, B. and Richter, C.F., "Seismicity of the Earth", Princeton University Press, Princeton (1954)
24. Kallberg, K.T., "Seismic Risk in Southern California". Research Report R69-31, Dept. of Civil Engineering, MIT (1969)
25. Faccioli, E. y Reséndiz, D., "Soil Dynamics: Behaviour Including Liquefaction", Capítulo 4 del libro "Seismic Risk and Engineering Decisions", editado por Lomnitz C. y Rosenblueth, E., Elsevier, Amsterdam (1976)
26. Reglamento de Construcciones de SOP, título: Requisitos Estructurales, capítulo 10 "Análisis Sísmico", SAHOP (1976)
27. Applied Technology Council. San Francisco, California, "An Evaluation of a response Spectrum Approach to Seismic Design of Buildings", Center for Building Technology, Institute of Applied Technology, National Bureau of Standards, Washington, D.C. (1974)
28. Instituto de Ingeniería, UNAM, "Manual de diseño por sismo, según el reglamento de construcciones para el Distrito Federal", Informe No 406
29. Comisión Federal de Electricidad, "Manual de diseño de obras civiles", México D. F. (1969).

PERIODO DE RECURRENCIA	MOVIMIENTO DEL TERRENO		AMORTIGUAMIENTO	FACTORES DE AMPLIFICACION		ENVOLVENTES DE LOS ESPECTROS	
	$T_r$ (años)	$a_r$ (cm/seg <sup>2</sup> )	$v_r$ (cm/seg)	$\xi$	$f_a$	$f_v$	$a^*$ (cm/seg <sup>2</sup> )
30	270	29	0.02	4.3	2.8	1161	81
50	331	38	0.02	4.3	2.8	1423	106
100	410	53	0.02	4.3	2.8	1763	148
30	270	29	0.05	2.6	1.9	702	55
50	331	38	0.05	2.6	1.9	860	72
100	410	53	0.05	2.6	1.9	1066	101

TABLA 1 VALORES MAXIMOS DE ACELERACIONES Y VELOCIDADES DEL TERRENO Y SU RELACION CON LAS ENVOLVENTES  
 DE LOS ESPECTROS DE DISEÑO



a) Epicentros x



b) Profundidad (km)

Fig 1. Características de los temblores con magnitud  $M \geq 4.5$  ocurridos de 1932 a 1980 seleccionados en el presente estudio

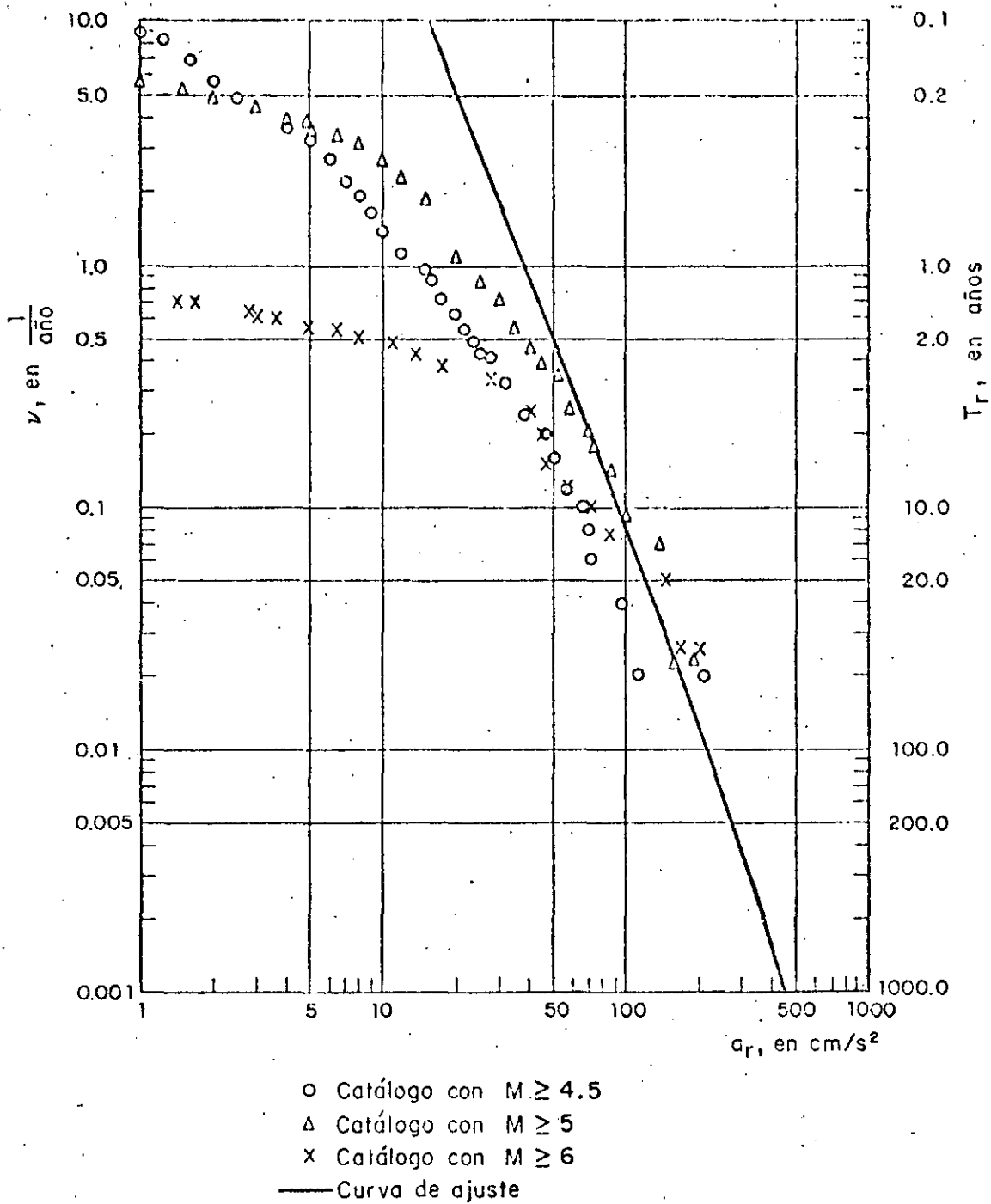


Fig 2. Curva de ajuste de las parejas de valores de la tasa media de excedencia  $\nu$  y aceleraciones máximas del terreno  $a_r$  obtenidas con datos de diversos catálogos, para Cerro Prieto B.C.

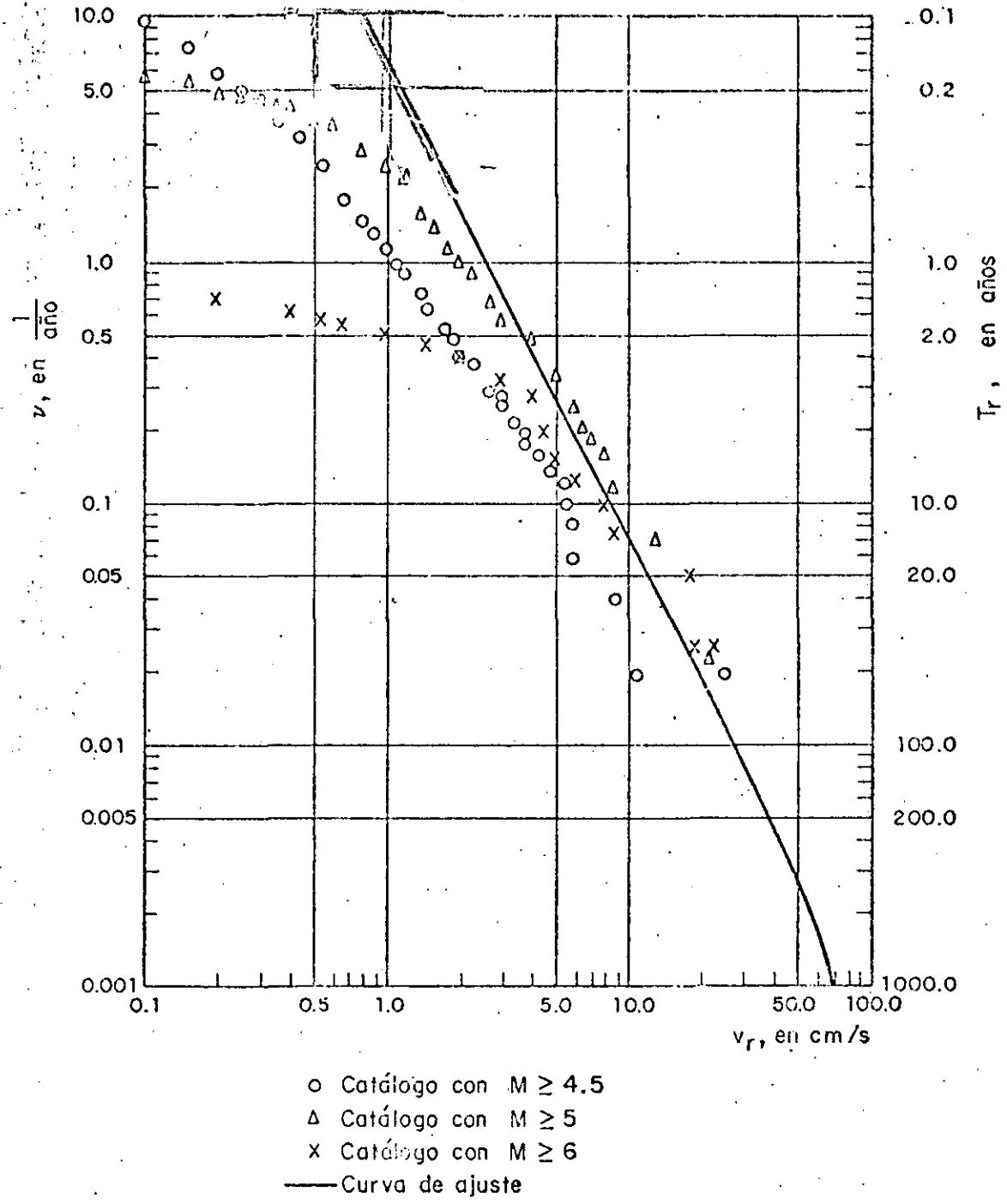


Fig 3. Curva de ajuste de las parejas de valores de la tasa media de excedencia  $\nu$  y velocidades máximas del terreno  $\nu_r$  obtenidas con datos de diversos catálogos, para Cerro Prieto B. C.

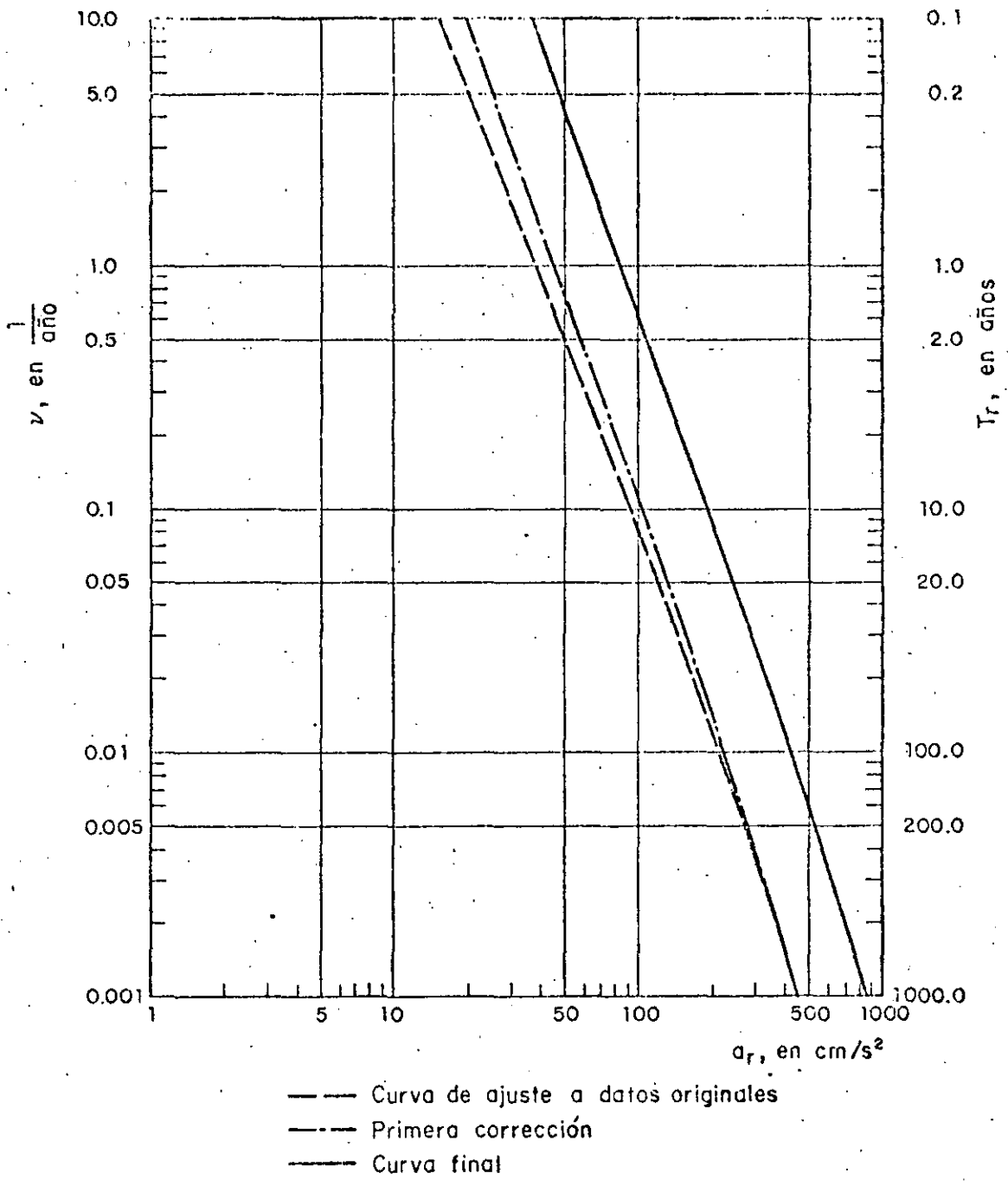


Fig 4. Tasa media de excedencia  $\nu$  (y periodo de recurrencia  $T_r$ ) vs aceleración máxima del terreno  $a_r$  para Cerro Prieto B. C.

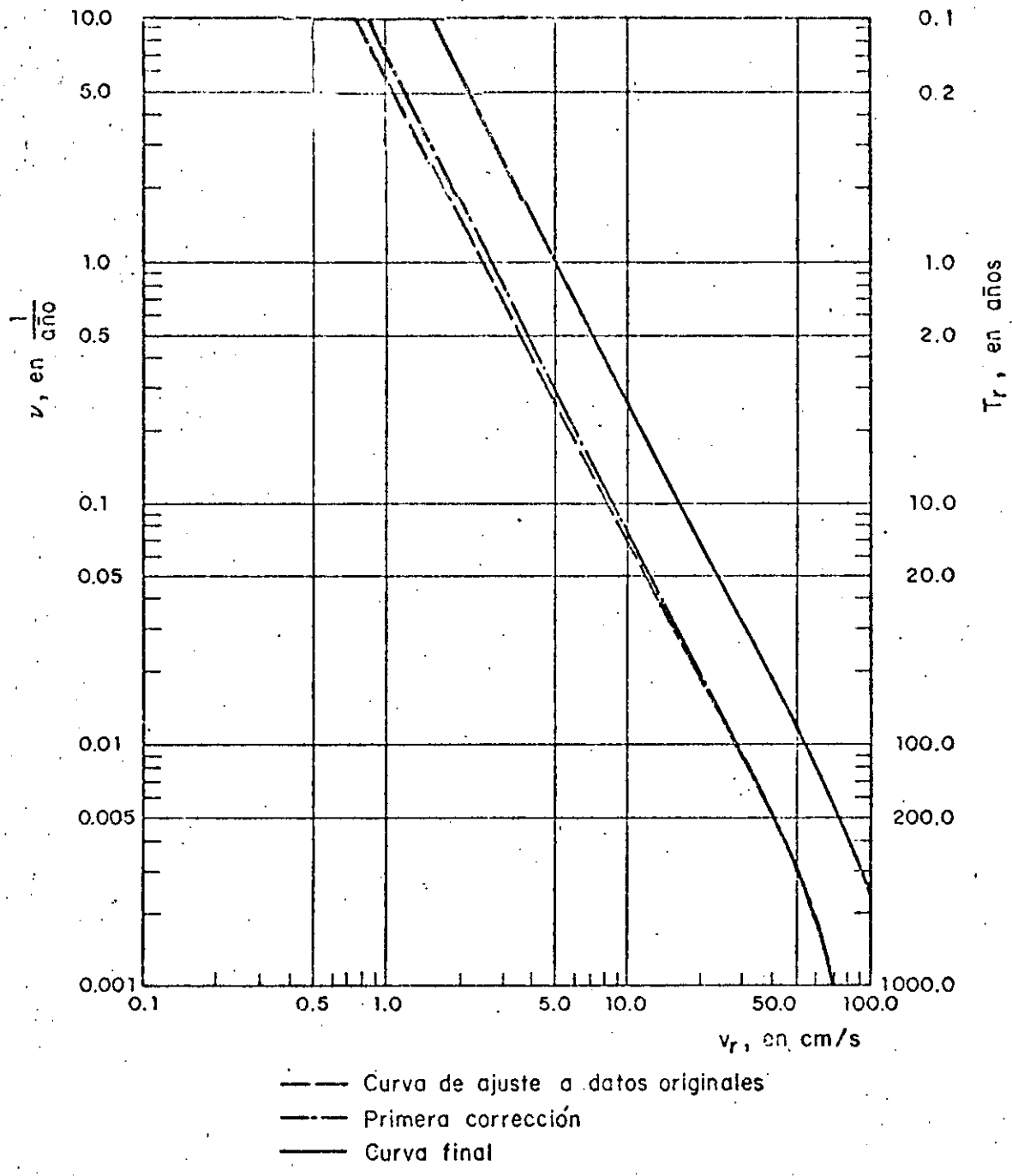


Fig 5. Tasa media de excedencia  $\nu$  (y periodo de recurrencia  $T_r$ ) vs velocidad máxima del terreno  $v_r$  para Cerro Prieto B. C.

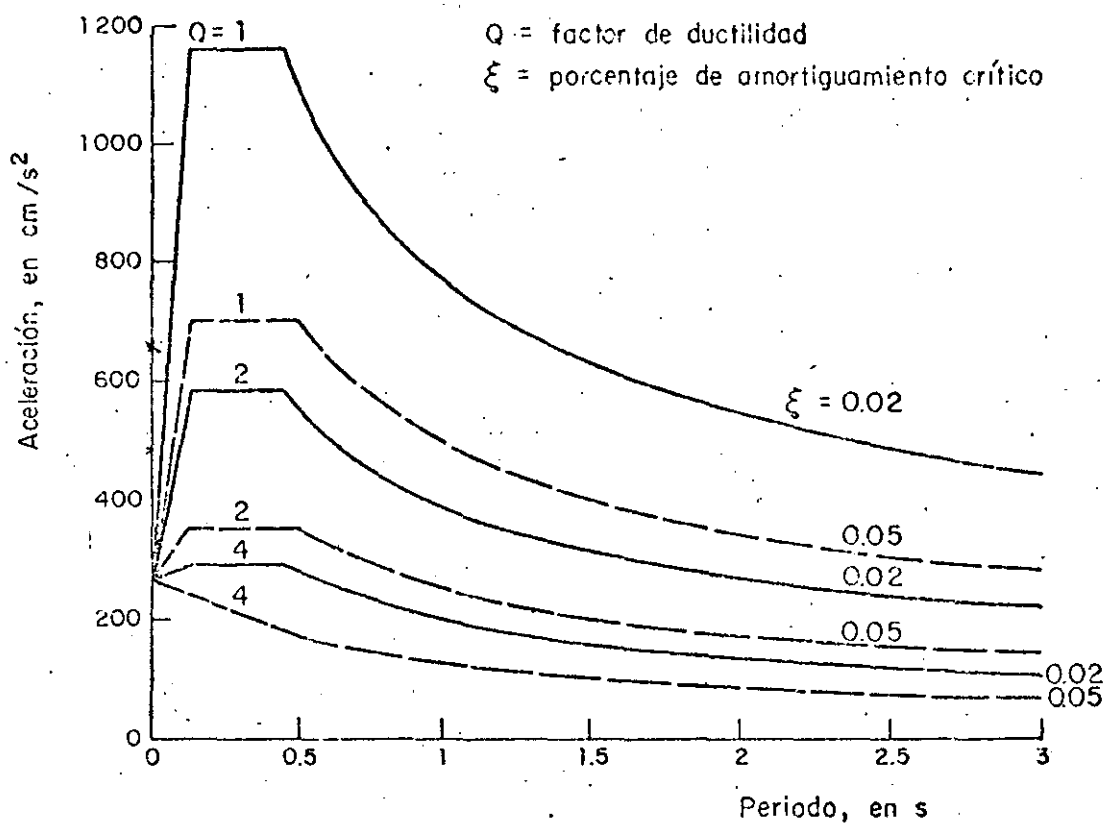


Fig 6. Espectro de diseño para terreno firme, periodo de recurrencia de 30 años, en Planta Geotérmica de Cerro Prieto, B. C.

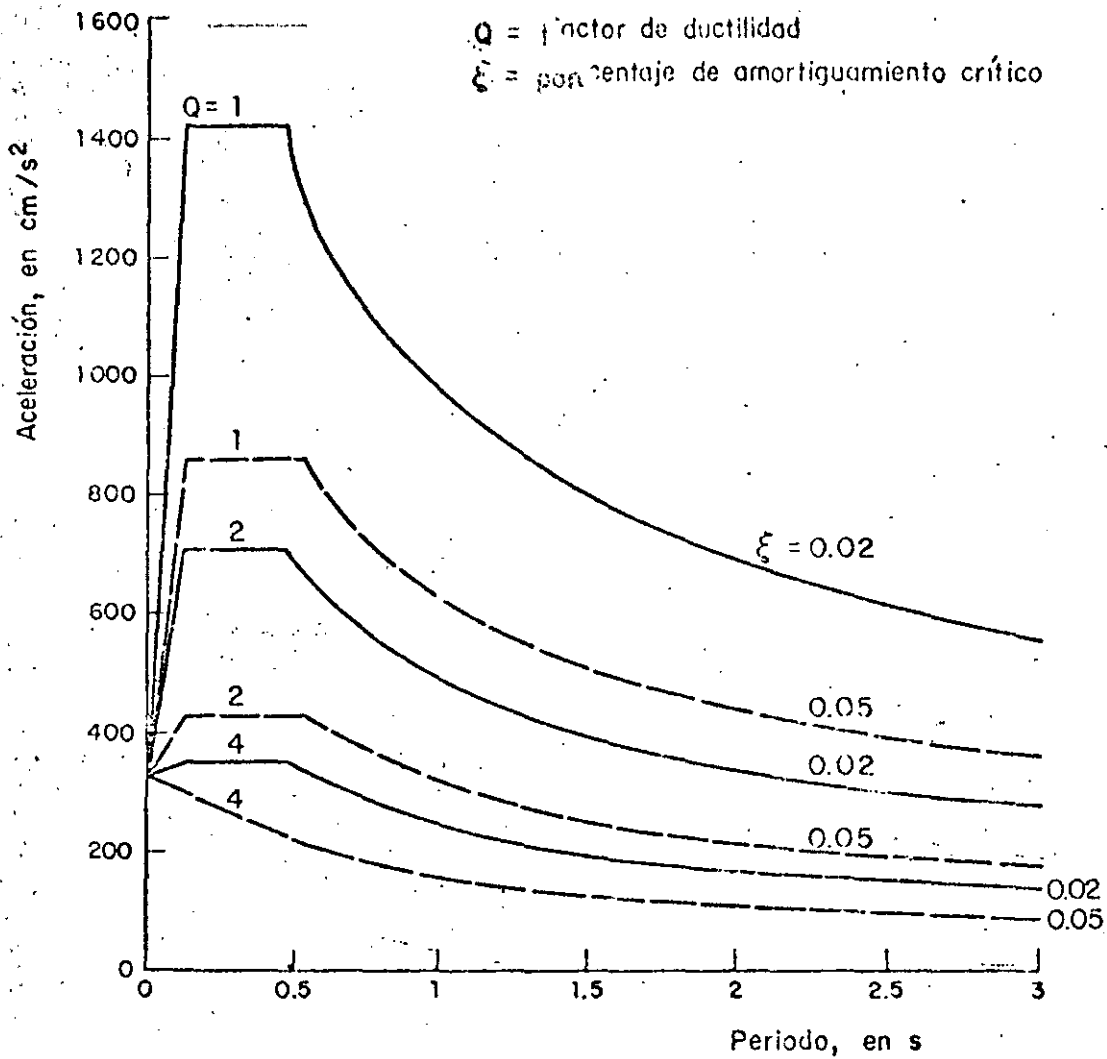


Fig 7. Espectro de diseño para terreno firme, periodo de recurrencia de 50 años, en Planta Geotérmica de Cerro Prieto, B. C.

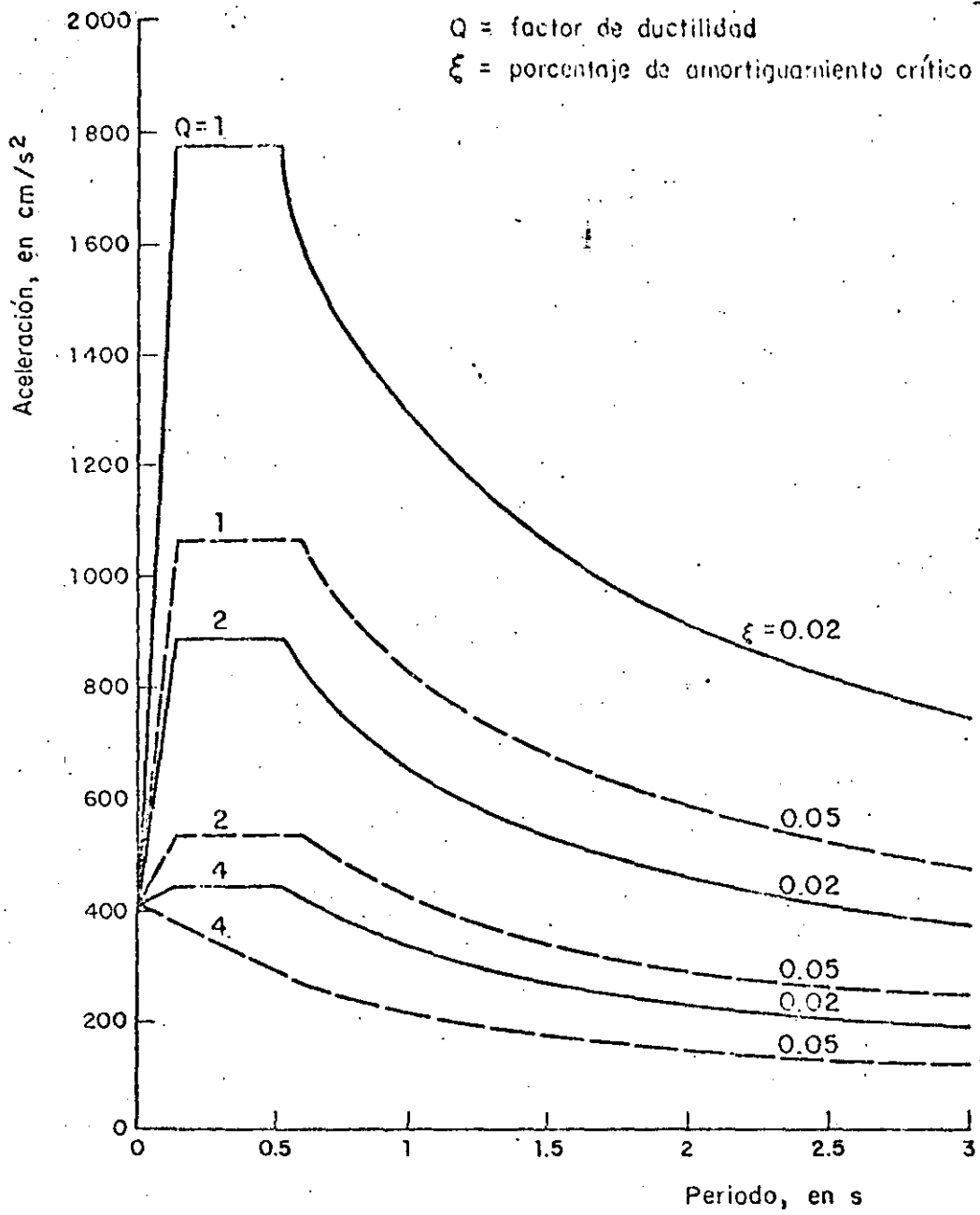


Fig 8. Espectro de diseño para terreno firme, periodo de recurrencia de 100 años, en Planta Geotérmica de Cerro Prieto, B. C.

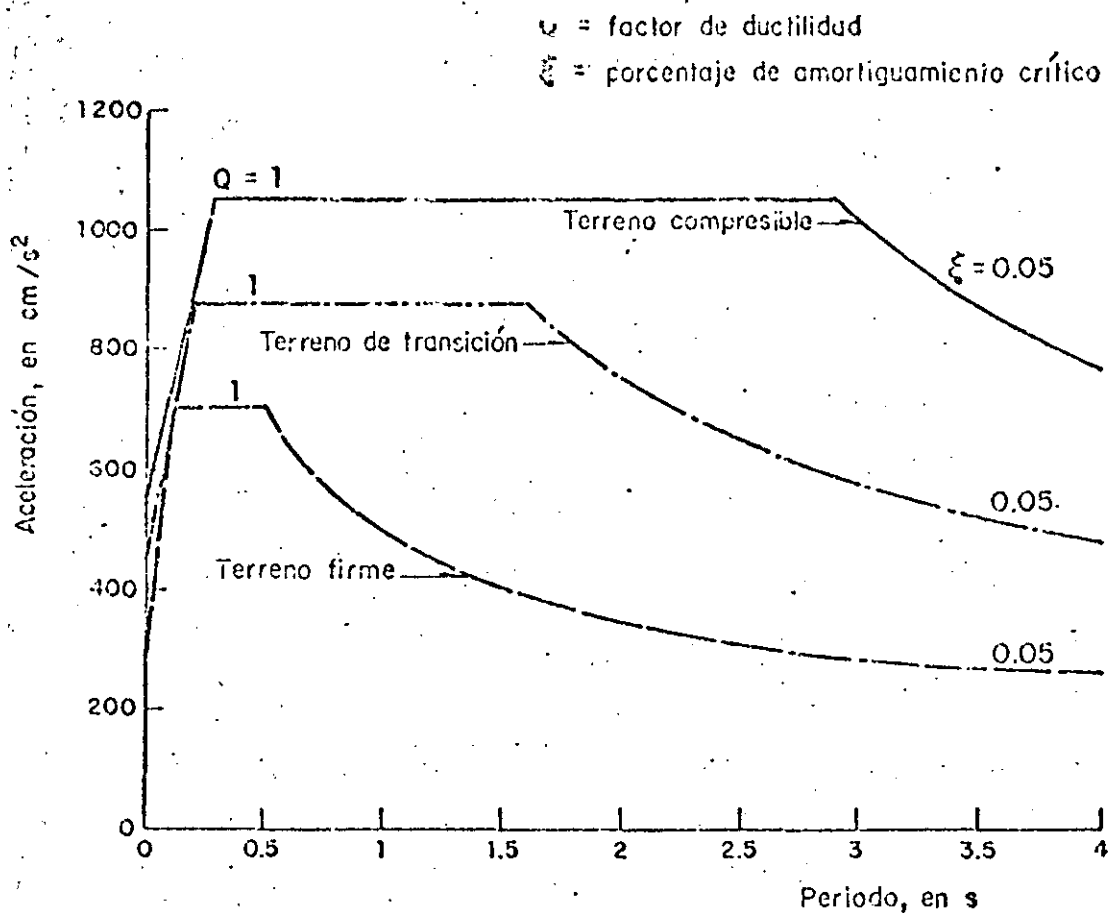
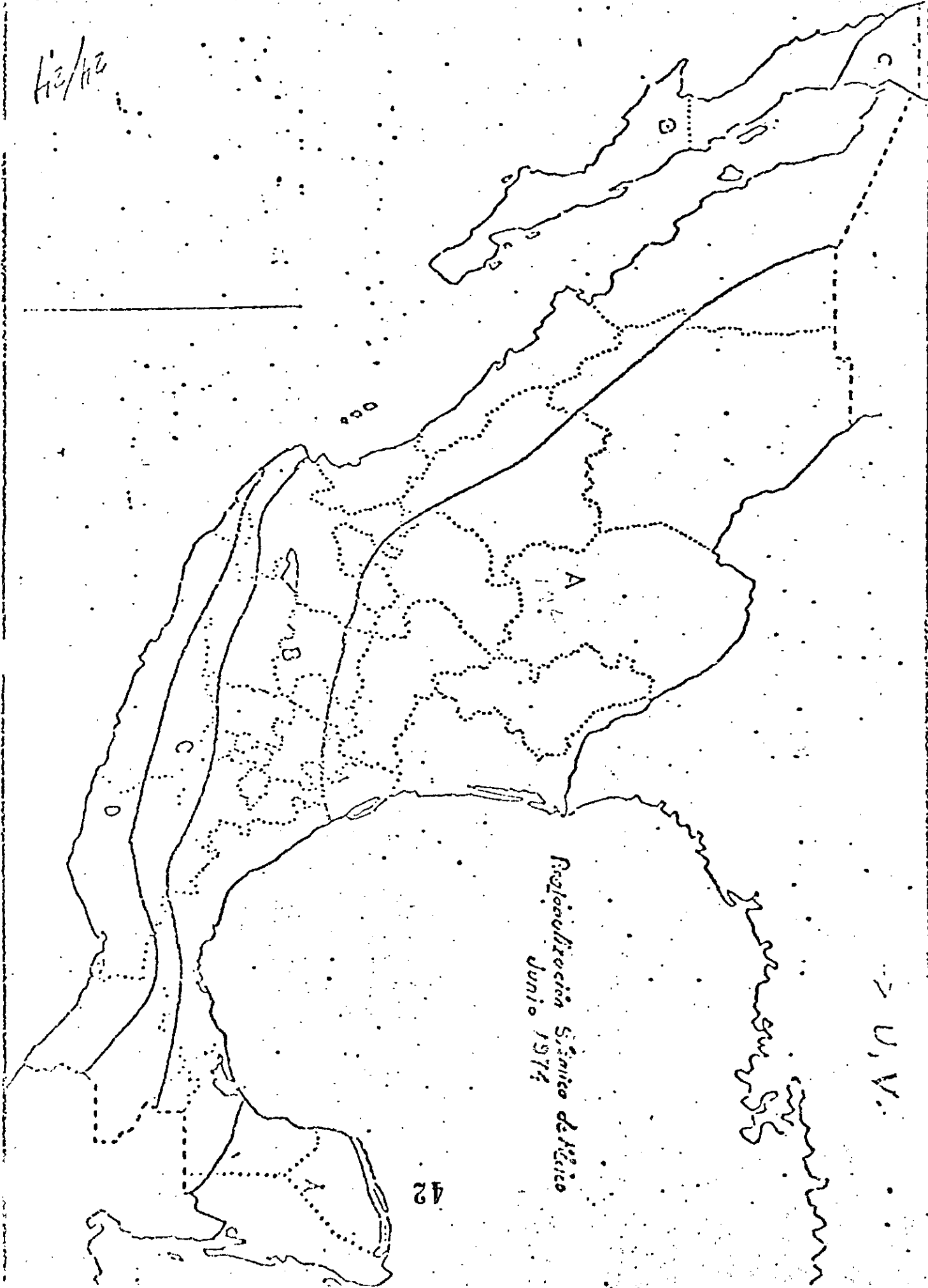


Fig 9. Espectro de diseño para terreno firme, de transición y compresible, periodo de recurrencia de 30 años, en Plania Geotérmica de Cerro Prieto, Baja California

REGIONALIZACION SISMICA  
DE MEXICO

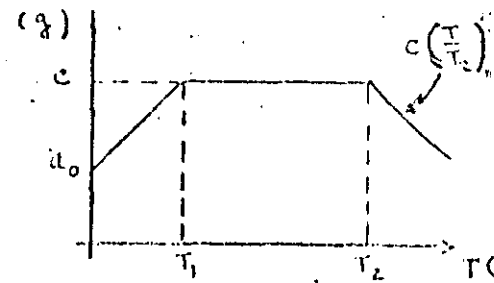
H2/H2



Recolección Sianito de H2O  
Junio 1974

U.V.

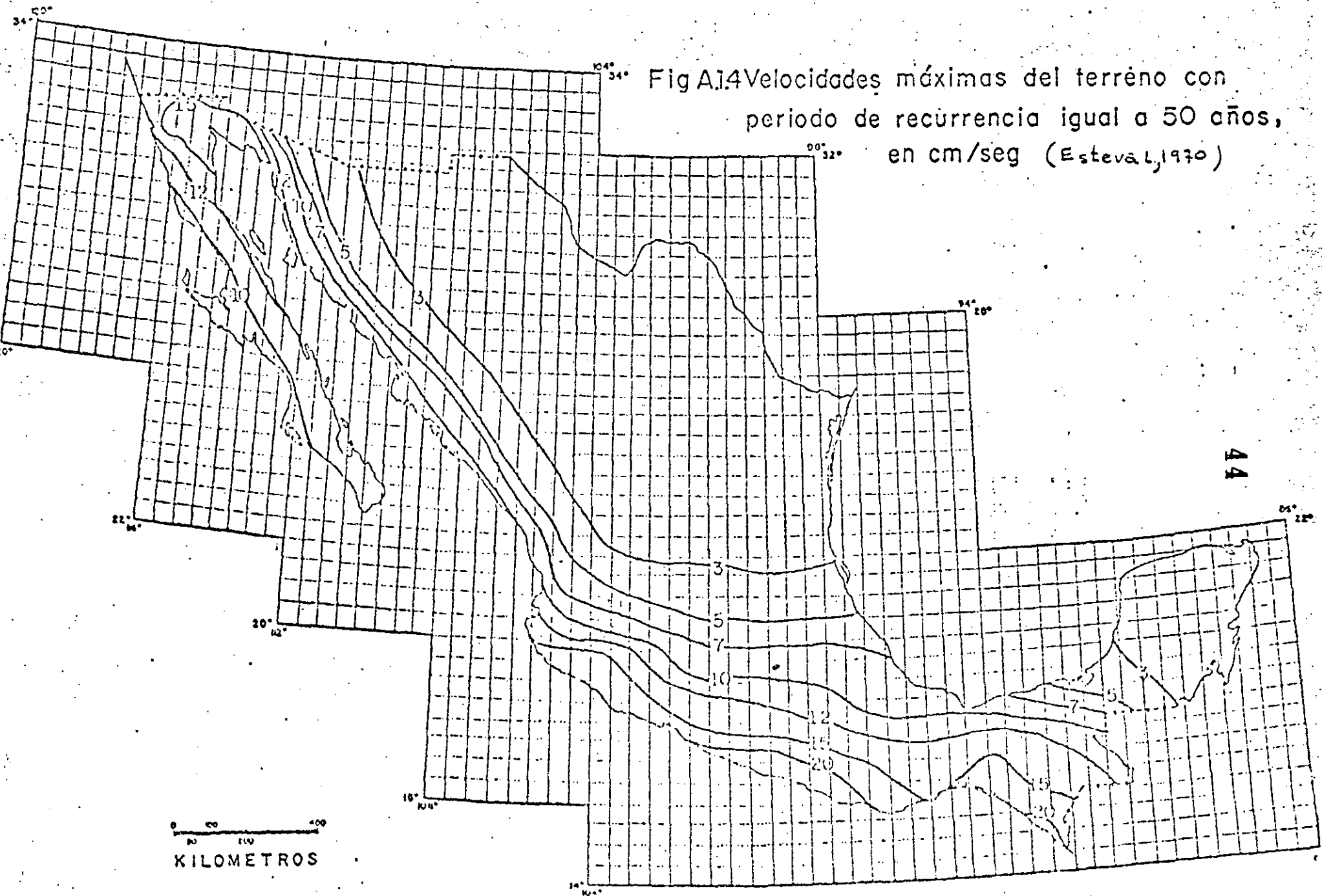
TABLA 10.3  
VALORES DE  $\alpha_0$ ,  $T_1$ ,  $T_2$  y  $r$ .



ZONA DE LA REPUBLICA	TIPO DE SUELO	$\alpha_0$	$c$	$T_1$	$T_2$	$r$
A	I	0.03	0.03	0.30	0.8	1/2
	II	0.045	0.12	0.55	2.0	2/3
	III	0.05	0.16	0.75	3.3	1
B	I	0.03	0.16	0.30	0.8	1/2
	II	0.045	0.20	0.50	2.0	2/3
	III	0.05	0.24	0.80	3.3	1
C	I	0.05	0.24	0.25	0.67	1/2
	II	0.08	0.30	0.45	1.6	2/3
	III	0.10	0.36	0.60	2.9	1
D	I	0.09	0.48	0.15	0.55	1/2
	II	0.14	0.56	0.30	1.4	2/3
	III	0.18	0.64	0.45	2.7	1

$T_1$  y  $T_2$  están en segundos.

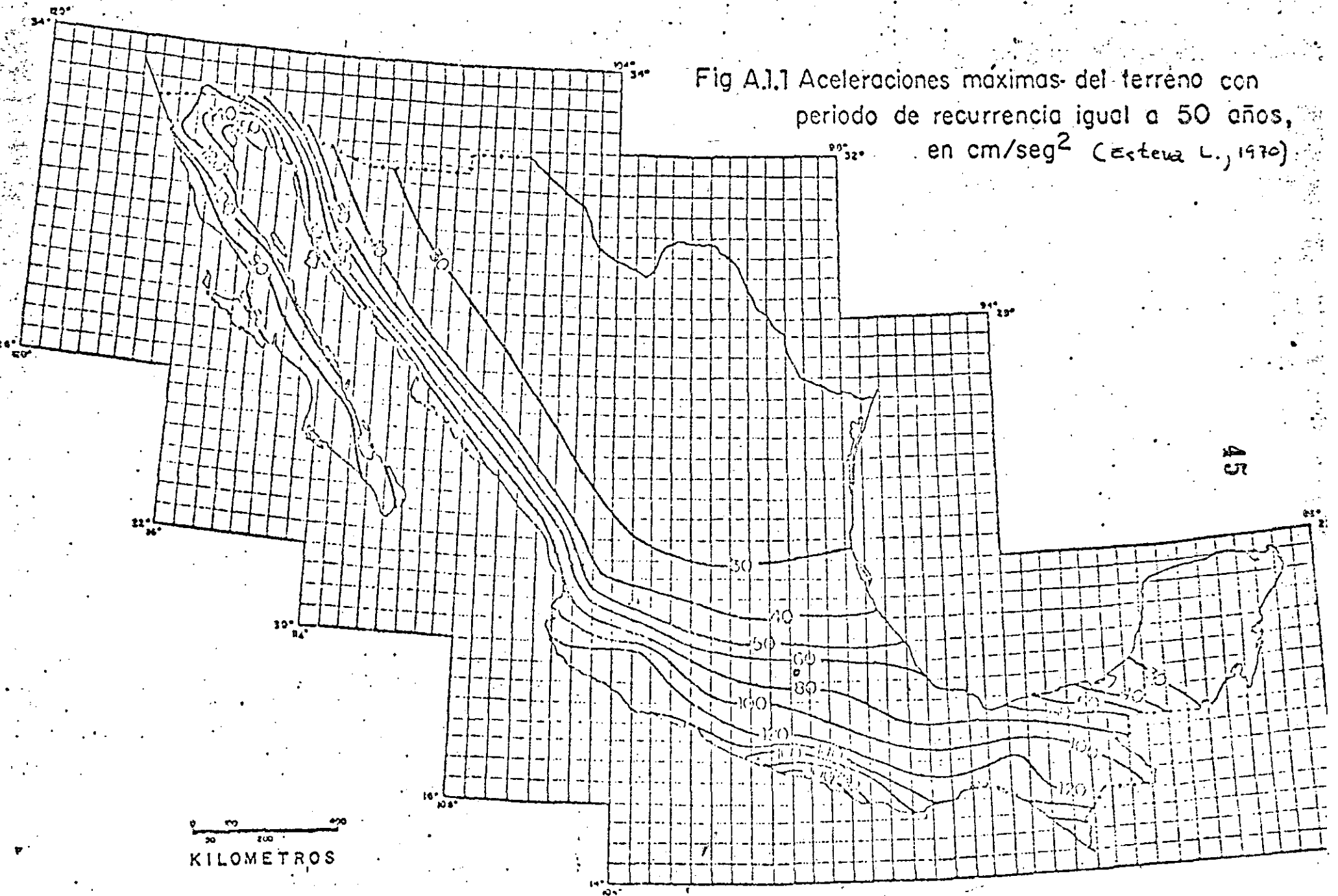
Fig A1.4 Velocidades máximas del terreno con periodo de recurrencia igual a 50 años, en cm/seg (Esteval, 1970)



0 50 100 150 200  
KILOMETROS

44

Fig A.1.1 Aceleraciones máximas del terreno con periodo de recurrencia igual a 50 años, en  $\text{cm}/\text{seg}^2$  (Estevez L., 1970)





**DIVISION DE EDUCACION CONTINUA  
FACULTAD DE INGENIERIA U.N.A.M.**

ANALISIS DE RIESGO SISMICO

PROPAGACION DE ONDAS ELASTICAS EN UN MEDIO SEMINFINITO.

DR. FRANCISCO SANCHEZ SESMA

JULIO, 1985

# PROPAGACION DE ONDAS ELASTICAS EN UN MEDIO SEMINFINITO

por

Francisco J Sánchez-Sesma

*Instituto de Ingeniería, Universidad Nacional Autónoma de México*

## 1. INTRODUCCION

Las ondas sísmicas se propagan desde la fuente de acuerdo con las propiedades mecánicas del medio en que viajan y, por supuesto, dependen también de las características de la fuente. La descripción del fenómeno ha podido hacerse de forma satisfactoria al recurrir a simplificaciones e hipótesis que llevan a la formulación de modelos que representan los aspectos más importantes de la propagación de ondas en la tierra. Es usual aceptar que la tierra es un medio elástico lineal, homogéneo e isotrópico. En un medio de esta naturaleza con extensión ilimitada se pueden propagar dos tipos de ondas elásticas; las ondas P o de compresión y las ondas S o de cortante. Las primeras se propagan con mayor velocidad y por eso se les suele llamar primarias mientras que las segundas reciben el nombre de secundarias. Existen diversas soluciones para las ecua-

ciones que gobiernan el fenómeno de propagación. Así, para una fuente puntual se podría hablar de ondas esféricas, que a grandes distancias de la fuente se pueden representar como ondas planas. En algunos casos se modela el problema de propagación como bidimensional y las soluciones para una fuente se dan en términos de ondas cilíndricas, que también a grandes distancias son aproximadamente planas. Un buen número de soluciones de las ecuaciones fundamentales puede encontrarse en el excelente texto de Ewing, Jardetzky y Press (1957).

La existencia de una superficie libre introduce reflexiones de las ondas al llegar a esta. Para estudiar la naturaleza de las reflexiones dicha superficie debe considerarse libre de esfuerzos. Dado que a grandes distancias de la fuente las ondas pueden suponerse planas y que para las longitudes de onda de interés la curvatura de la tierra es, comparativamente, pequeña se estudiará el problema de reflexión de ondas planas por la superficie de un medio elástico seminfinito. Dicha superficie se supondrá plana.

A continuación se presentan algunos aspectos de la propagación de ondas en un medio elástico de extensión ilimitada y se expresan las ecuaciones que gobiernan el fenómeno en términos de potenciales de desplazamiento. Posteriormente se discute la reflexión de ondas planas por la

frontera libre de un semiespacio elástico, homogéneo e isotrópico. La incidencia de ondas P y SV armónicas se estudia con detalle. Finalmente se presentan las ondas superficiales de Rayleigh y de Love, las primeras como caso límite en que la velocidad aparente es menor que las velocidades de propagación de las ondas de cuerpo y las segundas como ejemplo de propagación en el caso más simple de un medio estratificado.

## 2. PROPAGACION DE ONDAS EN UN MEDIO ELASTICO

Puede demostrarse que en un sólido elástico, homogéneo e isotrópico las ecuaciones de movimiento están dadas por

$$\begin{aligned}
 (\lambda+2\mu)\frac{\partial^2 u}{\partial x^2} + \mu\left(\frac{\partial^2 u}{\partial y^2} + \frac{\partial^2 u}{\partial z^2}\right) + (\lambda+\mu)\left(\frac{\partial^2 v}{\partial x\partial y} + \frac{\partial^2 w}{\partial x\partial z}\right) &= \rho \frac{\partial^2 u}{\partial t^2} \\
 (\lambda+2\mu)\frac{\partial^2 v}{\partial y^2} + \mu\left(\frac{\partial^2 v}{\partial x^2} + \frac{\partial^2 v}{\partial z^2}\right) + (\lambda+\mu)\left(\frac{\partial^2 u}{\partial x\partial y} + \frac{\partial^2 w}{\partial y\partial z}\right) &= \rho \frac{\partial^2 v}{\partial t^2} \\
 (\lambda+2\mu)\frac{\partial^2 w}{\partial z^2} + \mu\left(\frac{\partial^2 w}{\partial x^2} + \frac{\partial^2 w}{\partial y^2}\right) + (\lambda+\mu)\left(\frac{\partial^2 u}{\partial x\partial z} + \frac{\partial^2 v}{\partial y\partial z}\right) &= \rho \frac{\partial^2 w}{\partial t^2}
 \end{aligned} \tag{1}$$

donde  $u, v, w$  = desplazamientos en las direcciones  $x, y, z$ , respectivamente;  $\lambda, \mu$  = constantes de Lamé,  $\rho$  = densidad del medio y  $t$  = tiempo. Estas ecuaciones pueden escribirse de una manera compacta en notación vectorial, esto es

$$\mu \nabla^2 \bar{u} + (\lambda + \mu) \nabla \nabla \cdot \bar{u} = \rho \ddot{\bar{u}} \tag{2}$$

donde  $\bar{u} = (u, v, w)$  = vector desplazamiento,  $\nabla^2$  = operador Laplaciano y  $\nabla$  = operador gradiente.

Antes de considerar soluciones generales de las ecuaciones de movimiento dos ejemplos simples permitirán ilustrar las principales características de las ondas planas en un sólido elástico de extensión ilimitada.

Supongase que  $u \neq 0$ ,  $v = w = 0$  y que  $u$  es solo función de  $x$  y del tiempo. Las ecs 1 se reducen a la expresión

$$(\lambda + 2\mu) \frac{\partial^2 u}{\partial x^2} = \rho \frac{\partial^2 u}{\partial t^2} \quad (3)$$

una solución de esta ecuación es

$$u = f(t - x/\alpha) + g(t + x/\alpha) \quad (4)$$

donde  $\alpha^2 = (\lambda + 2\mu)/\rho$  y  $f, g$  son funciones de *una sola variable* que pueden describir una forma de onda arbitraria. Un simple análisis de los argumentos de  $f$  y  $g$  permite establecer que  $f(t - x/\alpha)$  representa una onda que viaja en la dirección positiva de  $x$  con velocidad  $\alpha$  y  $g(t + x/\alpha)$  describe una onda que viaja en la dirección negativa. Debe notarse que  $f(t - x/\alpha)$  puede representar una onda armónica estacionaria,  $\exp[i\omega(t - x/\alpha)]$  donde  $i = \sqrt{-1}$  y  $\omega$  = frecuencia circular del movimiento. Puede demostrarse que la ec 4 representa ondas de compresión o P.

Un segundo ejemplo simple se obtiene si se supone que  $u = w = 0$  y que  $v = v(x, t)$ . De las ecs 1 se obtiene que

$$\mu \frac{\partial^2 v}{\partial x^2} = \rho \frac{\partial^2 v}{\partial t^2} \quad (5)$$

y la solución tiene la misma forma que la ec 4 pero representa ondas que viajan con una velocidad  $\beta$ , donde  $\beta^2 = \mu/\rho$ . Debe notarse que el movimiento es perpendicular a la dirección de avance. Puede demostrarse que las soluciones de la ec 5 representan ondas de cortante, sin cambio de volumen.

Las ecuaciones de movimiento pueden resolverse de una manera más general por medio de *potenciales de desplazamiento*.

Si el vector desplazamiento se expresa como

$$\bar{u} = \nabla\phi + \nabla_x\bar{\psi}, \text{ con } \nabla \cdot \bar{\psi} = 0 \quad (6)$$

donde  $\phi$  es un potencial escalar y  $\bar{\psi}$  es un potencial vectorial, puede demostrarse que la ec 6 representa una solución de la ec 2 (o de la ec 1 en coordenadas rectangulares) si  $\phi$  y  $\bar{\psi}$  satisfacen, respectivamente, las ecuaciones de onda:

$$\nabla^2\phi = \frac{1}{\alpha^2} \frac{\partial^2\phi}{\partial t^2} \quad (7)$$

$$\nabla^2 \bar{\psi} = \frac{1}{\beta^2} \frac{\partial^2 \bar{\psi}}{\partial t^2} \quad (8)$$

Así, por ejemplo, una solución de la ec 7 que representa una onda plana de compresión que viaja en una dirección arbitraria, está dada por

$$\phi = f \left( t - \frac{x\ell + ym + zn}{\alpha} \right) \quad (9)$$

donde  $\ell, m, n$  = cosenos de los ángulos formados por la dirección de viaje y los tres ejes coordenados, respectivamente. Si  $\bar{r} = (x, y, z)$  y  $\bar{n} = (\ell, m, n)$  donde  $\bar{r}$  = vector de posición y  $\bar{n}$  = vector unitario que da la dirección de propagación, la ec 9 puede escribirse como

$$\phi = f(t - \bar{r} \cdot \bar{n} / \alpha) \quad (10)$$

Es evidente que soluciones similares pueden encontrarse para los tres componentes del potencial vectorial y representarían ondas de cortante viajando con una velocidad  $\beta$ .

En coordenadas rectangulares la ec 6 se desarrolla como

$$\begin{aligned} u &= \frac{\partial \phi}{\partial x} + \frac{\partial \psi_z}{\partial y} - \frac{\partial \psi_y}{\partial z} \\ v &= \frac{\partial \phi}{\partial y} - \frac{\partial \psi_z}{\partial x} + \frac{\partial \psi_x}{\partial z} \\ w &= \frac{\partial \phi}{\partial z} + \frac{\partial \psi_y}{\partial x} - \frac{\partial \psi_x}{\partial y} \end{aligned} \quad (11)$$

donde  $\bar{\psi} = (\psi_x, \psi_y, \psi_z)$ .

Los potenciales de desplazamiento  $\phi$  y  $\bar{\psi}$  permiten especificar ondas planas de compresión y cortante, respectivamente, que viajen en cualquier dirección y con cualquier forma. Además, dado el carácter lineal de las ecuaciones involucradas, cualquier combinación de soluciones sigue satisfaciendo las ecuaciones de movimiento de un sólido elástico, homogéneo e isotrópico de extensión ilimitada. La utilidad de este hecho se hace evidente cuando se hace necesario seleccionar una combinación particular de ondas planas que satisfaga una cierta condición de frontera o que describa una fuente. Tal es el caso en el problema que se aborda a continuación.

### 3. REFLEXION DE ONDAS PLANAS POR LA FRONTERA LIBRE DE UN SEMIESPACIO ELASTICO

Considérese que la frontera libre es el plano  $yz$  como se muestra en la fig 1. Además, sin perder generalidad, supóngase que las direcciones de avance de las ondas están alojadas en el plano  $xz$ .

Para describir el movimiento debido a ondas de cortante se introduce el concepto de planos de polarización. Así, se descompone el movimiento en la dirección de la coordenada  $y$  (ondas polarizadas horizontalmente o SH) y en la

dirección perpendicular a la dirección de avance en el plano vertical  $xz$  (ondas polarizadas verticalmente o SV). En la propagación de ondas P el movimiento es en la dirección de avance de la onda. Esto se ilustra en la fig 2.

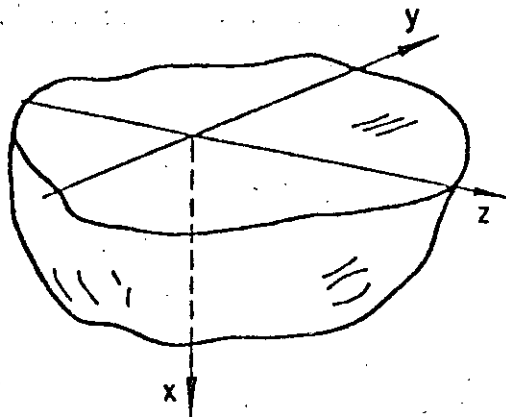


Fig 1. Sistema de coordenadas en el semiespacio elástico

La propagación de ondas SH está gobernada por la ecuación

$$\frac{\partial^2 v}{\partial x^2} + \frac{\partial^2 v}{\partial z^2} = \frac{1}{\beta^2} \frac{\partial^2 v}{\partial t^2} \quad (12)$$

Que es precisamente la ecuación de onda en dos dimensiones, en este caso no es necesario recurrir a la formulación del problema en términos de los potenciales de desplazamiento. Puede demostrarse que, en la reflexión de una onda SH plana por una frontera libre, el ángulo de incidencia es igual al ángulo de reflexión y la onda reflejada mantiene la forma de la onda incidente. Si la onda incidente está dada

por

$$e^{i(\omega t - \beta(z + \frac{x \cos \gamma - z \sin \gamma}{\beta}))} \quad (13)$$

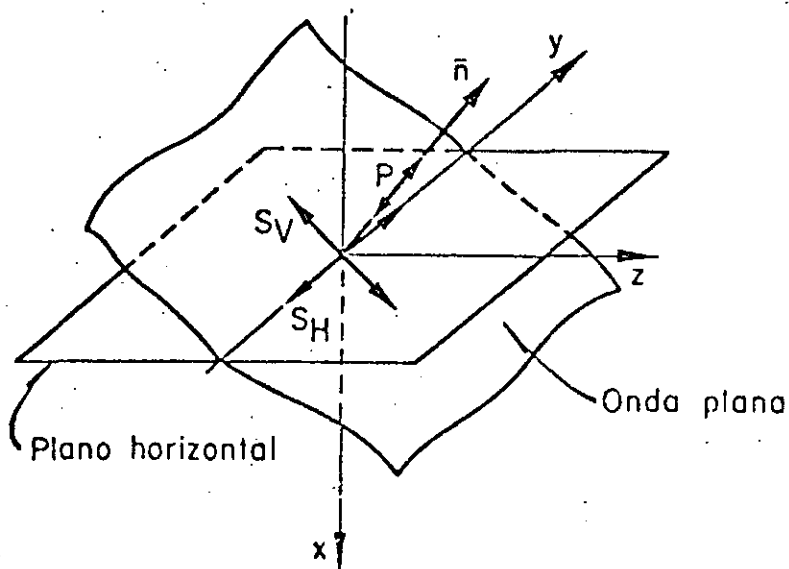


Fig 2. Nomenclatura para ondas planas

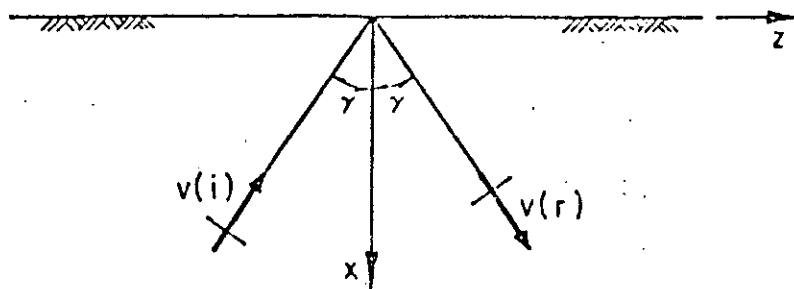


Fig 3. Ondas SH incidente y reflejada

la onda reflejada está dada simplemente por

$$v^{(r)} = f\left(t - \frac{x \cos \gamma + z \operatorname{sen} \gamma}{\beta}\right) \quad (14)$$

aquí  $\gamma$  = ángulo de incidencia. Puede verificarse que  $v = v^{(i)} + v^{(r)}$  satisface la ec 12 y la condición de que el plano  $x = 0$  esté libre de esfuerzo pues los únicos esfuerzos relevantes están dados por

$$\tau_{xy} = \mu \frac{\partial v}{\partial x}, \quad \tau_{yz} = \mu \frac{\partial v}{\partial z} \quad (15)$$

y combinando las ecs 13, 14 y 15 resulta que  $\tau_{xy} = 0$  en  $x = 0$ . Debe observarse que en estas condiciones el movimiento en  $x = 0$ , la superficie libre, se puede escribir como

$$v_{x=0} = 2 f\left(t - \frac{z \operatorname{sen} \gamma}{\beta}\right), \quad (16)$$

por lo que el factor de amplificación es dos.

En la propagación de ondas P y SV el movimiento está en el plano  $xz$ , es decir  $u = u(x, z, t)$ ,  $w = w(x, z, t)$  y  $v = 0$ . En este caso las ecuaciones de onda que deben satisfacer los potenciales, si  $\psi = \psi_y$ , son

$$\frac{\partial^2 \phi}{\partial x^2} + \frac{\partial^2 \phi}{\partial z^2} = \frac{1}{\alpha^2} \frac{\partial^2 \phi}{\partial t^2} \quad (17)$$

$$\frac{\partial^2 \psi}{\partial x^2} + \frac{\partial^2 \psi}{\partial z^2} = \frac{1}{\beta^2} \frac{\partial^2 \psi}{\partial t^2} \quad (18)$$

Los desplazamientos quedan como

$$u = \frac{\partial \phi}{\partial x} - \frac{\partial \psi}{\partial z} \quad (19)$$

$$w = \frac{\partial \phi}{\partial z} + \frac{\partial \psi}{\partial x} \quad (20)$$

Los esfuerzos que al valuarse en la superficie deben anularse son

$$\sigma_x = \lambda \left( \frac{\partial^2 \phi}{\partial x^2} + \frac{\partial^2 \psi}{\partial z^2} \right) + 2 \mu \left( \frac{\partial^2 \phi}{\partial x^2} - \frac{\partial^2 \psi}{\partial x \partial z} \right) \quad (21)$$

$$\tau_{xz} = \mu \left( 2 \frac{\partial^2 \phi}{\partial x \partial z} + \frac{\partial^2 \psi}{\partial x^2} - \frac{\partial^2 \psi}{\partial z^2} \right) \quad (22)$$

ya que  $\tau_{xy} = 0$ .

Considérense los casos mostrados en las figs 4 y 5, la incidencia de ondas P y de ondas SV, respectivamente.

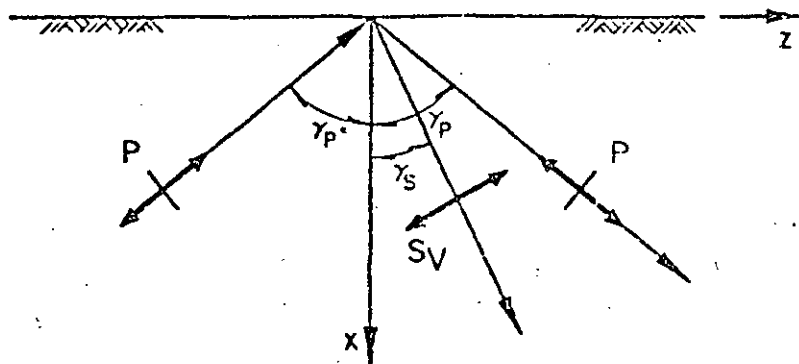


Fig 4. Incidencia de ondas P

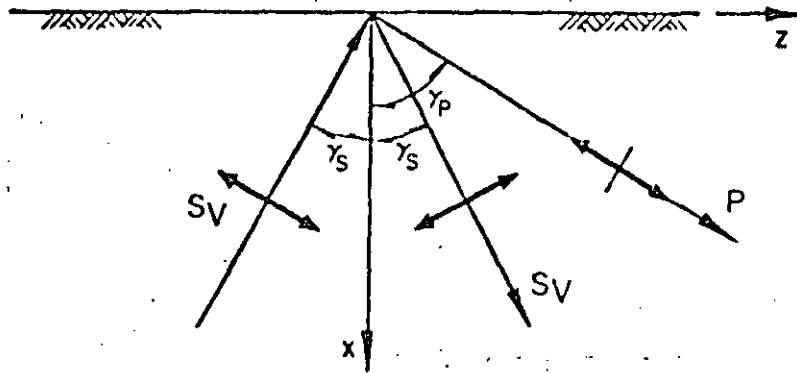


Fig 5. Incidencia de ondas SV

Mediante la técnica de separación de variables se puede demostrar que las soluciones de las ecs 17 y 18 son de la forma

$$\phi = A_0 e^{Mx} e^{Lz} e^{\Omega t} \quad (23)$$

$$\psi = B_0 e^{Kx} e^{Lz} e^{\Omega t} \quad (24)$$

donde

$$M^2 + L^2 = \frac{\Omega^2}{\alpha^2} \quad \text{y} \quad K^2 + L^2 = \frac{\Omega^2}{\beta^2} \quad (25)$$

Hasta ahora  $K$ ,  $L$ ,  $M$  y  $\Omega$  con valores complejos son posibles soluciones, pero para los actuales propósitos basta hacer

$$\Omega = i\omega \quad \text{y} \quad L = -i\ell \quad (26)$$

pues al tener a  $\Omega$  como número imaginario puro se garantiza

que los potenciales sean finitos. Al definir  $l$  como imaginario negativo con  $l = \omega/c$  se observa que el producto

$$e^{-l z} e^{i \omega t} = e^{i \omega (t - z/c)} \quad (27)$$

representa una onda armónica que viaja en la dirección positiva de  $z$  con una velocidad de fase  $c$ , si  $c$  es negativa la dirección de viaje es en la dirección negativa de  $z$ .

En términos de los ángulos de las figs 4 y 5 se tiene que

$$c = \frac{\alpha}{\text{sen } \gamma_p} = \frac{\beta}{\text{sen } \gamma_s} \quad (28)$$

Con estas definiciones  $M$  y  $K$  deben ser o reales o imaginarios pues, de las ecs 25 y 26, se tiene que

$$M^2 = l^2 - \omega^2/\alpha^2 = \omega^2(1/c^2 - 1/\alpha^2) \quad (29)$$

y

$$K^2 = l^2 - \omega^2/\beta^2 = \omega^2(1/c^2 - 1/\beta^2) \quad (30)$$

Así, para  $\beta < \alpha < |c|$ ,  $M$  y  $K$  son imaginarios; para  $\beta < |c| < \alpha$ ,  $M$  es real y  $K$  imaginario; para  $|c| < \beta < \alpha$ ,  $M$  y  $K$  son reales.

Para el primer caso,  $\beta < \alpha < |c|$ , se tienen los potenciales

$$\phi = (A_1 e^{i m x} + A_2 e^{-i m x}) e^{-l z} e^{i \omega t} \quad (31)$$

$$\psi = (B_1 e^{ikx} + B_2 e^{-ikx}) e^{-i\ell z} e^{i\omega t} \quad (32)$$

donde  $\ell = \omega/c$ ,  $m = \omega(1/\alpha^2 - 1/c^2)^{1/2}$  y  $k = \omega(1/\beta^2 - 1/c^2)^{1/2}$ .

Si  $B_1 = 0$  se tiene el caso mostrado en la fig 4 de incidencia de ondas P. En cambio si  $A_1 = 0$  se tendrá incidencia de ondas SV. Sustituyendo las ecs 31 y 32 en las ecs 21 y 22, haciendo que  $\sigma_x = \tau_{xz} = 0$  en  $x=0$  y resolviendo el sistema de ecuaciones resultante se obtiene que

a) Para  $B_1 = 0$

$$\frac{A_2}{A_1} = \frac{4 \cot \gamma_P \cot \gamma_S - (\cot^2 \gamma_S - 1)^2}{4 \cot \gamma_P \cot \gamma_S + (\cot^2 \gamma_S - 1)^2} \quad (33)$$

$$\frac{B_2}{A_1} = \frac{4 \cot \gamma_P (\cot^2 \gamma_S - 1)}{4 \cot \gamma_P \cot \gamma_S + (\cot^2 \gamma_S - 1)^2} \quad (34)$$

donde  $\gamma_P =$  ángulo de incidencia y de reflexión de la onda P y  $\gamma_S =$  ángulo de reflexión de la onda SV. Debe recordarse que la velocidad aparente está dada por

$$c = \frac{\alpha}{\text{sen } \gamma_P} = \frac{\beta}{\text{sen } \gamma_S} \quad (35)$$

b) Para  $A_1 = 0$

$$\frac{A_2}{B_1} = \frac{4 \cot \gamma_S (\cot^2 \gamma_S - 1)}{4 \cot \gamma_P \cot \gamma_S + (\cot^2 \gamma_S - 1)^2} \quad (36)$$

$$\frac{B_2}{B_1} = \frac{4 \cot \gamma_P \cot \gamma_S - (\cot^2 \gamma_S - 1)^2}{4 \cot \gamma_P \cot \gamma_S + (\cot^2 \gamma_S - 1)^2} \quad (37)$$

La incidencia de una onda P puede variar de vertical ( $c$  infinita) a horizontal ( $c = \alpha$ ) y las ecs 33 y 34 permiten calcular las amplitudes de los potenciales de las ondas reflejadas. Para la incidencia de una onda SV se tiene que  $0 \leq \gamma_S \leq \text{sen}^{-1}(\beta/\alpha)$ .

Si se toma la energía cinética por unidad de volumen como  $\frac{1}{2} \rho (\dot{u}^2 + \dot{w}^2)$ , puede calcularse el flujo de energía mediante el producto de la energía cinética por la velocidad de propagación y el área del frente de onda considerado. Para incidencia de una onda P puede demostrarse que las fracciones de energía reflejada como ondas P y SV están dadas, respectivamente, por

$$\frac{A_2^2}{A_1^2} \quad \text{y} \quad \frac{B_2^2 \tan \gamma_P}{A_1^2 \tan \gamma_S}$$

y, similarmente, para incidencia de una onda SV se tiene que

$$\frac{A_2^2 \tan \gamma_S}{B_1^2 \tan \gamma_P} \quad \text{y} \quad \frac{B_2^2}{B_1^2}$$

En las figs 6 y 7 se presentan valores de  $\sqrt{E/E_{\text{inc}}}$  para incidencia de ondas P y SV, respectivamente, en función del ángulo de incidencia y con diferentes relaciones  $\alpha/\beta$ .

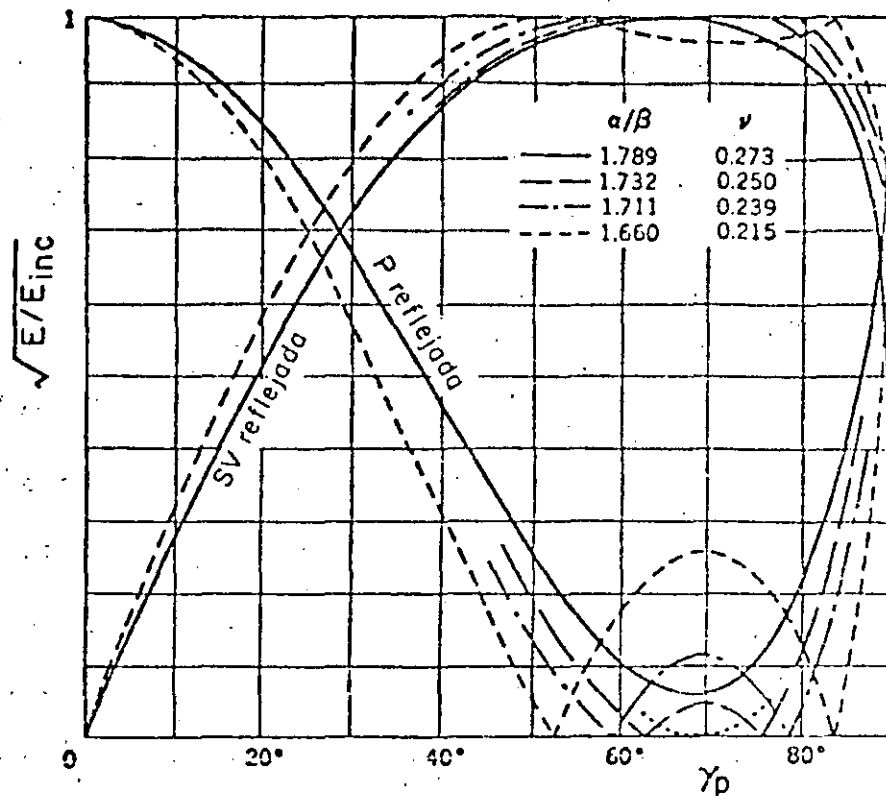


Fig 6. Raíz cuadrada de la relación de energía reflejada a energía incidente para una onda P incidente en una superficie libre

Para el segundo caso,  $\beta < |c| < \alpha$ , se tienen los potenciales

$$\phi = (A_1 e^{mx} + A_2 e^{-mx}) e^{-ilz} e^{i\omega t} \quad (38)$$

$$\psi = (B_1 e^{ikx} + B_2 e^{-ikx}) e^{ilz} e^{i\omega t} \quad (39)$$

donde  $l = \omega/c$ ,  $m = |\omega| (1/c^2 - 1/\alpha^2)^{1/2}$  y  $k = \omega(1/\beta^2 - 1/c^2)^{1/2}$ .

Para evitar que  $\phi$  crezca indefinidamente al aumentar  $x$  se hace que  $A_1 = 0$  por lo que no hay onda P incidente en este caso. Mediante un proceso análogo al del caso anterior se obtiene que

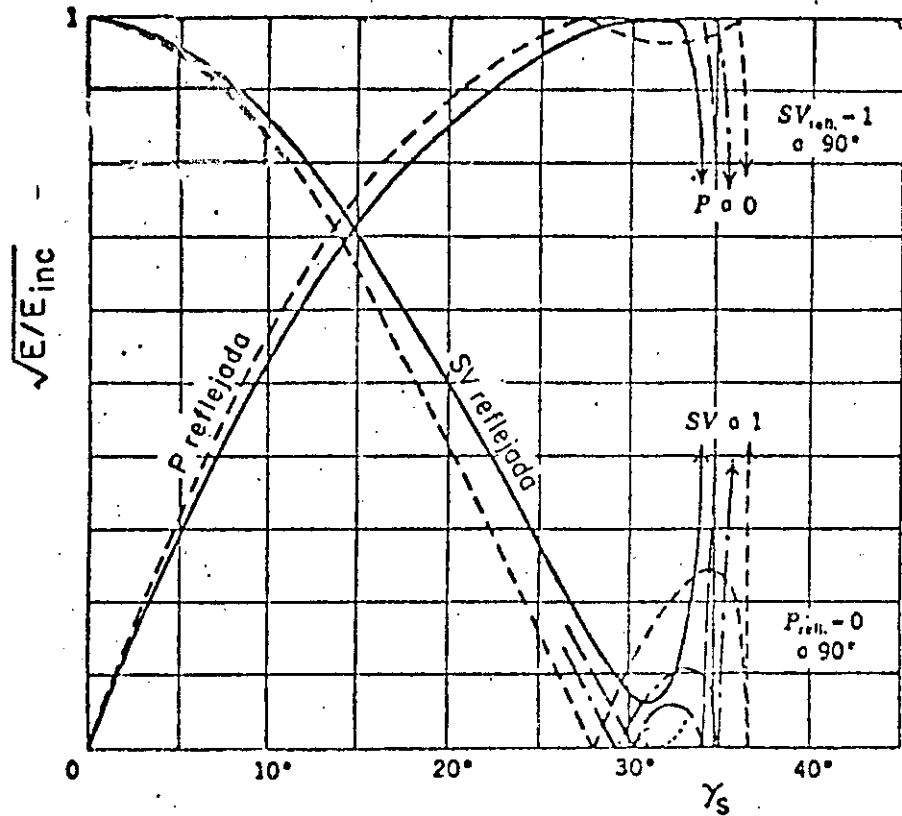


Fig 7. Raíz cuadrada de la relación de energía reflejada a energía incidente para una onda SV incidente en una superficie libre

$$\frac{A_2}{B_1} = - \frac{4 \cot \gamma_S (\cot^2 \gamma_S - 1)}{(\cot^2 \gamma_S - 1)^2 - 4i(1 - c^2/\alpha^2)^{1/2} \cot \gamma_S \operatorname{sgn} \omega} \quad (40)$$

$$\frac{B_2}{B_1} = - \frac{(\cot^2 \gamma_S - 1)^2 + 4i(1 - c^2/\alpha^2)^{1/2} \cot \gamma_S \operatorname{sgn} \omega}{(\cot^2 \gamma_S - 1)^2 - 4i(1 - c^2/\alpha^2)^{1/2} \cot \gamma_S \operatorname{sgn} \omega} \quad (41)$$

donde  $\operatorname{sgn} \omega = (-1$  si  $\omega < 0$  o  $1$  si  $\omega > 0$ ). En este caso, la incidencia de ondas SV con ángulos de incidencia  $\gamma_S$  mayores que  $\sin^{-1}(\beta/\alpha)$  genera ondas P no homogéneas que se atenúan con la profundidad.

## 4. ONDAS DE RAYLEIGH

Para el tercer caso,  $|c| < \beta < \alpha$ , se tiene que

$$\phi = A_2 e^{-mx} e^{-l\ell z} e^{i\omega t} \quad (42)$$

$$\psi = B_2 e^{-kx} e^{-l\ell z} e^{i\omega t} \quad (43)$$

donde  $m = |\omega| (1/c^2 - 1/\alpha^2)^{1/2}$  y  $k = |\omega| (1/c^2 - 1/\beta^2)^{1/2}$ . Se han eliminado  $A_1$  y  $B_1$  pues no representan ondas incidentes con potenciales finitos. Las ecuaciones de esfuerzos nulos en  $x = 0$  conducen a

$$\frac{A_2}{B_2} = \frac{2l(1-c^2/\beta^2)^{1/2} \operatorname{sgn} \omega}{2 - c^2/\beta^2} \quad (44)$$

$$\frac{A_2}{B_2} = \frac{2 - c^2/\beta^2}{2l(1-c^2/\alpha^2)^{1/2} \operatorname{sgn} \omega} \quad (45)$$

como las ecs 44 y 45 deben ser iguales se obtiene que la velocidad de fase,  $c$ , debe satisfacer la siguiente ecuación:

$$\left(2 - \frac{c^2}{\beta^2}\right)^2 - 4\left(1 - \frac{c^2}{\alpha^2}\right)^{1/2} \left(1 - \frac{c^2}{\beta^2}\right)^{1/2} = 0 \quad (46)$$

La raíz real de esta ecuación,  $c_R$ , encontrada por vez primera por Rayleigh, da la velocidad de las llamadas ondas de Rayleigh. En la fig 8 se presentan valores de  $c_R$  para

distintos valores del módulo de Poisson  $\nu$ . Las ondas de Rayleigh son ondas *superficiales* y debido a ello sufren

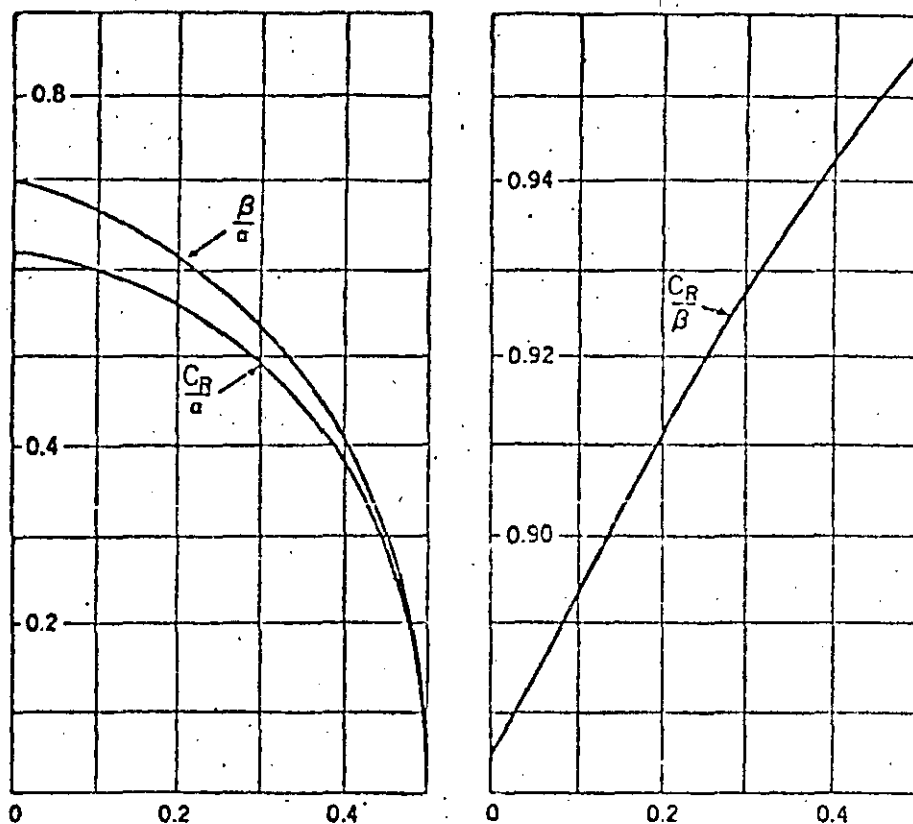


Fig 8. Relaciones  $\beta/\alpha$ ,  $c_R/\alpha$  y  $c_R/\beta$  como funciones del módulo de Poisson  $\nu$

menor atenuación geométrica. Puede demostrarse que el movimiento generado por ondas de Rayleigh hace que las partículas describan trayectorias elípticas con ciclos retrógrados, a diferencia de los ciclos progresivos que se presentan en las ondas superficiales en líquidos. La fig 9 muestra un dibujo esquemático de las ondas superficiales de Rayleigh.

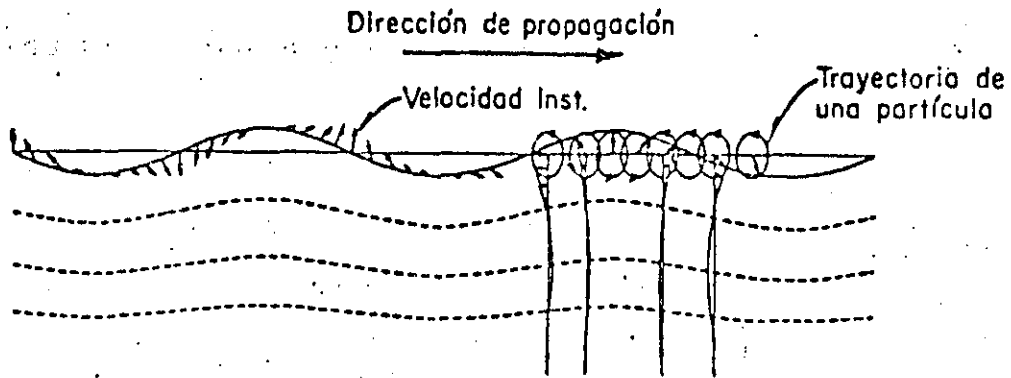


Fig 9. Ondas de Rayleigh

## 5. ONDAS DE LOVE

Puede demostrarse que la propagación de ondas superficiales (que se atenúen con la profundidad) del tipo SH es imposible en un semiespacio homogéneo. No obstante, las ondas SH superficiales se observan en la superficie de la tierra.

Love demostró que una teoría suficiente para explicar las ondas SH superficiales puede desarrollarse si se tiene un estrato homogéneo de espesor uniforme  $H$  con propiedades  $\mu_1$  y  $\beta_1$  sobre un semiespacio de propiedades  $\mu_2$  y  $\beta_2$  como se muestra en la fig 10. Supóngase que los desplazamientos son independientes de la coordenada  $y$ , y además que la variación con el tiempo está dada por  $e^{i\omega t}$ . El plano  $x = -H$  representa la superficie libre. Las ecuaciones de movimiento (ecs 1) se reducen a

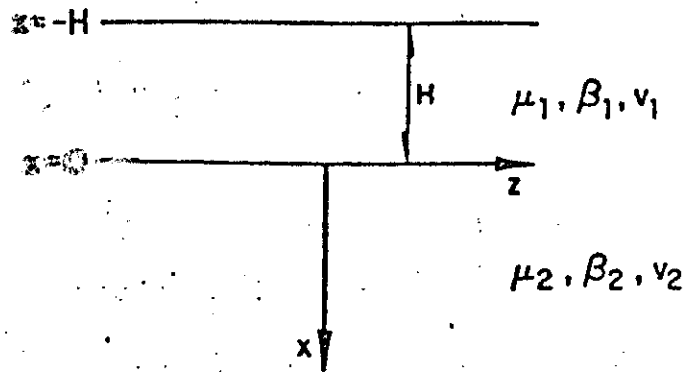


Fig 10. Notación para un estrato sobre un semiespacio elástico

para el estrato y

$$\frac{\partial^2 v_2}{\partial x^2} + \frac{\partial^2 v_2}{\partial z^2} + k_{\beta_2}^2 v_2 = 0 \quad (48)$$

donde  $k_{\beta_i} = \omega/\beta_i$ ,  $i = 1, 2$  para el semiespacio.

Haciendo uso de soluciones del tipo de las ecs 23 y 24 se puede escribir que

$$v_1 = (A e^{-k\gamma_1 x} + B e^{k\gamma_1 x}) e^{ik(z-ct)} \quad (49)$$

$$v_2 = C e^{-k\gamma_2 x} e^{ik'(z-ct)} \quad (50)$$

donde  $\gamma_1 = (1 - c^2/\beta_1^2)^{1/2}$  y  $\gamma_2 = (1 - c^2/\beta_2^2)^{1/2}$ . Se observa que si  $c < \beta_2$ ,  $v_2 \rightarrow 0$  cuando  $x \rightarrow \infty$ .

Las condiciones de frontera son que  $v_1 = v_2$  y  $(\tau_{xy})_1 = (\tau_{xy})_2$  en  $x=0$  y que  $\tau_{xy} = 0$  en  $x = -H$ . Estas condiciones conducen a un sistema de ecuaciones homogéneo en A, B y C. Para que se tenga solución diferente de cero el determinante del sistema debe anularse. Así, se tiene que

$$\tan k \gamma_1 H = i \frac{\mu_2 \gamma_2}{\mu_1 \gamma_1} = \frac{\mu_2 (1 - c^2/\beta_2^2)^{1/2}}{\mu_1 (c^2/\beta_1^2 - 1)^{1/2}} \quad (51)$$

es la ecuación para obtener la velocidad de las ondas de Love.

Si  $\beta_1 < \beta_2$  la ec 51 da valores reales de  $c$ , en el intervalo  $\beta_1 < c < \beta_2$ , que dependen de  $k$  y  $H$ . Pueden obtenerse ondas de Love de forma general superponiendo ondas de Love del tipo de la ec 49 con diferentes  $k$ .

La dependencia de la velocidad de propagación de la frecuencia ocasiona el fenómeno de *dispersión* y, en general, este es el caso en medios estratificados.

## 6. BIBLIOGRAFIA

Ewing, W M, Jardetzky, W S y Press, F, *Elastic waves in layered media*, Mc Graw-Hill Book Co, Nueva York, 1957

White, J E, *Seismic waves: radiation transmission and attenuation*, Mc Graw-Hill Book Co., Nueva York, 1965

Fung, Y C, *Foundations of solid mechanics*, Prentice-Hall, Inc, Englewood Cliffs, Nueva Jersey, 1965



**DIVISION DE EDUCACION CONTINUA  
FACULTAD DE INGENIERIA U.N.A.M.**

ANALISIS DE RIESGO SISMICO

NOCIONES ELEMENTALES

JULIO, 1985

Para estudiar el problema de propagación estudiemos primeramente el caso unidimensional. La ecuación que gobierna este movimiento es la llamada 'ecuación de onda unidimensional' y se escribe como

$$\frac{\partial^2 \phi}{\partial x^2} = \frac{1}{c^2} \frac{\partial^2 \phi}{\partial t^2} \quad (1)$$

donde  $\phi$  es por ejemplo la elevación de una onda en el que  $y$   $c$  es un coeficiente conocido como celeridad o velocidad de propagación.

Para obtener la solución general de la ec. 1 es conveniente hacer el siguiente cambio de variables,

$$u = x - ct$$

"

$$v = x + ct \quad (2)$$

este método conocido como de D'Alembert conduce a las siguientes transformaciones

$$\frac{\partial \phi}{\partial x} = \frac{\partial \phi}{\partial u} + \frac{\partial \phi}{\partial v}$$

$$\frac{\partial^2 \phi}{\partial x^2} = \frac{\partial^2 \phi}{\partial u^2} + 2 \frac{\partial^2 \phi}{\partial u \partial v} + \frac{\partial^2 \phi}{\partial v^2}$$

$$\frac{\partial \phi}{\partial t} = -c \frac{\partial \phi}{\partial u} + c \frac{\partial \phi}{\partial v}$$

$$\frac{\partial^2 \phi}{\partial t^2} = c^2 \left( \frac{\partial^2 \phi}{\partial u^2} - 2 \frac{\partial^2 \phi}{\partial u \partial v} + \frac{\partial^2 \phi}{\partial v^2} \right)$$

Now we add these two equations to get

$$\frac{(\lambda + 2G)q^2 - \lambda N^2}{2iGNs} = -\frac{2qiN}{s^2 + N^2} \quad (3-71)$$

and cross-multiply in Eq. (3-71) to obtain

$$4qGsN^2 = (s^2 + N^2)[(\lambda + 2G)q^2 - \lambda N^2] \quad (3-72)$$

Squaring both sides of Eq. (3-72) and introducing  $q$  from Eq. (3-59) and  $s$  from Eq. (3-60), we get

$$16G^2N^4 \left( N^2 - \frac{\omega^2}{v_p^2} \right) \left( N^2 - \frac{\omega^2}{v_s^2} \right) = \left[ (\lambda + 2G) \left( N^2 - \frac{\omega^2}{v_p^2} \right) - \lambda N^2 \right]^2 \left[ N^2 + \left( N^2 - \frac{\omega^2}{v_s^2} \right) \right]^2 \quad (3-73)$$

Now, dividing through by  $G^2N^2$ , we obtain

$$16 \left( 1 - \frac{\omega^2}{v_p^2 N^2} \right) \left( 1 - \frac{\omega^2}{v_s^2 N^2} \right) = \left[ 2 - \frac{(\lambda + 2G)}{G} \left( \frac{\omega^2}{v_p^2 N^2} \right) \right]^2 \left( 2 - \frac{\omega^2}{v_s^2 N^2} \right)^2 \quad (3-74)$$

Then, using the following relationships derived in the footnote\* gives

$$\frac{\omega^2}{v_p^2 N^2} = \frac{v_R^2}{v_p^2} = \alpha^2 K^2 \quad (3-75)$$

$$\frac{\omega^2}{v_s^2 N^2} = \frac{v_R^2}{v_s^2} = K^2 \quad (3-76)$$

$$\frac{\lambda + 2G}{G} = \frac{1}{\alpha^2} = \frac{2 - 2\nu}{1 - 2\nu} \quad (3-77)$$

\* By definition,

$$N = \frac{2\pi}{L}$$

or

$$L = \frac{2\pi}{N}$$

(Let  $L_s$  and  $v_s$  be the wave length and velocity, respectively, of the surface wave.)

Eq. (3-74) can be written

$$16(1 - \alpha^2 K^2)(1 - K^2) = \left( 2 - \frac{1}{\alpha^2} \alpha^2 K^2 \right)^2 (2 - K^2)^2 \quad (3-78)$$

After expansion and rearrangement, Eq. (3-78) becomes

$$K^4 - 8K^2 + (24 - 16\alpha^2)K^2 + 16(\alpha^2 - 1) = 0 \quad (3-79)$$

Equation (3-79) can be considered a cubic equation in  $K^2$  and real valued solutions can be found for given values of  $\nu$ . The quantity  $K$  represents a ratio between the velocity of the surface wave and the velocity of the shear wave.

Also,

$$L_s = \frac{v_s}{f} = \frac{2\pi v_s}{\omega}$$

and, from above,

$$L_s = \frac{2\pi}{N} = \frac{v_s 2\pi}{\omega}$$

therefore,

$$N = \frac{\omega}{v_s}$$

and

$$N^2 = \frac{\omega^2}{v_s^2}$$

Let  $K$  and  $\alpha$  be defined such that

$$\frac{v_R^2}{v_s^2} = K^2 \quad \text{and} \quad \frac{v_R^2}{v_p^2} = \alpha^2 K^2$$

Then

$$\frac{\omega^2}{v_p^2 N^2} = \frac{v_R^2}{v_p^2} = \alpha^2 K^2$$

and

$$\frac{\omega^2}{v_s^2 N^2} = \frac{v_R^2}{v_s^2} = K^2$$

Substitution of  $v_p$  and  $v_s$  from Eqs. (3-46) and (3-48) gives

$$\frac{1}{\alpha^2} = \frac{v_p^2}{v_s^2} = \frac{\lambda + 2G}{G} = \frac{\rho}{G} = \frac{\lambda + 2G}{G}$$

and using

$$\nu = \frac{\lambda}{2(\lambda + G)}$$

we get

$$\frac{\lambda + 2G}{G} = \frac{2 - 2\nu}{1 - 2\nu} = \frac{1}{\alpha^2}$$

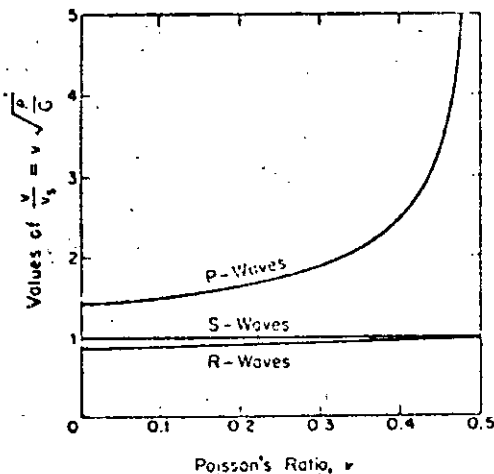


Figure 3-13. Relation between Poisson's ratio,  $\nu$ , and velocities of propagation of compression (P), shear (S), and Rayleigh (R) waves in a semi-infinite elastic medium (from Richart, 1962).

From this solution it is clear that  $K^*$  is independent of the frequency of the wave; consequently, the velocity of the surface wave is independent of frequency and is nondispersive.

Ratios of  $v_R/v_S$  and  $v_P/v_S$  can be obtained from Eq. (3-79) for values of Poisson's ratio  $\nu$  from 0 to 0.5. Curves of these ratios as a function of  $\nu$  are shown in Fig. 3-13.

#### Rayleigh-Wave Displacement

So far, a relationship for the ratio of the Rayleigh-wave velocity to the shear-wave velocity has been obtained, but additional information about the Rayleigh wave can be determined by obtaining the expressions for  $u$  and  $w$  in terms of known quantities. Upon substituting the expressions for  $\Phi$  and  $\Psi$  from Eqs. (3-65) and (3-66) into the expressions for  $u$  and  $w$ , we get

$$\begin{aligned} u &= \frac{\partial \Phi}{\partial x} + \frac{\partial \Psi}{\partial z} \\ &= -A_1 i N \exp[-qz + i(\omega t - Nx)] - A_2 s \exp[-sz + i(\omega t - Nx)] \end{aligned} \quad (3-80)$$

and

$$\begin{aligned} w &= \frac{\partial \Phi}{\partial z} - \frac{\partial \Psi}{\partial x} \\ &= -A_1 i N \exp[-qz + i(\omega t - Nx)] + A_2 i N \exp[-sz + i(\omega t - Nx)] \end{aligned} \quad (3-81)$$

From Eq. (3-70) we can get

$$A_2 = -\frac{2qiNA_1}{s^2 + N^2}$$

and substitution of  $A_2$  into Eqs. (3-80) and (3-81) gives

$$u = A_1 \left[ -iN \exp(-qz) + \frac{2iqsN}{s^2 + N^2} \exp(-sz) \right] \exp i(\omega t - Nx) \quad (3-82)$$

and

$$w = A_1 \left[ \frac{2qN^2}{s^2 + N^2} \exp(-sz) - q \exp(-qz) \right] \exp i(\omega t - Nx) \quad (3-83)$$

Equations (3-82) and (3-83) can be rewritten

$$u = A_1 N i \left\{ -\exp \left[ -\frac{q}{N}(zN) \right] + \frac{2 \frac{q}{N} \frac{s}{N}}{\frac{s^2}{N^2} + 1} \exp \left[ -\frac{s}{N}(zN) \right] \right\} \times \exp i(\omega t - Nx) \quad (3-84)$$

and

$$w = A_1 N \left\{ \frac{2 \frac{q}{N}}{\frac{s^2}{N^2} + 1} \exp \left[ -\frac{s}{N}(zN) \right] - \frac{q}{N} \exp \left[ -\frac{q}{N}(zN) \right] \right\} \times \exp i(\omega t - Nx) \quad (3-85)^*$$

Now, from Eqs. (3-84) and (3-85), the variation of  $u$  and  $w$  with depth can be expressed as

$$U(z) = -\exp \left[ -\frac{q}{N}(zN) \right] + \frac{2 \frac{q}{N} \frac{s}{N}}{\frac{s^2}{N^2} + 1} \exp \left[ -\frac{s}{N}(zN) \right] \quad (3-86)$$

and

$$W(z) = \frac{2 \frac{q}{N}}{\frac{s^2}{N^2} + 1} \exp \left[ -\frac{s}{N}(zN) \right] - \frac{q}{N} \exp \left[ -\frac{q}{N}(zN) \right] \quad (3-87)$$

\* The significance of the presence of  $i$  in the expression for  $u$  (Eq. 3-84) and its absence in the expression for  $w$  (Eq. 3-85) is that the  $u$ -component of displacement is  $90^\circ$  out of phase with the  $w$ -component of displacement.

EFFECT OF LOCAL SOIL CONDITIONS  
UPON EARTHQUAKE GROUND MOTIONS

by Robert V. Whitman

1. INTRODUCTION

It has long been recognized that local soil conditions can have a profound effect upon the damage caused by an earthquake. Such an effect was clearly evident in accounts of the great Lisbon earthquake of 1755, and in the accounts of almost every subsequent major earthquake that affected a large city. The effect of soil conditions upon damage during the 1906 San Francisco earthquake was well recognized in studies of that earthquake. The topic received considerable study following the Kanto (Tokyo) earthquake of 1923. The effect of local soil conditions upon earthquake damage is hardly a new problem. The seismic codes of most countries specifically require different earthquake resistance for different soil conditions. Codes now in effect in the United States contain no such requirement, but not because soil conditions are thought to be unimportant. The writers of the U.S. codes recognized the importance of soil conditions, but felt the problem was so complex and poorly understood that adequate code provisions could not be written. Without a doubt, soil conditions will be incorporated into U.S. seismic codes in the very near future.

Much of the earthquake damage to buildings built upon poor soils results from partial or complete failure of the soil. Such failures include slumping of river banks, failure of waterfront retaining structures, large landslides, foundation settlement and foundation failures. Seed (1970) has provided an excellent summary description of such failures. Many such failures are caused by total or partial liquefaction of loose saturated cohesionless soils. The possibility of such failures, especially liquefaction failures, in any given locale or site requires individual study by experts. Appendix B contains a very brief discussion of liquefaction.

This chapter considers the effect of local soil conditions upon earthquake ground motions, and hence upon the shaking of buildings.

when there is no failure of the soil. Field observations and theoretical studies of this effect have been summarized in recent papers by Ohsaki (1969) and Seed (1969). Much is now known about the problem, although by no means is there complete understanding. There are several ways in which this new knowledge can be put to practical use. One way is the development of site-conditioned earthquake motions for input to the analysis of important structures; this approach is now being used in the design of tall buildings in San Francisco and Tokyo. The second way is to guide the development of new building code provisions. This chapter deals primarily with the latter application. That is, the chapter will discuss how the base shear coefficient  $C$  should vary with soil conditions. A plot of  $C$  vs.  $T$ , the fundamental period of the building, will be called a seismic coefficient diagram.

Figure 1 illustrates several different forms of seismic coefficient diagrams incorporating soil conditions. The simplest forms are those in Figures 1a and 1b; here all ordinates are multiplied by a factor that is independent of period. That is:

$$C(T) = S C_0(T) \quad (1)$$

where  $S$  is a soil factor and  $C_0(T)$  is the seismic coefficient function for a reference soil condition. Ohsaki (1969) has tabulated values of  $S$  required by the codes of 13 countries. Table 1 gives examples of such factors, ranging from the very simple table used in Canada to the somewhat complex table in effect in Japan.

Figures 1c through 1f show more complicated proposals for introducing the effect of local soil conditions into seismic coefficient diagrams; now the effect of soil is varied depending upon the period  $T$ .

1. Figure 1c comes from the new Chilean code. The curve of  $C$  vs.  $T$  varies in shape depending upon a parameter  $T_0$ . The parameter  $T_0$  is related to the characteristic frequency of the site of the building being designed.
2. Figure 1d shows a seismic coefficient diagram proposed by Muto in Japan in 1963. Both the maximum seismic coefficient and the period scale are adjusted in accordance with the type of ground.

- 3. According to the proposed curves shown in Figure 1e, low stiff buildings having a small period  $T$  would be designed for a larger seismic coefficient if on hard ground than if on soft ground. For tall flexible buildings, the reverse would be true.
- 4. Figure 1f shows the code provisions developed for Mexico City, so as to account for the effect of the unusually soft and deep clay which underlies much of that city.

Thus, a great variety of methods have been proposed for incorporating the effects of soils conditions into the seismic provisions of building codes. A building official faced with the selection of a suitable provision, or an engineer faced with implementing such provisions, must understand the basic thinking lying behind the various proposals. To develop such basic understanding, it is useful to consider four categories of soil conditions:

- I. Shallow soil deposit with a distinct characteristic frequency.
- II. Deep deposit of firm soil.
- III. Shallow soft soil overlying deep deposit of firm soil.
- IV. Deep deposit of soft soil.

While these four cases do not encompass all possible soil conditions, they serve to bring out the fundamental considerations.

## 2. ROLE AND STATUS OF THEORY

In order to understand adequately the effect of local soil conditions, we must combine interpretations of actual accelerograph records together with theoretical analysis. Within the recent past, it has been necessary to rely very heavily upon theory, since the field data from accelerographs has been very scanty indeed. Because of the many accelerographs which have been installed within the past few years and will be installed within the near future, there soon should be many more records involving a variety of soil conditions. However, theory will continue to be of vital importance in helping to sort out and understand the potentially staggering quantity of rather confusing data.

The theory of ground amplification\* as it exists today is by no means perfect. However, in many cases predictions from the theory are in accord with observations (Seed, 1969). There now has been considerable experience in the practical use of the theory, and we understand both its limitations as well as how it can be used. Used with judgement, this theory is a very useful tool for understanding the effects of local soil conditions.

## 3. CASE I: SHALLOW SOIL DEPOSIT WITH DISTINCT CHARACTERISTIC FREQUENCY

For a uniform soil deposit (Fig. 2a), the fundamental period is given by:

$$T_0 = \frac{4H}{C_s} \quad (2)$$

where  $H$  = thickness of deposit  
 $C_s$  = shear wave velocity.

Case I is typified by  $T_0 < 0.5$  sec. The following tabulation indicates typical combinations of  $C_s$  and  $H$  satisfying this condition.

$C_s$ (m/sec)	$H$ (m)
100 (Very soft clay or silt)	< 12.5
200 (Loose sand, soft clay)	< 25
300 (Dense sand, stiff clay)	< 37.5
400 (Compact sand, hard clay)	< 50

Soil deposits with a depth greater than about 50 meters probably do not belong in Case I. The soil descriptions in the table are intended to give a very general idea of typical shear wave velocities in soils; for further discussion of the evaluation of soil properties for specific cases, see Appendix A and Whitman (1969). Since the soil is non-linear, the shear wave velocity and hence the fundamental period depend upon the intensity of the earthquake, decreasing as the intensity increases.

\* The nature of this theory is outlined in Appendix A.

where  $C_D$  is the dilatational, or compressive, wave velocity. The wave velocity for granite serves as a reference against which a soil is rated. The smaller this ratio, the more severe the expected damage during an earthquake.

2. The depth to the water table. The shallower the water table, the greater the expected damage.

These two factors are combined in the equation

$$n = 1.67 \log_{10} \left[ \frac{(\gamma C_D)_{\text{rock}}}{(\gamma C_D)_{\text{soil}}} \right] + e^{-0.04h^2} \quad (5)$$

where  $n$  is the increment in intensity units on a scale equivalent to the modified Mercalli scale, and  $h$  is the depth to the water table in meters. Eq. 5 typically gives an increase in 1 to 2 intensity units (equivalent to a 2 or 4 fold increase in acceleration) for soft ground as compared to firm ground. Medvedev's method was originally developed for use in connection with shallow soil deposits and buildings having only a few stories.

The relationship between Medvedev's method and amplification theory may be understood by means of the example in Figure 9. When the water table is very low, then the ratio  $C_D/C_S$  is the same for both the soil and the rock. Thus ratios 3 and 4 are equivalent, and Medvedev's method and amplification theory will predict the same trends. The soil in Figure 9b has the same  $C_S$  as in Figure 9a, and thus amplification theory would predict the same behavior for both cases. Raising the water table means that  $C_D$  increases considerably in the soil, and thus the first term in Medvedev's equation decreases. However, this decrease is compensated by an increase in the second term. Thus, Medvedev's two factors taken together give roughly the same result as amplification theory. Moreover, the increases in intensity predicted by Medvedev are consistent with increases in acceleration predicted by amplification theory.

## Summary

For the common case of shallow soil deposits, the predictions of amplification theory are generally in accord with actual experience during earthquakes and moreover are in accord with the semi-empirical methods of microzoning proposed by Kanai and Medvedev.

Figure 10 summarizes the effect of local soil and rock conditions upon response spectra (say for 5% damping) at a given distance from the epicenter of an earthquake. With increasing softness of the earth material, the peak of the spectra increases and shifts to a larger period. Thus, the response of low stiff buildings is strongly affected by soil conditions. On the other hand, a shallow soil deposit has little or no effect upon the response of the fundamental period of tall buildings having long natural periods (although the shallow soil will affect the response of the higher modes of such a building).

Based upon current knowledge, a seismic coefficient diagram such as type (b) in Figure 1 should be used to account for differences in near surface earth materials within a small region. That is to say, the soil factor  $S$  should be independent of period. There are several reasons for this recommendation.

1. Because of uncertainties in both the fundamental period of the soil and the predominant periods in the input ground motion, it is difficult to predict the predominant period in motion at the top of soil. Use of constant  $S$  for  $T < 0.5$  sec. covers these uncertainties.
2. Use of constant  $S$  for  $T > 0.5$  sec. recognizes that the contribution of the higher modes will be affected by soil conditions, and provides extra conservatism with regard to the design of tall buildings.

With further research, it may be possible to use a reduced value of  $S$  for  $T > 0.5$  sec.

Table 2 gives recommended soil factors. These factors are based upon both theory and experience, and consider possible settlement problems in addition to amplification effects. In the 2nd column of the table, hard crystalline rock found at considerable depth has been taken as the reference; the soil factor for a soft soil is 4. However, it generally is more practical to use surface exposures of rock as a reference (3rd column), and then the soil factor for soft soil is 2.2. In some localities, it may even be desirable to use firm soil as a reference (4th column), in which case the soil factor for soft soil is only 1.6.

#### 4. CASE II DEEP DEPOSIT OF FIRM SOIL

Several areas that have experienced major earthquakes are underlain by more than 100 meters of compact alluvium. Los Angeles, Caracas, Venezuela, and Santiago, Chile are prime examples.

##### Theoretical Considerations

Amplification spectra: Figure 11 illustrates the general nature of the amplification spectrum for this case. Now several peaks occur within the range of building periods of practical interest.

The fundamental period is greater than in Case I, and tends to coincide with the period of taller structures. Because the shear wave velocity of compact alluvium is rather high (300 to 450 m/sec) the radiation damping also is greater than in Case I, and hence the amplification at the fundamental peak generally is less than in Case I. Nonetheless, this amplification can be quite important.

The higher order peaks typically occur at periods less than 0.5 second; that is, within the same range of periods for which amplification occurred in Case I. Radiation damping is less important for these higher modes, and hence when internal damping is small--as during small earthquakes--the peaks corresponding to these modes may be nearly as high as the fundamental peak.

Peak accelerations: Figure 12 shows computed acceleration at ground surface, for conditions corresponding to Figure 10 (the input is the same as in Fig. 3, but with a peak acceleration of 0.03g). Peak acceleration is increased; typical increases are factors of 1.5 to 3, with the larger values applying to smaller earthquakes. This increase is caused by the higher modes of the soil; these modes have amplification peaks in the range of the predominant periods of the input motion. The fundamental mode does not cause an increase in peak acceleration, but does amplify the longer period components of ground motion.

Response spectra: Figure 13 compares response spectra for motions at the surface of several different depths of compact alluvium. Changing the depth of the alluvium has relatively little effect upon the general position of the spectra for  $T < 0.5$  second. However, increasing the depth of the alluvium has a very significant effect upon the spectra at larger periods corresponding to taller buildings.

##### Field Evidence

There is, to the author's knowledge, no adequate direct confirmation of these theoretical results, although Gutenberg (1957) has shown that deep deposits amplify the long period components of ground motion. Actual accelerograph records from nearby sites with very different depths of alluvium must be obtained before adequate confirmation is possible.

Observations of damage to buildings during the Caracas earthquake of July 1967 do provide strong indirect confirmation of the theory (Whitman, 1969; Seed et al, 1970). Caracas is underlain by a compact alluvium whose depth generally is less than 100 meters. However, under one portion of the city the depth is as much as 300 meters. Analysis of the patterns of damage shows:

1. For buildings having 8 stories or less, the percentage of buildings damaged is more-or-less constant for all parts of the city.

23

## Summary

For this situation, it is appropriate to use a seismic coefficient diagram of Type (f) in Fig 1. Now the seismic coefficient is less for very small periods than for intermediate periods. However, at this time use of such a diagram is justified only for sites where there is considerable actual experience which has been studied in detail.

## 7. PILE FOUNDATIONS

The evidence currently available suggests that piles usually do not alter the ground motions at the base of a building (Ohsaki, 1969). This is because piles generally are flexible enough to follow the horizontal motions of the soil (for example, see Yamamoto and Seki, 1970) However, piles may improve the ability of the building to resist the effects of the ground motion--by reducing both static settlements (that may use up some of the reserve strength of the building) and dynamic rocking motion. Because of the need for less conservatism, the soil factor  $S$  might be reduced somewhat for pile-supported buildings.

Large diameter caissons may be stiff enough to resist following the motions of a soft soil through which they pass (Ohsaki, 1969). Then the amplifying effect of the soil-caisson system will be more like that of a firm soil rather than a soft soil. Thus for caisson-supported buildings,  $T_0$  used in Eq. 7 could be somewhat less than the fundamental period of the soil.

Unfortunately, at the present time there are no sound rules for deciding just how much  $S$  and  $T_0$  might be modified in accordance with these considerations.

## 8. RESPONSE SPECTRA AND TIME HISTORIES

The emphasis in this chapter has been upon code provisions to

reflect soil conditions. However, there is a growing trend toward requiring dynamic analyses for tall or important buildings.

The principles discussed in connection with Cases I, II, and III can be used to suggest the possible form for a general design response spectrum incorporating soil conditions:

$$S_a = \begin{cases} S_{a0} S & T \leq T_0 \\ S_{a0} \frac{T_0}{T} \left[ (S-1) \frac{T_0}{T} + 1 \right] & T \geq T_0 \end{cases} \quad (8)$$

where  $S_a$  is the spectral acceleration and  $S_{a0}$  is the spectral acceleration for the reference soil condition. This equation is plotted in Figure 17. The soil factor  $S$ , which brings in the effect of the near-surface soil, might be less than in Table 2, since use of dynamic analysis means less need for conservatism. For example, the following values might be used:

<u>Ground condition</u>	<u>S</u>
Exposed rock	1.0
Firm soil	1.3
Soft soil	1.8

The effect of the near-surface soil upon spectral acceleration decreases for  $T > T_0$ . This is in contrast to Eq. 7 where there was need to account for the contributions from higher modes; when a dynamic analysis is performed, the response of higher modes is introduced directly

For  $T > 3$  seconds and  $T_0 > 1$  second, Eq. 8 becomes too conservative. Tezcan (1972) has recently presented a more general approach to development of response spectra including soil effects.

Time histories whose spectra lie above the spectra given by Eq. 8

would be suitable as input for dynamic analysis. Great caution should be followed in using individual time histories generated by the theoretical procedures described in Appendix A, since there are uncertainties both in the validity of the procedures and the selection of soil properties. If such procedures are used to generate site-conditioned time histories, it is very essential that a set of time histories be developed by varying the input assumptions.

### 9. FINAL COMMENTS

The four cases which have been discussed in this chapter certainly do not cover all possible soil conditions, and many problems remain to be solved by further theoretical research plus analysis of accelerograph records. For example, the line of demarcation between Cases II and IV is not at all clear. However, the current understanding of the effect of local soil conditions is almost equal-- and perhaps even equal--to the current understanding of the nature and amplitude of earthquake ground motions for average soil conditions. That is to say, the effect of soil conditions can be evaluated with almost as much confidence as can the reference seismic coefficient  $C_0$ .

Table 1

### EXAMPLES OF SOIL FACTORS

<u>Canada</u>		<u>Argentina</u>	
General	1.0	Hard	0.75
Soft	1.5	Medium	1.00
		Soft	1.25
		Very soft	1.50

### Japan

Ground/Structure	Wood	Steel	Reinf. Conc.
I Rock	0.6	0.6	0.8
II Diluvium	0.8	0.8	0.9
III Alluvium	1.0	1.0	1.0
IV Very soft	1.5	1.0	1.0

Table 2

RECOMMENDED SOIL FACTORS TO ACCOUNT FOR  
EFFECT OF NEAR SURFACE SOILS

Ground condition	Reference ground condition		
	Hard rock	Exposed rock	Firm soil
Hard crystalline rock at depth ( $C_s > 1200$ m/sec)	1.0	0.6	0.4
Exposed rock with minimal weathering ( $C_s = 700$ m/sec)	1.8	1.0	0.7
Firm clay, compact sand/gravel, deeply weathered rock ( $C_s = 350$ m/sec)	2.5	1.4	1.0
Soft clay or silt ( $C_s = 120$ m/sec)	4.0	2.2	1.6

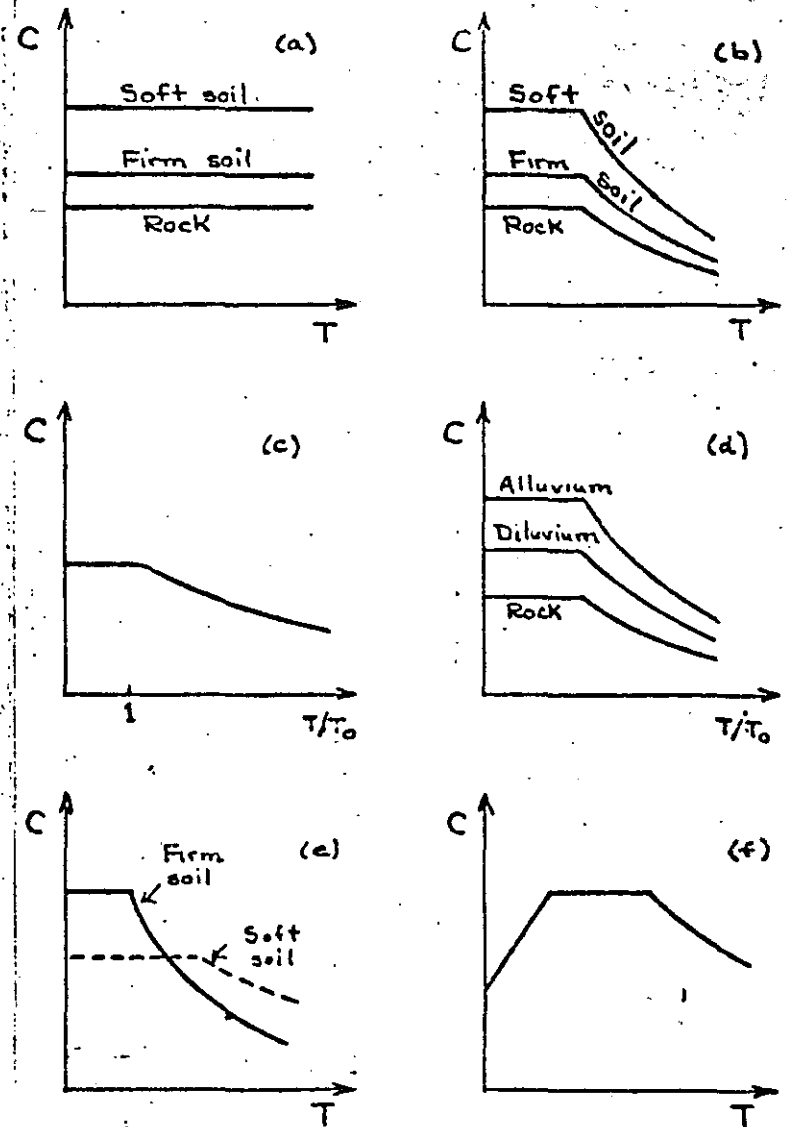
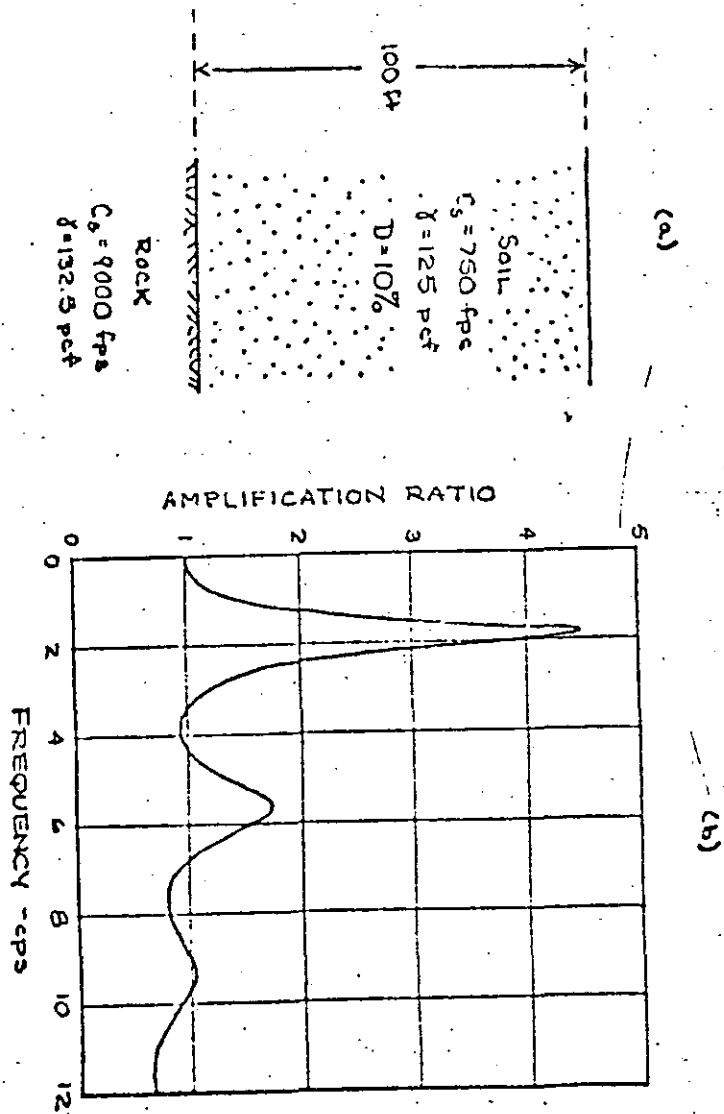
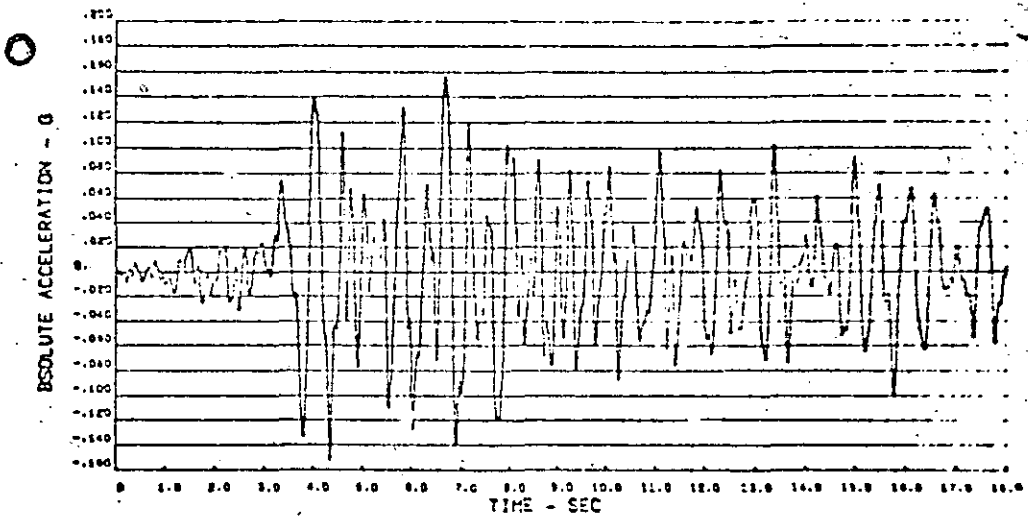


FIGURE 1 VARIOUS TYPES OF SEISMIC COEFFICIENT DIAGRAMS

FIGURE 2 AMPLIFICATION RATIO FOR SHALLOW SOIL PROFILE



TAFT NS9V EARTHQUAKE OF JULY 21, 1952 - NORMALIZED TO 0.1 G



TAFT NS9V EARTHQUAKE OF JULY 21, 1952 - NORMALIZED TO 0.1 G

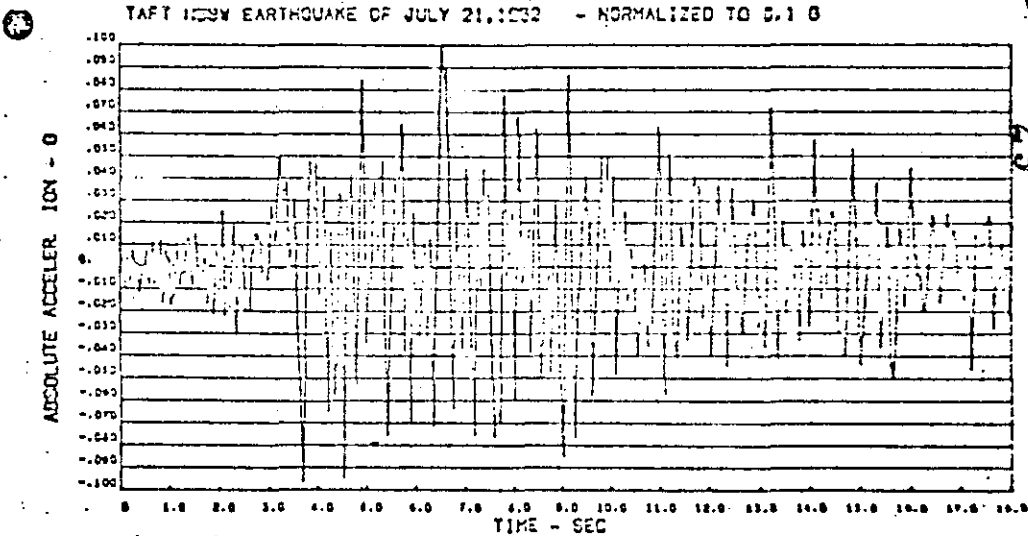


FIGURE 3 INPUT AND COMPUTED SURFACE MOTIONS FOR PROFILE IN FIGURE 2

TOKYO STA. AB SIMPLE AVE. 6 QUAKES

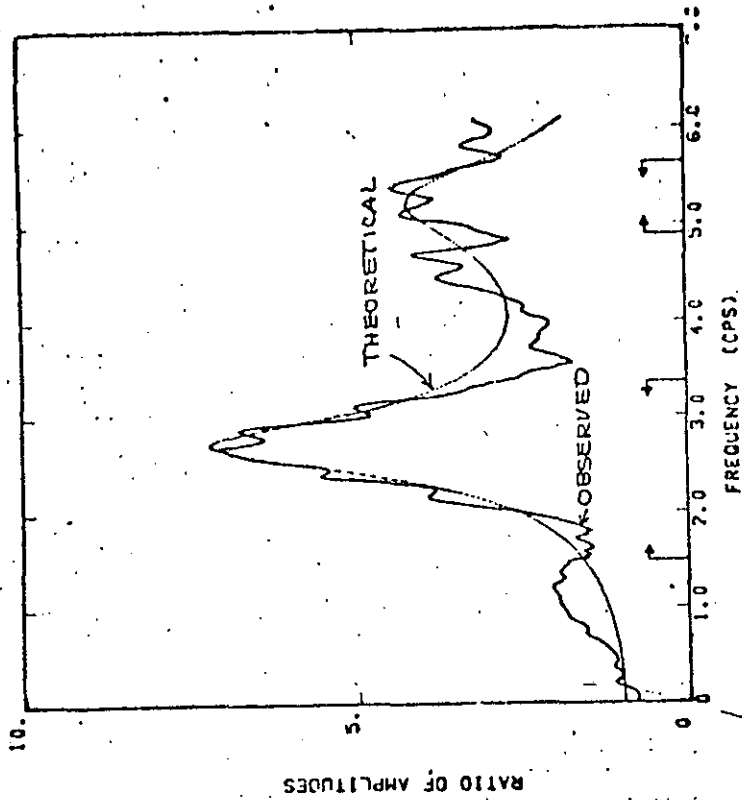


FIGURE 5 THEORETICAL AND OBSERVED AMPLIFICATION CURVES

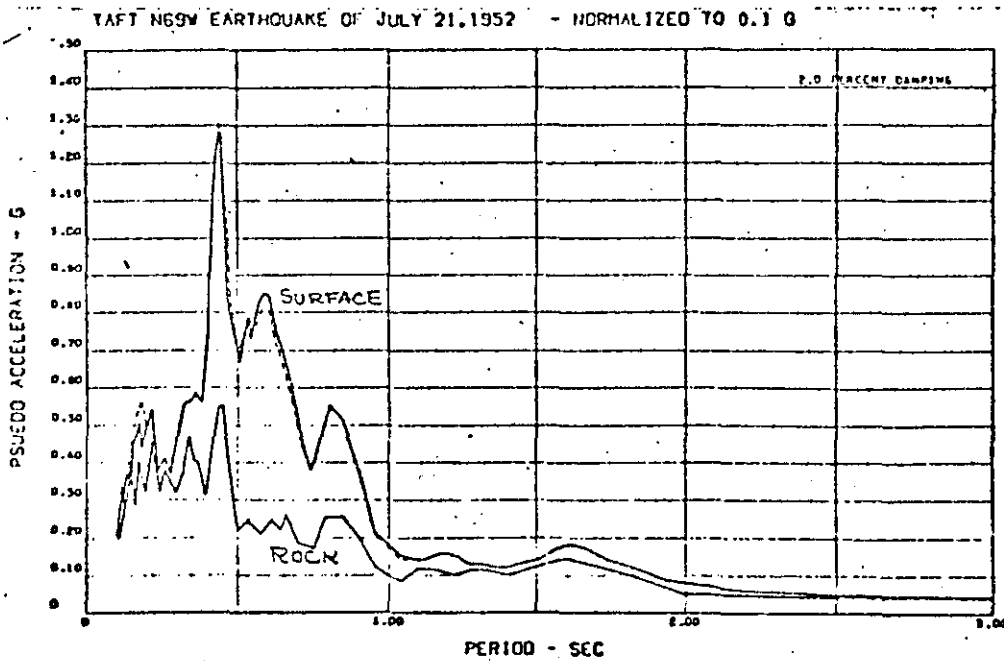


FIGURE 4 COMPARISON OF INPUT AND SURFACE RESPONSE SPECTRA FOR SHALLOW SOIL PROFILE

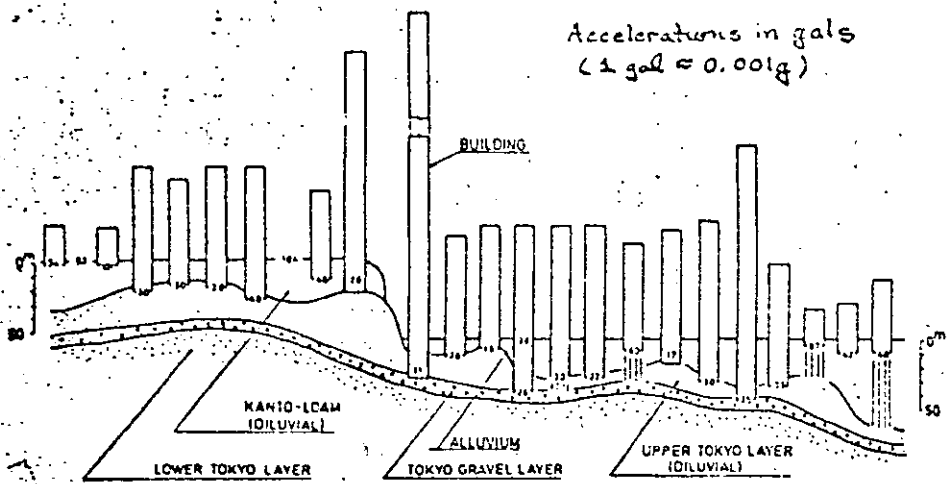


FIGURE 6 PEAK ACCELERATIONS FOR DIFFERENT SOILS AND DEPTHS IN TOKYO DURING EARTHQUAKE IN 1968 (from Ohnaki, 1969)

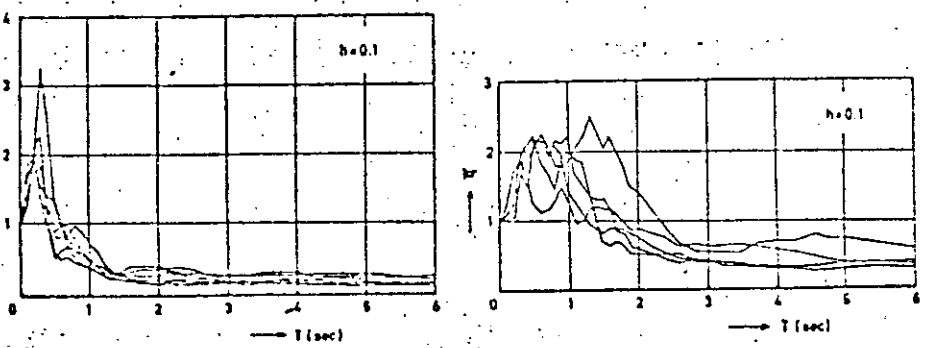
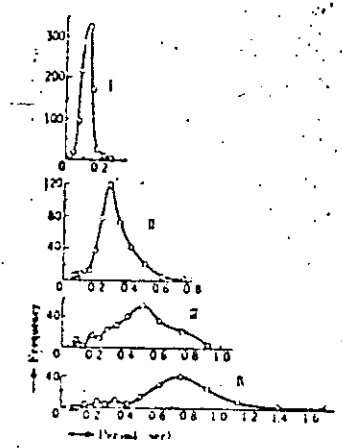
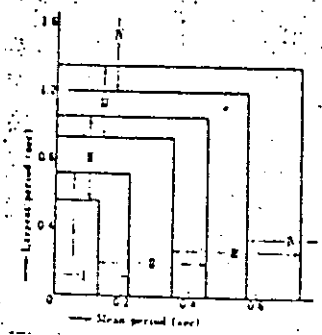
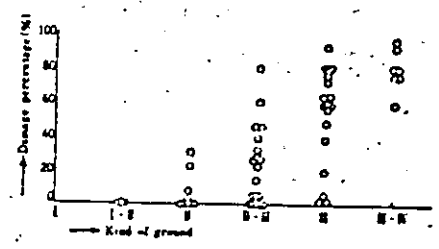


FIGURE 7 RESPONSE SPECTRA (normalized to peak acceleration) FOR DIFFERENT SOIL CONDITIONS IN TOKYO (from Ohnaki, 1969)

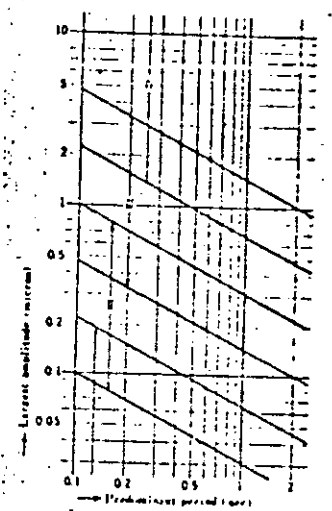
I ROCK  
II DILUVIUM  
III ALLUVIUM  
IV VERY SOFT



(a) Frequency of occurrence of various periods in microtremor records on different ground



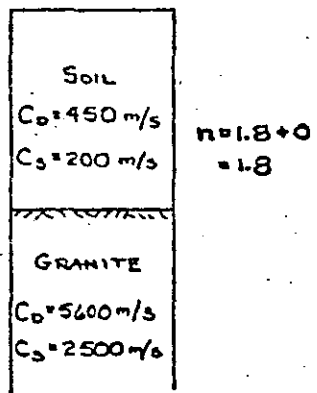
(c) Correlation of mean and largest period with ground type.



(d) Correlation of amplitude and predominant period with ground type

FIGURE 8 USE OF MICROTREMOR MEASUREMENTS TO CLASSIFY GROUND TYPE (after Kanai and Tanaka, 1961)

(a) Low water table



(b) High water table

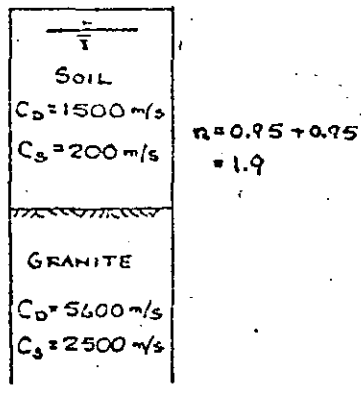


FIGURE 9 EXAMPLE OF MEDVEDEV METHOD

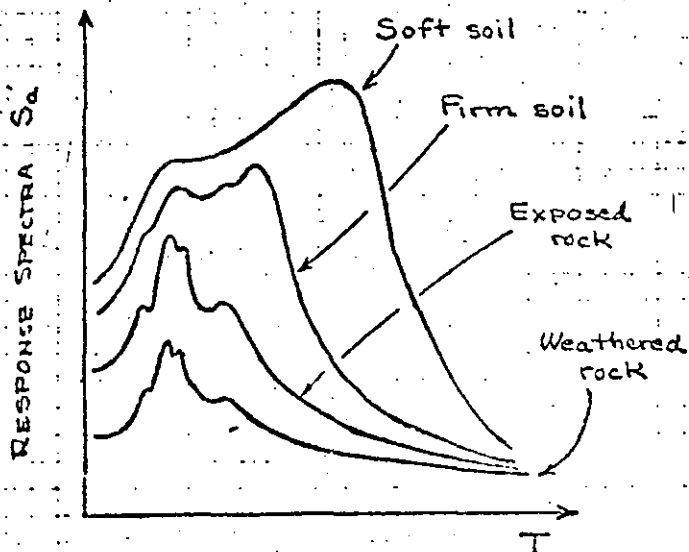


FIGURE 10 SUMMARY OF AMPLIFYING EFFECTS OF SHALLOW SOIL DEPOSIT

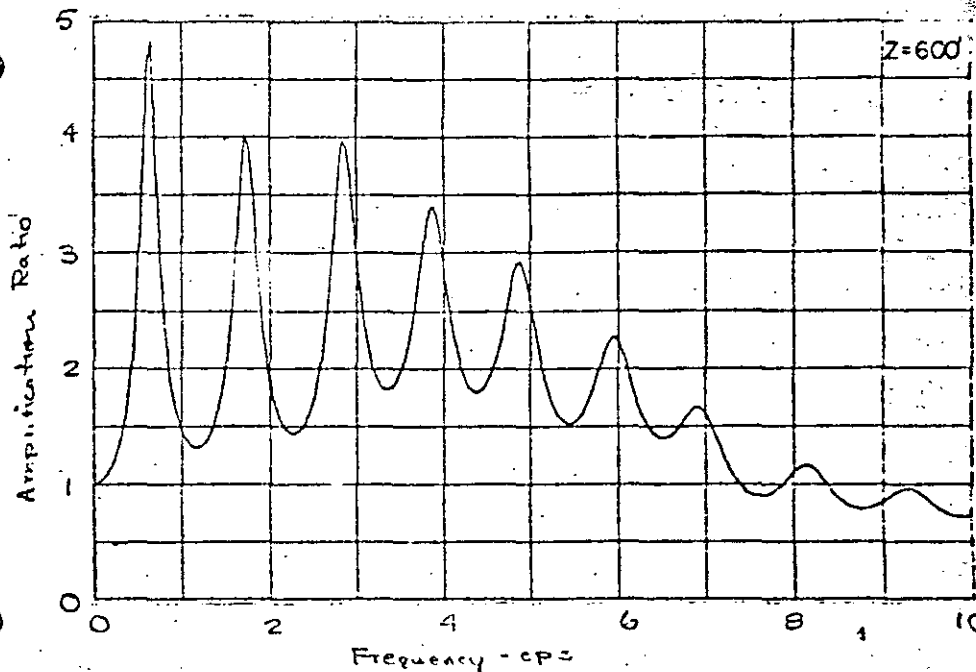


FIGURE 11 AMPLIFICATION SPECTRUM FOR 600 FOOT DEEP SOIL PROFILE

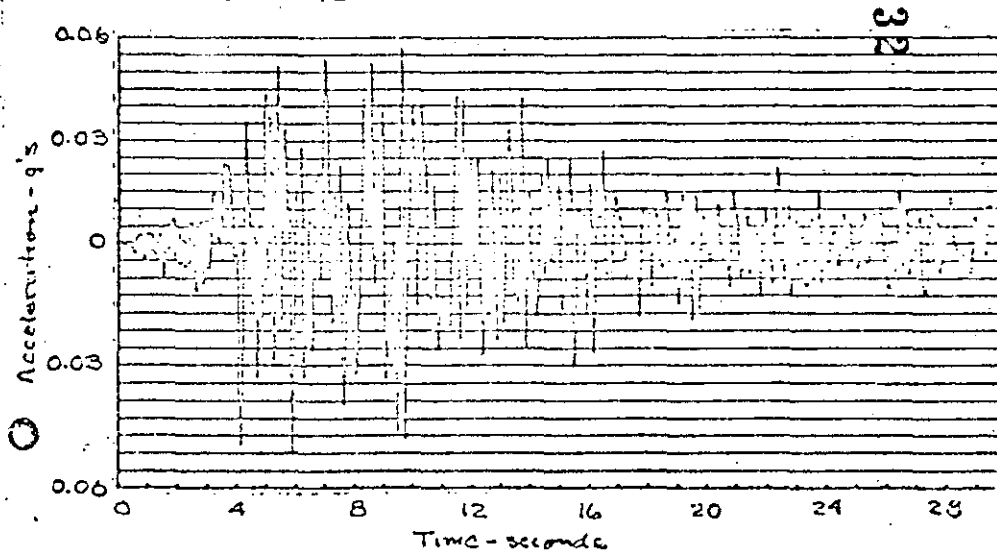


FIGURE 12 ACCELERATION COMPUTED AT 600' OF SOIL

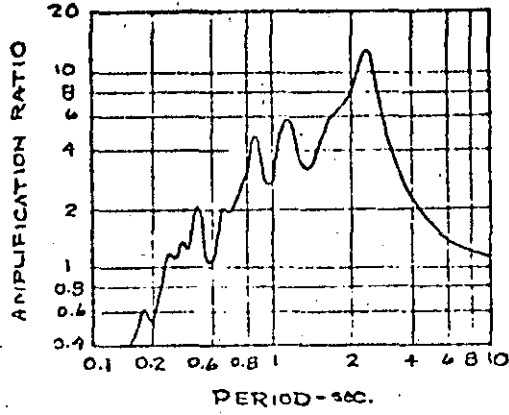
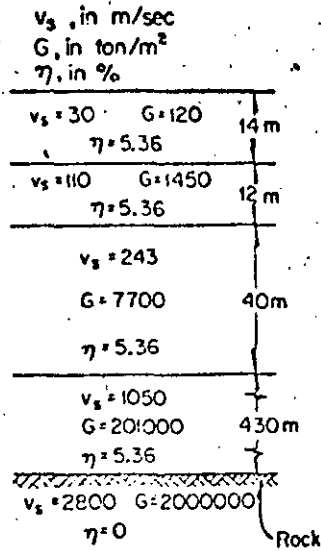


FIGURE 15 AMPLIFICATION SPECTRUM FOR DEEP PROFILE WITH VERY SOFT SOIL

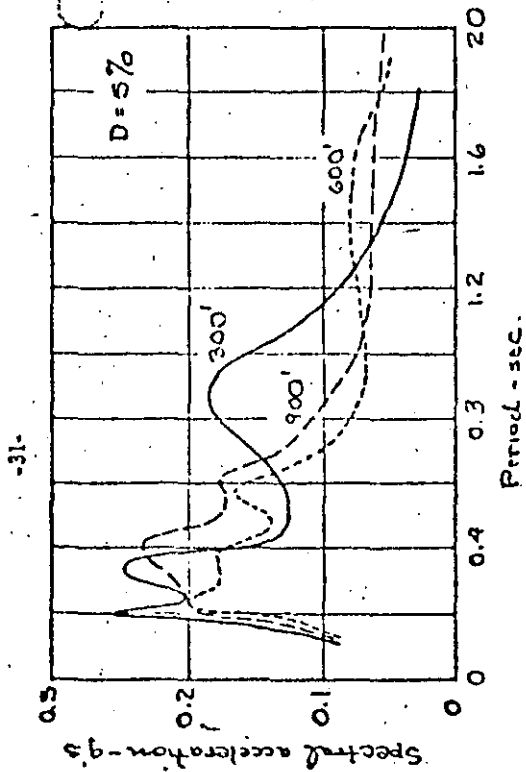


FIGURE 13 RESPONSE SPECTRA (smoothed average for several inputs) FOR DIFFERENT DEEP SOIL PROFILES



FIGURE 14 SHALLOW STRATA OF SOFT SOIL OVERLYING DEEP DEPOSIT OF FIRM SOIL

2219  
7/2/69

FUNDAMENTALS OF SOIL AMPLIFICATION

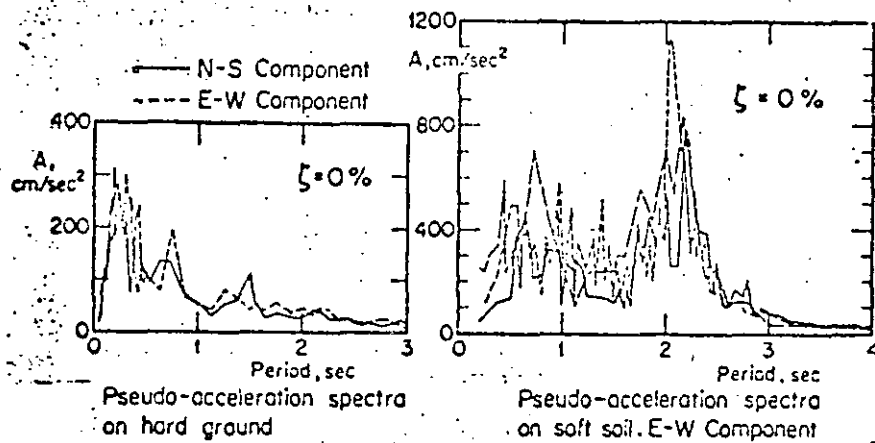


FIGURE 16 RESPONSE SPECTRA FOR HARD AND SOFT GROUND IN MEXICO CITY (from Esteva et al, 1969)

by

J. M. Roesset

Department of Civil Engineering  
Massachusetts Institute of Technology

March 1969

Preface

The purpose of these notes is to present some of the methods now available to include the effect of local soil conditions in the derivation of design earthquakes or response spectra.

The dynamic characteristics of a soil deposit can be expressed by its Transfer function representing the amplification experienced from bottom to top by a sinusoidal steady state motion. The derivation of amplification curves using both a continuous and a discrete solution is presented in II and the relative advantage of each method is discussed.

The general problem of considering an actual earthquake record and filtering it through the soil is discussed in III. Finally, approximate simplified methods are presented to obtain directly response spectra which include the effect of the soil from the knowledge of a response spectrum on firm ground or at bedrock.

Table of Contents

	Page
Preface	ii
I. INTRODUCTION	1
I-1. Statement of the Problem.	1
I-1. General Considerations	3
II. STEADY STATE PERIODIC MOTIONS - The Amplification Function	5
II-1. Continuous Solution	6
A. Uniform layer - Rigid rock	6
B. Uniform layer - Elastic rock	14
C. Multilayered system	23
II-2. Discrete Model	32
III. TRANSIENT MOTIONS	36
III-1. Continuous Solution	37
III-2. Discrete Model	48
IV. DERIVATION OF RESPONSE SPECTRA	51
References	62

by  
J. M. Roesset

## I - INTRODUCTION

## I.1 Statement of the Problem.

During the initial phases of development, Earthquake Engineering was mainly concerned with developing methods to estimate the response of a structure to given dynamic loads. While there are still many problems to be solved in the area of Structural Dynamics, particularly in the nonlinear range, it is somewhat disturbing to observe the large discrepancy between the accuracy sought by some methods of analysis and the uncertainty in the nature and magnitude of the loads to which the structure will be subjected. This inconsistency has been recognized in the last years and an increasing amount of effort is now being devoted to study the characteristics of earthquake motions as a function of magnitude, distance to the epicenter and local soil conditions. The purpose of this research is to arrive at simple, but realistic methods to represent the characteristics of the ground motion at a particular site. Among these methods one of the most powerful ones is through the use of design response spectra.

Determination of the appropriate earthquake motions at any given site involves two fundamental steps:

1. Evaluation of the seismic risk of the region. For an area with frequent strong earthquakes this step may be relatively easy and engineers may already know that a certain city is periodically subject to earthquakes of some average magnitudes with epicenters at some average distances. For regions with relatively scarce earthquake history, the determination of a design earthquake becomes much more complicated and requires in general geological and seismological studies, which attempt to identify possible sources of earthquakes or active faults.

\* c Massachusetts Institute of Technology, March 1969

The results of this step can take different forms, the simplest one being a series of values for probable magnitudes and associated epicentral distances. It is possible from these values, using the formulas suggested by Rosenblueth, to characterize each possible design earthquake by its maximum ground acceleration, velocity and displacement. Newmark has derived a simple approximate method by which the corresponding design spectra can be estimated, knowing these three characteristics. It is possible then to draw response spectra for each design earthquake and to find their average or envelope. Alternatively one can try to generate artificial earthquakes that would have the same average characteristics. It must be realized, however, that if this procedure is used it will not be enough to generate just one sample earthquake for a given set of values of magnitude and epicentral distance. Quite the contrary, a substantial number of samples should be generated and used for each possible earthquake, making the procedure extremely long and costly.

In any case the corresponding design earthquakes or response spectra will apply to an overall region for firm ground conditions.

2. Having obtained one or more earthquake records which could occur at the site on firm ground, or better, a set of design response spectra, the next step is to study how these motions would be modified by the local soil conditions of the particular site where the structure is going to be built. The effect of the soil is going to be one of filtering the motions, increasing their amplitude in some ranges of frequencies and decreasing it in others. This problem is normally referred to as soil amplification and will be the subject of the following discussion.

The particular problem under consideration can then be stated as: Given a soil profile and a design earthquake or response spectrum at bedrock, determine the corresponding earthquake or spectrum at the top of the soil.

It should be noticed that in order to be able to apply these results directly in the dynamic analysis of the structure, it must be

assumed that its mass is negligible in comparison to that of the underlying soil. Otherwise a third step is involved corresponding to the problem of soil-structure interaction. In other words it will not be possible to consider the structure and the soil as uncoupled systems.

1.2 General Considerations.

Earthquake motions may be decomposed into a series of waves which propagate from the focus in all directions. Given an infinite medium these waves are basically of two types: dilatational or compressional waves and shear waves. The first are normally called P waves. The second can be decomposed again by projecting the motion in two orthogonal directions. SV waves correspond to motions in a vertical plane, SH waves to horizontal motions. Of course when the direction of propagation is vertical, both SH and SV waves would correspond to horizontal motion.

When the waves propagating through a continuous medium find a free surface, a new type of wave is generated, normally referred to as surface or Rayleigh waves. If, in addition, the medium is not homogeneous, but there is a clear discontinuity at some depth from the free surface, a second type of surface wave, called Love wave, is generated. When there are several surfaces of discontinuities in the properties, other types of waves are created.

The overall problem of following an earthquake as it propagates from its focus is of course a three-dimensional wave propagation problem. By assuming for instance a line source of relatively large length or by considering only the effects at some distance from the epicenter, the problem can be reasonably reduced to a two-dimensional one for SV and P waves and a one-dimensional problem for the propagation of SH waves.

The methods described here relate all of them to the solution of the one-dimensional wave propagation equation. Their basic limitations are thus:

1. Only shear waves are considered, either SH or SV if they are propagating vertically, and only SH if they propagate at an angle. P waves propagating vertically could be considered by replacing the appropriate constants (modulus; wave propagation velocity). Surface waves are, however, neglected.
2. The different layers of soil are assumed to be parallel and extending in the horizontal direction for a distance several times larger than the total depth to bedrock.

In spite of these limitations, the solutions obtained by these methods seem to provide a useful and reasonable estimate of the filtering effect of the soil. Two-dimensional wave propagation problems can now be solved by the use of the finite element method. These techniques offer a promising future. Their application is, however, still limited and there are several questions which still have to be solved before they can be used with confidence.

The filtering effect of the soil can be measured in two different ways:

1. By considering a steady state harmonic oscillation of the soil and the underlying rock and determining the ratio of the amplitude at the free surface of the soil to the amplitude at bedrock or at the outcropping of rock (without any soil on top). This ratio will be a function of the frequency of the motion, and if there is damping, a complex function. It is normally referred to as the Transfer Function of the soil. Its modulus is the amplification function, amplification ratio or amplification spectrum.
2. By considering a given earthquake record (time history of acceleration) at bedrock or at the outcropping of rock, and determining the corresponding accelerogram at the free surface of the soil. The result in this case is not only a complete time history of acceleration at the free surface of the soil but also, if so desired, time histories of shear stresses and strains at any point within the soil. It provides therefore a much more complete solution, but it requires considerably

37

more computer time. Furthermore, because of the reasons previously mentioned, the complete analysis would have to be repeated for each earthquake sample, and it would make little sense to do it for just one record.

Both types of results can be obtained using two different mathematical models:

1. A continuous solution of the differential equation corresponding to the one-dimensional wave propagation problem.
2. A discrete solution replacing each layer of soil by a system of lumped masses and springs and applying standard procedures of Structural Dynamics.

The continuous model offers in general more flexibility and has an economic advantage if the results are desired only at a few points. At present the discrete model requires less computational time when complete histories of accelerations, velocities, strains and stresses are necessary at many points. Both models yield exactly the same results (except for small discrepancies due to different round-off and truncation errors) when:

- a) Damping is assumed constant in all modes and viscosity for each layer directly proportional to its modulus and inversely proportional to frequency.
- b) The underlying rock is assumed to be rigid or in other words the input motion is considered at bedrock with the soil on top, rather than at the outcropping of rock. For elastic rock, results can still be made to agree if an additional damping is inserted in the discrete model to simulate the loss of energy through radiation in the rock.

In the following pages the basis of both formulations will be presented, considering first the case of steady state periodic motions (determination of the amplification curve), then the case of transient motions. The application of these methods to obtain filtered earth-

quake records at the free surface of the soil is immediate. On the other hand, their application to design response spectra, modifying them to include the effect of the soil, is not so straightforward. This point and approximate solutions are discussed at the end.

## II - STEADY STATE PERIODIC MOTIONS

### The Amplification Function

#### II.1 Continuous Solution.

##### A. Uniform layer. Rigid rock.

Let us consider first a uniform layer of soil resting on rock. The equation of motion corresponding to the one-dimensional wave propagation problem is

$$\rho \frac{\partial^2 u}{\partial t^2} = G \frac{\partial^2 u}{\partial x^2} + n \frac{\partial^3 u}{\partial t \partial x^2}$$

where  $\rho$  = density or mass per unit volume =  $\frac{\gamma}{g}$

$\gamma$  = unit weight

$g$  = acceleration of gravity

$G$  = shear modulus

$n$  = viscosity constant

$u(x,t)$  = displacement of a point in the soil layer

If the rock is rigid but a displacement  $u_G(t)$  is imposed at the base of the soil, the boundary conditions are:

$$\frac{\partial u}{\partial x} = 0 \text{ at } x = 0$$

$$u = u_G(t) \text{ at } x = H$$

38

and the initial conditions:

$$u = 0 \text{ at } t = 0$$

$$\frac{\partial u}{\partial t} = 0 \text{ at } t = 0$$

By calling  $y = u - u_G$  the relative displacement, the equation can be rewritten as:

$$\rho \frac{\partial^2 y}{\partial t^2} = G \frac{\partial^2 y}{\partial x^2} + n \frac{\partial^3 y}{\partial x^2 \partial t} - \rho \frac{\partial^2 u_G}{\partial t^2}$$

with Initial Conditions

$$y = 0, \frac{\partial y}{\partial t} = 0 \quad \text{at } t = 0$$

and Boundary Conditions

$$y = 0 \quad \text{at } x = H$$

$$\frac{\partial y}{\partial x} = 0 \quad \text{at } x = 0$$

If  $u_G(t) = 0$ , the free vibrations can be investigated. Writing then

$$\rho \frac{\partial^2 y}{\partial t^2} = G \frac{\partial^2 y}{\partial x^2} + n \frac{\partial^3 y}{\partial x^2 \partial t}$$

and trying a solution of the form

$$y = U(x) \cdot V(t)$$

where  $U$  is a function only of  $x$

$V$  is a periodic function of  $t$  alone

$$\frac{U''}{U} = \rho \frac{V''}{GV + nV} = -p^2$$

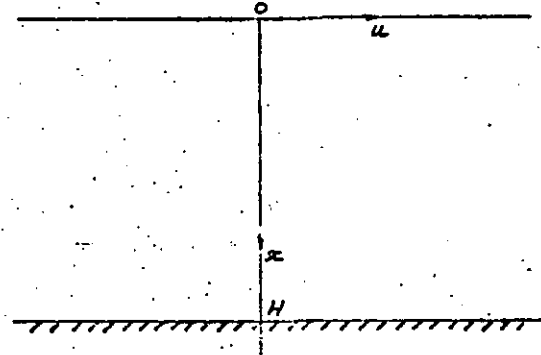


FIG. 1 - UNIFORM LAYER

The natural frequencies of the layer of soil are then given by

$$f_n = \frac{2n-1}{4H} \sqrt{\frac{G}{\rho}} = \frac{(2n-1)C_s}{4H}$$

$$\omega_n = \frac{(2n-1)\pi}{2H} \sqrt{\frac{G}{\rho}} = \frac{(2n-1)\pi C_s}{2H}$$

and the natural periods

$$T_n = \frac{4H}{2n-1} \sqrt{\frac{\rho}{G}} = \frac{4H}{(2n-1)C_s}$$

where  $C_s = \sqrt{\frac{G}{\rho}}$  is the shear wave velocity of the soil.

The corresponding modal shapes are

$$U = \cos \frac{(2n-1)\pi}{2H} x$$

If the soil has viscosity  $n \neq 0$  in order to have harmonic motion we must have

$$n < \frac{4H}{(2n-1)\pi} \sqrt{\frac{G}{\rho}} = \frac{2 \cdot 2\pi \cdot G}{(2n-1)\pi C_s} = \frac{4H}{(2n-1)\pi} \sqrt{\frac{G}{\rho}}$$

A critical value of viscosity can be established for each mode.

In particular in order to have at least 1 mode

$$n < n_{1 \text{ crit}} = \frac{4H}{\pi} \sqrt{\frac{G}{\rho}}$$

It is important to realize that if there is any viscosity the number of modes will be finite. (Higher modes will have damping higher than critical).

Considering now the forced vibration problem, it is convenient for a steady state periodic motion to represent the base displacement by

$$u_G(t) = C e^{i\omega t}$$

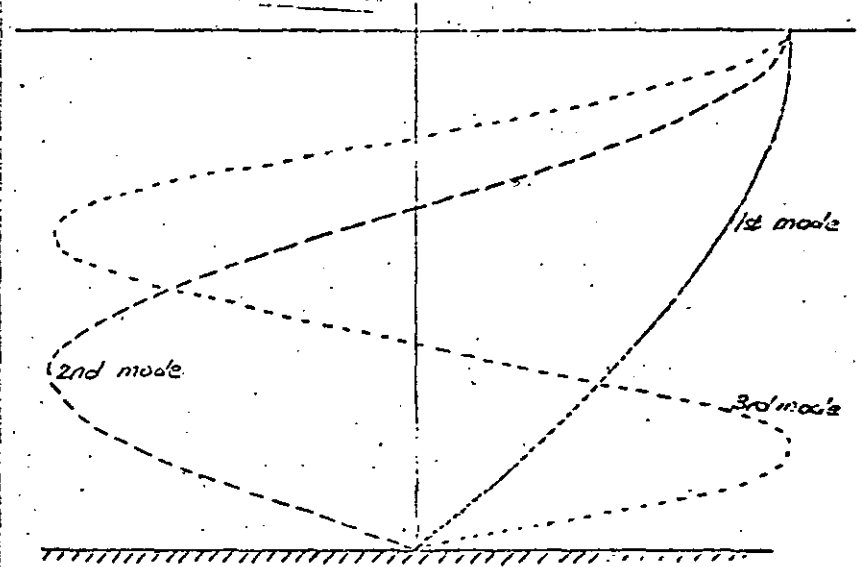


FIG. 2. MODAL SHAPES FOR A UNIFORM LAYER

and the solution by

$$y(x,t) = U(x)e^{int}$$

then

$$U = E \cos px + F \sin px - C$$

$$\text{with } p^2 = \frac{\rho n^2}{G + in\eta}$$

Imposing the boundary conditions

$$F = 0$$

$$E \cos p\ell = C$$

$$U = C \left( \frac{\cos px}{\cos p\ell} - 1 \right)$$

$$\text{and } \bar{y} = -n^2 C \left( \frac{\cos px}{\cos p\ell} - 1 \right) e^{int}$$

$$\bar{u} = \bar{y} + \bar{u}_G = -n^2 C \frac{\cos px}{\cos p\ell} e^{int}$$

and at the free surface of the soil the absolute acceleration becomes

$$\bar{u} = -n^2 C \frac{1}{\cos p\ell} e^{int}$$

Since the base motion was  $\bar{u}_G = -n^2 C e^{int}$

$$\bar{u} = \frac{1}{\cos p\ell} \bar{u}_G$$

The transfer function of the soil for absolute acceleration at the free surface is then defined as:

$$\text{TF}(\bar{u}) = \frac{1}{\cos p\ell}$$

It should be noticed that if there is viscosity,  $p$  is a complex variable and therefore  $\cos p\ell$  has to be interpreted as

$$1/2 (e^{ip\ell} + e^{-ip\ell})$$

or

$$\text{TF}(\bar{u}) = \frac{2}{e^{ip\ell} + e^{-ip\ell}}$$

The fact that the transfer function is complex indicates that there is both a change in amplitude and in phase. If only the change in amplitude is considered the Amplification Function is defined as the modulus of the transfer function.

$$A(\alpha) = \frac{2}{|e^{ip\ell} + e^{-ip\ell}|}$$

Calling

$$\alpha = \frac{1}{\sqrt{2}} \operatorname{Hn} \sqrt{\frac{\rho}{G}} \frac{\sqrt{1 + (n\eta/G)^2 - 1}}{1 + (n\eta/G)^2}$$

$$\beta = \frac{1}{\sqrt{2}} \operatorname{Hn} \sqrt{\frac{\rho}{G}} \frac{\sqrt{1 + (n\eta/G)^2 + 1}}{1 + (n\eta/G)^2}$$

$$A(\alpha) = \frac{1}{\sqrt{\cos^2 \alpha \cos^2 \beta + \sin^2 \alpha \sin^2 \beta}}$$

For small values of  $\frac{n\eta}{G}$

$$\alpha = \frac{1}{2} \operatorname{Hn} \sqrt{\frac{\rho}{G}} n \frac{\eta}{G} = \frac{1}{2} \frac{4 \eta^2}{\sqrt{G}}$$

$$\beta = \operatorname{Hn} \sqrt{\frac{\rho}{G}}$$

stresses in the soil during an earthquake to determine the factor of safety against liquefaction and to guide in the selection of suitable values for modulus and damping ratios.

In order to obtain these results several methods are still available using either the continuous or the discrete model.

### III.1 - Continuous Solution

Given a certain time history of acceleration representing an earthquake record at the outcropping of rock, or at the interface between soil and rock, the corresponding accelerogram at the free surface of the soil can be obtained by:

- a) Obtaining the Fourier transform of the input earthquake.
- b) Multiplying it by the Transfer function of the soil.
- c) Obtaining the inverse Fourier transform of the resulting function.

The Fourier transform of a function of time  $f(t)$  can be visualized as a limiting case of a Fourier series expansion. It is given by the formula

$$F(\omega) = \int_0^{\infty} f(t) e^{-i\omega t} dt = \int_{-\infty}^{\infty} f(t) e^{-i\omega t} dt \text{ (if } f(t) = 0 \text{ for } t < 0)$$

$f(t)$  is then said to be the inverse Fourier transform of  $F(\omega)$

$$f(t) = \frac{1}{2\pi} \int_{-\infty}^{\infty} F(\omega) e^{i\omega t} d\omega$$

It should be noticed that  $F(\omega)$  is a complex function, writing it as

$$F(\omega) = C(\omega) - iS(\omega)$$

$$C(\omega) = \int_0^{\infty} f(t) \cos \omega t dt \text{ (is the cosine transform)}$$

$$S(\omega) = \int_0^{\infty} f(t) \sin \omega t dt \text{ (is the sine transform)}$$

If on the other hand it is written as

$$F(\omega) = E(\omega) e^{-i\phi(\omega)t}$$

$$E(\omega) = \sqrt{C(\omega)^2 + S(\omega)^2}$$

$$\phi(\omega) = \tan^{-1} \frac{S(\omega)}{C(\omega)}$$

$E(\omega)$  represents the amplitude Fourier spectrum, and  $\phi(\omega)$  the phase spectrum. The amplitude spectrum has an important physical meaning. Given two values of frequency,  $\omega_1, \omega_2$ , the area under the curve  $E(\omega)$  from  $\omega_1$  to  $\omega_2$  gives the amplitude of the motion in this range of frequencies. A simple look at the Fourier amplitude spectrum (often referred to for short as Fourier spectrum) gives immediately an idea of the range of frequencies where most of the amplitude of the motion is contained. In fact Hudson has shown that this spectrum is a lower bound to the undamped velocity response spectrum and in general a very good approximation to it (they would coincide if the maximum response occurred after the end of the excitation). Arias has also shown that if  $E(\omega)$  is computed for different durations of the earthquake, the envelope of these spectra is an upper bound to the undamped velocity response spectrum.

The amplitude Fourier spectrum is of course closely related to the spectral density function  $S(\omega)$

$$S(\omega) = \frac{1}{2\pi} \frac{E(\omega)^2}{T}$$

and 
$$S^+(\omega) = \frac{1}{\pi} \frac{E(\omega)^2}{T}$$

where  $T$  is the duration of the excitation  $f(t)$

The area under the spectral density function between two frequencies  $\omega_1$  and  $\omega_2$  gives a measure of the energy of the excitation in that range.

The Fourier transform has not been used normally in Structural Dynamics. Its determination is, however, extremely fast and simple with a digital computer. Even if this method of analysis is not going to be used, the Fourier transform will provide significant information on the nature of the excitation and will help to answer such questions as how many modes should be included in a modal analysis.

The transfer function of the soil as determined in II is again a complex function. The product of these two complex functions can be accomplished by

Multiplying the Fourier amplitude spectrum of the input by the amplification function of the soil. The result is the Fourier amplitude spectrum of the earthquake at the free surface of the soil.

Adding to the Fourier phase spectrum the change in phase curve of the soil. The result is the Fourier phase spectrum of the output.

The inverse Fourier transform of this product will be again a real function representing the time history of acceleration on top of the soil. Notice that if the input represents the accelerogram at the interface between rock and soil the transfer function corresponding to rigid rock should be used. If on the other hand the input represents the accelerogram which would be recorded on the rock without any soil on top, the transfer function for elastic rock has to be used. The second approach seems more logical. However, at the present time, there is no clear way to determine what the earthquake records should be at bedrock with soil on top or at the outcropping of rock, since most accelerograms of real earthquakes have been obtained on ground (even if firm ground).

Figures 13 through 17 summarize the procedure as outlined. (The phase spectra are not plotted). Figure 13 shows a record of the Taft earthquake and Figure 14 its amplitude Fourier spectrum. Figure 15

FIG. 13. ACCELEROGRAM OF TAFT EARTHQUAKE

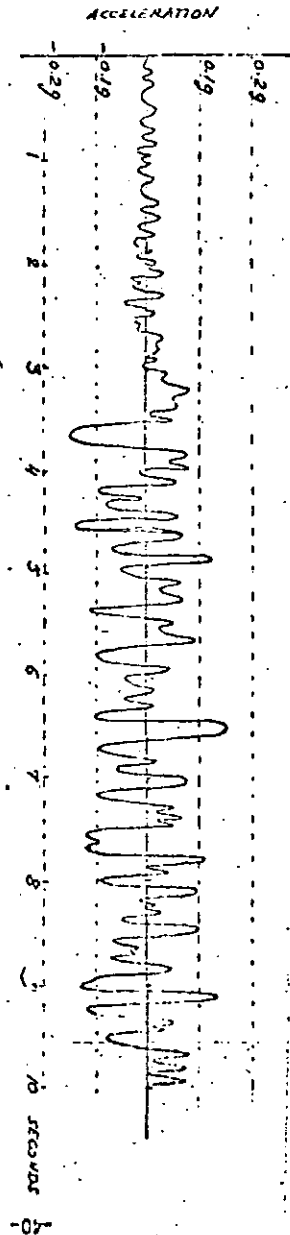
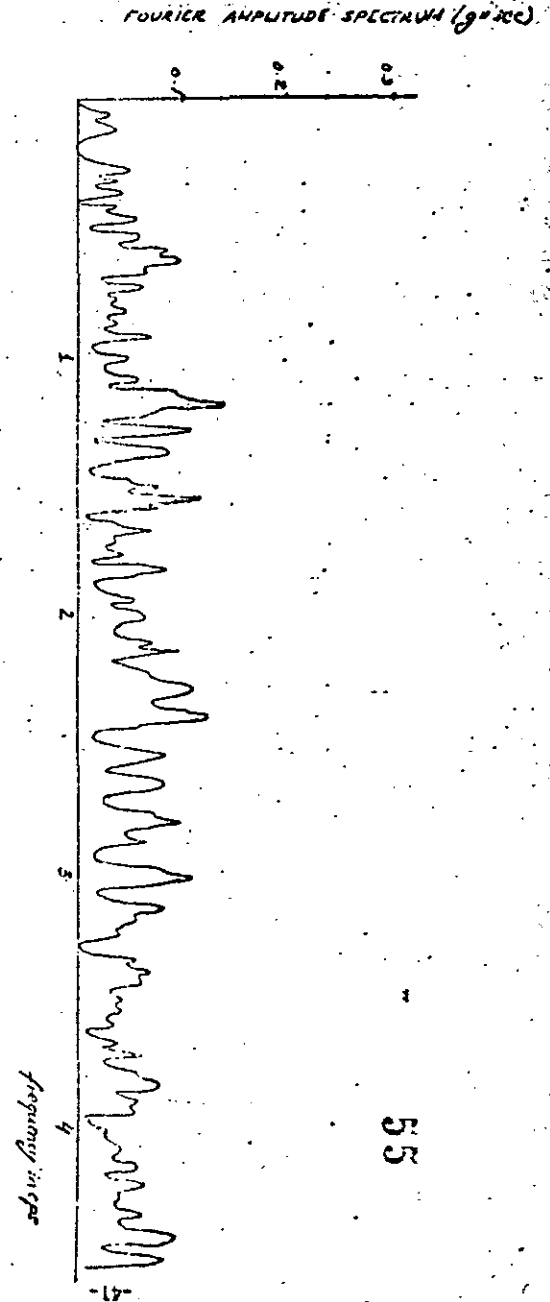


FIG. 14. FOURIER AMPLITUDE SPECTRUM FOR TAFT EARTHQUAKE



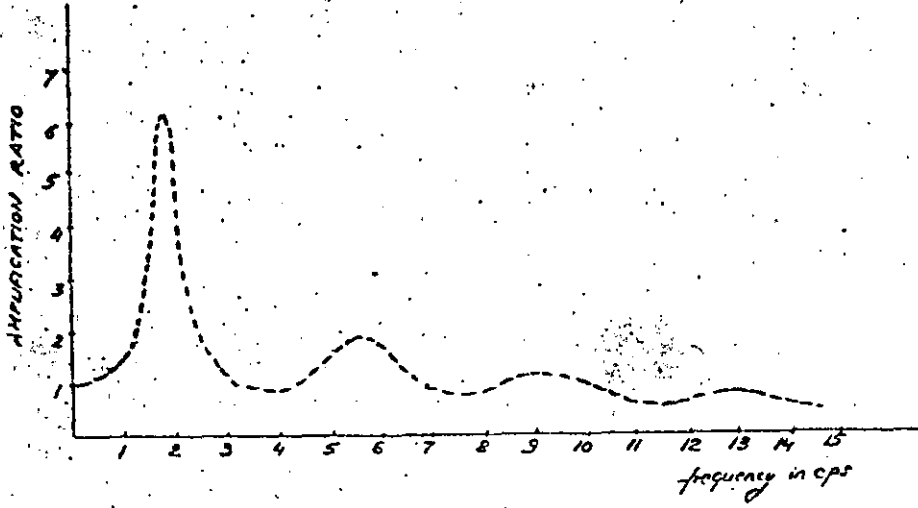


FIGURE 15. AMPLIFICATION FUNCTION OF SOIL

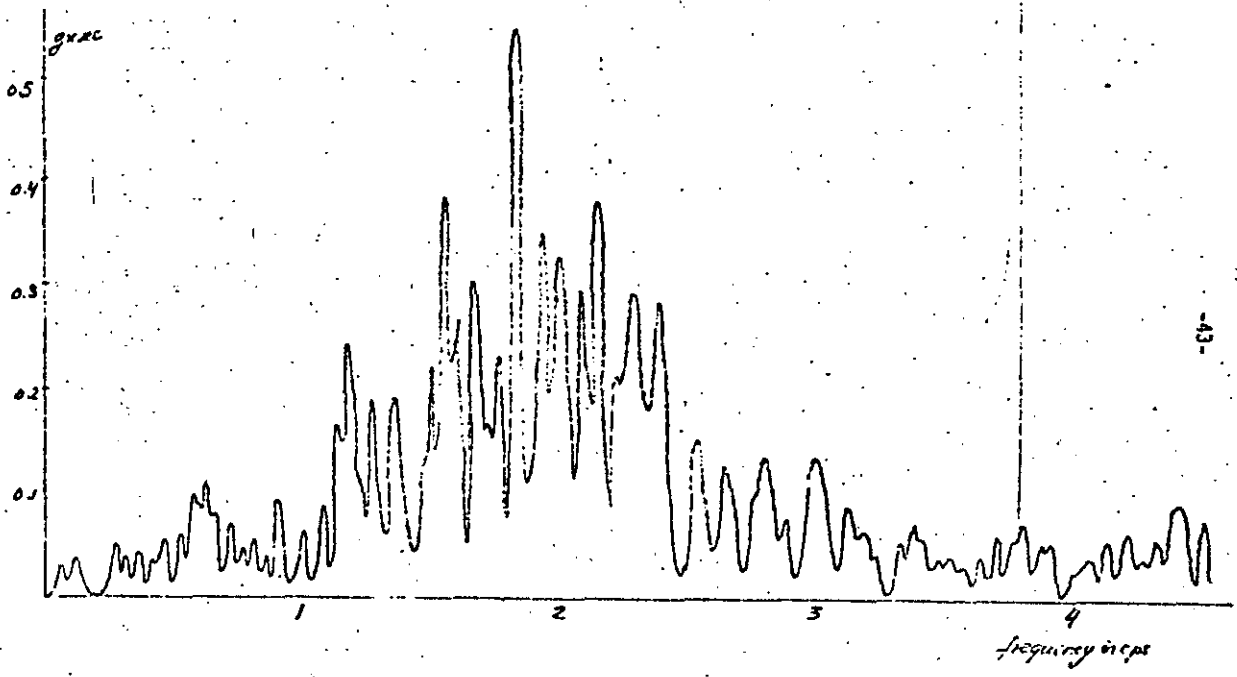


FIGURE 16. FOURIER AMPLITUDE SPECTRUM OF ACCELEROGRAM AT TOP OF SOIL

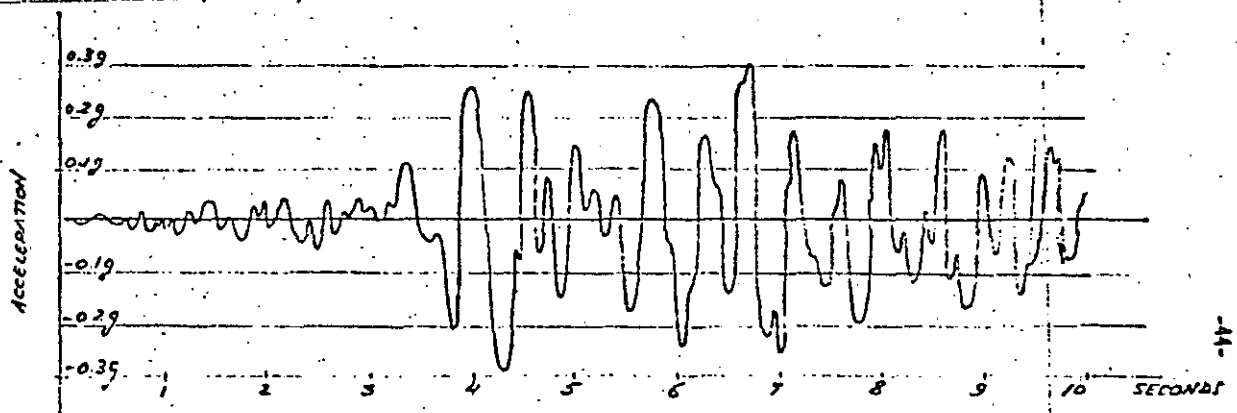


FIGURE 17. ACCELEROGRAM AT TOP OF SOIL

shows the amplification curve for a given soil profile (the uniform layer previously considered with rigid rock). The product of the Fourier spectrum of the input by the amplification function is shown in Figure 17.

Once the earthquake record at the surface of the soil has been obtained, design response spectra can be obtained in two different ways:

- a) From the Fourier transform of the output (before inverting it), by multiplying it by the Transfer function of a one-degree-of-freedom linear oscillator, then inverting the result and finding the maximum. The Transfer function of the one-degree-of-freedom system with frequency  $\omega_n$  and damping  $\delta_n$  is

$$H(\omega) = \frac{\omega_n^2}{\omega_n^2 - \omega^2 + 2i\delta_n\omega\omega_n}$$

- b) By integrating through a step-by-step procedure, the equation of motion of a one-degree-of-freedom system

$$y + 2\delta_n\omega_n\dot{y} + \omega_n^2 y = -\ddot{u}_s$$

where  $u_s$  is the acceleration time history on top of soil.

The first procedure is normally referred to as integration in the frequency domain whereas in the second case the solution is said to be carried out in the time domain. While the first method would represent a consistent continuation of the procedure followed up to that moment at the present time the second seems more economical as far as computer time is concerned.

Figure 18 shows the pseudo-acceleration response spectrum for the Taft earthquake filtered through the uniform soil deposit. The response spectrum of the input is also shown in the same figure. Figure 19 shows the ratio of both response spectra for 2 and 5%

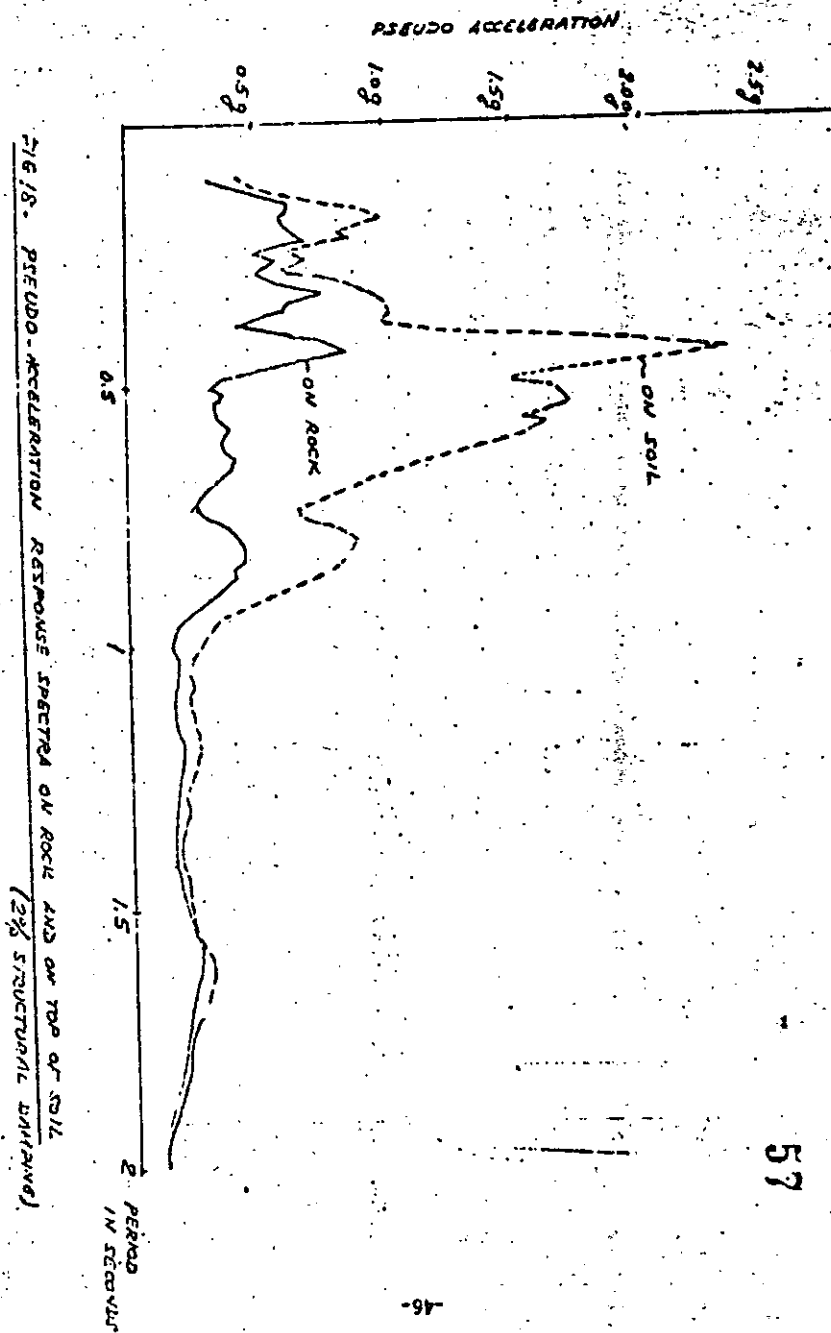


FIG. 18. PSEUDO-ACCELERATION RESPONSE SPECTRA ON ROCK AND ON TOP OF SOIL (2% STRUCTURAL DAMPING)

hysteretic dissipation of energy. Correspondingly both shear modulus and damping are functions of strain. If a non-linear analysis is to be performed only the discrete model with physical integration of the equations of motion would be applicable. Often, however, the system is considered linear, assuming values of shear modulus and damping, determining histories of strains, computing new values of modulus and damping and cycling until convergence of the process is obtained. For these preliminary runs the discrete model with modal analysis is convenient and it provides a faster, more economical solution. Once appropriate values of modulus and damping have been obtained, the continuous model can be used for a final series of analyses with different values of damping in each layer. (In the modal solutions the values of damping are averaged and expressed as modal damping, constant in all modes).

#### IV. DERIVATION OF RESPONSE SPECTRA

The methods previously outlined are mainly intended to consider an earthquake at the base of the soil, filter it and obtain the resulting time history of acceleration at the free surface. While it is possible to obtain then design response spectra on top of the soil, the procedure has for this purpose several difficulties:

- a) It requires as an input an actual accelerogram, be it that of a real earthquake, scaled or not, or an artificial earthquake obtained by a simulation process. While the area of Earthquake Simulation has seen a considerable progress in the last years, it is still harder to derive the time history of an earthquake corresponding to a certain magnitude and epicentral distance than it is to derive a response spectrum.
- b) In order to obtain reliable results the analysis cannot be done for just one input earthquake, but should be repeated for several inputs representing samples of earthquakes with the same average characteristics. The resulting response spectra should finally be smoothed by drawing an average or envelope. The process becomes then too long and expensive.

It would be therefore desirable to have simple and approximate ways by which smooth response spectra on top of the soil would be derived from response spectra at bedrock or on firm ground. Figure 19 showed the amplification curve for a given soil profile and the ratio of response spectra for 2 and 5% of structural damping. The similarity of these curves is apparent. In fact, if the Fourier spectrum were exactly the undamped velocity response spectrum, the amplification curve should coincide with the ratio of response spectra for no damping.

There are, however, several important differences between these two curves:

1. The amplification curve tends to zero as the frequency increases or as the period becomes very small. The ratio of response spectra on the other hand tends to a finite value which is the ratio of the maximum acceleration on top of the soil to the maximum acceleration of the input. (This ratio can be estimated from the design response spectra at bedrock if the modes of the soil are known). The ratio of response spectra is therefore highly dependent on the input earthquake in the high frequency range (or for very short periods, say T smaller than 0.1 seconds).
2. The amplification curve is a function of the soil properties only. The ratio of response spectra on the other hand will depend on the soil properties (periods and damping), the amount of structural damping and the selected earthquake input.
3. The ratio of response spectra is in general smoother than the amplification curve with lower peaks and higher valleys and it becomes smoother as the structural damping increases. For damping values of 20 or 25% the ratio of response spectra is practically constant over a long range of periods. On the other hand for very small values of structural damping or for undamped spectra, the ratio of the response spectra should be close to the amplification curve except in the range of very small periods.
4. It should also be expected that the agreement between the amplification curve and the ratio of response spectra would be better for

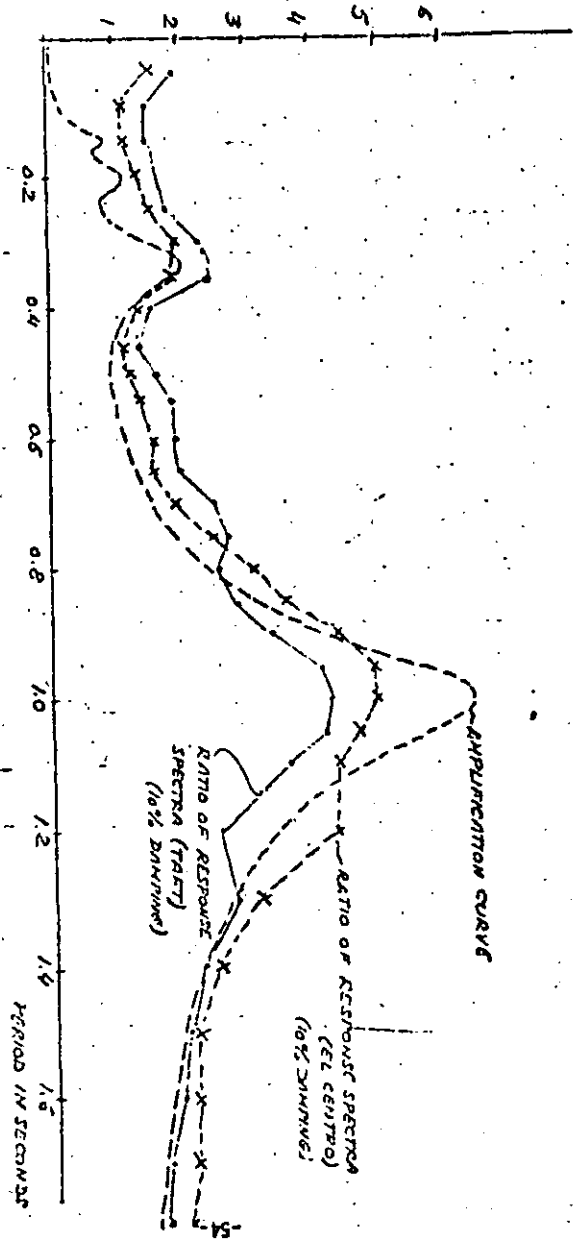
high values of damping in the soil since this would tend to eliminate the transients and furnish a motion closer to a periodic one.

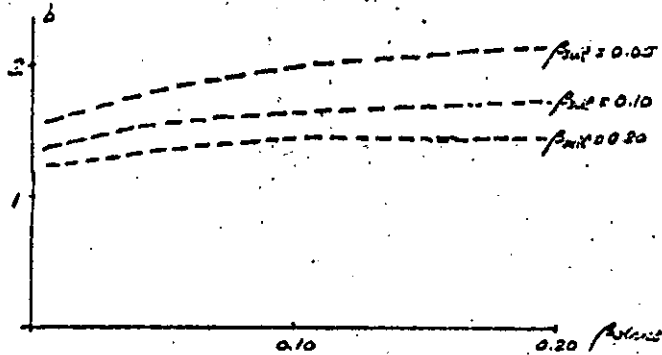
In order to determine the applicability of the amplification curve to reproduce the ratio of response spectra, the ratio between both curves b has been obtained at several points for uniform soils with varying fundamental periods and damping, subject to different earthquake inputs. The earthquake records considered are El Centro, Taft and five artificial earthquakes with a Tajimi type spectral density function.

Figure 20 shows for one of the cases studied the amplification curve and the ratio of response spectra for El Centro and Taft earthquakes. Figure 21 shows the average ratio of response spectra for the five artificial earthquakes, together with the 95% confidence levels (mean + 2σ). Most of the points of the curves for El Centro and Taft fall within this band. It must be therefore realized that even within samples of earthquakes with the same properties (magnitude and epicentral distance) a substantial variation is to be expected in the ratio of response spectra.

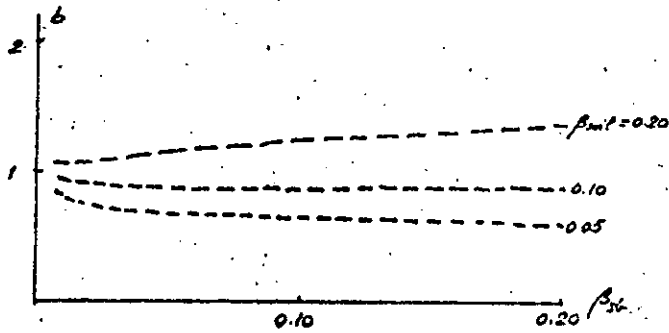
Figure 22 shows the effect of the natural period of the soil and the amount of damping in the value of b at different points. For  $T = 2T_1$  (1st natural period) the ratio is practically constant, independent of  $T_1$ . For  $T = T_1$  it has again little variation for periods larger than 0.3 seconds. For  $T = 0.5 T_1$  the variation is large for periods smaller than 0.5 seconds and for  $T = \frac{1}{3} T_1$  for periods smaller than 0.8 or 0.9 seconds. It should be noticed that in all cases the variation is small for values of T larger than 0.2 or 0.3 seconds. If it is accepted that in this range (say 0 to 0.2 or 0.3 seconds) the maximum acceleration at top of the soil controls the response spectrum, the values of b can be considered only slightly depending on the natural period of the soil over the range of application.

FIG. 20. COMPARISON OF AMPLIFICATION CURVE AND RATIO OF RESPONSE SPECTRA EL CENTRO AND TAFT EARTHQUAKES.





$T_1 = 1 \text{ sec}$   
 $T = 0.5 T_1$   
 $\omega = 2 \omega_1$



$T_1 = 1 \text{ sec}$   
 $T = \frac{1}{3} T_1$   
 $\omega = 3 \omega_1$

FIG 23 (CONTINUED)

While all the cases considered to derive the curves for the values  $b$  have corresponded to a uniform soil profile and further testing is necessary for multilayer systems, it is believed that such a procedure could also be applied for the latter taking the  $T_1$  as the period at which the maximum amplification occurs rather than the first fundamental period.

Figure 24 shows an example of application of the method. Curves of the standard deviation  $\sigma$  have also been obtained. From these curves it is then possible to draw not only the average ratio of response spectra but also confidence levels.

REFERENCES

1. Seed and Idriss, "Influence of Soil Conditions on Ground Motions during Earthquakes. State of the Art Symposium, Earthquake Engineering of Buildings, San Francisco, California - Feb. 1968 and Journal of Soil Mechanics and Foundations Division ASCE, Jan. 1969.
2. Donovan and Matthiesen, "Effects of Site Conditions on Ground Motions During Earthquakes." Same Symposium.
3. Herrera, Rosenblueth and Rascon, "Earthquake Spectrum Prediction for the Valley of Mexico. 3rd World Conference on Earthquake Engineering, 1965.
4. Idriss and Seed, "Seismic Response of Horizontal Soil Layers," Journal of the Soil Mechanics and Foundations Division, ASCE, July 1968.
5. Roesset and Whitman, "Effect of Local Soil Conditions upon Earthquake Damage - Theoretical Background." M.I.T. Dept. of Civil Engineering Report, 1969.
6. "The Use of Amplification Functions to Derive Response Spectra, Including the Effect of Local Soil Conditions," M.I.T. Civil Engineering Dept. Report, 1969.

AMPLIFICATION

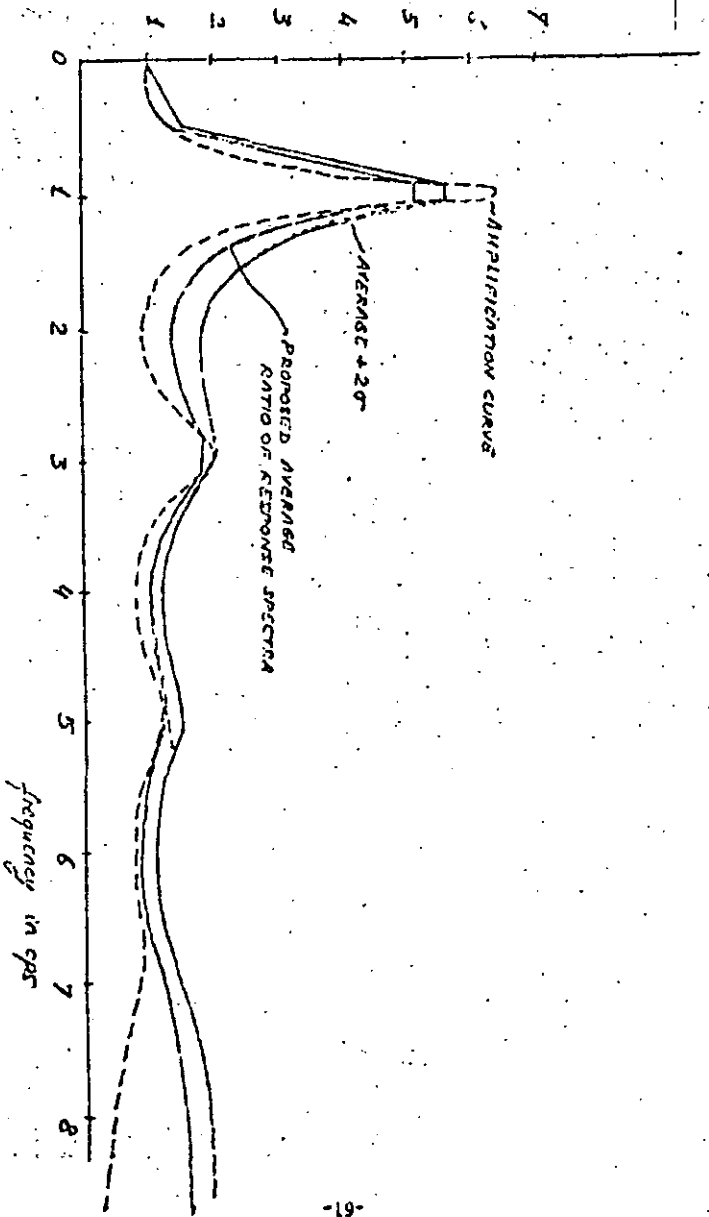


FIGURE 24. SUGGESTED RATIO OF RESPONSE SPECTRA (20% DAMPING)



**DIVISION DE EDUCACION CONTINUA  
FACULTAD DE INGENIERIA U.N.A.M.**

ANALISIS DE RIESGO SISMICO

INFLUENCIA DE LAS CONDICIONES LOCALES EN LAS  
CARACTERISTICAS DEL MOVIMIENTO SISMICO

DR. FRANCISCO SANCHEZ SESMA

JULIO, 1985

# INFLUENCIA DE LAS CONDICIONES LOCALES EN LAS CARACTERISTICAS DEL MOVIMIENTO SISMICO

Francisco J. Sánchez-Sesma  
*Instituto de Ingeniería, UNAM*

## INTRODUCCION

Las amplitudes y formas de las ondas sísmicas generadas en un temblor dependen del mecanismo focal y de la cantidad de energía liberada en la zona de ruptura. El mecanismo focal controla la manera en que las ondas son irradiadas en el espacio y en el tiempo. No obstante, las ondas sísmicas una vez emitidas por la fuente sufren modificaciones en su trayecto que dependen de las propiedades mecánicas de los medios en que se propagan y de las dimensiones de las inhomogeneidades o irregularidades con que se encuentren. Si los cambios de las propiedades en una interfase son grandes o si el tamaño de las irregularidades es comparable o mayor que la longitud de onda predominante de las ondas incidentes, se generarán cambios significativos en el movimiento debidos a reflexión, refracción y difracción de las ondas.

Interesa entender la naturaleza de esos cambios porque pueden ocasionar grandes amplificaciones locales y variaciones significativas del movimiento del terreno en distancias relativamente pequeñas. Este efecto es de particular importancia en la respuesta sísmica de estructuras grandes como presas, puentes o líneas de transmisión. Se trata de estructuras en las que los movimientos diferentes en los apoyos pueden ser muy peligrosos. Existe evidencia del papel que juegan los efectos de las condiciones locales en estudios de la distribución espacial del daño en temblores. Si bien el daño depende de la calidad de las

construcciones, en muchos casos los daños severos están asociados a fenómenos de amplificación. En muchos casos se han utilizado en éxito modelos de propagación unidimensional de ondas de cortante cuando la configuración del sitio en estudio esta formada por estratos aproximadamente horizontales. Debe notarse, sin embargo, que el uso indiscriminado de modelos unidimensionales puede dar lugar a errores de importancia cuando las irregularidades locales son significativas pues no se toma en cuenta la naturaleza física del problema.

Los temblores fuertes, de interés en ingeniería sísmica, tienen componentes importantes en la banda de frecuencias de 0.1 Hz a 15 o 20 Hz. Por otra parte, las velocidades de propagación cerca de la superficie de la tierra varían de unos 200 m/s a casi 2 km/s; de manera que las correspondientes longitudes de onda caen en el rango de las decenas de metros a las decenas de kilómetros.

Las irregularidades geológicas y topográficas con dimensiones comparables con las longitudes de onda predominantes tendrán, entonces, considerable influencia en el movimiento. La extensión y detalle con que deben estudiarse las condiciones locales podrá estimarse en términos de las longitudes de onda asociadas con los periodos de oscilación que son más significativos para un análisis particular. Para un edificio alto, una presa o un puente, por ejemplo, las dimensiones locales pueden ser de varios kilómetros. Para una estructura pequeña y rígida, en cambio esas dimensiones pueden ir de las decenas a los cientos de metros.

El problema de calcular el movimiento en la vecindad de una irregularidad topográfica o estratigráfica ante incidencia de ondas sísmicas ha sido tratado como un problema de difrac-

ción de ondas elásticas de un cierto tipo. No se han desarrollado aun criterios prácticos para determinar la contribución de los distintos tipos de ondas en un cierto temblor (es usual suponer que se trata de ondas SV propagándose verticalmente). En parte, esto es debido a que las técnicas para tratar la difracción de diversos tipos de ondas elásticas son relativamente recientes. El hecho de que sean pocos los estudios que consideren materiales no lineales es también ilustrativo de las dificultades que en este caso se presentan. La mayoría de los estudios de difracción de ondas elásticas consideran configuraciones bidimensionales y sólo algunos casos de incidencia de ondas SH admiten soluciones analíticas (en el dominio de la frecuencia). Si bien las soluciones bidimensionales son una aproximación, proporcionan información útil sobre la respuesta sísmica de irregularidades; de hecho, algunos resultados preliminares de difracción tridimensional son similares a los obtenidos para dos dimensiones,

Los métodos que se han empleado para estudiar el problema son de varios tipos (de acuerdo con cada caso particular) y en algunos casos son de reciente desarrollo. Se ha empleado el método de los elementos finitos, que permite una gran flexibilidad en el modelado de dominios irregulares y aun de materiales no lineales. Suele ser, sin embargo, costoso y requiere precauciones especiales para tratar las fronteras del dominio y definir apropiadamente la excitación. Los elementos finitos pueden combinarse con esquemas de diferencias finitas en el tiempo o con solución en el dominio de la frecuencia.

Se han aplicado con éxito esquemas de diferencias finitas en el espacio y en el tiempo, sin embargo, algunas de las restricciones mencionadas para los elementos finitos limitan el uso generalizado de esta técnica.

Los métodos de frontera, basados en representaciones integrales y/o en expansiones en términos de familias completas de soluciones, están en desarrollo y es de esperarse que no sufran las desventajas de otras técnicas; en particular, al tratar sólo las fronteras se reduce la dimensionalidad del problema.

Por algún tiempo seguirán faltando criterios para formular excitaciones en términos de tipos de ondas incidentes, ángulos de incidencia, contenidos de frecuencias, etc. No obstante, en tanto estos criterios se formulan, se continúa el desarrollo de las técnicas de análisis de la difracción.

Podría parecer que es aun lejana la aplicación de criterios prácticos en la evaluación de los efectos de una cierta irregularidad en la intensidad sísmica. Es probable que el empleo sistemático de medidas integrales de la intensidad sísmica permita construir tales criterios. Una medida integral con interesantes propiedades es la intensidad de Arias. Los valores relativos de la intensidad de Arias respecto a una intensidad de referencia permitirían definir un índice de efectos topográficos que serviría para estimar la variación espacial de las aceleraciones máximas. Sin embargo, al presente, se carece de suficientes registros para estudiar con finura la variación espacial de la intensidad.

El propósito de estas notas es dar una introducción muy general del problema de estimar los efectos de las condiciones locales en las características de los temblores. Preceden también a algunos textos más especializados que el autor ha reunido aquí.



**DIVISION DE EDUCACION CONTINUA  
FACULTAD DE INGENIERIA U.N.A.M.**

ANALISIS DE RIESGO SISMICO

DIFFRACTED WAVES AND DISPLACEMENT FIELD OVER  
TWO-DIMENSIONAL ELEVATED TOPOGRAPHICS

JULIO, 1985

## Diffracted waves and displacement field over two-dimensional elevated topographies

Pierre-Yves Bard *Laboratoire de Géophysique Interne (associé au CNRS: ERA 503) IRIGM, Université Scientifique et Médicale de Grenoble BP 53X, 38041 Grenoble Cedex, France*

Received 1982 April 14; in original form 1981 April 16

**Summary.** The Aki-Larner technique is used to perform, in both the time and frequency domains, an analysis of the effects of two-dimensional elevated topography on ground motion. Incident plane *SH*-, *SV*- and *P*-waves are considered and the respective influences of surface geometry, elastic parameters and the incident wave characteristics, as long as they remain within the limits of applicability of the A-L technique, are investigated in some detail.

Besides the well-known amplification/deamplification effect related to the surface curvature, wave scattering phenomena on the convex parts of the surface are shown to contribute significantly to the disturbances in the displacement field around the topographic structure. These scattered waves are *SH* in the case of incident *SH*-waves, and mainly Rayleigh waves in the *P* case, while both Rayleigh and horizontal *P*-waves, sometimes of large amplitude, develop in the *SV* case. The frequency dependence of this scattering, though complex, seems to be mainly controlled by the horizontal scale of the topographic structure. The parameter study points out the regular and intuitive behaviour of this wave scattering in both *SH* and *P* cases, while it exhibits a puzzling complexity for incident *SV*-waves, which is interpreted as resulting from the importance of the *S-P* reflections on mountain slopes in that case.

As to the ground motion, some general features may be pointed out. The amplification on mountain tops, which is systematically greater for incident *S*-waves than for *P*-waves, generally decreases as the average slope decreases or as the angle of incidence increases. Mountain slopes undergo either amplification or deamplification depending on site location, frequency and incidence angle, but they always undergo strong differential motion due to the lateral propagation of the scattered waves and their interference with the primary wave. Finally, all these effects may be greatly enhanced in the case of complex topographies, which moreover give rise to a significant prolongation of ground motion because of the large number of scattered waves.

## 1. Introduction

For many years, a great number of authors have pointed out the importance of site effects in many seismological problems, ranging from source parameter computation to seismic risk assessment. These site effects were at first related to the local sediment cover (resonance of surface layers, sand liquefaction, attenuation of high frequencies, etc.). More recently, however, observations have been made (e.g. Key 1967; Nason 1971; Trifunac & Hudson 1971) showing the influence of topography on surface ground motion.

Besides field studies (Davis & West 1973; Griffiths & Bollinger 1979), or model studies (Rogers, Katz & Bennett 1974; Ilan, Bond & Spivack 1979), the theoretical investigations have focused more on numerical solution rather than on a detailed study of the effects of topography on surface motion. A lot of numerical methods have been developed to investigate the scattered far-field (small perturbations: Gilbert & Knopoff 1960; Hudson & Knopoff 1967; Hudson 1967; MacIvor 1969; small perturbations and finite difference: Aboudi 1971; Alterman & Aboudi 1971), or the displacement field over the topography itself (analytical models: Trifunac 1973; Wong & Trifunac 1974; Singh & Sabina 1977; finite differences: Boore 1972; Alterman & Nathaniel 1975; Ilan 1977; Ilan *et al.* 1979; finite elements: Smith 1975; discrete wavenumber representation: Lerner 1970; Bouchon 1973; matched asymptotic expansion: Sabina & Willis 1975, 1977; integral equations: Wong & Jennings 1975; Sills 1978; Sanchez-Sesma & Rosenblueth 1979; and boundary methods: England, Sabina & Herrera 1980). All these theoretical models, involving a two-dimensional homogeneous elastic half-space with a simple topographic section (except Singh & Sabina 1977, who consider a three-dimensional hemispheric valley), provide results which quantitatively agree with one another, and qualitatively confirm the experimental observations: amplification usually occurs on convex parts of the ground surface (mountain tops or valley edges), and deamplification on concave parts and shadow zones. Our purpose here is therefore not to present yet another numerical method, but to try to gain a better understanding of these topographic effects, through their dependence on parameters such as incident wave type, frequency, incidence angle and anomaly height.

In other respects, all available theoretical results seem to underestimate the observed effects of topography on surface motion, as reported by Davis & West (1973), and Griffiths & Bollinger (1979). Since the model study values corroborate those obtained by numerical methods (Rogers *et al.* 1974; Ilan *et al.* 1979), it is believed that quantitative disagreement between theory and observation is due, at least partly, to the complexity of both incident signal and topography. It is therefore another aim of the present paper to show how a somewhat complicated topography can produce greater effects than isolated ridges or valleys, and that the surface motion at a particular site depends a lot on the topographic features of a wide area around.

We believe that the Aki-Lerner method is the best suited to this kind of study, since it is a very tractable and computationally cheap method, and because the discrete wavenumber representation provides useful information on the nature of the scattered elastic field. This

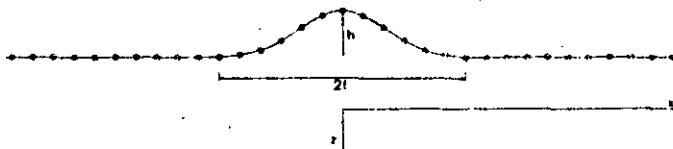


Figure 1. Geometrical shape of the mountain model introduced by Sills (1978), and corresponding to the cases investigated in Figs 2-17. The open circles indicate the sites where the synthetic seismograms of Figs 2, 3 and 14 are computed.

technique has already been presented with many details by Lamer (1970), Aki & Lamer (1970) and Bouchon (1973), and its reliability carefully discussed. The limitation of our investigations to topographic features having slopes lower than  $40^\circ$ , and to incident body waves only, with rather small incidence angles so as to avoid shadow zones, together with the experimental observations of Rogers *et al.* (1974) and Ilan *et al.* (1979) showing that the radiation lobes of the diffracted waves are directed essentially downwards, allow us to think that the Rayleigh ansatz error does not alter the accuracy of our results too much.

## 2 Effects of simple topography on incident plane waves — a parameter study

### 2.1 GENERALITIES

Our purpose is to evaluate the surface displacement and the scattered elastic field produced by a plane body wave impinging upon a two-dimensional topographic feature lying over an otherwise isotropic homogeneous elastic half-space, for various topography, half-space and incident wave characteristics.

Our computations rely on the same theoretical formulation as those presented by Bouchon (1973), except that we do not correct the displacement field for the residual stresses, since we remain well within the validity limits of the A-L technique. Furthermore, in order to investigate the ground motion in the time domain, we follow the approach described by Bard & Bouchon (1980a), making the computation at equally spaced frequencies having an imaginary part equal to half the frequency step. The disturbances induced by the structure periodicity  $L$  (required by the A-L method) are avoided by a suitable choice of both the frequency range and the time window.

Topographic effects then depend on three kinds of parameters:

#### 2.1.1 Topographic shape

This is the most difficult to quantify. For a better understanding of the diffraction and amplification/deamplification mechanisms, only simple topographic profiles are considered at first. The 'pseudo-realistic' mountain model of Sills (1978) is chosen, defined through the equation:

$$\zeta(x) = h(1 - a) \cdot \exp(-3a) \quad \text{with} \quad a = (x/l)^2$$

this topography is completely defined by its half-width  $l$  and its height  $h$ . Its shape is illustrated in Fig. 1.

#### 2.1.2 Half-space elastic parameters

These reduce to the shear and compressional velocities, respectively denoted as  $\beta$  and  $\alpha$ , since the material density has no influence.

#### 2.1.3 Incident wavefield characteristics

These are wave type, incidence angle, azimuth and frequency spectrum. Only incident plane waves are considered here, for simplicity and because nearfield studies introduce a lot of new parameters related to the source mechanism. Moreover, only incident body waves are taken into account. The effect of incident wave azimuth is not considered: only in plane and out of plane motions are investigated.

The remaining independent dimensionless parameters considered in this paper are therefore: the topography shape ratio  $h/l$ , the Poisson ratio  $\nu$ , the dimensionless frequency

$\eta = 2l/\lambda$  (which is scaled to the  $S$  wavelength  $\lambda = \beta/f$ ), and the incidence angle  $\theta$ , measured from the vertical axis.

For time domain studies, we generally choose an input signal in form of a Ricker wavelet, having a time dependence:

$$f(t) = (a - 0.5) \exp(-a) \quad \text{with} \quad a = |\pi(t - t_s)/t_p|^2$$

where  $t_s$  is the time of maximum amplitude, and  $t_p$  the characteristic period. We also sometimes use a combination of several Ricker wavelets.

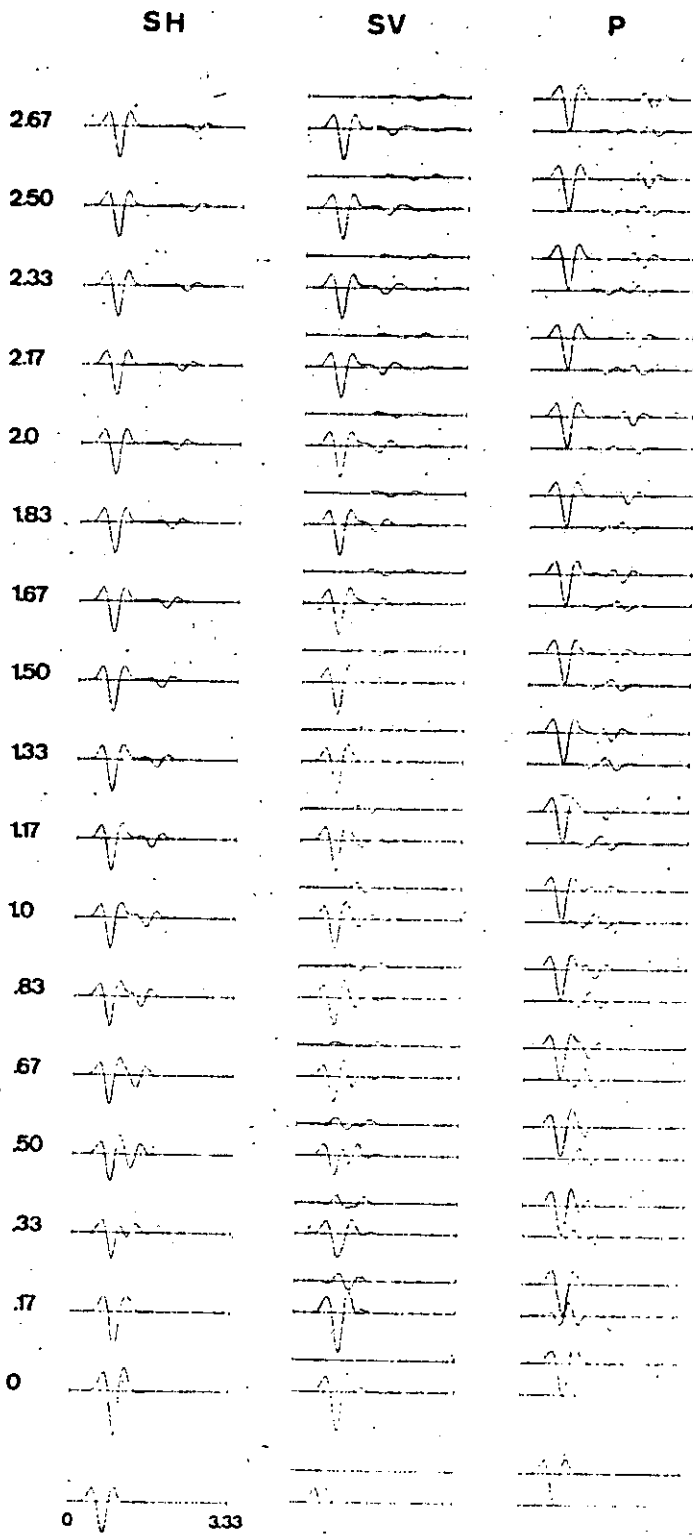
## 2.2 GENERAL CHARACTERISTICS OF TOPOGRAPHIC EFFECTS IN THE VERTICAL INCIDENCE CASE

In this section the case of  $P$ ,  $SV$  and  $SH$  plane waves vertically incident on two topographic features is investigated, a mountain having a shape ratio  $h/l$  equal to 0.375, and a symmetric depression. Materials with Poisson's ratio  $\nu = 0.25$  are considered until Section 2.5.

### 2.2.1 Time domain study

Fig. 2 illustrates the time history of ground motion at several sites located over the topographic elevation and some distance apart, for an incident Ricker signal having a characteristic dimensionless frequency of  $\eta_p = 1.83$ , in each of the three  $SH$ ,  $SV$  and  $P$  incident cases. The well-known amplification pattern on mountain tops appears on each of the three components, but it is more important in the case of incident  $S$ -waves (43 per cent for  $SH$  and 30 per cent for  $SV$ ) than in the case of incident  $P$ -waves (only 10 per cent). Moreover the computed motions do not exhibit much change in signal waveform or duration. On the contrary, on mountain slopes, significant alterations appear; while the ground displacement amplitude is reduced, its duration is increased. The amplitude reduction is more important for horizontal components (the maximum attenuation is about 25 per cent for  $SH$ , 40 per cent for  $SV$  and only 10 per cent for incident  $P$ -waves). In the  $SH$  case, seismograms away from the topography show an outward propagating signal having roughly the same shape as the incident signal and an amplitude of about 20 per cent at a distance  $2l$  from the mountain top. The phase velocity of this diffracted wave, together with the space dependence of its amplitude, which fits an  $x^{-1/2}$  decay, are consistent with a horizontal  $SH$ -wave generated near the mountain top. In the  $P$  and  $SV$  cases, seismograms exhibit a somewhat greater complication, because of the outward propagation of two such diffracted waves. Their phase velocities, vertical/horizontal component ratio, and spatial decay ( $x^{-1/2}$  for the fastest wave, and nearly constant for the slowest), allow their identification as a horizontal  $P$ -wave and Rayleigh wave, respectively. The relative importance of these two waves undergoes great changes with the incident wave type. In the  $SV$  case, the horizontal  $P$ -wave is the main disturbance and is associated with a horizontal displacement around 20 per cent of the direct one (measured at the same reference site  $x = 2l$ ), whereas in the  $P$  case,

Figure 2. Response of the mountain illustrated in Fig. 1 ( $h/l = 0.375$ ) to vertically incident, respectively,  $SH$ ,  $SV$  and  $P$  Ricker wavelets of characteristic dimensionless frequency  $\eta_p = 1.83$ . The traces represent the time history of the displacement at surface receivers, spaced from 0 to  $2.5l$  from the mountain top (numbers on the left represent the site location in dimensionless values  $x/l$ ). In the  $SH$  case, only the transverse horizontal component,  $v$ , is represented, while in the  $P$  and  $SV$  cases, both horizontal motion along the  $x$ -axis ( $u$ , lower trace) and vertical motion ( $w$ , upper trace), are depicted. The bottom traces represent the ground motion for a plane free surface. The dimensionless length of the time window is 3.33. Here  $\nu = 0.25$ .



Incident signal :  $\eta_p = 1.83$

emphasized in the *SV* case. The deamplification pattern on the near side is combined with the great sensitivity of the surface horizontal displacement on the incidence angle (that is with the local surface slope), and, at low frequencies, with the interference between the back scattered Rayleigh and *P*-waves and the primary wave. The mountain top here exhibits a low frequency strong deamplification pattern, and the point of maximum amplification is located very near the middle of the slope. The vertical displacement is maximum near mountain top, and slightly greater on the far side than on the near one.

Synthetic seismograms in Fig. 14 provide a good illustration of all these features. The directivity effect appears very clearly for both *P* and *SV* cases. For instance, the forward scattered Rayleigh wave is five times larger than the back scattered one in the *SV* case. For incident *P*-waves, this ratio is greater since the back scattered Rayleigh is very weak. On the contrary, Fig. 15 shows a very clear back scattered *P*-wave, in this case, while there is no forward scattered such wave. The maximum displacement values undergo important changes over the topography, for both vertical and horizontal components in the *SV* case, and mainly for the horizontal component in the *P* case. As an example, the deamplification on the near side reaches 80 per cent in the *SV* case for the horizontal motion. An interesting feature is the motion at the mountain top in the *SV* case where horizontal or vertical components appear to be completely decoupled: the horizontal motion is of rather low frequency while the vertical motion attains much higher frequencies, and the apparent arrival time of the *SV*-wave is different on the two components (about 0.4 dimensionless time later on the vertical one).

## 2.5 ASPECTS OF THE INFLUENCE OF THE POISSON RATIO

The vast majority of Earth components have a Poisson ratio very near 0.25. Nevertheless, this value may be significantly greater for some surface materials, such as poorly consoli-

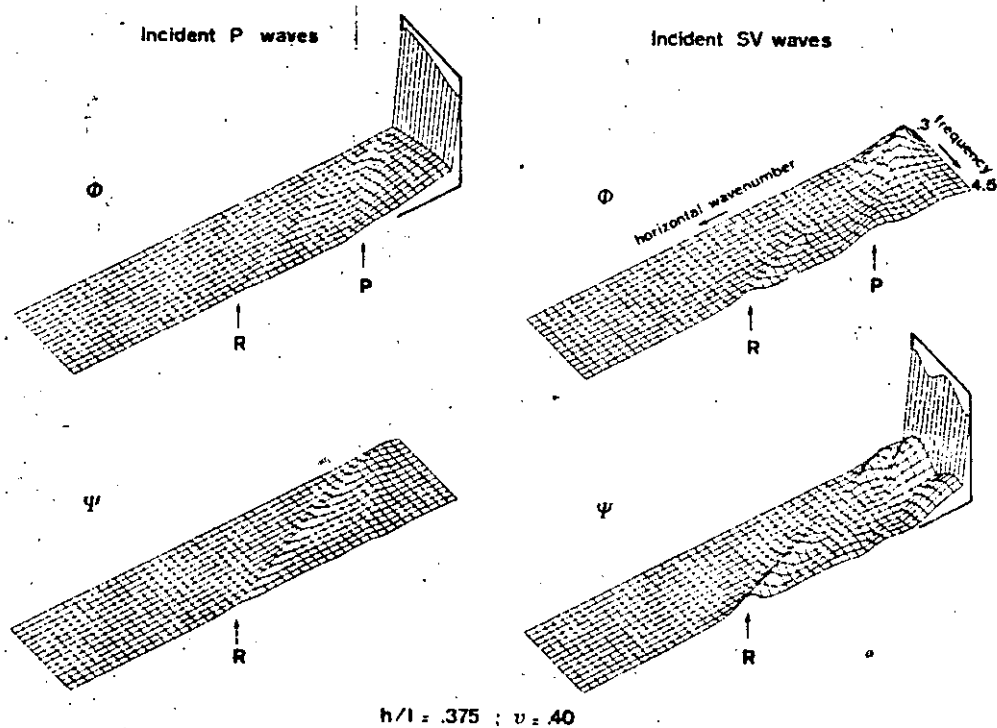


Figure 16. The same as Fig. 5, for a mountain of same shape but having a larger Poisson ratio, i.e.  $\nu = 0.40$ .

dated sediments or artificial fills. In order to get an idea of the upper limit of the changes in the diffraction and amplification/deamplification phenomena due to the Poisson ratio, we have investigated the case of a medium size mountain ( $h/l = 0.375$ ) having a Poisson ratio of 0.40 (that is a shear to compressional velocity ratio of 0.41) impinged by vertical  $P$ - and  $SV$ -waves, for a dimensionless frequency up to 4.5.

As shown in Figs 16 and 17, these variations of the Poisson ratio induce significant variations on the scattered Rayleigh wave. For incident  $P$ -waves, its amplitude is much smaller for  $\nu = 0.40$ , especially at high frequencies: around one-half for  $\eta < 2.5$ , and one-third for  $\eta > 3$ . In the  $SV$  incident case, we observe a slight reduction too in the low frequency domain ( $\eta < 1.5$ ), then the Rayleigh wave disappears, as in the  $\nu = 0.25$  case, for dimensionless frequencies between 1.5 and 2.4, and, for higher frequencies, its amplitude is similar in both cases, and even a little greater for  $\nu = 0.40$ .

The horizontally diffracted  $P$ -wave is still very weak for incident  $P$ -waves, though slightly greater in the high Poisson ratio case. For incident  $SV$ -waves, its amplitude is comparable in both cases at dimensionless frequencies below 2.5, and it is then significantly lower (around one-half) in the high Poisson ratio case.

Also noticeable are a slight decrease in the amplitude of the homogeneous waves for low-frequency incident  $P$ -waves, and their opposite small increase for low-frequency incident  $SV$ -waves.

These variations in the diffracted field are obviously reverberating on the surface motion. At some distance from the topographic feature, the weakening of the main scattered waves (the  $P$ -wave for incident  $SV$ -waves, and the Rayleigh one in the  $P$  incident case), together with the slight increase in the amplitude of the other diffracted wave (respectively Rayleigh and  $P$ ), somewhat lessen and disturb the oscillating pattern of the horizontal and vertical displacement spectra (Fig. 17).

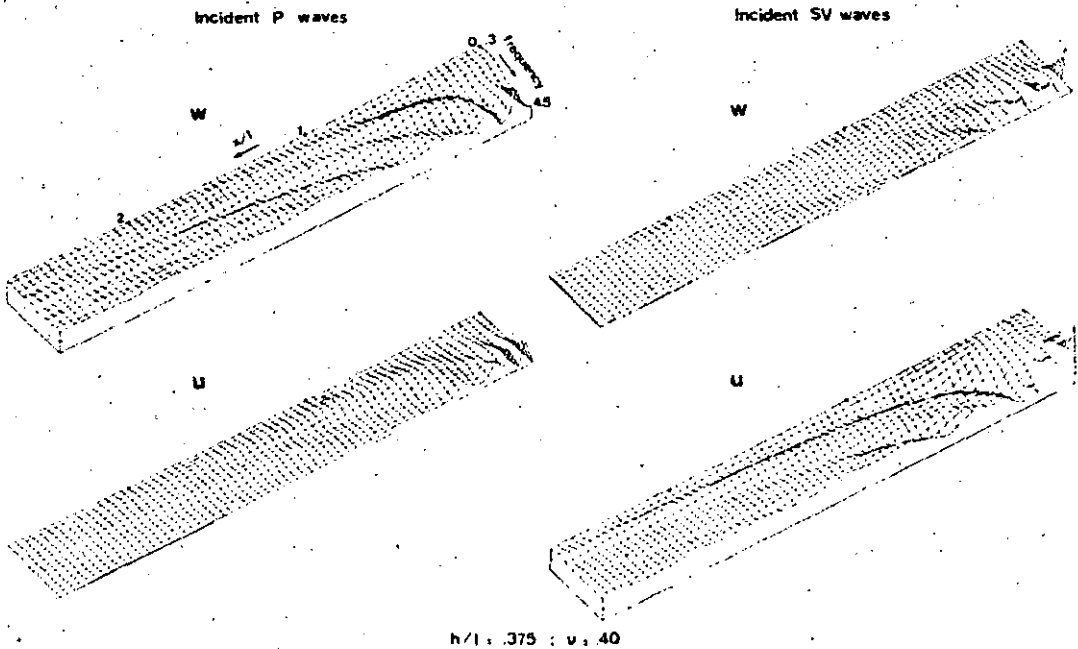


Figure 17. Displacement amplitude as a function of site location and frequency for the large Poisson ratio case ( $\nu = 0.40$ ), and for incident  $P$ -waves (left) and  $SV$ -waves (right). The top diagrams represent the vertical component, and the bottom diagrams the horizontal component.

- Nason, R. D., 1971. Shattered earth at Wallaby Street, Sylmar, *Prof. Pap. US geol. Surv.*, 733, 97-98.
- Rogers, A. M., Katz, L. J. & Bennett, T. J., 1974. Topographic effects of ground motion for incident *P* waves - a model study, *Bull. seism. Soc. Am.*, 64, 437-456.
- Sabina, F. J. & Willis, J. R., 1975. Scattering of *SH* waves by a rough half-space of arbitrary slope, *Geophys. J. R. astr. Soc.*, 42, 685-703.
- Sabina, F. J. & Willis, J. R., 1977. Scattering of Rayleigh waves by a ridge, *J. Geophys.*, 43, 401-419.
- Sanchez-Sesma, F. J. & Rosenblueth, E., 1979. Ground motion at canyons of arbitrary shape under incident *SH* waves, *Int. J. Earthq. Eng. Struct. Dyn.*, 7, 441-450.
- Sills, L. B., 1978. Scattering of horizontally polarized shear waves by surface irregularities, *Geophys. J. R. astr. Soc.*, 54, 319-348.
- Singh, S. K. & Sabina, F. J., 1977. Ground motion amplification by topographic depressions for incident *P* waves under acoustic approximation, *Bull. seism. Soc. Am.*, 67, 345-352.
- Smith, W. D., 1975. The application of finite element analysis to body wave propagation problems, *Geophys. J.*, 42, 747-768.
- Trifunac, M. D., 1973. Scattering of plane *SH* waves by a semi-cylindrical canyon, *Int. J. Earthq. Eng. Struct. Dyn.*, 1, 267-281.
- Trifunac, M. D. & Hudson, D. E., 1971. Analysis of the Pacoima Dam accelerogram. San Fernando, California, earthquake of 1971, *Bull. seism. Soc. Am.*, 61, 1393-1411.
- Wong, H. L. & Jennings, P. C., 1975. Effect of canyon topography on strong ground motion, *Bull. seism. Soc. Am.*, 65, 1239-1257.
- Wong, H. L. & Trifunac, M. D., 1974. Scattering of plane *SH* waves by a semi-elliptical canyon, *Int. J. Earthq. Eng. Struct. Dyn.*, 3, 157-169.



**DIVISION DE EDUCACION CONTINUA  
FACULTAD DE INGENIERIA U.N.A.M.**

ANALISIS DE RIESGO SISMICO

THE EFFECTS OF LOCAL IRREGULARITIES ON  
SEISMIC GROUND MOTION

DR. FRANCISCO SANCHEZ SESMA

JULIO, 1985

# THE EFFECTS OF LOCAL IRREGULARITIES ON SEISMIC GROUND MOTION

By

Francisco J. Sánchez-Sesma\*

## ABSTRACT

The effects of topographical and geological irregularities on seismic ground motion are discussed. A short description is given of some of the available techniques to calculate such effects. Some comments are made on the importance of local conditions in the assessment of seismic risk.

## INTRODUCTION

It has long been recognized that local topography and geology can significantly affect the ground motion at a site (Figure 1). The contribution of topography could serve to explain the high acceleration recorded at the Pacoima Dam (1.25 g) during the San Fernando, California earthquake of February 9, 1971 (Trifunac and Hudson, 1971; Boore, 1972c). For the aftershocks of the same earthquake Davis and West (1973) in a series of observations have found significant local amplifications due to topographical relief. In a field

---

\* Instituto de Ingeniería, UNAM; Cd. Universitaria  
Apdo. 70-472, Coyoacán 04510, México, D.F., MEXICO

study in the Appalachian Mountains using distant mine blasts as sources, average amplitude ratios between mountaintop and valley sites were determined (Griffiths and Bollinger, 1979). These average ratios showed that the seismic wave amplitudes at the crests were amplified by factors from 1.7 to 3.4. In Figure 2 three seismograms for the same event in the Powell Mountain area are shown. The positions of recording sites are also displayed in the figure.

The effect of soil conditions in ground motion has been observed in well-documented earthquakes (Sozen *et al.*, 1968; Jennings, 1971) and in regression analyses of strong motion data. There is significant evidence that subsurface topography, *i.e.* lateral heterogeneities, are related to localized damage distribution in the Skopje, Yugoslavia earthquake of July 26, 1963 (Poceski, 1969). It has been suggested that focusing of the wave energy, by irregular interfaces, generated large motion amplification in limited zones of the city (Jackson, 1971). Damage statistics of buried utility pipes in the Miyagiken-Oki, Japan earthquake of June 12, 1978 have shown spectacular increase in the number of occurred failures near the cut and fill boundary of a newly developed area (Kubo and Isoyama, 1980).

Local conditions can generate large amplifications and important spatial variations of seismic ground motion. These effects are of particular significance in the assessment of seismic risk, in studies of microzonation, in planning and in the seismic design of important facilities (Esteve, 1977; Ruiz, 1977). In particular, local irregularities can be relevant in calculating the seismic response of long structures (see Figure 3) like dams, bridges or life-line systems (*e.g.* Esquivel and Sánchez-Sesma, 1980; Ruiz and Esteve, 1981).

As pointed out by Trifunac (1980), the strong earthquake shaking of interest in earthquake engineering falls in the frequency range from about 0.1 Hz to about 20 Hz and since the seismic wave velocities near the earth's surface lie in the range from about 0.1 km/s to about 3 km/s, it can be seen that the corresponding wave lengths are from tens of meters to tens of kilometers. Thus, the topographical and geological irregularities of dimensions near to this range will have considerable influence on the corresponding waves. It follows that the extent and detail of local conditions required to study their effects should be considered in terms of the wave lengths associated with the periods of motion which are more important for a particular analysis. For a tall building, a dam or a bridge, for example, these local site dimensions might be of several kilometers. On the other hand, for stiff structures or small buildings, these dimensions can be from tens to hundreds of meters.

Although recent work has emphasized the physical understanding of local effects so that quantitative predictions can be made, as stated in a recent review by Boore (1983), there is still lack of criteria for dealing with the problem taking into account source, path and local conditions. Active research is needed to predict more accurately the local effects, given the source parameters. Indeed, it is encouraging the recent progress on strong motion prediction using mathematical modeling techniques (Aki, 1982). Much of the research is concentrated on the understanding of fault mechanics and wave propagation in the Earth. It is generally accepted that high frequency radiation, which controls accelerations, comes from very localized parts of the fault. A powerful asymptotic theory of high frequency radiation has been recently developed (Madariaga, 1983). Applications of the theory are coming. However, it should be noted that the foci of future earthquakes are not known;

their location, mechanism and amount of released energy can only be speculated in terms of regional seismicity models (Esteva, 1976). On the other hand, the knowledge of geological details is generally small to justify the use of very refined models of wave propagation, particularly for the high frequencies. It is then clear, in view of the mentioned uncertainties, that the problem of seismic risk assessment must be dealt with a probabilistic framework. A promising approach seems to be the use of integral measures of intensity such as the Arias' (1970) using stochastic descriptions of the input and simplified models of the local irregularities (Sánchez-Sesma *et al.*, 1983).

The aim of this work is to review the problem of calculating the effects of topographical and geological irregularities on ground motion given certain input, *i.e.* some kind of seismic waves. For this purpose the current formulation of the problem, the known analytical solutions and the available numerical methods are discussed in brief. This review is by no means complete and reflects the particular trends of the author. Nevertheless, it is hoped that this work could serve to stimulate discussion and interest on the problem.

## FORMULATION OF THE PROBLEM

There is no doubt that the source mechanism governs the way in which the released seismic energy is radiated in space and time. However, seismic waves, once emitted by the source, are dependent on the mechanical properties of earth materials and the heterogeneities encountered in their path. This is also true dealing with irregular local conditions. Moderate changes in mechanical impedances or irregularities with size comparable to incident wave lengths can generate significant amplifications and spatial variations of ground motion (Boore, 1972b).

Plane waves are reflected back and refracted forward as they arrive at a plane interface. The amounts of reflected and transmitted energy depend on the mechanical properties of the media involved. Reflection and refraction in elastic wave propagation can well be described by geometrical means. Let us call diffraction to every change in the waves' path that can not be described as reflection or refraction. For studying diffraction of elastic waves it is necessary to solve a boundary value problem for the governing equations of linear elasticity (e.g. Achenbach, 1973; Aki and Richards, 1980).

To fix ideas, consider an elastic, homogeneous and isotropic half-space with an irregular surface. Under incidence of elastic waves the irregularity will diffract the incident waves (diffraction is frequently called scattering). Diffracted waves must satisfy, together with incident waves, the governing equations (Navier equations) and the boundary conditions (traction-free surface). Moreover, the diffracted fields must satisfy the Sommerfeld (1949) radiation condition at infinity, which means that the diffracted fields must scatter to infinity; i.e., no energy

may be radiated from infinity into the irregular region. The Sommerfeld radiation condition has been extended to elastic wave fields by Kupradze (1965).

### ANALYTICAL SOLUTIONS

The simplest problems in elastic wave diffraction are the two-dimensional SH-wave problems because they can be analyzed separately from other body waves. The governing equation for this case is the scalar wave equation. Then, analytical solutions can be obtained for geometries of the scatterer which allow separation of variables (Mow and Pao, 1971). Using this method, exact solutions have been obtained for the diffraction of SH-waves by canyons and alluvial valleys with semi-circular (Trifunac, 1971, 1973) or semi-elliptical shapes (Wong and Trifunac, 1974a, b). Even with these simple models of local irregularities, complicated interference patterns were found and the obtained surface displacement fields vary strongly in space (see Figure 4). They are very sensitive to the incidence angle and the frequency. Results for alluvial valleys show the importance of the two-dimensional behaviour which gives much larger amplifications than those obtained from unidimensional calculations. These analytical solutions have shown the importance of the problem and they provide a check for numerical procedures.

For the more difficult cases of P- or SV-incident waves the orthogonal wave functions developed in classical physics are not separable for the half-space surface due to the coupling of boundary conditions. Lee (1978, 1982) overcome this difficulty for a semi-spherical canyon by expanding the spherical wave functions further into a power series which matched all the boundary conditions successfully. However,

this approach is limited to small frequencies because the resulting matrix equations, which are infinite, can only be solved approximately for this case.

Under additional simplifying assumptions, other analytical solutions have been obtained using orthogonal wave functions. For an acoustic medium the exact expressions for the scattered fields generated by incidence of P-waves on canyons of semi-circular and semi-spherical shapes (Singh and Sabina, 1977) have been obtained. However, the results are of small utility because the acoustic assumption can hardly be met in real cases. The problem of vertically incident P-waves upon a semi-ellipsoidal three-dimensional scatterer has been exactly solved for an elastic medium in which horizontal displacements are restricted (Sánchez-Sesma, 1983b). Results for vertical displacement are in reasonable agreement with those from more reliable computations for a truly elastic medium (Sánchez-Sesma, 1983a).

Under the assumption of small-slope irregularities a perturbation solution has been obtained for the elastic scattered field by two-dimensional geometries (Gilbert and Knopoff, 1960). The approximation is based on replacing the irregularity by an equivalent stress distribution. An application of this method by Hudson (1967) deals with small-slope three-dimensional scatterers. With this approach reasonable estimates have been obtained of the scattered Rayleigh waves as compared with observations even in cases in which slope angles are as large as  $25^\circ$  or, say,  $30^\circ$  (Hudson and Boore, 1980).

The method of matched asymptotic expansions has no restrictions on the slope of the irregularity. It is based in matching the first terms of an outer expansion of the near field with those of an inner expansion of the far field

(Sabina and Willis, 1975, 1977). Although the method is limited to very small frequencies, results are in qualitative agreement with observations.

#### NUMERICAL METHODS

A powerful technique has been developed by Aki and Larner (1970) to treat scattering of SH-waves by irregular interfaces. In the Aki-Larner method, incidence is assumed of a plane single-frequency wave which causes a displacement field. This field is represented by superposition of plane waves of unknown complex amplitudes propagating in many directions. Inhomogeneous plane waves are allowed. The total motion is obtained from integration over horizontal wave number. Under the assumption of horizontal periodicity of the irregularity, the integral is replaced by an infinite sum. Truncation of this sum and application of the interface conditions of continuity of stress and displacement leads to a system of linear equations for the complex scattering coefficients. This method, which is restricted to small-slope irregularities, has been applied by Bouchon (1973) to study the effects of two-dimensional irregular topographies on ground motion for incidence of SH, SV and P waves. An extension of the method has been advanced by Bouchon and Aki (1977a, b) to represent with this discrete-wave-number technique near seismic source fields in a layered medium with irregular interfaces. Another extension of the method, now to time domain calculations, has been developed to study the seismic response of alluvial valleys (Bard and Bouchon, 1980a, b) under incidence of SH, P and SV waves. The Aki-Larner technique has been recently used by Bard (1982) to analyze the effects of two-dimensional elevated topography on ground motion. The comprehensive studies by Bard and Bouchon throw light on the subject and

on the physics of the problem. The method has been used to model the fields generated by real faults (Bouchon, 1979; Campillo, 1983). It can be used to model ground motion considering together the effects of source, path and local conditions. However, in this case the numerical computations may become very expensive -if they can be performed- for many real cases.

The finite difference method is also a powerful tool in elastic wave propagation studies (Alterman and Karal, 1968; Boore, 1972a). It has been applied to modelate two-dimensional irregular interfaces (Boore *et al.*, 1971) and ridges (Boore, 1972b) in the SH case and also for incident of P and SV-waves upon a sedimentary basin (Harmsen and Harding, 1981) and a step-like topography (Boore *et al.*, 1981). Interesting results have been found concerning the significant generation of Rayleigh surface waves by lateral irregularities. For incidence of P waves upon a surface slot the computations by Ilan and Bond (1981) give good agreement with experiments. It was found that the amplitude of the scattered Rayleigh wave is, as expected, dependent on incidence angle. A finite difference analysis of axisymmetric topographical irregularities has been presented to study the effects of vertically incident shear waves (Zhenpeng *et al.*, 1980). Spectral ratios were obtained and comparison with observations gives reasonable agreement. The finite difference method is theoretically unlimited to model details and nonlinear behaviour of materials, but the size of the problem can easily exceed the capacity of major computing facilities.

The finite element method also allows a detailed description of site topography and layering. It is possible with this method to calculate the response of two-dimensional soil configurations with truly nonlinear stress-strain relations

(Streeter *et al.*, 1974; Joyner and Chen, 1975; Joyner, 1975). The major disadvantage of the method is its low-frequency limit and high cost. Usually, real time analysis must be shortened to avoid the reflections from the artificial boundaries. The use of different transmitting techniques can reduce the spurious waves to some extent (e.g. Smith, 1974, 1975; Ayala and Aranda, 1977; Clayton and Engquist, 1977; Castellani *et al.*, 1981; Liao and Wong, 1981). A successful criterion has been developed for damping out the unwanted reflections by means of non-uniform element size (Day, 1977). Finite elements have been used to treat problems of irregular layering (Lysmer and Drake, 1972; Drake, 1972; Aranda and Ayala, 1978) and two-dimensional topographical irregularities (Castellani *et al.*, 1982) under idealized conditions. Nevertheless, a realistic wave analysis is quite costly.

In recent years boundary methods have gained increasing popularity. This fact is mainly due to the availability of high speed computers. Boundary methods are well suited to deal with wave propagation problems because they avoid the introduction of fictitious boundaries and reduce by one the dimensionality of the problem. These facts yield numerical advantages. Moreover, boundary methods can be used together with the finite element method (Zienkiewics *et al.*, 1977). Then, the region modeled with finite elements can be smaller (e.g. Ayala and Gómez, 1979; Shah *et al.*, 1982).

There are two main approaches for the formulation of boundary methods; one is based on the use of boundary integral equations (Cruse and Rizzo, 1968a, b; Brebbia, 1978; Cole *et al.*, 1978; Alarcón *et al.*, 1979), and the other, on the use of complete systems of solutions (Herrera and Sabina, 1978; Herrera, 1980). The scattering of incident SH-waves from two-dimensional irregular topographies has

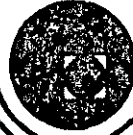
been formulated with integral equations by Wong and Jennings (1975) for arbitrarily shaped canyon-like profiles and by Sills (1978) for ridges and mixed shapes. This method has been applied with success to calculate the effects of a dipping layer of alluvium of an SH-wave source on the surface (Wong *et al.*, 1977). Results compare favorably with observations during a full-scale low-amplitude propagation test. A powerful approach which combines the boundary integral equation method with finite differences in time has been presented (Cole *et al.*, 1978) for solving elastodynamic problems. The performance of the method was found to be good in a simple numerical problem. A boundary method has been recently developed and applied to solve two-dimensional scattering of harmonic elastic waves by canyons (Sánchez-Sesma, 1978, 1981; Sabina *et al.*, 1979; Sánchez-Sesma and Rosenblueth, 1979; Wong, 1979, 1982; England *et al.*, 1980; Sánchez-Sesma *et al.*, 1982a), alluvial deposits (Sánchez-Sesma and Esquivel, 1979; Dravinski, 1982a, b, 1983) and ridges (Sánchez-Sesma and Esquivel, 1980; Sánchez-Sesma *et al.*, 1982b) for different types of waves and shapes of the scatterers. The method consists of constructing the scattered fields with linear combinations of members of a  $c$ -complete family of wave functions (Herrera and Sabina, 1978). These families of functions, which are solutions of the governing equations of the problem, can be constructed in a very general way, with single or multipolar sources having their singularities outside the region of interest. Coefficients of the linear forms thus constructed are obtained from a least-squares matching of boundary conditions. As pointed out by Wong (1982), the method can be considered as a generalized inverse one. In doing this, Wong suggested a procedure which improves the solution numerically. A general framework for the method is given by a recent algebraic theory of boundary value problems (Herrera, 1979, 1980 a, b).

- Sánchez-Sesma, F.J. (1983a). Diffraction of elastic waves by three-dimensional surface irregularities, *Bull. Seism. Soc. Am.*, in press.
- Sánchez-Sesma, F.J. (1983b). Ground motion on three-dimensional depressions for vertically incident P waves using a simplified elastic medium, in process.
- Sánchez-Sesma, F.J. and E. Rosenblueth (1979). Ground motion at canyons of arbitrary shape under incident SH waves, *Int. J. Earthquake Eng. Struct. Dyn.* 7, 441-450.
- Sánchez-Sesma, F.J. and J.A. Esquivel (1979). Ground motion on alluvial valleys under incident plane SH waves, *Bull. Seism. Soc. Am.*, 69, 1107-1120.
- Sánchez-Sesma, F.J. and J.A. Esquivel (1980). Ground motion on ridges under incident SH waves, *Proc. World Conf. Earthquake Eng.*, 7th, Istanbul, 1, 33-40.
- Sánchez-Sesma, F.J., I. Herrera and M.A. Bravo (1982a). Difracción de ondas P, SV y de Rayleigh en un semiespacio elástico. *Instituto de Ingeniería, UNAM, Mexico.*
- Sánchez-Sesma, F.J., I. Herrera and J. Avilés (1982b). A boundary method for elastic wave diffraction. Application to scattering of SH waves by surface irregularities, *Bull. Seism. Soc. Am.*, 72, 473-490.
- Sánchez-Sesma, F.J., E. Faccioli and R. Fregonese (1983). An index for measuring the effects of topography on seismic ground motion intensity, *Bull. Seism. Soc. Am.*, submitted for publication.

- Shah, A.H., K.C. Wong and S.K. Datta (1982). Diffraction of plane SH waves in a half-space. *Int. J. Earthquake Eng. Struct. Dyn.*, **10**, 519-528.
- Sills, L.B. (1978). Scattering of horizontally polarized shear waves by surface irregularities, *Geophys.*, *J.R. Astr. Soc.*, **54**, 319-348.
- Singh, S.K. and F.J. Sabina (1977). Ground motion amplification by topographic depressions for incident P waves under acoustic approximation, *Bull. Seism. Soc. Am.*, **67**, 345-352.
- Smith, W.D. (1974). A nonreflecting boundary for wave propagation problems, *J. Computational Phys.*, **15**, 492-503.
- Smith, W.D. (1975). The application of finite element analysis to body wave propagation problems, *Geophys.*, *J.R. Astr. Soc.*, **42**, 747-768.
- Sommerfeld, A. (1949). *Partial differential equations in physics*, Academic Press, Inc., New York.
- Sozen, M.A., P.C. Jennings, R.B. Matthiesen, G.W. Housner and N.M. Newmark (1968). *Engineering Report on the Caracas Earthquake of July 29, 1967*, National Academy of Sciences, Washington, D.C.
- Streeter, V.L., E.B. Wylie and F.E. Richard, Jr. (1974). Soil motion computations by characteristics method, *Proc. Am. Soc. Civil Eng., J. Geotech. Eng. Div.*, **100**, 247-263.
- Takeuchi, H. and M. Saito (1972). Seismic surface waves, in *Methods in Computational Physics*, **11**, B.A. Bolt, ed., Academic Press, New York.

- Trifunac, M.D. (1971). Surface motion of a semi-cylindrical alluvial valley for incident plane SH waves, *Bull. Seism. Soc. Am.*, **61**, 1755-1770.
- Trifunac, M.D. (1973). Scattering of plane SH waves by a semi-cylindrical canyon, *Int. J. Earthquake Eng. Struct. Dyn.*, **1**, 267-281.
- Trifunac, M.D. (1980). Effects of site geology on amplitudes of strong motion, *Proc. World Conf. Earthquake Eng.*, *7th*, Istanbul, **2**, 145-152.
- Trifunac, M.D. and D.E. Hudson (1971). Analysis of the Pacoima Dam accelerogram - San Fernando, California, earthquake of 1971, *Bull. Seism. Soc. Am.*, **61**, 1393-1411.
- Wong, H.L. (1975). Dynamic soil-structure interaction, *Earthquake Eng. Res. Lab., Report No. EERL 75-01*, California Inst. of Tech., Pasadena, California.
- Wong, H.L. (1979). Diffraction of P, SV and Rayleigh waves by surface topographies, *Report CE 79-05*, Department of Civil Engineering, University of Southern California, Los Angeles, California.
- Wong, H.L. (1982). Effect of surface topography on the diffraction of P, SV and Rayleigh waves, *Bull. Seism. Soc. Am.*, **72**, 1167-1183.
- Wong, H.L. and M.D. Trifunac (1974a). Scattering of plane SH wave by a semi-elliptical canyon, *Int. J. Earthquake Eng. Struct. Dyn.*, **3**, 157-169.

- Wong, H.L. and M.D. Trifunac (1974b). Surface motion of a semi-elliptical alluvial valley for incident plane SH wave, *Bull. Seism. Soc. Am.*, 64, 1389-1408.
- Wong, H.L. and P.C. Jennings (1975). Effect of canyon topography on strong ground motion. *Bull. Seism. Soc. Am.*, 65, 1239-1257.
- Wong, H.L., Trifunac, M.D. and B. Westermo (1977). Effects of surface and subsurface irregularities on the amplitude of monochromatic waves, *Bull. Seism. Soc. Am.*, 67, 353-368.
- Zhenpeng, L., Y. Baipo and Y. Yifan (1980). Effect of three-dimensional topography on earthquake ground motion, *Proc. World Conf. Earthquake Eng.*, 7th, Istanbul, 2, 161-168.
- Zienkiewicz, O.C., D.W. Kelly and P. Bettess (1977). The coupling of the finite element method and boundary solution procedures, *Intern. J. Num. Meth. Eng.*, 11, 355-377.



**DIVISION DE EDUCACION CONTINUA  
FACULTAD DE INGENIERIA U.N.A.M.**

ANALISIS DE RIESGO SISMICO

GROUND MOTION AT CANYONS OF ARBITRARY SHAPE  
UNDER INCIDENT SH WAVES

DR. FRANCISCO SANCHEZ SESMA

JULIO, 1985

## GROUND MOTION AT CANYONS OF ARBITRARY SHAPE UNDER INCIDENT SH WAVES

FRANCISCO J. SÁNCHEZ-SESMA\* AND EMILIO ROSENBLUETH†

*Instituto de Ingeniería, Universidad Nacional Autónoma de México, México*

### SUMMARY

A method for calculating the two-dimensional scattering of incident SH waves by canyons of arbitrary shape is presented. The problem is formulated in terms of a Fredholm integral equation of the first kind with the integration path outside the boundary. Point-source discretization and a least-squares scheme are used. Numerical results are compared with the known analytic solution for a semi-cylindrical canyon. Spatial variations of surface amplitudes are computed for triangular and half-cycle sinusoidal canyons as well.

### INTRODUCTION

Influence of local conditions on ground motion due to earthquakes has been recognized as a significant feature in seismic design.<sup>1,2</sup> Topographic effects can introduce appreciable differences on seismic movements between neighbouring sites, even when the distance from the active fault and predominant incident angles do not change.

The subject has been treated in the literature as a problem of elastic-wave diffraction. Analytic solutions for semi-cylindrical and semi-elliptical canyons under incident SH waves have been obtained.<sup>3,4</sup> An acoustic approximation has been used for a similar problem where only vertically incident P waves are considered in detail.<sup>5</sup> By means of matched asymptotic expansions, expressions for the solution of the SH-wave diffraction problem have also been obtained.<sup>11</sup> This solution is restricted to low frequencies. Another approach assumes periodicity of surface shape and uses discretized integral equations to describe the movement in the neighbourhood of topographic irregularities with small slopes under low-frequency incident waves.<sup>6</sup> The SH-wave diffraction problem for canyons of arbitrary shape has been formulated in terms of a Fredholm integral equation of the second kind and applied to the study of topographic effects at Pacoima Canyon<sup>7</sup>. Large amplifications and decrements were found in harmonic analysis but computed response spectra showed small differences, save for the range of high frequencies. For the same problem a multipole expansion in terms of Hankel functions about the origin and the least-squares method have been used.<sup>15</sup> Comparison of results with some known exact solutions yields very good agreement.

In the present work an alternative method is developed for solving SH-wave diffraction problems in arbitrarily shaped canyons. The method makes use of an integral representation of scattered waves as a simple layer potential<sup>8</sup> applied at interior points thus avoiding singularities in the kernel of the integral equation. The idea is similar to Copley's<sup>9</sup> for Weber's equation and has been applied by De Mey<sup>10</sup> to the solution of Laplace's interior problem.

The resulting Fredholm integral equation of the first kind is *discretized* with line sources concentrated at an interior curve. Emphasis is on field representation rather than on solution of the integral equation itself. Thus, the Fredholm integral equation serves as an intermediate step in the problem formulation and provides a useful tool to investigate some of the singularities of the operator.

Once the boundary conditions are established, a system of equations is obtained which is solved in the least-squares sense.

\* Associate Professor of Engineering.

† Professor of Engineering.

The method has been applied to solve scattering and diffraction of P and SV waves by canyons<sup>17</sup> as well as ground motion of alluvial valleys under incident SH waves.<sup>18</sup>

Questions arise on completeness of the set of sources and convergence of the method. We will not deal with them in this work. It can be shown that the set of line sources located on an interior curve is complete so that no additional sources are required to approximate the field outside the canyon and its boundary. The proof is similar to that used by Millar<sup>16</sup> to establish the completeness of the multipole expansion and its normal derivatives. Given that the set is complete, it can be shown that the least-squares solution, when applied on the boundary as done here, leads to an approximate solution that converges uniformly in the mean to the exact solution as the number of sources tends to infinity.

For the semi-cylindrical canyon numerical results obtained by this method are compared with Trifunac's exact solution.<sup>3</sup> Convergence is illustrated showing results for increasing number of sources. Results are provided also for half-cycle sinusoidal and triangular canyons.

### PROBLEM FORMULATION

For the propagation of polarized SH waves, displacements in the  $z$  direction satisfy the scalar wave equation

$$\frac{\partial^2 u}{\partial x^2} + \frac{\partial^2 u}{\partial y^2} = \frac{1}{c^2} \frac{\partial^2 u}{\partial t^2} \quad (1)$$

where  $c = (\mu/\rho)^{1/2}$  is the shear wave velocity,  $\mu$  the shear modulus, and  $\rho$  the mass density of the medium. For harmonic waves of the form  $u \exp(i\omega t)$ , equation (1) can be transformed into the Helmholtz equation

$$\frac{\partial^2 u}{\partial x^2} + \frac{\partial^2 u}{\partial y^2} + k^2 u = 0 \quad (2)$$

where  $k = \omega/c$  is the wave number and  $\omega$  the circular frequency.

The traction-free boundary condition implies that at the free surface

$$\frac{\partial u}{\partial \mathbf{n}} = 0 \quad (3)$$

where  $\mathbf{n}$  is the normal vector to the half-space surface or to the canyon surface (Figure 1).

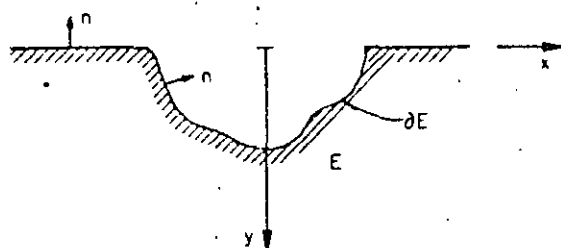


Figure 1. Canyon geometry

Assume that the solution has the form

$$u = u^{(0)} + u^{(d)} \quad (4)$$

where  $u^{(0)}$  is the free-field displacement (without surface irregularities) and  $u^{(d)}$  the contribution of the diffracted waves.

For illustration, consider a plane wave of unit amplitude that propagates towards the half-space surface

$$u^{(i)} = \exp \left[ i\omega \left( t - \frac{x}{c_x} + \frac{y}{c_y} \right) \right] \quad (5)$$

where  $c_x = c/\sin \gamma$ ,  $c_y = c/\cos \gamma$  and  $\gamma$  is the incidence angle (Figure 2). To satisfy the free boundary conditions at  $y = 0$ , a reflected wave must be given by

$$u^{(r)} = \exp \left[ i\omega \left( t - \frac{x}{c_x} - \frac{y}{c_y} \right) \right] \quad (6)$$

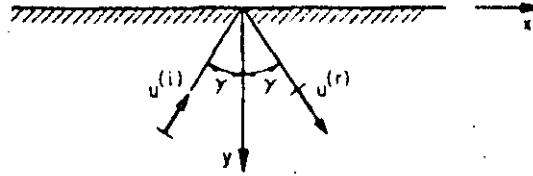


Figure 2. Incident and reflected plane SH waves, free-field

Thus the free-field solution is obtained as  $u^{(0)} = u^{(i)} + u^{(r)}$ , which may be written as

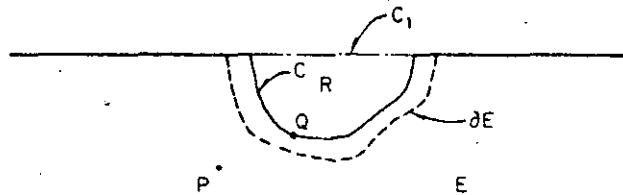
$$u^{(0)} = 2 \cos\left(\frac{\omega y}{c_y}\right) \exp i\omega \left[ \left( t - \frac{x}{c_x} \right) \right] \quad (7)$$

Assume that displacement  $u^{(d)}$  can be expressed as a simple layer potential at interior curve  $C$

$$u^{(d)}(P) = \int_C \sigma(Q) G(P, Q) dS_Q \quad (8)$$

where  $Q \in C$ ,  $P \in E \cup \partial E$  (Figure 3),  $\sigma(Q)$  is the simple layer density—an unknown function to be determined from the boundary conditions—and  $G(P, Q)$  is Green's function for a point  $Q$  in the half-space, that is,  $G(P, Q)$  satisfies

$$\left( \frac{\partial^2}{\partial x^2} + \frac{\partial^2}{\partial y^2} + k^2 \right) G(P, Q) = -\delta(|\vec{r} - \vec{r}_0|) \quad (9)$$

Figure 3. Definition of regions  $R$  and  $E$  and curves  $C$ ,  $C_1$  and  $\partial E$ 

with the free-surface condition

$$\frac{\partial G}{\partial y} = 0 \quad \text{at } y = 0 \quad (10)$$

where  $\delta(\cdot)$  is Dirac's delta function,  $\vec{r}$  the position vector of point  $P$  and  $\vec{r}_0$  the position vector of point  $Q$ . Green's function is given by

$$G(P, Q) = \frac{i}{4} [H_0^{(2)}(kr_1) + H_0^{(2)}(kr_2)] \exp(i\omega t) \quad (11)$$

where  $H_0^{(2)}(\cdot)$  is Hankel's function of the second kind and order zero,  $r_1 = [(x-x_0)^2 + (y-y_0)^2]^{\frac{1}{2}}$ , the distance from point  $Q(x_0, y_0)$  to point  $P(x, y)$ , and  $r_2 = [(x-x_0)^2 + (y+y_0)^2]^{\frac{1}{2}}$  is the distance from  $P$  to the image point of  $Q$  with co-ordinates  $(x_0, -y_0)$ . In this equation Hankel's function represents cylindrical SH waves that propagate towards infinity with speed  $c$  and satisfy Sommerfeld's radiation condition.<sup>12</sup>

From equations (4) and (8) one can write

$$u(P) = u^{(0)}(P) + \int_C \sigma(Q) G(P, Q) dS_Q \quad (12)$$

where  $P \in E \cup \partial E$ .

Replacing equation (12) in equation (3) for  $P \in \partial E$ , the resulting Fredholm integral equation of the first kind is

$$\int_C \sigma(Q) \frac{\partial G(P, Q)}{\partial n_P} dS_Q = -\frac{\partial u^{(0)}(P)}{\partial n_P}, \quad P \in \partial E \quad (13)$$

where  $n_P$  is the normal vector to boundary  $\partial E$  at point  $P$ .

To investigate conditions for which the solution of (13) is non-unique, we will look for non-trivial solutions  $\sigma$  of the homogeneous problem

$$\int_C \sigma(Q) \frac{\partial G(P, Q)}{\partial n_P} dS_Q = 0, \quad P \in \partial E \quad (14)$$

Let  $\phi$  be the solution of

$$\frac{\partial^2 \phi}{\partial x^2} + \frac{\partial^2 \phi}{\partial y^2} + k^2 \phi = 0 \quad (15)$$

in a region  $R$ , limited by  $C$  and  $C_1$  (Figure 3). For a point  $P$  outside this region, applying Green's theorem<sup>12</sup> we get

$$\int_{C \cup C_1} \left[ \frac{\partial \phi(Q)}{\partial n_Q} G(P, Q) - \phi(Q) \frac{\partial G(P, Q)}{\partial n_Q} \right] dS_Q = 0 \quad (16)$$

Let  $\phi = 0$  at  $C$  and  $\partial \phi / \partial n = 0$  at  $C_1$ ; that is,  $\phi$  is an eigenfunction of the problem

$$\left. \begin{aligned} \frac{\partial^2 \phi}{\partial x^2} + \frac{\partial^2 \phi}{\partial y^2} + k^2 \phi &= 0 && \text{in } R \\ \phi &= 0 && \text{at } C \\ \frac{\partial \phi}{\partial n} &= 0 && \text{at } C_1 \end{aligned} \right\} \quad (17)$$

Furthermore, by construction

$$\frac{\partial G(P, Q)}{\partial n_Q} = 0 \quad \text{at } C_1 \quad (18)$$

Then, from equation (16), for  $P$  outside region  $R$  we get  $(Q)$

$$\int_C \frac{\partial \phi(Q)}{\partial n_Q} G(P, Q) dS_Q = 0 \quad (19)$$

For  $P \in \partial E$ , from equation (19) we may write

$$\int_C \frac{\partial \phi(Q)}{\partial n_Q} \frac{\partial G(P, Q)}{\partial n_P} dS_Q = 0 \quad (20)$$

That is, there are non-trivial solutions  $\sigma(Q) = \partial \phi(Q) / \partial n_Q$  when  $k$  coincides with the eigenvalues of the problem defined by equations (17).

In particular, when  $R$  is a semi-circle with radius  $a_0$  the eigenvalues are given by

$$k_{m,n} = \frac{j_{m,n}}{a_0} \quad (21)$$

where  $j_{m,n}$  is the  $n$ th root of the equation  $J_m(x) = 0$ ,  $J_m(\cdot)$  is the Bessel function of the first kind and order  $m$ ,  $m = 0, 1, 2, \dots$  and  $n = 1, 2, \dots$

Given an arbitrary region  $R$ , there exists an infinite sequence of eigenvalues  $k$  for which the problem of equations (17) has a continuous solution.<sup>12</sup>

Nevertheless, there may be other non-trivial solutions of equation (14). The eigenfunctions of the problem defined by equations (17) provide only some of them. This suggests use of a suitable numerical approach to avoid the lack of uniqueness.

We seek a solution in the least-squares sense, that is, one for which the mean square error

$$\int_{\partial E} \left| \frac{\partial u^{(0)}(P)}{\partial n_P} + \frac{\partial u^{(1)}(P)}{\partial n_P} \right|^2 dS_P \quad (22)$$

is minimum. This criterion and the source-discretization scheme shown below lead us to a method which, apparently, does not suffer lack of uniqueness. Thus, emphasis is laid on field representation rather than on

the solution of the integral equation itself. On the other hand, it can be shown that the set of line sources is complete if we take a *dense* subset on  $C$ ; it suffices to select equally spaced points. Uniform convergence to the exact solution in the mean is thus ensured. These ideas parallel those in the work of Millar.<sup>16</sup>

### SOURCE-DISCRETIZATION AND NUMERICAL SOLUTION

Let  $\sigma(Q)$  be of the form

$$\sigma(Q) = \sum_{n=1}^N b_n \delta(|Q - Q_n|) \quad (23)$$

where  $N$  is the number of sources of amplitude  $b_n$  at points  $Q_n \in C$ . Equations (12) and (13) can then be written as

$$u(P) = u^{(0)}(P) + \sum_{n=1}^N b_n G(P, Q_n) \quad (24)$$

and

$$\sum_{n=1}^N b_n \frac{\partial G(P, Q_n)}{\partial n_P} = -\frac{\partial u^{(0)}(P)}{\partial n_P} \quad (25)$$

In order to find the  $N$  unknowns  $b_n$ ,  $n = 1, 2, \dots, N$ , impose the condition from equation (13) at  $M$  points  $P_m$  on the boundary of the canyon

$$\sum_{n=1}^N b_n \frac{\partial G(P_m, Q_n)}{\partial n_{P_m}} = -\frac{\partial u^{(0)}(P_m)}{\partial n_{P_m}}, \quad m = 1, 2, \dots, M \quad (26)$$

Equations (26) represent the standard problem of linear algebra of  $M$  equations with  $N$  unknowns

$$[A_{mn}] \{b_n\} = \{f_m\} \quad (27)$$

Good results can be obtained when  $M = N$ , but this case requires care in the choice of curve  $C$ . For instance, when  $k$  coincides with or is very close to the eigenvalues of the interior problem (17), numerical difficulties arise (e.g. unrealistically large displacements or ill-conditioned operator). Modifying the choice of curve  $C$  changes the interior problem and removes the singularity.

It is convenient, though, to take  $M > N$  and solve in the least-squares sense<sup>14</sup> by means of

$$[A_{mn}^*]^T [A_{mn}] \{b_n\} = [A_{mn}^*]^T \{f_m\} \quad (28)$$

where  $[A_{mn}^*]^T$  is the transposed conjugate of the coefficients matrix. The resulting system of equations is of order  $N \times N$ .

Once the values of  $b_n$ ,  $n = 1, 2, \dots, N$ , are obtained, equation (24) allows us to calculate the displacement at any point of the region  $E$  and its boundary. Solution of equation (28) is equivalent to obtaining a minimum for the mean square error in expression (22).

### RESULTS

In order to gauge the method's accuracy, displacements at point of a semi-cylindrical canyon have been calculated for several incidence angles and normalized frequencies

$$\eta = \frac{ka}{\pi} = \frac{2a}{\lambda} \quad (29)$$

where  $\lambda$  is the incident wave length,  $a$  the radius of the canyon and thus  $\eta$  is the canyon width-to-wave-length ratio.

Values of real and imaginary parts of  $u$  at some points are presented in Table I for  $\eta = 2.0$  and  $\gamma = 30, 60, 90$  degrees using several values of  $N$  for the calculation. Comparison is provided with the exact values given by Trifunac's solution.<sup>3</sup> For the interior curve  $C$ , a semi-circumference with radius  $0.8a$  and 99 collocation points at the boundary were used.

Table I. Comparison of results to exact solution, semi-cylindrical canyon,  $\eta = 2.00$ 

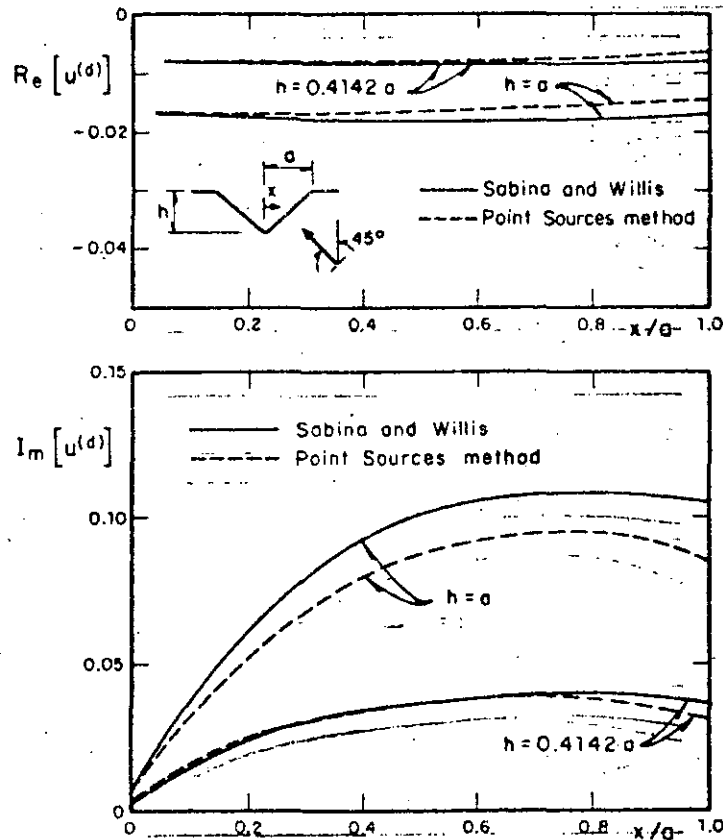
$x/a$	$[y = 30^\circ]$						Exact	
	$M = 10$		$M = 15$		$M = 20$			
-1.50	0.74091	-1.15704	0.70448	-1.13299	0.70317	-1.12942	0.70319	-1.12941
-1.00	-3.40383	-0.18822	-3.46605	-0.37223	-3.47828	-0.42692	-3.47834	-0.42714
-0.50	1.28720	0.48138	1.25202	0.49594	1.25098	0.49759	1.25097	0.49748
0.00	1.62731	-1.78459	1.59742	-1.76556	1.59831	-1.76382	1.59843	-1.76378
0.50	-1.79672	0.20781	-1.76972	0.20801	-1.76331	0.20677	-1.76347	0.20669
1.00	1.43898	0.38959	1.42650	0.63539	1.42391	0.72468	1.42407	0.72470
1.50	-0.12401	2.04079	-0.05495	2.06556	-0.05054	2.06386	-0.05053	2.06384

$x/a$	$[y = 60^\circ]$						Exact	
	$M = 10$		$M = 15$		$M = 20$			
-1.50	-1.83283	2.46628	-1.76901	2.55157	-1.76450	2.55561	-1.76450	2.55559
-1.00	2.92025	-3.02770	2.85687	-2.74221	2.80912	-2.63566	2.80893	-2.63559
-0.50	2.64131	-1.31221	2.72037	-1.24558	2.73097	-1.24294	2.73078	-1.24296
0.00	-2.40835	0.07178	-2.44644	0.14278	-2.45132	0.14889	-2.45120	0.14878
0.50	1.51314	-0.37793	1.51624	-0.37835	1.52035	-0.37156	1.52027	-0.37135
1.00	0.70125	-0.67186	0.47134	-0.86228	0.38808	-0.89220	0.38792	-0.89198
1.50	-0.94335	-0.85681	-0.99280	-0.74464	-0.99267	0.73442	-0.99266	-0.73446

$x/a$	$[y = 90^\circ]$						Exact	
	$M = 10$		$M = 15$		$M = 20$			
-1.50	-3.41897	-0.42424	-3.40347	-0.18771	-3.39576	-0.17178	-3.39574	-0.17174
-1.00	4.70441	0.08372	4.13223	0.19777	3.92585	0.27071	3.92598	0.27041
-0.50	-3.53599	-0.48741	-3.48763	-0.44017	-3.47836	-0.42708	-3.47834	-0.42725
0.00	2.60129	0.04269	2.66496	0.13720	2.65254	1.49088	2.65257	0.14950
0.50	-1.53581	0.61482	-1.43244	0.71927	-1.42397	0.72545	-1.42407	0.72483
1.00	-0.06127	0.69389	-0.01917	0.76622	-0.04852	0.84105	-0.04860	0.84038
1.50	0.95417	0.13408	0.99010	0.23138	0.99196	0.24013	0.99201	0.24020

Figure 4. Comparison for real and imaginary parts of  $u^{(d)}$  between numerical solution and solution obtained using matched asymptotic expansions<sup>11</sup> at part of the surface of the triangular canyon for  $\eta = 0.1/\pi$

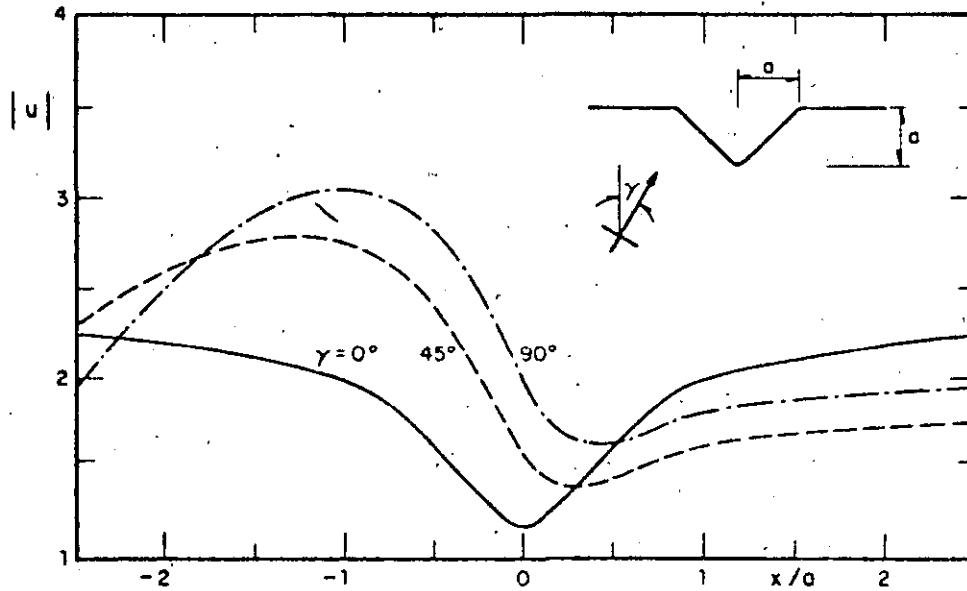


Figure 5. Displacement amplitudes at the surface of a triangular canyon with  $45^\circ$  slopes for different incidence angles  $\gamma$  and normalized frequency  $\eta = 0.25$

The method also has been applied to a semi-elliptical canyon;<sup>13</sup> agreement with the published exact solution<sup>4</sup> is excellent.

Real and imaginary parts of the diffracted field at a portion of the surface of a triangular canyon for two different depths, incidence angle  $\gamma = -45$  degrees and normalized frequency  $\eta = 0.1/\pi$  are shown in Figure 4. The solution is compared with the one obtained by means of matched asymptotic expansions.<sup>11</sup>

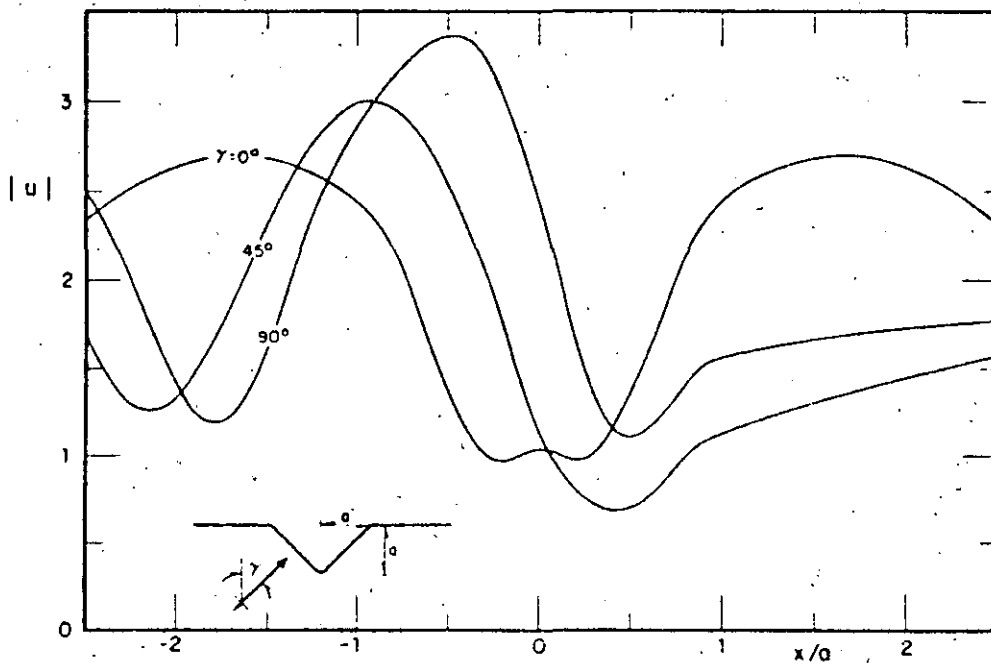


Figure 6. Displacement amplitudes at the surface of a triangular canyon with  $45^\circ$  slopes for different incidence angles  $\gamma$  and normalized frequency  $\eta = 0.5$

for two-dimensional problems (Sánchez-Sesma, 1978, 1981; Sánchez-Sesma and Rosenblueth, 1979; Sánchez-Sesma and Esquivel, 1979, 1980; Wong, 1979, 1982; England *et al.*, 1980; Dravinski, 1982a, b; Sánchez-Sesma *et al.*, 1982a, b) is extended here to three-dimensional cases. The method consists of constructing the scattered fields with linear combinations of members of a  $c$ -complete family of wave functions (Herrera and Sabina, 1978) which are solutions of Navier's equations. Coefficients of the linear forms thus constructed are obtained from a collocation, least-squares matching of boundary conditions. As pointed out by Wong (1982), the method can be considered as a generalized inverse one. In doing this, Wong suggested a procedure which improves the solution numerically.

The families of solutions can be formed in a very general way with sources having their singularities outside the region of interest and fulfilling radiation conditions if the region is infinite. A general framework for the method is given by a recent algebraic theory of boundary value problems (Herrera, 1979, 1980a, b).

It is convenient that the mentioned solutions satisfy boundary conditions on the free surface of the half-space leaving only the region of the irregularity for numerical treatment. However, in some cases this requirement introduces severe restrictions in numerical calculations because of the lengthy computations needed to obtain such solutions. It has been found in a recent, two-dimensional analysis of the scattering of  $P$ ,  $SV$  and Rayleigh waves (Sánchez-Sesma *et al.*, 1982a) that the use of solutions that actually do not satisfy free-boundary conditions gives results which agree very well with those of Wong (1979, 1982) for a semi-circular canyon. These solutions for the displacement fields were constructed using only Hankel and trigonometric functions. Of course, the numerical treatment included the free boundary. However, the computational effort, even with the addition of part of the half-space surface, was greatly reduced. A relatively small part of the free surface (three times the radius of the canyon at both sides of it) needed to be considered to obtain convergent results for the range of frequencies considered; i.e.,  $\omega \leq \pi\beta/2a$ , where  $a$  = radius and  $\beta$  = velocity of shear waves (Sánchez-Sesma *et al.*, 1982a).

In this work, the three-dimensional scattered displacement fields are constructed with linear combinations of solutions of Navier's equations, which are given in terms of spherical Hankel and Bessel functions, associated with Legendre and trigonometric functions (Takeuchi and Saito, 1972; Aki and Richards, 1980). Since each of these solutions does not satisfy in itself the free-boundary conditions, the numerical treatment is extended to part of the half-space surface, as has already been mentioned. These solutions have been widely used in seismology to deal, for example, with the free oscillations of the earth. Here, the origin of the spherical coordinate system is on the surface of the half-space.

In the present approach, axial symmetry of the scatterer is assumed in order to allow azimuthal decomposition. That is to say, the problem is split into "two-dimensional" problems. For normal incidence of  $P$  or  $SV$  waves, only one azimuthal number is required. For nearly vertical incidences or long wavelengths of the apparent incident surface field, only a few terms of the azimuthal decomposition are needed to give good results.

Some numerical examples are given for vertically incident  $P$  waves on different surface irregularities.

#### THE PROBLEM

Consider the elastic half-space and a three-dimensional surface irregularity represented in Figure 1 by regions  $E$  and  $R$ , respectively. Let  $\partial_1 E$  and  $\partial_1 R$  be the free

boundaries of the regions, and  $\partial_2 E = \partial_2 R$  be the common boundary between them. Under incidence of elastic waves, the irregularity generates diffracted fields that should be superimposed on the free-field solution, that is to say, on the fields in *absence* of irregularity.

Under the assumption of time dependence given by  $\exp(i\omega t)$ , where  $i = \sqrt{-1}$ ,  $\omega =$  circular frequency, and  $t =$  time, the displacement vector,  $\bar{u}$ , must satisfy the reduced Navier equation, which in vector form is given by

$$\mu \nabla^2 \bar{u} + (\lambda + \mu) \nabla \nabla \cdot \bar{u} + \rho \omega^2 \bar{u} = 0. \quad (1)$$

Here  $\lambda, \mu =$  Lamé constants, and  $\rho =$  mass density. These constants should be particularized for each medium.

We can write the total fields as

$$\bar{u}^E = \bar{u}^{(0)} + \bar{u}^{(s)} \quad (2)$$

for the region  $E$ , and

$$\bar{u}^R = \bar{u}^{(r)} \quad (3)$$

for region  $R$ . In equation (2)  $\bar{u}^{(0)}$  is the displacement vector of the free-field solution. In equations (2) and (3),  $\bar{u}^{(s)}$  and  $\bar{u}^{(r)}$  represent the scattered and refracted fields in the half-space and the irregularity, respectively.

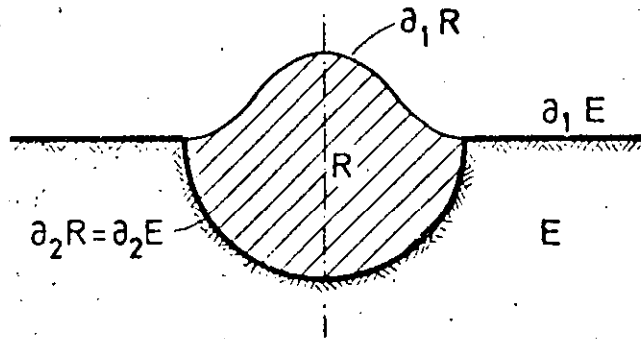


FIG. 1. Definition of regions  $E$  and  $R$  and their boundaries.

The boundary conditions that must be satisfied by the total fields are given by

$$\bar{\sigma}(\bar{u}^E) = 0 \quad \text{in } \partial_1 E, \quad (4)$$

$$\bar{\sigma}(\bar{u}^R) = 0 \quad \text{in } \partial_1 R, \quad (5)$$

$$\bar{\sigma}(\bar{u}^E) = \bar{\sigma}(\bar{u}^R) \quad \text{in } \partial_2 E, \quad \text{and} \quad (6)$$

$$\bar{u}^E = \bar{u}^R \quad \text{in } \partial_2 E. \quad (7)$$

In these equations,  $\bar{\sigma}$  stands for the traction vector associated with a particular displacement field and with the normal vector to the boundary. Assume, for definiteness, that the normal vector on the common boundary is directed toward  $R$ . The first two of equations (4) to (7) are the boundary conditions of free surface,

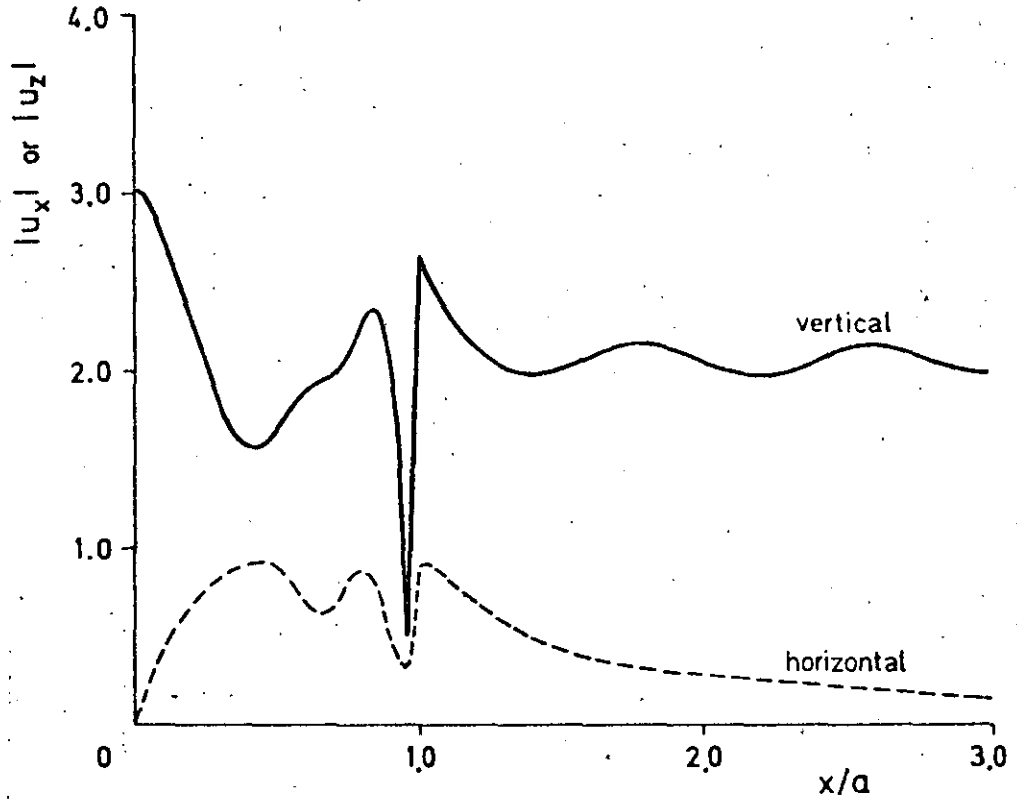
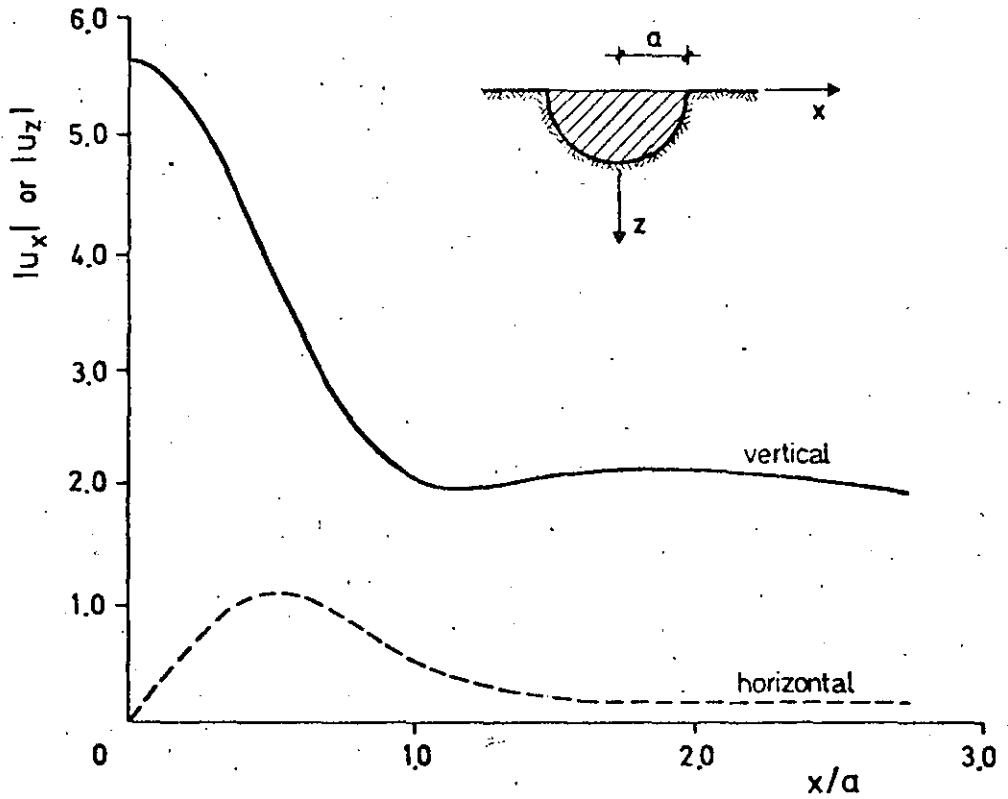


FIG. 7. Surface amplitudes of vertical and horizontal displacements. Semi-spherical cavity. Normalized frequency  $\eta_0 = 1.50$ . Poisson coefficient  $\nu = 0.25$ .



A ridge was also studied with a shape given by the negative of equation (31). Figure 10 shows the displacement amplitudes for vertical incidence of  $P$  waves with a normalized frequency  $\eta_0 = 0.5$ . Poisson's coefficient is  $\nu = 0.3$ . Here, 90 collocation points were used distributed as follows: 30 in the fictitious interface; 20 in the surface of the ridge itself; and 40 in part of the free surface in a length of  $3a$ , where  $2a =$  maximum horizontal dimension of the ridge. The orders of expansions were 15 for the internal and external regions. Residual tractions do not exceed 4 per cent of the reference value. An amplification of vertical motion of 60 per cent at the top of the ridge and a reduction of about 25 per cent near the base can be observed. In this example, horizontal motion has small relative amplitudes. The results for the

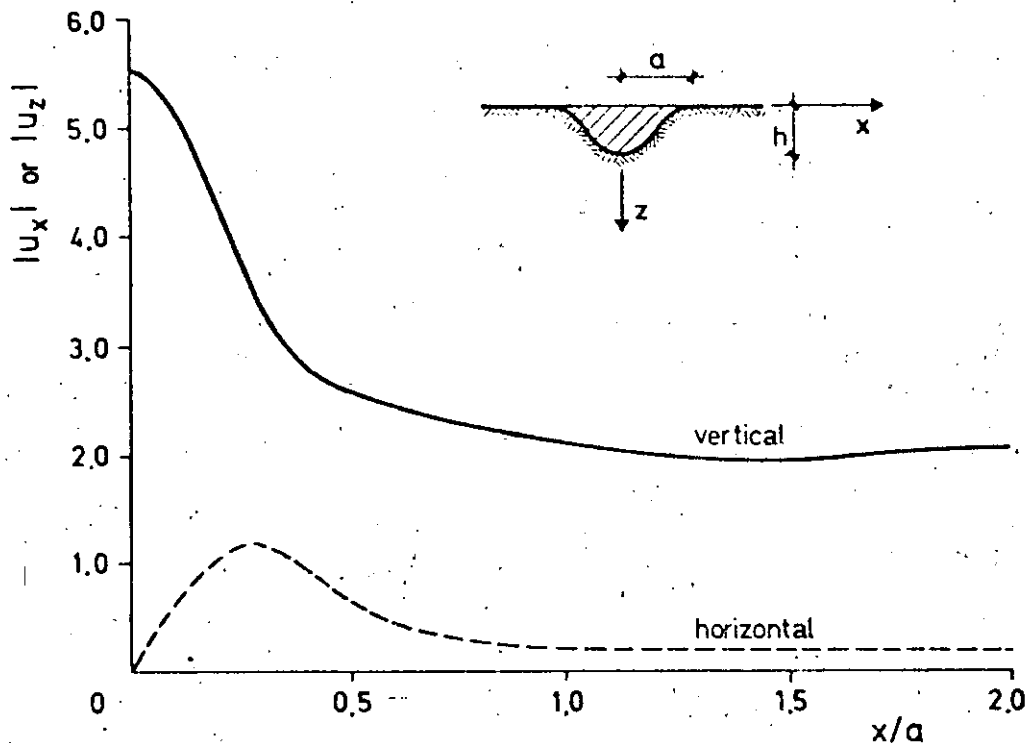


FIG. 9. Surface amplitudes of vertical and horizontal displacements. Axisymmetric alluvial deposit with  $h/a = 0.5$ . Normalized frequency  $\eta_0 = 1.0$ . Poisson coefficients  $\nu_R = 0.30$  and  $\nu_E = 0.25$ . Material properties  $\mu_R/\mu_E = 0.3$  and  $\rho_R/\rho_E = 0.6$ .

ridge studied are similar to those obtained for incident  $SH$  waves on a two-dimensional ridge (Sills, 1978; Sánchez-Sesma *et al.*, 1982b).

The results presented in this section were obtained from a "trial and error" procedure to determine the order of expansions and the number and location of collocation points. This procedure was based upon the error analysis on boundary conditions and the stability of the calculated surface field. Typically, when the residual tractions are less than, say, 5 per cent of the reference value, the calculated displacement fields of various analyses do not present significant changes. Additional research is needed to generate rules for practical assessment of the calculation parameters.

FIG. 8. Surface amplitudes of vertical and horizontal displacements. Semi-spherical alluvial deposit. Normalized frequency  $\eta_0 = 0.5$ . Poisson coefficients  $\nu_R = 0.30$  and  $\nu_E = 0.25$ . Material properties  $\mu_R/\mu_E = 0.3$  and  $\rho_R/\rho_E = 0.6$ .

Sean las soluciones de la ec 1 de las formas

$$\bar{u}^E = \bar{u}^{(0)} + \sum_{j=1}^3 \sum_{n=0}^N \sum_{m=0}^n A_{jnm}^N \bar{w}_{jnm}^E \quad (2)$$

$$\bar{u}^R = \sum_{j=1}^3 \sum_{n=0}^N \sum_{m=0}^n B_{jnm}^N \bar{w}_{jnm}^R \quad (3)$$

para las regiones E y R, respectivamente. En la ec 2,  $\bar{u}^{(0)}$  = vector de desplazamientos de campo libre y  $\bar{w}_{jnm}^E$  = elemento del conjunto completo de soluciones de la ec 1 en E que satisface la condición de irradiación al infinito. En la ec 3,  $\bar{w}_{jnm}^R$  = elemento del conjunto completo de soluciones de la ec 1 en R.  $A_{jnm}^N$  y  $B_{jnm}^N$  son coeficientes indeterminados y N es el orden de las aproximaciones.

A partir de las ecs 2 y 3 y las condiciones de frontera se obtienen ecuaciones para cada punto de la frontera (3 en  $\partial_1 E$  o  $\partial_1 R$  o 6 en  $\partial_2 E = \partial_2 R$ ). Imponiendo dichas condiciones en un número suficiente de puntos de colocación y buscando que el error cuadrático a lo largo de la frontera sea mínimo se obtienen los coeficientes de las ecs 2 y 3. Este criterio de colocación y mínimos cuadrados ha sido probado en problemas bidimensionales (20, 22, 23).

CAMPO LIBRE Y CAMPOS DIFRACTADOS

Puede demostrarse (19) que los campos libres y difractados admiten representación en series de Fourier con respecto a la coordenada azimutal  $\phi$ , que aparece en la Fig 2 donde se muestra el sistema de coordenadas esféricas. En el caso del campo libre la representación se obtiene a partir del desarrollo del factor de propagación exponencial en una serie de funciones de Bessel y cosenos de múltiplos de  $\phi$ . Por otra parte, los campos difractados son de tres tipos: esferoidales de ondas P y S y toroidales de ondas S y son, en general, vectores de la forma

$$f_n(r) \bar{F}_n^m(\theta, \phi) \quad (4)$$

donde  $f_n(r)$  = función escalar que se expresa en sus diferentes formas mediante funciones esféricas de Bessel o de Hankel y  $\bar{F}_n^m$  = función vectorial que se expresa con funciones trigonométricas de  $\theta$  y la función

$$Y_n^m(\theta, \phi) = P_n^m(\cos \theta) e^{im\phi} \quad (5)$$

y sus primeras derivadas. En la ec 5  $P_n^m(.)$  = función de Legendre con  $m = 0, \pm 1, \pm 2, \dots, \pm n$ . Puede verse que también para los campos difractados se tienen expresiones en donde aparecen separadamente senos y cosenos de  $m\phi$ , donde m = número azimu

tal. Si el difractor es axisimétrico se encuentra que la ortogonalidad de las funciones trigonométricas del ángulo azimutal  $\phi$  permite resolver el problema como *bidimensional*, para cada número azimutal. Para incidencia vertical de ondas P o S basta tomar  $m = 0$  ó  $1$ , respectivamente.

### RESULTADOS NUMERICOS

Se presentan resultados numéricos para el caso de incidencia normal de ondas SV y P a dos tipos de irregularidades topográficas: valles aluviales y promontorios. Las ondas incidentes, así como las difractadas, son función de las frecuencias normalizadas

$$\eta_k = \frac{ka}{\pi} = \frac{2a}{\Lambda_k} \quad \text{o} \quad \eta_q = \frac{qa}{\pi} = \frac{2a}{\Lambda_q} \quad (6)$$

donde  $\Lambda_k, \Lambda_q$  = longitud de las ondas incidentes SV y P, respectivamente,  $a$  = semiancho de la irregularidad,  $k, q$  = número de onda de cortante y compresión, respectivamente y  $\eta_k, \eta_q$  = frecuencia normalizada de cortante y compresión, respectivamente. Todos los resultados que se presentan corresponden a ondas incidentes con frecuencia normalizada  $\eta_k$  o  $\eta_q$  igual a 1.0.

Para determinar el orden de los desarrollos así como el número y la posición de los puntos de colocación se emplea un procedimiento de *prueba y error*. Dicho procedimiento se basa en el análisis del error en las condiciones de frontera y de la estabilidad del campo de superficie libre. Para los cálculos, el orden de los desarrollos fue de 10 y el número de puntos de colocación de 30 distribuidos uniformemente en  $\partial_2 R, \partial_1 R$  y una porción de  $\partial_1 E$  con longitud de  $2a$ , con lo cual se obtuvieron tracciones residuales que no excedieron el 6% del máximo esfuerzo en la solución de campo libre.

En la Fig 3 se presentan resultados para el caso de incidencia de ondas P a un promontorio definido por

$$z = h [1 - 3\xi^2 + 2\xi^3], \quad 0 \leq \xi \leq 1 \quad (7)$$

donde  $h$  = máxima altura o profundidad de la irregularidad y  $\xi = (x^2 + y^2)^{1/2}/a$ . Las amplitudes de los desplazamientos corresponden a una relación de aspecto,  $h/a$ , igual a 1.0 y un módulo de Poisson,  $\nu_E$ , igual a 0.25. Para el mismo ejemplo, pero para incidencia de ondas SV se obtuvieron los resultados que se muestran en la Fig 4. En ambos casos se presentan amplificaciones importantes con órdenes máximos de 2 para ondas P y 2.5 para SV.

En las Fig 5 y Fig 6 se presentan resultados para un valle aluvial, definido por la ec 7, cuando inciden ondas P y SV, respectivamente. En ambos casos los parámetros son  $h/a = 0.5$ ,  $\nu_R/\nu_E = 0.25$ ,  $\rho_R/\rho_E = 0.75$ ,  $\nu_R = 0.30$  y  $\nu_E = 0.25$ . En este ti

po de irregularidad también se presentan amplificaciones importantes, con órdenes máximos de 2.0 para ondas P y 3.0 para SV.

Para la frecuencia adimensional considerada, en el promontorio se encontraron importantes amplificaciones y reducciones de las amplitudes de los desplazamientos, mientras que en el valle solo se encontraron amplificaciones.

### CONCLUSIONES

Se ha aplicado un método de frontera para resolver el problema de difracción de ondas elásticas por irregularidades topográficas tridimensionales. Los resultados obtenidos muestran la generación de amplificaciones importantes en la superficie libre de las irregularidades, por lo que la influencia de estas en el movimiento sísmico puede ser significativa en diseño.

En este trabajo se estudiaron irregularidades axisimétricas e incidencia vertical. Es importante estudiar los casos de incidencia oblicua de ondas de cuerpo así como de ondas superficiales. Es de esperarse que los efectos de cambios del ángulo de incidencia sean significativos.

En análisis posteriores será importante estudiar la variación de los resultados para un rango de frecuencias suficientemente amplio.

### REFERENCIAS

1. Aki, K., "Strong motion prediction using mathematical modeling techniques", *Bull. Seism. Soc. Am.*, 72, 1982, 529-541.
2. Boore, D.M., "A note on the effect of simple topography on seismic SH waves", *Bull. Seism. Soc. Am.*, 62, 1972, 275-284.
3. Boore, D.M., "The effect of simple topography on seismic waves. Implications for the accelerations recorded at Pacoima Dam, San Fernando Valley, California", *Bull. Seism. Soc. Am.*, 63, 1973, 1603-1609.
4. Bouchon, M., "Effect of topography on surface motion", *Bull. Seism. Soc. Am.*, 63, 1973, 615-632.
5. Davis, L.L. y West, L.R., "Observed effects of topography on ground motion", *Bull. Seism. Soc. Am.*, 63, 1973, 283-298.
6. Dravinski, M., "Influence of interface depth upon strong ground motion", *Bull. Seism. Soc. Am.*, 72, 1982, 597-614.
7. Esquivel, J.A. y Sánchez-Sesma, F.J., "Effects of canyon topography on dynamic soil-bridge interaction for incident plane SH waves", *Proc. World Conf. Earthquake Eng.*, 7th, Istanbul, 2, 1980, 153-160.

8. Esteva, L., "Seismicity", *Seismic risk and engineering decisions*, C. Lomnitz y E. Rosenblueth (eds), Elsevier, Amsterdam, 1976.
9. Griffiths, D.W. y Bollinger, G.A., "The effect of the Appalachian Mountain topography on seismic waves", *Bull. Seism. Soc. Am.*, 69, 1979, 1081-1105.
10. Herrera, I. y Sabina, F.J., "Connectivity as an alternative to boundary integral equations. Construction of bases", *Proc. Nat'l. Acad. Sci., U.S.A.*, 75, 1978, 2059-2063.
11. Hudson, J.A. y Boore, D.M., "Comments on scattered surface waves from a surface obstacle", *Geophys. J. R. Astr. Soc.*, 60, 1980, 123-127.
12. Jackson, P.S., "The focusing of earthquakes", *Bull. Seism. Soc. Am.*, 61, 1971, 685-695.
13. Kupradze, V.D., "Potential methods in the theory of elasticity", *Israel Program for Scientific Translations*, Jerusalem, 1965.
14. Lee, V.W., "A note on the scattering of elastic plane waves by a hemispherical canyon", *Soil Dynamics and Earthquake Engineering*, 1, 1982, 122-129.
15. Poceski, A., "The ground effects of the Skopje July 26, 1963 earthquake", *Bull. Seism. Soc. Am.*, 59, 1969, 1-29.
16. Ruiz, S.E., "Influencia de las condiciones locales en las características de los sismos", *Instituto de Ingeniería, UNAM*, 387, 1977, México.
17. Ruiz, S.E. y Esteva, L., "Probabilistic response of multi-support structures on non uniform soil conditions", *Int. Conf. on Recent Advances in Geotechnical Earthquake Engineering and Soil Dynamics*, St. Louis, Missouri, 1, 1981, 351-354.
18. Sánchez-Sesma, F.J., "A boundary method applied to elastic scattering problems", *Arch. Mech.*, 33, 1981, 167-179.
19. Sánchez-Sesma, F.J., "Diffraction of elastic waves by three-dimensional surface irregularities", *Bull. Seism. Soc. Am.*, 73, 1983, en prensa.
20. Sánchez-Sesma, F.J. y Esquivel, J.A., "Ground motion on alluvial valleys under incident plane SH waves", *Bull. Seism. Soc. Am.*, 69, 1979, 1107-1120.
21. Sánchez-Sesma, F.J., Herrera, I. y Avilés, J., "A boundary method for elastic wave diffraction. Application to scattering of SH waves by surface irregularities", *Bull. Seism.*

Soc. Am., 72, 1982, 473-490.

22. Sánchez-Sesma, F.J., Herrera, I. y Bravo, M. A., "Difracción de ondas P, SV y de Rayleigh en un semiespacio elástico", Instituto de Ingeniería, UNAM, 1982, México.

23. Sánchez-Sesma, F.J. y Rosenblueth, E., "Ground motion at canyons of arbitrary shape under incident SH waves", *Int. J. Earthquake Eng. Struct. Dyn.*, 7, 1979, 441-450.

24. Singh, S.K. y Sabina, F.J., "Ground motion amplification by topographic depressions for incident P waves under acoustic approximation", *Bull. Seism. Soc. Am.*, 67, 1977, 345-352.

25. Sommerfeld, A., *Partial differential equations in physics*, Academic Press, New York, 1949.

26. Takeuchi, H. y Saito, M., "Seismic surface waves", *Methods in computational physics*, Academic Press, New York, 1972.

27. Trifunac, M.D., "Surface motion of a semi-cylindrical alluvial valley for incident plane SH waves", *Bull. Seism. Soc. Am.*, 61, 1971, 1755-1770.

28. Trifunac, M. D. y Hudson, D.E., "Analysis of the Pacoima Dam accelerogram-San Fernando, California, earthquake of 1971", *Bull. Seism. Soc. Am.*, 61, 1971, 1393-1411.

29. Wong, H. L., "Effect of surface topography on the diffraction of P, SV and Rayleigh waves", *Bull. Seism. Soc. Am.*, 72, 1982, 1167-1183.

30. Wong, H.L. y Jennings, P.C., "Effect of canyon topography on strong ground motion", *Bull. Seism. Soc. Am.*, 65, 1975, 1239-1257.

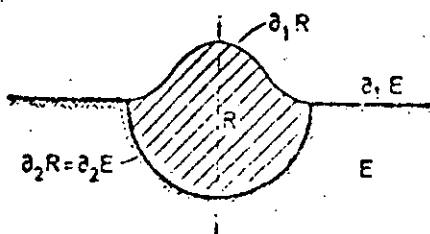


Fig 1. Definición de las regiones E y R y sus fronteras

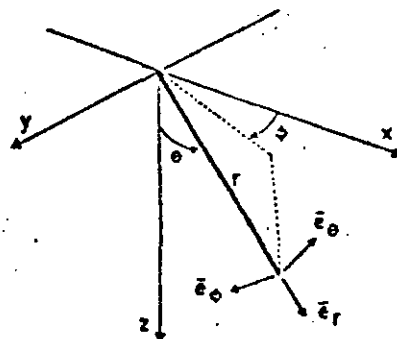


Fig 2. Sistema de coordenadas cartesianas y esféricas. Vectores unitarios en el sistema esférico



**DIVISION DE EDUCACION CONTINUA  
FACULTAD DE INGENIERIA U.N.A.M.**

ANALISIS DE RIESGO SISMICO

SEISMICITY

DR. LUIS ESTEVA MARABOTO

JULIO, 1985

## Chapter 6

### SEISMICITY

LUIS ESTEVA

*Instituto de Ingeniería, Universidad Nacional Autónoma de México, Mexico*

#### 6.1 ON SEISMICITY MODELS

Rational formulation of engineering decisions in seismic areas requires quantitative descriptions of seismicity. These descriptions should conform with their intended applications: in some instances, simultaneous intensities during each earthquake have to be predicted at several locations, while in others it suffices to make independent evaluations of the probable effects of earthquakes at each of those locations.

The second model is adequate for the selection of design parameters of individual components of a regional system (the structures in a region or country) when no significant interaction exists between response or damage of several such individual components, or between any of them and the system as a whole. In other words, it applies when the damage — or negative utility — inflicted upon the system by an earthquake can be taken simply as the addition of the losses in the individual components.

The linearity between monetary values and utilities implied in the second model is not always applicable. Such is the case, for instance, when a significant portion of the national wealth or of the production system is concentrated in a relatively narrow area, or when failure of life-line components may disrupt emergency and relief actions just after an earthquake. Evaluation of risk for the whole regional system has then to be based on seismicity models of the first type, that is, models that predict simultaneous intensities at several locations during each event; for the purpose of decision making, nonlinearity between monetary values and utilities can be accounted for by means of adequate scale transformations. These models are also of interest to insurance companies, when the probability distribution of the maximum loss in a given region during a given time interval is to be estimated.

Whatever the category to which a seismic risk problem belongs, it requires the prediction of probability distributions of certain ground motion characteristics (such as peak ground acceleration or velocity, spectral density, response or Fourier spectra, duration) at a given site during a single shock or of maximum values of some of those characteristics in earthquakes occurring during given time intervals. When the reference interval tends to infinity, the probability distribution of the maximum value of a given characteristic ap-

proaches that of its maximum *possible* value. Because different systems or subsystems are sensitive to different ground motion characteristics, the term *intensity characteristic* will be used throughout this chapter to mean a particular parameter or set of parameters of an earthquake motion, in terms of which the response is to be predicted. Thus, when dealing with the failure probability of a structure, intensity can be alternatively measured — with different degrees of correlation with structural response — by the ordinate of the response spectrum for the corresponding period and damping, the peak ground acceleration, or the peak ground velocity.

In general, local instrumental information does not suffice for estimating the probability distributions of maximum intensity characteristics, and use has to be made of data on subjective measures of intensities of past earthquakes, of models of *local seismicity*, and of expressions relating characteristics with magnitude and site-to-source distance. Models of local seismicity consist, at least, of expressions relating magnitudes of earthquakes generated in given volumes of the earth's crust with their return periods. More often than not, a more detailed description of local seismicity is required, including estimates of the maximum magnitude that can be generated in these volumes, as well as probabilistic (stochastic process) models of the possible histories of seismic events (defined by magnitudes and coordinates).

This chapter deals with the various steps to be followed in the evaluation of seismic risk at sites where information other than direct instrumental records of intensities has to be used: identifying potential sources of activity near the site, formulating mathematical models of local seismicity for each source, obtaining the contribution of each source to seismic risk at the site and adding up contributions of the various sources and combining information obtained from local seismicity of sources near the site with data on instrumental or subjective intensities observed at the site.

The foregoing steps consider use of information stemming from sources of different nature. Quantitative values derived therefrom are ordinarily tied to wide uncertainty margins. Hence they demand probabilistic evaluation, even though they cannot always be interpreted in terms of relative frequencies of outcomes of given experiments. Thus, geologists talk of the maximum magnitude that can be generated in a given area, assessed by looking at the dimensions of the geological accidents and by extrapolating the observations of other regions which available evidence allows to brand as similar to the one of interest; the estimates produced are obviously uncertain, and the degree of uncertainty should be expressed together with the most probable value. Following nearly parallel lines, some geophysicists estimate the energy that can be liberated by a single shock in a given area by making quantitative assumptions about source dimensions, dislocation amplitude and stress drop, consistent with tectonic models of the region and, again, with comparisons with areas of similar tectonic characteristics.

Uncertainties attached to estimates of the type just described are in gen-

eral extremely large: some studies relating fault rupture area, stress drop, and magnitude (Brune, 1968) show that, considering not unusually high stress drops, it does not take very large source dimensions to get magnitudes 8.0 and greater, and those studies are practically restricted to the simplest types of fault displacement. It is not clear, therefore, that realistic bounds can always be assigned to potential magnitudes in given areas or that, when this is feasible, those bounds are sufficiently low, so that designing structures to withstand the corresponding intensities is economically sound, particularly when occurrence of those intensities is not very likely in the near future. Because uncertainties in maximum feasible magnitudes and in other parameters defining magnitude-recurrence laws can be as significant as their mean values when trying to make rational seismic design decisions, those uncertainties have to be explicitly recognized and accounted for by means of adequate probabilistic criteria. A corollary is that geophysically based estimates of seismicity parameters should be accompanied with corresponding uncertainty measures.

Seismic risk estimates are often based only on statistical information (observed magnitudes and hypocentral coordinates). When this is done, a wealth of relevant geophysical information is neglected, while the probabilistic prediction of the future is made to rely on a sample that is often small and of little value, particularly if the sampling period is short as compared with the desirable return period of the events capable of severely damaging a given system.

The criterion advocated here intends to unify the foregoing approaches and rationally to assimilate the corresponding pieces of information. Its philosophy consists in using the geological, geophysical, and all other available non-statistical evidence for producing a set of alternate assumptions concerning a mathematical (stochastic process) model of seismicity in a given source area. An initial probability distribution is assigned to the set of hypotheses, and the statistical information is then used to improve that probability assignment. The criterion is based on application of *Bayes theorem*, also called the *theorem of the probabilities of hypotheses*. Since estimates of risk depend largely on conceptual models of the geophysical processes involved, and these are known with different degrees of uncertainty in different zones of the earth's crust, those estimates will be derived from stochastic process models with uncertain forms or parameters. The degree to which these uncertainties can be reduced depends on the limitations of the state of the art of geophysical sciences and on the effort that can be put into compilation and interpretation of geophysical and statistical information. This is an economical problem that should be handled, formally or informally, by the criteria of decision making under uncertainty.

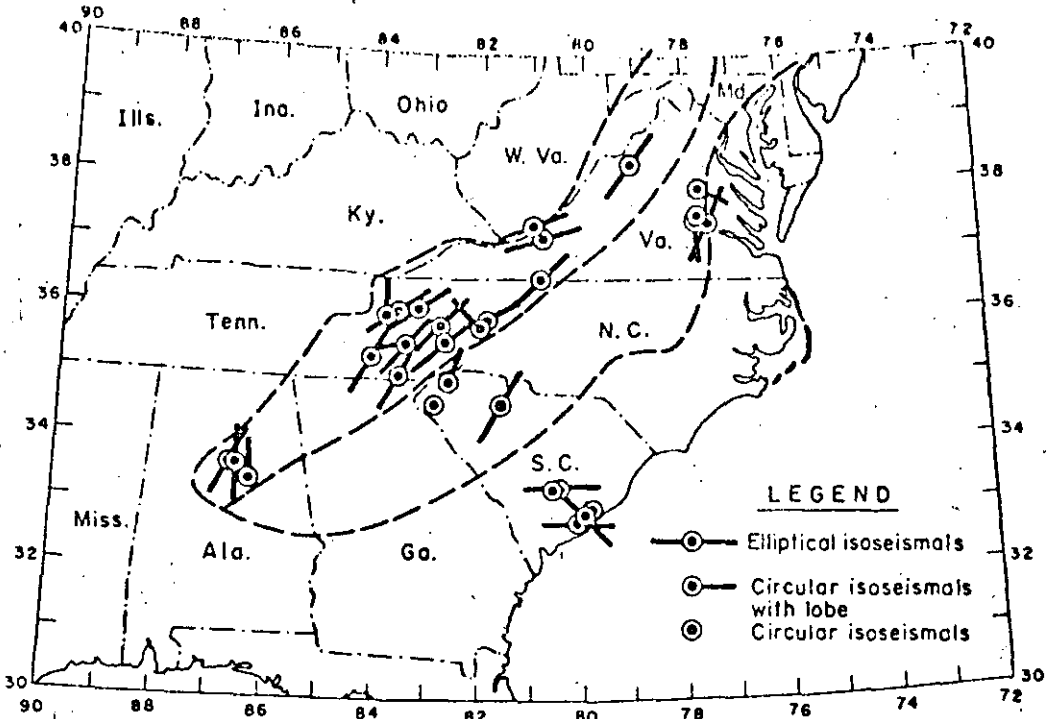


Fig. 6.2. Elongation of isoseismals in the southeastern United States. (After Bollinger, 1973.)

lowing expression relating magnitude  $M$ , hypocentral distance  $R$  (in kilometers) and intensity  $I$  (Esteva, 1968):

$$I = 1.45 M - 5.7 \log_{10} R + 7.9 \quad (6.1)$$

The prediction error, defined as the difference between observed and computed intensity, is roughly normally distributed, with a standard deviation of 2.04, which means that there is a probability of 60% that an observed intensity is more than one degree greater or smaller than its predicted value.

#### 6.2.1.2 Peak ground accelerations and velocities

A few of the available expressions will be described. Their comparison will show how cautiously a designer intending to use them should proceed.

Housner studied the attenuation of peak ground accelerations in several regions of the United States and presented his results graphically (1969) in terms of fault length (in turn a function of magnitude), shapes of isoseismals and areas experiencing intensities greater than given values (Fig. 6.4 and 6.5).

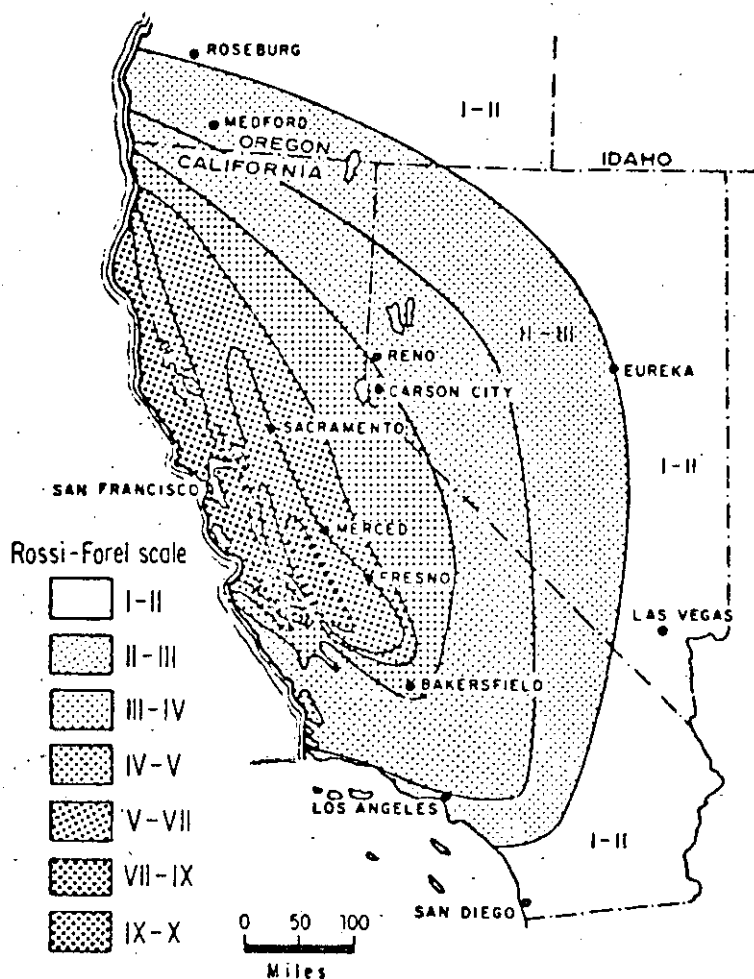


Fig. 6.3. Isoseismals in California. (After Bolt, 1970.)

He showed that intensities attenuate faster with distance on the west coast than in the rest of the country. This comparison is in agreement with Milne and Davenport (1969), who performed a similar analysis for Canada. From observations of strong earthquakes in California and in British Columbia, they developed the following expression for  $a$ , the peak ground acceleration, as a fraction of gravity:

$$a/g = 0.0069 e^{1.6M} / (1.1 e^{1.1M} + R^2) \quad (6.2)$$

Here,  $R$  is epicentral distance in kilometers. The acceleration varies roughly as  $e^{1.64M} R^{-2}$  for large  $R$ , and as  $e^{0.54M}$  where  $R$  approaches zero. This reflects to some extent the fact that energy is released not at a single point but from a finite volume. A later study by Davenport (1972) led him

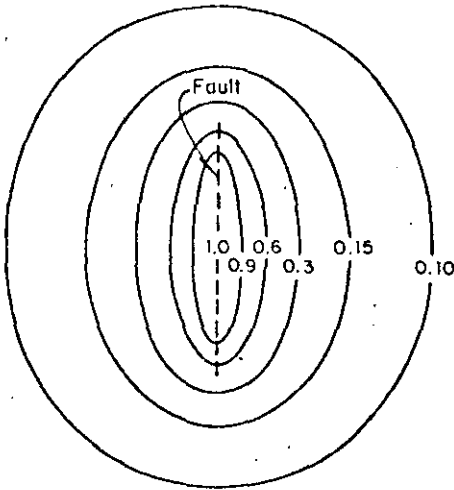


Fig. 6.4. Idealized contour lines of intensity of ground shaking. (After Housner, 1969.)

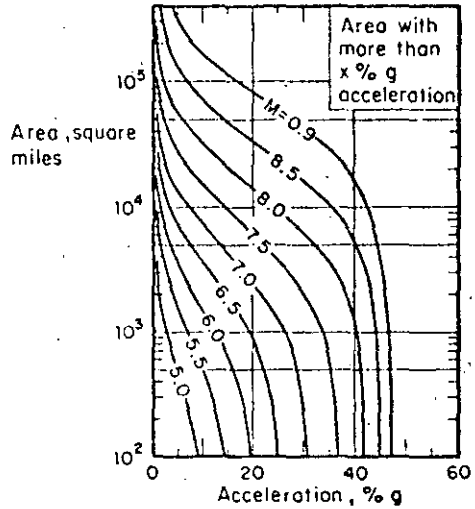


Fig. 6.5. Area in square miles experiencing shaking of  $x\%g$  or greater for shocks of different magnitudes. (After Housner, 1969.)

to propose the expression:

$$a/g = 0.279 e^{0.8M}/R^{1.64} \tag{6.3}$$

The statistical error of this equation was studied by fitting a lognormal probability distribution to the ratios of observed to computed accelerations. A standard deviation of 0.74 was found in the natural logarithms of those ratios.

Esteva and Villaverde (1973), on the basis of accelerations reported by Hudson (1971, 1972a,b), derived expressions for peak ground accelerations and velocities, as follows:

$$a/g = 5.7 e^{0.8M}/(R + 40)^2 \tag{6.4}$$

$$v = 32 e^M/(R + 25)^{1.7} \tag{6.5}$$

Here  $v$  is peak ground velocity in cm/sec and the other symbols mean the same as above. The standard deviation of the natural logarithm of the ratio of observed to predicted intensity is 0.64 for accelerations and 0.74 for velocities. If judged by this parameter, eqs. 6.3 and 6.4 seem equally reliable. However, as shown by Fig. 6.6, their mean values differ significantly in some ranges.

With the exception of eq. 6.2, all the foregoing attenuation expressions are products of a function of  $R$  and a function of  $M$ . This form, which is acceptable when the dimensions of the energy-liberating source are small com-

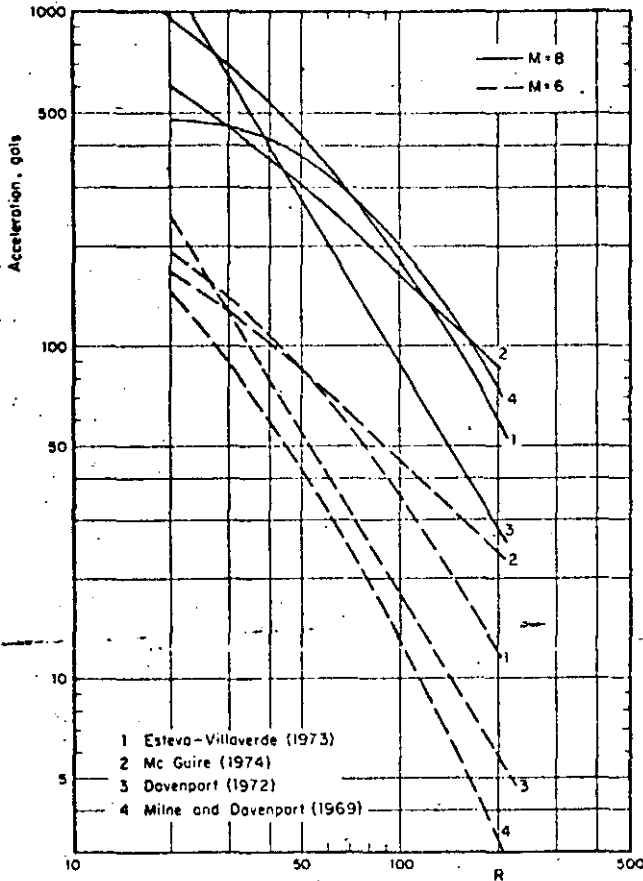


Fig. 6.6. Comparison of several attenuation expressions.

pared with  $R$ , is inadequate when dealing with earthquake sources whose dimensions are of the order of moderate hypocentral distances, and often greater than them. Although equation errors (probability distributions of the ratio of observed to predicted intensities) have been evaluated by Davenport (1972) and Esteva and Villaverde (1973), their dependence on  $M$  and  $R$  has not been analyzed. Because seismic risk estimates are very sensitive to the attenuation expressions in the range of large magnitudes and short distances, more detailed studies should be undertaken, aiming at improving those expressions in the mentioned range, and at evaluating the influence of  $M$  and  $R$  on equation error. Information on strong-motion records will probably be scanty for those studies, and hence they will have to be largely based on analytical or physical models of the generation and propagation of seismic waves. Although significant progress has been lately attained in this direction (Trifunac, 1973) the results from such models have hardly influenced the

practice of seismic risk estimation because they have remained either unknown to or imperfectly appreciated by engineers in charge of the corresponding decisions.

### 6.2.1.3 Response spectra

Peak ground acceleration and displacement are fairly good indicators of the response of structures possessing respectively very high and very small natural frequencies. Peak velocity is correlated with the response of intermediate-period systems, but the correlation is less precise than that tying the former parameters; hence, it is natural to formulate seismic risk evaluation and engineering design criteria in terms of spectral ordinates.

Response spectrum prediction for given magnitude and hypocentral or site-to-fault distance usually entails a two-step process, according to which peak ground acceleration, velocity and displacement are initially estimated and then used as reference values for prediction of the ordinates of the response spectrum. Let the second step in the process be represented by the operation  $y_s = \alpha y_R$ , where  $y_s$  is an ordinate of the response spectrum for a given natural period and damping ratio, and  $y_R$  is a parameter (such as peak ground acceleration or velocity) that can be directly obtained from the time-history record of a given shock regardless of the dynamic properties of the systems whose response is to be predicted. For given  $M$  and  $R$ ,  $y_R$  is random and so is  $y_s/y_R = \alpha$ ; the mean and standard deviation of  $y_s$  depend on those of  $y_R$  and  $\alpha$  and on the coefficient of correlation of the latter variables. As shown above,  $y_R$  can only be predicted within wide uncertainty limits, often wider than those tied to  $y_s$  (Estevá and Villaverde, 1973). The coefficient of variation of  $y_s$  given  $M$  and  $R$  can be smaller than that of  $y_R$  only if  $\alpha$  and  $y_R$  are negatively correlated, which is often the case: the greater the deviation of an observed value of  $y_R$  with respect to its expectation for given  $M$  and  $R$ , the lower is likely to be  $\alpha$ . In other words, it seems that in the intermediate range of natural periods the expected values of spectral ordinates for given damping ratios can be predicted directly in terms of magnitude and focal distance with narrower (or at most equal) margins of uncertainty than those tied to predicted peak ground velocities. For the ranges of very short or very long natural periods, peak amplitudes of ground motion and spectral ordinates approach each other and their standard errors are therefore nearly equal.

McGuire (1974) has derived attenuation expressions for the conditional values (given  $M$  and  $R$ ) of the mean and of various percentiles of the probability distributions of the ordinates of the response spectra for given natural periods and damping ratios. Those expressions have the same form as eqs. 6.4 and 6.5, but their parameters show that the rates of attenuation of spectral ordinates differ significantly from those of peak ground accelerations or velocities. For instance, McGuire finds that peak ground velocity attenuates in proportion to  $(R + 25)^{-1.20}$ , while the mean of the pseudovelocity for a

TABLE 6.1

McGuire's attenuation expressions  $y = b_1 10^{b_2 M} (R + 25)^{-b_3}$ 

$y$	$b_1$	$b_2$	$b_3$	$V(y) = \text{coeff. of var. of } y$
$a$ gals	472.3	0.278	1.301	0.548
$v$ cm/sec	5.64	0.401	1.202	0.696
$d$ cm	0.393	0.434	0.885	0.883
Undamped spectral pseudovelocities				
$T = 0.1$ sec	11.0	0.278	1.346	0.941
0.5	3.05	0.391	1.001	0.636
1.0	0.631	0.378	0.549	0.768
2.0	0.0768	0.469	0.419	0.989
5.0	0.0834	0.564	0.897	1.344
5% damped spectral pseudovelocities				
$T = 0.1$ sec	10.09	0.233	1.341	0.651
0.5	5.74	0.356	1.197	0.591
1.0	0.432	0.399	0.704	0.703
2.0	0.122	0.466	0.675	0.941
5.0	0.0706	0.557	0.938	1.193

natural period of 1 sec and a damping ratio of 2% attenuates in proportion to  $(R + 25)^{-0.59}$ . These results stem from the way that frequency content changes with  $R$  and lead to the conclusion that the ratio of spectral velocity should be taken as a function of  $M$  and  $R$ .

Table 6.1 summarizes McGuire's attenuation expressions and their coefficients of variation for ordinates of the pseudovelocity spectra and for peak ground acceleration, velocity and displacement. Similar expressions were derived by Esteva and Villaverde (1973), but they are intended to predict only the maxima of the expected acceleration and velocity spectra, regardless of the periods associated with those maxima. No analysis has been performed of the relative validity of McGuire's and Esteva and Villaverde's expressions for various ranges of  $M$  and  $R$ .

### 6.3 LOCAL SEISMICITY

The term *local seismicity* will be used here to designate the degree of seismic activity in a given volume of the earth's crust; it can be quantitatively described according to various criteria, each providing a different amount of information. Most usual criteria are based on upper bounds to the magnitudes of earthquakes that can originate in a given seismic source, on the

amount of energy liberated by shocks per unit volume and per unit time or on more detailed statistical descriptions of the process.

### 6.3.1 Magnitude-recurrence expressions

Gutenberg and Richter (1954) obtained expressions relating earthquake magnitudes with their rates of occurrence for several zones of the earth. Their results can be put in the form:

$$\lambda = \alpha e^{-\beta M} \quad (6.6)$$

where  $\lambda$  is the mean number of earthquakes per unit volume and per unit time having magnitude greater than  $M$  and  $\alpha$  and  $\beta$  are zone-dependent constants;  $\alpha$  varies widely from point to point, as evidenced by the map of epicenters shown in Fig. 6.7, while  $\beta$  remains within a relatively narrow range, as shown in Fig. 6.8. Equation 6.6 implies a distribution of the energy liberated per shock which is very similar to that observed in the process of microfracturing of laboratory specimens of several types of rock subjected to gradually increasing compressive or bending strain (Mogi, 1962; Scholz, 1968). The values of  $\beta$  determined in the laboratory are of the same order as those obtained from seismic events, and have been shown to depend on the heterogeneity of the specimens and on their ability to yield locally. Thus, in heterogeneous specimens made of brittle materials many small shocks precede a major fracture, while in homogeneous or plastic materials the number of small shocks is relatively small. These cases correspond to large and small  $\beta$ -values, respectively. No general relationship is known to the writer between  $\beta$  and geotectonic features of seismic provinces: complexity of crustal structure and of stress gradients precludes extrapolation of laboratory results; and statistical records for relatively small zones of the earth are not, as a rule, adequate for establishing local values of  $\beta$ . Figure 6.8 shows that for very high magnitudes the observed frequency of events is lower than predicted by eq. 6.6. In addition, Rosenblueth (1969) has shown that  $\beta$  cannot be smaller than 3.46, since that would imply an infinite amount of energy liberated per unit time. However, Fig. 6.8 shows that the values of  $\beta$  which result from fitting expressions of the form 6.6 to observed data are smaller than 3.46; hence, for very high values of  $M$  (above 7, approximately) the curve should bend down, in accordance with statistical evidence.

Expressions alternative to eq. 6.6 have been proposed, attempting to represent more adequately the observed magnitude-recurrence data (Rosenblueth, 1964; Merz and Cornell, 1973). Most of these expressions also fail to recognize the existence of an upper bound to the magnitude that can be generated in a given source. Although no precise estimates of this upper bound can yet be obtained, recognition of its existence and of its dependence on the geotectonic characteristics of the source is inescapable. Indeed, the prac-

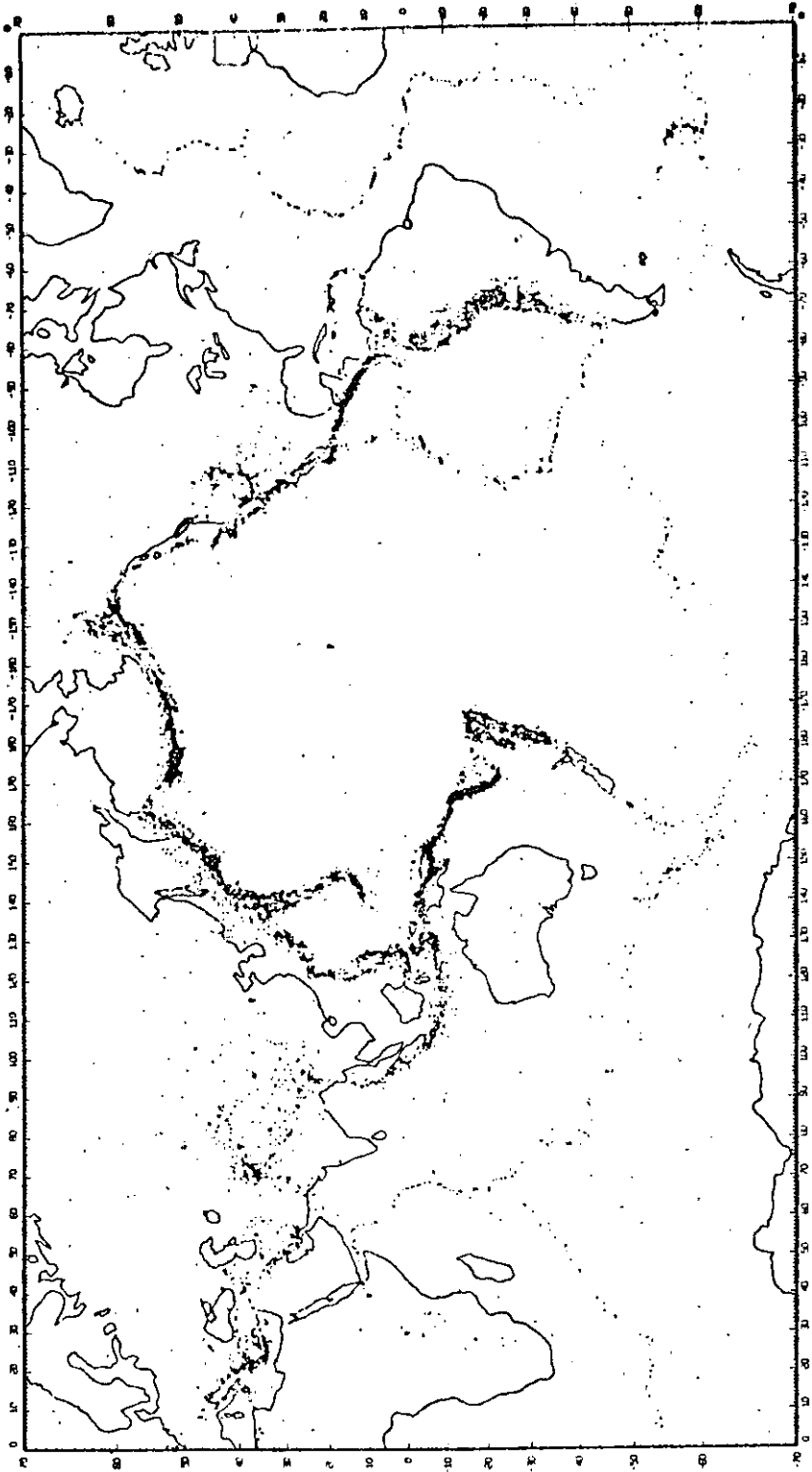


Fig. 6.7. Map showing epicenters for the interval 1961-1967. (After Newmark and Rosenblueth, 1971.)

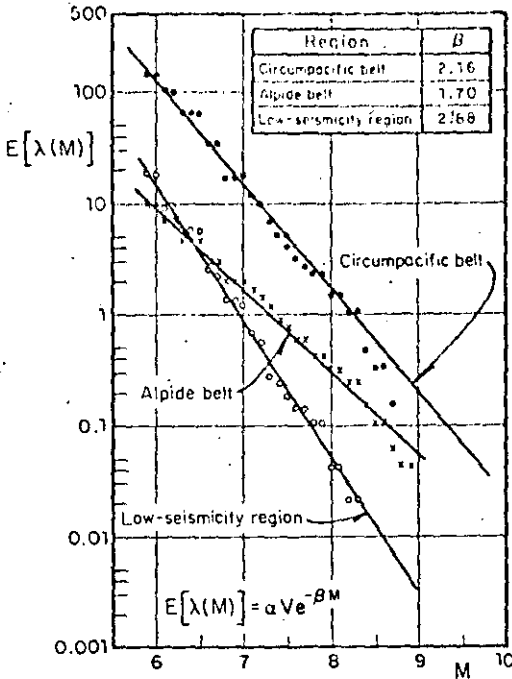


Fig. 6.8. Seismicity of macrozones. (After Esteva, 1968.)

tice of seismic zoning in the Soviet Union has been based on this concept (Gzovsky, 1962; Ananiin et al., 1968) and in many countries design spectra for very important structures, such as nuclear reactors or large dams, are usually derived from the assumption of a maximum credible intensity at a site; that intensity is ordinarily obtained by taking the maximum of the intensities that result at the site when at each of the potential sources an earthquake with magnitude equal to the maximum feasible value for that source is generated at the most unfavourable location within the same source. When this criterion is applied no attention is usually paid to the uncertainty in the maximum feasible magnitude nor to the probability that an earthquake with that magnitude will occur during a given time period. The need to formulate seismic-risk-related decisions that account both for upper bounds to magnitudes and for their probabilities of occurrence suggests adoption of magnitude recurrence expressions of the form:

$$\begin{aligned}
 \lambda &= \lambda_L G^*(M) && \text{for } M_L \leq M \leq M_U \\
 &= \lambda_L && \text{for } M < M_L \\
 &= 0 && \text{for } M > M_U
 \end{aligned} \tag{6.7}$$

where  $M_L$  = lowest magnitude whose contribution to risk is significant,  $M_U$

= maximum feasible magnitude, and  $G^*(M)$  = complementary cumulative probability distribution of magnitudes every time that an event ( $M \geq M_L$ ) occurs. A particular form of  $G^*(M)$  that lends itself to analytical derivations is:

$$G^*(M) = A_0 + A_1 \exp(-\beta M) - A_2 \exp[-(\beta - \beta_1)M] \quad (6.8)$$

where:

$$A_0 = A\beta_1 \exp[-\beta(M_U - M_L)]$$

$$A_1 = A(\beta - \beta_1) \exp(\beta M_L)$$

$$A_2 = A\beta \exp(-\beta_1 M_U + \beta M_L)$$

$$A = [\beta\{1 - \exp[-\beta_1(M_U - M_L)]\} - \beta_1\{1 - \exp[-\beta(M_U - M_L)]\}]^{-1}$$

As  $M$  tends to  $M_L$  from above, eq. 6.7 approaches eq. 6.6. Adoption of adequate values of  $M_U$  and  $\beta_1$  permits satisfying two additional conditions: the maximum feasible magnitude and the rate of variation of  $\lambda$  in its vicinity. When  $\beta_1 \rightarrow \infty$ , eq. 6.8 tends to an expression proposed by Cornell and Vanmarcke (1969).

Yegulalp and Kuo (1974) have applied the theory of extreme values to estimating the probabilities that given magnitudes are exceeded in given time intervals. They assume those probabilities to fit an extreme type-III distribution given by:

$$F_{M_{\max}}(M|t) = \exp[-C(M_U - M)^k t] \quad \text{for } M \leq M_U \\ = 0 \quad \text{for } M > M_U \quad (6.9)$$

Here  $F_{M_{\max}}(M|t)$  indicates the probability that the maximum magnitude observed in  $t$  years is smaller than  $M$ ,  $M_U$  has the same meaning as above, and  $C$  and  $K$  are zone-dependent parameters. This distribution is consistent with the assumption that earthquakes with magnitudes greater than  $M$  take place in accordance with a Poisson process with mean rate  $\lambda$  equal to  $C(M_U - M)^k$ . Equation 6.9 produces magnitude recurrence curves that fit closely the statistical data on which they are based for magnitudes above 5.2 and return periods from 1 to 50 years, even though the values of  $M_U$  that result from pure statistical analysis are not reliable measures of the upper bound to magnitudes, since in many cases they turn out inadmissibly high.

For low magnitudes, only a fraction of the number of shocks that take place is detected. As a consequence,  $\lambda$ -values based on statistical information lie below those computed according to eqs. 6.6 and 6.8 for  $M$  smaller than about 5.5. In addition, Fig. 6.9, taken from Yegulalp and Kuo (1974), shows that the numbers of detected shocks fit the extreme type III in eq. 6.9 better than the extreme type-I distribution implied by eq. 6.6., coupled with the assumption of Poisson distribution of the number of events. It is not

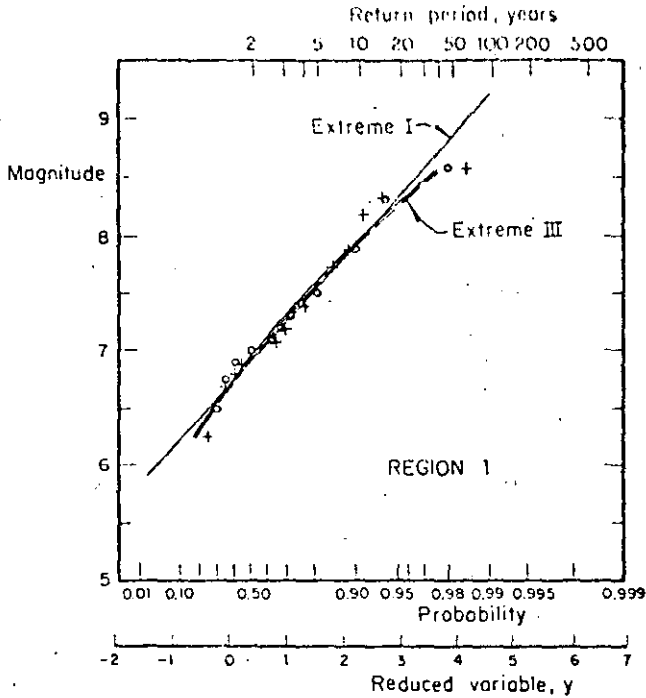


Fig. 6.9. Magnitude statistics in the Aleutian Islands region. (After Yegulalp and Kuo, 1974.)

clear what portion of the deviation from the extreme type-I distribution is due to the low values of the detectability levels and what portion comes from differences between the actual form of variation of  $\lambda$  with  $M$  and that given by eq. 6.6. The problem deserves attention because estimates of expected losses due to nonstructural damage may be sensitive to the values of  $\lambda$  for small magnitudes (say below 5.5) and because the evaluation of the level of seismic activity in a region is often made to depend on the recorded numbers of small magnitude shocks and on assumed detectability levels, i.e. of ratios of numbers of detected and occurred earthquakes (Kaila and Narain 1971; Kaila et al., 1972, 1974).

None of the expressions for  $\lambda$  presented in this chapter possess the desirable property that its applicability over a number of non-overlapping regions of the earth's crust implies the validity of an expression of the same form over the addition of those regions, unless some restrictions are imposed on the parameters of each  $\lambda$ . For instance, the addition of expressions like 6.6 gives place to an expression of the same form only if  $\beta$  is the same for all terms in the sum. Similar objections can be made to eq. 6.8. In what follows these forms will be preserved, however, as their accuracy is consistent with

the amount of available information and their adoption offers significant advantages in the evaluation of regional seismicity, as shown later.

### 6.3.2 Variation with depth

Depth of prevailing seismic activity in a region depends on its tectonic structure. For instance, most of the activity in the western coast of the United States and Canada consists of shocks with hypocentral depths in the range of 20–30 km. In other areas, such as the southern coast of Mexico, seismic events can be grouped into two ensembles: one of small shallow shocks and one of earthquakes with magnitudes comprised in a wide range, and with depths whose mean value increases with distance from the shoreline (Fig. 6.10). Figure 6.11 shows the depth distribution of earthquakes with magnitude above 5.9 for the whole circum-Pacific belt.

### 6.3.3 Stochastic models of earthquake occurrence

Mean exceedance rates of given magnitudes are expected averages during long time intervals. For decision-making purposes the times of earthquake occurrence are also significant. At present those times can only be predicted within a probabilistic context.

Let  $t_i$  ( $i = 1, \dots, n$ ) be the unknown times of occurrence of earthquakes generated in a given volume of the earth's crust during a given time interval, and let  $M_i$  be the corresponding magnitudes. For the moment it will be assumed that the risk is uniformly distributed throughout the given volume, and hence no attention will be paid to the focal coordinates of each shock.

Classical methods of time-series analysis have been applied by different researchers attempting to devise analytical models for random earthquake sequences. The following approaches are often found in the literature:

(a) Plotting of histograms of waiting times between shocks (Knopoff, 1964; Aki, 1963).

(b) Evaluation of Poisson's index of dispersion, that is of the ratio of the sample variance of the number of shocks to its expected value (Vere-Jones, 1970; Shlien and Toksöz, 1970). This index equals unity for Poisson processes, is smaller for nearly periodic sequences, and is greater than one when events tend to cluster.

(c) Determination of autocovariance functions, that is, of functions representing the covariance of the numbers of events observed in given time intervals, expressed in terms of the time elapsed between those intervals (Vere-Jones, 1970; Shlien and Toksöz, 1970). The autocovariance function of a Poisson process is a Dirac delta function. This feature is characteristic for the Poisson model since it does not hold for any other stochastic process.

(d) The hazard function  $h(t)$ , defined so that  $h(t) dt$  is the conditional probability that an event will take place in the interval  $(t, t + dt)$  given that

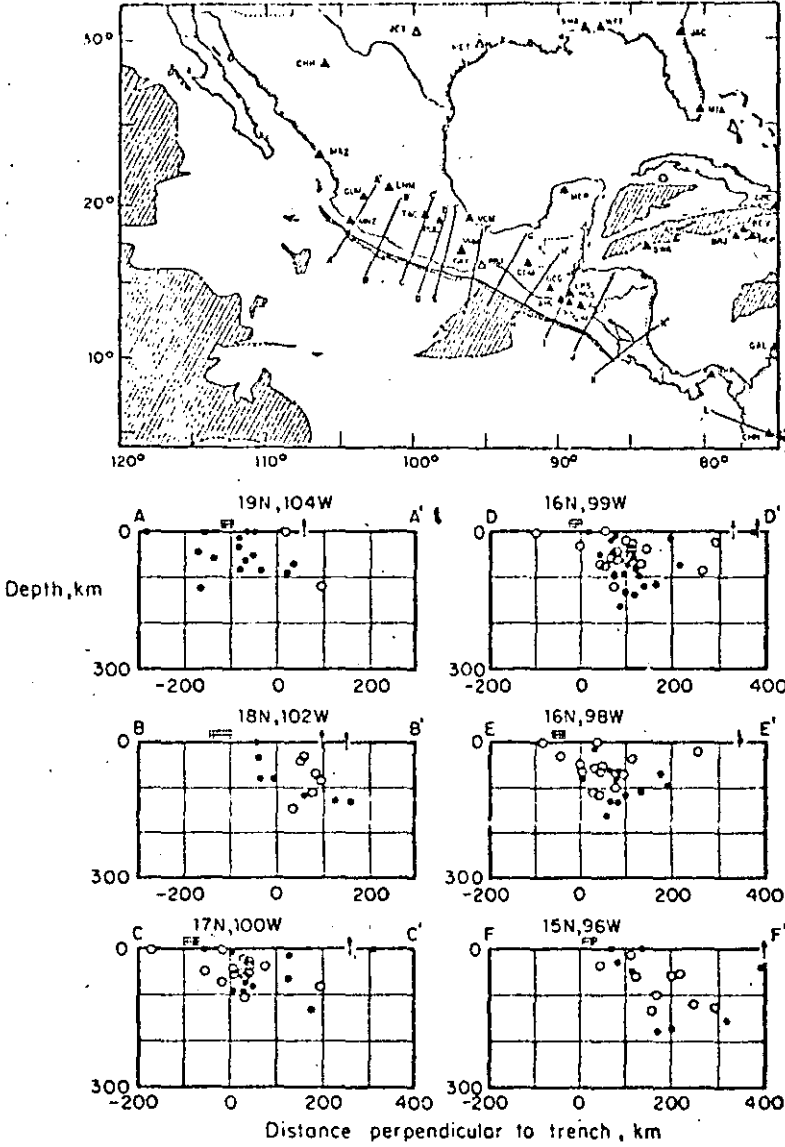


Fig. 6.10. Earthquake hypocenters projected onto a series of vertical sections through Mexico (After Molnar and Sykes, 1969.)

no events have occurred before  $t$ . If  $F(t)$  is the cumulative probability distribution of the time between events:

$$h(t) = f(t)/[1 - F(t)] \tag{6.10}$$

where  $f(t) = \partial F(t)/\partial t$ .

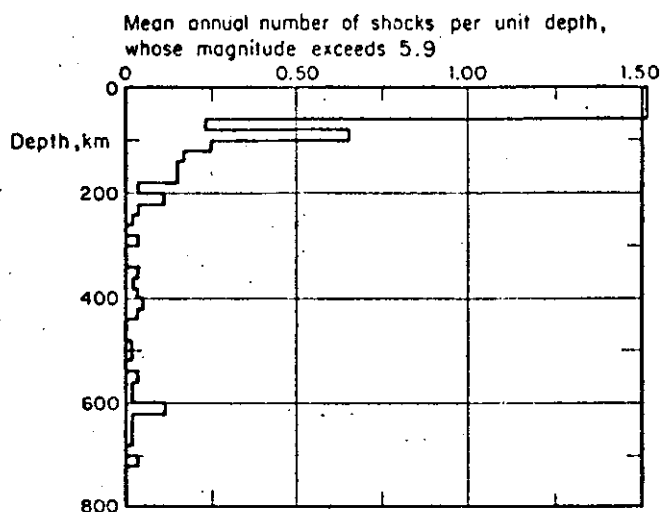


Fig. 6.11. Variation of seismicity with depth. Circum-Pacific Belt, (After Newmark and Rosenblueth, 1971.)

For the Poisson model,  $h(t)$  is a constant equal to the mean rate of the process.

### 6.3.3.1 Poisson model

Most commonly applied stochastic models of seismicity assume that the events of earthquake occurrence constitute a Poisson process and that the  $M_i$ 's are independent and identically distributed. This assumption implies that the probability of having  $N$  earthquakes with magnitude exceeding  $M$  during time interval  $(0, t)$  equals:

$$p_N = [\exp(-\nu_M t)(\nu_M t)^N] / N! \quad (6.11)$$

where  $\nu_M$  is the mean rate of exceedance of magnitude  $M$  in the given volume. If  $N$  is taken equal to zero in eq. 6.11, one obtains that the probability distribution of the maximum magnitude during time interval  $t$  is equal to  $\exp(-\nu_M t)$ . If  $\nu_M$  is given by eq. 6.6, the extreme type-I distribution is obtained.

Some weaknesses of this model become evident in the light of statistical information and of an analysis of the physical processes involved: the Poisson assumption implies that the distribution of the waiting time to the next event is not modified by the knowledge of the time elapsed since the last one, while physical models of gradually accumulated and suddenly released energy call for a more general renewal process such that, unlike what happens in the Poisson process, the expected time to the next event decreases as time goes on (Esteva, 1974). Statistical data show that the Poisson assump-

tion may be acceptable when dealing with large shocks throughout the world (Ben-Menahem, 1960), implying lack of correlation between seismicities of different regions; however, when considering small volumes of the earth, of the order of those that can significantly contribute to seismic risk at a site, data often contradict Poisson's model, usually because of clustering of earthquakes in time: the observed numbers of short intervals between events are significantly higher than predicted by the exponential distribution, and values of Poisson's index of dispersion are well above unity (Figs. 6.12 and 6.13). In some instances, however, deviations in the opposite direction have been observed: waiting times tend to be more nearly periodic, Poisson's index of dispersion is smaller than one, and the process can be represented by a renewal model. This condition has been reported, for instance, in the southern coast of Mexico (Esteve, 1974), and in the Kamchatka and Pamir-Hindu Kush regions (Gaisky, 1966 and 1967). The models under discussion also fail to account for clustering in space (Tsuboi, 1958; Gajardo and Lomnitz, 1960), for the evolution of seismicity with time, and for the systematic shifting of active sources along geologic accidents (Allen, Chapter 3 of this book). On account of its simplicity, however, the Poisson process model provides a valuable tool for the formulation of some seismic-risk-related decisions, particularly of those that are sensitive only to magnitudes of events having very long return periods.

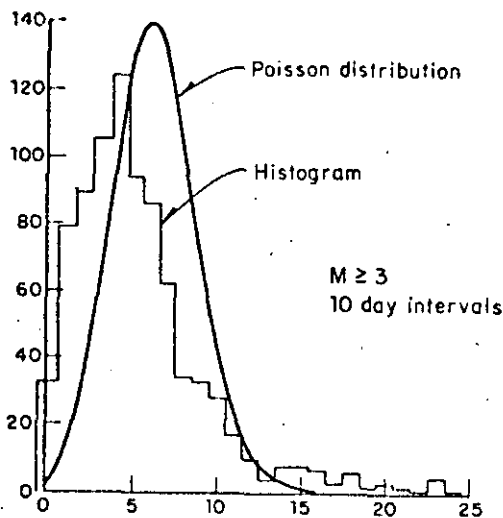
### 6.3.3.2 Trigger models

Statistical analysis of waiting times between earthquakes does not favor the adoption of the Poisson model or of other forms of renewal processes, such as those that assume that waiting times are mutually independent with lognormal or gamma distributions (Shlien and Toksöz, 1970). Alternative models have been developed, most of them of the 'trigger type' (Vere-Jones, 1970), i.e. the overall process of earthquake generation is considered as the superposition of a number of time series, each having a different origin, where the origin times are the events of a Poisson process. In general, let  $N$  be the number of events that take place during time interval  $(0, t)$ ,  $\tau_m$  = origin time of the  $m$ th series,  $W_m(t, \tau_m)$  the corresponding number of events up to instant  $t$ , and  $n$ , the random number of time series initiated in the interval  $(0, t)$ . The total number of events that occur before instant  $t$  is then:

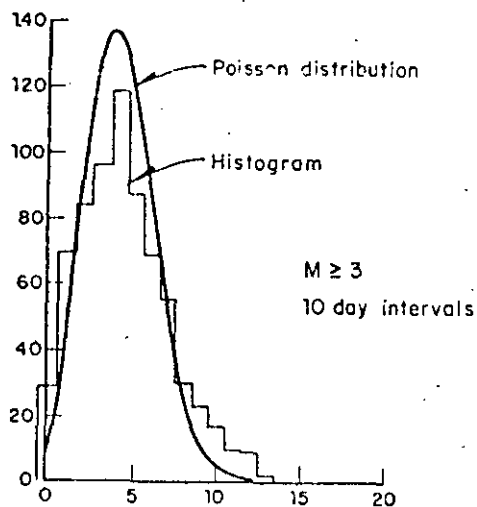
$$N = \sum_m^{n_t} W_m(t, \tau_m) \quad (6.12)$$

If origin times are distributed according to a homogeneous Poisson process with mean rate  $\nu$ , and all  $W_m$ 's are identically distributed stochastic processes with respect to  $(t - \tau_m)$ , it can be shown (Parzen, 1962) that the mean and variance of  $N$  can be obtained from:

$$E(N) = \nu \int_0^t E[W(t, \tau)] d\tau \quad (6.13)$$



a) Including swarms



b) Eliminating swarms

Fig. 6.12. Evaluation of Poisson process assumption. (After Knopoff, 1964.)

$$\text{var}(N) = \nu \int_0^t E[W^2(t, \tau)] d\tau \quad (6.14)$$

Parzen (1962) gives also an expression for the probability generating function  $\psi_N(Z; t)$  of the distribution of  $N$  in terms of  $\psi_W(Z; t, \tau)$ , the generat-

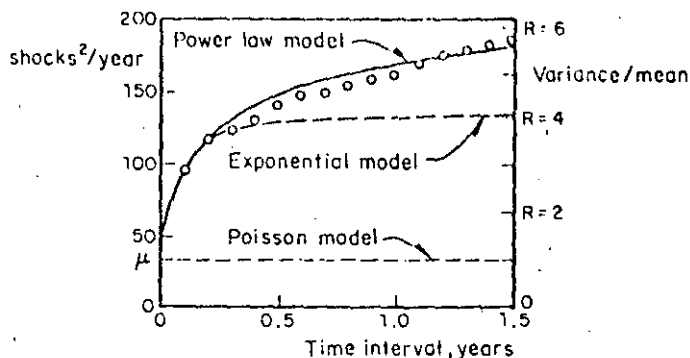


Fig. 6.13. Variance-time curve for New Zealand shallow shocks. (After Vere-Jones, 1966.)

ing function of each of the component processes:

$$\psi_N(Z; t) = \exp \left[ -\nu t + \nu \int_0^t \psi_W(Z; t, \tau) d\tau \right] \quad (6.15)$$

where:

$$\psi_W(Z; t, \tau) = \sum_{n=0}^{\infty} Z^n P\{W(t, \tau) = n\} \quad (6.16)$$

and the probability mass function of  $N$  can be obtained from  $\psi_N(Z; t)$  by recalling that:

$$\psi_N(Z; t) = \sum_{n=0}^{\infty} Z^n P\{N = n\}$$

expanding  $\psi_N$  in power series of  $Z$ , and taking  $P\{N = n\}$  equal to the coefficient of  $Z^n$  in that expansion. For instance, if it is of interest to compute  $P\{N = 0\}$ , expansion of  $\psi_N(Z; t)$  in a Taylor's series with respect to  $Z = 0$  leads to:

$$\psi_N(Z; t) = \psi_N(0; t) + Z\psi'_N(0; t) + \frac{Z^2}{2!}\psi''_N(0; t) + \dots \quad (6.17)$$

where the prime signifies derivative with respect to  $Z$ . From the definition of  $\psi_N$ ,  $P\{N = 0\} = \psi_N(0; t)$ .

Because the component processes of 'trigger'-type time series appear overlapped in sample histories, their analytical representation usually entails study of a number of alternative models, estimation of their parameters, and comparison of model and sample properties -- often second-order properties (Cox and Lewis, 1966).

*Vere-Jones models.* Applicability of some general 'trigger' models to rep-

resent local seismicity processes was discussed in a comprehensive paper by Vere-Jones (1970), who calibrated them mainly against records of seismic activity in New Zealand. In addition to simple and compound Poisson processes (Parzen, 1962), he considered Neyman-Scott and Bartlett-Lewis models, both of which assume that earthquakes occur in clusters and that the number of events in each cluster is stochastically independent of its origin time. In the Neyman-Scott model, the process of clusters is assumed stationary and Poisson, and each cluster is defined by  $p_N$ , the probability mass function of its number of events, and  $\Lambda(t)$ , the cumulative distribution function of the time of an event corresponding to a given cluster, measured from the cluster origin. The Bartlett-Lewis model is a special case of the former, where each cluster is a renewal process that ends after a finite number of renewals. In these models the conditional probability of an event taking place during the interval  $(t, t + dt)$ , given that the cluster consists of  $N$  shocks, is equal to  $N\lambda(t)dt$ , where  $\lambda(t) = \partial\Lambda(t)/\partial t$ .

Because clusters overlap in time they cannot easily be identified and separated. Estimation of process parameters is accomplished by assuming different sets of those parameters and evaluating the corresponding goodness of fit with observed data.

Various alternative forms of Neyman-Scott's model were compared by Vere-Jones with observed data on the basis of first- and second-order statistics: hazard functions, interval distributions (in the form of power spectra) and variance time curves. The statistical record comprises about one thousand New Zealand earthquakes with magnitudes greater than 4.5, recorded from 1942 to 1961. Figures 6.13–6.15 show results of the analysis for shallow New Zealand shocks as well as the comparison of observed data with sev-

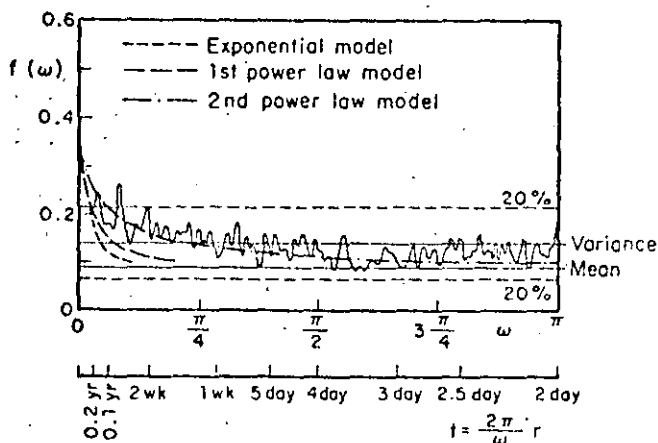


Fig. 6.14. Smoothed periodogram for New Zealand shallow shocks. (After Vere-Jones, 1966.)

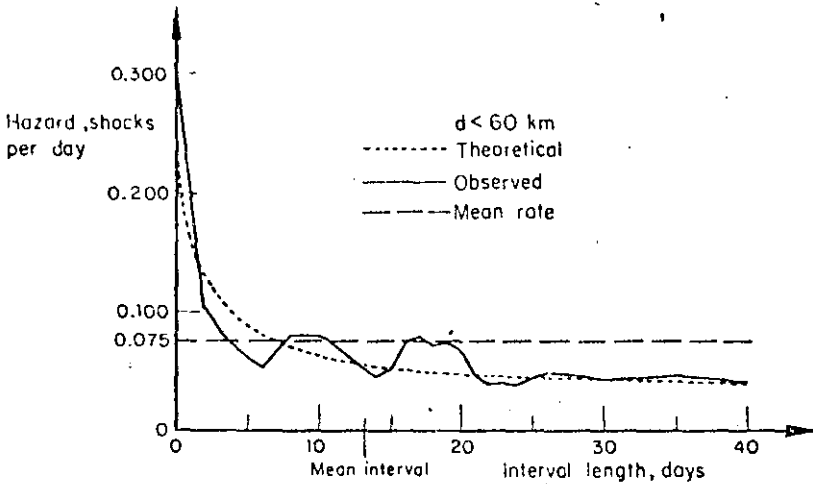


Fig. 6.15. Hazard function for New Zealand shallow shocks. (After Vere-Jones, 1970.)

eral alternative models. The process of cluster origins is Poisson in all cases, but the distributions of cluster sizes ( $N$ ) and of times of events within clusters differ among the various instances: in the Poisson model no clustering takes place (the distribution of  $N$  is a Dirac delta function centered at  $N = 1$ ) while in the exponential and in the power-law models the distribution of  $N$  is extremely skewed towards  $N = 1$ , and  $\Lambda(t)$  is taken respectively as  $1 - e^{-\lambda t}$

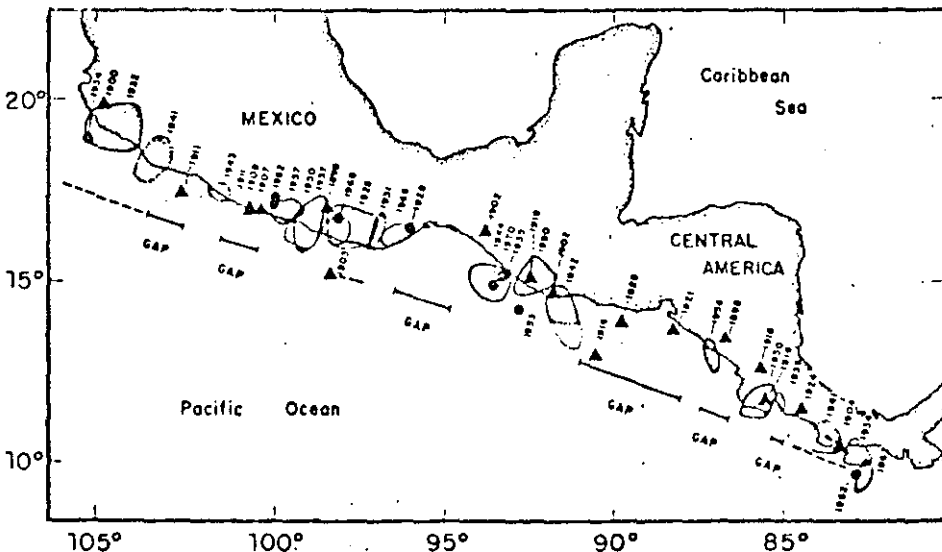


Fig. 6.16. Rupture zones and epicenters of large shallow Middle American earthquakes of this century. (After Kelleher et al., 1973.)

and  $1 - [c/(c + t)]^\delta$  for  $t \geq 0$ , and as zero for  $t < 0$ , where  $\lambda$ ,  $c$ , and  $\delta$  are positive parameters. In Figs. 6.13–6.15,  $\delta = 0.25$ ,  $c = 2.3$  days, and  $\lambda = 0.061$  shocks/day. The significance of clustering is evidenced by the high value of Poisson's dispersion index in Fig. 6.13, while no significant periodicity can be inferred from Fig. 6.14. Both figures show that the power-law model provides the best fit to the statistics of the samples. A similar analysis for New Zealand's deep shocks shows much less clustering: Poisson's dispersion index equals 2, and the hazard function is nearly constant with time.

Still, data reported by Gaisky (1967) have hazard functions that suggest models where the cluster origins as well as the clusters themselves may be represented by renewal processes. Mean return periods are of the order of several months, and hence these processes do not correspond, at least in the time scale, to the process of alternate periods of activity and quiescence of some geological structures cited by Kelleher et al. (1973), which have led to the concept of 'temporal seismic gaps', discussed below.

*Simplified trigger models.* Shlien and Toksöz (1970) proposed a simple particular case of the Neyman-Scott process; they lumped together all earthquakes taking place during non-overlapping time intervals of a given length and defined them as clusters for which  $\lambda(t)$  was a Dirac delta function. Working with one-day intervals, they assumed the number of events per cluster to be distributed in accordance with the discrete Pareto law and applied a maximum-likelihood criterion to the information consisting of 35 000 earthquakes reported by the USCGS from January 1971 to August 1968. The model proposed represents reasonably well both the distribution of the number of earthquakes in one-day intervals and the dispersion index. However, owing to the assumption that no cluster lasts more than one day, the model fails to represent the autocorrelation function of the daily numbers of shocks for small time lags. The degree of clustering is shown to be a regional function, and to diminish with the magnitude threshold value and with the focal depth.

*Aftershock sequences.* The trigger processes described have been branded as reasonable representations of regional seismic activity, even when aftershock sequences and earthquake swarms are suppressed from statistical records, however arbitrary that suppression may be. The most significant instances of clustering are related, however, to aftershock sequences which often follow shallow shocks and only rarely intermediate and deep events. Persistence of large numbers of aftershocks for a few days or weeks has propitiated the detailed statistical analysis of those sequences since last century. Omori (1894) pointed out the decay in the mean rate of aftershock occurrence with  $t$ , the time elapsed since the main shock; he expressed that rate as inversely proportional to  $t + q$ , where  $q$  is an empirical constant. Utsu (1961) proposed a more general expression, proportional to  $(t + c)^{-\zeta}$  where  $\zeta$  is a constant; Utsu's proposal is consistent with the power-law expression for  $\Lambda(t)$  presented above.

Lomnitz and Hax (1966) proposed a clustering model to represent aftershock sequences; it is a modified version of Neyman and Scott's model, where the process of cluster origins is non-homogeneous Poisson with mean rate decaying in accordance with Omori's law, the number of events in each cluster has a Poisson distribution, and  $\Lambda(t)$  is exponential. All the results and methods of analysis described by Vere-Jones (1970) for the stationary process of cluster origins can be applied to the nonstationary case through a transformation of the time scale. Fitting of parameters to four aftershock sequences was accomplished through use of the second-order information of the sample defined on a transformed time scale. By applying this criterion to earthquake sets having magnitudes above different threshold values it was noticed that the degree of clustering decreases as the threshold value increases.

The magnitude of the main shock influences the number of aftershocks and the distribution of their magnitudes and, although the rate of activity decreases with time, the distribution of magnitudes remains stable throughout each sequence (Lomnitz, 1966; Utsu, 1962; Drakopoulos, 1971). Equation 6.6 represents fairly well the distribution of magnitudes observed in most aftershock sequences. Values of  $\beta$  range from 0.9 to 3.9 and decrease as the depth increases. Since values of  $\beta$  for regular (main) earthquakes are usually estimated from relatively small numbers of shocks generated throughout crust volumes much wider than those active during aftershock sequences, no relation has been established among  $\beta$ -values for series of both types of events. The parameters of Utsu's expression for the decay of aftershock activity with time have been estimated for several sequences, for instance those following the Aleutian earthquake of March 9, 1957, the Central Alaska earthquake of April 7, 1958, and the Southeastern Alaska earthquake of July 10, 1958 (Utsu, 1962), with magnitudes equal to 8.3, 7.3, and 7.9, respectively;  $c$  (in days) was 0.37, 0.40, and 0.01, while  $\zeta$  was 1.05, 1.05 and 1.13, respectively. The relationship of the total number of aftershocks whose magnitude exceeds a given value with the magnitude of the main shock was studied by Drakopoulos (1971) for 140 aftershock sequences in Greece from 1912 to 1968. His results can be expressed by  $N(M) = A \exp(-\beta M)$ , where  $N(M)$  is the total number of aftershocks with magnitude greater than  $M$ , and  $A$  is a function of  $M_0$ , the magnitude of the main shock:

$$A = \exp(3.62 \beta + 1.1M_0 - 3.46) \quad (6.18)$$

Formulation of stochastic process models for given earthquake sequences is feasible once this relationship and the activity decay law are available for the source of interest. For seismic-risk estimation at a given site the spatial distribution of aftershocks may be as significant as the distribution of magnitudes and the time variation of activity, particularly for sources of relatively large dimensions.

### 6.3.3.3 *Renewal process models*

The trigger models described are based on information about earthquakes with magnitudes above relatively low thresholds recorded during time intervals of at most ten years. The degrees of clustering observed and the distributions of times between clusters cannot be extrapolated to higher magnitude thresholds and longer time intervals without further study.

Available information shows beyond doubt that significant clustering is the rule, at least when dealing with shallow shocks. However, there is considerable ground for discussion on the nature of the process of cluster origins during intervals of the order of one century or longer. While lack of statistical data hinders the formulation of seismicity models valid over long time intervals, qualitative consideration of the physical processes of earthquake generation may point to models which at least are consistent with the state of knowledge of geophysical sciences. Thus, if strain energy stored in a region grows in a more or less systematic manner, the hazard function should grow with the time elapsed since the last event, and not remain constant as the Poisson assumption implies. The concept of a growing hazard function is consistent with the conclusions of Kelleher et al. (1973) concerning the theory of periodic activation of *seismic gaps*. This theory is partially supported by results of nearly qualitative analysis of the migration of seismic activity along a number of geological structures. An instance is provided by the southern coast of Mexico, one of the most active regions in the world. Large shallow shocks are generated probably by the interaction of the continental mass and the subductive oceanic Cocos plate that underthrusts it and by compressive or flexural failure of the latter (Chapter 2). Seismological data show significant gaps of activity along the coast during the present century and not much is known about previous history (Fig. 6.16). Along these gaps, seismic-risk estimates based solely on observed intensities are quite low, although no significant difference is evident in the geological structure of these regions with respect to the rest of the coast, save some transverse faults which divide the continental formation into several blocks. Without looking at the statistical records a geophysicist would assign equal risk throughout the area. On the basis of seismicity data, Kelleher et al. have concluded that activity migrates along the region, in such a manner that large earthquakes tend to occur at seismic gaps, thus implying that the hazard function grows with time since the last earthquake. Similar phenomena have been observed in other regions; of particular interest is the North Anatolian fault where activity has shifted systematically along it from east to west during the last forty years (Allen, 1969).

Conclusions relative to activation of seismic gaps are controversial because the observation periods have not exceeded one cycle of each process. Nevertheless, those conclusions point to the formulation of stochastic models of seismicity that reflect plausible features of the geophysical processes.

These considerations suggest the use of renewal-process models to rep-

resent sequences of individual shocks or of clusters. Such models are characterized because times between events are independent and identically distributed. The Poisson process is a particular renewal model for which the distribution of the waiting time is exponential. Wider generality is achieved, without much loss of mathematical tractability, if inter-event times are supposed to be distributed in accordance with a gamma function:

$$f_T(t) = \frac{\nu}{(k-1)!} (\nu t)^{k-1} e^{-\nu t} \quad (6.19)$$

which becomes the exponential distribution when  $k = 1$ . If  $k < 1$ , short intervals are more frequent and the coefficient of variation is greater than in the Poisson model; if  $k > 1$ , the reverse is true. Shlien and Toksöz (1970) found that gamma models were unable to represent the sequences of individual shocks they analyzed; but these authors handled time intervals at least an order of magnitude shorter than those referred to in this section.

On the basis of hazard function estimated from sequences of small shocks in the Hindu-Kush, Vere-Jones (1970) deduces the validity of 'branching renewal process' models, in which the intervals between cluster centers, as well as those between cluster members, constitute renewal processes.

Owing to the scarcity of statistical information, reliable comparisons between alternate models will have to rest partially on simulation of the process of storage and liberation of strain energy (Burridge and Knopoff, 1967; Veneziano and Cornell, 1973).

#### 6.3.4 Influence of the seismicity model on seismic risk

Nominal values of investments made at a given instant increase with time when placing them at compound interest rates, i.e. when capitalizing them. Their real value — and not only the nominal one — will also grow, provided the interest rate overshadows inflation. Conversely, for the purpose of making design decisions, nominal values of expected utilities and costs inflicted upon in the future have to be converted into present or actualized values, which can be directly compared with initial expenditures. Descriptions of seismic risk at a site are insufficient for that purpose unless the probability distributions of the times of occurrence of different intensities — or magnitudes at neighbouring sources — are stipulated; this entails more than simple magnitude-recurrence graphs or even than maximum feasible magnitude estimates.

Immediately after the occurrence of a large earthquake, seismic risk is abnormally high due to aftershock activity and to the probability that damage inflicted by the main shock may have weakened natural or man-made structures if emergency measures are not taken in time. When aftershock activity has ceased and damaged systems have been repaired, a normal risk level is attained, which depends on the probability-density functions of the waiting times to the ensuing damaging earthquakes.

For the purpose of illustration, let it be assumed that a fixed and deterministically known damage  $D_0$  occurs whenever a magnitude above a given value is generated at a given source. If  $f(t)$  is the probability-density function of the waiting time to the occurrence of the damaging event, and if the risk level is sufficiently low that only the first failure is of concern, the expected value of the actualized cost of damage is (see Chapter 9):

$$\bar{D} = D_0 \int_0^{\infty} e^{-\gamma t} f(t) dt \quad (6.20)$$

where  $\gamma$  is the discount (or compound interest) coefficient and the overbar denotes expectation. If the process is Poisson with mean rate  $\nu$ , then  $f(t)$  is exponential and  $\bar{D} \cong D_0 \nu/\gamma$ ; however, if damaging events take place in clusters and most of the damage produced by each cluster corresponds to its first event, the computation of  $\bar{D}$  should make use of the mean rate  $\nu$  corresponding to the clusters, instead of that applicable to individual events. Table 6.II shows a comparison of seismic risk determined under the alternative assumptions of a Poisson and a gamma model ( $k = 2$ ), both with the same mean return period,  $k/\nu$  (Esteva, 1974). Three descriptions of risk are presented as functions of the time  $t_0$  elapsed since the last damaging event:  $T_1$ , the expected time to the next event, measured from instant  $t_0$ ; the expected value of the present cost of failure computed from eq. 6.20, and the hazard function (or mean failure rate). Since clustering is neglected, risk of aftershock occurrence must be either included in  $D_0$  or superimposed on that displayed in the table.

This table shows very significant differences among risk levels for both processes. At small values of  $t_0$ , risk is lower for the gamma process, but it

TABLE 6.II  
Comparison of Poisson and gamma processes

$t_0 \nu/k$	$\bar{T}_1 \nu/k$	Poisson process, $k = 1$			$hk/\nu$	$T_1 \nu/k$	Gamma process, $k = 2$		$hk/\nu$
		$D/D_0$		$D/D_0$			$\bar{D}$		
		$\gamma k/\nu = 10$	$\gamma k/\nu = 100$	$\gamma k/\nu = 10$			$bk/\nu = 100$		
0					1.0	0.0278	0.0004	0	
0.1					0.92	0.0511	0.0036	0.367	
0.2					0.86	0.0675	0.0059	0.667	
0.5					0.75	0.0973	0.0100	1.333	
1	1.0	0.0909	0.0099	1.0	0.67	0.120	0.0132	2.000	
2					0.60	0.139	0.0158	2.667	
5					0.54	0.154	0.0179	3.333	
10					0.52	0.160	0.0187	3.633	
					0.50	0.167	0.0196	4.000	

grows with time, until it outrides that for the Poisson process, which remains constant. The differences shown clearly affect engineering decisions.

#### 6.4 ASSESSMENT OF LOCAL SEISMICITY

Only exceptionally can magnitude-recurrence relations for small volumes of the earth's crust and statistical correlation functions of the process of earthquake generation be derived exclusively from statistical analysis of recorded shocks. In most cases this information is too limited for that purpose and it does not always reflect geological evidence. Since the latter, as well as its connection with seismicity, is beset with wide uncertainty margins, information of different nature has to be evaluated, its uncertainty analyzed, and conclusions reached consistent with all pieces of information. A probabilistic criterion that accomplishes this is presented here: on the basis of geotectonic data and of conceptual models of the physical processes involved, a set of alternate assumptions can be made concerning the functions in question (magnitude recurrence, time, and space correlation) and an initial probability distribution assigned thereto; statistical information is used to judge the likelihood of each assumption, and a posterior probability distribution is obtained. How statistical information contributes to the posterior probabilities of the alternate assumptions depends on the extent of that information and on the degree of uncertainty implied by the initial probabilities. Thus, if geological evidence supports confidence in a particular assumption or range of assumptions, statistical information should not greatly modify the initial probabilities. If, on the other hand, a long and reliable statistical record is available, it practically determines the form and parameters of the mathematical model selected to represent local seismicity.

##### 6.4.1 *Bayesian estimation of seismicity*

Bayesian statistics provide a framework for probabilistic inference that accounts for prior probabilities assigned to a set of alternate hypothetical models of a given phenomenon as well as for statistical samples of events related to that phenomenon. Unlike conventional methods of statistical inference, Bayesian methods give weight to probability measures obtained from samples or from other sources; numbers, coordinates and magnitudes of earthquakes observed in given time intervals serve to ascertain the probable validity of each of the alternative models of local seismicity that can be postulated on the grounds of geological evidence. Any criterion intended to weigh information of different nature and different degrees of uncertainty should lead to probabilistic conclusions consistent with the degree of confidence attached to each source of information. This is accomplished by Bayesian methods.

Let  $H_i$  ( $i = 1, \dots, n$ ) be a comprehensive set of mutually exclusive assumptions concerning a given, imperfectly known phenomenon and let  $A$  be the observed outcome of such a phenomenon. Before observing outcome  $A$  we assign an initial probability  $P(H_i)$  to each hypothesis. If  $P(A|H_i)$  is the probability of  $A$  in case hypothesis  $H_i$  is true, then Bayes' theorem (Raiffa and Schlaifer, 1968) states that:

$$P(H_i|A) = P(H_i) \frac{P(A|H_i)}{\sum_j P(H_j)P(A|H_j)} \quad (6.21)$$

The first member in this equation is the (posterior) probability that assumption  $H_i$  is true, given the observed outcome  $A$ .

In the evaluation of seismic risk, Bayes' theorem can be used to improve initial estimates of  $\lambda(M)$  and its variation with depth in a given area as well as those of the parameters that define the shape of  $\lambda(M)$  or, equivalently, the conditional distribution of magnitudes given the occurrence of an earthquake. For that purpose, take  $\lambda(M)$  as the product of a rate function  $\lambda_L = \lambda(M_L)$  by a shape function  $G^*(M, B)$ , equal to the conditional complementary distribution of magnitudes given the occurrence of an earthquake with  $M \geq M_L$ , where  $M_L$  is the magnitude threshold of the set of statistical data used in the estimation, and  $B$  is the vector of (uncertain) parameters  $B_1, \dots, B_r$  that define the shape of  $\lambda(M)$ . For instance, if  $\lambda(M)$  is taken as given by eq. 6.8,  $B$  is a vector of three elements equal respectively to  $\beta, \beta_1$ , and  $M_U$ ; if eq. 6.9 is adopted,  $B$  is defined by  $k$  and  $M_U$ .

The initial distribution of seismicity is in this case expressed by the initial joint probability density function of  $\lambda_L$  and  $B$ :  $f'(\lambda_L, B)$ . The observed outcome  $A$  can be expressed by the magnitudes of all earthquakes generated in a given source during a given time interval. For instance, suppose that  $N$  earthquakes were observed during time interval  $t$  and that their magnitudes were  $m_1, m_2, \dots, m_N$ . Bayes' expression takes the form:

$$f''(\lambda_L, B|m_1, \dots, m_N; t) = f'(\lambda_L, B) \frac{P[m_1, m_2, \dots, m_N; t|\lambda_L, B]}{\int \int P[m_1, m_2, \dots, m_N; t|l, b] f'(l, b) dl db} \quad (6.22)$$

where  $f''(\cdot)$  is the posterior probability density function, and  $l$  and  $b$  are dummy variables that stand for all values that may be taken by  $\lambda_L$  and  $B$ , respectively. Estimation of  $\lambda_L$  can usually be formulated independently of that of the other parameters. The observed fact is then expressed by  $N_L$ , the number of earthquakes with magnitude above  $M_L$  during time  $t$ , and the following expression is obtained, as a first step in the estimation of  $\lambda(M)$ :

$$f'(\lambda_L|N_L; t) = f'(\lambda_L) \frac{P(N_L; t|\lambda_L)}{\int P(N_L; t|l) f'(l) dl} \quad (6.23)$$

#### 6.4.1.1 Initial probabilities of hypothetical models

Where statistical information is scarce, seismicity estimates will be very

sensitive to initial probabilities assigned to alternative hypothetical models; the opinions of geologists and geophysicists about probable models, about the parameters of these models, and the corresponding margins of uncertainty should be adequately interpreted and expressed in terms of a function  $f'$ , as required by equations similar to 6.22 and 6.23. Ideally, these opinions should be based on the formulation of potential earthquake sources and on their comparison with possibly similar geotectonic structures. This is usually done by geologists, more qualitatively than quantitatively, when they estimate  $M_U$ . Initial estimates of  $\lambda_L$  are seldom made, despite the significance of this parameter for the design of moderately important structures (see Chapter 9).

Analysis of geological information must consider local details as well as general structure and evolution. In some areas it is clear that all potential earthquake sources can be identified by surface faults, and their displacements in recent geological times measured. When mean displacements per unit time can be estimated, the order of magnitude of creep and of energy liberated by shocks and hence of the recurrence intervals of given magnitudes can be established (Wallace, 1970; Davies and Brune, 1971), the corresponding uncertainty evaluated, and an initial probability distribution assigned. The fact that magnitude-recurrence relations are only weakly correlated with the size of recent displacements is reflected in large uncertainties (Petrushesky, 1966).

Application of the criterion described in the foregoing paragraph can be unfeasible or inadequate in many problems, as in areas where the abundance of faults of different sizes, ages, and activity, and the insufficient accuracy with which focal coordinates are determined preclude a differentiation of all sources. Regional seismicity may then be evaluated under the assumption that at least part of the seismic activity is distributed in a given volume rather than concentrated in faults of different importance. The same situation would be faced when dealing with active zones where there is no surface evidence of motions. Hence, consideration of the overall behavior of complex geological structures is often more significant than the study of local details.

Not much work has been done in the analysis of the overall behavior of large geological structures with respect to the energy that can be expected to be liberated per unit volume and per unit time in given portions of those structures. Important research and applications should be expected, however, since, as a result of the contribution of plate-tectonics theory to the understanding of large-scale tectonic processes, the numerical values of some of the variables correlated with energy liberation are being determined, and can be used at least to obtain orders of magnitude of expected activity along plate boundaries. Far less well understood are the occurrence of shocks in apparently inactive regions of continental shields and the behavior of complex continental blocks or regions of intense folding, but even there some

progress is expected in the study of accumulation of stresses in the crust.

Knowledge of the geological structure can serve to formulate initial probability distributions of seismicity even when quantitative use of geophysical information seems beyond reach. Initial probability distributions of local seismicity parameters  $\lambda_L$ ,  $B$  in the small volumes of the earth's crust that contribute significantly to seismic risk at a site, can be assigned by comparison with the average seismicity observed in wider areas of similar tectonic characteristics, or where the extent and completeness of statistical information warrant reliable estimates of magnitude-recurrence curves (Esteve, 1969). In this manner we can, for instance, use the information about the average distribution of the depths of earthquakes of different magnitudes throughout a seismic province to estimate the corresponding distribution in an area of that province, where activity has been low during the observation interval, even though there might be no apparent geophysical reason to account for the difference. Similarly, the expected value and coefficient of variation of  $\lambda_L$  in a given area of moderate or low seismicity (as a continental shield) can be obtained from the statistics of the motions originated at all the supposedly stable or aseismic regions in the world.

The significance of initial probabilities in seismic risk estimates, against the weight given to purely statistical information, becomes evident in the example of Fig. 6.16: if Kelleher's theory about activation of seismic gaps is true, risk is greater at the gaps than anywhere else along the coast; if Poisson models are deemed representative of the process of energy liberation, the extent of statistical information is enough to substantiate the hypothesis of reduced risk at gaps. Because both models are still controversial, and represent at most two extreme positions concerning the properties of the actual process, risk estimates will necessarily reflect subjective opinions.

#### 6.4.1.2 Significance of statistical information

*Estimation of  $\lambda_L$ .* Application of eq. 6.23 to estimate  $\lambda_L$  independently of other parameters will be first discussed, because it is a relatively simple problem and because  $\lambda_L$  is usually more uncertain than  $M_U$  and much more so than  $\beta$ .

A model as defined by eq. 6.19 will be assumed to apply. If the possible assumptions concerning the values of  $\lambda_L$  constitute a continuous interval, the initial probabilities of the alternative hypotheses can be expressed in terms of a probability-density function of  $\lambda_L$ . If, in addition, a certain assumption is made concerning the form of this probability-density function, only the initial values of  $E(\lambda_L)$  and  $V(\lambda_L)$  have to be assumed. It is advantageous to assign to  $\nu = k/E(T)$  a gamma distribution. Then, if  $\rho$  and  $\mu$  are the parameters of this initial distribution of  $\nu$ , if  $k$  is assumed to be known, and if the observed outcome is expressed as the time  $t_n$  elapsed during  $n + 1$  consecutive events (earthquakes with magnitude  $\geq M_L$ ), application of eq. 6.23 leads to the conclusion that the posterior probability function of  $\nu$  is

also gamma, now with parameters  $\rho + nk$  and  $\mu + t_n$ . The initial and the posterior expected values of  $\nu$  are respectively equal to  $\rho/\mu$ , and to  $(\rho + nk)/(\mu + t_n)$ . When initial uncertainty about  $\nu$  is small,  $\rho$  and  $\mu$  will be large and the initial and the posterior expected values of  $\nu$  will not differ greatly. On the other hand, if only statistical information were deemed significant,  $\rho$  and  $\mu$  should be given very small values in the initial distribution, and  $E(\nu)$ , and hence  $\lambda_L$ , will be practically defined by  $n$ ,  $k$ , and  $t_n$ . This means that the initial estimates of geologists should not only include expected or most probable values of the different parameters, but also statements about ranges of possible values and degrees of confidence attached to each.

In the case studied above only a portion of the statistical information was used. In most cases, especially if seismic activity has been low during the observation interval, significant information is provided by the durations of the intervals elapsed from the initiation of observations to the first of the  $n + 1$  events considered, and from the last of these events until the end of the observation period. Here, application of eq. 6.23 leads to expressions slightly more complicated than those obtained when only information about  $t_n$  is used.

The particular case when the statistical record reports no events during at least an interval  $(0, t_0)$  comes up frequently in practical problems. The probability-density function of the time  $T_1$  from  $t_0$  to the occurrence of the first event must account for the corresponding shifting of the time axis. Furthermore, if the time of occurrence of the last event before the origin is unknown, the distribution of the waiting time from  $t = 0$  to the first event coincides with that of the *excess life* in a renewal process at an arbitrary value of  $t$  that approaches infinity (Parzen, 1962). For the particular case when the waiting times constitute a gamma process,  $T_1$  is measured from  $t = 0$ ,  $T$  is the waiting time between consecutive events, and it is known that  $T_1 \geq t_0$ , the conditional density function of  $\tau_1 = (T_1 - t_0)/E(T)$  is given by eq. 6.24 (Esteve, 1974), where  $u_0 = t_0/E(T)$ :

$$f_{\tau_1}(u|T_1 \geq t_0) = \frac{\sum_{m=1}^k \frac{k}{(m-1)!} [k(u+u_0)]^{m-1}}{\sum_{m=1}^k \sum_{n=1}^m \frac{1}{(n-1)!} (ku_0)^{n-1}} e^{-ku} \quad (6.24)$$

Consider now the implications of Bayesian analysis when applied to one of the seismic gaps in Fig. 6.16, under the conditions implicit in eq. 6.24. An initial set of assumptions and corresponding probabilities was adopted as described in the following. From previous studies referring to all the southern coast of Mexico, local seismicity in the gap area (measured in terms of  $\lambda$  for  $M \geq 6.5$ ) was represented by a gamma process with  $k = 2$ . An initial

probability density function for  $\nu$  was adopted such that the expected value of  $\lambda(6.5)$  for the region coincided with its average throughout the complete seismic province. Two values of  $\rho$  were considered: 2 and 10, which correspond to coefficients of variation of 0.71 and 0.32, respectively. Values in Table 6.III were obtained for the ratio of the final to the initial expected values of  $\nu$ , in terms of  $u_0$ .

The last two columns in the table contain the ratios of the computed values of  $E''(T_1)$  and  $E'(T)$  when  $\nu$  is taken as equal respectively to its initial or to its posterior expected value. This table shows that, for  $\rho = 10$ , that is, when uncertainty attached to the geologically based assumptions is low, the expected value of the time to the next event keeps decreasing, in accordance with the conclusions of Kelleher et al. (1973). However, as time goes on and no events occur, the statistical evidence leads to a reduction in the estimated risk, which shows in the increased conditional expected values of  $T_1$ . For  $\rho = 2$ , the geological evidence is less significant and risk estimates decrease at a faster rate.

#### 6.4.1.3 Bayesian estimation of jointly distributed parameters

In the general case, estimation of  $B$  will consist in the determination of the posterior Bayesian joint probability function of its components, taking as statistical evidence the relative frequencies of observed magnitudes. Thus, if event  $A$  is described as the occurrence of  $N$  shocks, with magnitudes  $m_1, \dots, m_N$ , and  $b_i$  ( $i = 1, \dots, r$ ) are values that may be adopted by the components of vector  $B$  being estimated, eq. 6.21 becomes:

$$f_B(b_1, \dots, b_r | A) = \frac{f_B(b_1, \dots, b_r) P(A | b_1, \dots, b_r)}{\int \dots \int f_B(u_1, \dots, u_r) P(A | u_1, \dots, u_r) du_1, \dots, du_r} \quad (6.25)$$

where  $P(A | u_1, \dots, u_r)$  is proportional to:

$$\prod_{i=1}^N g(m_i | u_1, \dots, u_r)$$

and  $g(m) = -\partial G^*(m) / \partial m$ .

Closed-form solutions for  $f''$  as given by eq. 6.25 are not feasible in general. For the purpose of evaluating risk, however, estimates of the posterior first and second moments of  $f''$  can be obtained from eq. 6.25, making use of available first-order approximations (Benjamin and Cornell, 1970; Rosenblueth, 1975). Thus, the posterior expected value of  $B_i$  is given by  $\int f_{B_i}''(u) u du$ , where  $f_{B_i}''(u) = \int \dots \int f_B''(u_1, \dots, u_r) du_1, \dots, du_n$  and the multiple integral is of order  $r - 1$ , because it is not extended to the dominion of  $B_i$ . Hence:

$$E''(B_i) = \frac{E'_B [B_i P(A | B_1, \dots, B_r)]}{E'_B [P(A | B_1, \dots, B_r)]} \quad (6.26)$$

TABLE 6.III

Bayesian estimates of seismicity in one seismic gap

$u_0 = t_0/E'(T)$	$E''(\nu)/E'(\nu)$		$E''(T_1 T_1 > t_0)/E'(T)$	
	$\rho = 2$	$\rho = 10$	$\rho = 2$	$\rho = 10$
0	1.0	1.0	0.75	0.75
0.1	0.95	0.99	0.76	0.74
0.5	0.75	0.94	0.91	0.71
1	0.58	0.87	1.14	0.73
5	0.20	0.54	3.11	1.05
10	0.11	0.36	5.47	1.55
20	0.06	0.22	10.50	2.48

where  $E'$  and  $E''$  stand for initial and posterior expectation, and subscript  $B$  means that expectation is taken with respect to all the components of  $B$ . Likewise, the following *posterior moments* can be obtained:

Covariance of  $B_i$  and  $B_j$

$$\text{Cov}''(B_i, B_j) = \frac{E'_B[B_i B_j P(A|B_1, \dots, B_r)]}{E'_B[P(A|B_1, \dots, B_r)]} - E''(B_i)E''(B_j) \quad (6.27)$$

Expected value of  $\lambda(M)$

$$\begin{aligned} E''[\lambda(M)] &= E''(\lambda_1)E''[G^*(M; B)] \\ &= E''(\lambda_1) \frac{E'_B[G^*(M; B)P(A|B_1, \dots, B_r)]}{E'_B[P(A|B_1, \dots, B_r)]} \end{aligned} \quad (6.28)$$

*Marginal distributions.* The posterior expectation of  $\lambda(M)$  is in some cases all that is required to describe seismicity for decision-making purposes. Often, however, uncertainty in  $\lambda(M)$  must also be accounted for. For instance, the probability of exceedance of a given magnitude during a given time interval has to be obtained as the expectation of the corresponding probabilities over all alternative hypotheses concerning  $\lambda(M)$ . In this manner it can be shown that, if the occurrence of earthquakes is a Poisson process and the Bayesian distribution of  $\lambda_L$  is gamma with mean  $\bar{\lambda}_L$  and coefficient of variation  $V_L$ , the marginal distribution of the number of earthquakes is negative binomial with mean  $\bar{\lambda}_L$ . In particular, the marginal probability of zero events during time interval  $t$  — equivalently, the complementary distribution function of the waiting time between events — is equal to  $(1 + t/t'')^{-r''}$ , where  $r'' = V_L^2$  and  $t'' = r''/\bar{\lambda}_L$ . The marginal probability-density function of the waiting time, that should be substituted in eq. 6.20, is  $\bar{\lambda}_L(1 + t/t'')^{-r''-1}$ , which tends to the exponential probability function as  $r''$  and  $t''$  tend to infinity (and  $V_L \rightarrow 0$ ) while their ratio remains equal to  $\bar{\lambda}_L$ .

Bayesian uncertainty tied to the joint distribution of all seismicity parameters ( $\lambda_L, B_1, \dots, B_r$ ) can be included in the computation of the probability of occurrence of a given event  $Z$  by taking the expectation of that probability with respect to all parameters:

$$P(Z) = E_{\lambda_L, B} [P(Z); \lambda_L, B_1, \dots, B_r] \quad (6.29)$$

When the joint distribution of  $\lambda_L, B$  stems from Bayesian analysis of an initial distribution and an observed event,  $A$ , this equation adopts the form:

$$P'(Z) = \frac{E'_{\lambda_L, B} [P(Z|\lambda_L, B)P(A|\lambda_L, B)]}{E'_{\lambda_L, B} [P(A|\lambda_L, B)]} \quad (6.30)$$

where ' and " stand for initial and posterior, respectively.

*Spatial variability.* Figure 6.17 shows a map of geotectonic provinces of Mexico, according to F. Mooser. Each province is characterized by the large-scale features of its tectonic structure, but significant local perturbations to the overall patterns can be identified. Take for instance zone 1, whose seismotectonic features were described above, and are schematically shown in Fig. 6.18 (Singh, 1975): the Pacific plate underthrusts the continental block and is thought to break into several blocks, separated by faults transverse to the coast, that dip at different angles. The continental mass is also

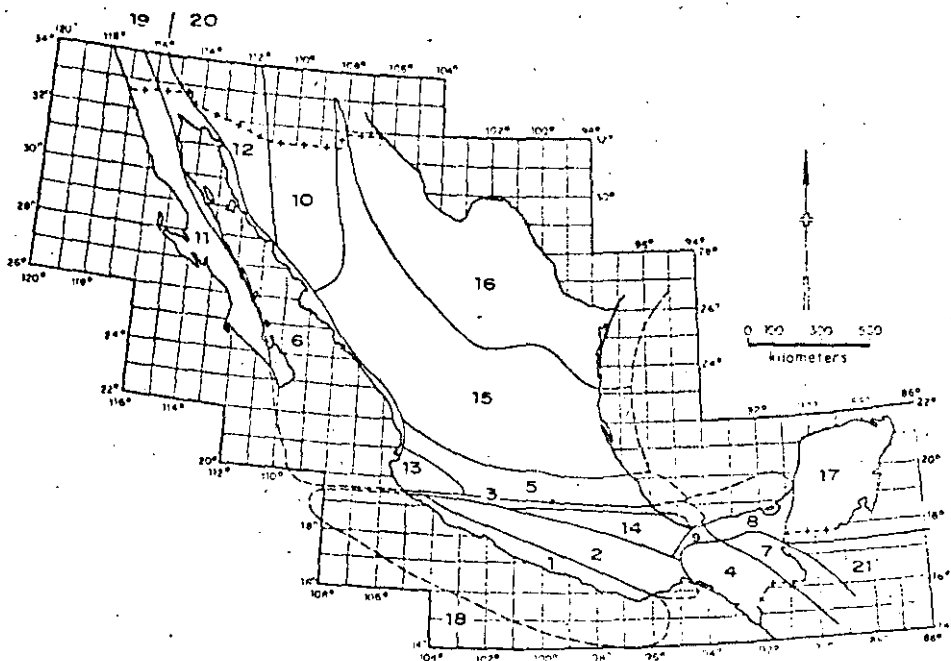


Fig. 6.17. Seismotectonic provinces of Mexico. (After F. Mooser.)

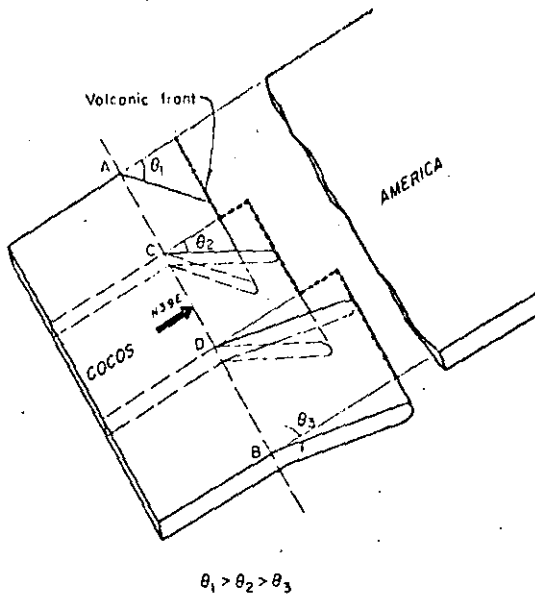


Fig. 6.18. Schematic drawing of the segmenting of Cocos plate as it subducts below American plate. (After Singh, 1974.)

made up of several large blocks. Seismic activity at the underthrusting plate or at its interface with the continental mass is characterized by magnitudes that may reach very high values and by the increase of mean hypocentral depth with distance from the coast; small and moderate shallow shocks are generated at the blocks themselves. Variability of statistical data along the whole tectonic system was discussed above and is apparent in Fig. 6.10. Bayesian estimation of local seismicity averaged throughout the system is a matter of applying eq. 6.21 or any of its special forms (eqs. 6.22 and 6.23), taking as statistical evidence the information corresponding to the whole system. However, seismic risk estimates are sensitive to values of local seismicity averaged over much smaller volumes of the earth's crust; hence the need to develop criteria for probabilistic inference of possible patterns of space variability of seismicity along tectonically homogeneous zones.

On the basis of seismotectonic information, the system under consideration can first be subdivided into the underthrusting plate and the subsystem of shallow sources; each subsystem can then be separately analyzed. Take for instance the underthrusting plate and subdivide it into  $s$  sufficiently small equal-volume subzones. Let  $\nu_L$  be the rate of exceedance of magnitude  $M_L$  throughout the main system,  $\nu_{L_i}$  the corresponding rate at each subzone, and define  $p_i$  as  $\nu_{L_i}/\nu_L$ , with  $p_i$  independent of  $\nu_L$  ( $p_i$  is equal to the probability that an earthquake known to have been generated in the overall system originated at subzone  $i$ ). Initial information about possible space variability of

$\nu_{L_i}$  can be expressed in terms of an initial probability distribution of  $p_i$  and of the correlation among  $p_i$  and  $p_j$  for any  $i$  and  $j$ . Because  $\Sigma \nu_{L_i} = \nu_L$ , one obtains  $\Sigma p_i = 1$ . This imposes two restrictions on the initial joint probability distribution of the  $p_i$ 's:  $E'(p_i) = 1/s$ ,  $\text{var}' \Sigma p_i = 0$ . If all  $p_i$ 's are assigned equal expectations and all pairs  $p_i, p_j, i \neq j$  are assumed to possess the same correlation coefficient  $\rho_{ij} = \rho'$ , the restrictions mentioned lead to  $E'(p_i) = 1/s$  and  $\rho' = -1/(s-1)$ . Posterior values of  $E(p_i)$  and  $\rho_{ij}$  are obtained according to the same principles that led to eqs. 6.25–6.28. Statistical evidence is in this case described by  $N$ , the total number of earthquakes generated in the system, and  $n_i$  ( $i = 1, \dots, s$ ) the corresponding numbers for the subzones. Given the  $p_i$ 's, the probability of this event is the multinomial distribution:

$$P[A|p_1, \dots, p_s] = \frac{N!}{n_1! \dots n_s!} p_1^{n_1} \dots p_s^{n_s} \quad (6.31)$$

If the correlation coefficients among seismicities of the various subzones can be neglected, each  $p_i$  can be separately estimated. Because  $p_i$  has to be comprised between 0 and 1, it is natural to assign it a beta initial probability distribution, defined by its parameters  $n_i'$  and  $N_i'$ , such that  $E'(p_i) = n_i'/N_i'$  and  $\text{var}'(p_i) = n_i'(N_i' - n_i')/[N_i'^2(N_i' + 1)]$  (Raiffa and Schlaifer, 1968). The parameters of the posterior distribution will be:

$$n_i'' = n_i' + n_i, N_i'' = N_i' + N$$

Take for instance a zone whose prior distribution of  $\lambda_L$  is assumed gamma with expected value  $\lambda_L'$  and coefficient of variation  $V_L'$ . Suppose that, on the basis of geological evidence and of the dimensions involved, it is decided to subdivide the zone into four subzones of equal dimensions; a-priori considerations lead to the assignment of expected values and coefficients of variation of  $p_i$  for those subzones, say  $E'(p_i) = 0.25, V'(p_i) = 0.25$  ( $i = 1, \dots, 4$ ). From previous considerations for  $s = 4$  take  $\rho_{ij}' = -1/3$  for  $i \neq j$ . Suppose now that, during a given time interval  $t$ , ten earthquakes were observed in the zone, of which 0, 1, 3, and 6 occurred respectively in each subzone. If the Poisson process model is adopted,  $\lambda_L'$  and  $V_L'$  can be expressed in terms of a fictitious number of events  $n' = V_L'^{-2}$  occurred during a fictitious time interval  $t' = n'/\lambda_L'$ ; after observing  $n$  earthquakes during an interval  $t$ , the Bayesian mean and coefficient of variation of  $\lambda_L$  will be  $\lambda_L'' = (n' + n)/(t' + t)$ ,  $V_L'' = (n' + n)^{-1/2}$  (Esteva, 1968). Hence:

$$\lambda_L'' = (V_L'^{-2} + 10)/(V_L'^{-2} \lambda_L'^{-1} + t), \quad V_L'' = (V_L'^{-2} + 10)^{-1/2}$$

Local deviations of seismicity in each subzone with respect to the average  $\lambda_L$  can be analyzed in terms of  $p_i$  ( $i = 1, \dots, 4$ ); Bayesian analysis of the proportion in which the ten earthquakes were distributed among the subzones proceeds according to:

$$E''(p_i|A) = \frac{E'[p_i P(A|p_1, \dots, p_4)]}{E'[P(A|p_1, \dots, p_4)]} \quad (6.32)$$

The expectations that appear in this equation have to be computed with respect to the initial joint distribution of the  $p_i$ 's. In practice, adequate approximations are required. For instance, Benjamin and Cornell's (1970) first-order approximation leads to  $E''(p_1) = 0.226$ ,  $E''(p_4) = 0.294$ .

If correlation among subzone seismicities is neglected, and statistical information of each subzone is independently analyzed, when the  $p_i$ 's are assigned beta probability-density functions with means and coefficients of variation as defined above, one obtains  $E''(p_1) = 0.206$ ,  $E''(p_4) = 0.311$ , which are not very different from those formerly obtained; however, when  $E'(p_i) = 0.25$  and  $V'(p_i) = 0.5$ , the first criterion leads to  $E''(p_i) = 0.206$ ,  $E''(p_4) = 0.314$ , while the second produces 0.131 and 0.416, respectively. Part of the difference may be due to neglect of  $\rho'_{ij}$ , but probably a significant part stems from inaccuracies of the first-order approximation to the expectations that appear in eq. 6.32; alternate approximations are therefore desirable.

*Incomplete data.* Statistical information is known to be fairly reliable only for magnitudes above threshold values that depend on the region considered, its level of activity, and the quality of local and nearby seismic instrumentation. Even incomplete statistical records may be significant when evaluating some seismicity parameters; their use has to be accompanied by estimates of detectability values, that is, of ratios of the numbers of events recorded to total numbers of events in given ranges (Esteva, 1970; Kaila and Narain, 1971).

## 6.5 REGIONAL SEISMICITY

The final goal of local seismicity assessment is the estimation of regional seismicity, that is, of probability distributions of intensities at given sites, and of probabilistic correlations among them. These functions are obtained by integrating the contributions of local seismicities of nearby sources, and hence their estimates reflect Bayesian uncertainties tied to those seismicities. In the following, regional seismicity will be expressed in terms of mean rates of exceedance of given intensities; more detailed probabilistic descriptions would entail adoption of specific hypotheses concerning space and time correlations of earthquake generation.

### 6.5.1 Intensity-recurrence curves

The case when uncertainty in seismicity parameters is neglected will be discussed first. Consider an elementary seismic source with volume  $dV$  and local seismicity  $\lambda(M)$  per unit volume, distant  $R$  from a site  $S$ , where intensity-recurrence functions are to be estimated. Every time that a magnitude  $M$  shock is generated at that source, the intensity at  $S$  equals:

$$Y = \epsilon Y_p = \epsilon b_1 \exp(b_2 M) g(R) \quad (6.33)$$

(see eqs. 6.4 and 6.5), where  $\epsilon$  is a random factor and  $Y$  and  $Y_p$  stand for actual and predicted intensities,  $b_1$  and  $b_2$  are given constants, and  $g(R)$  is a function of hypocentral distance. The probability that an earthquake originating at the source will have an intensity greater than  $y$  is equal to the probability that  $\epsilon Y_p > y$ . If  $Y_p$  is expressed in terms of  $M$  and randomness in  $\epsilon$  is accounted for, one obtains:

$$\nu(y) = \int_{\alpha_u}^{\alpha_L} \nu_p(y/u) f_\epsilon(u) du \quad (6.34)$$

where  $\nu$  and  $\nu_p$  are respectively mean rates at which actual and predicted intensities exceed given values,  $\alpha_U = y/y_U$ ,  $\alpha_L = y/y_L$ ,  $y_U$ , and  $y_L$  are the predicted intensities that correspond to  $M_U$  and  $M_L$ , and  $f_\epsilon$  the probability-density function of  $\epsilon$ . If eq. 6.33 is assumed to hold:

$$\nu_p(y) = K_0 + K_1 y^{-r_1} - K_2 y^{-r_2} \quad (6.35)$$

where:

$$K_i = [b_1 g(R)]^{r_i} A_i \lambda_i dV \quad (i = 0, 1, 2) \quad (6.36)$$

$$r_0 = 0, \quad r_1 = \beta/b_2, \quad r_2 = (\beta - \beta_1)/b_2 \quad (6.37)$$

Substitution of eq. 6.35 into 6.34, coupled with the assumption that  $\ln \epsilon$  is normally distributed with mean  $m$  and standard deviation  $\sigma$  leads to:

$$\nu(y) = c_0 K_0 + c_1 K_1 y^{-r_1} - c_2 K_2 y^{-r_2} \quad (6.38)$$

where:

$$c_i = \exp(Q_i) \left[ \Phi \left( \frac{\ln \alpha_L - u_i}{\sigma} \right) - \Phi \left( \frac{\ln \alpha_U - u_i}{\sigma} \right) \right] \quad (6.39)$$

$\Phi$  is the standard normal cumulative distribution function,  $Q_i = 1/2 \sigma^2 r_i^2 + m r_i$ , and  $u_i = m + \sigma^2 r_i$ . Similar expressions have been presented by Merz and Cornell (1973) for the special case of eq. 6.8 when  $\beta_1 \rightarrow \infty$  and for a quadratic form of the relation between magnitude and logarithm of exceedance rate. Closed-form solutions in terms of incomplete gamma functions are obtained when magnitudes are assumed to possess extreme type-III distributions (eq. 6.9).

Intensity-recurrence curves at given sites are obtained by integration of the contributions of all significant sources. Uncertainties in local seismicities can be handled by describing regional seismicity in terms of means and variances of  $\nu(y)$  and estimating these moments from eq. 6.34 and suitable first- and second-moment approximations. Influence of these uncertainties in design decisions has been discussed by Rosenblueth (in preparation).

- McGuire, R.K., 1974. Seismic structural response risk analysis incorporating peak response regressions on earthquake magnitude and distance. *Mass. Inst. Technol., Dep. Civ. Eng.*, R74-51.
- Merz, H.A. and Cornell, C.A., 1973. Seismic risk analysis based on a quadratic magnitude-frequency law. *Bull. Seismol. Soc. Am.*, 63 (6): 1999-2006.
- Milne, W.G. and Davenport, A.G., 1969. Earthquake probability. *Proc. 4th World Conf. Earthquake Eng., Santiago*.
- Mogi, K., 1962. Study of elastic shocks caused by the fracture of heterogeneous materials and its relations to earthquake phenomena. *Bull. Earthquake Res. Inst. Tokyo*, 40: 125-173.
- Molnar, P. and Sykes, L.R., 1969. Tectonics of the Caribbean and Middle America regions from focal mechanisms and seismicity. *Geol. Soc. Am. Bull.*, 80: 1639.
- Newark, N.M. and Rosenblueth, E., 1971. *Fundamentals of Earthquake Engineering*. Prentice-Hall, Englewood Cliffs.
- Omori, F., 1894. On the aftershocks of earthquakes. *J. Coll. Sci. Imp. Univ. Tokyo*, 7: 111-200.
- Parzen, E., 1962. *Stochastic Processes*. Holden Day, San Francisco.
- Petrushkevsky, B.A., 1966. *The Geological Fundamentals of Seismic Zoning*. Scientific Translation Service, order 5032, Ann Arbor, USA.
- Raiffa, H. and Schlaifer, R., 1968. *Applied Statistical Decision Theory*, MIT Press.
- Rosenblueth, E., 1964. Probabilistic design to resist earthquakes. *Am. Soc. Civ. Eng., J. Eng. Mech. Div.*, 90 (EM5): 189-249.
- Rosenblueth, E., 1969. Seismicity and earthquake simulation. *Rep. NSF-UCEER Conf. Earthquake Eng. Res., Pasadena*, pp. 47-64.
- Rosenblueth, E., 1975. *Point Estimates for Probability Moments*. National University of Mexico, Institute of Engineering, Mexico City.
- Rosenblueth, E., in preparation. Optimum design for infrequent disturbances.
- Rukos, E., 1974. *Análisis dinámico de la margen izquierda de Chicoasén*. National University of Mexico, Institute of Engineering, Mexico City.
- Salt, P.E., 1974. Seismic site response. *Bull. N. Z. Natl. Soc. Earthquake Eng.*, 7 (2): 63-77.
- Scholz, C.H., 1968. The frequency-magnitude relation of microfracturing and its relation to earthquakes. *Bull. Seismol. Soc. Am.*, 58: 399-417.
- Shlien, S. and Toksöz, M.N., 1970. A clustering model for earthquake occurrences. *Bull. Seismol. Soc. Am.*, 60 (6): 1765-1787.
- Singh, S.K., 1975. *Mexican Volcanic Belt: Some Comments on a Model Proposed by F. Mooser*. National University of Mexico, Institute of Engineering, Mexico City.
- Trifunac, M.D., 1973. Characterization of response spectra by parameters governing the gross nature of earthquake source mechanisms. *Proc. 5th World Conf. Earthquake Eng., Rome*, pp. 701-704.
- Tsuboi, C., 1958. Earthquake province. Domain of sympathetic seismic activities. *J. Phys. Earth.*, 6 (1): 35-49.
- Utsu, T., 1961. A statistical study on the occurrence of aftershocks. *Geophys. Mag., Tokyo*, 30: 521-605.
- Utsu, T., 1962. On the nature of three Alaska aftershock sequences of 1957 and 1958. *Bull. Seismol. Soc. Am.*, 52: 179-297.
- Veneziano, D. and Cornell, C.A., 1973. Earthquake models with spatial and temporal memory for engineering seismic risk analysis. *Mass. Inst. Technol., Dep. Civ. Eng.*
- Vere-Jones, D., 1970. Stochastic models for earthquake occurrence. *J. R. Stat. Soc.*, 32 (1): 1-45.
- Wallace, R.E., 1970. Earthquake recurrence intervals on the San Andreas Fault. *Geol. Soc. Am. Bull.*, 81: 2875-2890.
- Yegulalp, T.M. and Kuo, J.T., 1974. Statistical prediction of the occurrences of maximum magnitude earthquakes. *Bull. Seismol. Soc. Am.*, 64 (2): 393-414.



**DIVISION DE EDUCACION CONTINUA  
FACULTAD DE INGENIERIA U.N.A.M.**

ANALISIS DE RIESGO SISMICO

BAYESIAN ANALYSIS OF SEISMIC HAZARD: AN UPDATING OF  
CONCEPTS, CRITERIA AND MODELS

DR. LUIS ESTEVA MARABOTO

JULIO, 1985

BAYESIAN ANALYSIS OF SEISMIC HAZARD:  
AN UPDATING OF CONCEPTS, CRITERIA AND MODELS

L. Esteva\*

INTRODUCTION

Probabilistic models of hazard and risk constitute the basis for rational engineering decisions in the face of uncertainty. They provide a framework for the definition of quantitative criteria and rules for measuring safety, for balancing it with costs (both, initial and maintenance) and benefits, for making decisions relative to maximum tolerable risks and for stating policies with regards to desirable marginal expenditures aimed at protecting human lives.

Probabilities are usually deemed as properties of nature. According to this conception, evaluating them is a matter of observing a phenomenon a large number of times, quantifying the corresponding outcomes and plotting their histograms; if the number of observations is small, the probabilistic model itself is said to be uncertain or else the validity of a probabilistic formulation of the decision making process is denied. Consistently with the bayesian approach, the uncertainty about a probabilistic model of nature can be assimilated to the uncertainties intrinsic to that model\*\* and used together with the

---

\* Institute of Engineering, National University of Mexico.

\*\* What we understand by *intrinsic* here depends on the variables that we use to describe the model: a large portion of the uncertainty *intrinsic* to the generation of earthquakes along a fault described by its size and rate of slip would be dispelled if we had a time history of the state of stresses throughout a region including the fault. That part of the uncertainty would now be ascribed to the model adopted, while the remaining portion would be called *intrinsic*.

latter with the aim of making decisions based on what we know and how well we know it. Thus, probability is not a property of nature (or not only, at least), but of our uncertainty about its past, present and future. The probability distributions that we would determine on the exclusive basis of direct statistical observations are conventionally branded as *objective* probabilities, while the uncertainty that arises from the practical difficulties to collect enough *objective* information constitutes the realm of *subjective* probabilities.

The arguments favoring and detracting the validity of subjective probabilities for making of engineering decisions have been discussed in extenso elsewhere (1, 2). Those arguments support the adoption of a bayesian framework for assimilating information and making decisions for hazardous environments. Rather than repeating those arguments, this paper concentrates on recent developments and criteria which have resulted from the experience gained in practical applications. The following concepts are given special attention:

- a) Recent discoveries which contradict widely accepted assumptions about the shape of magnitude-recurrence curves.
- b) Improved criteria for processing statistical information from seismic sources similar to those of interest when trying to propose prior probability distributions of the forms and parameters of seismicity models.
- c) Study of simplified seismicity models represented by stochastic processes other than Poisson.

- d) Discussion of decision criteria related to safety levels and analysis of the implications of bayesian uncertainty.

#### MAGNITUDE-RECURRENCE CURVES

Statistical studies about the occurrence of earthquakes in large regions of the earth have led to frequency recurrence curves similar to those depicted in fig. 1, which will be represented in this paper by an expression of the following form:

$$\lambda(M) = \alpha e^{-\beta M} (1 - e^{\gamma(M - M_u)}), \quad M < M_u \quad (1)$$

$$= 0 \quad , \quad M \geq M_u$$

Here,  $\lambda(M)$  is the mean number of earthquakes with magnitude larger than  $M$  occurring per unit time in a given (unit) volume of the earth's crust within a given seismic source,  $M_u$  is the upper bound to the magnitudes that can be generated in the seismic source of interest, and  $\alpha$ ,  $\beta$ ,  $\gamma$  are parameters obtained by statistical curve fitting.  $\alpha$  and  $\beta$  determine  $\lambda$  for small values of  $M$ , and if the parenthesis in the second member of eq. 1 is taken as unity (i.e. if  $\gamma$  is taken as infinity), we obtain the well known Gutenberg-Richter exponential expression, which provides the possibility of estimating an upper bound to the expected rates of occurrence of large magnitude earthquakes on the basis of the statistical information about small magnitudes.

Careful studies recently developed show that at least in some regions eq. 1 does not hold. For instance, ref. 3 reports the results of analyzing the catalogues of NOAA Hypocentral Data File and of Preliminary Determination of Epicenters from 1963 to 1981 related to the Mexican

subduction zone ( $H \leq 65$  km; fig. 2). Figure 3 shows some results of the analysis for the Oaxaca portion of the subduction zone: solid squares represent numbers of earthquakes having body-wave magnitudes ( $m_b$ ) larger than given values, while the solid circles correspond to surface-wave magnitudes ( $M_s$ ); hollow squares and circles correspond to numbers of earthquakes in magnitude increments of 0.1. It is seen that, whereas magnitude-recurrence curves similar to those of fig. 1 are valid for body-wave magnitudes, the data of surface-wave magnitudes lead to a bulge in the range of large values of the latter; this bulge precludes the possibility of extrapolating magnitude-recurrence statistics from small to large magnitude intervals. Similar situations have been found elsewhere (5-7). When  $m_b$  values are used this effect is concealed because of saturation.

An explanation for the bulge in the  $\lambda(M_s)$  curve for the Oaxaca seismic province can be provided by a model similar to that proposed in ref. 4. The plate interface in the region can be subdivided into a few large simple fault zones (40 to 100 km in length), the lateral boundaries of which terminate in barriers imposed by geometry or by abrupt strength variations. Each fault ruptures cyclically over its entire dimension without giving rise to smaller events in the manner required by eq. 1. The aftershocks, the background seismicity, and the foreshocks, taken together, follow eq. 1, but the maximum magnitudes of these sequences are well below the main-shock magnitude.

For the purpose of seismic hazard analysis, the following equation is used to represent magnitude-recurrence curves as shown in fig. 4:

$$\lambda(M) = \alpha(e^{-\beta M} - e^{-\beta M_1}) + \delta(1 - e^{-\gamma(M - M_r)}) \quad (2)$$

The first and second terms in this equation represent the background and mainshock activities, respectively; each of them must be taken equal to zero if  $M \geq M_1$  or  $M \geq M_u$ , respectively. According to the observations,  $M$  can be substantially lower than  $M_u$ , but when trying to fit the parameters of eq. 2 to a set of data, practically equal results are obtained if  $M_1$  is made equal to  $M_u$ , thus reducing by one the number of parameters to be estimated.

For the purpose of bayesian estimation of the parameters of  $\lambda(M)$  in eqs. 1 and 2, it is necessary to propose prior joint probability distributions of those parameters. This is better achieved if a change of variables is performed, such that the new parameters can be taken as stochastically independent in their joint bayesian distribution, and if their marginal probability density functions can be easily related with indirect observations (by comparison with other seismic regions) or with quantitative models of the process of energy accumulation and release at seismic sources similar to that of interest.

When eq. 1 is applicable, the requirements in the foregoing paragraph are nearly satisfied if  $\lambda(M)$  is expressed in terms of  $E_0$ ,  $\beta$ ,  $\gamma$  and  $M_u$ , where  $E_0$  is the energy dissipated per unit time by generation of earthquakes with magnitude larger than a threshold magnitude  $M_0$ , and the other parameters were defined above. The prior marginal probability density functions of  $E_0$ ,  $\beta$  and  $M_u$  can be postulated independently; those of  $E_0$  and  $M_u$  may be based on both physical considerations and observations in similar regions, whereas that of  $\beta$  will in general be based exclusively on the latter type of concepts, and very little can be said a priori about  $\gamma$ . If the natural logarithm of the energy dissipated by a shock of magnitude  $M$  is expressed as  $A + BM$ , then  $E_0$  is given as follows:

$$E_0 = D_1 (e^{k_1 M_u} - e^{k_1 M_0}) + D_2 (e^{k_2 M_u} - e^{k_2 M_0}) \quad (3)$$

where  $D_1 = -\alpha\beta e^A k_1^{-1}$  ,  $D_2 = -\alpha(\gamma - \beta)e^A - \gamma M_u k_2^{-1}$

$$k_1 = B - \beta \quad , \quad k_2 = B - \beta + \gamma$$

From eq. 3,  $\alpha$  can be obtained as a function of  $E_0$ ,  $\beta$ ,  $\gamma$ ,  $M_u$ , for any specified  $M_0$ .

Similarly, if eq. 2 is applicable, and it is decided to take  $M_1 = M_u$ , it may be convenient to take as independent parameters  $E_0$ ,  $\mu$ ,  $\beta$ ,  $\gamma$  and  $M_u$ , where  $\mu$  is the ratio of the energies dissipated by the first and second processes considered by eq. 1. These energies are, respectively,

$$E_{01} = D_3 (e^{k_3 M_u} - e^{k_3 M_0}) \quad (4a)$$

$$E_{02} = D_4 (e^{k_4 M_u} - e^{k_4 M_0}) \quad (4b)$$

where  $D_3 = -\alpha\beta e^A k_3^{-1}$  ,  $D_4 = -\gamma\delta e^A - \gamma M_u k_4^{-1}$

$$k_3 = B - \beta \quad , \quad k_4 = B + \gamma$$

Given  $E_0$ ,  $\mu$ ,  $\beta$ ,  $\gamma$  and  $M_u$ , it is easy to obtain  $\alpha$  and  $\delta$ .

#### MULTI-PARAMETER BAYESIAN SEISMIC HAZARD ANALYSIS

The assessment of seismic hazard in practice is based as a rule on information about concepts of different nature, including, among others, statistical data about the activity of seismic sources and qualitative or quantitative descriptions of the geotectonic environment. The latter information is usually taken by geologists and geophysicists as the basis for making estimates of maximum magnitudes that can be generated at given sources. These estimates are obtained by extrapolation of magnitudes

observed in other regions with comparable geotectonic conditions; they include significant subjective components, such as selecting the sources from which extrapolations are made, or deciding about the maximum length of a particular fault that can rupture during the largest possible earthquake. The estimates mentioned tend systematically to err on the safe side, which is reasonable under minimax decision rules: risk to facilities should be kept to a minimum, regardless of cost.

If decisions are to account for a proper balance between costs, benefits and risk, the latter must be expressed in quantitative terms. This entails assigning quantitative measures to uncertainties tied to hazard estimates (maximum possible magnitude, rate of activity) based on geology, and defining probabilistic models capable of assimilating the mentioned uncertainties with those attached to predicting the seismic history on the basis of maximum possible magnitude and rate of activity. All this can be achieved through bayesian analysis, which is not a substitute for geotectonic and statistical information, but an efficient tool for processing available knowledge consistently. A well founded criticism which can be made to the subjective assignment of probabilities by individual experts to alternate hypotheses concerning the nature and parameters of seismotectonic processes is the possibility of arriving at prior bayesian distributions which do not reflect the levels of uncertainty implied by the available information. In fact, we even lack a criterion for judging about the consistency between that information and the assigned probabilities. Under some conditions, the analysis of statistical data for a number of seismotectonic regions similar to that of interest may serve to gage the consistency in question, as shown below. In other, we shall have to pursue consistency by a mechanism permitting the analysis by a group of experts of the subjective

probabilities assigned (including, of course, the basis for those assignments) by a number of independent experts or groups of experts.

In this section and in the following, we consider that the seismicity of a given source is defined by its activity rate  $\lambda(M)$ , and therefore we deal with the problem of making bayesian estimates of the parameters of  $\lambda(M)$  in eqs. 1 and 2. This section is devoted to the practical application of Bayes theorem, while next section concentrates on the formulation of the prior distribution of the mentioned parameters.

Let  $\epsilon$  be the vector of parameters that determine  $\lambda(M)$  (for instance, if we work with eq. 1,  $\epsilon^T = [\alpha \ \beta \ \gamma \ M_u]$ ). If  $H$  represents the observed seismic history, Bayes theorem states that

$$f_{\epsilon}''(e|H) = K f_{\epsilon}'(e) p(H|e) \quad (5)$$

where  $f_{\epsilon}'$  and  $f_{\epsilon}''$  are respectively prior and posterior joint bayesian probability density functions of  $\epsilon$ ,  $p(H|e)$  is the likelihood of  $H$  given  $e$  and  $K$  is a normalizing constant such that the multiple integral of  $f_{\epsilon}''(e|H)$  over the region of definition of  $\epsilon$  equals unity.

In general,  $H$  will consist of the magnitudes and times ( $M_i, t_i; i = 1, \dots, N$ ) of earthquakes occurred during time interval  $t$ . If  $H$  is an observed realization of the process of occurrence of earthquakes above the threshold value  $M_0$ , and it is assumed to be a Poisson process with all magnitudes identically distributed and mutually independent, then

$$p(H|e) \propto e^{-\lambda(M_0)t} \prod_{i=1}^N (-\lambda'(M_i)) \quad (6)$$

where  $\lambda' = d\lambda/dM$ . An equation similar to eq. 6 is given in ref. 1 for the case in which seismicity is expressed by the rate of exceedance of different intensity values at a given site.

The determination of  $K$  in eq. 5 implies carrying out a multifold integration, unless  $f_e'$  can be factorized. Otherwise, in practical applications we may have to recourse to numerical integration, Monte Carlo simulation or discrete distribution techniques (8). In some cases, and provided the conditional probability density function of magnitudes given the occurrence of a random event is independent of time and previous history, it may prove advantageous to split the parameter estimation process in two steps: first, estimating the parameters of the conditional distribution of  $M$ , and second, estimating a parameter proportional to the energy dissipated per unit time. If eq. 1 is adopted, this is tantamount to obtaining initially the joint bayesian p.d.f. of  $\beta$ ,  $\gamma$  and  $M_u$ , and then the conditional p.d.f. of  $\alpha$  for given values of these parameters. For the first part, and starting for instance from eq. 1, one obtains that the conditional p.d.f. of  $M$  given that an earthquake occurs is as follows:

$$f_M(m) = -Ae^{-\beta m} [\beta + (\gamma - \beta)e^{-\gamma(M_u - m)}] \quad (7)$$

where  $A = e^{\beta M_0} [1 - e^{-\gamma(M_u - M_0)}]^{-1}$ . The likelihood function to be used in eq. 5 is given by eq. 8.

$$p(H|e) \propto \prod_{i=1}^N f_M(m_i; \beta, \gamma, M_u) \quad (8)$$

For the purpose of updating the conditional distribution of  $\alpha$  for given values of  $\beta$ ,  $\gamma$  and  $M_u$ , we can use as statistical information the number of earthquakes with magnitudes greater than the threshold value  $M$  occurred during time

interval  $t$ . If we substitute  $M_u$  for  $M$  in eq. 1 and then express the latter in the form  $\lambda(M_0) = \alpha G(\beta, \gamma, M_u)$ , the conditional distribution of  $\alpha$  can be readily obtained from that of  $\lambda(M_0)$ : updating of the latter distribution on the basis of the statistical information is straightforward (9).

The criterion described by eqs. 5-8 is applied in the following to a fictitious example represented by a simulated record of earthquake magnitudes. A hypothetical source with  $f_M(m)$  given by eq. 7 with  $\beta = 2$ ,  $\gamma = 3$ ,  $M_0 = 5.5$ ,  $M_u = 7.5$  was assumed and a set of 150 stochastically independent magnitude values was simulated from that p.d.f. In order to study the variability of the seismicity estimates with the sample size, Bayes theorem was applied to determine the joint distribution of  $\beta$ ,  $\gamma$  and  $M_u$ , considering successively the complete set of simulated magnitudes and two subsets of sizes 50 and 100. These simulated magnitude values are shown in a cumulative magnitude-recurrence plot in fig. 7 together with the theoretical  $\lambda(M)$  curve from which the simulated record was obtained. The bayesian probability distributions of  $\beta$ ,  $\gamma$  and  $M_u$  were supposed to be discretized at all combinations of the following feasible values of each parameter:  $\beta = 1.8, 2.6$ ;  $\gamma = 0.5, 2, 4$ ;  $M_u = 7.3, 8$ . The feasible values assumed for  $\gamma$  were obtained by inspection from the simulated records of fig. 7; those for  $\beta$  were arbitrarily adopted, and the value  $M_u = 7.3$  was proposed from the condition that it should have to be greater than the maximum simulated value, i.e., 7.18. Thus, the domain of the multiparameter bayesian distribution considered is that of the twelve cases included in Table 1. The prior bayesian probabilities are 1/12 for each case. The posterior distributions derived from application of eqs. 5-8 to the three sample sizes ( $N = 50, 100, 150$ ) are shown in the same table. Table 2

summarizes the means and variation coefficients of  $\beta$ ,  $\gamma$ ,  $M_u$  as well as of the complementary cumulative magnitude distributions,  $\bar{F}_M(m)$ . The corresponding deterministic values are shown for comparison in the last column.

Although the means of all parameters and functions seem to approach systematically their deterministic values, significant random deviations disturb those trends. The deviations corresponding to  $\beta$ ,  $\gamma$  and  $M_u$  are more pronounced than those affecting  $\bar{F}_M(m)$ . Similar statements can be made about the systematic decrease in the variation coefficients with increasing sample size. Further analysis of fig. 7 and of the results of similar cases shows that adoption of discretized distributions of the seismicity parameters must be done with caution, considering, among others, the following problems.

- a) In some cases the statistical information may warrant posterior probability distributions having a pronounced peak in the vicinity of one or more parameters (for instance, those cases in which  $\beta$  is very well defined). Such a peak cannot be reproduced unless the discrete mesh adopted a priori includes one or more points sufficiently close to its maximum; otherwise, the posterior distribution will overestimate uncertainty with respect to the mentioned parameters.
- b) In regions where the slopes of the likelihood function of the seismicity parameters given the sample are large the posterior bayesian probability masses may concentrate excessively on one or few points, failing to represent the uncertainty determined by the continuous posterior distribution corresponding to the rigorous solution.

Bayesian analysis of seismicity under assumptions more general than Poisson process is a topic practically unexplored, in spite of the significantly more sophisticated models which have been developed (10-12), capable of

representing effects as complex and as relevant as systematic variation of hazard with time, aftershock sequences and more general types of clustering. This omission results from the complexities arising from having to cope simultaneously with too many parameters as well as from the difficulties involved in obtaining likelihood functions.

If fore- and aftershocks are ignored, one can think of adopting renewal process models other than Poisson.

Reference 9 deals with the bayesian analysis of a renewal process with inter-arrival times ( $T$ ) distributed in accordance with a gamma function:

$$f_T(t) = \frac{\nu}{(k-1)!} (\nu t)^{k-1} e^{-\nu t} \quad (9)$$

where  $\nu$  and  $k$  are the parameters to be estimated. Only very simple cases are covered, assuming  $k$  known. It is obtained, for instance, that if the prior p.d.f. of  $\nu$  is gamma with parameters  $\rho$  and  $\mu$ , and if  $H$  is expressed as the time  $T_n$  elapsed between  $n+1$  consecutive events, then the posterior p.d.f. of  $\nu$  is also gamma, now with parameters  $\rho + nk$  and  $\mu + t_n$ . In the latter case, only a portion of the relevant statistical information is used. In most cases, specially if seismic activity has been low during the observation interval, significant information is provided by the durations of the intervals elapsed from the initiation of observations to the first of the  $n+1$  events considered and from the last of those events to the end of the observation interval. Here, the posterior p.d.f. of  $\nu$  has to be obtained by application of eq. 5 with the following likelihood function:

$$p\{H|e\} \propto f_{T_1}(t_1) \cdot f_{T_{n-1}}(t_n - t_1) \cdot [1 - F_T(t_f - t_n)] \quad (10)$$

The first factor in the second member of this equation is the probability density function of the waiting time to the first (delayed) event.  $T_1$  can be taken as the excess life in a renewal process at an arbitrary value of time that tends to infinity and its p.d.f. can be obtained as  $\frac{1}{\bar{T}}|1 - F_T(t)|$ , where  $T$  is the random time between consecutive events,  $F_T$  is its cumulative probability distribution function and  $\bar{T}$  is its expected value (13). The second factor is the probability density function of the time between events 1 and  $n$ , evaluated at  $t_n - t_1$ , and  $t_f$  in the last factor is the end of the observation interval. For the particular case where the statistical record reports no events during the time interval  $(0, t_f)$ , the second member of eq. 10 must be replaced with  $p\{T_1 \geq t_f\}$ . This particular case is typical of seismic gaps, and is studied in ref. 9. The results show that the posterior expected value of  $T_1$ , the waiting time to the first event, conditional to no occurrence of events up to instant  $t$  may start decreasing as  $t$  grows, in accordance with the behaviour of ordinary renewal processes; however, as time goes on and no events occur, the statistical evidence makes the estimated risk to decrease, and therefore the conditional expected value of  $T_1$  to increase with  $t$ . The smaller the value of  $k$  in eq. 9, the faster the decreasing of risk estimates.

A summary is presented in ref. 2 of the results of an analysis of the influence of  $k$  on the ratio of the present value of expected failure costs for gamma and Poisson processes. The structures considered have deterministic properties. Because the coefficient of variation of the waiting time between events is inversely proportional to the square root of  $k$ , the greater  $k$  the lesser the uncertainty about the waiting time to next event. The ratio of expected failure costs for gamma and Poisson processes is smaller than unity for small values of the

time elapsed since last event and grows with that time. The greater  $k$  the more pronounced are these variations.

A likelihood function as given by eq. 10 is meaningful if we define as *events* all earthquakes with magnitudes larger than a given value; if we assume that the distribution of each magnitude is independent of time and history (renewal process with independent random selection), bayesian estimates of risk can be made on the basis of eq. 8 together with application of eq. 10 for all earthquakes with magnitudes larger than  $M_0$ ; but the assumption of independent selection is inconsistent with the concept that the times required for the accumulation of the energy amount necessary to produce shocks of given magnitudes should grow with those magnitudes, and that the time elapsed since the occurrence of a small magnitude earthquake should not affect significantly the energy available for large shocks. If we could filter out fore- and aftershocks (which is much more easily said than done), it would be reasonable to conceive the occurrence of earthquakes above a given magnitude  $M_0$  as a renewal process with parameter  $k$  dependent on  $M_0$ . A low value of  $M_0$  considers the occurrence of many small and a few large earthquakes; a random event would very unlikely give place to a significant change in the energy available for future shocks, and the assumption of Poisson process ( $k = 1$ ) would be warranted. For large  $M_0$  values this assumption is untenable; therefore, we arrive at the problem of assimilating a set of statistical data relative to different magnitude ranges, and using it as an ensemble for estimating the parameters of a complex process, which cannot be represented as a renewal process with independent random selection. The problem is solved if we relate the hazard at any instant with the previous history of energy dissipation. For this purpose we adopt an extended version of a seismicity model proposed in ref. 10.

Suppose first that the seismic record does not contain any fore- or aftershock. Represent that record by a Markov process with system states specified by the values of the hazard function  $\lambda(t)$ , where  $\lambda(t)dt$  is the conditional probability that there will be one earthquake (of any magnitude) during time interval  $t, t + dt$  given that none has occurred. It is assumed that the distribution of the energy (or magnitude) of an earthquake is independent of history; it is also assumed that  $\lambda(t)$  decreases sharply every time there is an earthquake and that the size of the discontinuity can be deterministically related to the energy of the earthquake producing it, in terms of parameters to be estimated.

A typical sample of the process (where, of course, the values of  $\lambda$  are non-observable variables) is shown in fig. 5. If  $\lambda$  is deterministically related to the strain energy stored in the system, and if this energy increases at constant rate during time intervals between shocks, it follows that all segments of the  $\lambda(t)$  curve can be obtained by translation of the initial hazard function. Also, the size of each discontinuity can be determined from the corresponding earthquake energy by considering that the time origin of the  $\lambda(t)$  curve is translated an amount equal to the length of time required to store the mentioned energy:

$$\tau_{k+1} - \tau_k = E_{k+1}/\omega$$

Here,  $E_k$  is the energy liberated by the  $k$ -th shock and  $\omega$  is the rate of energy accumulation. The latter is one of the parameters to be estimated.

Before talking about the problem of bayesian estimation of parameters, let us discuss a possible family of hazard functions and their application when trying to relate  $E$  with jumps in  $\lambda$ . A particular case of the Weibull distribution corresponds to the following p.d.f. (13):

$$f(t) = \frac{k}{v} \left(\frac{t}{v}\right)^{k-1} \exp\left(-\left(\frac{t}{v}\right)^k\right) \quad \begin{array}{l} v \geq 0 \\ k \geq 1 \\ t \geq 0 \end{array} \quad (11)$$

If the waiting time between earthquakes is assumed to possess this distribution, the hazard function is:

$$\lambda(t) = \frac{k}{v} \left(\frac{t}{v}\right)^{k-1} \quad (12)$$

If  $k = 1$ , one has Poisson process with  $\lambda(t) = 1/v$ . For other values of  $k$  one gets the types of hazard function shown in fig. 6.

Let us take for simplicity  $A = k/v^k$ ,  $n = k - 1$ . Then  $\lambda = At^n$ . Immediately prior to the  $(k+1)$ th shock, the hazard function is  $\lambda'_k = At^n$ , and just after a shock with energy  $E_k$  it is  $\lambda_{k+1} = A(t - E/w)^n$ . Thus,  $\lambda_{k+1}$  can be expressed in terms of  $\lambda'_k$ :

$$\lambda_{k+1} = A \left[ \left( \frac{\lambda'_k}{A} \right)^{1/n} - \frac{E_{k+1}}{w} \right]^n$$

Suppose  $\lambda_0$ ,  $A$  and  $n$  were known. Then time history  $(t_1, E_1; t_2, E_2; \dots t_n, E_n)$  would determine  $\lambda(t)$  for any  $t$ . The only function we need in order to complete the model is the conditional p.d.f. of energy for any shock. This may have for instance a form consistent with eq. 1. It will be represented as  $f_E(e; \epsilon)$ , where  $\epsilon$  is a vector of parameters to be estimated.

If eq. 1 applies,  $\epsilon^T = \{\alpha \ \beta \ \gamma \ M_u\}$ . Given  $B^T = \{\lambda_0 \ A \ \mu \ \epsilon^T \ \omega\}$  (the vector of parameters to be estimated) one can obtain their likelihood. Once this is done, the problem of bayesian updating of the proposed seismicity model is solved (at least in theory). The mentioned likelihood is obtained as follows:

$$L(t_1, t_2, \dots, t_n; e_1, e_2, \dots, e_n | \tau_0, A, \mu, \epsilon, \omega) = \prod_{j=1}^n f_T(t_j - \tau_{j-1}) f_E(e_j) (1 - F_T(t_f - \tau_n))$$

where  $t_j$  is the time of occurrence of the  $j$ -th earthquake,  $t_f$  is the end of the observation interval,  $f_T$  is the probability density function of the waiting time from the fictitious time origin of the hazard function (see fig. 5),  $f_E$  the p.d.f. of the energy liberated by a randomly selected earthquake,  $e_j$  the energy liberated by the  $j$ -th earthquake; because  $\tau_j$  is a deterministic function of  $\tau_0, A, \mu$ , and all observed values  $t_k, e_k, k = 1, \dots, n$ , the second member in the last equation is a function of the variables in vector  $B$  defined above.

#### ON THE CONSISTENCY OF PRIOR BAYESIAN DISTRIBUTIONS OF SEISMICITY PARAMETERS

The prior distribution of the seismicity parameters of a potential seismic source is an efficient description of the estimates that a team of experts can make concerning those parameters before looking at the local seismic record. That distribution should account for all available knowledge about the local geologic structures and tectonic processes, as well as for the seismicity patterns observed at other regions with similar geologic and tectonic characteristics. Also, that distribution summarizes the extrapolations that a capable team of experts in the geophysical sciences can make on the basis

of observations throughout the globe; therefore, it must reflect the degree of uncertainty tied to those extrapolations. A simple way of expressing that uncertainty is by formulating a comprehensive and mutually exclusive set of hypotheses about the possible models of the seismic process at a source and assigning to each hypothesis a weight, taken by definition as proportional to the bayesian probability of its being the correct representation of the natural process (in reality, due to the fact that the set of hypotheses does not cover the universe of all possible models, we understand by "the correct representation of the natural process" that model within the set which best represents nature). But no uniquely determined criteria have been proposed capable of transforming information other than direct statistical data into prior bayesian probability distributions: no doubt, subjective probabilities can be used as descriptors of degrees of belief, and then used for decision making under uncertain risk conditions, but the decision maker faced with stating subjective probability distributions reflecting his beliefs does not know what a subjective probability should measure, what consistency rules should it satisfy and how well founded are his degrees of belief. This kind of problems requires immediate attention by those interested in decision making on the basis of quantitative risk information. A partial solution can be provided by having groups of experts assigning, evaluating and correcting probability values and calibrating the final decisions with those that would be obtained by a rational analysis of the mentioned probabilities. In some cases the adequacy of given probability distributions of seismicity parameters assigned on the basis of the information available for a number of *comparable* regions can be judged by contrasting them with the statistics observed on those regions. The concepts and criteria which may be used for such evaluations are exemplified in the sequel.

Take a set of potential seismic sources corresponding to regions with similar geologic and tectonic characteristics. They may differ in some quantitative aspects, such as size of faults, intensity of faulting (cross area of faults per square kilometer of ground surface) or rate of crust deformation or fault slip; they may, instead, be undistinguishable as far as the mentioned features are concerned. In the first case the statistical seismicity information can be used to estimate the parameters of a predictive model of expected seismic activity in sources of the type considered in terms of quantitative measures of the geologic and tectonic structures and processes. In the second case all the regions may be considered to be samples obtained from a population characterized by the probability distribution of the seismicity parameters of a randomly selected region. This distribution, if known, might be taken as the prior bayesian probability distribution of the mentioned parameter for a new region of interest, assumed to belong to the same population. Thus, the regions included in the original set shall be called *auxiliary regions* and the collective statistical information available for them shall be used as the basis for stating a prior probability distribution for the seismicity parameters of the new region. The statistical information for the latter should then be combined with the mentioned prior probability distribution in order to obtain the corresponding posterior distribution through use of eqs. 5-8.

Returning to the set of auxiliary regions, let  $\epsilon_i$ ,  $i = 1, \dots, N$ , be the vector of parameters of an expression similar to the second member of eqs. 1 or 2, that is, of a given magnitude-recurrence expression,  $\lambda_M(m; \epsilon_i)$ , valid for the  $i$ -th auxiliary region. Let  $f_{\epsilon|u}(e|m)$  be the bayesian p.d.f. of vector  $e$  for a randomly selected

region, and  $\mu$  the parameters determining that p.d.f. Because  $\mu$  is uncertain we have to solve the problem of obtaining its bayesian probability distribution  $f_{\mu}(m)$ ; for this purpose we shall recourse to the observed seismic history  $h$  at all the regions. If this information were sufficient to permit obtaining accurate estimates of  $\varepsilon_i$  for  $i = 1, \dots, N$ , the bayesian estimation of  $f_{\mu}(m)$  would be formulated as follows:

$$f_{\mu|\varepsilon}''(m|e) = K_1 f_{\mu}'(m) f_{\varepsilon|\mu}(e|m) \quad (15)$$

Here,  $f_{\varepsilon|\mu}(e|m)$  is the likelihood function of  $\mu = m$  conditioned to  $\varepsilon = e$ ,  $K_1$  is a normalizing constant and  $f_{\mu}'$ ,  $f_{\mu|\varepsilon}''$  are respectively prior and posterior bayesian density functions of  $\mu$ . As a rule,  $h$  does not suffice for making sufficiently accurate estimates of  $\varepsilon$ . In other words,  $\varepsilon$  is not observable and therefore eq. 15 cannot be applied directly. We must instead try to obtain a posterior distribution of  $\mu$  conditioned to the observed seismic history:  $H = h$ . This is expressed as follows:

$$f_{\mu|H}''(m|h) = K_2 f_{\mu}'(m) p_{H|\mu}(h|m) \quad (16)$$

where  $K_2$  is a normalizing constant,  $f_{\mu}'$  and  $f_{\mu|H}''$  are prior and posterior distributions and, in accordance with the rules of conditional probabilities,

$$p_{H|\mu}(h|m) = \int p_{H|\varepsilon}(h|e) f_{\varepsilon|\mu}(e|m) de \quad (17)$$

The marginal posterior p.d.f. of  $\varepsilon$  for a randomly selected region is, therefore,

$$f_{\varepsilon|H}''(e|h) = \int f_{\varepsilon|\mu}(e|m) f_{\mu|H}''(m|h) dm \quad (18)$$

The latter p.d.f. would be taken as the prior p.d.f. of  $\epsilon$  for a new seismic region assumed to belong to the same population as the original set.

The team of experts analyzing the characteristics of the different regions may assume a priori a certain degree of correlation among vectors  $\epsilon_i$  and  $\epsilon_j$ . This assumption will be reflected in  $f_{\epsilon|\mu}(e|m)$ . Thus, if  $\epsilon_i$  and  $\epsilon_j$  are independent,

$$f_{\epsilon|\mu}(e|m) = \prod_{i=1}^N f_{\epsilon_i|\mu}(e_i|m) \quad (19)$$

while in a more general case the correlation matrix may form part of  $\mu$ . Either for practical reasons or on the grounds of geophysical similarity, it may be justified to assume at least some parameters of the correlation matrix. In the extreme case when all regions are so similar that they are assumed to possess the same  $\epsilon$ , we obtain the condition of perfect correlation, which is tantamount to taking together all the regions and all the statistical information and using it as a single block in the estimation of the vector  $\epsilon$  valid throughout all regions.

The use of eqs. 15-18 is illustrated in the following for a hypothetical set of two regions. For simplicity, it is assumed that we are interested only in the rate of activity above a given threshold value, and therefore vectors  $\epsilon_i$  will have only one component each, the corresponding rate  $\lambda_i$ ,  $i = 1, 2$ . The complete set of seismicity parameters is therefore  $\epsilon^T = [\lambda_1 \lambda_2]$ . The observed history is described by  $N_i$  and  $t_i$ ,  $i = 1, 2$ , the number of events observed and the duration of the observation interval for each region. The following values are assumed here:

$N_1 = 3$ ,  $t_1 = 50$  years,  $N_2 = 3$ ,  $t_2 = 80$  years; the corresponding estimates of  $\lambda_i$  are therefore 0.06 and 0.0375, respectively.

$\lambda_1$  and  $\lambda_2$  are assumed independent, with their bayesian distributions discretized at three points. The vector  $\mu$  of parameters of the bayesian distributions of  $\lambda_1$  and  $\lambda_2$  is  $\mu^T = [E(\lambda_1), E(\lambda_2), V(\lambda_1), V(\lambda_2)]$ , where  $E(\cdot)$  denotes expectation and  $V(\cdot)$  variation coefficient.

The distribution of  $\mu$  is discretized in the following values:  $E(\lambda_i) = 0.02, 0.08$ ;  $V(\lambda_i) = 0.2, 0.6$ ;  $i = 1, 2$ . The prior distribution of  $\mu$  assigns equal values to each of the possible combinations of these parameter values. Table 3 summarizes the probability mass function of  $\epsilon_j$  for each  $E(\lambda_i)$  and  $V(\lambda_i)$ .

The likelihood functions for each  $\mu = m$  are obtained as follows:

$$p_{H|\mu}(h|m) = \sum_{ij} p(h|\ell_i, \ell_j) p\{\lambda_1 = \ell_i, \lambda_2 = \ell_j|m\}$$

and because the prior distribution of  $\mu$  is uniform, the posterior distribution is proportional to the likelihood function:

$m: \bar{\lambda}_i, V_{\lambda_i}$	$p(h m)$	$p''(m h)$
0.02, 0.2	$8.209 \times 10^{-3}$	0.217
0.02, 0.6	$6.435 \times 10^{-3}$	0.170
0.08, 0.2	$1.269 \times 10^{-2}$	0.363
0.08, 0.6	$9.416 \times 10^{-3}$	0.249

The marginal probability mass function of  $\epsilon$  is, therefore,

$$p''_{\lambda_i | H}(\ell_i | h) = \sum_j p_{\lambda_i | \nu}(\ell_i | m_j) p''_{\nu | H}(m_j | h)$$

which leads to:

$\ell_i$	$p''(\ell_i   h)$	
0.01	0.0399	$E''(\lambda_i) = 0.0567$
0.02	0.4200	
0.08	0.4799	$V''(\lambda_i) = 0.633$
0.16	0.0595	

The foregoing analysis assumed  $\lambda_1$  independent from  $\lambda_2$ . An alternate assumption might have considered  $\lambda_i = r_i \lambda$ , with  $r_i$  and  $\lambda$  independent and the distribution of  $r_i$  prescribed. Considering this case, taking the distribution of  $r_i$  as discretized at points 0.7 and 1.3 with equal probabilities, and the prior distribution of  $\lambda$  as discretized at points 0.02 and 0.08, also with equal probabilities, we obtain the following posterior distribution of  $\lambda$ :  $p_{\lambda}(0.02) = 0.332$ ,  $p_{\lambda}(0.08) = 0.668$ . From this distribution and that of  $r_i$  we obtain for  $\lambda$  the following posterior distribution:

$\ell_i$	$p_{\lambda}(\ell_i)$	
0.014	0.166	$E''(\lambda_i) = 0.06$
0.026	0.166	$V''(\lambda_i) = 0.576$
0.056	0.332	
0.104	0.332	

If  $r_i$  is taken deterministically equal to unity,  $E''(\lambda_i) = 0.057$  and  $V''(\lambda_i) = 0.503$ .

pages 24 to 30  
are to be replaced by a  
new version

25.2.18

and informal criteria will improve our knowledge and understanding of the scales of values and decision rules that best serve the interests and goals of the human groups to be affected by the decisions under discussion.

#### REFERENCES

1. Esteva, L., "Uncertainty, reliability and decisions in structural engineering", *ICOSSAR 3*, Trondheim (1981).
2. Esteva, L., and Chávez, M., "Analysis of uncertainty on seismic risk estimates", *Proc. Third International Earthquake Microzonation Conference*, Seattle (1982).
3. Singh, S.K., Rodríguez, M., and Esteva, L., "Statistics of small earthquakes along the Mexican subduction zone", *Institute of Geophysics, National University of Mexico* (1983), submitted for publication to *Bulletin of the Seismological Society of America*.
4. Wesnousky, S., Scholz, C.H., Shimazaki, K., and Matsuda, T., "Earthquake frequency distribution and the mechanics of faulting" (1983), submitted for publication to *Journal of Geophysical Research*.
5. Utsu, T., "Aftershocks and earthquake statistics, III", *Journal of the Faculty of Science, Hokkaido University, Series VII*, 3, 379-442 (1971).
6. Purcaru, G., "A new magnitude-frequency relation for earthquakes and a classification of relation types", *Geophysical Journal of the Royal Astronomical Society*, 42, 61-79 (1975).

7. Lahr, J.C., and Stephens, C.D., "Alaska seismic zone: possible example of non-linear magnitude distribution for faults", *Earthquake notes*, 53, 66 (1982).
8. Rosenblueth, E., "Point estimates for probability moments", *Proc. National Academy of Sciences, USA*, 72, 10, 3812-14 (1975).
9. Esteva, L., "Seismicity", Chapter 6 of *Seismic risk and engineering decisions*, edited by C. Lomnitz and E. Rosenblueth, Elsevier, Amsterdam (1976).
10. Knopolf, L., "A stochastic model for the occurrence of main-sequence earthquakes", *Reviews of Geophysics and Space Physics*, 9, 1 (1971).
11. Vere Jones, D., "Stochastic models for earthquake occurrences", *Journal of the Royal Statistical Society*, 32, 1-62 (1970).
12. Vere Jones, D., "Stochastic models for earthquake sequences", *Geophysical Journal of the Royal Astronomical Society*, 21, 323-335 (1975).
13. Parzen, E., "*Stochastic processes*", Holden Day, San Francisco (1964).
14. Rosenblueth, E., "Optimum design for infrequent disturbances", *Journal of the Structural Division, ASCE*, 102, ST9 (1976).
15. Starr, C., "Social benefit vs. technological risk", *Science*, 165 (1969).

16. Okrent, D., "A general evaluation approach to risk-benefit for large technological systems and its application to nuclear power", University of California, Los Angeles (1977).
17. Paté, M.E., "Public policy in earthquake effects mitigation: earthquake engineering and earthquake prediction", Technical report 30, The John A. Blume Earthquake Engineering Center, Stanford University (1978).
18. Grandori, G. and Benedetti, D., "On the choice of the acceptable seismic risk", *Earthquake Engineering and Structural Dynamics*, 2, 1, 3-10 (1973).
19. Raiffa, H., and Schlaiffer, R., "Applied Statistical Decision Theory", MIT Press, Cambridge, Mass. (1968).

TABLE 1. Posterior bayesian probabilities for three sample sizes

case	Assumption			Probabilities		
	$\beta$	$\gamma$	$\mu$	$N=50$	100	150
1	1.8	0.5	7.3	0.0407	0.0363	0.2550
2		✓	8.0	0.0083	0.0021	0.0154
3		2	7.3	0.0039	0.0008	0.0266
4		✓	8.0	0.0010	0	0.0004
5		4	7.3	0.0013	0.0001	0.0052
6		✓	8.0	0.0007	0	0.0001
7	2.6	0.5	7.3	0.2037	0.1331	0.0015
8		✓	8.0	0.1767	0.1539	0.0141
9		2	7.3	0.1820	0.2439	0.1205
10		✓	8.0	0.1207	0.1179	0.0680
11		4	7.3	0.1529	0.2138	0.4297
12		✓	8.0	0.1081	0.0979	0.0635

TABLE 2. Means and coefficients of variation of seismicity parameters and of complementary cumulative magnitude distributions

Parameter X	E(X)			V(X)			Deterministic values
	N = 50	100	150	N = 50	100	150	
B	2.56	2.57	2.36	0.072	0.062	0.156	2
$\gamma$	1.88	2.14	2.57	0.752	0.656	0.592	3
$M_U$	7.59	7.56	7.41	0.045	0.047	0.035	7.5
$\bar{F}_M(6.0)$	0.257	0.259	0.288	0.110	0.088	0.113	0.36
$\bar{F}_M(6.5)$	0.062	0.063	0.078	0.253	0.194	0.211	0.13
$\bar{F}_M(6.75)$	0.029	0.030	0.038	0.346	0.261	0.257	0.072
$\bar{F}_M(7.0)$	0.012	0.012	0.016	0.477	0.377	0.335	0.038

TABLE 3. Discrete bayesian distributions of  $\lambda_i$  for each  $E(\lambda_i)$  and  $V(\lambda_i)$

$E(\lambda_i)$	$V(\lambda_i)$	$\lambda_i$			
		0.01	0.02	0.08	0.16
0.02	0.2	0.0229	0.973	0.0038	0
	0.6	0.2057	0.760	0.0343	0
0.08	0.2	0	0.0305	0.947	0.0229
	0.6	0	0.2743	0.520	0.2057

TABLE 4. Values of  $p_F/\tilde{p}_F$ 

$E(v)t$	$\rho$				
	0.1	0.3	1	3	10
0.001	0.9950	0.9983	0.9995	0.9998	1.0
0.01	0.9533	0.9838	0.9951	0.9984	0.9995
0.1	0.7037	0.8689	0.9553	0.9845	0.9953
1.0	0.3373	0.5630	0.7910	0.9146	0.9721

TABLE 5. Values of  $E(v(y_D)) / E(v(y_{D1}))$  for  $\kappa = 2$ 

A	n	$\eta_1$						
		1	0.5	0.2	0.1	0.05	0.02	0.01
$10^{-7}$	2	1.0	1.0	1.0	0.999	0.990	0.799	0.465
	4	1.0	2.0	0.977	0.589	0.235	0.0631	0.0234
$10^{-2}$	2	0.994	0.919	0.518	0.257	0.120	0.0426	0.0193
	4	0.994	0.713	0.218	0.0808	0.0296	0.0078	0.0029

TABLE 6. Values of  $E(v(y_D)) / E(v(y_{D1}))$  and  $n/\eta_1$  for  
 $c = 0.01$ ,  $n = 2$ ,  $\kappa = 2$ ,  $\eta_1 = 0.01$ 

$v_k$	0	0.10	0.20	0.30	0.50	0.70	1.0
$E(v(y_D))/E(v(y_{D1}))$	0.191	0.189	0.185	0.178	0.159	0.137	0.107
$n/\eta_1$	2.288	2.300	2.325	2.370	2.508	2.701	3.057

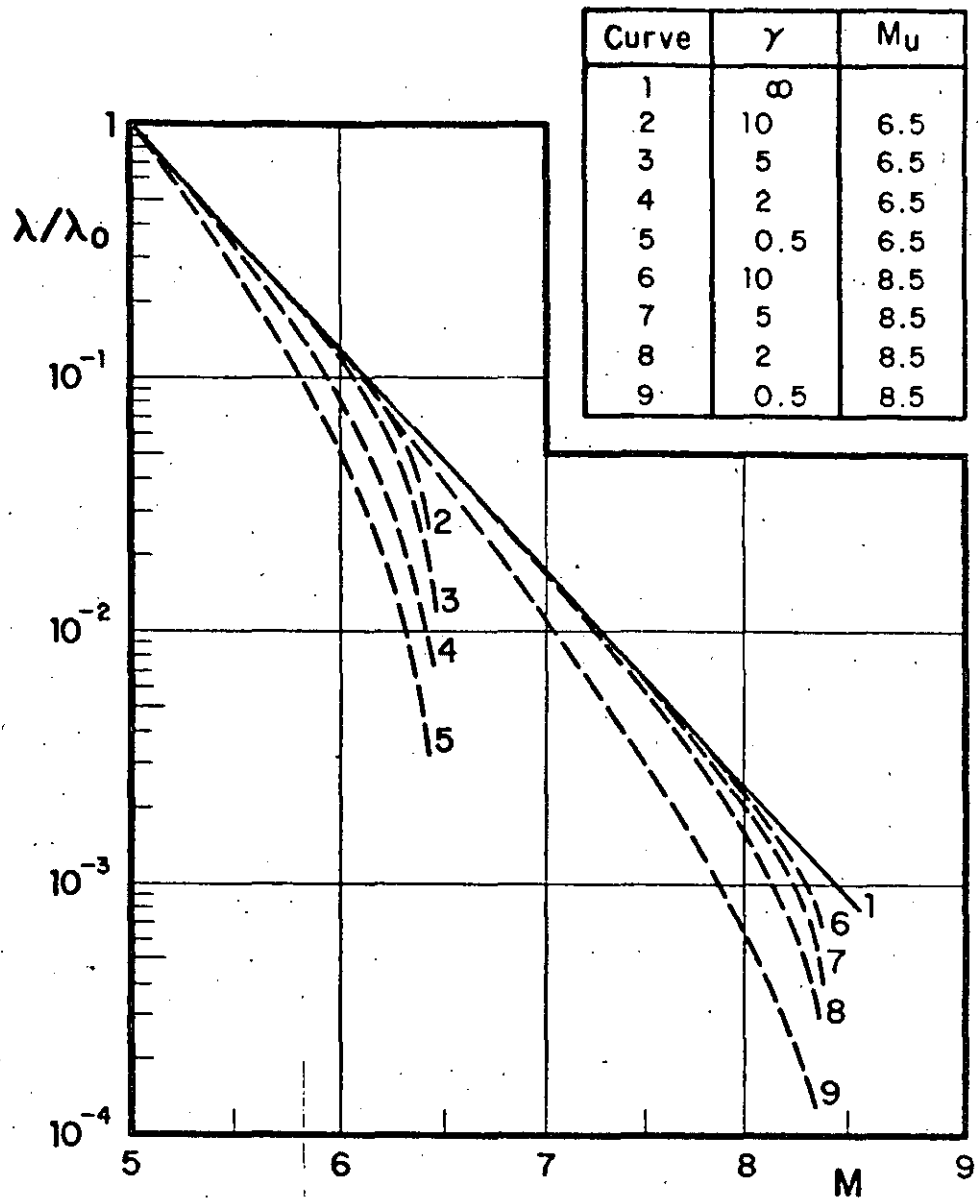


Fig 1. Influence of  $\gamma$  and  $M$  on  $\lambda(M)$  for  $\beta=2$

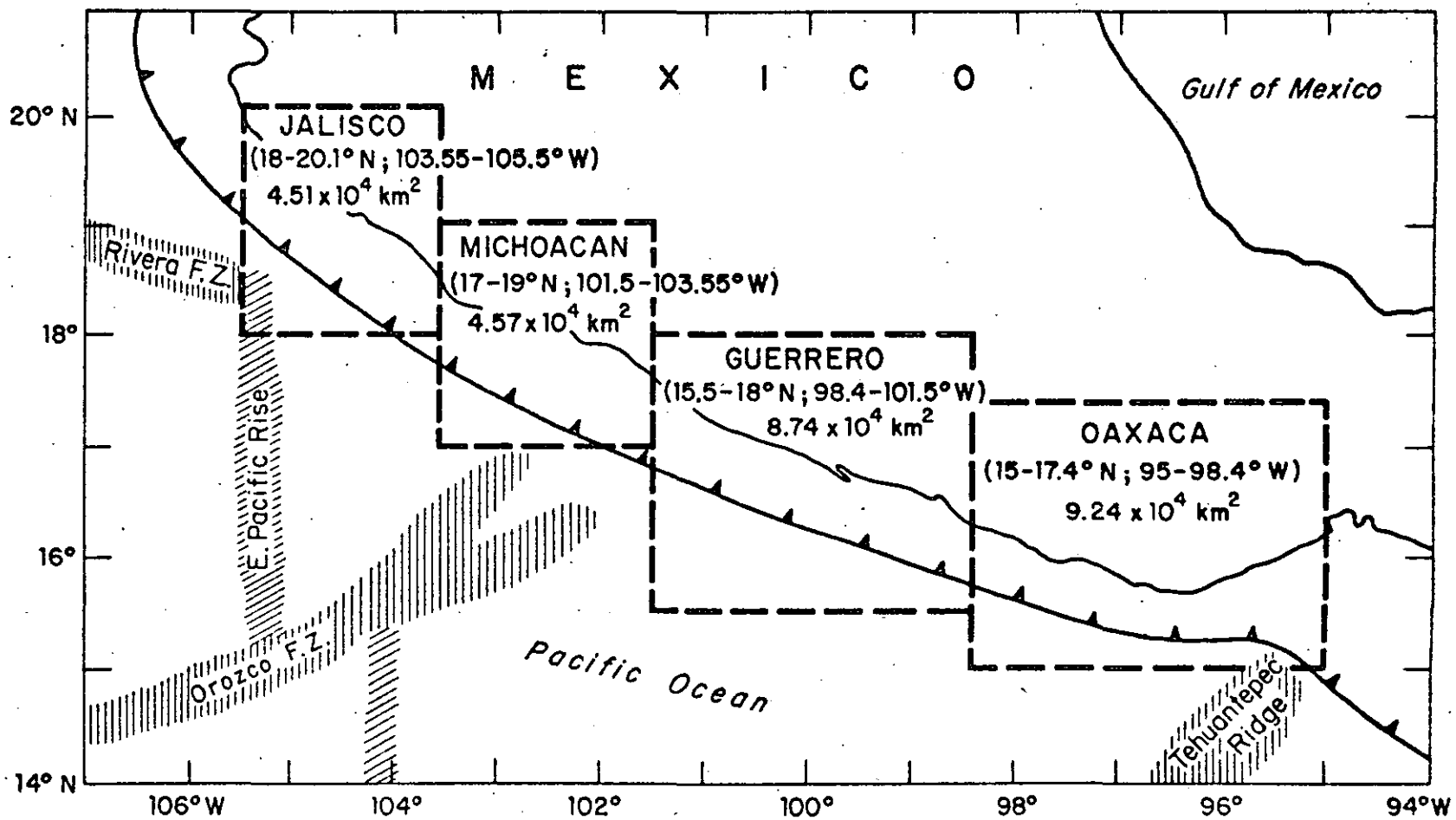


Fig 2. Mexican subduction zone



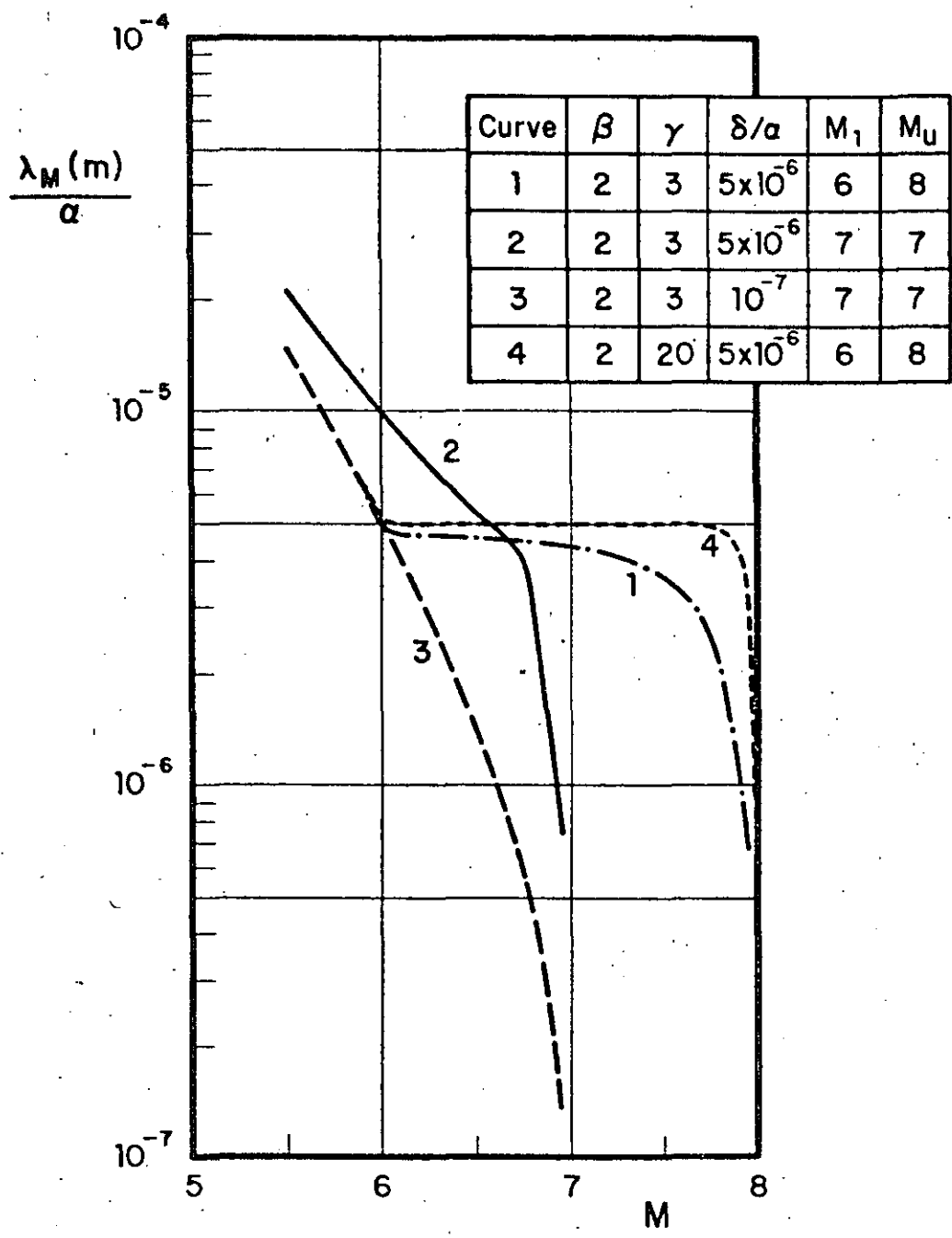


Fig 4. General shapes of magnitude recurrence curves given by eq 2

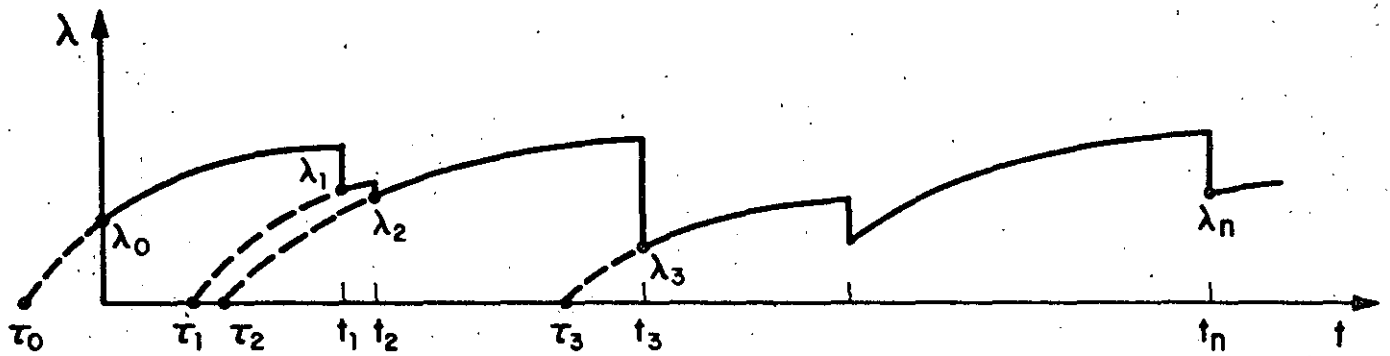


Fig 5. Hazard function for a sample of a Markov process model of seismicity neglecting clustering

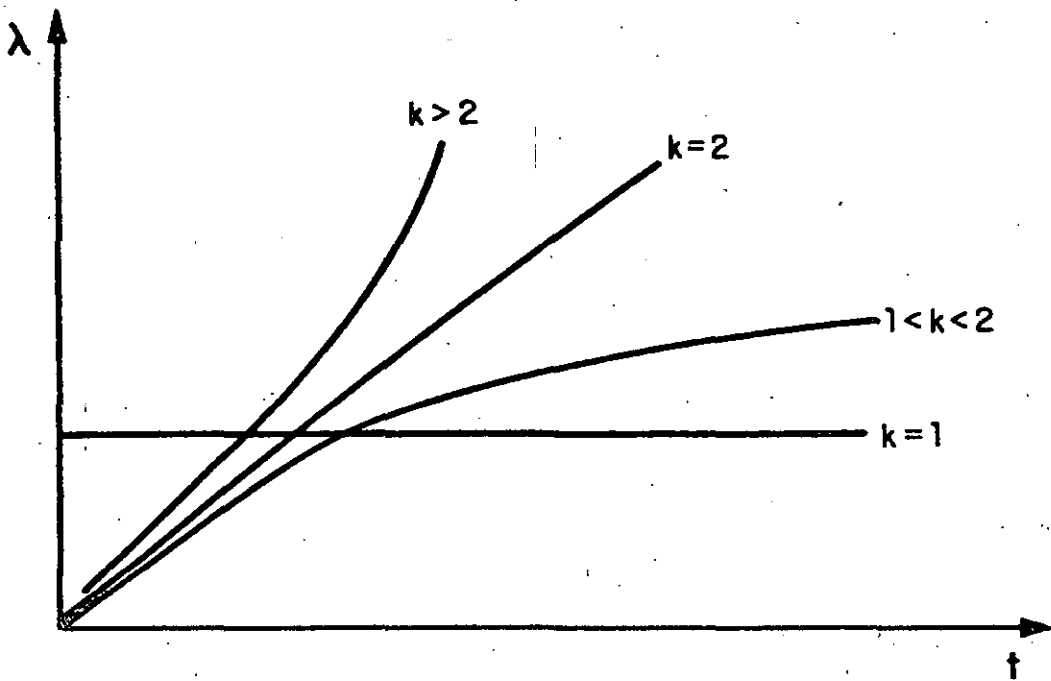


Fig 6. Shapes of hazard functions for Weibull distribution of inter-arrival times

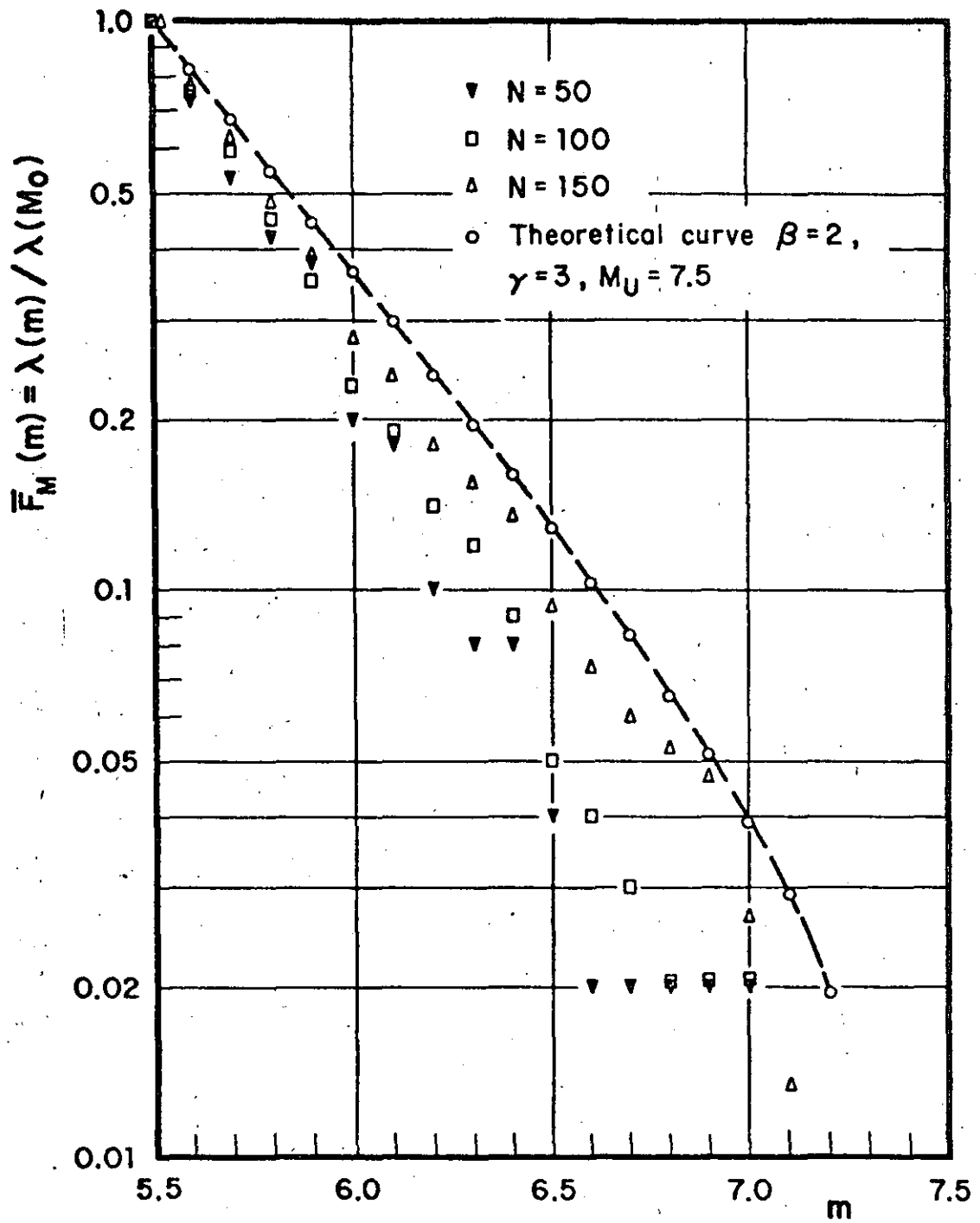


Fig 7. Summary of simulated seismic records

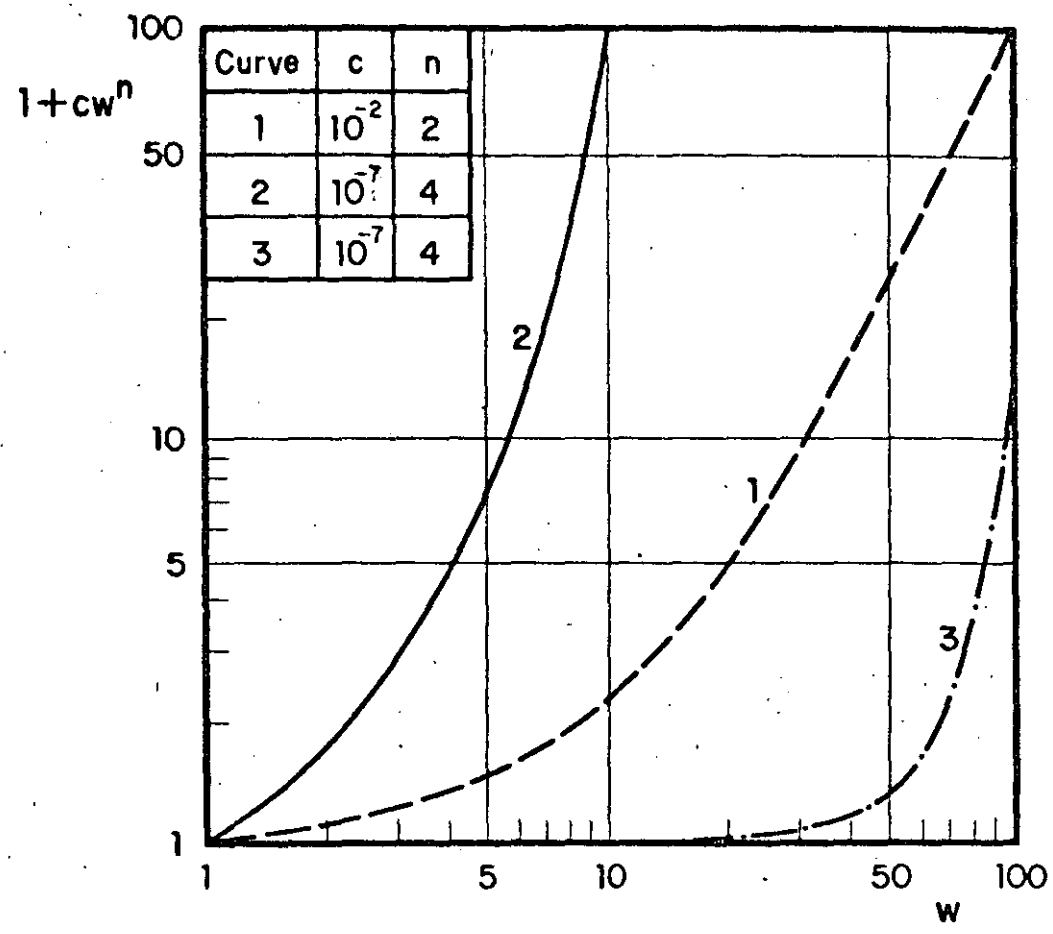
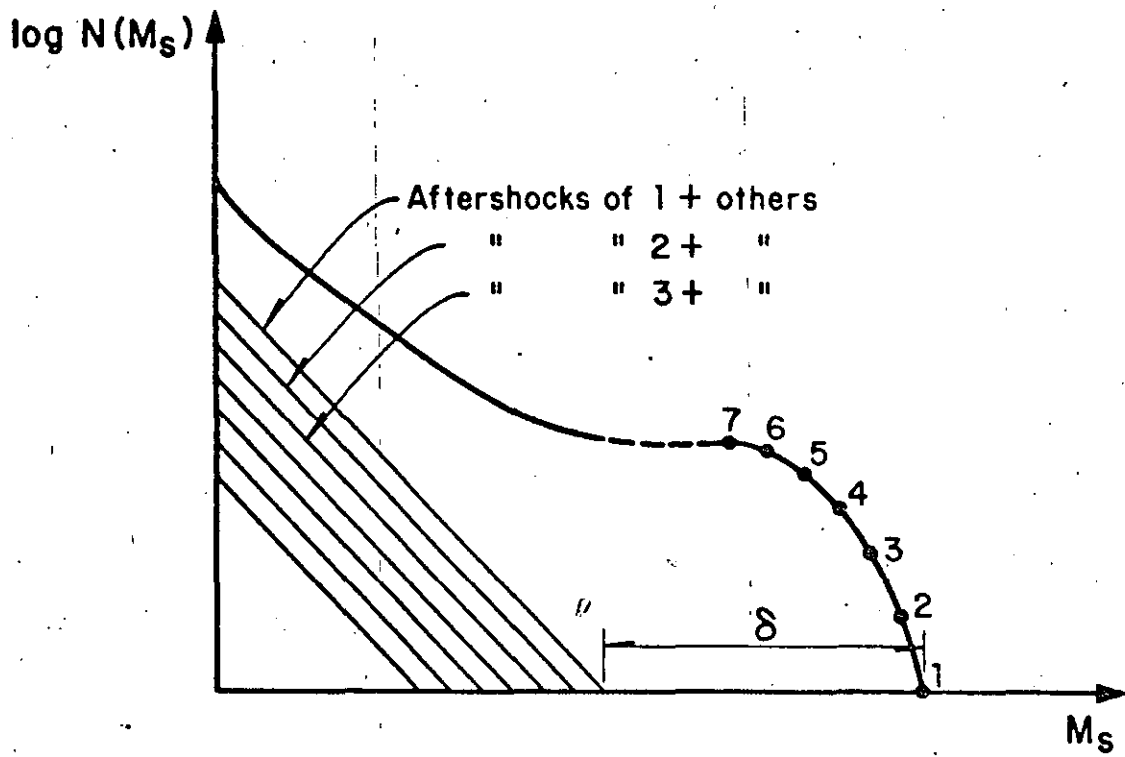


Fig 8. Utility functions for risk aversion





**DIVISION DE EDUCACION CONTINUA  
FACULTAD DE INGENIERIA U.N.A.M.**

ANALISIS DE RIESGO SISMICO

EMPIRICAL BAYES ESTIMATION OF SEISMICITY PARAMETERS

JULIO, 1985

# EMPIRICAL BAYES ESTIMATION OF SEISMICITY PARAMETERS

A.M. Hasofer

University of New South Wales, P.O. Box 1, Kensington, N.S.W. 2033 (Australia)

and

L. Esteva

Instituto de Ingenieria UNAM, Ciudad Universitaria, DF 04510, Coyoacan (Mexico)

(Received May 24, 1983)

**Key words:** Seismicity, empirical Bayes method, negative exponential distribution

---

## ABSTRACT

*A methodology based on the framework of Empirical Bayes Estimation is presented for the estimation of local seismicity in a given region, using statistical information concerning that region together with additional information derived from other regions having similar geotech-*

*nic characteristics.*

*The methodology is applied to estimation of seismicity in Southern Mexico, using additional information from nine other regions around the Pacific Ocean.*

---

## 1. INTRODUCTION

The estimation of seismicity parameters in regions where only scanty data are available is fraught with uncertainties. To increase the precision of the estimation, it has often been suggested that use be made of statistical data from other regions of the world which have similar geotechnic characteristics, but it is almost always the case that the various data

cannot be considered as a random sample from a single distribution. The underlying parameters obviously vary.

Empirical Bayes Estimation is a statistical technique which has been specially developed for this particular purpose.

The data of the various regions are supposed to be the result of a two-stage sampling process: first a sampling process from an underlying parameter distribution which yields

the various parameter sets corresponding to the considered regions, and then a second sampling process in each region, yielding the observed data. The Empirical Bayes method estimates the underlying parameter distribution, and then estimates the *a posteriori* distribution of the parameters in each region, given the data.

In this paper, the Empirical Bayes method is applied to the determination of the seismicity parameters in a region of Mexico, making use of the local data as well as of the data from nine auxiliary regions having similar geotechnic characteristics.

For a presentation of the Empirical Bayes method, see Maritz [1].

## 2. OUTLINE OF EMPIRICAL BAYES TECHNIQUE

The Empirical Bayes technique has been developed in order to handle the following type of problem.

Suppose we have a sequence of observation vectors  $x_1, x_2, \dots, x_n$  such that the likelihood function of  $x$  is  $f(x|\lambda)$  which depends on the value of a vector of parameters,  $\lambda$ , which is assumed to vary from one observation vector to another.

The conceptual model used to handle the above situation assumes that the parameter  $\lambda$  is a random variable, and that the successive observations correspond to values of  $\lambda$  which are a random sample from a given distribution  $G(\lambda)$ .

The marginal likelihood function of  $x$ ,  $f_G(x)$ , will then be given by

$$f_G(x) = \int f(x|\lambda) dG(\lambda) \quad (1)$$

The above assumptions are equivalent to assuming that the  $x_r$  are a random sample from the density function  $f_G(x)$ , i.e. that their likelihood function is

$$L = f_G(x_1) f_G(x_2) \dots f_G(x_n). \quad (2)$$

The problem is to estimate the distribution function  $G(\lambda)$  from the observations  $x_1, \dots, x_n$ .

In general, two basic approaches are used:

### (1) Parametrization of $G(\lambda)$

If it can be assumed that  $G(\lambda)$  has a known form depending on some vector of parameters  $\theta$ , then  $f_G(x)$  becomes a function of  $\theta$ , and the problem reduces itself to a classical parameter-estimation problem which can be handled by any of the standard techniques.

### (2) Discretization of $G(\lambda)$

When no reasonable parametrization of  $G(\lambda)$  is available, we assume that  $G$  has concentrations of mass at the points  $\lambda_i$  ( $i = 1, \dots, k$ ). Let:

$$P(\lambda_i) = \theta_i. \quad (3)$$

Then the problem reduces itself to estimating either the  $\lambda_i$ , or the  $\theta_i$ , or both.

## 3. A SPECIAL CASE WHICH IS EASY TO TREAT

Suppose we choose  $k = n$ , i.e. we assume that the number of points where  $G$  has concentrations of mass is equal to the number of observations. For each observation vector  $x$ , we calculate by some method, e.g. the method of moments or maximum likelihood, an estimate of the parameter vector  $\lambda$ . Thus we have  $n$  values  $\lambda_1, \dots, \lambda_n$ .

The marginal density function of  $x$  is then

$$f_G(x) = \sum_{r=1}^n \theta_r f(x|\lambda_r). \quad (4)$$

Finally, the likelihood  $L$  is given by

$$L = f_G(x_1) \dots f_G(x_n). \quad (5)$$

The method of maximum likelihood is now used to estimate the  $\theta_i$  (see Maritz [1] p. 42).

Let  $f(x_s | \lambda_r) = p_{rs}$ .

Then

$$\ln L = \sum_{s=1}^n \ln \left[ \sum_{r=1}^n p_{rs} \theta_r \right].$$

In order to maximize  $\ln L$ , subject to the condition  $\theta_1 + \dots + \theta_n = 1$ , we use a Lagrange multiplier,  $\gamma$ . This gives:

$$\frac{\partial}{\partial \theta_r} [\ln L - \gamma(\theta_1 + \dots + \theta_n)] = \sum_{s=1}^n \frac{p_{rs}}{\sum_{r=1}^n p_{rs} \theta_r} - \gamma = 0. \quad (6)$$

Let

$$\frac{1}{\sum_{r=1}^n p_{rs} \theta_r} = \xi_s.$$

Then

$$\sum_{s=1}^n p_{rs} \xi_s = \gamma, \quad r = 1, \dots, n, \quad (7)$$

and

$$\sum_{r=1}^n p_{rs} \theta_r = \frac{1}{\xi_s}, \quad s = 1, \dots, n. \quad (8)$$

Suppose that the determinant of  $p_{rs}$ ,  $\Delta$ , does not vanish. Then, denoting the cofactor of  $p_{rs}$  in  $\Delta$  by  $P_{rs}$ , gives: from (7)

$$\xi_r = \frac{\gamma}{\Delta} \sum_{s=1}^n P_{rs}, \quad (9)$$

and from (8)

$$\theta_s = \frac{1}{\Delta} \sum_{r=1}^n P_{rs} \xi_r^{-1}. \quad (10)$$

Replacing  $\xi_r$  in (10) by its value in (9)

$$\theta_s = \gamma^{-1} \sum_{r=1}^n P_{rs} \left( \sum_{s=1}^n P_{rs} \right)^{-1}.$$

To find  $\gamma$ , we use the relation  $\sum_{s=1}^n \theta_s = 1$ ,

from which

$$1 = \gamma^{-1} \sum_{r=1}^n \left\{ \frac{\sum_{s=1}^n P_{rs}}{\sum_{s=1}^n P_{rs}} \right\} = \gamma^{-1} n.$$

Thus  $\gamma = n$ , and we finally have

$$\theta_s = \frac{1}{n} \sum_{r=1}^n P_{rs} \left( \sum_{s=1}^n P_{rs} \right)^{-1}. \quad (11)$$

#### 4. A POSTERIORI ESTIMATE OF THE PARAMETERS $\lambda_s$

The values of  $\theta_i$  given by eqn. (11) constitute the *a priori* distribution of  $\lambda_s$  for any new region which can be assumed to belong to the same population.

Once the value of the  $\theta_i$  are obtained, it is easy to calculate the *a posteriori* estimate  $\lambda_s$ . This is given by  $\bar{\lambda}_s = E(\lambda_s | x_s)$  and it is easy to see that this is given by

$$\bar{\lambda}_s = \frac{\sum_r \lambda_r \theta_r p_{rs}}{\sum_r \theta_r p_{rs}}. \quad (12)$$

#### 5. APPLICATION TO THE ESTIMATION OF SEISMICITY

##### (1) Statistical data

Following Esteva and Bazan, [2], the seismicity of a region on the southern coast of Mexico is estimated by using statistical data referring to the region itself, as well as data referring to nine auxiliary regions with similar geotechnic characteristics. Designations and some characteristics of the considered regions are given in Table 1.

Two sets of statistical data are available for each region, namely  $n'$  earthquakes with mag-

TABLE 1

List of seismic regions

No	Designation	Coordinates		Area (1000 km <sup>2</sup> )
		Latitude	Longitude	
1	South Chile	33°-45°S	60°-90°W	242
2	Central Chile	27°-33°S	60°-90°W	378
3	North Chile-South Peru	15°-27°S	60°-90°W	285
4	Central/North Peru and South Ecuador	2°-15°S	60°-90°W	818
5	Central America	8°-16°N	83°-94°W	83
6	Alaska	50°-64°N	142°-164°W	366
7	Aleutian Islands	50°-60°N	165°E-160°W	459
8	Kamchatka	48°-55°N	155°-165°E	302
9	Kuriles	42°-48°N	145°-155°E	169
10	Mexico (Region of Interest)	14°-20°N	94°-105°W	778

nitudes  $m'_j \geq M'_0$ , ( $j = 1, \dots, n'$ ;  $M'_0 = 7$ ) during the period  $T'$  (1918-1952; 35 years) and  $n''$  with magnitudes  $m''_j \geq M''_0$ , ( $j = 1, \dots, n''$ ;  $M''_0 = 6$ ) during the period  $T''$  (1953-1974; 22 years).

## (2) A model for seismicity

Occurrence of earthquakes with magnitudes greater than or equal to  $M$  generated in a given seismic region will be represented by a Poisson process with mean rate  $\lambda(M)$  per unit area and unit time. The function  $\lambda(M)$  will be assumed to be of the form [2]

$$\lambda(M) = \begin{cases} \alpha(e^{-\beta M} - e^{-\beta M_1}) & \text{for } M < M_1, \\ = 0 & \text{for } M > M_1. \end{cases} \quad (13)$$

The statistical data described above may be considered to be generated as follows for each region.

Consider first the time interval  $T'$ . The data can be assumed to be generated by a simple Poisson process with parameter  $\mu'$  given by

$$\mu' = w\alpha(e^{-\beta M'_0} - e^{-\beta M_1}), \quad (14)$$

where  $w$  is the area of the region.

To each event  $t_i$  from this Poisson process, we attach a random variable  $X'_i$  with density function

$$g(m) = \begin{cases} \frac{\beta e^{-\beta m}}{(e^{-\beta M'_0} - e^{-\beta M_1})} & \text{for } M'_0 \leq m \leq M_1, \\ = 0 & \text{elsewhere.} \end{cases} \quad (15)$$

Moreover, the random variables  $X'_i$  are independent and identically distributed.

For the time interval  $T''$ , the model is the same, except that  $M''_0$  is substituted for  $M'_0$ . In other words, the data for each region of realizations consist of two Compound Poisson processes.

The likelihood function of the two sets of data turns out to be

$$f(x|\alpha, \beta, M_1) = (w\alpha\beta)^{n'+n''} \times \exp[-w\alpha(\kappa'T' + \kappa''T'') - \beta S] \quad (16)$$

where  $\kappa' = e^{-\beta M'_0} - e^{-\beta M_1}$ ;  $\kappa'' = e^{-\beta M''_0} - e^{-\beta M_1}$ ; and  $S = \sum m'_j + \sum m''_j$ . For the derivation see the Appendix.

### (3) Preliminary estimation of the parameters in each region

#### (a) Estimation of the upper bound, $M_1$

Following Cooke [3], as estimator for the upper bound of the  $X$ 's we use:

$$\hat{M}_1 = (1 + r^{-1})Y_1 - r^{-1}Y_r, \quad (17)$$

where  $Y_1$  is the largest value of the sample, and  $Y_r$  is the  $r$ th largest value. The value of  $r$  can be taken to be fairly small, and the value of the estimator is insensitive to  $r$ . In the calculations given later in the paper,  $r$  will be taken to be 10.

#### (b) Estimation of $\alpha$ and $\beta$

Given the value of  $M_1$ , the parameters  $\alpha$  and  $\beta$  are estimated by maximum likelihood. The equations are:

$$\frac{\partial}{\partial \alpha} (\ln f) = \frac{n}{\alpha} - w(\kappa'T' + \kappa''T'') \quad (18)$$

$$\frac{\partial}{\partial \beta} (\ln f) = \frac{n}{\beta} - w\alpha(R'T' + R''T'') - S = 0. \quad (19)$$

where  $R' = M_1 e^{-\beta M_1} - M_0' e^{-\beta M_0'}$ ;  $R'' = M_1 e^{-\beta M_1} - M_0'' e^{-\beta M_0''}$ ; and  $n = n' + n''$ .

Replacing  $\alpha$  in (19) by its value from (18), we find

$$n \left( \frac{1}{\beta} - \frac{R'T' + R''T''}{\kappa'T' + \kappa''T''} \right) - S = 0. \quad (20)$$

This equation must be solved numerically for  $\beta$ , and it turns out that a better form is  $n - \beta(S + nF) = 0$ , where  $F = (R'T' + R''T'')/(\kappa'T' + \kappa''T'')$ .

Once  $\hat{\beta}$  is calculated,  $\hat{\alpha}$  is obtained by the formula  $\hat{\alpha} = n/(\kappa'T' + \kappa''T'')w$ .

### (4) Numerical results of preliminary estimation

The values given in Table 2 were obtained for each of the 10 considered regions. (Note that the units of  $\alpha$  are earthquakes per year per km<sup>2</sup>).

TABLE 2

Statistical data and preliminary parameter estimates

Region No	$S$	$n$	$M_1$	$\alpha$	$\beta$
1	495	75	8.41	4.85	2.1
2	253	38	8.43	0.51	2.0
3	559.7	83	8.18	0.19	1.6
4	309.2	46	8.08	0.04	1.6
5	408.8	63	7.98	105.8	2.5
6	701.1	110	8.64	3053.0	3.2
7	1850	290	8.34	4876.0	3.2
8	851.5	132	8.43	291.1	2.8
9	959.1	147	8.83	94.16	2.5
10	387.1	58	8.16	0.18	1.8

### (5) Calculation of the *a priori* distribution of the parameters

As explained in section 3, the *a priori* distribution of the parameter set  $(\alpha, \beta, M_1)$  was taken to be discrete, taking each of the ten sets of values given in Table 1 with probability  $\theta_i (i = 1, \dots, 10)$ .

Using formula (16), the matrix of conditional likelihoods  $(p_{rs})$  was calculated. Some difficulties were encountered on account of the very large numbers generated. In this connection it is important to note that the solution of the set of eqns. (7) and (8) depends only on the ratio of the elements in any particular column. One should also note that, since  $M_1$  does not vary very significantly, and since  $\alpha$  and  $\beta$  were calculated by using a maximum-likelihood method, the diagonal elements of the matrix  $(p_{rs})$  tend to be the largest elements in each column.

The procedure adopted was to calculate first the matrix of elements  $\ln(p_{rs})$ , then to subtract from each column the largest element, which turned out to be the diagonal element. Next, the matrix of likelihoods was calculated. It turned out to have ones along the main diagonal, with much smaller elements elsewhere.

Finally, the  $\theta_i$  were calculated, and the values obtained were: 0.10, 0.07, 0.10, 0.09, 0, 0.10, 0.10, 0.10, 0.21, 0.13.

## (6) Calculation of the *a posteriori* estimators for region 10

This is easily done, using formula (12). The values obtained are:  $\hat{\alpha}_{10} = 0.1779$ ;  $\hat{\beta}_{10} = 1.826$ ;  $\hat{M}_{1(10)} = 8.164$ .

## 6. CONCLUSION

The method described above provides a general procedure for combining relevant data which cannot be considered as identically distributed. While the idea of combining such data for estimating seismicity is already outlined in Esteva and Bazan [2], this paper provides for the first time a precise mathematical and statistical model for such a procedure.

As in most empirical Bayes applications, it is not possible to derive simple formulae for the bias and variance of the estimators. All what one can say in general is that, on account of formula (12), the empirical Bayes estimators are averages of the estimators in the various regions. If  $n$  is the number of regions, and the estimators have comparable variances, the Bayes estimator's variance can be expected to be improved by a factor of about  $n$  against the estimator based on one region alone. Also the Bayes estimator can be expected to show very little bias. (See Maritz [1]).

For the particular case at hand, the only way to obtain precise figures is to resort to simulation. Work is proceeding at present on this aspect of the investigation, and the results will be given in a forthcoming paper.

Of course, as with every other probabilistic model, the accuracy of the estimation and its variance will depend on the validity of the assumptions on which the model is based, namely

- (i) the Poisson occurrence of the earthquakes,
- (ii) the truncated negative exponential distribution

for the distribution of earthquake magnitudes,

- (iii) that the parameters in each of the ten regions are random values from a population of parameters which can be approximated by a discrete distribution.

The model is certainly highly plausible, but its eventual value will only be judged by its long-run success in practical applications.

## 7. ACKNOWLEDGEMENT

The research embodied in this paper was carried out while the second author was on a visiting appointment at the Instituto de Ingenieria, Mexico.

## APPENDIX

### Derivation of the likelihood function of the data

#### 1. Likelihood of a compound Poisson process.

Consider a realization of a Poisson process with parameter  $\lambda$  over a time interval  $T$ . Let  $(t_1, \dots, t_n)$  be the points of time at which the occurrences of the process are located.

Divide the time interval  $T$  into small intervals of length  $h$ . Let  $h$  be so small that in each small interval either one occurrence or no occurrence is located. The probability of  $(t_1, \dots, t_n)$  is then  $\exp(-\lambda T)\lambda^n h^n$  and is independent of the exact values of  $t_1, \dots, t_n$ .

As  $h \rightarrow 0$  the likelihood remains proportional to  $\exp(-\lambda T)\lambda^n$  and is a function of  $n$  only.

If  $g(x)$  is the common density function of the random variables located at  $(t_1, \dots, t_n)$ , and  $(x_1, \dots, x_n)$  is the set of observed values, the likelihood function, given  $n$ , is  $g(x_1) \dots g(x_n)$ .

Finally, the likelihood of the observations  $(t_1, \dots, t_n)$  and  $(x_1, \dots, x_n)$  is

$$\exp(-\lambda T)\lambda^n g(x_1) \dots g(x_n). \quad (21)$$

**REFERENCES**

- 1 J.S. Maritz, Empirical Bayes Methods. Methuen & Co. Ltd., London, 1970.
- 2 L. Esteva and E. Bazan, Seismicity and seismic risk related to subduction zones. Second International Seminar on Microzonation, San Francisco, California, 1978.
- 3 P. Cooke, Optimal linear estimation of bounds of random variables. *Biometrika*, 67(1) (1980) 257-258.



**DIVISION DE EDUCACION CONTINUA  
FACULTAD DE INGENIERIA U.N.A.M.**

XI CURSO INTERNACIONAL DE INGENIERIA SISMICA

ANALISIS DE RIESGO SISMICO

USE OF STATISTICAL DATA IN ASSESSING LOCAL SEISMICITY

JULIO, 1985

As long as we idealize earthquake generation as a Poisson process we need only assess the exceedance rate as a function of magnitude. More realistic models demand evaluation of more than one quantity for every given magnitude. In turn the exceedance rate must be defined by two or more parameters, depending on the refinement desired.

The bayesian treatment is entirely general. Details of its application to the examples chosen here are, however, tied to the assumption that we deal with a Poisson process and to the particular shape of the exceedance-rate curves. The choice is justified for a wide range of applications.

### GENERAL SOLUTION FOR A SINGLE REGION

Assume that we deal with a Poisson process. Let  $\lambda = \lambda(M; \underline{\theta})$  denote the exceedance rate: the expected number of earthquakes with magnitude greater than  $M$  that occur per unit time; it is a function of  $M$  with parameters vector  $\underline{\theta}$ . Let  $M_0$  denote the smallest magnitude for which there are complete, reliable observations over a period  $t$ , and  $M_u$  the maximum possible magnitude within the region in question. Divide the interval  $M_0, M_u$  into segments of size  $\Delta M$  small enough that the probability is negligible of there having occurred more than one earthquake in any one given segment during the period of observation. The probability that an earthquake with magnitude  $M_i$  occurred is, save for higher-order terms,  $-\lambda'_i t \Delta M e^{\lambda'_i t \Delta M}$  where  $\lambda'_i = d\lambda/dM$  at  $M = M_i$ . Again save for higher-order terms, the probability that no earthquake occurred with magnitude in the segment containing  $M_j$  is  $e^{\lambda'_j t \Delta M}$ . Hence, the likelihood of the event  $\epsilon$ , consisting in the occurrence of earthquakes with magnitudes  $M_i$ ,  $i = 1, \dots, n$ , given  $\underline{\theta}$  is

$$L_{\epsilon | \underline{\theta}} = \prod_i (-\lambda'_i)^{\epsilon_i} \exp(\sum_k \lambda'_k t \Delta M), \quad k = i, j$$

Now make  $\Delta M$  tend to zero. In the limit,

$$L_{\epsilon | \underline{\theta}} = \prod_i (-\lambda'_i)^{\epsilon_i} \exp\left(t \int_{M_0}^{M_u} \lambda' dM\right)$$

$$= -\prod_i \lambda_i^{\epsilon_i} \exp[(\lambda_u - \lambda_0)t] \quad (1)$$

where  $\lambda' = d\lambda/dM$ ,  $\lambda_0 = \lambda(M_0)$ , and  $\lambda_u = \lambda(M_u)$ .

We must often aggregate seismic data gathered over periods of observation having different  $M_0$ s. Let then subscript  $k$  identify such periods and recast equation (1) in the form

$$L_{\epsilon|\underline{\theta}} = \frac{-\pi\lambda'}{\lambda} \exp\left[\sum_k (\lambda_u - \lambda_{0k}) t_k\right] \quad (2)$$

Subscript  $i$  covers the totality of observed earthquakes.

Now let  $\ell'_{\underline{\theta}}$  denote the prior likelihood function of the parameter vector. Bayes' theorem gives us the posterior likelihood,

$$\ell''_{\underline{\theta}} = \ell_{\epsilon|\underline{\theta}} \ell'_{\underline{\theta}} \quad (3)$$

We get the joint posterior probability density function  $p''_{\underline{\theta}}$  by normalizing  $\ell''_{\underline{\theta}}$  so that its integral over the domain of  $\underline{\theta}$  be one. (As is customary in Bayesian statistics, here we use the single prime to denote prior values, the double prime for the posterior ones, and no prime for statistical data.)

We are interested in the probability density of  $\lambda$  as a function of  $M$ . This we obtain from  $p''_{\underline{\theta}}$ . In most practical cases, though, it suffices with the calculation of the expectation of  $\lambda$  and perhaps of its variance. This allows computing the corresponding parameters of the exceedance rates of the seismic effects at the site of interest. Results from all pertinent regions are finally combined to provide a basis for design. In the present paper we will stop at the calculation of  $p''_{\underline{\theta}}$ .

### EXCEEDANCE-RATE CURVES AND THE POISSON ASSUMPTION

With basis on work by Gutenberg and Richter<sup>1</sup> it was established practice for decades to idealize as linear the relation between the logarithm of the exceedance rate,  $\ln \lambda$ , and the magnitude  $M$  of the earthquakes generated in any volume of the earth's crust, sometimes introducing a cutoff at the estimated maximum possible value of  $M$  (Figure 1). Owing to inaccuracies in the magnitude, to the combination of data

from seismic provinces having different cutoff magnitudes, and presumably to other causes, the right-hand end of the curve was found to be rounded, as in Figure 1; and among other things because many small earthquakes are not registered, the rather irrelevant left-hand end was also rounded.

If  $\ln \lambda$  is a linear function of  $M$  with a cutoff, so is  $\ln(-d\lambda/dM)$  save for a concentrated pulse at the cutoff magnitude. That a linear relation should hold given the nature of tectonic mechanisms has been proved in an analytical study<sup>2</sup>. However, the same study concludes that there must be a second process, superimposed on the first, originating high-magnitude motions and thus causing the hump in Figure 2. The second process corresponds to earthquakes triggered by slips at asperities in geologic faults. The overall seismicity is associated with the sum of the exceedance rates for both processes. By integrating  $-d\lambda/dM$  we get curves like the one in Figure 3, in which there is nearly a magnitude gap over some range. This is in close agreement with results of studies in which reported magnitudes and focal coordinates have been very carefully reevaluated<sup>3-7</sup>. Except for aftershocks and swarms, earthquakes not associated with the hump seem to occur in approximate accord with Poisson processes, but perhaps not these due to the second process. Seismicity studies are doubtless due in for a nosy revision.

For illustration we will take the exceedance rate to be of the form

$$\lambda = \alpha(e^{-\beta M} - e^{-\beta M_u}) \quad (4)$$

where  $\alpha, \beta$ , and  $M_u$  are parameters dependent on the region. This relation closely resembles the ones found by Gutenberg and Richter. Theoretically<sup>2</sup>  $\beta$  should be 2.25 but somewhat different values occur in nature.

The Poisson assumption is justified when assessing seismicity for design of not very important structures in areas of high seismicity. Governing earthquakes are then mostly of moderate magnitude and originate through roughly independent processes, which makes their arrival times nearly Poisson. For the same reasons the tail-end bumps and fairly sharp cutoffs will be blurred, justifying use of equation 4.

### PRIOR DISTRIBUTION FUNCTIONS

Aside from theoretical considerations that furnish a very rough estimate of  $\beta$  and aside from information on seismic activity there are no sound bases for assigning a prior distribution to the seismicity parameters. The orders of magnitude of radioactive and geothermal energies available for earthquake generation are too high to be of much use while estimates based exclusively on fault size and stress drop get us into circular reasoning, as the stress drop has been inferred from data on earthquakes.

The maximum possible magnitude is ordinarily inferred from comparisons of the sizes of local faults and other tectonic features with those of other regions, from empirical correlations, and from earthquake history. There is no evidence, either historical, archeological, or geological, that there has ever occurred an earthquake of tectonic origin with magnitude greater than 9, while some arguments favor assigning the 1755 Lisbon earthquake a magnitude approaching this value<sup>8</sup>. On the other hand, even in regions having no active faults we cannot rule out the possibility that some might eventually form. Pending a careful assessment it seems reasonable to recognize that in every region there is a possibility that  $M_u$  will exceed 3. We would like for the prior density function of  $M_u$  rapidly to approach zero as  $M_u$  tends to some value slightly in excess of 9, say 9.2, as well as when it tends to 3. The beta distribution with likelihood function,

$$L'_{M_u} = (M_u - x_1)^{a_1 - 1} (x_2 - M_u)^{a_2 - 1} \quad (5)$$

will do this if we set  $x_1 = 3$ ,  $x_2 = 9.2$  and if  $a_1$  and  $a_2$  exceed 1. For purposes of illustration we will choose  $a_1 = 5$ ,  $a_2 = 3$ . For the beta distribution,  $E'M = (a_1 x_2 + a_2 x_1) / (a_1 + a_2)$  and  $c'M_u = [(x_2 - x_1) / (a_1 x_2 + a_2 x_1)] [a_1 a_2 / (a_1 + a_2)]^{1/2}$  where  $E$  and  $c$  denote expectation and coefficient of variation, respectively. With the values assigned to the parameters we get  $E'M_u = 6.875$ ,  $c'M_u = 0.1544$ .

With basis on local studies it should be possible to raise  $a_1$  and  $a_2$  and it may be possible to narrow the range  $x_2 - x_1$ , making

$$z = \frac{M - x_1}{x_2 - x_1}$$

the distribution more peaked on both counts.

When seismic data have been collected over a single time interval — in other words, with  $M_0$  constant, — substituting  $\lambda$  from equation (4) into (1) gives,

$$L_{\epsilon|\underline{\theta}} = \alpha^n \beta^n e^{-\alpha\tau - \beta\delta} \quad (6)$$

where  $\tau = (e^{-\beta M_0} - e^{-\beta M_u})t$  and  $\delta = \sum M_i$ . This has the disadvantage that  $\alpha$  and  $\beta$  are strongly coupled since  $M_0$  is almost always appreciably greater than zero. We improve matters by moving the origin of magnitudes to  $M_0$  (after all, the zero in the magnitude scale is quite arbitrary) and rewriting equation (6) as

$$L_{\epsilon|\underline{\theta}} = \tilde{\alpha}^n \tilde{\beta}^n e^{-\tilde{\alpha}\tilde{\tau} - \tilde{\beta}\tilde{\delta}} \quad (7)$$

where  $\tilde{\alpha}\tilde{\tau} = \lambda_0 t$ ,  $\tilde{\tau} = (1 - e^{-\beta M_u})t$ ,  $\tilde{\delta} = \sum \tilde{M}_i$ , and  $\tilde{M}_i = M_i - M_0$ . An uncoupled, approximate solution now obtains by replacing  $\beta$  and  $M_u$  with their expectations in the expression for  $\tilde{\tau}$ , and  $\tilde{\alpha}$  with its expectation when it comes to  $M_u$ . Indeed we can write,

$$L_{\epsilon|\underline{\theta}} \approx L_{\epsilon|\alpha} L_{\epsilon|\beta} L_{\epsilon|M_u} \quad (8)$$

$$L_{\epsilon|\alpha} = \tilde{\alpha}^n e^{-\tilde{\alpha}\tilde{\tau}}, \quad \tilde{\tau} = (1 - e^{-\beta M_u})t \quad (9)$$

$$L_{\epsilon|\beta} = \tilde{\beta}^n e^{-\tilde{\beta}\tilde{\delta}} \quad (10)$$

$$L_{\epsilon|M_u} = e^{-\tilde{\alpha}\tilde{\tau}} \quad (11)$$

where the overbar denotes expectation. The required expectations can be obtained iteratively. We will see in the numerical examples that the errors involved are quite small. Greater accuracy results from writing  $\tilde{\beta}$  for  $\beta$ , where  $\tilde{\beta}$  is such that

$$\tilde{\alpha} \tilde{\tau} - \tilde{\beta} \tilde{\delta} = \alpha \tau - \beta \delta$$

or  $\bar{\beta} = \tilde{\beta}$  and

$$\beta = \tilde{\alpha} (\tilde{\tau} - \tau) / \tilde{\delta} + \tilde{\beta}$$

$$\approx \tilde{\alpha} \bar{M}_u (\tilde{\beta} - \bar{\beta}) e^{-\bar{\beta} \bar{M}_u} + \tilde{\beta} \tag{12}$$

When data come from time intervals having different values of  $M_0$ , equations (2) and (4) yield equation (6) with  $n = \sum_k n_k \delta_k = \sum_k k \delta_k$ ,  $\tau = \sum_k (e^{-\beta M_{0k}} - e^{-\beta M_u}) t_k$  where subscript  $k$  identifies each such interval. Again coupling is reduced by moving the origin of  $M$  to some convenient magnitude, such as the smallest  $M_{0k}$ . Should coupling between  $\tilde{\alpha}$  and  $\tilde{\beta}$  still be excessive after applying equation (12), one can make  $\beta$  a quadratic function of  $\tilde{\beta}$ , perhaps  $\alpha$  a linear function of  $\tilde{\alpha}$  and  $\tilde{\beta}$  (which amounts to further shifting of the origin of  $M$ ), or even use numerical integration in two or three dimensions. As we will see, though, even the use of equation (12) will rarely be justified.

Because prior estimates of  $\alpha$  and  $\beta$  come essentially from comparisons with other regions and because the use of natural conjugate distributions appreciably simplifies the mathematical treatment it is desirable to assign such distributions to these parameters. For Poisson processes a natural conjugate is the gamma-1 distribution<sup>9</sup>, with prior density function

$$\rho'_{\lambda_0} = \frac{\lambda_0^{n'-1} t'^{n'} e^{-\lambda_0 t'}}{\Gamma(n')} \tag{13}$$

where  $n'$  and  $t'$  are prior parameters. Similar expressions hold for  $\tilde{\alpha}$  and for  $\beta$  (or  $\tilde{\beta}$ ) after replacing  $t'$  with  $\tilde{\tau}$  and with  $\tilde{\delta}'$  respectively. The  $n'$  for  $\tilde{\alpha}$  must be the same as for  $\lambda_0$  but that for  $\beta$  will usually be much greater. It follows from equation 13 that

$$E'\lambda_0 = n'/t' \quad (14)$$

$$c'\lambda_0 = n' \cdot t'^{-1/2} \quad (15)$$

The posterior densities  $p''_{\lambda_0}$ , and  $p''_{\beta}$  are obtained by replacing  $n'$ ,  $t'$ ,  $\tilde{\tau}'$ , and  $\tilde{\delta}'$  with  $n'' = n' + n$ ,  $t'' = t' + t$ ,  $\tilde{\tau}'' = \tilde{\tau}' + \tilde{\tau}$ , and  $\tilde{\delta}'' = \tilde{\delta}' + \tilde{\delta}$ , respectively.

Forcing matters a bit, when data come from a single period of observation, according to equation (11) we can multiply  $\ell'_{M_u}$  in equation (5) by  $\exp[-\tilde{\alpha}(1 - e^{-\tilde{\beta}M_u})t]$  where  $t'$  is some prior parameter that needs not be the same as that used in the prior distribution of  $\lambda_0$  nor in the calculation of  $\tilde{\tau}'$ . Then we can say that not very orthodoxly,  $\ell'_{M_u}$  is a natural conjugate distribution (not very orthodoxly because it contains more than the least possible number of parameters; still it retains its form as we incorporate data and  $t'$  changes into  $t'' = t' + t$  to give us the posterior likelihood function of  $M_u$ .) The net results usually differ little from assuming that both prior and posterior distributions of  $M_u$  are beta with parameters  $a_1$ ,  $a_2$ ,  $x_1$ , and  $x_2$  but that the posterior distribution is zero for  $M_u \leq M_1$ , where  $M_1$  is the largest observed magnitude.

The prior likelihoods can heuristically be regarded as the outcomes of a fictitious, conceptual experiment in which we register  $n'$  earthquakes having some  $\tilde{\delta}' = \Sigma \tilde{M}_i$  over a time interval  $t'$ . The experiment being imaginary there is no objection to  $n'$  assuming non-integer values, but  $n'$ ,  $t'$ , and  $\tilde{\delta}'$  must not be negative. Incorporation of real data is equivalent to joining the fictitious experiment with the observations, making a wider, partially real experiment come about.

Prior to the gathering or at least to the processing of empirical data the distributions assigned to  $\lambda_0$  and to  $\tilde{\alpha}$  must be diffuse. On the other hand, local studies of tectonics allow us to pool data from similar regions. One should accordingly begin by setting  $n'$  and  $t'$  equal to zero; then one should incorporate data from the pertinent macrozone of the earth's crust (the Circumpacific belt,

the Alpine belt, or the low seismicity macrozone; see Reference 8); and proceed to smaller, tectonically similar regions.

We should apply the same approach for the distribution of  $\beta$  save that rather than using a diffuse prior we should begin with a flat one, assigning small values to  $n'$  and  $\delta'$ , as we have some theoretical basis for the estimate of  $\beta$ .

The treatment described here for  $\lambda_0$  and for parameters  $\alpha$  and  $\beta$  can be applied to other parameters should one seek a more accurate definition of the exceedance-rate curves.

### POOLING

We will begin with  $\lambda_0 = \lambda(M_0)$ , which for the purpose we will designate as  $\lambda$ , as a quantity to be assessed using data about earthquakes originating in regions tectonically similar to the one in which we are interested. Let us write  $\lambda_j = \xi_j \lambda$ ,  $j = 1, \dots, N$ , where subscript  $j$  refers to the  $j$ th region, no subscript to the set of  $N$  similar regions, and  $\lambda$  and  $\xi_j$  are statistically independent variables for all  $j$ , save that  $\sum_1^N \xi_j = 1$ . Before we process seismic data from the set of regions the only relevant information is their areas  $A_j$  and the degrees of correlation we expect between pairs of the  $\lambda_j$ 's. We must therefore take  $E'\xi_j = A_j/A$  where  $A = \sum_1^N A_j$  while the degrees of correlation are decreasing functions of the coefficients of variation of the  $\xi_j$ 's. (With additional local tectonic information we may choose  $E'\xi_j \neq A_j/A$  but must still comply with the condition  $\sum_1^N \xi_j = 1$ .)

Let  $n_j$  denote the number of earthquakes with magnitude greater than  $M_0$  observed to occur in region  $j$  during a period of observation  $t_j$ . The probability of the event consisting in the occurrence of  $n_j$  such earthquakes,  $j=1, \dots, N$ , given  $\xi_j$ ,  $j=1, \dots, N$ , is

$$P_{\epsilon} | \underline{\xi}, \lambda = \left[ \prod_j \frac{(\xi_j \lambda t_j)^{n_j}}{n_j} \right] e^{-\sum_j \xi_j \lambda t_j} \quad (16)$$

where  $\underline{\xi}$  is the vector of the  $\xi_j$ 's. If all the  $t_j$ 's are equal, say to  $t$ , the exponent of  $e$  becomes  $-\lambda t$ . Hence the likelihood function

$$L_{\epsilon|\underline{\xi}} = \prod_j \xi_j^{n_j} \quad (17)$$

This suggests for the prior joint distribution of the  $\xi_j$ 's the multinomial beta, which is a natural conjugate of  $L_{\epsilon|\underline{\xi}}$ :

$$p'_{\underline{\xi}} = \Gamma(m') \prod_j \frac{\xi_j^{m'_j - 1}}{\Gamma(m'_j)} \quad (18)$$

in which  $\sum_j^N m'_j = m'$ . (If the only relevant information about the regions are their areas and their similarity, then  $m'_j = m' A_j / A$  but this must generally be modified when we have additional local tectonic information.) Hence also the posterior joint likelihood function

$$L''_{\underline{\xi}} = \Gamma(m'') \prod_j \frac{\xi_j^{m''_j - 1}}{\Gamma(m''_j)} \propto \prod_j \xi_j^{m''_j - 1} \quad (19)$$

where  $m''_j = m'_j + n_j$ . Here  $m'$  needs not be related with the  $n'$  in the prior distribution of  $\lambda$ . We conclude from equation (19) that the posterior marginal expectation of  $\xi_j$  is  $E'' \xi_j = m''_j / m''$  and that the corresponding coefficient of variation squared is

$$c''^2 \xi_j = \frac{m'' - m'_j}{m''_j (m'' + 1)} \quad (20)$$

where  $m'' = \sum_1^N m''_j = m' + \sum_1^N n_j$ .

Actually  $m'$ , which measures the degrees of correlation between pairs of  $\lambda_j$ 's, is a quantity about which we have little experience. We should therefore assign it a prior probability distribution and update it in the light of the observed numbers of earthquakes.

This can be done by using equation (19), from which it follows that

$$\begin{aligned}
 L_{\epsilon|m'} &= \int \dots \int \ell_{\underline{\epsilon}}'' d\epsilon_1 \dots d\epsilon_N \\
 &\quad \epsilon_j \geq 0, \quad \sum_1^N \epsilon_j = 1 \\
 &= \frac{\Gamma(m')}{\Gamma(m'')} \prod_j \frac{\Gamma(m_j'')}{\Gamma(m_j')}
 \end{aligned} \tag{21}$$

so, if we assign  $m'$  the prior likelihood function  $\ell_m'$ , we find the posterior one,  $\ell_m'' = L_{\epsilon|m'} \ell_m'$ .

From the assumed independence between  $\epsilon_j$  and  $\lambda$  it follows that

$$\begin{aligned}
 E''\lambda_j &= E''\epsilon_j E''\lambda \\
 &= (m_j''/m'') (n''/t'')
 \end{aligned} \tag{22}$$

$$\begin{aligned}
 c''^2 \lambda_j &= c''^2 \epsilon_j + c''^2 \epsilon_j c''^2 \lambda + c''^2 \lambda \\
 &= c''^2 \epsilon_j (1 + 1/m'') + 1/n''
 \end{aligned} \tag{23}$$

from equation (15);  $c''^2 \epsilon_j$  is given by equation (20).

There remains for us to provide guidelines for assigning  $m'$  a prior distribution. Analysis of a great many regions in groups of equal areas has shown that the relation

$$c^2 \epsilon_j = (A/A_j)^\delta - 1 \tag{24}$$

gives satisfactory results [8, 10]. Here  $\delta$  is a positive constant, found to be about 0.25 for regions as dissimilar as those which comprise the Circumpacific belt, and about 0.50 for the rest of the world. For regions deemed tectonically similar, values of  $\delta$  between 0.05 and 0.20 are to be expected. (This expression cannot hold for regions of any size since  $c^2 \epsilon_j$  and  $c^2(1 - \epsilon_j)$  must be related to each other through the condition that the variances

of  $\xi_j$  and of  $1 - \xi_j$  must be equal, which, if equation (24) always held, would only be true when  $E\xi_j = 0.5$  and/or  $\delta = 1$ . However, the empirical confirmation is vast for the case  $E\xi_j = 1/N$  and  $2 \leq N \leq 100$ .) By equating  $c^2 \xi_j$  from equations (20) and (24), replacing the double primes with single primes, and making  $m'/m'_j = A/A_j = N$  we get

$$m' = \frac{N - N^\delta}{N^\delta - 1} \quad (25)$$

Secondly, if we have an idea of the correlation coefficient between pairs of  $\lambda_j$ s we can make use of the expression

cho → 
$$\rho''_{jk} = \frac{c''^2 \lambda}{c''_{\lambda_j} c''_{\lambda_k}} \quad (26)$$

where  $\rho'_{jk}$  is the correlation coefficient between  $\lambda_j$  and  $\lambda_k$ . By expressing  $c''_{\lambda_j}$  and  $c''_{\lambda_k}$  as functions of  $c''_{\lambda}$ ,  $m'_j$ , and  $m'_k$  through equations (20) and (23) (after replacing the double primes with single primes) and the latter in terms of  $m'$ , we can solve for  $m'$  as a function of a specified  $\rho'_{jk}$ . The different values of  $m'$  thus found give an idea of its order of magnitude. For example, if  $m'_j = m'_k = m'/N$ , equation (26) gives us

$$m' = \frac{(N - 1)(1/c''^2 \lambda + 1)}{1/\rho'_{jk} - 1} \quad (27)$$

*we have already seen that, from some total of a priori hypotheses, we can estimate the function*

For a given  $N$ ,  $\rho'_{jk}$  is not very sensitive to moderate differences between  $m'_j$  and  $m'_k$  if  $m'$  is found from equation (27). For example, with  $c''_{\lambda} = 0.2$ ,  $\rho'_{jk} = 0.1$ , and  $m'_j = m'_k = m'/2$ , equation (17) gives  $m' = 1.89$ . If now  $m'_j = m'/3$  and  $m'_k = 2m'/3$ ,  $m' = 1.89$  yields  $\rho'_{jk} = 0.0979$ . Whatever the value of  $c''_{\lambda}$ , the  $m'$  that results in  $\rho'_{jk} = 0.5$  according to equation (27) when  $m'_j = m'_k = m'/20$ , will give  $\rho'_{jk} = 0.5825$  if  $m'_j = m'/20$  but  $m'_k = m'/10$ , while it results in  $\rho'_{jk} = 0.4047$  when  $m'_j = m'/20$  and  $m'_k = m'/40$ .

Finally, the maximum entropy criterion subject only to the restrictions that the  $\xi_j$ s have a joint beta distribution (Appendix 2) yields

$$m' = 1/\min_j E' \xi_j \quad (28)$$

while if the  $m_j$ 's do not differ from each other,  $m' < N$ .

Since equations (25) and (27) are valid when all  $m_j$ 's are equal, we may use the first two expressions for an estimate of  $m'$  when we postulate that the  $m_j$ 's are approximately equal to each other and center the prior distribution of  $m'$  around these values but subject it to the condition  $m' \geq 1/\min_j E' \xi_j$ , as we usually know more about the relative seismicities than implied by equation (28). When the  $m_j$ 's differ significantly from each other, we must dispense of equation (25) and replace (27) with (26).

This approach cannot be used when the times of observation  $t_j$  are not all equal to each other, for we cannot then apply the simplification that produced equation (17), and we may have to use numerical integration. We may still resort to a simplifying artifice by noticing that the exponent of  $e$  in the resulting expression for  $p_{\xi, \lambda}''$  is  $-\lambda \sum_j \xi_j t_j''$  so that the assumption that  $\lambda$  and the  $\xi_j$ 's are statistically independent implies that  $\sum_j \xi_j t_j''$  is a constant. If we denote this constant by  $t''$  and make it equal, say, to  $\sum_j E' \xi_j t_j''$ , we can apply the former scheme by replacing  $\xi_j$  with  $\xi_j t_j''/t'' = \eta_j$ , say. Again we find  $E'' \eta_j = m_j''/m''$ , from which  $E'' \xi_j = (t''/t_j'')(m_j''/m'')$ , while equations (20), (21), and (23) are still valid.

A similar artifice can be used when the magnitudes  $M_0$  are not equal for all the regions provided we know the values of  $\beta$  and  $M_{u_j}$ . When these are uncertain we get approximate results if we replace them with their expectations.

The approach we have described in connection with  $\lambda_0$  is directly applicable in the pooling of information for the assessment of  $\tilde{\alpha}$ , as it suffices to replace  $t$  with  $\tilde{\tau}$  (see equation (7)). In general, though, the  $\tilde{\tau}_j$ 's will differ from each other and their dependence on the uncertain parameters  $\beta_j$  and  $M_{u_j}$  introduces coupling between them and  $\tilde{\alpha}$ . Again the coupling is approximately overcome through the replacement of the uncertain parameters with their expectations and use of the scheme we introduced for the assessment of  $\lambda_j$  when the  $t_j$ 's differ from each other.

The first step consists, then in assessing  $\beta$ , since it is independent of  $\tilde{\alpha}$  and  $\tilde{M}_u$  (see equation (10)). Let now  $\beta_j = \xi_j \beta$  where  $\beta$  is statistically independent of the  $\xi_j$ 's. It follows from equation (10) that

$$L_{\epsilon | \underline{\xi}, \beta} = \left[ \prod_j (\xi_j \beta)^{n_j} \right] e^{-\beta \sum_j \tilde{\delta}_j \xi_j} \quad (29)$$

if we let

$$p'_{\underline{\xi}, \beta} = \Gamma(m') \left[ \prod_j \frac{(\xi_j \beta)^{m'_j - 1}}{\Gamma(m'_j)} \right] e^{-\beta \sum_j \tilde{\delta}'_j \xi_j} \quad (30)$$

we get

$$L''_{\underline{\xi}, \beta} = \Gamma(m'') \left[ \prod_j \frac{(\xi_j \beta)^{m''_j - 1}}{\Gamma(m''_j)} \right] e^{-\beta \sum_j \tilde{\delta}''_j \xi_j} \quad (31)$$

where we have set  $\tilde{\delta}''_j = \sum_j \tilde{\delta}_j \xi_j$ , a constant because of the assumed independence between  $\beta$  and the  $\xi_j$ 's. Integrating with respect to  $\beta$  we get

$$L''_{\underline{\xi}} = \Gamma(m'') \prod_j \frac{n_j^{m''_j - 1}}{\Gamma(m''_j)} \propto \prod_j n_j^{m''_j - 1} \quad (32)$$

where  $n_j$  is now  $\xi_j \tilde{\delta}''_j / \tilde{\delta}''$  and  $\sum_j n_j = 1$ . Finally,  $E'' \xi_j = (m''_j / m'')$  ( $\tilde{\delta}'' / \tilde{\delta}''_j$ ) while the second member in equation (2) now gives us  $c''^2 \xi_j$  and mutatis mutandis equations (21)-(23) still hold. Notice that  $n'$  and  $m'$  as related to  $\beta$  are ordinarily greater than those associated with  $\lambda_0$  and  $\alpha$ . Notice also that when not all the  $\beta_j$ 's are equal,  $\ln \lambda$  does not comply with equation (4), so  $\beta$  plays then the mere role of an arbitrary parameter.

The approach is of course inapplicable to the distributions of  $M_{u_j}$ . For each region the distribution must be based on local tectonic information if available, and blind correlations with other regions play no role.

## EXAMPLES

With the purpose of illustrating first the more basic concepts we will present examples in which we meet problems in roughly the reverse order to that in which they are met in practice.

1 Single region with one period of observation. Consider a single region for which  $M_0 = 4$ , we have arrived at rather flat prior distributions of  $\tilde{\alpha}$  and  $\beta$ , and there are no studies of local tectonic conditions. We have assigned  $\tilde{\alpha}$  and  $\beta$  gamma-2 distributions with  $n' = 0.1$  for  $\tilde{\alpha}$  and 1 for  $\beta$ ,  $\tilde{\tau}' = 0.4$  yr, and  $\delta' = 0.5$ . (In practice  $n'$  would almost surely exceed 4 for  $\beta$ , say  $n' = 6$  and  $\delta' = 3$  would have been more representative. We chose the lower values to accentuate differences between successive cycles.) We adopt equation (5) with  $x_1 = 3$ ,  $x_2 = 9.2$ ,  $a_1 = 5$ , and  $a_2 = 3$  for the prior likelihood function of  $M_u$ . Seismic data for an 80-yr period of observation were generated through simulation (see Appendix 1) using  $\tilde{\alpha} = 0.25/\text{yr}$ ,  $\beta = 2$ , and  $M_u = 8$ . Table 1 displays the results of two simulation runs.

We begin by using equations (7)-(11) for calculating posterior distributions on the basis of the first run. Since  $M_1$  exceeds 3,  $E''M_u$  will be greater than 6.875. We will tentatively use 7.4,  $E''\tilde{M}_u = 7.4 - 4 = 3.4$ . Also tentatively,  $E''\beta = E'\beta = 1/0.5 = 2$ . Then  $\tilde{\tau} = (1 - e^{-2 \times 3.4}) \times 80 = 79.91$  yr and so  $\tilde{\tau}'' = 80.31$  yr. According to the table,  $n = 23$ ,  $\tilde{\delta} = 100.08 - 23 \times 4 = 8.08$ . Hence,  $E''\tilde{\alpha} = 23.1/80.31 = 0.2876/\text{yr}$ ,  $c''\tilde{\alpha} = 1/\sqrt{23.1} = 0.2081$ ,  $E''\beta = 24/8.58 = 2.7972$ , and  $c''\beta = 1/\sqrt{24} = 0.2041$ . We evaluate  $E''M_u$  and  $c''M_u$  numerically using the likelihood function of the observations (equation (11)) and the prior likelihood function of  $M_u$  (equation (5)) and noticing that the posterior is zero for  $M_u \leq M_1$ . We get  $E''M_u = 6.90$ ,  $c''M_u = 0.1353$ . (Had we merely used equation (5) for the posterior likelihood truncating it at  $M_u = 5.14$  we would have found  $E''M_u = 6.99$ ,  $c''M_u = 0.1267$ .) Now we go through a second cycle of computations using the expected values we have just gotten. To the number of significant figures given, none of our results changes save that now  $E''\tilde{\alpha} = 0.2874/\text{yr}$ .

Use of equation (12) yields  $|e - \hat{\beta}| < 10^{-9} |\hat{\beta} - \beta|$ , and so no further refinement is justified.

Finally we repeat our analysis with data from the second run. We get  $E^{\hat{\alpha}} = 0.2263$ ,  $c^{\hat{\alpha}} = 0.2351$ ,  $E^{\beta} = 1.4022$ ,  $c^{\beta} = 0.2249$ ,  $E^{M_u} = 7.92$ ,  $c^{M_u} = 0.0493$ . (Using equation (5) for the posterior likelihood of  $M_u$ , truncated at  $M_u = 7.37$ , would have yielded  $E^{M_u} = 7.94$ ,  $c^{M_u} = 0.0494$ .)

Comparison of results for the two runs with the parameters used in the simulation shows that such small samples of earthquake magnitudes can be quite misleading. We also conclude that a single cycle of the iteration procedure is ordinarily sufficient, that the refinement consisting in use of equation (12) is rarely if ever justified, and that the conservative estimate of  $E^{M_u}$  and  $c^{M_u}$ , in which  $\ell_{M_u}''$  is taken equal to  $\ell_{M_u}'$  truncated at  $M_1$ , is often adequate. (It can be shown to be always conservative in that it overestimates both  $E^{M_u}$  and  $c^{M_u}$ .)

2 Single region with two observation periods. Earthquakes in the region considered in Example 1 have also been observed during an 80-yr period with  $M_{01} = 4$ . Prior to this all earthquakes with  $M > 6$  were registered over a period of 800 yr. Now  $\hat{\tau} = 80(1 - e^{-\beta M_u}) + 800(e^{-2\beta} - e^{-\beta M_u})$ . We will take  $n'$ ,  $\hat{\tau}'$ , and  $\hat{\delta}'$  as for Example 1 and again assume there are no studies of local tectonics. Results of simulation using the same parameters as for Example 1 but both values of  $M_{0k}$  and both of  $t_k$  appear in Table 2.

We will tentatively employ  $E^{M_u} = 7.9$  and  $E^{\beta} = 2$ . Then  $\hat{\tau} = 94.36$  yr,  $\hat{\tau}'' = 94.76$  yr, and since  $n = 26$  and  $\hat{\delta} = 120.01 - 4 \times 26 = 16.01$ , we get  $E^{\hat{\alpha}} = 0.2754/\text{yr}$ ,  $c^{\hat{\alpha}} = 0.1957$ ,  $E^{\beta} = 1.6354$ , and  $c^{\beta} = 0.1925$ . Consequently,  $E^{M_u} = 8.24$ ,  $c^{M_u} = 0.0344$ . A second cycle changes  $E^{\hat{\alpha}}$  into 0.2374/yr but does not alter the other values computed, up to their last significant figures.

From equation (12),  $\beta = 9.7 \times 10^{-5} + 0.99994\hat{\beta}$ , and we can say that it is  $\hat{\beta}$  that has the gamma-1 distribution with the parameters we obtained and that the distribution of  $\beta$  can be obtained therefrom.

3 Three tectonically similar regions. Data for this problem are contained in Table 3. For the assessment of  $\lambda_0$  and  $\alpha$  we choose  $n' = 1$ ,  $t' = 1$  yr while for that of  $\beta$ ,  $n' = 2$ ,  $\hat{\delta}' = 0.8$ . In

assessing  $\xi_j$ , we take the regions to be sufficiently similar so that  $\delta = 0.1$  or, if they were of equal size,  $\rho'_{jk} = 0.6$ . There are no local studies to allow improving on the estimates of maximum possible magnitudes beyond what is given by equation (5) with  $a_1 = 5$ ,  $a_2 = 3$ ,  $x_1 = 3$ ,  $x_2 = 9.2$  and by seismic data.

For  $\lambda_0$  we get  $n'' = 1 + 85 = 86$ ,  $t'' = 1 + 42 = 43$  yr and so  $E''\lambda = 86/43 = 2.00/\text{yr}$  and  $c''^2\lambda = 1/86 = 0.0116$ .

From equation (25) with  $\delta = 0.1$  and  $N = 3$ ,  $m' = 16.22$  for the prior distributions of  $\xi_j$ . According to equation (27),  $m' \approx 19$ , and from equation (28),  $m' \geq 6$ . We will assign  $m'$  a prior distribution discretized as in Table 4. Application of equation (21) gives the posterior probabilities in the third column. Then using  $m' = 12$  for example, we get  $m'_1 = 12/6 = 2$ ,  $m''_1 = 2 + 5 = 7$ ,  $m'' = 12 + 85 = 97$ ,  $E''\xi_1 = 7/97 = 0.07216$ ,  $c''^2\xi_1 = 90/7 \times 98 = 0.1312$ . Next we compute the weighted mean of  $E''\xi_1$ , 0.07758. The variance of these values is  $1.012 \times 10^{-5}$ , which we add to the weighted mean of the individual variances to get  $6.8775 \times 10^{-4}$ , whence  $c''^2\xi_1 = 0.1160$ . Consequently,  $E''\lambda_1 = 0.07758 \times 2.00 = 0.1552/\text{yr}$  from equation (22), and  $c''\lambda_1 = 0.1289$  from equation (23),  $c''\lambda_1 = 0.3591$ . Had we disregarded information from the other two regions we would have arrived at  $E''\lambda_1 = (5 + 1/6)/43 = 0.1202$ ,  $c''\lambda_1 = 1/\sqrt{16 + 5} = 0.4399$ .

For  $\beta$  we get  $n'' = 87$ ,  $\tilde{\lambda} = 34.8$ , so  $E''\beta = 2.50$ ,  $c''^2\beta = 0.0092$ .

We now assign  $m'$  the prior distribution discretized as in Table 5. From equation (21) we get the posterior distribution in the third column. We take  $E'\xi_j = 1$  for all  $j$ . Now, using  $m' = 30$  for example, we obtain  $m'' = 30 + 85 = 115$  and  $\tilde{\lambda}'' = 115/2.5 = 46$ , whence  $\tilde{\lambda}' = 46 - 34 = 12$ , which we distribute among the regions in proportion to  $V_j$ . By adding  $\delta'_j$  to  $\delta_j$  we get the  $\delta''_j$  shown. It follows that  $E''\beta_1 = 10/5 = 2.0000$ ,  $c''^2\xi_1 = 105/100 \times 116 = 0.0905$ , and so on. Proceeding as we did with  $\lambda_j$  we find  $E''\beta_1 = 2.0350$ ,  $c''\beta_1 = 0.3041$ . These results compare with the ones we would have obtained disregarding information from the other zones:  $E''\beta_1 = (2/6 + 5)/(0.8/6 + 3) = 1.7021$ ,  $c''\beta_1 = 0.4330$ .

By assigning  $M_{uj}$  the beta distribution in equation (5) truncated at  $M_{1j}$  we get the first estimates of  $E''M_{uj}$  in Table 6. These, together with the computed  $E''\beta_j$ , furnish a first approximation to  $\tilde{\tau}''_j$ . Next when  $m' = 12$ , we compute  $E''\tilde{\alpha} = 7/42.97 +$

$34/42.99 + 59/43.00 = 2.0002/\text{yr}$ ,  $c''^2 \tilde{\alpha} = c''^2 \lambda$ ,  $\tilde{\tau}'' = 0.07216 \times 42.97 + 0.35052 \times 42.99 + 0.57732 \times 43.00 = 42.9941 \text{ yr}$ , and repeat for  $m' = 18$  and  $24$ . We obtain  $E'' \tilde{\alpha}_j$  and  $c'' \tilde{\alpha}_j$  as we did for  $\beta_j$ . Using equation (11) we recompute  $E'' M_{uj}$  and obtain  $c'' M_{uj}$ . The expected maximum possible magnitudes are sufficiently close to their first approximation as not to justify a second cycle.

### SUMMARY AND CONCLUSIONS

In assessing local seismicity we must rely heavily on empirical information. This consists of seismic data from the region of interest and from regions geotectonically similar to it. The latter, together with the meager theoretical bases available, permits constructing prior distributions of the seismicity parameters. Through use of Bayes' theorem one can combine these distributions with data from the region in question to obtain a posterior, probabilistic description of seismicity.

In many cases it is justified to idealize the earthquake generating process as Poisson. A general bayesian solution is given for this situation. Under the same circumstances it is also reasonable to approximate the exceedance rate as  $\lambda(M) = \alpha(e^{-\beta M} - e^{-\beta M_u})$  where  $\lambda$  is the expected number of times per year that magnitude  $M$  is exceeded,  $M \geq M_0 =$  threshold magnitude beyond which there are complete data,  $M_u =$  maximum possible magnitude, and  $\alpha$  and  $\beta =$  parameters. To  $\lambda(M_0)$  is assigned a natural conjugate gamma-1 distribution. Parameters  $\alpha$ ,  $\beta$ , and  $M_u$  are statistically coupled through the likelihood function  $L_{\epsilon|\underline{\theta}}$  where  $\epsilon$  is the event observed and  $\underline{\theta}$  is the vector of seismicity parameters. However, by shifting the origin of magnitudes, which changes  $\alpha$  and  $M_u$  into  $\tilde{\alpha}$  and  $\tilde{M}_u$ , we can write with good accuracy  $L_{\epsilon|\underline{\theta}} = L_{\epsilon|\tilde{\alpha}} L_{\epsilon|\beta} L_{\epsilon|\tilde{M}_u}$ . Then  $\tilde{\alpha}$  and  $\beta$  are given a treatment similar to  $(M_0)$  while for  $M_u$  we choose as prior a beta distribution. Results can be refined through use of a simple scheme which, however, is rarely if ever justified. An approximation is introduced to deal with cases in which data come from periods of observation having different  $M_0$ s. It is found that in all cases the truncation, at the maximum observed magnitude, of the prior distribution of  $M_u$  gives satisfactory results.

To make explicit use of data from similar regions it is postulated that the  $\lambda(M_0)$  for the  $j$ th region can be written as  $\xi_j \lambda(M_0)$  where  $\lambda(M_0)$  refers to the set of  $N$  similar regions and  $\lambda(M_0)$  and the  $\xi_j$ s are statistically independent save that  $\sum_1^N \xi_j = 1$ . The joint natural conjugate prior likelihood function for  $\xi$  is the multinomial beta  $\prod_j \xi_j^{m_j-1}$  where the  $m_j$ 's are prior parameters. These are taken proportional to the prior expected numbers of earthquakes in each region. Their sum,  $m' = \sum_1^N m_j$ , measures the degree of correlation expected among the seismicities of the various regions. Since there is little experience in choosing  $m'$ , guidelines are supplied for the purpose. One criterion is based on empirical data, another on the postulated coefficients of correlation between  $\lambda(M_0)$ s for the various regions, and a third criterion, based on entropy maximization, gives a lower bound on  $m'$ .

A similar approach is used for the  $\beta$ s of the different regions, save that the condition  $\sum_1^N \xi_j = 1$  is replaced with the constraint that a certain linear combination of these variables be constant. The same scheme applies to  $\lambda(M_0)$  when the times of observation differ from region to region. Parameters  $\alpha_j$  are given much the same treatment.

Numerical examples illustrate the methods described and show the adequacy of the approximations involved.

#### APPENDIX 1 SIMULATION

We wish to simulate a multiple Poisson process that generates earthquakes with magnitudes  $M_i$ ,  $i = 1, \dots, n$ ,  $M_j \leq M_i$  if  $j > i$ , when the exceedance rate is given by equation (4). Let  $y = \alpha t e^{-\beta M}$ ; so  $\lambda t = y - y_u$ ,  $y_u = y(M_u)$ ,

$$y_{i+1} = y_i - \ln x_i, x_i \text{ uniformly distributed in } 0, 1$$

$$y_1 = y_u - \ln x_0$$

$$M_i = \frac{1}{\beta} \ln \frac{\alpha t}{y_i}$$

The procedure follows immediately from treating the Poisson nature of the generation process, in which  $M_i$  are the magnitudes  $M$ .

The simulation is a simple matter to generate such as from a digital base. The only difficulty is to generate the  $x_i$  values. This can be done by using a random number generator which produces values between 0 and 1.

APPENDIX 2 MAXIMUM-ENTROPY CRITERION FOR  $m'$ 

Let  $\xi_j$ ,  $j = 1, \dots, N$  be a set of random variables about which all we know is that  $0 \leq \xi_j \leq 1$  for all  $j$  and  $\sum_1^N \xi_j = 1$ . We wish to find the joint probability density function of  $\underline{\xi}$  such that  $-\int_0^1 \dots \int_0^1 p_{\underline{\xi}} \ln p_{\underline{\xi}} d\xi_1 \dots d\xi_N$  be maximum. Suppose first that all  $\xi_j$  were fixed except  $\xi_1$  and  $\xi_2$ . It is known that the conditional distribution of  $\xi_1$  giving maximum entropy would then be uniform between 0 and  $1 - \sum_3^N \xi_j$  and that hence,  $\xi_2$  is distributed identically. Since this is true for all pairs of  $\xi_j$ , the joint likelihood function is  $\prod_j \xi_j^{m_j - 1}$  with  $m_j = 1$  for all  $j$  and so  $m' = N$ .

In no case can any of the  $m_j$ 's be smaller than 1, for  $S$  would be  $-\infty$  while it is finite when  $m_j \geq 1$  for all  $j$ . Hence, when not all the expected  $\xi_j$ 's are equal,  $m' \geq 1/\min_j E'\xi_j$ . Now let  $S_j$  be the entropy of the marginal probability density function of  $\xi_j$ . We can show that when  $m_j \geq 1$ ,  $S_j$  decreases with  $m_j$ . Therefore the equal sign gives the maximum  $S$ . Hence, in all cases  $m' \geq 1/\min_j E'\xi_j$ .

## ACKNOWLEDGMENTS

A major part of this paper was done while I was visiting professor at the Politecnico de Milano. I am grateful to Luis Esteva for his inspiration, encouragement, and critical review of the manuscript. The work was sponsored by the Comisión Federal de Electricidad.

## REFERENCES

1. B. Gutenberg and C.F. Richter, *Seismicity of the Earth (and Associated Phenomena)*, Princeton University Press, Princeton, NJ (1942).
2. J. Lomnitz-Adler, "On the magnitude frequency relation of asperity models", to be published.
3. S.K. Singh, M. Rodríguez, and L. Esteva, "Statistics of small earthquakes and frequency of occurrence of large earthquakes along the Mexican subduction zone", *Bull. Seismol. Soc. Amer.*, **73**, 1779-96.

4. S. Wesnousky, C.H. Scholz, K. Shimazaki, and T. Matsuda, "Earthquake frequency distribution and the mechanics of faulting", submitted for pub to *Jour. Geophys. Res.* (1983).
5. T. Utsu, "Aftershocks and earthquake statistics", *III Jour. Fac. of Sci., Hokkaido Univ., Series VII, 3*, 379-442 (1971).
6. G. Purcaru, "A new magnitude-frequency relation for earthquakes and a classification of relation types", *Geophys. Jour. Royal Astron. Soc.*, **42**, 61-79 (1975).
7. J.C. Lahr and C.D. Stephens, "Alaska seismic zone: possible example of nonlinear magnitude distribution for faults", *Earthquake Notes*, **53**, 66 (1982).
8. N.M. Newmark and E. Rosenblueth, *Fundamentals of Earthquake Engineering*, Prentice-Hall, Inc. Englewood Cliffs, NJ (1971).
9. H. Raiffa and R. Schlaifer, *Applied Statistical Decision Theory*, Harvard University Press., Cambridge, MA (1961).
10. L. Estevea, "Bases para la formulaci3n de decisiones de dise1o s3smico", doctoral thesis, Univ. Nac. Aut. de M3x., Mexico (1968).

Table 1. Simulation runs for Example 1

$i$	$M_i$		$i$	$M_i$	
	Run 1	Run 2		Run 1	Run 2
1	5.14	7.37	13	4.15	4.29
2	4.99	5.32	14	4.15	4.28
3	4.96	5.31	15	4.14	4.27
4	4.77	4.92	16	4.12	4.25
5	4.63	4.78	17	4.12	4.21
6	4.62	4.66	18	4.10	4.12
7	4.44	4.64	19	4.08	
8	4.41	4.62	20	4.06	
9	4.39	4.59	21	4.05	
10	4.37	4.54	22	4.02	
11	4.21	4.50	23	4.00	
12	4.16	4.38	Sum	100.08	85.05

Table 2. Simulation run for Example 1

$i$	$M_i$	$i$	$M_i$	$i$	$M_i$
1	7.85	11	4.27	21	4.12
2	6.47	12	4.20	22	4.10
3	6.14	13	4.20	23	4.04
4	5.77	14	4.19	24	4.04
5	5.05	15	4.16	25	4.04
6	4.67	16	4.16	26	4.00
7	4.63	17	4.14	Sum	120.01
8	4.63	18	4.14		
9	4.37	19	4.14		
10	4.36	20	4.13		

Table 3. Data for Example 3

$j$	$A_j$	$n_j$	$\tilde{\delta}_j$	$M_{1j}$
1	1/6	5	3	6.84
2	2/6	30	14	7.51
3	3/6	50	17	7.89
Sum	1	85	34	

$$t = 42 \text{ yr}, M_u = 4$$

Table 4. Assessment of  $\xi_1$ , Example 3

$m'$	$P'_{m'}$	$P''_{m'}$	$m'_1$	$m''_1$	$m'$	$E''\xi_1$	$c''^2\xi_1$
12	0.2	0.1927	2	7	97	0.07216	0.1312
18	0.6	0.6096	3	8	103	0.07767	0.1142
24	0.2	0.1977	4	9	109	0.08257	0.1010

Table 5. Assessment of  $\beta_\lambda$ , Example 3

$m'$	$P'_{m'}$	$P''_{m'}$	$m'_1$	$m''_1$	$m''$	$\tilde{\delta}'_1$	$\tilde{\delta}''_1$	$E''\beta_\lambda$	$c''^2\beta_\lambda$	$E''\beta_2$	$E''\beta_3$
30	0.2	0.2142	5	10	115	2	5	2.0000	0.0905	2.2222	2.8261
36	0.6	0.5998	6	11	121	2.4	5.4	2.0370	0.0820	2.2340	2.8099
42	0.2	0.1860	7	12	127	2.8	5.8	2.0690	0.0749	2.2449	2.7953

Table 6. Assessment of  $\tilde{\alpha}$  and  $M_{uj}$ 

$j$	$E''B_j$	First Approximation		Results of first cycle		
		$E''M_{uj}$	$\tilde{\tau}_{uj}$	$E''\tilde{\alpha}_j$	$E''M_{uj}$	$c'M_{uj}$
1	2.0350	7.64	42.97	0.1553	7.6360	0.0677
2	2.2335	8.03	42.99	0.6991	8.0252	0.0448
3	2.8107	8.27	43.00	1.1458	8.2691	0.0330



**DIVISION DE EDUCACION CONTINUA  
FACULTAD DE INGENIERIA U.N.A.M.**

ANALISIS DE RIESGO SISMICO

MICROZONING: MODELS AND REALITY

DR. LUIS ESTEVA

JULIO, 1985

## MICROZONING: MODELS AND REALITY

Contribution to a panel session on Ground Motion Characteristics

6WCEE, Delhi, 1977

by

Luis Esteva<sup>1</sup>

### INTRODUCTION

Nobody doubts that local conditions usually have a significant influence on the characteristics of earthquake ground motion. What is not agreed upon, however, is the manner in which that influence must be evaluated. When one talks about microzoning, attention is usually focused on shear-beam models of stratified soil formations and in unidimensional, vertically traveling shear waves. But strong-motion and seismological records have shown that those models can only be applied to a much narrower range of conditions than is usually believed, and that many other geologic or topographic features can have a more pronounced influence on ground motion than the presence of sediments. More general analytical models have been developed in order to account for two-dimensional and three-dimensional response and various types of arriving waves, but their validity and range of applicability have not been determined yet. Because of this, and because of the greater complexity of these models as compared with shear-beam amplification models, they have not gained wide acceptance in the solution of actual engineering problems.

Not only is the shear-beam amplification model the object of strong controversy with respect to the types of waves that significantly contribute to the earthquake motion at a site, but also with respect to the lack of consistent criteria intended to define base rock level, i.e., the level at which usual intensity-attenuation laws are supposed to be valid, and above which local soil contributes to modify intensity and frequency content of seismic motions. In other words, it cannot be uniquely defined what constitutes local conditions and what is a portion of the path. Those criteria can be objected also on the grounds that the influence of local soil conditions is often accounted for twice when making estimates of seismic risk: as a random factor associated with the path when establishing empirical attenuation laws and as a systematic correction associated with local conditions when studying amplification.

But microzoning is not only a matter of ground-motion amplification; it also implies formulation of consistent criteria to define design spectra at different sites, and evaluation of liquefaction potential. The former point requires consideration of the different laws that govern amplification of different types of waves and different directions of arrival, as well as their corresponding probabilities; the latter is not covered by this discussion, as it will be included in another panel session. Thus, the paper deals with the problems of ground motion characteristics, under the framework of conceptual models, analytic results and observed facts. The paper is not intended to be a state-of-the-art report although it is based on one

---

<sup>1</sup> Institute of Engineering, National University of Mexico

(Ruiz, 1976) The intention of the author is mainly to point out some basic questions pertinent to the topic, aiming at the generation of vivid and fruitful discussion.

## SEISMIC WAVES

The results of some analytical studies show that the influence of local soil on the ground motion is strongly dependent on the nature of the incoming seismic waves. Hence, analytical prediction of the amplitudes of ground motion at a site characterized by given local conditions as compared with those that would occur under standard conditions requires both the decomposition of the motion into various types of incoming waves, and the formulation of models adequate for the study of amplification and transformation of those types of waves. Despite the very significant effort devoted by seismologists to the formulation of analytical models for the study of wave amplification and transformation, very little of their contributions is either available or of use to engineers, as those models deal in general with the types of waves that are recorded at large epicentral distances (far field), or consider highly idealized topographical features. These results should not be overlooked, however, as they can provide a qualitative insight to many engineering problems.

If a reasonable degree of success is to be attained in the prediction of the influence of local conditions for a sufficiently wide range of cases, a lot of understanding has to be previously achieved about the decomposition of ground motion into different types of seismic waves in the near and intermediate fields. Obviously, the detailed source mechanism and the propagation path can be decisive in the directions and relative amplitudes of the most significant incoming waves, and hence on the laws governing ground motion amplification.

## MECHANISM, PATH AND LOCAL CONDITIONS

The profusion of heterogeneities, irregularities and discontinuities in the earth's crust (Fig 1) is responsible for the complex patterns of reflection, refraction, and scattering that seismic waves suffer in their path from source to site. Hence, it is not surprising that the influence of mechanism and path on ground motion characteristics is in some instances more pronounced than that of local conditions. This influence stems both from the modification of the surface ground motion itself, independent of local conditions, and from the fact that the different types of seismic waves resulting from mechanism and path effects are modified by local soil in different manners.

Fig 2 shows the two main paths followed by seismic energy from the source to a site of interest: through the interior of the crust, in the form of body waves, and along the surface, in the form of surface waves. But this picture still displays an oversimplified conception of the process: the source is not a point, but a large volume, and the influence of path is much more pronounced and complex than is implied by Fig 2.

The general type of source mechanism, and not only the detailed history of relative displacement along a fault, has a strong influence on the types of seismic waves generated, and hence on the motion characteristics for standard ground conditions, and in the manner in which local conditions modify them. Thus, strike-slip motion tends to produce a higher proportion of SH and Love waves, while subduction faults tend to produce higher proportions of P, SV and Rayleigh waves. The fact that seismic waves are generated from a large volume that may extend as far as the ground surface or its close proximity means that a significant portion of the motion at the near field should be made up of the contribution

of body waves that travel at very low angles with respect to the horizontal (Fig 3). These waves are probably guided along stratified formations and then modified by local conditions according to patterns similar to those affecting surface waves. Besides, it is likely that they give place to conventional surface waves that significantly contribute to ground motion at short epicentral distances and in the range of small and moderate frequencies. This pattern of energy travel seems plausible, and provides an explanation to the failure of conventional amplification theory to adequately predict the influence of local conditions.

The complexity of the path followed by waves is another reason for stating that surface ground motion at the near field is not the result of the superposition of a short number of wave trains: every wave impinging on a crust heterogeneity, subsurface discontinuity or topographic feature, gives place to a number of secondary trains of all types of waves (Fig 4).

Whatever the mechanism and the path of the waves for a given shock, it is of interest to assess the influence of local conditions; but, as Fig 5 shows, that influence cannot in general be made to depend only on the stratified soil formations underlying the site of interest: as an important portion of the energy may be traveling in the horizontal direction, the meaning of the term *local conditions* should be extended to include geologic and topographic features in the immediate vicinity of the site. Local amplification would hence be sensitive to the direction of wave arrival.

Even in the case that adequate tools were available for estimating the influence of local conditions on the amplification functions for the various significant types of seismic waves, the problem would remain of determining the trains of waves of different types that would arrive from a given direction. This is probably not feasible, when dealing with near-field problems, first because of the possible occurrence of a large number of significant wave trains of different types incoming from different directions, and second because it is not always clear whether a given geologic or topographic accident should be taken as portion of the path—the influence of which would be included as a random factor in the experimental error of an *intensity attenuation expression* (expression relating intensity with magnitude and distance)—or of the local conditions—the influence of which should be included as a systematic correction—when trying to predict ground motion produced by seismic waves arriving from a given direction. For instance, coming back to Fig 5, a promontory such as *B* could be taken as a part of the path or of the local conditions for the purpose of assessing the contribution of surface waves coming from the left to ground motion at *A*, depending on whether the local zone is assumed to be bounded by line 1 or 2, respectively. Because the absence or presence of features such as these has not been explicitly included in empirical attenuation expressions, a unique criterion cannot be easily established. For the purpose of microzoning, however, a great deal of information is provided by ratios of surface wave amplitudes at *A* and *B*—and not necessarily their absolute values— for earthquakes originated at the left of the figure.

### OBSERVED FACTS

Before the San Fernando earthquake of 1971, conceptual models of soil-related intensity amplification had gained their main support from nearly qualitative comparisons of observed differences between intensities on firm ground and on sedimentary deposits at a number of sites, notably Tokyo, San Francisco, Mexico City and Caracas. A more quantitative support to models based on the concept of vertically traveling SV waves had been provided by the comparison of predicted and observed response of the soft clay

deposits underlying Mexico City (Herrera *l. et al.*, 1965); but conclusions valid for very peculiar conditions—existence of a very pronounced contrast between shear wave velocities of soil and underlying material—were being indiscriminately extrapolated, in spite of the fact that, in order to apply the same criterion, arbitrary decisions had often to be made concerning the portion of the ground profile that should be considered as a filter that would amplify standard-conditions-ground-motion. But records obtained during San Fernando earthquake disclosed the limitations of the mentioned criterion. Although a large portion of the area affected by that earthquake is known to be underlain by deep sedimentary formations (Fig 6), no pronounced contrast between shear wave velocities is apparent. Fig 7 (from Hudson, 1972) shows a sampling of peak accelerations measured at different sites. Included are all sites for which a clear distinction could be made between rock and alluvium as the basic site condition. It is evident that many factors other than distance and local site characteristics must be important.

Influence on ground motion of fault mechanism and propagation path has been disclosed by recordings obtained at a number of sites during several events. Thus, Udawadia and Trifunac (1973) analyzed a group of 15 events recorded at El Centro, California, characterized by short epicentral distances and magnitudes ranging from 3 to 6.8; the same authors (Trifunac and Udawadia, 1974) studied the records obtained at 6 stations located in the metropolitan area of Los Angeles during three different earthquakes, and Hudson (1972) analyzed the records of a number of seismoscopes and accelerographs obtained within an area of 40 square miles during San Fernando earthquake.

The 15 events recorded at El Centro were classified into four sub-groups, according to source azimuth with respect to the station, and Fourier spectra of records within each sub-group were compared. Group I included four events, three of them having the same epicenter, but different magnitudes. Spectral shapes of the components corresponding to the various events differ considerably among themselves. As propagation path and local conditions are the same, differences can only be ascribed to differences in fault mechanism and perhaps to nonlinear effects. Group II includes four events with different magnitudes and origins and, again, no similarity attributable to path or local conditions can be detected in the records. For one event in particular, predominant frequencies are very low, which can be explained in terms of predominance of surface waves. Group III includes the Imperial Valley earthquake of 1940, the record of which has been analyzed (Trifunac, 1971a) leading to the conclusion that it actually consisted of the superposition of several events, each starting a few seconds after the previous one. Horizontal components are similar, but the vertical component of the Imperial Valley earthquake shows significantly higher ordinates for high frequencies. This is probably a consequence of the short epicentral distance, that implies low attenuation of body waves, and of the peculiar source mechanism. Finally, the last group included events with large epicentral distances—about 150 km—and records were characterized by the low frequencies typical of surface waves. Despite very clear similarities between magnitude and origin of events in this group, their spectral shapes are significantly different, thus suggesting predominance of source effects over path and local conditions.

Similar conclusions are obtained from Trifunac and Udawadia's study concerning the records obtained at six stations during Borrego Mountain (1968), Lytle Creek (1970) and San Fernando (1971) earthquakes: source mechanism and epicentral distance significantly affected the records, while local conditions played only a secondary role. Of the six stations, four lie within Los Angeles Metropolitan area, two of them less than 1 km apart; two are located on base-rock and the other four—those within Los Angeles—on deep sediments of intermediate stiffness. In no case are dominant ground periods evident. An analysis of

records obtained at the four sites on sediments makes apparent the influence of source mechanism. For the Borrego Mountain shock, for instance, transverse displacements are systematically larger than radial ones, thus suggesting significant contribution of Love waves; the shapes of the displacement and velocity records are the same at all four sites, but their amplitudes differ, probably as a consequence of variations in the depth of alluvium from station to station, within a distance of 12 km. Records and spectra corresponding to the San Fernando earthquake are also very similar among themselves, but they differ in shape and in relative frequency content from those obtained during the other shocks. Large amplitudes of radial and transverse displacements have been ascribed (Hanks, 1975) to Rayleigh and Love waves, respectively. Fourier spectra of Borrego Mountain records at the four Los Angeles stations shown are very similar in the range of frequencies smaller than 1 hz; the similarity should not be ascribed to dominant group periods, but to the predominance of surface waves, given the long epicentral distance—about 200 km. For San Fernando earthquake, instead, the contribution of high frequencies is rather important, as could be expected, given the proximity of the source—40 km.

Hudson's observations during San Fernando earthquake covered a wide range of ground conditions, from crystalline rock to alluvial deposits 300 m deep. Notorious discrepancies were observed in seismoscope traces even for sites with very similar ground conditions, stressing the importance of other factors, such as topography or subsurface irregularities, pointed out, for instance, by Jackson (1971) and Boore (1972). A comparison of response spectra corresponding to rock and alluvium sites fails to show any systematic influence of local soil. The author concludes that the properties of response spectra at the same sites during another earthquake would probably show quite different relative variations. This implies that formulation of microzoning maps must be based on the analysis of records obtained during a sufficiently large number of intense earthquakes.

Some interesting cases have been presented in the literature, describing the overall response of some soil formations during strong earthquakes. Although the influence of local conditions was shown to be clear in those cases, it was also clear that it may not suffice to study the influence of the soil directly underneath the structure of interest, but that an analysis of the response of a wider area can explain observed facts. Two instances will be described in this respect: one corresponds to the Skopje earthquake of 1963, and the other to two records obtained at Hutt Valley, New Zealand.

Pocski (1969) describes the geological setting of Skopje: the city is located in a long valley along which flows the Vardar river. A cross section of the valley shows a large discontinuity of the sediment thickness along a line that follows the river course (Fig 8). The greatest intensity of damage on constructions was observed directly above the discontinuity, and was ascribed to the hypothetical occurrence of large rotational components of the ground motion with respect to a vertical axis, motivated by the also hypothetical difference in the horizontal response of the alluvial deposits at each side of the discontinuity.

The rotational response of a large volume of alluvium was actually detected by Stephenson (1974), when he analyzed the records obtained at two sites near Hutt Valley. The sites are 900 m apart, and are underlain by saturated recent alluvial deposits with shear wave velocities of about 100 m/sec. Spectral densities of acceleration at both sites show each a predominant direction of response, with a high statistical correlation between the corresponding predominant components, thus suggesting the torsional oscillation of a large mass of alluvium.

How should microzoning be influenced by effects such as those described in this section?

## EFFECTS OF TOPOGRAPHY

The largest acceleration ever recorded occurred at one of the abutments of Pacoima dam during the San Fernando earthquake and implied, according to Reimer *et al* (1973) a three-fold amplification of its peak value. Ratios of up to 30 between the peak ordinates of the Fourier spectrum of the velocity record obtained at the top and at the base of Kagel mountain were computed for several aftershocks of the mentioned event, while the corresponding ratios of peak ground velocities "only" reached 3.95. This implies a resonant effect of the mountain, which was explained by Davis and West (1973) in terms of the ratio of its average width and the length of shear waves. The values indicated are not necessarily amplifications with respect to standard conditions (whatever they are), as analytical studies show (see Fig. 9) that at some frequencies wave amplitudes tend to be amplified at the top of promontories and reduced at their base (Bouchon, 1973; Aki & Larner, 1970; Boore, 1972), but the fact remains that the effects of surface topography cannot be overlooked. Similar considerations can be made regarding the significance of subsurface topography: the distribution of structural damage in Skopje in 1963 was ascribed to excessive torsional oscillations in the region directly above a sharp discontinuity of soft layer thickness (Fig. 8) for incident waves that possessed significant horizontal components parallel to the discontinuity; and analytical studies predict focusing of waves in the vicinity of subsurface irregularities (Jackson, 1971). The interaction of subsurface topography and direction of wave arrival is illustrated in Fig 10 (Trifunac, 1971b), which shows relative amplitudes of the motion produced at the surface by SH waves arriving at a semicylindrical valley. Amplitudes vary with site location and with incidence angle at a fast rate, thus suggesting that detailed knowledge of subsurface topography and of directions and types of incoming waves would be required for the deterministic prediction of the influence of topographic features. As this knowledge is not easy to achieve at present, careful judgement must be exercised when trying to employ analytical results as those shown here in the predictions of seismic risk.

A further question stemming from the significance of surface and subsurface irregularities is that related to the homogeneity of the data set that has been used by different investigators in the derivations of empirical attenuation expressions: unless those sites for which the topographic conditions are suspected to have a significant systematic influence on ground motion are eliminated from the data set used to derive those attenuation expressions, we face the danger of accounting for the mentioned conditions twice: as random effects in one step and as systematic effects in another.

## MODELS AND REALITY

Theoretical considerations and observed facts concerning mechanism, path and local conditions, point at the complexities involved in the formulation of mathematical models intended to predict the influence of local conditions on ground motion.

Hence, the question arises of whether the role of those models is too limited to be of practical significance. This is probably too pessimistic an outlook although detailed simulations of near-field motions based on physical models that account for source, path and local conditions are probably beyond reach of present engineering practice, the writer believes that a fair degree of understanding of the parameters and mechanisms that affect ground motion amplification and attenuation can be gained by means of simplified analytical models that consider alternate patterns of energy liberation and propagation.

The significance of models as related to reality and to decision making in engineering is dramatically illustrated by the applicability of the vertically-traveling-shear wave model to the study of ground motion amplification in the valley of Mexico: this is the site on earth where that model has been most beautifully supported by instrumental evidence, and however, the shallow depths and large epicentral distances of earthquakes usually observed there imply that practically all energy must arrive in the form of surface waves. It is easy to understand that the apparent confirmation of the unidimensional-shear-wave model in this case stems from the fact that the large lengths of the incoming surface waves lead to the response of the soft soil formation far away from the borders of the valley according to a pattern very similar to that of the shear beam model. The agreement is accentuated because very little energy is radiated back to the base, and because a significant portion of it is radiated in accordance with the shear beam model. This form of soil response and the small ratio of energy radiation are responsible for the occurrence of dominant ground periods. For the same reasons, dominant ground periods determined by means of excitation applied at the surface coincide with those resulting from earthquake excitation. But the conditions that favor the practical applicability of the mentioned model in the case where a pronounced contrast exists between the soft formations and the base do not appear in the absence of that contrast, and conditions other than sediment properties may dominate the local pattern of intensity variations.

In an attempt at developing a unified approach to the combined intensity-attenuation and local-amplification effects for site underlain by stratified soil formations, Sanchez and Esteva (1977) made use of available data for the derivation of attenuation expressions that directly account for the systematic influence of local soil, while random deviations were dealt with as equation errors. Data of earthquakes recently recorded at sites where detailed information was available about local soil conditions (this means 50 horizontal components at 10 different sites) provided the basis for semiempirical attenuation expressions for Fourier spectra at the ground surface. These expressions are of the form  $F(\omega) = G(\omega; R, M) g(\omega; s)$ , where  $F(\omega)$  is the ordinate of Fourier spectrum for frequency  $\omega$ ,  $G$  accounts for source ( $M$ ) and path ( $R$ ) effects, and  $g$  is a function that accounts for amplification effects in terms of local soil properties ( $s$ ).  $G$  was assumed of the form  $b_1(R + c)^{-b_2} \exp(b_2 M)$ , and  $g$  was taken as the amplification function of an equivalent single-degree-of-freedom model of a linear shear beam assumed to represent the soil layers above firm ground. A number of expressions were derived for seven values of  $\omega$ , in accordance with three alternate definitions of firm ground: the surface material itself, or those with shear wave velocities of 400 and 800 m/sec, respectively. The results were disappointing: the ratio of observed to predicted ordinates of Fourier spectra was systematically greater than unity for the components recorded at the particular site where the computed values of  $g$  were highest (i.e., where a thick layer of very soft materials existed), and the standard deviation of that ratio for the whole ensemble of sites and records was very high and independent of the definition of firm ground. But Mohraz (1976) obtained significantly different intensity attenuation expressions for different alluvium thickness. A similar study was carried out by Faccioli (1976), who classified ground properties into four categories: crystalline rock, sedimentary rock (including stiff conglomerates and very compact sands), typical alluvial deposits with intermediate stiffness and soft deposits (loose sands and soft clays). He succeeded in obtaining empirical attenuation expressions for each of these categories, for which the standard deviation of error is lower than that associated with previous expressions that neglected the influence of local conditions (Esteva and Villaverde, 1973; Mc Guire, 1974). The systematic influence of such conditions is thus confirmed, as well as the inadequacy of the shear beam model to predict them.

Two-dimensional models as shown in Fig 11 can perhaps suffice for the qualitative study of

the overall patterns of wave generation and transformation. They should also prove useful for the understanding of the possible influence of irregularities and discontinuities found by different types of waves along their path, and for the assessment of local variability of intensities in the neighborhood of some geological or topographical accidents. Probably, they can even help at gaining some insight into the general patterns of waves arriving at a site, thus permitting the formulation of adequate amplification models. There are instances, however, where three-dimensional models may be required. One such case is the study of the amplified motion recorded at one of the abutments of Pacoima Dam during San Fernando earthquake; another would be the study of the response of an alluvial formation where torsional oscillations might be of importance.

Given a train of incoming waves, predictions of the resulting motion at a site with heterogeneous properties or irregular topography can be dealt with as a diffraction problem. However, standard analytical formulation (Morse & Feshbach, 1953) can only be applied in practice to simplified idealizations of actual conditions (see, for instance, Aki and Larner, 1970; Bouchon, 1973; Trifunac, 1971b). For more general applications, finite difference solutions of the wave equation (Boore, 1972), finite element wave-propagation investigations (Smith, 1974) and dynamic response studies of finite-element models of small local regions (Lysmer & Drake, 1971; Ayala & Aranda, 1977) have been undertaken. The latter formulation is very attractive to engineers, because it permits direct application of standard programs of frequency-domain or time-response dynamic analysis. But adequate boundary conditions have to be defined at the edges of the region under study in order to allow transmittal of incoming and outgoing waves without excessive energy losses or reflections. When incoming and outgoing waves are of the same type and have the same direction, theoretically exact boundary conditions can be established, expressed in terms of equivalent damping units (Lysmer & Drake, 1971; Tsai, 1969). Approximate solutions have also been formulated for the case of outgoing body waves of known type and unknown direction (Lysmer & Kuhlenmeyer, 1969) and these solutions have been extended to the combination of incoming and outgoing waves (Ayala & Aranda, 1977), but the general case of known incoming waves and unknown outgoing wave types and directions has not been sufficiently studied.

Despite these problems, criteria based on the time-history analysis of finite element models will probably gain wide acceptance in view of their ability to account for nonlinear soil behavior. But despite the importance usually ascribed to nonlinearities when trying to explain discrepancies between observed and predicted local amplification effects, it must be recognized that their influence is often overshadowed by the overall patterns of shock generation and propagation. It is this consideration that supports the usefulness of frequency-domain studies as advocated above.

### CONCLUDING REMARKS

Microzonation implies much more than influence of stratified soil formations. It implies a better knowledge of the fault mechanisms of earthquakes that significantly contribute to seismic risk at a site, study of the possible influence of path characteristics on the types of arriving seismic waves and hence on the manner in which local conditions will affect them. More general analytical models for the study of all factors affecting seismic waves from their source will have to be developed, adapted and implemented by engineers. But, as a consequence of the complexities inherent in the phenomena under study, those models should only play a role complementary to instrumental observations. Because path and

mechanism effects have been shown to affect local variations of ground motion, a large number of events will have to be recorded at every site of interest and its neighborhood before reliable conclusions can be drawn concerning those variations. Hence, small magnitude shocks should be given increased attention, as they will probably constitute the main source of information at some sites, in spite of their inability to provide information about the influence of nonlinear soil behavior associated with severe shocks. Deployment, operation and interpretation of the records of local instrumental networks should aim at the description of earthquake motion variability throughout small regions, and at the understanding of the patterns of seismic waves giving place to that variability.

#### ACKNOWLEDGEMENTS

The author wishes to express his gratitude to S. E. Ruiz for her assistance in the revision and interpretation of the literature, through the preparation of a state-of-the-art report. Critical reading of the manuscript by G. Ayala and J. Bielak is also gratefully acknowledged.

#### REFERENCES

- Aki, K. & Larner K., 1970, "Surface motion of a layered medium having an irregular interface due to incident plane SH waves", *J. Geophys Res.*, 75, pp. 933-954
- Ayala, G. & Aranda R., 1977 "Boundary conditions in soil amplification studies", 6WCEE, Delhi
- Boore D. M., 1972, "A note on the effect of simple topography on seismic SH waves", *Bull. Seism. Soc. Am.*, Vol 62, No. 1, pp. 275-284
- Bouchon, M., 1973, "Effect of topography on surface motion", *Bull. Seism. Soc. Am.*, Vol 63, No. 3, pp. 615-632
- Davis, L. L. & West, L. R., 1973, "Observed effects of topography on ground motion", *Bull. Seism. Soc. Am.*, Vol 63, No. 1, pp. 283-298
- Esteva, L. & Villaverde, L., 1973, "Seismic risk, design spectra and structural reliability", *Proc. 5WCEE*, Rome
- Faccioli, 1976, personal communication
- Hanks, T. C., 1975, "Strong ground motion following the San Fernando, California, earthquake. 1. Ground displacements", mentioned by Trifunac and Udvardia, 1974
- Herrera, I., Rosenblueth, E. & Rascón, O. A., 1965, "Earthquake spectrum prediction for the valley of Mexico", *Proc. 3WCEE*, Vol 1, pp 161-174
- Hudson, D. E., 1972, "Local distribution of strong earthquake ground motions", *Bull of the Seismological Soc. of America*, Vol 62, No. 6, pp. 1765-1786
- Jackson, P. S., 1971, "The focusing of earthquakes", *Bull. Seism. Soc. Am.*, Vol 61, No. 3, pp. 685-695
- Lysmer, J. & Drake, L. A., 1971, "A finite element method for seismology", *Methods in Computational Physics*, Cap. VI, University of California, Berkeley
- Lysmer, J. & Kuhlemeyer, R. L., 1969, "Finite dynamic model for infinite media", *Journ. Eng. Mech. Div. ASCE*, Vol 95, No. EM4, pp. 859-877

- Mohraz, B., "A study of earthquake response spectra for different geologic conditions", Bull. Seism. Soc. Am., Vol 66, No. 3, pp. 915-936
- Morse, & Feshbach, 1953, "Methods of Theoretical Physics", McGraw-Hill, Kogakusha, Tokyo
- Poceski, A., 1969, "The ground effects of the Skopje July 26, 1963 earthquake", Bull. Seism. Soc. Am., Vol 59, No. 1, pp. 1-29
- Reimer, R. B., Clough, R. W. and Raphael, J. M., 1974, "Evaluation of the Pacoima Dam accelerogram", SWCEB, Vol 2, pp. 2328-2337
- Ruiz, S. E., 1976, "Influencia de las condiciones locales en las características de los sismos", M S Thesis, Faculty of Engineering, National University of Mexico
- Sánchez-Sesma, F. J. & Esteva, L., 1977, "Intensity attenuation and local amplification: a unified approach", Institute of Engineering, National University of Mexico
- Smith, W. D., 1974, "A non reflecting plane boundary for wave propagation problems", Journal of Computational Physics, Vol 15, No. 4, pp. 492-503
- Stephenson, W. R., 1974, "Earthquake induced resonant motion of alluvium", Bull. New Zealand Nat. Soc. for Earthquake Engng, Vol 7, No. 3
- Trifunac, M. D., 1971a, "Response envelope spectrum and interpretation of strong earthquake ground motion", Bull. Seism. Soc. Am., Vol 61, No. 2, pp. 343-356
- Trifunac, M. D., 1971b, "Surface motion of a semi-cylindrical alluvial valley for incident plane SH waves", Bull. Seism. Soc. Am., Vol 61, pp. 1755-1770
- Trifunac, M. D. & Udawadia, F. E., 1974, "Variations of strong earthquake ground shaking in the Los Angeles area", Bull. Seism. Soc. Am., Vol. 64, No. 5, pp. 1429-1454
- Tsai, N., 1969, "Influence of local geology on earthquake motion", Ph. D. Thesis, California Institute of Technology, Pasadena, Calif
- Udawadia, F. E. & Trifunac, M. D., 1973, "Comparison of earthquake and microtremor ground motions in El Centro California", Bull. of the Seismological Soc. of America, Vol 63, No. 4, pp. 1227-1253

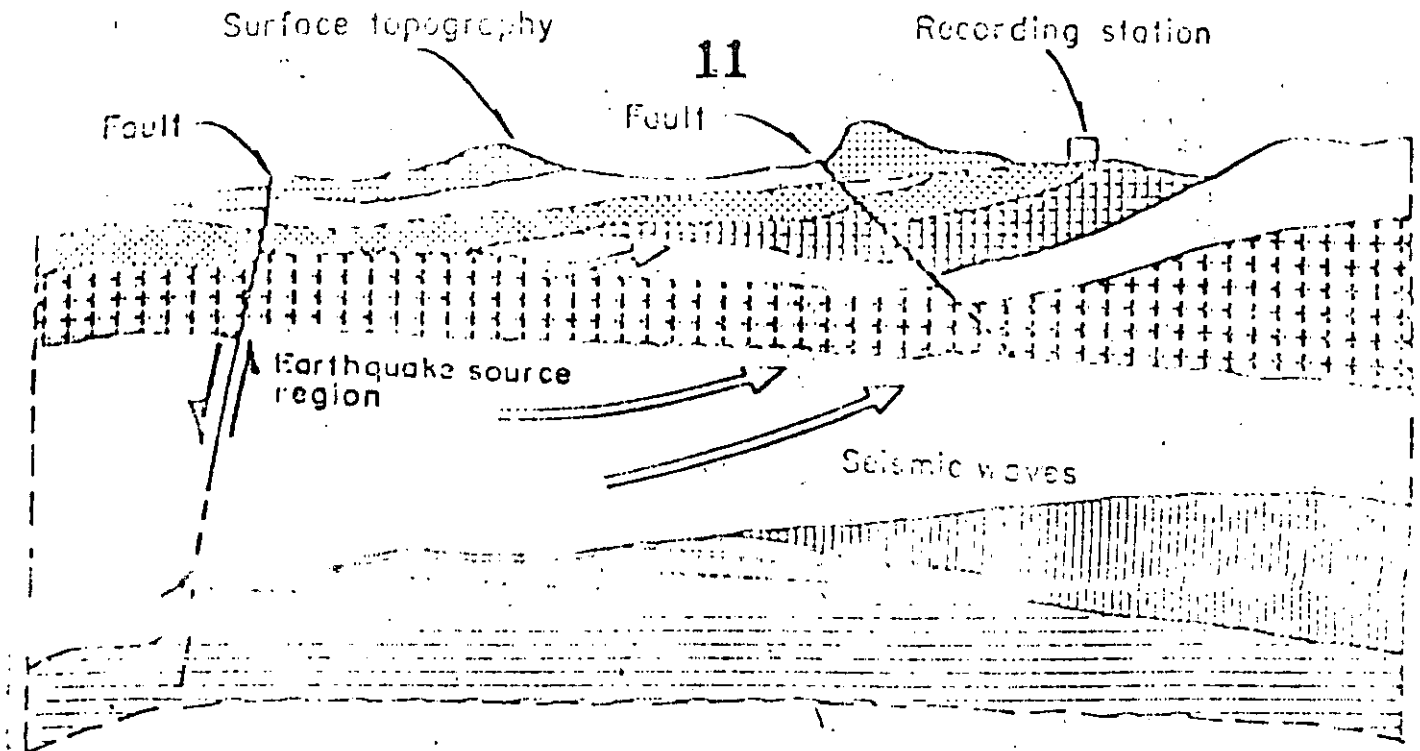


Fig. 1 Source, path and local conditions (Hudson, 1972)

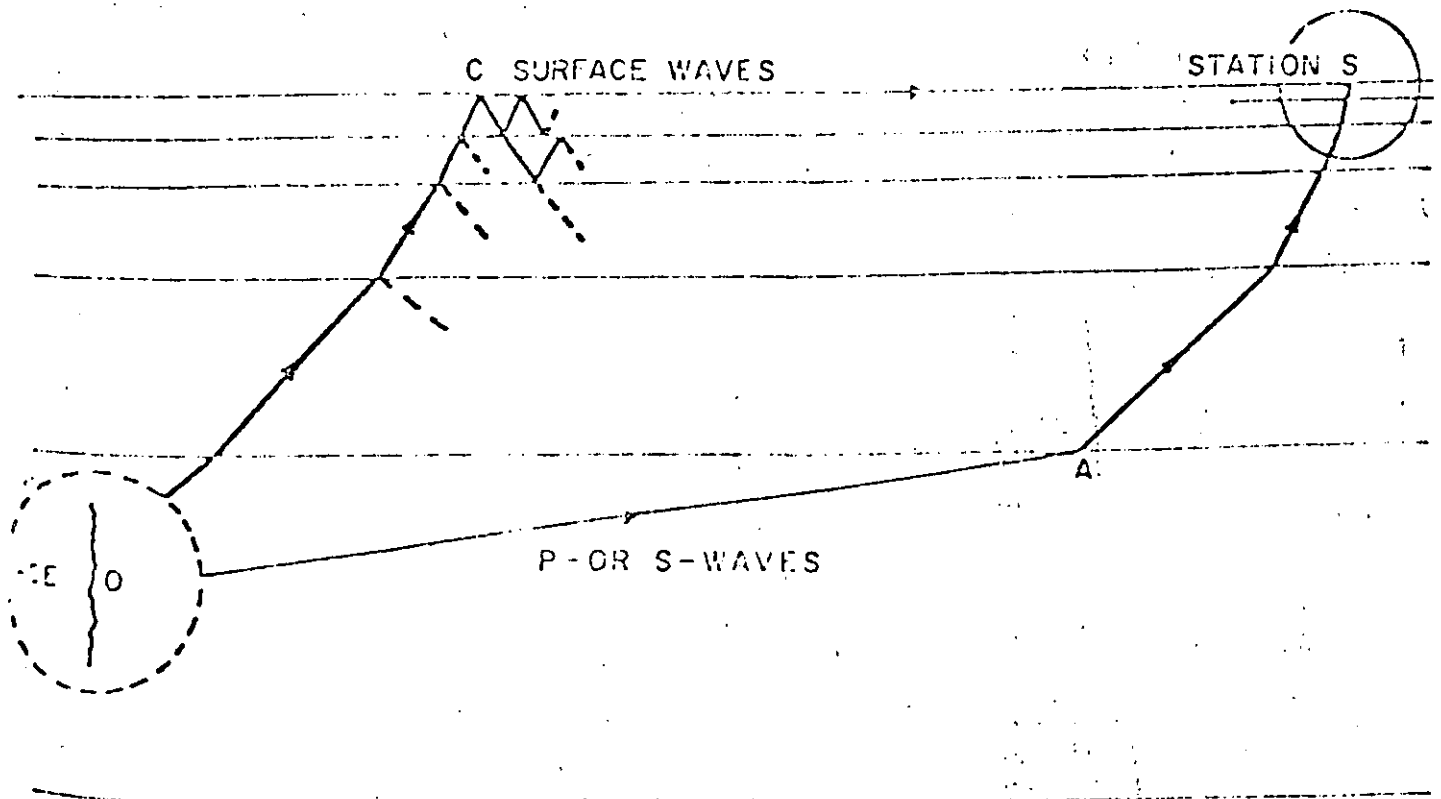


Fig. 2 Seismic waves (Foti, 1969)

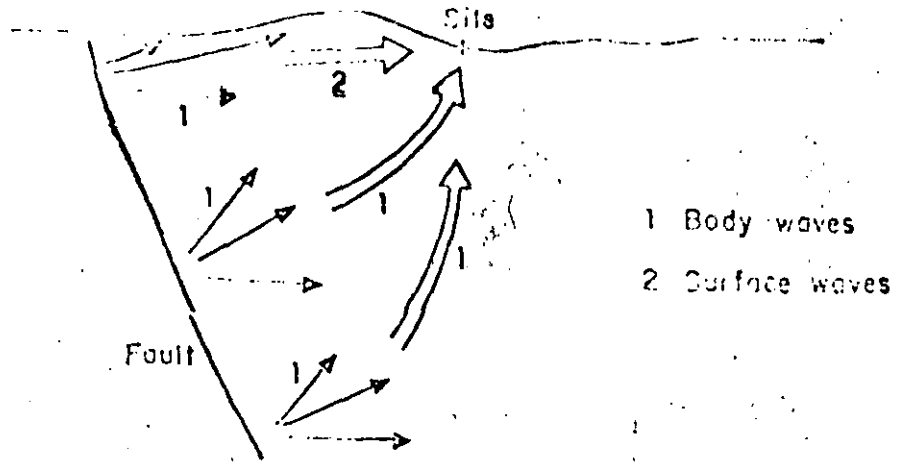


Fig. 3 Seismic waves in the near field

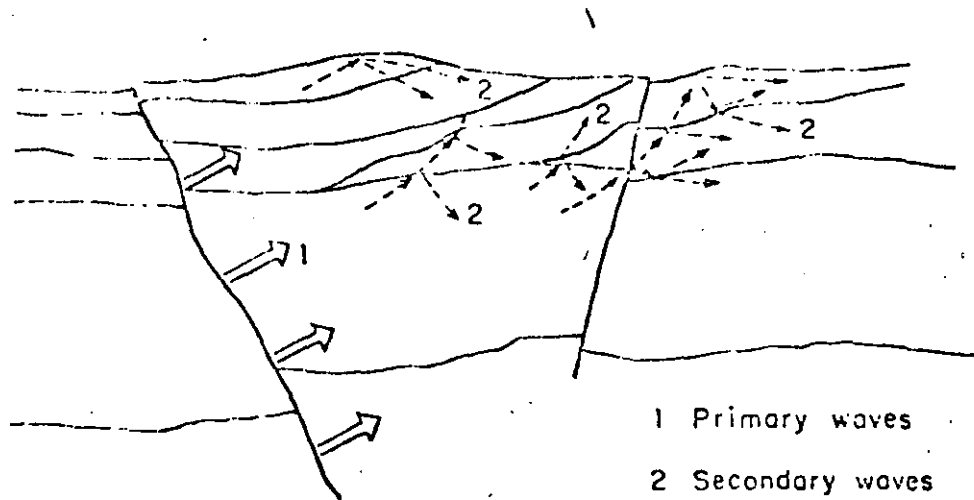


Fig. 4 Secondary wave trains

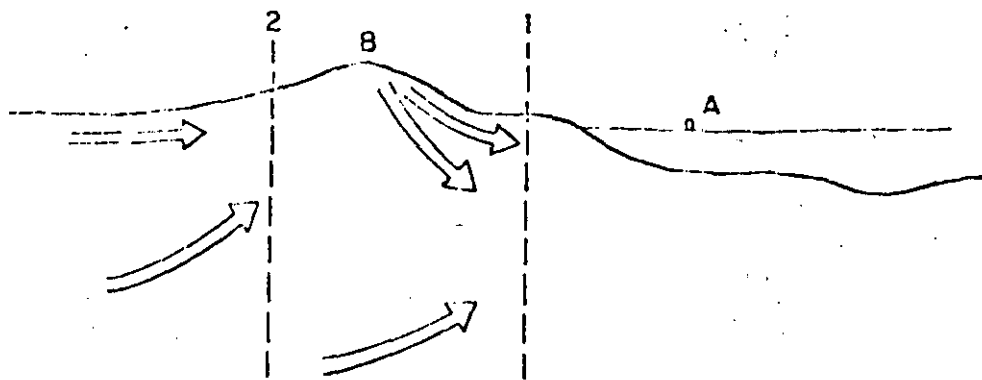
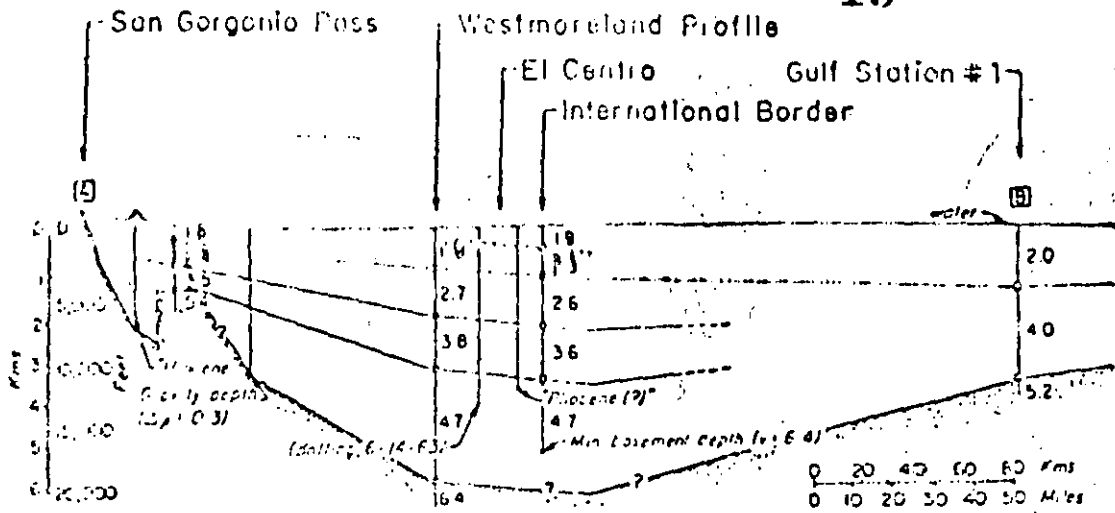


Fig. 5 Path and local conditions

SECTION A-B

← N 35° W

13



SECTION C-D

← East

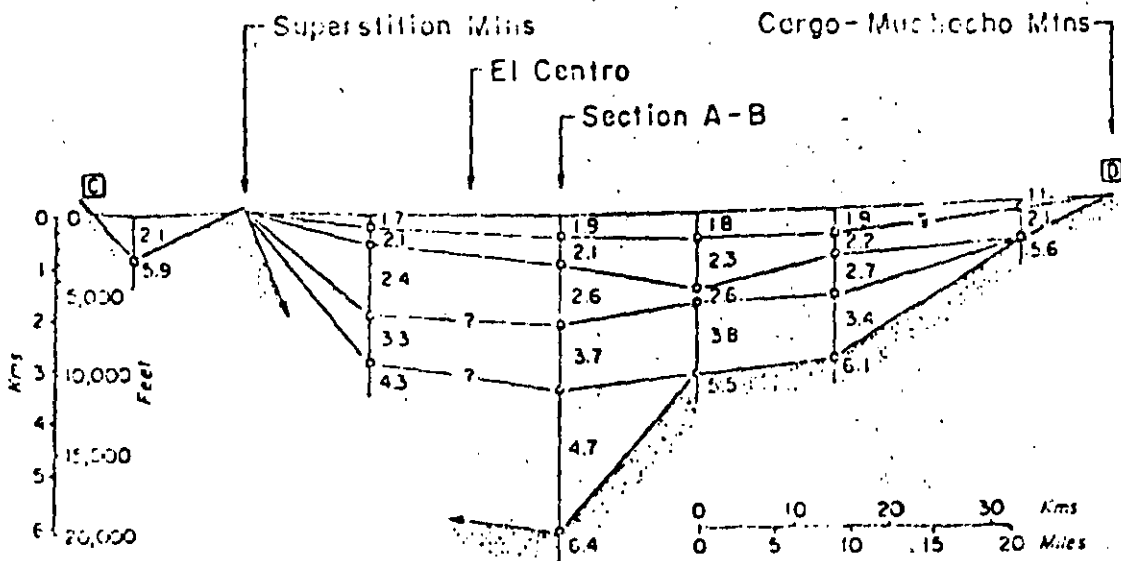
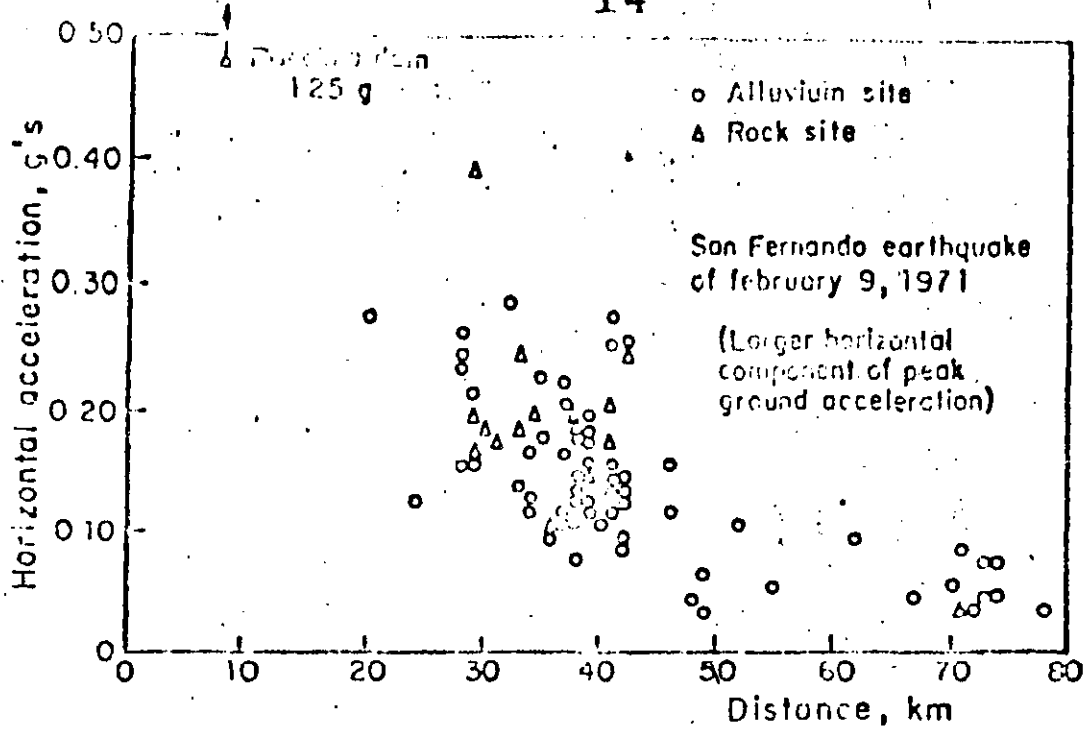


Fig. 6 Geologic cross section, Los Angeles area (Udwalid and Trifunac, 1973)



Peak ground acceleration versus distance

Fig. 7 Peak accelerations and ground conditions (Hudson, 1972)

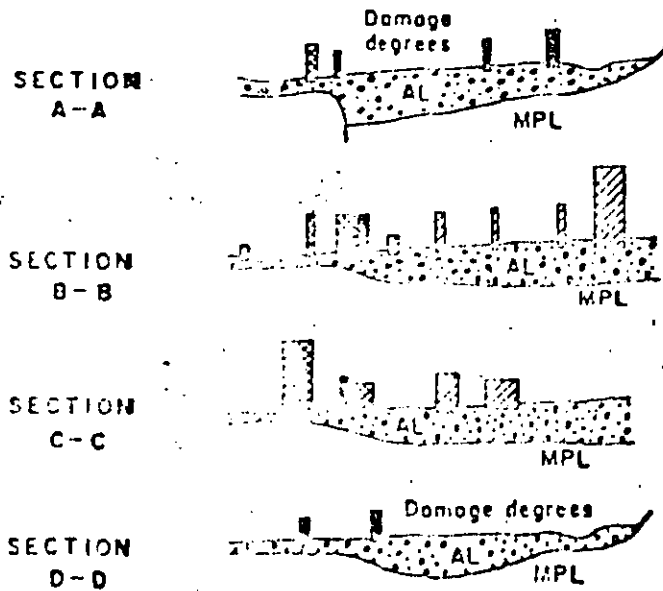


Fig. 8 Geologic cross section of Skopje (Focessit, 1969)

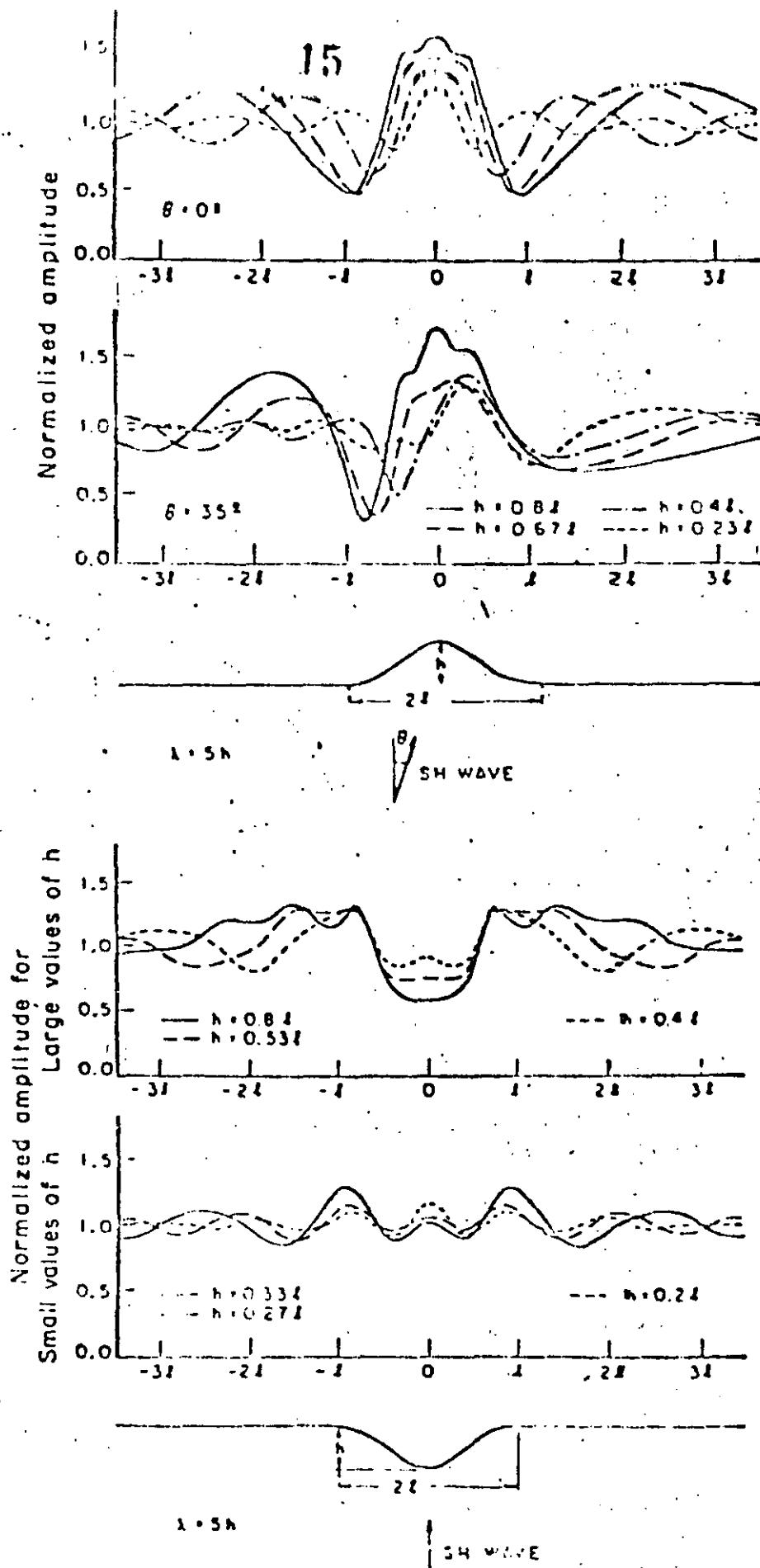


Fig. 9 Normalized amplitudes of motion produced by SH waves (Bowling, 1973)

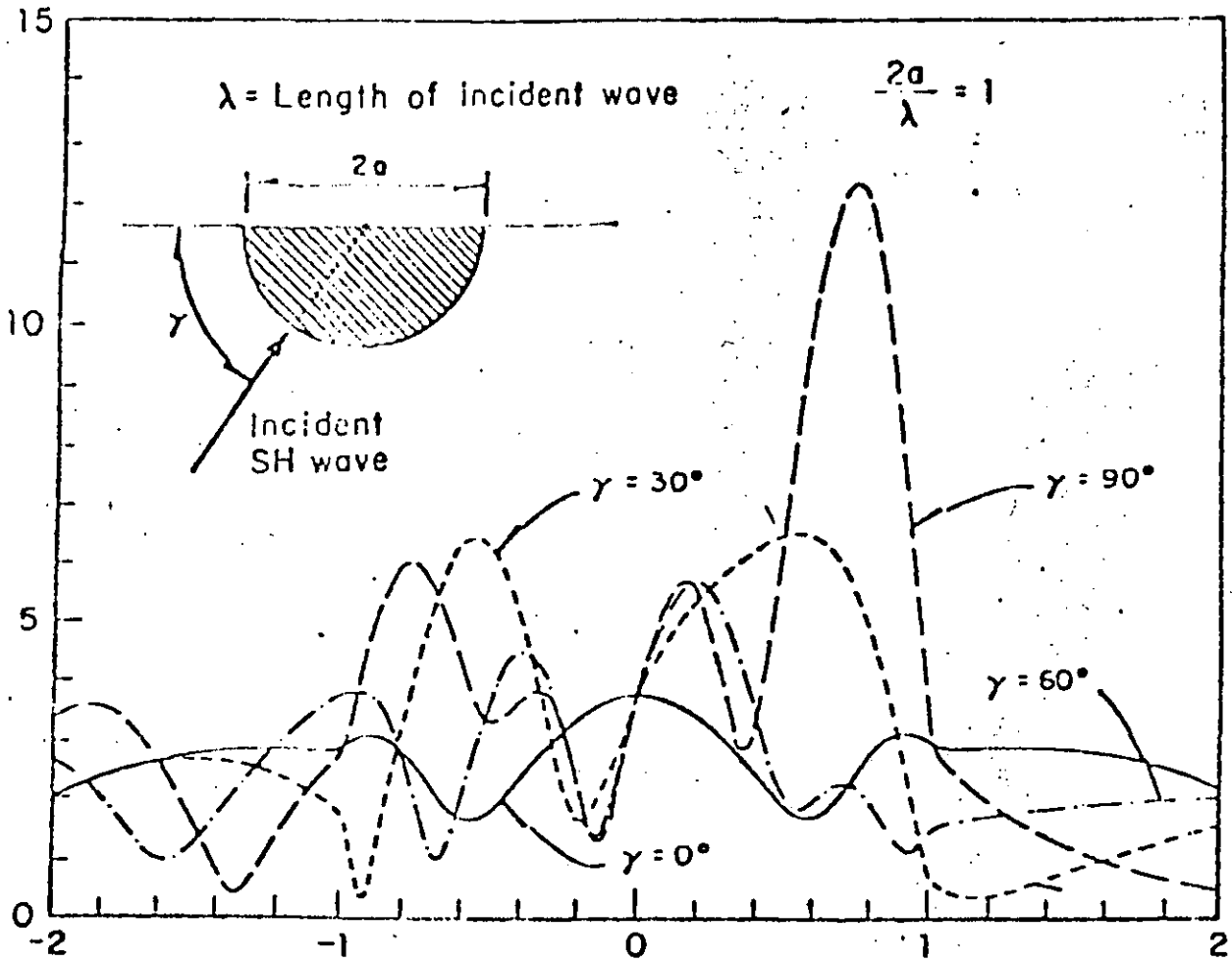


Fig. 10 Displacement amplitudes at the surface of a semicylindrical valley  
 (Trifunac, 1971b)

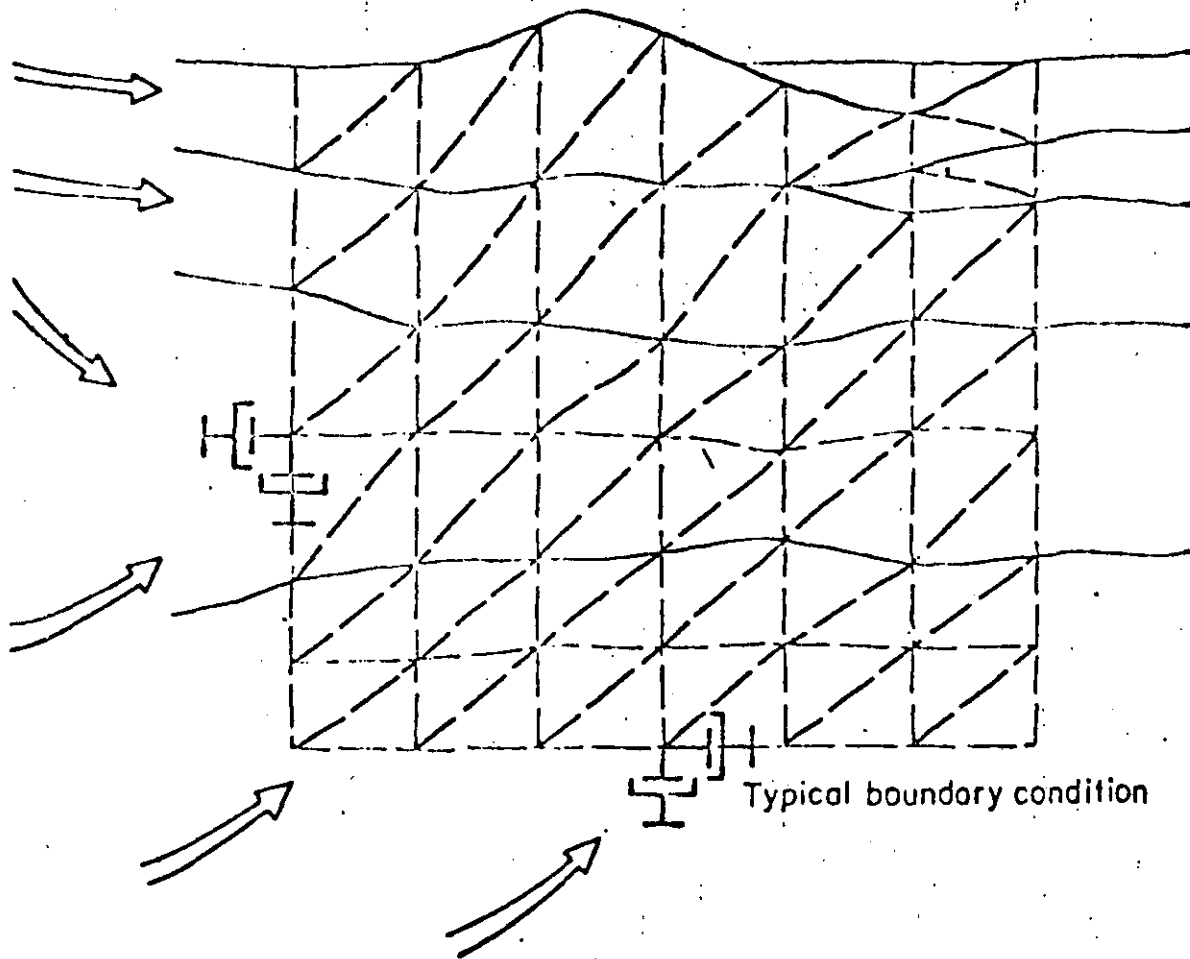


Fig. 11. Two-dimensional finite element models.



**DIVISION DE EDUCACION CONTINUA  
FACULTAD DE INGENIERIA U.N.A.M.**

ANALISIS DE RIESGO SISMICO

SOIL AMPLIFICATION: SOME REFINEMENTS

EDUARDO KAUSEL

JULIO, 1985

# Soil amplification: some refinements

EDUARDO KAUSEL

*Associate Professor of Civil Engineering, Massachusetts Institute of Technology, Cambridge, MA 02139, USA*

JOSÉ M. ROËSSET

*Professor of Civil Engineering, University of Texas, Austin, Texas, USA*

The most widely used techniques for the study of one-dimensional amplification of vertically propagating seismic waves involve solution of the dynamic equations in the frequency domain with linearly viscoelastic material properties. Material nonlinearities are approximately modeled by iterative use of linear solutions, adjusting values of modulus and damping until they are compatible with computed levels of strain. The program SHAKE is the best known example of a code using this procedure.

Several refinements to the iterative scheme originally proposed by Seed and Idriss are presented in this paper. In particular, it is shown that the solution for the layers underlying the control motion can be obtained in one single step, when the mass matrix is diagonal. Use of the shear stress in place of the shear strain as the controlling parameter in determining material properties gives faster convergence and identifies cases of potential non-convergence. Trivial modifications are also proposed to the standard scheme that would enable the researcher to study the amplification or deconvolution of non-vertically incident *S*/*H* waves with a code like SHAKE. These modifications consist simply in changing the mass density of the soil, and redefining the characteristic strain.

**Key Words:** soil dynamics, earthquake engineering.

## INTRODUCTION

It has become a standard practice among earthquake engineers to use linear wave propagation theory to assess the effects of local soil conditions on the amplitude and frequency contents of seismic motions in soil deposits. Usually the soils are idealized as horizontally layered strata overlying rock, and the incident waves are assumed to be plane waves propagating in a known direction through the rock half-space. Most of the practical applications have been limited to the study of shear waves propagating vertically, i.e. to the problem of one-dimensional soil amplification. The analytical solution to the soil amplification problem, which was described by Thomson as early as 1950,<sup>1</sup> was the subject of intense research in the 1960s.<sup>2-6</sup> More recent work has considered the amplification of generalized body waves<sup>7</sup> and surface waves.<sup>8</sup>

While it is theoretically possible to perform true incremental analyses, in which the properties of the soil are varied according to the load path and instantaneous levels of strain,<sup>9</sup> such procedures are seldom used in practice. Instead, approximate linear solutions are obtained by an iterative scheme originally proposed by Seed and Idriss.<sup>4</sup> Each iteration assumes constant values of soil properties during the earthquake, but the properties are chosen at the beginning of each iteration so as to be consistent with the levels of strain computed in the previous iteration. These levels of strain are usually measured by a characteristic

strain, which is either the peak<sup>10</sup> or the root mean square<sup>11</sup> value of the principal shearing strain. While the linear theory and the iterative solution do not provide exact solutions and have a limited range of application, they provide acceptable results for engineering purposes.<sup>9</sup> SHAKE<sup>12</sup> is the best known computer program using these procedures.

## IMPROVED ITERATION FOR LAYERS BELOW CONTROL MOTION

The iterative algorithm works well for many cases, but it can diverge when a large amplitude of motion is specified at or near the surface of a deep deposit of soft soil. The failure of the iterations to converge is the result of a number of factors:

- (a) The soil may be required to transmit a higher level of motion than it can accommodate. There is necessarily a limit to the stress that can be sustained by a layer of soil.
- (b) The soil may be required to transmit too much energy at high frequencies. The motion specified at the free surface may have a frequency content inconsistent with the properties of the soil and particularly the damping.

A typical amplification function from a depth *z* to the free surface of a soil deposit with linear hysteretic damping is shown in Fig. 1a. It can be seen that the amplitude tends to zero for increasing

Received March 1984. Discussion closes September 1984.

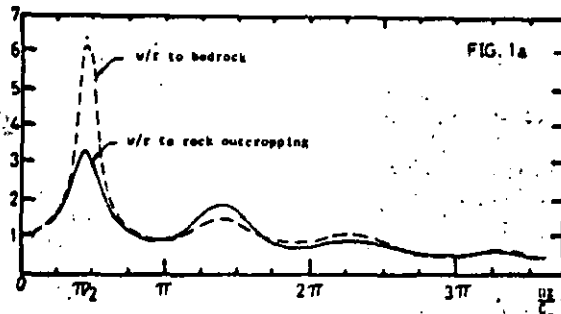


Figure 1a. Amplification functions: amplitude of motion at free surface for unit harmonic motion prescribed at depth  $z$

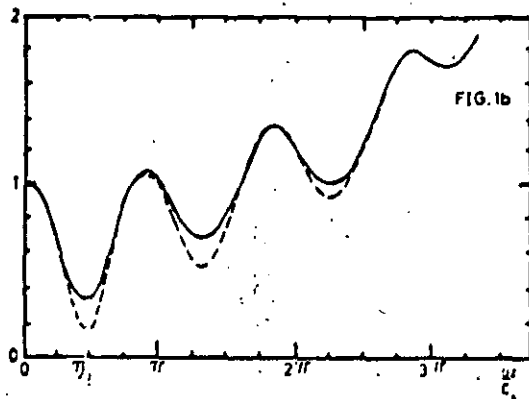


Figure 1b. Deamplification functions: amplitude of motion at depth  $z$  for unit harmonic motion prescribed at free surface

values of the parameter  $\Omega z/C_s$ , where  $\Omega$  is the frequency,  $z$  the depth and  $C_s$  the shear wave velocity. The function needed to determine the motion at depth  $z$  from a specified motion at the surface is the inverse of this curve, as shown in Fig. 1b. This function increases with  $\Omega z/C_s$  without bound. For given values of  $\Omega$  and  $C_s$  there is a depth  $z$  at which any given value will be exceeded.

- (c) The assumption of a linear hysteretic damping, independent of frequency is only an approximation. Since material damping is a function of amplitude, high frequencies associated with small amplitude cycles of vibration may have substantially less damping than the predominant frequencies of the layer. Figure 2 illustrates this point by comparing for a soil profile the amplification function resulting from the last cycle of a linear iterative analysis and the result of dividing the Fourier transform of the motion at the free surface by the Fourier transform of the motion at the bottom of the layer, with both motions having been computed through a nonlinear analysis in the time domain (non-linear transfer function).

Divergence may occur only below the elevation at which the earthquake motion, also called 'control motion', is specified. Thus, the algorithm always converges (although

not necessarily to a unique solution) for the soil above the elevation where the control motion is specified, and, in particular, it converges for the entire soil deposit when the motion is prescribed at bedrock.

As shown in the appendix (and in more detail in ref. 13), the solution of the iterative linear problem for a given layer below the elevation of the control motion depends only on the properties of that layer and the solution for the overlying layers. It is independent of the properties of the solutions for soils lying below the layer under consideration. Therefore, the iterative algorithm can be applied to that layer without considering underlying layers, and this fact leads to the following improved procedure:

1. Solve by the standard iterative method for all materials lying above the elevation of the control motion until the solution has converged satisfactorily.
2. Without further iterations on the overlying materials, solve for one layer below the control motion with iterations on the properties of that layer until satisfactory convergence is obtained.
3. Repeat the procedure of step 2 for each successively lower layer in the profile.

In this way, one does not proceed to the next lower layer until all overlying layers have converged. This modification results in an algorithm that is somewhat faster than the classical scheme in which all layers are analyzed simultaneously, and it identifies explicitly the layer in which the iterative procedure diverges without losing the solution for the overlying layers. This eliminates the need to preselect an arbitrary depth for the soil profile when bedrock is not clearly identified, or to engage in a trial and error procedure varying the depth of the layer or the frequency content of the input motion when convergence is not achieved.

**PROPERTIES DEPENDENT ON STRESS LEVEL**

The iterative linear approximation to the non-linear amplification problem involves computing values of damping and secant modulus from some characteristic measure of strain. When the control motion is prescribed at the free surface,

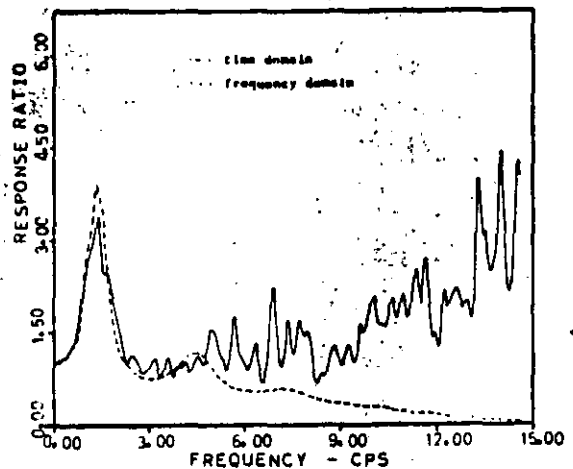


Figure 2. Amplification functions: non-linear time-domain analysis versus frequency-domain simulation with linear hysteretic damping

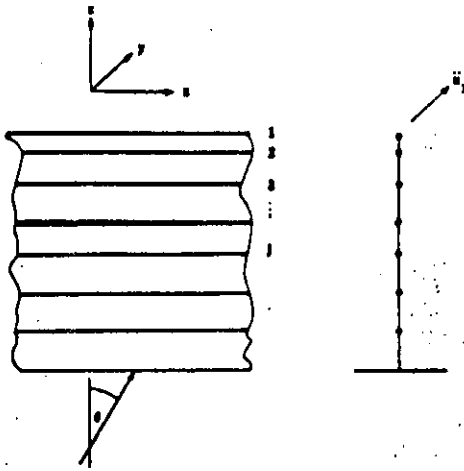


Figure 3. Lumped mass idealization of soil column.

this can be greatly improved by describing the properties in terms of characteristic levels of stress instead. To understand why this is so, consider the lumped mass representation of the soil column shown in Fig. 3. Let  $\tau_j, u_j$  be the shearing stress and displacement of the  $j$ th interface, and  $\rho_j, G_j, h_j$  the mass density, shear modulus, and thickness of the  $j$ th layer. The control motion is specified at interface (mass) 1. Regardless of material properties, equilibrium requires that for each frequency  $\Omega$ , in an analysis in the frequency domain

$$\tau_1 + \frac{1}{2} \rho_1 h_1 \ddot{u}_1 = 0 \quad (1)$$

so the frequency variation of  $\tau_1$  (or its time history when the inverse Fourier transform is applied) and any characteristic or average values, can be computed directly from that of  $\ddot{u}_1$ . If the secant modulus and damping of layer 1 were known in terms of  $\tau_1$ , one could compute their values directly without iterations. Once the material properties are known for layer 1, a one step linear solution of the vertical wave propagation problem for layer 1 gives the frequency variation of the acceleration  $\ddot{u}_2$ .

$$\ddot{u}_2 = \ddot{u}_1 + \frac{h_1}{G_1} \Omega^2 \tau_1 \quad (2a)$$

Equilibrium requires that

$$\tau_2 = \tau_1 - \frac{1}{2} (\rho_1 h_1 + \rho_2 h_2) \ddot{u}_2 \quad (2b)$$

This is then solved for the frequency variation of  $\tau_2$ , and the material properties are obtained for layer 2. The procedure is repeated for layer 3, and so on. The algorithm can be summarized by stating that, for any layer  $j$ ,

$$\ddot{u}_j = \ddot{u}_{j-1} + h_{j-1} \Omega^2 \tau_{j-1} / G_{j-1} \quad (3a)$$

$$\tau_j = \tau_{j-1} - \frac{1}{2} (\rho_{j-1} h_{j-1} + \rho_j h_j) \ddot{u}_j \quad (3b)$$

where  $\rho_0$  and  $h_0$  are zero. The procedure is then:

1. Solve for  $\tau_1$  from equation (1).
2. Evaluate material properties of layer 1 from  $\tau_1$ .
3. Solve for  $\ddot{u}_2$  from equation (3a).
4. Solve for  $\tau_2$  from equation (3b).
5. Repeat steps 2-4 for each layer in turn.

When the soil is not represented by lumped masses but by continuous layers, as in the SHAKE program, equation (3)

does not apply directly, but the equivalent equation for the continuous case in the frequency domain is nearly as simple. For materials lying above the control motion, the iterative linear solution must be obtained as before, except that soil properties are described in terms of stress rather than strain.

Curves of damping and secant modulus versus the logarithm of shear strain are easily replotted as curves versus logarithm of shear stress. For example, the average curves of shear modulus and damping versus shear strain for sands and clays (Figs. 5.6, 5.13, and 5.9, 5.14 of ref. 14) are replotted in Figs. 4 and 5. Similar transformations could be applied to other, more recent revisions of these curves (particularly for clays).

One objection to this procedure is that the stress-strain curve may be peaked, precluding a unique relation between secant modulus and stress level. However, this is mitigated by the following facts:

1. The levels of strain are usually smaller than those required to get past the peak of the stress-strain curve.
2. The moduli do not represent the stress-strain curve for the first application of load but reflect the effects of many cycles of loading, which tend to eliminate peaks in stress-strain curves.
3. When a genuine peak exists, iterative linear solutions may not be unique by any method. The use of shear stress as the controlling parameter identifies a potential problem in such a case.

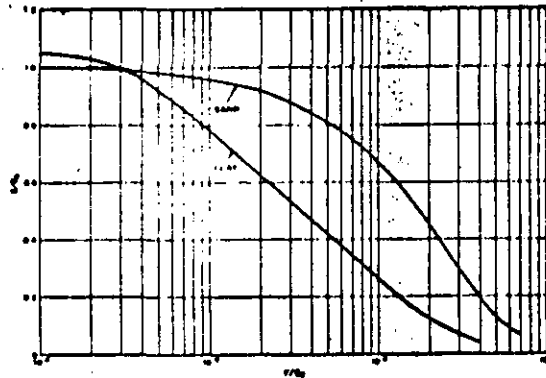


Figure 4. Shear modulus versus stress.

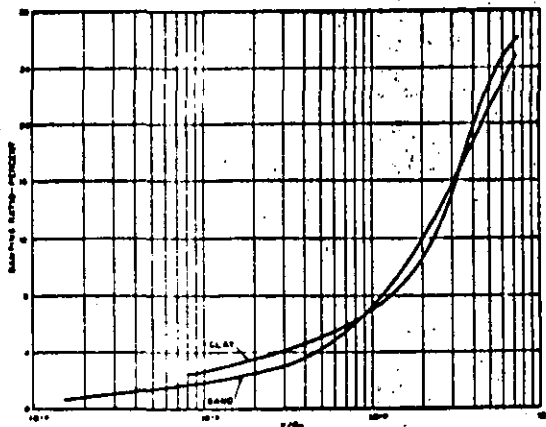


Fig. 5. Damping versus stress.

The proposed use of the shear stress as the controlling parameter permits achieving convergence in a single iteration, as opposed to the various iterations that are necessary when shear strain is the controlling parameter. It specifically identifies conditions in which the required shear stress exceeds the available shear strength. In addition it is more logical from a geotechnical point of view since it allows to account directly for the shear strength of the material.

**NON-VERTICALLY INCIDENT SH WAVES**

The study of wave amplification in layered soils subjected to nonvertically incident SH waves can be accomplished with the well known Thompson-Haskell algorithm. It will be demonstrated in the following, however, how a simple (but exact) solution to this problem can be obtained also with programs such as SHAKE by merely redefining the mass-density of the soil and the characteristic strain. These changes are as follows:

$$\rho_e = \rho_s \left[ 1 - \left( \frac{C_s}{C_r} \right)^2 \sin^2 \theta \right] \quad (4)$$

In which  $\rho_s, \rho_r$  are the real and the equivalent soil densities of the soil layers;  $C_s$  is the shear wave velocity in the layer under consideration;  $C_r$  is the shear wave velocity in the underlying bedrock; and  $\theta$  is the angle of incidence (w/r to the vertical) of the SH waves in the underlying rock. Also

$$\Gamma = \sqrt{\left| \frac{u_j - u_{j+1}}{h} \right|^2 + \left( \frac{\Omega}{C_r} \right)^2 \sin^2 \theta \left| \frac{u_j + u_{j+1}}{2} \right|^2} \quad (5)$$

is the amplification function for the maximum strain;  $\Omega$  = excitation frequency;  $h$  = layer thickness; and  $u$  = the frequency response function (transfer function times the Fourier spectrum of the input) for the displacement at the middle of the  $j$ th layer. The subindices  $j$  and  $j + 1$  refer to the interfaces bounding the  $j$ th layer under consideration. The actual characteristic strain is then computed as in ref. 13, via the RMS value of the strain obtained as an integral (summation) in the frequency domain<sup>13</sup>

$$\gamma_{RMS} = \sqrt{\frac{1}{2\pi T} \int_{-\infty}^{\infty} \Gamma^2 d\Omega} \quad (6)$$

$$\gamma_{char} = \frac{2 \text{ peak input acceleration}}{3 \text{ RMS input acceleration}} \times \gamma_{RMS} \quad (7)$$

(the  $T$  factor is the duration of the record, which is irrelevant since it cancels in the above ratio with an identical term in the RMS acceleration). These modifications will be proved in the following.

**1. Equivalent soil properties**

The propagation of plane SH waves in a horizontally layered soil is characterized by the wave equation (with  $u \equiv u_y$ )

$$\frac{\partial^2 u}{\partial x^2} + \frac{\partial^2 u}{\partial z^2} = \frac{1}{C_s^2} \frac{\partial^2 u}{\partial t^2} \quad (8)$$

Solutions to this equation representing plane harmonic SH waves are of the form

$$u = [A_1 \exp(-inz) + A_2 \exp(inz)] \exp(-ikx) \quad (9)$$

where  $k, n$  are the wavenumbers,  $A_1, A_2$  are wave ampli-

tudes and an implied factor  $\exp(i\Omega t)$  has been omitted. The wavenumbers satisfy the dispersion relation

$$k^2 + n^2 = \left( \frac{\Omega}{C_s} \right)^2 \quad (10)$$

For SH waves propagating in the halfspace (rock) with an angle  $\theta$  w/r to the vertical, the phase velocity is

$$V = \frac{C_r}{\sin \theta} \quad (11)$$

In which  $C_r$  = shear wave velocity in the underlying rock. Hence

$$k = \frac{\omega}{V} = \frac{\omega}{C_r} \sin \theta \quad (12)$$

which can be used to solve for  $n$

$$n^2 = \left( \frac{\Omega}{C_s} \right)^2 - \left( \frac{\Omega}{C_r} \right)^2 \sin^2 \theta \quad (13)$$

$$n = \left( \frac{\Omega}{C_s} \right) \left[ 1 - \left( \frac{C_s}{C_r} \right)^2 \sin^2 \theta \right]^{1/2} \quad (14)$$

Defining the equivalent shear wave velocity  $C_e$  as

$$C_e = \frac{C_s}{\sqrt{1 - (C_s/C_r)^2 \sin^2 \theta}} \quad (15)$$

we obtain

$$n = \frac{\Omega}{C_e} \quad (16)$$

Equation (9) transforms then into

$$u = \left[ A_1 \exp\left(-i \frac{\omega}{C_e} z\right) + A_2 \exp\left(i \frac{\omega}{C_e} z\right) \right] \exp(-ikx) \quad (17)$$

The term in brackets is identical to the solution for the one-dimensional wave equation

$$\frac{d^2 u}{dz^2} = C_e^2 \frac{d^2 u}{dz^2} \quad (18)$$

which characterizes the problem of vertically propagating SH waves. Since the exponential factor in  $(kx)$  is the same in all layers (and can thus be factored out), it follows that the one-dimensional solution with equivalent shear wave velocity is identical to that of the two-dimensional wave propagation problem with non-vertical incidence. It remains to establish the equivalent properties  $\rho_e, C_e$  that provide the appropriate shear-wave velocity  $C_e$ . These are obtained from the continuity requirements for the shearing stresses ( $\tau_{yz}$ ) across the interfaces.

The strain components (in the frequency domain)  $\Gamma_{xy}, \Gamma_{yz}$  are

$$\Gamma_{xy} = \frac{\partial u}{\partial x} = -iku \quad (19a)$$

$$\Gamma_{yz} = \frac{\partial u}{\partial z} = -in [A_1 \exp(-inz) - A_2 \exp(inz)] \exp(-ikx) \quad (19b)$$

Hence, the shearing stresses in horizontal planes  $\tau_{yz}$  are

given by

$$\tau_{yz} = G\Gamma_{yz} = -i\omega(z) [A_1 \exp(-i\omega z) - A_2 \exp(i\omega z)] \exp(-ikx) \quad (20)$$

By comparison, the stress  $\tau_{yz}$  associated with a one-dimensional model with properties  $C_e, G_e$  would be

$$\tau_{yz} = -i\frac{\Omega}{C_e} G_e \left[ A_1 \exp\left(-i\frac{\Omega}{C_e} z\right) - A_2 \exp\left(i\frac{\Omega}{C_e} z\right) \right] \quad (21)$$

Hence, to simulate the interface stresses of the two-dimensional model with the one-dimensional model, one must have

$$nG = \frac{\Omega}{C_e} G_e \quad (22)$$

which requires  $G_e = G$ , since  $n = \Omega/C_e$ . It follows that

$$\begin{aligned} \rho_e &= \frac{G_e}{C_e^2} = \frac{G}{C_e^2} \left[ 1 - \left(\frac{C_e}{C_r}\right)^2 \sin^2 \theta \right] \\ &= \rho \left[ 1 - \left(\frac{C_e}{C_r}\right)^2 \sin^2 \theta \right] \end{aligned} \quad (23)$$

Again, the exponential factor in  $(kx)$  is common to all layers, so that it drops out when establishing the continuity of the stresses across the interfaces. Thus, a program like SHAKE could be used (with slight modifications) to study obliquely incident SH waves. It suffices to replace in each layer the actual properties by the equivalent soil properties as described earlier.

This simple (but exact) procedure has various interesting consequences:

(a) In general,  $C_e/C_r < 1$ . Hence

$$0 < 1 - \frac{C_e^2}{C_r^2} \sin^2 \theta < 1 \quad (24)$$

so that

$$\rho_e < \rho \quad (25)$$

Since the equivalent soil profile is 'lighter', the amplification peaks for nonvertical incidence will evidence a shift towards the higher frequencies of the order of  $C_e/C_r$ . For a soil deposit overlying a much stiffer rock,  $C_e \ll C_r$ , so that  $C_e \approx C_r$ , and no shift would be observed. For a halfspace (deep alluvium),  $C_e/C_r = 1$ , and the peaks (valleys) shift by a factor  $\sqrt{1 - \sin^2 \theta} = \cos \theta$ .

(b) For bedrock,  $C_e \equiv C_r$ , so that

$$\rho_{er} = (1 - \sin^2 \theta) \rho_r \quad (26a)$$

$$C_{er} = \frac{C_r}{\sqrt{1 - \sin^2 \theta}} = \frac{C_r}{\cos \theta} \quad (26b)$$

The impedance contrast for a uniform soil layer on elastic rock would then be:

$$\begin{aligned} R_e &= \frac{\rho_e C_e}{\rho_r C_{er}} = \frac{\rho_e C_e \sqrt{1 - (C_e/C_r)^2 \sin^2 \theta}}{\rho_r C_r \sqrt{1 - \sin^2 \theta}} \\ &= R \frac{\sqrt{1 - (C_e/C_r)^2 \sin^2 \theta}}{\sqrt{1 - \sin^2 \theta}} \approx \frac{R}{\cos \theta} \end{aligned} \quad (27)$$

Hence, the effective radiation damping

$$\beta_e = \frac{1}{2} R_e = \frac{1}{2} \frac{R}{\cos \theta} \quad (28)$$

increases with increasing angle of incidence. The amplification peaks with respect to rock outcropping must then decrease approximately by a factor of  $\cos \theta$ .

(c) The amplification functions from a depth  $z$  in the soil to the surface are (almost) independent of the angle of incidence, except for the shift in frequency axis  $\sqrt{\rho_e/\rho_e}$ . For example, if  $C_e/C_r \approx 100/200 = 1/2$ , then

$$\frac{\rho_e}{\rho_e} = \frac{1}{\sqrt{1 - \frac{1}{4} \sin^2 \theta}} \quad (29)$$

An incidence angle of  $45^\circ$  would then shift the apparent period at depth  $z$  by a factor  $\sqrt{1 - (\frac{1}{2})^2} = 0.935$ , which differs little from unity.

For the same reason, the peaks of the transfer functions with respect to rock (not outcropping!) would essentially not change, but merely shift.

(d) The distortions in amplitude and frequency may not be negligible in clearly stratified soils (i.e. alternating soft and stiff layers).

To illustrate further these points, Figs. 6 and 7 show the amplification functions with respect to outcropping (elastic rock case) and bedrock (rigid rock case) for a soil profile with the properties listed on Table 1. Table 2 shows the angles of incidence of the waves in the different layers for various angles of incidence in the rock. It should be noticed that even for an extreme angle of  $90^\circ$  in the rock the angle of incidence in the top layer is of the order of  $5^\circ$  (i.e. an

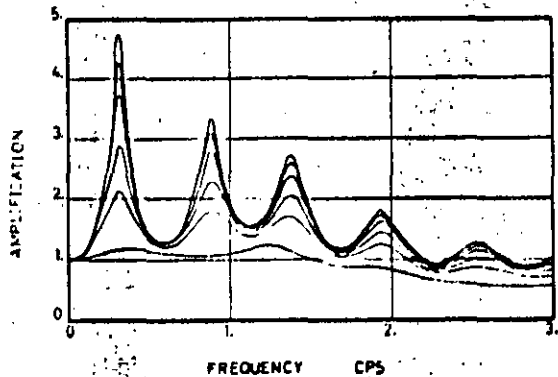


Figure 6. Amplification functions with respect to rock outcropping for various angles of SH-wave incidence

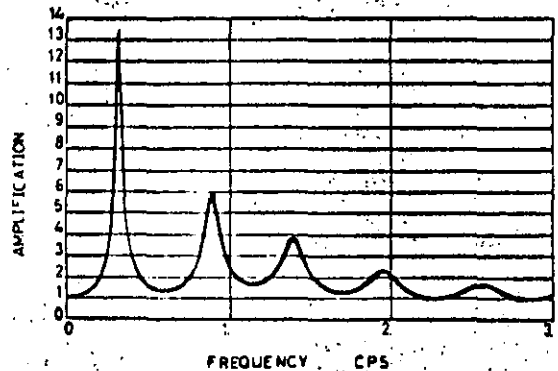


Figure 7. Amplification functions with respect to bedrock for various angles of SH-wave incidence

Table 1. Soil properties

Layer	Depth (ft)	Shear wave velocity (ft/s)	Unit weight (lb <sub>a</sub> /ft <sup>3</sup> )
1	10	714	100
2	150	897	120
3	70	1200	125
4	500	1300	125
5	400	1500	135
Rock		8000	150

Table 2. Angles of wave propagation through the layers

$\theta_1$	$\theta_2$	$\theta_3$	$\theta_4$	$\theta_5$	$\theta_6$
0	0	0	0	0	0
10°	1° 50'	1° 40'	1° 30'	1° 10'	0° 55'
20°	3° 40'	3°	2° 50'	2° 10'	1° 45'
30°	5° 25'	4° 40'	4° 20'	3° 10'	2° 30'
40°	7° 25'	6° 10'	5° 40'	4° 15'	3° 25'
45°	7° 40'	6° 40'	6° 05'	4° 35'	3° 35'
50°	8° 15'	7° 10'	6° 36'	4° 55'	3° 55'
60°	9° 20'	8° 10'	7° 30'	5° 40'	4° 25'
70°	10° 10'	8° 50'	8° 05'	6°	4° 50'
80°	10° 36'	9° 12'	8° 30'	6° 20'	5°
90°	10° 50'	9° 25'	8° 40'	6° 30'	5° 10'

almost vertical incidence). Because of the large difference in properties between the soil and the underlying rock, the shift in the frequencies of the peaks is very small. Thus, the effect of the angle of incidence on the amplification with respect to bedrock is negligible, illustrating the impossibility (or great difficulty) in assessing the angle of incidence of the waves from records obtained at various depths. On the other hand, the effect on the amplification with respect to outcropping can be substantial.

## 2. Characteristic strain

If non-linear effects are also to be computed (at least in an iterative sense) for the non-vertically incident *S*<sub>1</sub>-waves amplification problem, then some modification in the characteristic strain used are necessary to account for the second strain component that exists in this case. If the underlying bedrock (halfspace) has no material damping, then the wave number  $k$  is real and the amplitudes of the strains in the soil do not change in horizontal planes. This is true even if the soil itself has damping. However, in such a case, the equivalent mass density  $\rho_e$  would be a complex number. On the other hand, if the halfspace has material damping, the incident and reflected waves are attenuated in the horizontal direction of propagation and the maximum strains would depend on the abscissa. Hence, in this case, one could obtain only approximate solutions for a given cross section and the material properties would no longer be constant in horizontal planes. Nevertheless, for practical application, the damping in the underlying rock can be neglected, so that neither the change in peak strain nor the variation of soil properties with the abscissa need be considered.

The displacement field and associated strain components are given by equations (9) and (19) respectively. Choosing the origin of coordinates at the middle of the layer, one can determine the amplitudes  $A_1, A_2$  in terms of the interface displacements  $u_j, u_{j+1}$  (having vertical coordinates  $z = h/2$  and  $z = -h/2$  respectively)

$$u_j = \left[ A_1 \exp\left(-in\frac{h}{2}\right) + A_2 \exp\left(in\frac{h}{2}\right) \right] \exp(-ikx) \quad (30a)$$

$$u_{j+1} = \left[ A_1 \exp\left(in\frac{h}{2}\right) + A_2 \exp\left(-in\frac{h}{2}\right) \right] \exp(-ikx) \quad (30b)$$

From here, we obtain

$$A_1 = \frac{1}{\exp(-inh) - \exp(inh)} \times \left[ u_j \exp\left(-in\frac{h}{2}\right) - u_{j+1} \exp\left(in\frac{h}{2}\right) \right] \exp(ikx) \quad (31a)$$

$$A_2 = \frac{1}{\exp(-inh) - \exp(inh)} \times \left[ -u_j \exp\left(in\frac{h}{2}\right) + u_{j+1} \exp\left(-in\frac{h}{2}\right) \right] \exp(ikx) \quad (31b)$$

At the middle of the layer, we have then,

$$\begin{aligned} \Gamma_{yz} &= -in(A_1 - A_2) \exp(-ikx) \\ &= \frac{-in}{\exp(-inh) - \exp(inh)} \left[ \exp\left(in\frac{h}{2}\right) + \exp\left(-in\frac{h}{2}\right) \right] \\ &\quad \times (u_j - u_{j+1}) \\ &= \frac{n}{\sin nh} \cos \frac{nh}{2} (u_j - u_{j+1}) \end{aligned} \quad (32)$$

If  $h$  is small, then  $\cos n(h/2) \approx 1$ ,  $\sin nh \approx nh$  and

$$\Gamma_{yz} \approx \frac{u_j - u_{j+1}}{h} \quad (33)$$

Also,

$$\begin{aligned} u &= (A_1 + A_2) \exp(-ikx) \\ &= \frac{1}{\exp(-inh) - \exp(inh)} \left[ \exp\left(-in\frac{h}{2}\right) - \exp\left(in\frac{h}{2}\right) \right] \\ &\quad \times (u_j + u_{j+1}) \\ &= \frac{\sin n(h/2)}{\sin nh} (u_j + u_{j+1}) \end{aligned} \quad (34)$$

which for thin layers reduces to

$$u \approx \frac{1}{2} (u_j + u_{j+1}) \quad (35)$$

The strain components are then

$$\Gamma_{xy} = \frac{-ik}{2} (u_j + u_{j+1}) = \frac{-i\Omega \sin \theta}{C_p} \frac{u_j + u_{j+1}}{2} \quad (36a)$$

$$\Gamma_{yz} = \frac{u_j - u_{j+1}}{h} \quad (36b)$$

and the frequency spectrum for the maximum strain is

$$\begin{aligned} \Gamma^2 &= |\Gamma_{xy}|^2 + |\Gamma_{yz}|^2 \\ &= \left| \frac{u_j - u_{j+1}}{h} \right|^2 + \frac{\Omega^2 \sin^2 \theta}{C_p^2} \left| \frac{u_j + u_{j+1}}{2} \right|^2 \end{aligned} \quad (37)$$

which is based on Parseval's relationship

$$\begin{aligned} \int \gamma^2 dt &= \int (\gamma_{xy}^2 + \gamma_{yx}^2) dt \\ &= \frac{1}{2\pi} \int_{-\infty}^{\infty} (|\Gamma_{xy}|^2 + |\Gamma_{yx}|^2) d\Omega \\ &= \frac{1}{2\pi} \int_{-\infty}^{\infty} \Gamma^2 d\Omega \end{aligned} \quad (38)$$

Since  $|\exp(-ikx)| = 1$ , it follows that the amplitudes of the strains do not change with  $x$ . The iterative computation would then be performed as follows:

1. Define the equivalent soil properties in each layer.
2. Solve for the (absolute) displacement frequency response functions in the usual way. (These represent the amplitudes at  $x = 0$ ).
3. Compute the strains or stresses with the modified formula.
4. Modify the shear modulus in the standard fashion.

Implementation of the above procedure in a program such as SHAKE should require only minor programming effort.

#### APPENDIX

The analytical solution of the soil amplification problem was outlined by Thomson as early as 1950<sup>1</sup> and was the subject of intense research during the 1960s.<sup>2-4,15</sup> More recent studies in the amplification of generalized body<sup>2</sup> and surface<sup>3</sup> waves are also available.

For a horizontally stratified soil deposit under plane strain conditions, the general solution for steady state harmonic motion can be written for a particular layer<sup>1</sup> (see also Fig. 3).

$$X_{i+1} = T_i X_i \quad (39)$$

where  $X_i = (U^T, S^T)^T$  is the vector of displacements and stresses at the  $i$ th interface and is referred to as the 'state vector'. Also,  $T_i$  is a transfer matrix depending only on the elastic and geometric properties of the  $i$ th layer under consideration, the frequency of excitation, and the directional parameters of the incident waves. The exact form of the transfer matrix is not important in the present context (see for instance refs. 7 and 15).

(a) Soil column above control point (if any): from equation (39), it follows that:

$$\begin{aligned} X_j &= (T_1 T_2 T_3 \dots T_{j-1}) X_1 \\ &= \left( \prod_{i=1}^{j-1} T_i \right) X_1 = F X_1 \end{aligned} \quad (40)$$

where  $j$  defines the interface at which the control motion is specified;  $X_1$  contains the displacements and stresses at the free surface. Partitioning  $F$  into four submatrices, it is possible to write

$$\begin{Bmatrix} U \\ S \end{Bmatrix}_j = \begin{Bmatrix} F_{11} & F_{12} \\ F_{21} & F_{22} \end{Bmatrix} \begin{Bmatrix} U \\ S \end{Bmatrix}_1 \quad (41)$$

The boundary conditions are  $S_1 = 0$  at the free surface and  $U_j = U_c$ , at the control interface, where  $U_c$  is the control

motion. It follows finally

$$U_1 = F_{11}^{-1} U_c \quad (42a)$$

$$S_j = F_{21} F_{11}^{-1} U_c = S_c \quad (42b)$$

Equations (42) show that the motion at the free surface and at any other point between the free surface and the control surface) is a function of the elastic properties of the entire soil column above the control surface; however, it is independent of the properties and solution below the control surface. When the response of non-linear material is simulated by iterating a series of linear cases, each iteration for the material above the control point is independent of the material below the control point. Hence, the iterated solution for the column of soil above the control point can be obtained in the usual way, without consideration of layers underlying the control surface.

(b) Soil column below the control point: from equations (42), it follows that:

$$X_c = \begin{Bmatrix} U_c \\ S_c \end{Bmatrix} = \begin{Bmatrix} U_c \\ F_{21} F_{11}^{-1} U_c \end{Bmatrix} \begin{Bmatrix} U_c \\ S_c \end{Bmatrix} \quad (43)$$

defines the displacements and stresses at the control interface.  $S_c$  is computed with the iterated soil properties above the control point (equation (42b)). If the motion is defined at the free surface, then  $S_c = 0$ . The solution for the first interface below the control surface is simply

$$X_{c+1} = T_c X_c \quad (44)$$

Note that this motion depends only on the solution of the preceding interface, and on the elastic properties of the layer under consideration. Therefore, the iterative algorithm can be applied to that layer without consideration of the underlying layers. Once the iterated solution has converged (if at all), one proceeds to the next layer, using

$$X_{c+2} = T_{c+1} X_{c+1} \quad (45)$$

and so on. Hence, only one layer is considered at a time, and unnecessary computations for the overlying layers are avoided. In the classical scheme, all layers (both above and below the control point) are treated simultaneously. Therefore, the upper layers converge typically to a tolerance much smaller than that specified by the engineer, since the lower regions usually require more iterations to converge. On the other hand, the revised algorithm affords the possibility of identifying 'problem' layers and taking appropriate remedial action.

When the classical method of iterating all layers simultaneously diverges, it is usually found that the diverging layers are located in the lower part of the profile. The divergence becomes apparent when the computer automatically stops calculations because of the numerical overflow. Information on the behavior of overlying layers is lost, and the engineer must reformulate and resubmit the calculation for a reduced profile. The entire trial and error process can be quite expensive in both manhours and computer time. The revised algorithm described here identifies the critical nonconverging layer directly, provides a full solution for the overlying layers, and avoids the need for trial and error reductions of the profile used in calculations.

#### REFERENCES

- 1 Thomson, W. T. Transmission of elastic waves through a stratified solid medium, *J. Appl. Phys.* 1950, 21

- 2 Donovan, N. C. and Matthiesen, R. B. Effects of site conditions on ground motions during earthquakes, *State of Art Symposium, San Francisco, California*, February 1968
- 3 Rösset, J. M. and Whitman, R. V. Theoretical background for amplification studies, *M.I.T. Research Report R69-15*, Soils Publication No. 231, March 1969
- 4 Seed, H. B. and Idriss, I. M. Influence of soil conditions on ground motions during earthquakes, *J. Soil Mech. and Found. Div., ASCE*, 1969, 95 (SM1)
- 5 Seed, H. B. The influence of local soil conditions on earthquake damage, *Proc. 7th Int. Conf. on Soil Mech. and Found. Eng., Mexico City, Mexico*, August 1969
- 6 Tsai, W. C. Influence of local geology on earthquake ground motions, *Ph.D. Thesis*, California Institute of Technology, 1969
- 7 Jones, T. J., Rösset, J. M. Soil amplification of SV and P waves, *M.I.T. Research Report, R70-3*, Civil Engineering Department, January 1970
- 8 Michalopoulos, E. Amplifications of generalized surface waves, *M.S. Thesis*, M.I.T., Cambridge, MA, May 1976
- 9 Constantopoulos, I. V., Rösset, J. M. and Christian, J. T. A comparison of linear and exact nonlinear analyses of soil amplification, *5th World Conference on Earthquake Engineering, Rome*, 1973
- 10 Seed, H. B. and Idriss, I. M. Soil moduli and damping factors for dynamic response analysis, *Report No. EERC 70-10*, December 1970, Univ. of Calif., Berkeley
- 11 Kausel, R., Rösset, J. M. and Christian, J. T. Nonlinear behaviour in soil-structure interaction, *J. Geotech. Eng. Div., ASCE*, 1976
- 12 Schnabel, P. B., Lysmer, J. and Seed, H. B. SHAKE - a computer program for earthquake response analysis of horizontally layered sites, *Report No. EERC 72-12*, December 1972, Earthquake Engineering Research Center, University of California, Berkeley
- 13 Kausel, E., Christian, J. T., LaPlante, F. J. An improved algorithm for non-linear soil amplification, *Proc. 4th Int. Conf. on Structural Mechanics in Reactor Technology (SMIRT)*, paper K1/14, San Francisco, August 1977
- 14 Soil behavior under earthquake loading conditions, State of the Art Evaluation of Soil Characteristics for Seismic Response Analyses, *Report for US AEC* prepared by Shannon & Wilson Inc. and Agbabian Jacobsen Assoc., January 1972
- 15 Rösset, J. M. Soil amplification, Course on Soil Dynamics for Earthquake Design, *Lecture Series No. 2/76*, International Center for Computer Aided Design (ICCAD), Genoa, Italy

#### BIBLIOGRAPHY

- Kausel, E. and Rösset, J. M. Stiffness matrices for layered soils, *Bull. Seism. Soc. Am.* 1981, 71 (6)



**DIVISION DE EDUCACION CONTINUA  
FACULTAD DE INGENIERIA U.N.A.M.**

ANALISIS DE RIESGO SISMICO

EFFECT OF LOCAL SOIL CONDITIONS  
UPON EARTHQUAKE GROUND MOTIONS

ROBERT V. WHITMAN

JULIO, 1985

EFFECT OF LOCAL SOIL CONDITIONS  
UPON EARTHQUAKE GROUND MOTIONS

by Robert V. Whitman

1. INTRODUCTION

It has long been recognized that local soil conditions can have a profound effect upon the damage caused by an earthquake. Such an effect was clearly evident in accounts of the great Lisbon earthquake of 1755, and in the accounts of almost every subsequent major earthquake that affected a large city. The effect of soil conditions upon damage during the 1906 San Francisco earthquake was well recognized in studies of that earthquake. The topic received considerable study following the Kanto (Tokyo) earthquake of 1923. The effect of local soil conditions upon earthquake damage is hardly a new problem. The seismic codes of most countries specifically require different earthquake resistance for different soil conditions. Codes now in effect in the United States contain no such requirement, but not because soil conditions are thought to be unimportant. The writers of the U.S. codes recognized the importance of soil conditions, but felt the problem was so complex and poorly understood that adequate code provisions could not be written. Without a doubt, soil conditions will be incorporated into U.S. seismic codes in the very near future.

Much of the earthquake damage to buildings built upon poor soils results from partial or complete failure of the soil. Such failures include slumping of river banks, failure of waterfront retaining structures, large landslides, foundation settlement and foundation failures. Seed (1970) has provided an excellent summary description of such failures. Many such failures are caused by total or partial liquefaction of loose saturated cohesionless soils. The possibility of such failures, especially liquefaction failures, in any given locale or site requires individual study by experts. Appendix B contains a very brief discussion of liquefaction.

This chapter considers the effect of local soil conditions upon earthquake ground motions, and hence upon the shaking of buildings,

when there is no failure of the soil. Field observations and theoretical studies of this effect have been summarized in recent papers by Ohsaki (1969) and Seed (1969). Much is now known about the problem, although by no means is there complete understanding. There are several ways in which this new knowledge can be put to practical use. One way is the development of site-conditioned earthquake motions for input to the analysis of important structures; this approach is now being used in the design of tall buildings in San Francisco and Tokyo. The second way is to guide the development of new building code provisions. This chapter deals primarily with the latter application. That is, the chapter will discuss how the base shear coefficient  $C$  should vary with soil conditions. A plot of  $C$  vs.  $T$ , the fundamental period of the building, will be called a seismic coefficient diagram.

Figure 1 illustrates several different forms of seismic coefficient diagrams incorporating soil conditions. The simplest forms are those in Figures 1a and 1b; here all ordinates are multiplied by a factor that is independent of period. That is:

$$C(T) = S C_0(T) \quad (1)$$

where  $S$  is a soil factor and  $C_0(T)$  is the seismic coefficient function for a reference soil condition. Ohsaki (1969) has tabulated values of  $S$  required by the codes of 13 countries. Table 1 gives examples of such factors, ranging from the very simple table used in Canada to the somewhat complex table in effect in Japan.

Figures 1c through 1f show more complicated proposals for introducing the effect of local soil conditions into seismic coefficient diagrams; now the effect of soil is varied depending upon the period  $T$ .

1. Figure 1c comes from the new Chilean code. The curve of  $C$  vs.  $T$  varies in shape depending upon a parameter  $T_0$ . The parameter  $T_0$  is related to the characteristic frequency of the site of the building being designed.
2. Figure 1d shows a seismic coefficient diagram proposed by Muto in Japan in 1963. Both the maximum seismic coefficient and the period scale are adjusted in accordance with the type of ground.

- 3. According to the proposed curves shown in Figure 1e, low stiff buildings having a small period  $T$  would be designed for a larger seismic coefficient if on hard ground than if on soft ground. For tall flexible buildings, the reverse would be true.
- 4. Figure 1f shows the code provisions developed for Mexico City, so as to account for the effect of the unusually soft and deep clay which underlies much of that city.

Thus, a great variety of methods have been proposed for incorporating the effects of soils conditions into the seismic provisions of building codes. A building official faced with the selection of a suitable provision, or an engineer faced with implementing such provisions, must understand the basic thinking lying behind the various proposals. To develop such basic understanding, it is useful to consider four categories of soil conditions:

- I. Shallow soil deposit with a distinct characteristic frequency.
- II. Deep deposit of firm soil.
- III. Shallow soft soil overlying deep deposit of firm soil.
- IV. Deep deposit of soft soil.

While these four cases do not encompass all possible soil conditions, they serve to bring out the fundamental considerations.

2. ROLE AND STATUS OF THEORY

In order to understand adequately the effect of local soil conditions, we must combine interpretations of actual accelerograph records together with theoretical analysis. Within the recent past, it has been necessary to rely very heavily upon theory, since the field data from accelerographs has been very scanty indeed. Because of the many accelerographs which have been installed within the past few years and will be installed within the near future, there soon should be many more records involving a variety of soil conditions. However, theory will continue to be of vital importance in helping to sort out and understand the potentially staggering quantity of rather confusing data.

The theory of ground amplification as it exists today is by no means perfect. However, in many cases predictions from the theory are in accord with observations (Seed, 1969). There now has been considerable experience in the practical use of the theory, and we understand both its limitations as well as how it can be used. Used with judgement, this theory is a very useful tool for understanding the effects of local soil conditions.

3. CASE I: SHALLOW SOIL DEPOSIT WITH DISTINCT CHARACTERISTIC FREQUENCY

For a uniform soil deposit (Fig. 2a), the fundamental period is given by:

$$T_0 = \frac{4H}{C_s} \quad (2)$$

where  $H$  = thickness of deposit  
 $C_s$  = shear wave velocity

Case I is typified by  $T_0 < 0.5$  sec. The following tabulation indicates typical combinations of  $C_s$  and  $H$  satisfying this condition.

$C_s$ (m/sec)	$H$ (m)
100 (Very soft clay or silt)	< 12.5
200 (Loose sand, soft clay)	< 25
300 (Dense sand, stiff clay)	< 37.5
400 (Compact sand, hard clay)	< 50

Soil deposits with a depth greater than about 50 meters probably do not belong in Case I. The soil descriptions in the table are intended to give a very general idea of typical shear wave velocities in soils; for further discussion of the evaluation of soil properties for specific cases, see Appendix A and Whitman (1969). Since the soil is non-linear, the shear wave velocity and hence the fundamental period depend upon the intensity of the earthquake, decreasing as the intensity increases.

The nature of this theory is outlined in Appendix A.

Theoretical Considerations

The theory of soil amplification may conveniently be used to indicate the expected effects of a shallow soil deposit.

Amplification spectrum: An amplification spectrum is the ratio of the Fourier amplitude spectra for motions atop the soil to the Fourier amplitude spectra for motions of the underlying rock. Thus an amplification spectrum shows how the various frequency components in earthquake motion are amplified by the soil.

Figure 2b shows a typical amplification spectrum for a shallow soil deposit. It is characterized by a predominant peak, which occurs at the period given by Eq. 3. Smaller, unimportant peaks may occur at very small periods. The peak amplification ratio is a function of:

1. The ratio of the seismic impedance of the soil to the seismic impedance of the underlying rock:

$$\frac{(\gamma C_s)_{\text{soil}}}{(\gamma C_s)_{\text{rock}}} \quad (3)$$

where  $\gamma$  denotes unit weight. As discussed in Appendix A, this factor accounts for the loss of energy back into the underlying rock. The smaller this ratio, the greater the amplification. Thus, for a given rock, the peak amplification ratio increases as the overlying soil becomes softer.

2. The internal damping within the soil: This damping is determined primarily by the magnitude of the dynamic strains which occur within the soil. Thus, the stronger the earthquake, the greater the damping and the smaller the amplification.

One point from the theory is worth emphasizing: the amplification from an outcropping of rock to the surface of soil is less than the amplification from the interface between soil and rock to the surface of the soil. Thus, comparison of motions measured at several depths may overestimate the amplification between the surface outcroppings of different soil or rock.

For cases of interest, the peak amplification ratio between soil and an outcropping of underlying rock is typically between 3 and 6, with the larger values applying to the softer soils during smaller earthquakes.

Peak acceleration: For Case I,  $T_0$  lies within the range of the predominant periods in earthquake ground motions. Hence the amplifying effect of a shallow soil layer causes the peak acceleration at the ground surface to exceed that at an outcrop of the underlying rock. Figure 3 compares computed ground motions for the case corresponding to Fig. 2. As the peak of the amplification spectrum increases, the ratio of peak accelerations increases; however, the increase in peak acceleration is less than the peak amplification ratio. For typical cases the computed ratio of peak accelerations is from 1.5 to 4, with the larger values during smaller earthquakes. In Figure 3, note also the obvious change in predominant frequency.

Response spectra: Figure 4 compares response spectra computed from the motions on soil and on rock. At a period corresponding to the fundamental period of the soil, the ordinates of the spectra from soil motions are considerably greater than those for the spectra from rock motions. Thus, a building whose fundamental period is approximately the same as the fundamental period of the soil will respond much more strongly if on the soil than if on the rock.

A diagram formed by taking the ratio of the response spectra at each period is very similar to the amplification spectrum, although the peak of the former is not so high as the peak of the latter.

Field Evidence

While there are many pieces of evidence which support the general conclusions of the theory (see the papers by Ohsaki and Seed), it is not possible at this time to present evidence which totally substantiates the theory. In particular, there are very few instances of records from instruments placed over very different soils in the same immediate vicinity. A sampling of the available evidence is presented in the following subsections.

Amplification spectra: Figure 5 shows a comparison of actual and predicted amplification spectra (Cobry, 1971). The heavy line is an average of amplification spectra for six earthquakes at a given site, based on measurements made at different depths in Japan. Considering that there are uncertainties in the actual amplification data introduced by the processing of the data, the theoretical curve follows the actual behavior very well.

Peak accelerations: There are a number of examples within the Japanese literature showing that peak acceleration increases as the ground surface is approached, in accordance with the theory. As observed in rather small earthquakes, during which the internal damping is small, this increase is typically in the ratio of 3 or 4. Figure 6 shows peak accelerations observed, mostly in basements of buildings, at various depths beneath the surface of the ground in Tokyo. It should be emphasized that such an increase occurs in rock as well as in soil, because the stiffness of soil decreases near the surface, partly because of weathering and partly because of decrease in overburden stress.

Response spectra: Figure 7 compares response spectra computed from ground motions measured on soft soil and firm soil during the same earthquake. In each diagram, the spectral ordinates have been normalized to the peak acceleration, and hence the effect of soil conditions shows only in the shape and not in the ordinates of the spectra. The shift in the period at which the spectra peak is the result of amplification by the soil.

Damage to buildings: Most of the evidence concerning the effect of local soil conditions is indirect: in the form of differences in damage to buildings founded over different soils (Ohsaki, 1969; Duke and Leeds, 1953). Small buildings, whose fundamental period is in the range from 0.2 to 0.5 second, generally experience greater damage when founded over soft soil than when founded upon firm soil. These observations for the most part are consistent with the theory. However, some of the differences in damage may have resulted from partial failure of softer soils in addition to differences in ground motions.

Perspective from field evidence: Considering the available comparisons between predictions and observations, it may be concluded that the theory may be used to guide the choice of seismic coefficient diagrams for practical work. However, it is also clear that more actual experience is necessary before greater accuracy can be expected from theory.

Microtremor Studies

Kanai and Tanaka (1961) have proposed a method of microzonings based upon measurement of ambient vibrations. The measured vibrations are plotted in the form of an amplitude spectra; in Kanai's original work this spectra was constructed in an approximate way, but more recently Fourier analysis has been used for this purpose. Figure 8 shows some typical results; for identification of the soil types, see Table 1. Both the period and the magnitude of the peak of the spectra are used to determine the seismic zone; the longer the period and the higher the peak, the more severe the expected damage during an earthquake. Kanai has correlated the observed period and amplitude to the four types of ground considered in the Japanese seismic code.

This approach was specifically developed to predict the effect of shallow soil deposits upon damage to buildings having only a few stories. For these conditions, the predictions made by Kanai's approach are entirely consistent with the predictions of amplification theory. Thus, there is a sound reason why Kanai's approach has been in accord with experience during actual earthquakes.

Medvedev's Method

The Russian seismologist Medvedev (1952) has proposed a method for estimating the effect of ground conditions upon earthquake intensity, based upon two factors:

1. The ratio

$$\frac{(\gamma C_0) \text{ soil}}{(\gamma C_0) \text{ granite}} \quad (4)$$

where  $C_D$  is the dilatational, or compressive, wave velocity. The wave velocity for granite serves as a reference against which a soil is rated. The smaller this ratio, the more severe the expected damage during an earthquake.

2. The depth to the water table. The shallower the water table, the greater the expected damage.

These two factors are combined in the equation

$$n = 1.67 \log_{10} \left[ \frac{(\gamma C_D)_{\text{rock}}}{(\gamma C_D)_{\text{soil}}} \right] + e^{-0.04h^2} \quad (5)$$

where  $n$  is the increment in intensity units on a scale equivalent to the modified Mercalli scale, and  $h$  is the depth to the water table in meters. Eq. 5 typically gives an increase in 1 to 2 intensity units (equivalent to a 2 or 4 fold increase in acceleration) for soft ground as compared to firm ground. Medvedev's method was originally developed for use in connection with shallow soil deposits and buildings having only a few stories.

The relationship between Medvedev's method and amplification theory may be understood by means of the example in Figure 9. When the water table is very low, then the ratio  $C_D/\gamma$  is the same for both the soil and the rock. Thus ratios 3 and 4 are equivalent, and Medvedev's method and amplification theory will predict the same trends. The soil in Figure 9b has the same  $C_D$  as in Figure 9a, and thus amplification theory would predict the same behavior for both cases. Raising the water table means that  $C_D$  increases considerably in the soil, and thus the first term in Medvedev's equation decreases. However, this decrease is compensated by an increase in the second term. Thus, Medvedev's two factors taken together give roughly the same result as amplification theory. Moreover, the increases in intensity predicted by Medvedev are consistent with increases in acceleration predicted by amplification theory.

### Summary

For the common case of shallow soil deposits, the predictions of amplification theory are generally in accord with actual experience during earthquakes and moreover are in accord with the semi-empirical methods of microzoning proposed by Kanai and Medvedev.

Figure 10 summarizes the effect of local soil and rock conditions upon response spectra (say for 5% damping) at a given distance from the epicenter of an earthquake. With increasing softness of the earth material, the peak of the spectra increases and shifts to a larger period. Thus, the response of low stiff buildings is strongly affected by soil conditions. On the other hand, a shallow soil deposit has little or no effect upon the response of the fundamental period of tall buildings having long natural periods (although the shallow soil will affect the response of the higher modes of such a building).

Based upon current knowledge, a seismic coefficient diagram such as type (b) in Figure 1 should be used to account for differences in near surface earth materials within a small region. That is to say, the soil factor  $S$  should be independent of period. There are several reasons for this recommendation.

1. Because of uncertainties in both the fundamental period of the soil and the predominant periods in the input ground motion, it is difficult to predict the predominant period in motion at the top of soil. Use of constant  $S$  for  $T < 0.5$  sec. covers these uncertainties.
2. Use of constant  $S$  for  $T > 0.5$  sec. recognizes that the contribution of the higher modes will be affected by soil conditions, and provides extra conservatism with regard to the design of tall buildings.

With further research, it may be possible to use a reduced value of  $S$  for  $T > 0.5$  sec.

Table 2 gives recommended soil factors. These factors are based upon both theory and experience, and consider possible settlement problems in addition to amplification effects. In the 2nd column of the table, hard crystalline rock found at considerable depth has been taken as the reference; the soil factor for a soft soil is 4. However, it generally is more practical to use surface exposures of rock as a reference (3rd column), and then the soil factor for soft soil is 2.2. In some localities, it may even be desirable to use firm soil as a reference (4th column), in which case the soil factor for soft soil is only 1.6.

#### 4. CASE II DEEP DEPOSIT OF FIRM SOIL

Several areas that have experienced major earthquakes are underlain by more than 100 meters of compact alluvium. Los Angeles, Caracas, Venezuela, and Santiago, Chile are prime examples.

##### Theoretical Considerations

Amplification spectra: Figure 11 illustrates the general nature of the amplification spectrum for this case. Now several peaks occur within the range of building periods of practical interest.

The fundamental period is greater than in Case I, and tends to coincide with the period of taller structures. Because the shear wave velocity of compact alluvium is rather high (300 to 450 m/sec) the radiation damping also is greater than in Case I, and hence the amplification at the fundamental peak generally is less than in Case I. Nonetheless, this amplification can be quite important.

The higher order peaks typically occur at periods less than 0.5 second; that is, within the same range of periods for which amplification occurred in Case I. Radiation damping is less important for these higher modes, and hence when internal damping is small--as during small earthquakes--the peaks corresponding to these modes may be nearly as high as the fundamental peak.

Peak accelerations: Figure 12 shows computed acceleration at ground surface, for conditions corresponding to Figure 10 (the input is the same as in Fig. 3, but with a peak acceleration of 0.03g). Peak acceleration is increased; typical increases are factors of 1.5 to 3, with the larger values applying to smaller earthquakes. This increase is caused by the higher modes of the soil; these modes have amplification peaks in the range of the predominant periods of the input motion. The fundamental mode does not cause an increase in peak acceleration, but does amplify the longer period components of ground motion.

Response spectra: Figure 13 compares response spectra for motions at the surface of several different depths of compact alluvium. Changing the depth of the alluvium has relatively little effect upon the general position of the spectra for  $T < 0.5$  second. However, increasing the depth of the alluvium has a very significant effect upon the spectra at larger periods corresponding to taller buildings.

##### Field Evidence

There is, to the author's knowledge, no adequate direct confirmation of these theoretical results, although Gutenberg (1957) has shown that deep deposits amplify the long period components of ground motion. Actual accelerograph records from nearby sites with very different depths of alluvium must be obtained before adequate confirmation is possible.

Observations of damage to buildings during the Caracas earthquake of July 1967 do provide strong indirect confirmation of the theory (Whitman, 1969; Seed et al, 1970). Caracas is underlain by a compact alluvium whose depth generally is less than 100 meters. However, under one portion of the city the depth is as much as 300 meters. Analysis of the patterns of damage shows:

1. For buildings having 8 stories or less, the percentage of buildings damaged is more-or-less constant for all parts of the city.

- 2. Buildings having more than 8 stories, and particularly those having more than 15 stories, were much more heavily damaged in the part of the city over the very deep alluvium than elsewhere in the city.

These observations show clearly that a great depth of alluvium significantly amplifies the earthquake threat to tall buildings.

Summary

The theory, together with the evidence from the Caracas earthquake shows the need to guard against the strong shaking that can occur when the fundamental period of a tall building coincides with the fundamental period of a deep soil deposit. Thus, the fundamental period of the soil must enter into the code. When differences in depth of soil, rather than differences in the nature of the soil, are of concern, it appears that a seismic coefficient diagram of type (c) in Figure 1 is suitable. An example is the following formula from the Chilean code:

$$c = \begin{cases} c_0 & T \leq T_0 \\ c_0 \left[ \frac{2 T/T_0}{1+(T/T_0)^2} \right] & T \geq T_0 \end{cases} \quad (6)$$

The soil period  $T_0$  must be determined from a combination of experience, careful analysis of earthquake records and theoretical studies. Usually it is not possible to determine  $T_0$  by measurement of microtremors, since the high frequencies present in ambient vibrations mask the low frequencies associated with the fundamental period. When using Eq. 6,  $T_0$  should always be at least 0.4 even if the fundamental period is smaller than this limit.

5. CASE III SHALLOW SOFT SOIL OVERLYING DEEP DEPOSIT OF FIRM SOIL

Theoretical Considerations

As yet, this case (which is sketched in figure 14) has not been studied completely from a theoretical standpoint. The effect of the soft shallow deposits enter through the higher modes and the response of these higher modes is quite sensitive to the details of the analysis-- especially the assumptions concerning damping. The theoretical results which have been computed are not entirely satisfactory.

However, in a general way it may be said that Case III is a combination of Case I and Case II. Thus the fundamental mode of the deep compact alluvium will amplify long period motions while the higher modes of the deep alluvium will also amplify shorter period motions. The shallow soil deposits will further amplify the short period motions. With respect to the effect upon buildings, the following can be expected:

1. Buildings with  $T < 0.5$  second. Damage will be greater if these buildings are founded upon the soft soil than if they rest upon firm alluvium. The depth of the firm alluvium beneath a building has little effect upon the damage to that building. Thus conclusions applicable to Case I apply.
2. Buildings with  $T > 0.5$  second. Damage will be greater if a building is founded over a great depth of firm alluvium than if it rests upon a shallow depth of this alluvium. The presence or absence of soft soil near the surface has less effect upon the damage. Thus conclusions applicable to Case II apply.

Field Evidence

Damage in Valdivia and Concepción during the 1960 earthquakes has been studied extensively (Duke and Leeds, 1963, and subsequent studies at the University of Chile). This damage was greatest where there was soft soil at the surface. The great majority of this damage was to 1 and 2 story buildings. Thus the behavior during these earthquakes is consistent with Case I. Hence it is not surprising that predictions based upon Kanai's and Medvedev's methods correlated well with the damage patterns.

At both of these cities, there exist deep deposits of firm soil. Using amplification theory, attempts have been made to correlate damage to this total depth. However, since there were very few buildings having periods greater than 0.5 second, no such correlation was possible. Moreover, since the theory for a soft shallow layer over a deep stiff layer is still not reliable, the theory often did not show correctly the effect of the shallow layer.

Thus the experience from the 1960 earthquakes showed the effect of shallow soft deposits but gave no indication as to the effect of varying depths of the compact alluvium. However, the effect of the deep alluvium must not be ignored when establishing microregionalization or building code provisions for future construction, because more and more tall buildings certainly will be constructed in these and other cities with similar soil conditions.

Summary

A seismic coefficient diagram for this case must recognize both the effect of shallow soft deposits upon buildings having  $T < 2.5$  second and also the effect of deep soil upon buildings having longer periods. These requirements might be met by combining Eqs. 1 and 6:

$$C = \begin{cases} C_0 S & T \leq T_0 \\ C_0 S \left[ \frac{2T/T_0}{1+(T/T_0)^2} \right] & T \geq T_0 \end{cases} \quad (7)$$

The soil factor  $S$  would be chosen based upon the shear wave velocity of the near-surface soils, while  $T_0$  would bring in the effect of the deep deposit. Such a code provision might apply to many cities, such as Boston for example, where very poor soils at the surface overlie deep deposits of clay. Such a provision probably should be used only for  $T < 1.5$  seconds. If the fundamental period of the soil is greater, special provisions such as that described in the next section are warranted. As before, the minimum  $T_0$  is 0.4.

6. CASE IV DEEP DEPOSIT OF SOFT SOIL

Theoretical Considerations

Amplification spectra: Figure 15 shows an amplification spectra for a deep deposit of very soft clay. This spectrum is similar to that in Fig. 10, with one important difference: now the peak amplification at the fundamental mode is distinctly greater than that for the higher modes. This change occurs because, with a deep deposit of soft soil, radiation damping is less important and strains (and hence internal damping) are larger.

Response spectra: Figure 16 compares response spectra from motions measured on top of the soil with that from motions at an outcropping of the underlying hard soil. There is an increase in the ordinates at low periods. However, the remarkable feature is the very great increase in the range from 2 to 2.5 seconds. Now the peak of the spectra has been shifted to a much larger period.

Peak acceleration: In the case corresponding to Figure 16, peak acceleration on top of the soil was twice that on the hard outcropping. In other cases which have been investigated theoretically, peak acceleration is decreased.

Field Evidence

The classic example of this case is the soft deep deposit of clay underlying Mexico City. The examples in Figs 15 and 16 apply for the soil conditions in Mexico City, and have been confirmed by actual accelerograph records

It has often been suggested that a deep soft deposit can actually cause a decrease in peak acceleration. While there is little or no field evidence to prove this, such might occur during a strong earthquake when the internal damping within the soil would be increased.

22

Summary

For this situation, it is appropriate to use a seismic coefficient diagram of Type (f) in Fig 1. Now the seismic coefficient is less for very small periods than for intermediate periods. However, at this time use of such a diagram is justified only for sites where there is considerable actual experience which has been studied in detail.

7. PILE FOUNDATIONS

The evidence currently available suggests that piles usually do not alter the ground motions at the base of a building (Ohsaki, 1969). This is because piles generally are flexible enough to follow the horizontal motions of the soil (for example, see Yamamoto and Seki, 1970) However, piles may improve the ability of the building to resist the effects of the ground motion--by reducing both static settlements (that may use up some of the reserve strength of the building) and dynamic rocking motion. Because of the need for less conservatism, the soil factor S might be reduced somewhat for pile-supported buildings.

Large diameter caissons may be stiff enough to resist following the motions of a soft soil through which they pass (Ohsaki, 1969). Then the amplifying effect of the soil-caisson system will be more like that of a firm soil rather than a soft soil. Thus for caisson-supported buildings,  $T_0$  used in Eq. 7 could be somewhat less than the fundamental period of the soil.

Unfortunately, at the present time there are no sound rules for deciding just how much S and  $T_0$  might be modified in accordance with these considerations.

8. RESPONSE SPECTRA AND TIME HISTORIES

The emphasis in this chapter has been upon code provisions to

reflect soil conditions. However, there is a growing trend toward requiring dynamic analyses for tall or important buildings.

The principles discussed in connection with Cases I, II, and III can be used to suggest the possible form for a general design response spectrum incorporating soil conditions:

$$S_a = \begin{cases} S_{a0} S & T \leq T_0 \\ S_{a0} \frac{T_0}{T} \left[ (S-1) \frac{T_0}{T} + 1 \right] & T \geq T_0 \end{cases} \quad (8)$$

where  $S_a$  is the spectral acceleration and  $S_{a0}$  is the spectral acceleration for the reference soil condition. This equation is plotted in Figure 17. The soil factor S, which brings in the effect of the near-surface soil, might be less than in Table 2, since use of dynamic analysis means less need for conservatism. For example, the following values might be used:

<u>Ground condition</u>	<u>S</u>
Exposed rock	1.0
Firm soil	1.3
Soft soil	1.8

The effect of the near-surface soil upon spectral acceleration decreases for  $T > T_0$ . This is in contrast to Eq. 7 where there was need to account for the contributions from higher modes; when a dynamic analysis is performed, the response of higher modes is introduced directly

For  $T > 3$  seconds and  $T_0 > 1$  second, Eq. 8 becomes too conservative. Tezcan (1972) has recently presented a more general approach to development of response spectra including soil effects.

Time histories whose spectra lie above the spectra given by Eq. 8

26

would be suitable as input for dynamic analysis. Great caution should be followed in using individual time histories generated by the theoretical procedures described in Appendix A, since there are uncertainties both in the validity of the procedures and the selection of soil properties. If such procedures are used to generate site-conditioned time histories, it is very essential that a set of time histories be developed by varying the input assumptions.

9. FINAL COMMENTS

The four cases which have been discussed in this chapter certainly do not cover all possible soil conditions, and many problems remain to be solved by further theoretical research plus analysis of accelerograph records. For example, the line of demarcation between Cases II and IV is not at all clear. However, the current understanding of the effect of local soil conditions is almost equal-- and perhaps even equal--to the current understanding of the nature and amplitude of earthquake ground motions for average soil conditions. That is to say, the effect of soil conditions can be evaluated with almost as much confidence as can the reference seismic coefficient  $C_0$ .

Table 1

EXAMPLES OF SOIL FACTORS

<u>Canada</u>		<u>Argentina</u>	
General	1.0	Hard	0.75
Soft	1.5	Medium	1.00
		Soft	1.25
		Very soft	1.50

Japan

Ground/Structure	Wood	Steel	Reinf. Conc.
I Rock	0.6	0.6	0.8
II Diluvium	0.8	0.8	0.9
III Alluvium	1.0	1.0	1.0
IV Very soft	1.5	1.0	1.0

Table 2

RECOMMENDED SOIL FACTORS TO ACCOUNT FOR  
EFFECT OF NEAR SURFACE SOILS

Ground condition	Reference ground condition		
	Hard rock	Exposed rock	Firm soil
Hard crystalline rock at depth ( $C_s > 1200$ m/sec)	1.0	0.5	0.4
Exposed rock with minimal weathering ( $C_s = 700$ m/sec)	1.8	1.0	0.7
Firm clay, compact sand/gravel, deeply weathered rock ( $C_s = 350$ m/sec)	2.5	1.4	1.0
Soft clay or silt ( $C_s = 120$ m/sec)	4.0	2.2	1.6

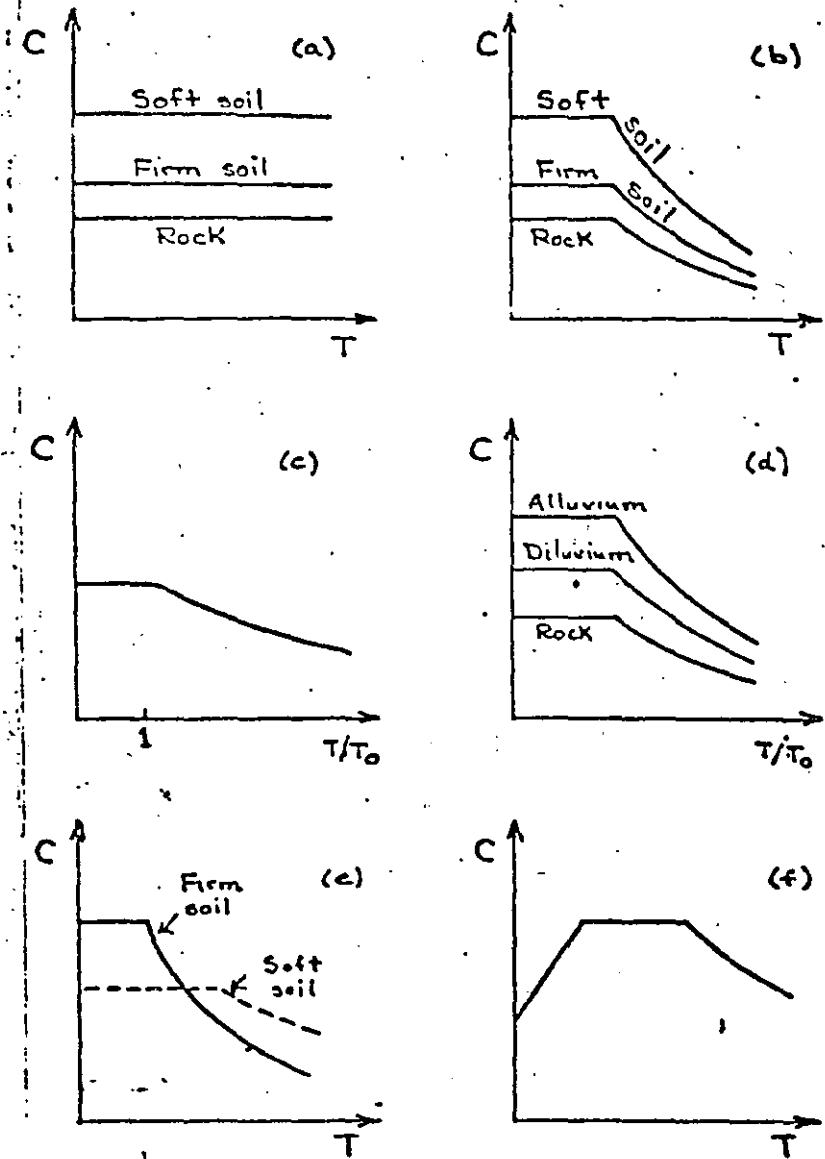
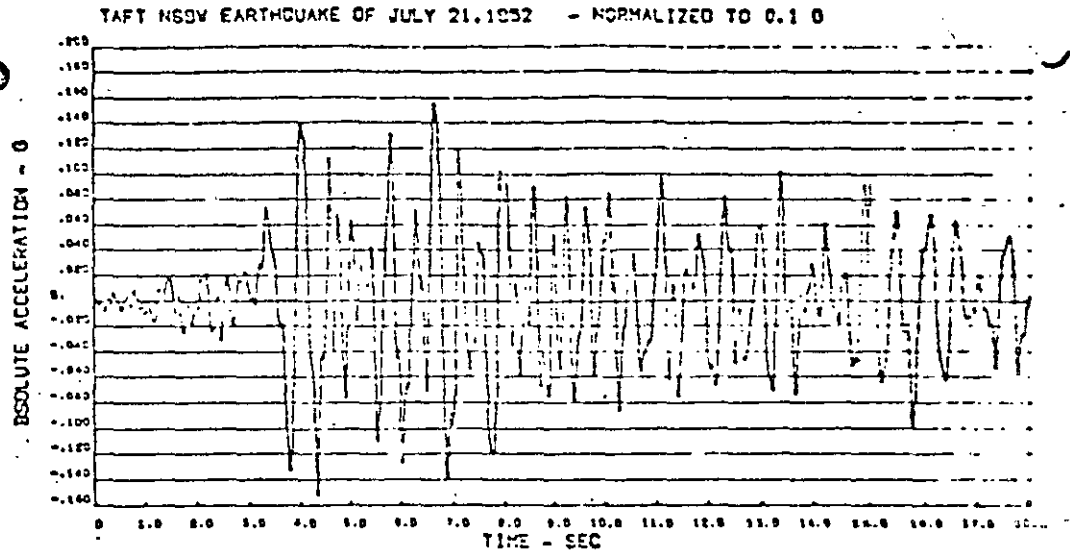
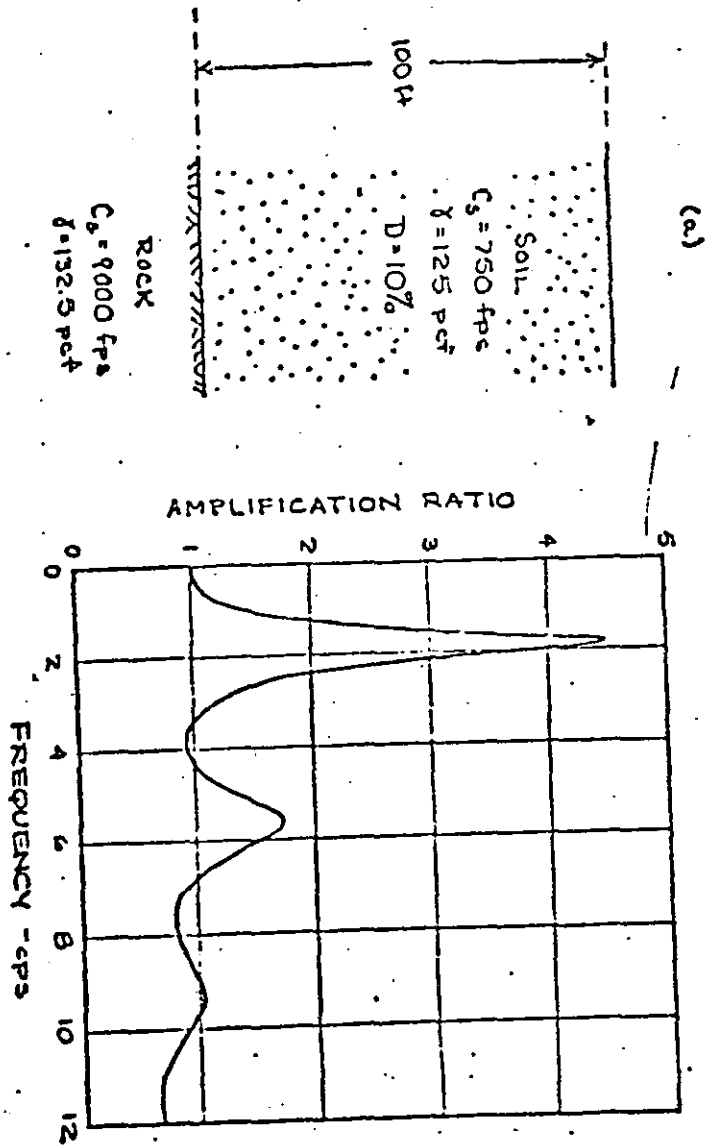
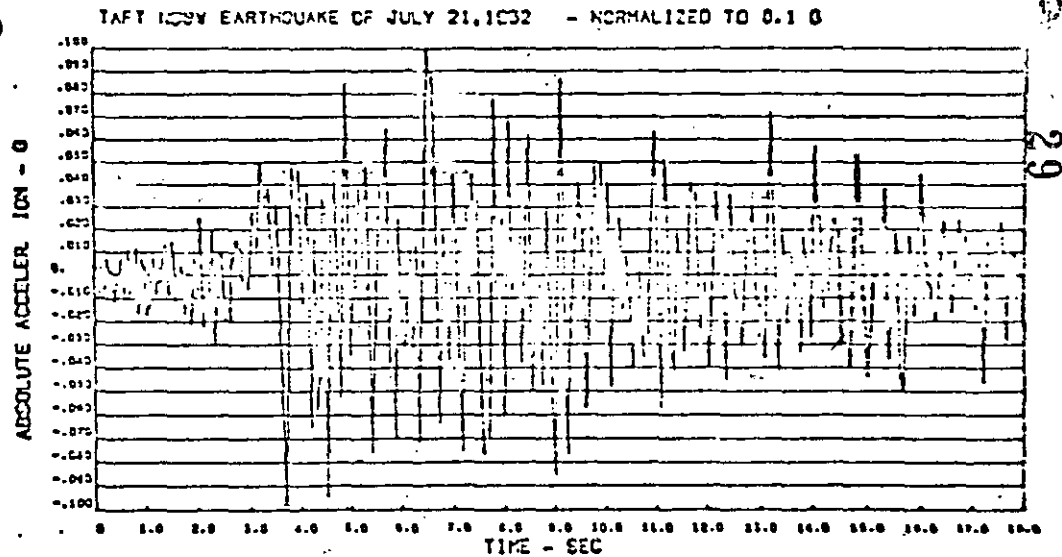


FIGURE 1 VARIOUS TYPES OF SEISMIC COEFFICIENT DIAGRAMS

FIGURE 2 AMPLIFICATION RATIO FOR SHALLOW/ SOIL PROFILE



(a) AT SURFACE



(b) AT OUTCROPPING OF UNDERLYING ROCK

FIGURE 3 INPUT AND COMPUTED SURFACE MOTIONS FOR PROFILE IN FIGURE 2

26-

TKYD STA. AB SIMPLE AVE. 6 QUAKES

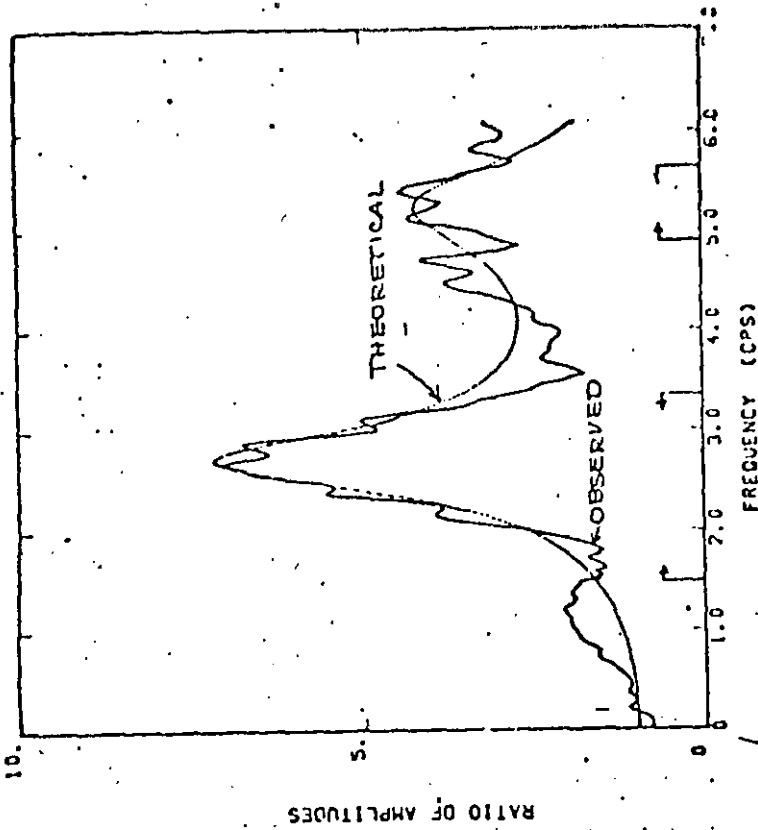


FIGURE 5 THEORETICAL AND OBSERVED AMPLIFICATION CURVES

TAFT NGDV EARTHQUAKE OF JULY 21, 1952 - NORMALIZED TO 0.1 G

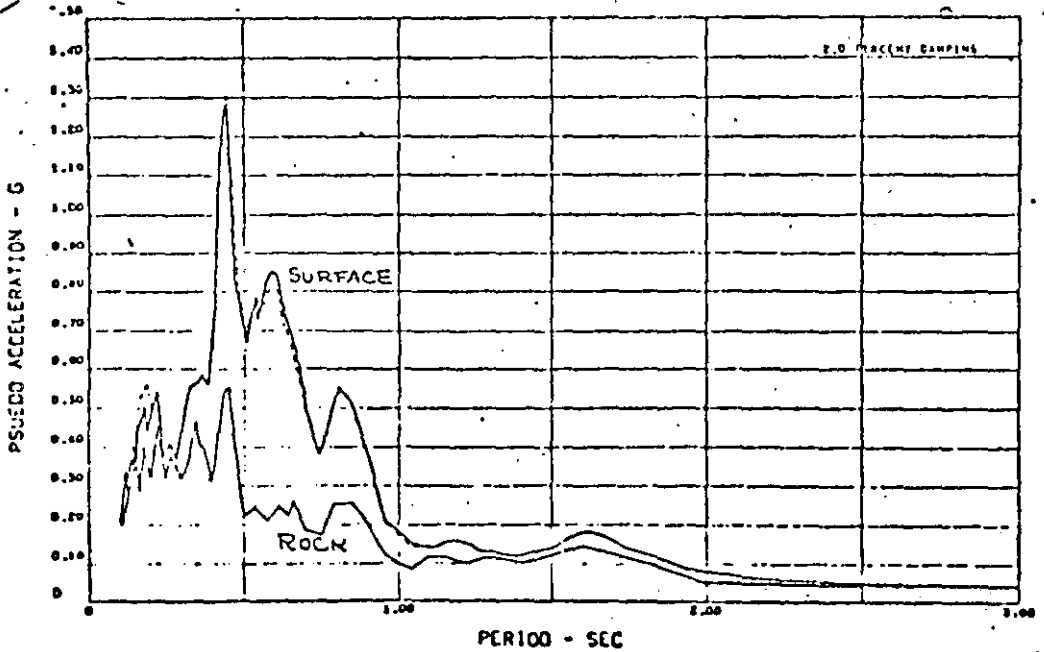


FIGURE 4 COMPARISON OF INPUT AND SURFACE RESPONSE SPECTRA FOR SHALLOW SOIL PROFILE

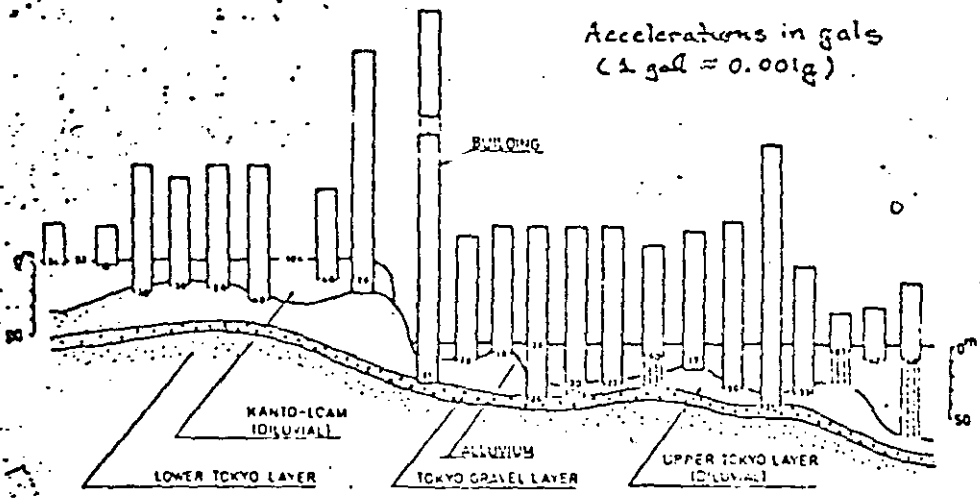


FIGURE 6 PEAK ACCELERATIONS FOR DIFFERENT SOILS AND DEPTHS IN TOKYO DURING EARTHQUAKE IN 1968 (from Ohnoki, 1969)

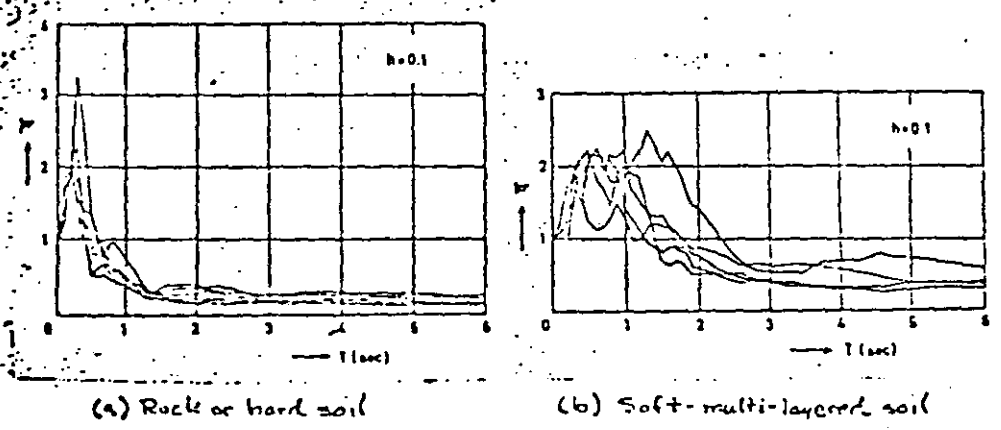
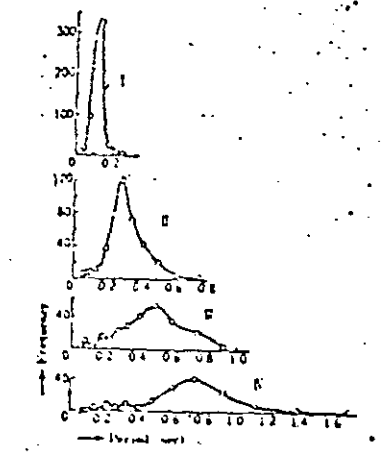
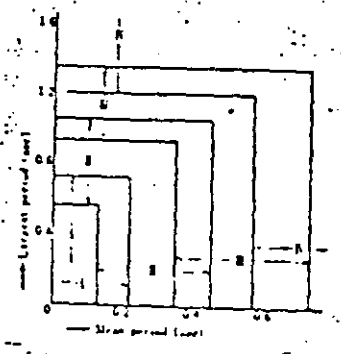


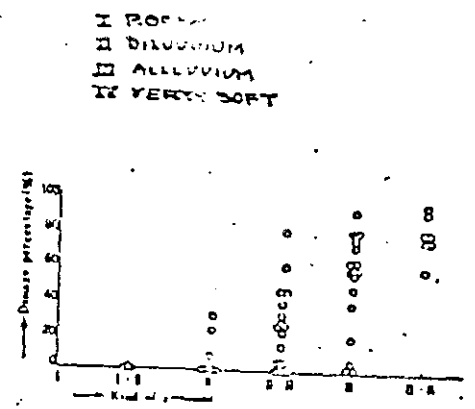
FIGURE 7 RESPONSE SPECTRA (normalized to peak acceleration) FOR DIFFERENT SOIL CONDITIONS IN TOKYO (from Ohnoki, 1969)



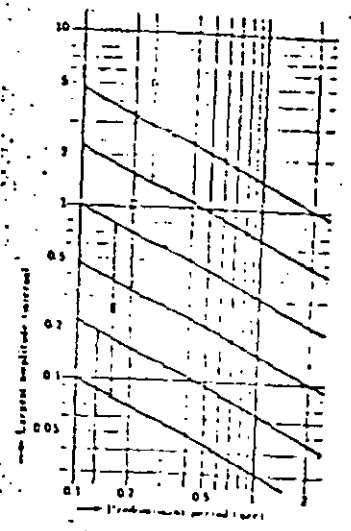
(a) Frequency of occurrence of various periods in microtremor records on different ground



(c) Correlation of mean and largest period with ground type.



(b) Correlation between type of ground and damage to slender buildings during 1923 earthquake.



(d) Correlation of amplitude and predominant period with ground type

FIGURE 8 USE OF MICROTREMOR MEASUREMENTS TO CLASSIFY GROUND TYPE (after Kanai and Tanaka, 1961)

a) Low water table

Soil
$C_0 = 450 \text{ m/s}$
$C_s = 200 \text{ m/s}$
GRANITE
$C_0 = 5100 \text{ m/s}$
$C_s = 2500 \text{ m/s}$

$n = 1.8 + 0$   
 $= 1.8$

(b) High water table

Soil
$C_0 = 1500 \text{ m/s}$
$C_s = 200 \text{ m/s}$
GRANITE
$C_0 = 5100 \text{ m/s}$
$C_s = 2500 \text{ m/s}$

$n = 0.95 + 0.95$   
 $= 1.9$

FIGURE 9 EXAMPLE OF MEDVEDEV METHOD

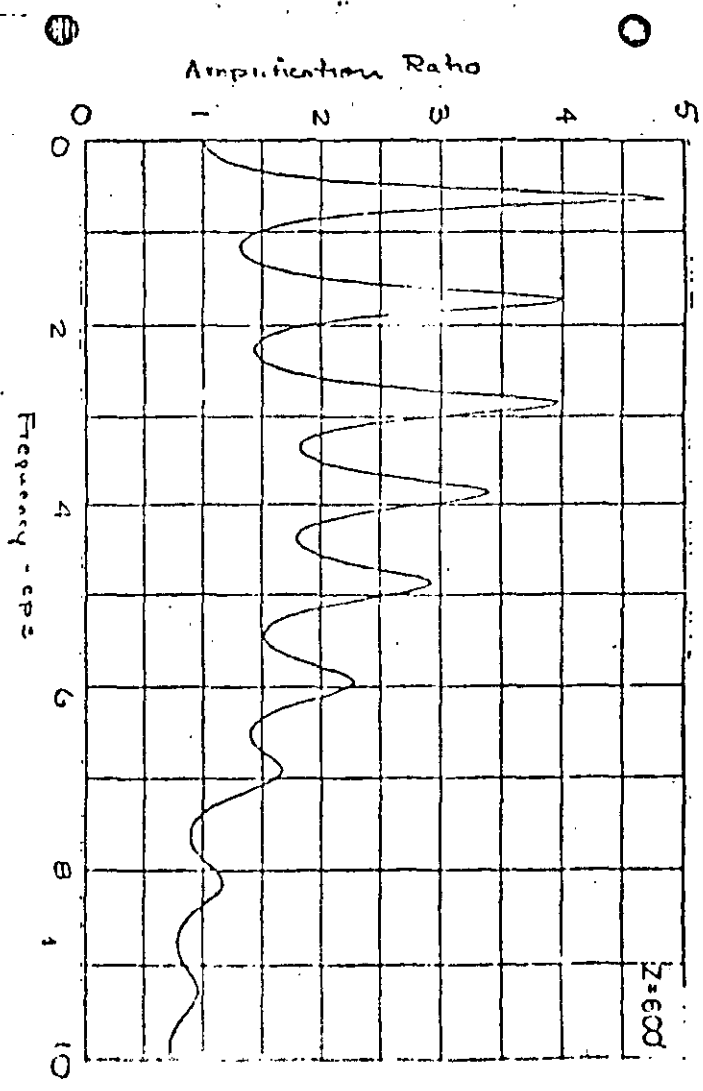


FIGURE 11 AMPLIFICATION SPECTRUM FOR 600 FEET DEEP SOIL PROFILE

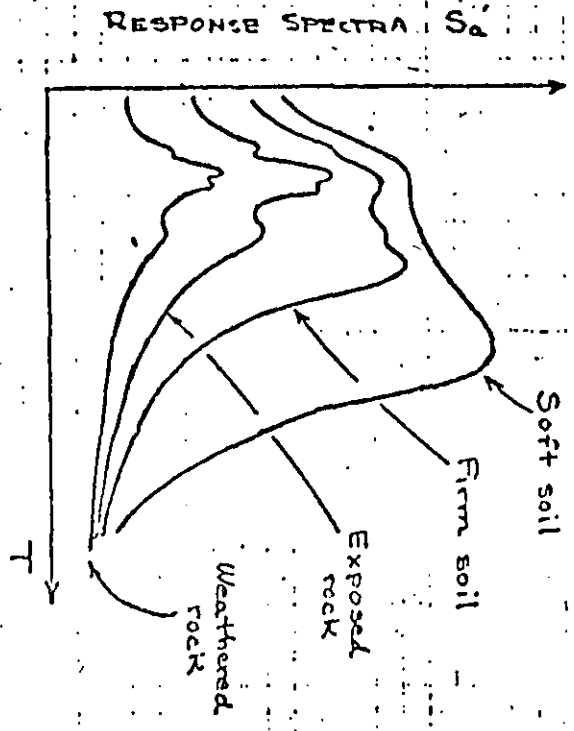


FIGURE 10 SUMMARY OF AMPLIFYING EFFECTS OF SHALLOW SOIL DEPOSIT

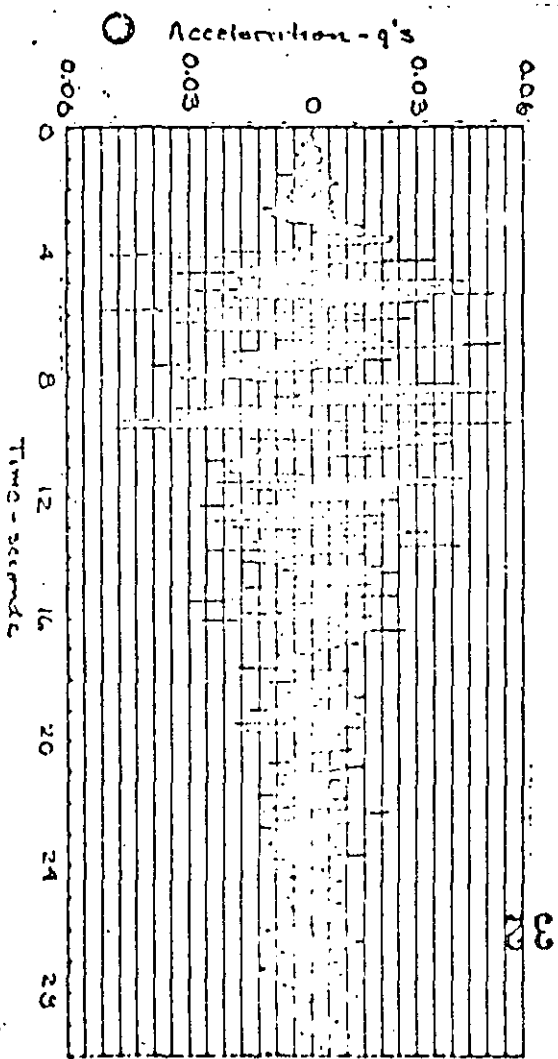


FIGURE 12 ACCELERATION COMPUTED AND PLOTTED AT 600 FEET DEEP

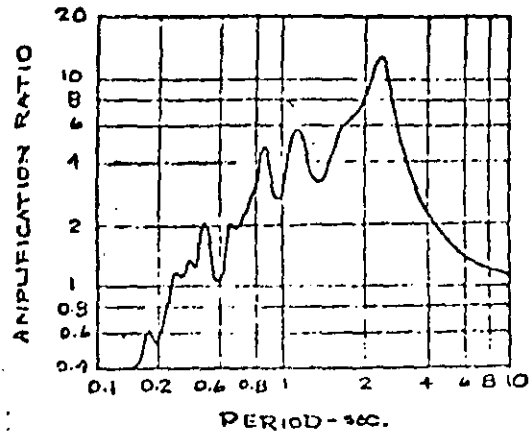
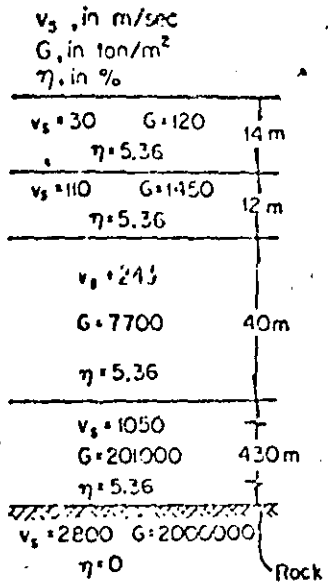


FIGURE 15 AMPLIFICATION SPECTRUM FOR DEEP PROFILE WITH VERY SOFT SOIL

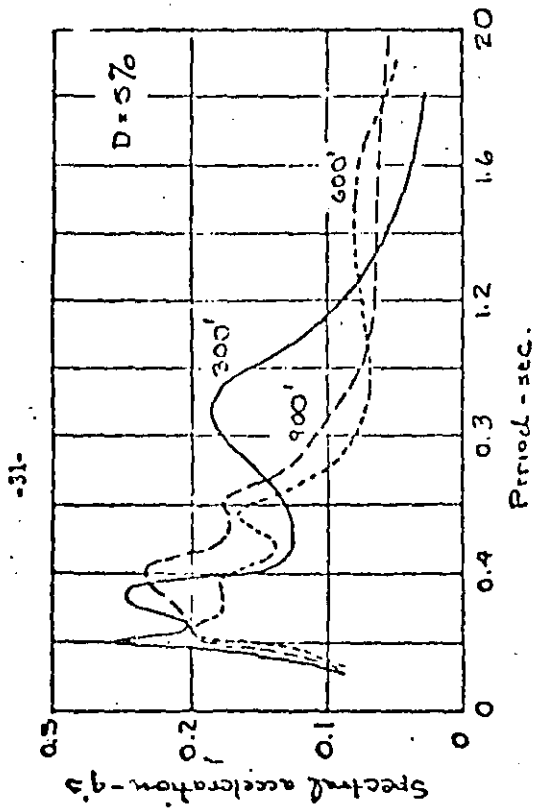


FIGURE 13 RESPONSE SPECTRA (smoothed average for several inputs) FOR DIFFERENT DEEP SOIL PROFILES

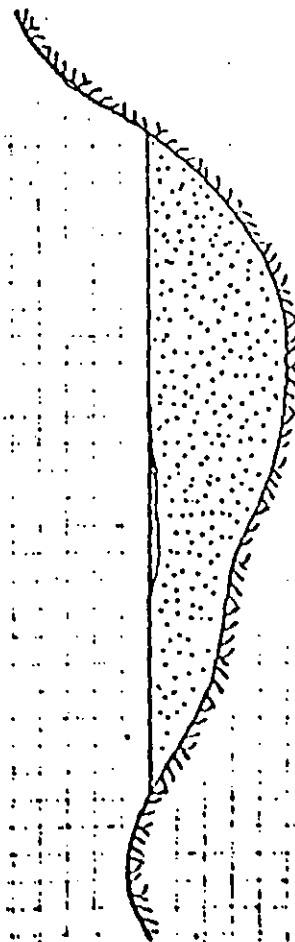


FIGURE 14 SHALLOW STRATA OF SOFT SOIL OVERLYING DEEP DEPOSIT OF FIRM SOIL

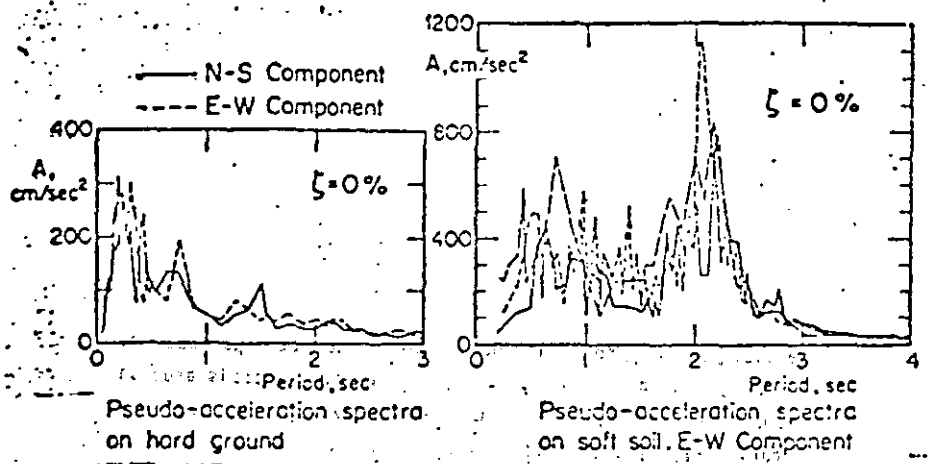


FIGURE 16. RESPONSE SPECTRA FOR HARD AND SOFT GROUND IN MEXICO CITY (from Esteva et al., 1969)

FUNDAMENTALS OF SOIL AMPLIFICATION

by  
J. M. Roesset

Department of Civil Engineering  
Massachusetts Institute of Technology

March 1969

Preface

The purpose of these notes is to present some of the methods now available to include the effect of local soil conditions in the derivation of design earthquakes or response spectra.

The dynamic characteristics of a soil deposit can be expressed by its Transfer function representing the amplification experienced from bottom to top by a sinusoidal steady state motion. The derivation of amplification curves using both a continuous and a discrete solution is presented in II and the relative advantage of each method is discussed.

The general problem of considering an actual earthquake record and filtering it through the soil is discussed in III. Finally, approximate simplified methods are presented to obtain directly response spectra which include the effect of the soil from the knowledge of a response spectrum on firm ground or at bedrock.

Table of Contents

	Page
Preface	ii
I. INTRODUCTION	1
I-1. Statement of the Problem.	1
I-1. General Considerations	3
II. STEADY STATE PERIODIC MOTIONS - The Amplification Function	5
II-1. Continuous Solution	6
A. Uniform layer - Rigid rock	6
B. Uniform layer - Elastic rock	14
C. Multilayered system	23
II-2. Discrete Model	32
III. TRANSIENT MOTIONS	36
III-1. Continuous Solution	37
III-2. Discrete Model	48
IV. DERIVATION OF RESPONSE SPECTRA	51
References	62

by

J. M. Roesset

## I - INTRODUCTION

## I.1 Statement of the Problem.

During the initial phases of development, Earthquake Engineering was mainly concerned with developing methods to estimate the response of a structure to given dynamic loads. While there are still many problems to be solved in the area of Structural Dynamics, particularly in the nonlinear range, it is somewhat disturbing to observe the large discrepancy between the accuracy sought by some methods of analysis and the uncertainty in the nature and magnitude of the loads to which the structure will be subjected. This inconsistency has been recognized in the last years and an increasing amount of effort is now being devoted to study the characteristics of earthquake motions as a function of magnitude, distance to the epicenter and local soil conditions. The purpose of this research is to arrive at simple, but realistic methods to represent the characteristics of the ground motion at a particular site. Among these methods one of the most powerful ones is through the use of design response spectra.

Determination of the appropriate earthquake motions at any given site involves two fundamental steps:

1. Evaluation of the seismic risk of the region. For an area with frequent strong earthquakes this step may be relatively easy and engineers may already know that a certain city is periodically subject to earthquakes of some average magnitudes with epicenters at some average distances. For regions with relatively scarce earthquake history, the determination of a design earthquake becomes much more complicated and requires in general geological and seismological studies, which attempt to identify possible sources of earthquakes or active faults.

\* c Massachusetts Institute of Technology, March 1969

The results of this step can take different forms, the simplest one being a series of values for probable magnitudes and associated epicentral distances. It is possible from these values, using the formulas suggested by Rosenblueth, to characterize each possible design earthquake by its maximum ground acceleration, velocity and displacement. Newmark has derived a simple approximate method by which the corresponding design spectra can be estimated, knowing these three characteristics. It is possible then to draw response spectra for each design earthquake and to find their average or envelope. Alternatively one can try to generate artificial earthquakes that would have the same average characteristics. It must be realized, however, that if this procedure is used it will not be enough to generate just one sample earthquake for a given set of values of magnitude and epicentral distance. Quite the contrary, a substantial number of samples should be generated and used for each possible earthquake, making the procedure extremely long and costly.

In any case the corresponding design earthquakes or response spectra will apply to an overall region for firm ground conditions.

2. Having obtained one or more earthquake records which could occur at the site on firm ground, or better, a set of design response spectra, the next step is to study how these motions would be modified by the local soil conditions of the particular site where the structure is going to be built. The effect of the soil is going to be one of filtering the motions, increasing their amplitude in some ranges of frequencies and decreasing it in others. This problem is normally referred to as soil amplification and will be the subject of the following discussion.

The particular problem under consideration can then be stated as: Given a soil profile and a design earthquake or response spectrum at bedrock, determine the corresponding earthquake or spectrum at the top of the soil.

It should be noticed that in order to be able to apply these results directly in the dynamic analysis of the structure, it must be

assumed that its mass is negligible in comparison to that of the underlying soil. Otherwise a third step is involved corresponding to the problem of soil-structure interaction. In other words it will not be possible to consider the structure and the soil as uncoupled systems.

### 1.2 General Considerations.

Earthquake motions may be decomposed into a series of waves which propagate from the focus in all directions. Given an infinite medium these waves are basically of two types: dilatational or compressional waves and shear waves. The first are normally called P waves. The second can be decomposed again by projecting the motion in two orthogonal directions. SV waves correspond to motions in a vertical plane, SH waves to horizontal motions. Of course when the direction of propagation is vertical, both SH and SV waves would correspond to horizontal motion.

When the waves propagating through a continuous medium find a free surface, a new type of wave is generated, normally referred to as surface or Rayleigh waves. If, in addition, the medium is not homogeneous, but there is a clear discontinuity at some depth from the free surface, a second type of surface wave, called Love wave, is generated. When there are several surfaces of discontinuities in the properties, other types of waves are created.

The overall problem of following an earthquake as it propagates from its focus is of course a three-dimensional wave propagation problem. By assuming for instance a line source of relatively large length or by considering only the effects at some distance from the epicenter, the problem can be reasonably reduced to a two-dimensional one for SV and P waves and a one-dimensional problem for the propagation of SH waves.

The methods described here relate all of them to the solution of the one-dimensional wave propagation equation. Their basic limitations are thus:

1. Only shear waves are considered, either SH or SV if they are propagating vertically, and only SH if they propagate at an angle. P waves propagating vertically could be considered by replacing the appropriate constants (modulus, wave propagation velocity). Surface waves are, however, neglected.

2. The different layers of soil are assumed to be parallel and extending in the horizontal direction for a distance several times larger than the total depth to bedrock.

In spite of these limitations, the solutions obtained by these methods seem to provide a useful and reasonable estimate of the filtering effect of the soil. Two-dimensional wave propagation problems can now be solved by the use of the finite element method. These techniques offer a promising future. Their application is, however, still limited and there are several questions which still have to be solved before they can be used with confidence.

The filtering effect of the soil can be measured in two different ways:

1. By considering a steady state harmonic oscillation of the soil and the underlying rock and determining the ratio of the amplitude at the free surface of the soil to the amplitude at bedrock or at the outcropping of rock (without any soil on top). This ratio will be a function of the frequency of the motion, and if there is damping, a complex function. It is normally referred to as the Transfer Function of the soil. Its modulus is the amplification function, amplification ratio or amplification spectrum.

2. By considering a given earthquake record (time history of acceleration) at bedrock or at the outcropping of rock, and determining the corresponding accelerogram at the free surface of the soil. The result in this case is not only a complete time history of acceleration at the free surface of the soil but also, if so desired, time histories of shear stresses and strains at any point within the soil. It provides therefore a much more complete solution, but it requires considerably

more computer time. Furthermore, because of the reasons previously mentioned, the complete analysis would have to be repeated for each earthquake sample, and it would make little sense to do it for just one record.

Both types of results can be obtained using two different mathematical models:

1. A continuous solution of the differential equation corresponding to the one-dimensional wave propagation problem.
2. A discrete solution replacing each layer of soil by a system of lumped masses and springs and applying standard procedures of Structural Dynamics.

The continuous model offers in general more flexibility and has an economic advantage if the results are desired only at a few points. At present the discrete model requires less computational time when complete histories of accelerations, velocities, strains and stresses are necessary at many points. Both models yield exactly the same results (except for small discrepancies due to different round-off and truncation errors) when:

- a) Damping is assumed constant in all modes and viscosity for each layer directly proportional to its modulus and inversely proportional to frequency.
- b) The underlying rock is assumed to be rigid or in other words the input motion is considered at bedrock with the soil on top, rather than at the outcropping of rock. For elastic rock, results can still be made to agree if an additional damping is inserted in the discrete model to simulate the loss of energy through radiation in the rock.

In the following pages the basis of both formulations will be presented, considering first the case of steady state periodic motions (determination of the amplification curve), then the case of transient motions. The application of these methods to obtain filtered earth-

quake records at the free surface of the soil is immediate. On the other hand, their application to design response spectra, modifying them to include the effect of the soil, is not so straightforward. This point and approximate solutions are discussed at the end.

## II - STEADY STATE PERIODIC MOTIONS

### The Amplification Function

#### II.1 Continuous Solution.

##### A. Uniform layer. Rigid rock.

Let us consider first a uniform layer of soil resting on rock. The equation of motion corresponding to the one-dimensional wave propagation problem is

$$\rho \frac{\partial^2 u}{\partial t^2} = G \frac{\partial^2 u}{\partial x^2} + n \frac{\partial^3 u}{\partial t \partial x^2}$$

where  $\rho$  = density or mass per unit volume =  $\frac{\gamma}{g}$

$\gamma$  = unit weight.

$g$  = acceleration of gravity

$G$  = shear modulus

$n$  = viscosity constant

$u(x,t)$  = displacement of a point in the soil layer

If the rock is rigid but a displacement  $u_G(t)$  is imposed at the base of the soil, the boundary conditions are:

$$\frac{\partial u}{\partial x} = 0 \text{ at } x = 0$$

$$u = u_G(t) \text{ at } x = H$$

38

and the initial conditions:

$$u = 0 \text{ at } t = 0$$

$$\frac{\partial u}{\partial t} = 0 \text{ at } t = 0$$

By calling  $y = u - u_G$  the relative displacement, the equation can be rewritten as:

$$\rho \frac{\partial^2 y}{\partial t^2} = G \frac{\partial^2 y}{\partial x^2} + n \frac{\partial^3 y}{\partial x^2 \partial t} - \rho \frac{\partial^2 u_G}{\partial t^2}$$

with Initial Conditions

$$y = 0, \frac{\partial y}{\partial t} = 0 \text{ at } t = 0$$

and Boundary Conditions

$$y = 0 \text{ at } x = H$$

$$\frac{\partial y}{\partial x} = 0 \text{ at } x = 0$$

If  $u_G(t) = 0$ , the free vibrations can be investigated. Writing then

$$\rho \frac{\partial^2 y}{\partial t^2} = G \frac{\partial^2 y}{\partial x^2} + n \frac{\partial^3 y}{\partial x^2 \partial t}$$

and trying a solution of the form

$$y = U(x) \cdot V(t)$$

where  $U$  is a function only of  $x$

$V$  is a periodic function of  $t$  alone

$$\frac{U''}{U} = \rho \frac{V''}{GV + nV} = -p^2$$

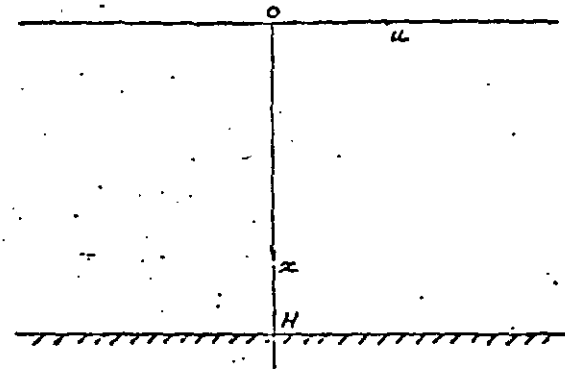


FIG. 1 - UNIFORM LAYER

and the solution by

$$y(x,t) = U(x)e^{i\omega t}$$

then

$$U = E \cos px + F \sin px + C$$

$$\text{with } p^2 = \frac{\rho \omega^2}{G + i\eta\omega}$$

Imposing the boundary conditions

$$F = 0$$

$$E \cos pL = C$$

$$U = C \left( \frac{\cos px}{\cos pL} - 1 \right)$$

$$\text{and } \bar{y} = -\alpha^2 C \left( \frac{\cos px}{\cos pL} - 1 \right) e^{i\omega t}$$

$$\bar{u} = \bar{y} + \bar{u}_G = -\alpha^2 C \frac{\cos px}{\cos pL} e^{i\omega t}$$

and at the free surface of the soil the absolute acceleration becomes

$$\bar{u} = -\alpha^2 C \frac{1}{\cos pL} e^{i\omega t}$$

Since the base motion was  $\bar{u}_G = -\alpha^2 C e^{i\omega t}$

$$\bar{u} = \frac{1}{\cos pL} \bar{u}_G$$

The transfer function of the soil for absolute acceleration at the free surface is then defined as:

$$TF(\bar{u}) = \frac{1}{\cos pL}$$

It should be noticed that if there is viscosity,  $p$  is a complex variable and therefore  $\cos pL$  has to be interpreted as

$$1/2 (e^{ipL} + e^{-ipL})$$

or

$$TF(\bar{u}) = \frac{2}{e^{ipL} + e^{-ipL}}$$

The fact that the transfer function is complex indicates that there is both a change in amplitude and in phase. If only the change in amplitude is considered the Amplification Function is defined as the modulus of the transfer function.

$$A(\alpha) = \frac{2}{|e^{ipL} + e^{-ipL}|}$$

Calling

$$a = \frac{1}{\sqrt{2}} H\alpha \sqrt{\frac{\rho}{G}} \sqrt{\frac{\sqrt{1 + (\eta\alpha/G)^2} - 1}{1 + (\eta\alpha/G)^2}}$$

$$b = \frac{1}{\sqrt{2}} H\alpha \sqrt{\frac{\rho}{G}} \sqrt{\frac{\sqrt{1 + (\eta\alpha/G)^2} + 1}{1 + (\eta\alpha/G)^2}}$$

$$A(\alpha) = \frac{1}{\sqrt{\cos^2 h^2 a \cos^2 b + \sin^2 h^2 a \sin^2 b}}$$

For small values of  $\frac{\eta}{G}$

$$a = \frac{1}{2} H\alpha \sqrt{\frac{\rho}{G}} \approx \frac{1}{2} H \frac{\alpha^2}{\sqrt{G}}$$

$$b = H\alpha \sqrt{\frac{\rho}{G}}$$

The natural frequencies of the layer of soil are then given by

$$f_n = \frac{2n-1}{4H} \sqrt{\frac{G}{\rho}} = \frac{(2n-1)C_s}{4H}$$

$$\omega_n = \frac{(2n-1)\pi}{2H} \sqrt{\frac{G}{\rho}} = \frac{(2n-1)C_s}{2H}$$

and the natural periods

$$T_n = \frac{4H}{2n-1} \sqrt{\frac{\rho}{G}} = \frac{4H}{(2n-1)C_s}$$

where  $C_s = \sqrt{\frac{G}{\rho}}$  is the shear wave velocity of the soil.

The corresponding modal shapes are

$$U = \sin \frac{(2n-1)\pi}{2H} x$$

If the soil has viscosity  $n \neq 0$  in order to have harmonic motion we must have

$$n < \frac{4H}{(2n-1)\pi} \sqrt{\frac{G}{\rho}} = \frac{2\pi G}{(2n-1)\pi C_s} = \frac{2\pi G}{(2n-1)\pi C_s}$$

A critical value of viscosity can be established for each mode.

In particular in order to have at least 1 mode

$$n < n_1 \text{ crit} = \frac{4H}{\pi} \sqrt{\frac{G}{\rho}}$$

It is important to realize that if there is any viscosity, the number of modes will be finite. (Higher modes will have damping higher than critical).

Considering now the forced vibration problem, it is convenient for a steady state periodic motion to represent the base displacement by

$$u_G(t) = C e^{i\omega t}$$

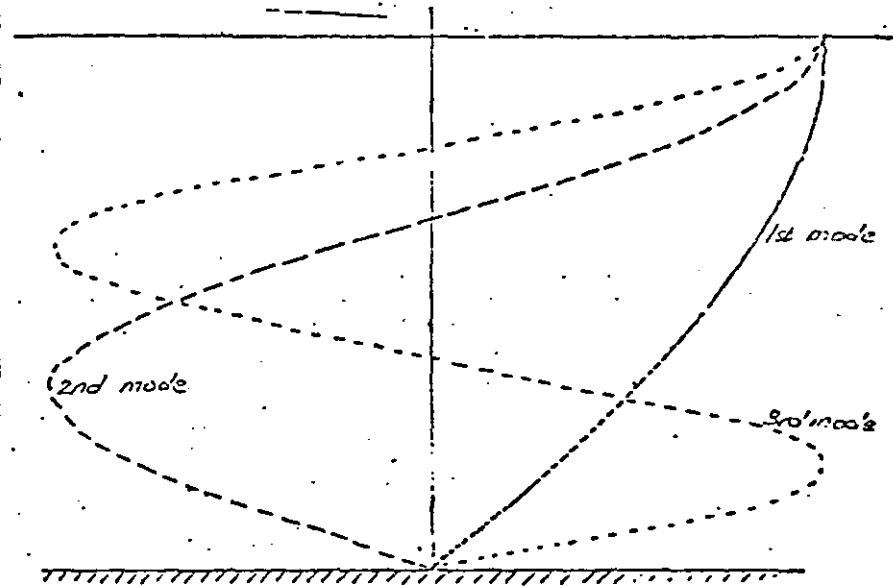


FIG. 2. MODAL SHAPES FOR A UNIFORM LAYER

and 
$$A(\alpha) = \frac{1}{\sqrt{\cos^2 \beta + \alpha^2 \sin^2 \beta}}$$

In particular if there is no viscosity  $n = 0$

$$A(\alpha) = \frac{1}{\cos \beta}$$

and the amplification will become infinity at  $\beta = \frac{(2n-1)\pi}{2}$  which corresponds to  $\alpha = \frac{(2n-1)\pi}{2H} \sqrt{\frac{G}{\rho}} = \omega_n$ , nth natural frequency of the layer.

On the other hand, if  $n \neq 0$ , the amplification will not become infinity. Two cases can then be considered:

1. If the value of  $n$  is constant as  $\alpha$  increases, the first expression will have to be used since  $\frac{n}{\alpha G}$  will not be small any longer. As  $\alpha$  increases  $A(\alpha)$  tends to zero, which means that for very large input frequencies the top of the layer remains at rest. The amplification function will have only a finite number of peaks corresponding to those natural frequencies of the layer which have damping less than critical.

For values of  $\alpha$  such that  $\frac{n}{\alpha G}$  is still small, the amplification at  $\alpha = \omega_n$ , nth natural frequency of the layer, becomes

$$A(\omega_n) = \frac{4}{(2n-1)^2} \frac{1}{n\omega_n/G} = \frac{2\pi r_1}{\pi n} \frac{1}{(2n-1)^2}$$

This shows that the amplitude of the peak at the second natural frequency of the layer will be  $\frac{1}{9}$  of that at the first, the amplitude of the third will be  $\frac{1}{25}$  etc. . .

2. If it is assumed that the viscosity is inversely proportional to the frequency so that  $\frac{n}{\alpha G} = \tan \delta$  is a constant, for small values of  $\frac{n}{\alpha G}$

$$A(\omega_n) = \frac{4}{(2n-1)^2 \tan \delta} = \frac{4}{(2n-1)^2} \frac{1}{2\delta}$$

with  $\delta = \frac{1}{2} \tan \delta =$  fraction of critical damping

In this case the amplitude of the second peak will be 1/3 that of the 1st, the amplitude of the third peak 1/5 and so on.

Comparing these results with those for a lumped mass discrete system as normally encountered in Structural Dynamics, we can say that a constant value of viscosity  $n$  corresponds to an increasing percentage of damping in each mode, whereas a constant value of  $\frac{n}{\alpha G}$  corresponds to constant damping in all modes.

Figures 3 and 4 show the amplification curves for a uniform soil layer with the following characteristics:

Depth	$h = 100'$
Shear wave velocity	$c_s = 750$ ft/sec.
Unit weight	$\gamma = 125$ lbs/cubic ft.

8. Uniform layer. Elastic rock

Taking now two sets of axes, one with origin at the free surface of the soil, the second with origin at the top of the rock, the motions in the soil and the rock can be expressed as

$$u_s = E_s e^{i(p_s x_s + \alpha t)} + F_s e^{-i(p_s x_s - \alpha t)}$$

$$-u_r = E_r e^{i(p_r x_r + \alpha t)} + F_r e^{-i(p_r x_r - \alpha t)}$$

where

$$p_s^2 = \frac{\rho_s \alpha^2}{G_s + i n_s \alpha}$$

$$p_r^2 = \frac{\rho_r \alpha^2}{G_r + i n_r \alpha}$$

The boundary conditions are now

$$\frac{\partial u_s}{\partial x_s} = 0 \text{ at } x_s = 0$$

$$u_s(x_s = H) = u_r(x_r = 0)$$

$$(G_s + i\eta_s \rho) \frac{\partial u_s}{\partial x_s} (x_s = H) = (G_r + i\eta_r \rho) \frac{\partial u_r}{\partial x_r} (x_r = 0)$$

The result is

$$E_s = F_s$$

$$u_s = E_s e^{int} (e^{ip_s x_s} + e^{-ip_s x_s})$$

$$E_s = \frac{2E_r}{e^{ip_s H} (1+\nu) + e^{-ip_s H} (1-\nu)}$$

$$F_r = E_r \frac{e^{ip_s H} (1-\nu) + e^{-ip_s H} (1+\nu)}{e^{ip_s H} (1+\nu) + e^{-ip_s H} (1-\nu)}$$

with

$$\nu = \frac{\rho_s (G_s + i\eta_s \rho)}{\rho_r (G_r + i\eta_r \rho)}$$

$$u_s(x_s = 0) = 2E_s e^{int}$$

$$u_s(x_s = H) = u_r(x_r = 0) = (E_r + F_r) e^{int} = E_s (e^{ip_s H} + e^{-ip_s H}) e^{int}$$

The ratio between the displacement (or acceleration)  $u$  at the free surface of the soil, and the displacement (or acceleration) at the interface between rock and soil can then be expressed as

$$TF = \frac{2}{e^{ip_s H} + e^{-ip_s H}}$$

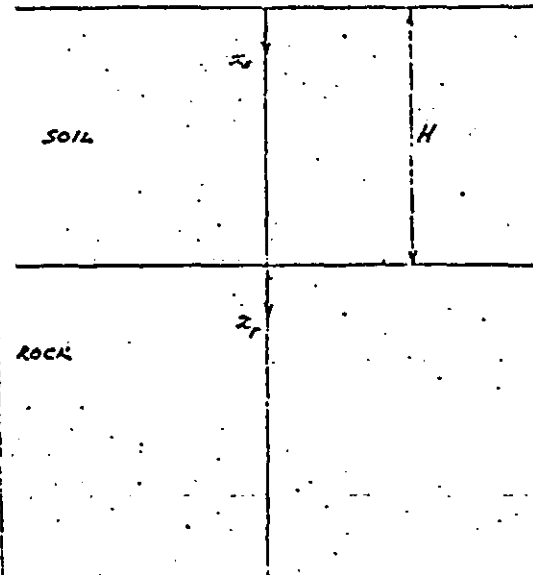


FIGURE 5. UNIFORM LAYER ON ELASTIC ROCK

44

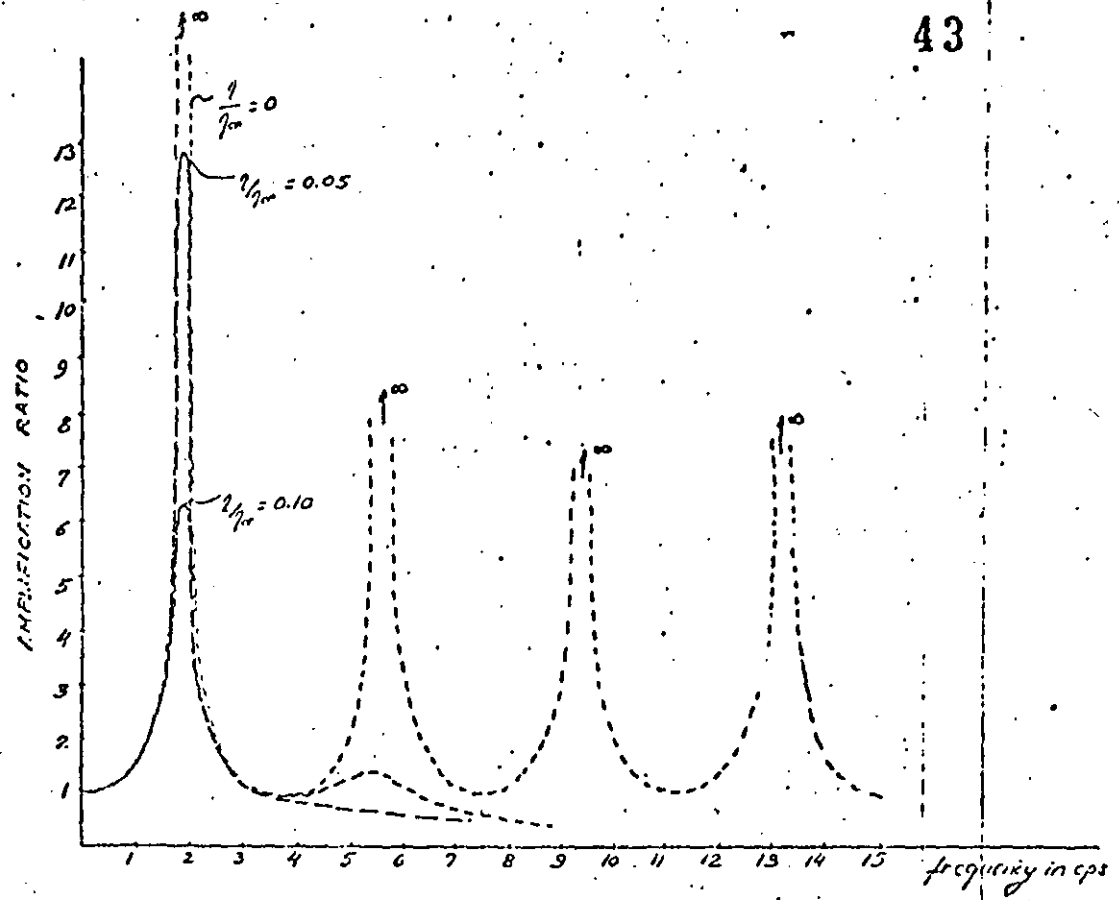


FIG. 3. AMPLIFICATION CURVE FOR UNIFORM LAYER  
RIGID ROCK - CONSTANT VISCOSITY

-15-

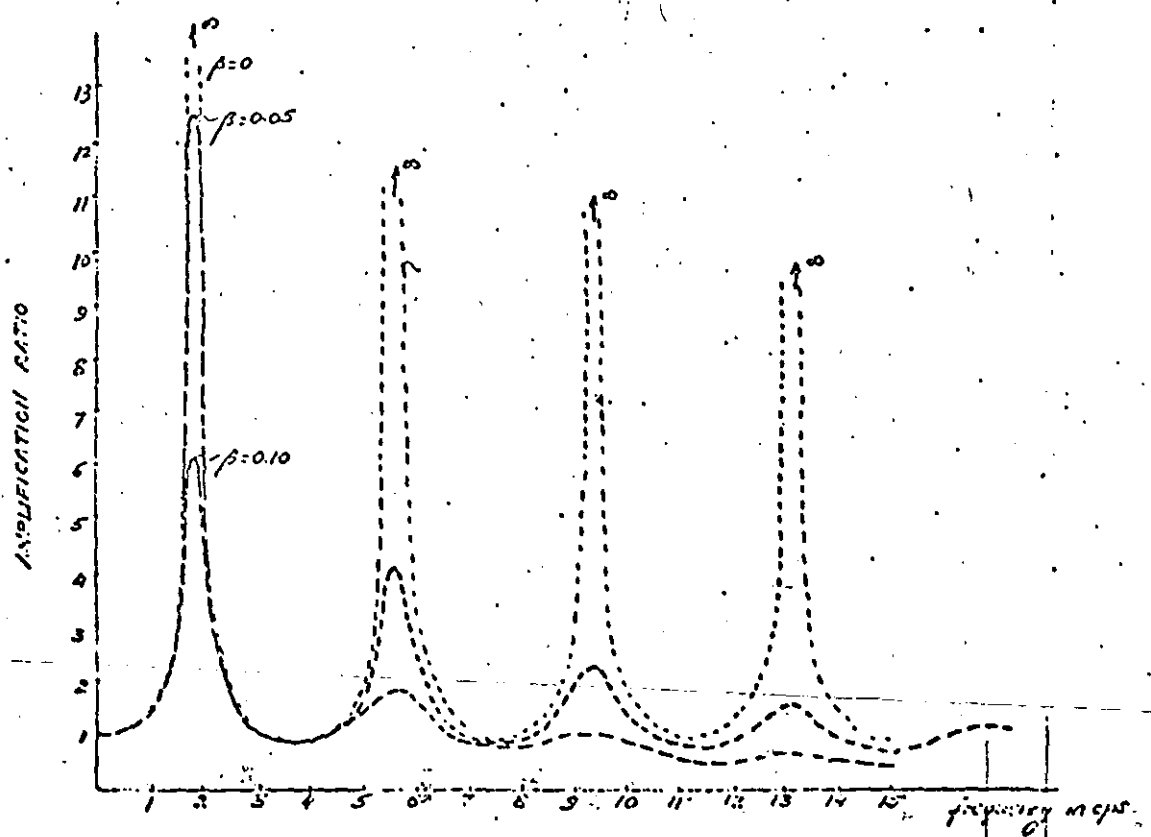


FIG. 4. AMPLIFICATION CURVE FOR UNIFORM LAYER  
RIGID ROCK - CONSTANT NORMAL DAMPING

-16-

which is the same expression previously obtained for rigid rock.

If on the other hand one considers the situation of the rock without soil on top, the motion at the outcropping of rock would be

$$u = 2E_r e^{int}$$

and the ratio between the displacement (or acceleration) at the free surface of the soil, and the displacement (or acceleration) at the outcropping of rock would be

$$A = \frac{2}{e^{ip_s H} (1+\nu) + e^{-ip_s H} (1-\nu)}$$

A second amplification function can thus be defined by considering the elastic properties of the rock. This function gives now the ratio between amplitudes of motion on top of the soil to the amplitude of the motion that would be felt on top of the rock if the soil were not there.

$$A(n) = \frac{2}{|e^{ip_s H} (1+\nu) + e^{-ip_s H} (1-\nu)|}$$

In this case if there is no viscosity  $n_s = n_r = 0$

$$p_s = \frac{n}{c_s} \quad p_r = \frac{n}{c_r}$$

$$A = \frac{p_s G_s}{p_r G_r} = \frac{G_s c_r}{G_r c_s} = \sqrt{\frac{G_s \rho_s}{G_r \rho_r}} = \sqrt{\frac{G_s \gamma_s}{G_r \gamma_r}} = \frac{\gamma_s c_s}{\gamma_r c_r}$$

and

$$A(n) = \frac{1}{|\cos p_s H + \nu \sin p_s H|}$$

At the natural frequencies of the layer  $\alpha = \omega_n \cos p_s H = 0$  and  $\sin p_s H = (-1)^n$

$$A(\omega_n) = \frac{\gamma_r c_r}{\gamma_s c_s}$$

It can be seen that this amplification ratio does not become infinity even if the soil has no viscosity.

If the rock has no viscosity  $n_r = 0$ , and the soil has a viscosity  $n_s$  so that  $n_s n / G_s$  is small, one can again derive an approximate formula for the amplification at the natural frequencies  $\alpha = \omega_n$

$$A(\omega_n) = \frac{\gamma_r c_r}{\gamma_s c_s} \cdot \frac{1}{1 + \frac{(2n-1) \gamma_r c_r}{\gamma_s c_s} \cdot \frac{n_s \omega_n}{G_s}}$$

For the case of constant viscosity  $n_s$

$$A(\omega_n) = \frac{\gamma_r c_r}{\gamma_s c_s} \cdot \frac{1}{1 + \frac{\gamma_r c_r}{\gamma_s c_s} \cdot \frac{n_s}{n_s \text{ crit}} (2n-1)^2 \frac{\omega_n}{2}}$$

and for the case of constant  $\frac{n_s n}{G} = 2\delta$

$$A(\omega_n) = \frac{\gamma_r c_r}{\gamma_s c_s} \cdot \frac{1}{1 + \frac{\gamma_r c_r}{\gamma_s c_s} \cdot 2\delta \cdot \frac{(2n-1)\omega_n}{4}}$$

Figures 6 and 7 show amplification functions with elastic rock for the same uniform layer of soil previously considered ( $\gamma_r = 140$ ,  $c_r = 4500$ ).

The main difference between both cases is the fact that the rock considered as an elastic half space is dissipating energy by radiation. Both solutions are then approximately related by the

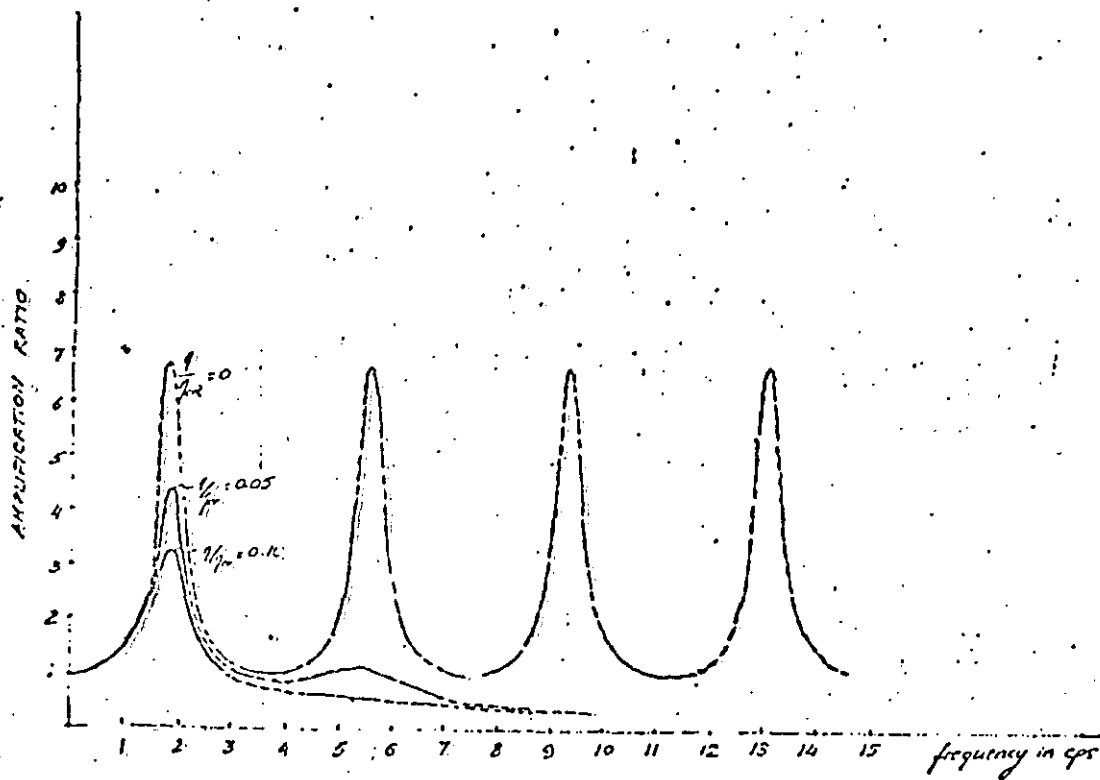


FIG. 6. AMPLIFICATION CURVE FOR UNIFORM LAYER.  
ELASTIC ROCK - CONSTANT VISCOSITY

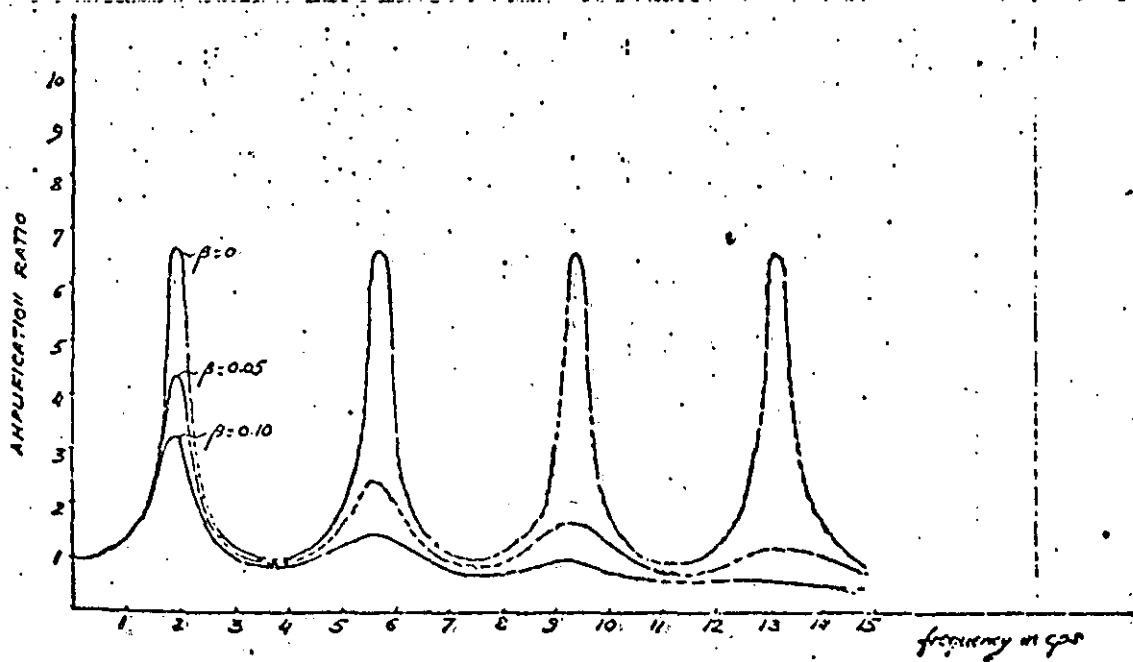


FIG. 7. AMPLIFICATION CURVE FOR UNIFORM LAYER  
ELASTIC ROCK - CONSTANT MASS DAMPING.

expression

$$\frac{1}{A_2(\omega)} = \frac{\gamma_s C_s}{\gamma_r C_r} + \frac{1}{A_1(\omega)}$$

where  $A_1(\omega)$  is the amplification function with rigid rock

$A_2(\omega)$  is the amplification function with elastic rock.

This formula can be reproduced by adding to the first case an equivalent radiation damping, function of frequency

$$B_{eq} = \frac{2}{\pi} \cdot \frac{\gamma_s C_s}{\gamma_r C_r} \cdot \frac{1}{2n-1}$$

or

$$s_{eq} = \frac{2}{\pi} \cdot \frac{\gamma_s C_s}{\gamma_r C_r} \cdot \frac{\omega_1}{\omega}$$

since  $\eta \frac{\omega}{G} = 2B$  this represents

$$\eta_{eq} = \frac{G}{\omega} 2B_{eq} = \frac{4}{\pi} G_s \frac{\gamma_s C_s}{\gamma_r C_r} \cdot \frac{\omega_1}{\omega^2}$$

C. Multilayered System.

When the soil deposit is made of several layers with different properties (Fig. B) one can define for each layer j

- $h_j$  = thickness
- $G_j$  = shear modulus
- $\gamma_j$  = unit weight
- $C_j$  = shear wave velocity
- $\eta_j$  = viscosity coefficient

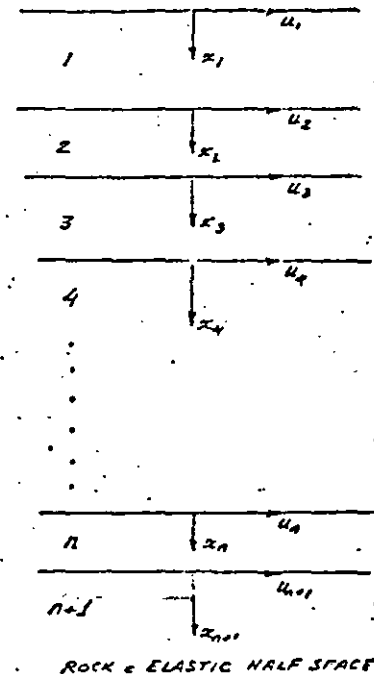


FIG. B. MULTIPLE STRATA OVER ELASTIC ROCK.

$$p_j^2 = \frac{\rho_j \omega^2}{G_j + i n_j \omega}$$

and

$$v_j = \frac{p_j (G_j + i n_j \omega)}{p_{j+1} (G_{j+1} + i n_{j+1} \omega)}$$

Displacement in each layer with respect to a local set of coordinate axes with origin at the top of the layer can then be expressed as

$$v_j = E_j e^{i(p_j x_j + \omega t)} + F_j e^{-i(p_j x_j - \omega t)}$$

By establishing compatibility between each layer and the next, one can write

$$F_1 = E_1 \text{ (because of the free surface condition)}$$

$$2E_2 = E_1 [e^{ip_1 h_1 (1+\nu_1)} + e^{-ip_1 h_1 (1-\nu_1)}]$$

$$2F_2 = E_1 [e^{ip_1 h_1 (1-\nu_1)} + e^{-ip_1 h_1 (1+\nu_1)}]$$

$$2E_3 = E_2 (1+\nu_2) e^{ip_2 h_2} + F_2 (1-\nu_2) e^{-ip_2 h_2}$$

$$2F_3 = E_2 (1-\nu_2) e^{ip_2 h_2} + F_2 (1+\nu_2) e^{-ip_2 h_2}$$

and

$$2E_{n+1} = E_n (1+\nu_n) e^{ip_n h_n} + F_n (1-\nu_n) e^{-ip_n h_n}$$

$$2F_{n+1} = E_n (1-\nu_n) e^{ip_n h_n} + F_n (1+\nu_n) e^{-ip_n h_n}$$

By replacing into the expressions for  $E_3, F_3$  the values of  $E_2, F_2$  in terms of  $E_1$ , then these ones into the expressions for  $E_4, F_4$  and so on one can finally obtain

$$E_{n+1} = a E_1$$

$$F_{n+1} = b E_1$$

The amplification function with rigid rock (ratio of displacement or acceleration at top of soil to displacement or acceleration at bedrock) is then

$$A_1(n) = \left| \frac{2E_1}{E_{n+1} + F_{n+1}} \right| = \frac{2}{|a+b|}$$

The amplification function with elastic rock (ratio of displacement or acceleration at top of soil to displacement or acceleration at the outcropping of rock) is

$$A_2(n) = \frac{|2E_1|}{|2E_{n+1}|} = \frac{1}{|a|} \quad \text{Q}$$

The explicit expression for the amplification function in terms of the soil properties becomes too long even for two layers. However, the numerical computation proceeding from layer to layer is simple and adapts itself very well to be programmed in a digital computer.

It is possible to have any kind of viscosity (constant or an arbitrary function of frequency) in any layer. On the other hand for the purpose of comparing the results with those obtained by other methods (modal analysis of the discrete model) a case which becomes easy to interpret is that in which  $\eta/G$  is equal for all layers.

Then if  $\frac{\eta_j}{G}$  is constant, independent of frequency, the resulting amplification function will have in each natural frequency a percentage of critical damping increasing linearly with the frequency  $\omega$ . The magnitude of the amplification in the  $n$ th natural frequency will thus be proportional to  $1/\omega_n^2$ .

If  $\frac{\eta_j}{G_j} \cdot n = 2\delta$  is constant, the resulting amplification function will have a constant percentage of critical damping in all the modes. The magnitude of the amplification will thus be proportional to  $1/\omega_n$ .

While it is not possible to find an exact simple formula to reproduce the effect of the elastic rock, it has been found that good results can be obtained by taking some average properties for the soil

$$\gamma_s \text{ average} = \frac{\sum \gamma_j h_j}{\sum h_j}$$

$$c_s \text{ average} = \frac{\sum c_{sj} h_j}{\sum h_j}$$

and writing

$$\frac{1}{A_2(\omega)} = \frac{\gamma_{save} c_{save}}{\gamma_r c_r} + \frac{1}{A_1(\omega)}$$

or adding an equivalent radiation damping.

$$b_{eq} = \frac{2}{\pi} \cdot \frac{\gamma_{save} c_{save}}{\gamma_r c_r} \frac{\omega_1}{\omega}$$

(The correct formula would be

$$A_2(\omega) = \frac{A_1(\omega)}{1 + \frac{\tau_b}{\sigma_r c_r u_b \omega}} = \frac{A_1(\omega)}{1 - \frac{\tau_b \omega}{c_r c_r u_b}}$$

where  $\tau_b$  is the shear stress at the base of the soil  
 $u_b$  the base displacement  
 $\omega_b$  the base acceleration.

Figures 9 and 10 show the amplification functions for a multi-layered soil profile with the following characteristics:

FIG. 9. AMPLIFICATION CURVE FOR COVERED SOIL  
 ELASTIC ROCK - CONSTANT VISCOSITY RATIO

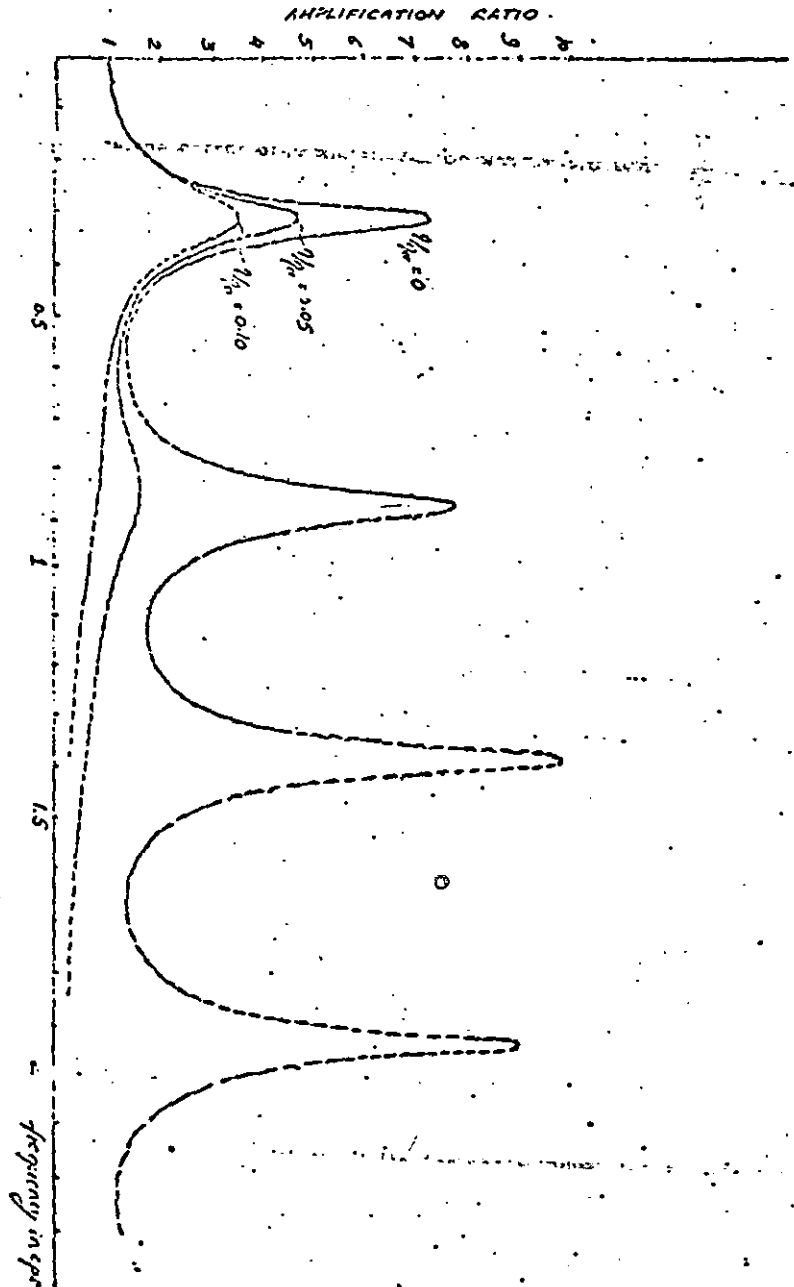
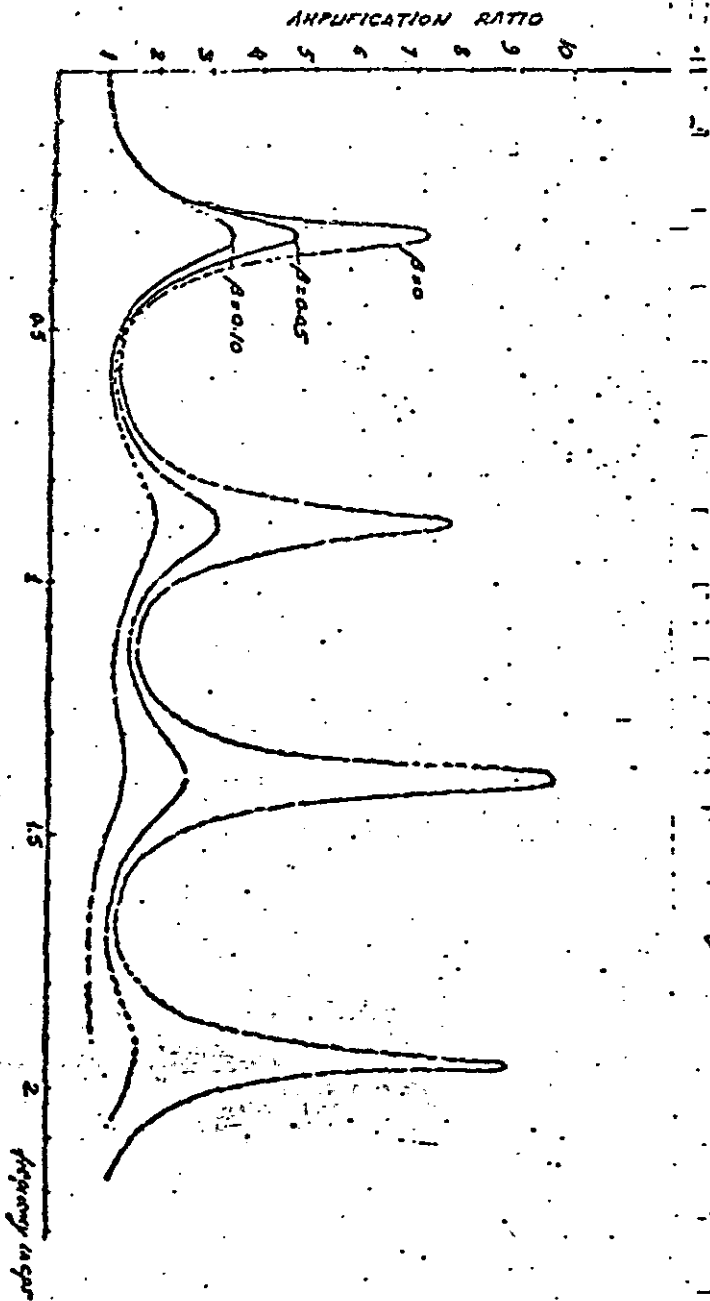


FIG. 10. AMPLIFICATION CURVE FOR LAYERED SOIL  
 ELASTIC ROCK - CONSTANT MODAL DAMPING.



-30-

Layer No.	Thickness ft.	Shear Wave Velocity ft./sec.	Unit Weight lb./ft. <sup>3</sup>
1	10	714	100
2	150	897	120
3	70	1200	125
4	500	1300	125
5	400	1500	135
Rock		8000	150

In both cases it has been assumed that the ratio  $\nu/G$  is the same for all layers. It should be noticed that for  $\nu = 0$  the maximum amplification does not occur at the first natural frequency but at the third one. This effect is more evident when different values of damping are considered for each layer, particularly in the case of soft layers of soil over relatively hard strata. Figure 11 shows the amplification curve for a soil profile which would correspond to the conditions at El Centro, California. It can be seen in this case that the amplification curve is basically the product of two functions: one corresponding to the relatively hard bottom of 11,000 feet with a fundamental frequency of about 0.1 cps, the other corresponding to the top 100 feet of soft soil with a fundamental frequency of about 1.5 cps. The amplification due to these top 100 feet is larger than that due to the remainder of the soil and the maximum peak in the combined amplification curve occurs in the range of 1.5 cps. It is important to notice that this simplified approach, lumping several layers of soil with similar properties into one layer with average properties and reducing the total system to just two layers which can be considered independently, can often be successfully applied for preliminary estimates. Of course to be able to treat the two resulting layers independently, multiplying the corresponding amplification functions at each point, it is necessary to be able to treat them as uncoupled, or what is the same, the mass of the top layer should be considerably smaller than that of the bottom layer.

### II.2 Discrete Model.

The basis for the discrete model is to replace each layer of soil by a series of lumped masses connected by a spring and dashpot. The resulting system (Fig. 12) is of course a familiar one for engineers working in Structural Dynamics.

For any given layer of thickness  $h_j$ , shear modulus  $G_j$ , unit weight  $\gamma_j$  and viscosity coefficient  $n_j$ , replaced by  $n_j$  discrete masses, one would have

$$M_1 = \frac{1}{2} \frac{\gamma_j}{g} \cdot \frac{h_j}{n_j}$$

$$M_2 = M_3 = M_4 = \dots = M_{n_j} = \frac{\gamma_j}{g} \frac{h_j}{n_j}$$

Of course at the interface between two layers the total lumped mass would be

$$\frac{1}{2g} \left( \frac{\gamma_j h_j}{n_j} + \frac{\gamma_{j+1} h_{j+1}}{n_{j+1}} \right)$$

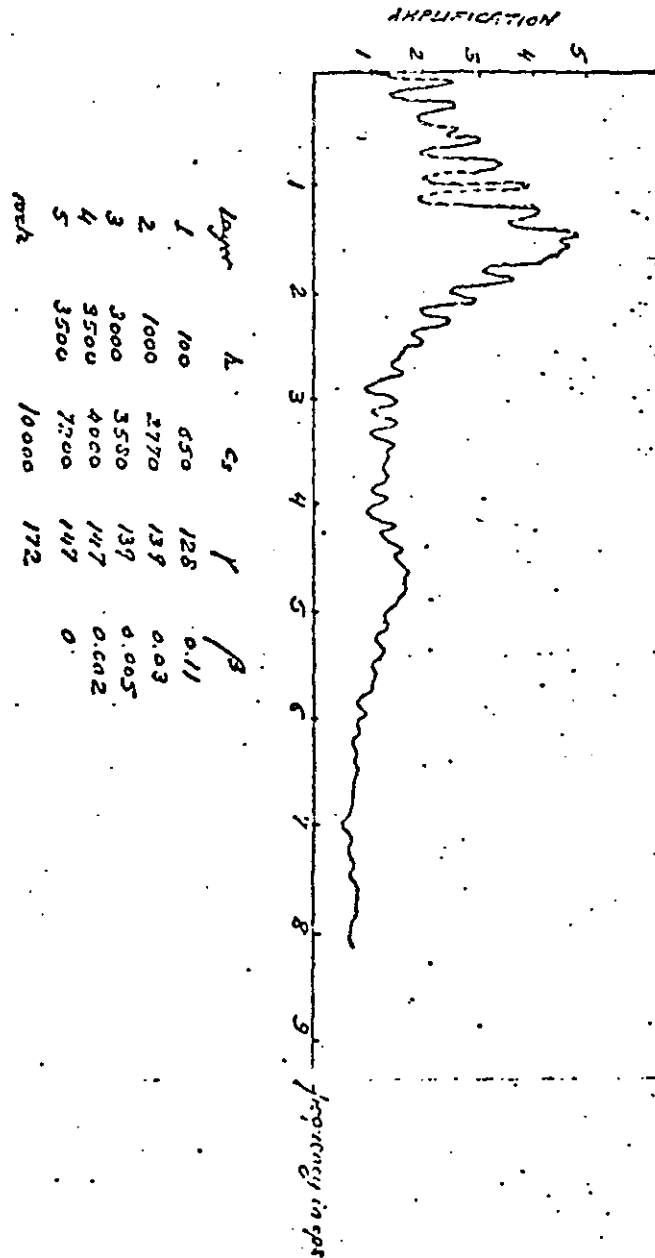
$$k_1 = k_2 = k_3 = \dots = k_{n_j} = \frac{G_j n_j}{h_j}$$

and 
$$C_1 = C_2 = C_3 \dots = \frac{n_j n_{j+1}}{h_j}$$

where  $C_i$  are the dashpot constants.

It is thus possible to write the equation of motion for each mass forming a stiffness matrix, a damping matrix and a mass matrix (diagonal). The solution of the problem falls then within the classical methods of Structural Dynamics and requires no further explanation here. It is important to notice, however, that if the dashpot constants are arbitrary ( $n/G$  variable from one layer to another) it is necessary to solve the problem by physical integration of the equations of motion.

FIG. 11. AMPLIFICATION CURVE FOR LAYERED SOIL (EL CENTRO)  
ELASTIC ROCK - VARIOUS DAMPING IN LAYERS.



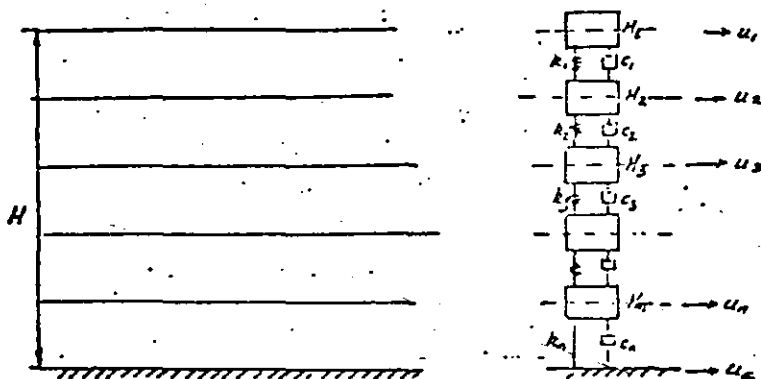


FIG 12. EQUIVALENT LUMPED MASS SYSTEM

In other words it is not possible in general to find an equivalent system with modal damping. If on the other hand the damping matrix can be expressed as a polynomial expression of  $K^{-1}M$  or  $M^{-1}K$  of the form

$$C = \sum_{r=m}^{r=m+n-1} d_r K(H^{-1}K)^r$$

or

$$C = \sum_{r=m}^{r=m+n-1} e_r M(K^{-1}M)^r$$

corresponding values of modal damping can be found and a normal modal analysis can be performed with damping in the  $i$ th mode,

$$2B_i \omega_i = \sum_{r=m}^{r=m+n-1} d_r \omega_i^{2r+2}$$

or

$$B_i = \frac{1}{2} \sum_{r=m}^{m+n-1} d_r \omega_i^{2r+1}$$

It can be shown that for the free vibration problem as the number of masses increases the natural periods and modal shapes tend to those given by the continuous solution. It has been found that a period  $T$  is reproduced with sufficient accuracy if the number of masses is

$$n \geq 5 \left( \frac{H}{TC_s} + \sqrt{\frac{H}{TC_s}} \right)$$

For a multilayered soil this condition should be verified for each layer independently and for the total deposit with an average shear wave velocity.

Knowing the natural periods or frequencies and the corresponding modal shapes, the participation factor of each mode for a base motion is

$$r_n = (-1)^{n-1} \frac{4}{(2n-1)\pi} \text{ for a uniform layer.}$$

In general the participation factor can be found by the normal procedures of Structural Dynamics. If M is the mass matrix and  $\phi_n$  the nth eigenvector

$$r_n = \frac{\phi_n^T M \mathbf{1}}{\phi_n^T M \phi_n}$$

where  $\mathbf{1}$  is a vector with all components unity.

If  $\phi_{n1}$  is the component of the eigenvector at the free surface of the soil calling  $g_n = r_n \phi_{n1}$  the amplification function can be written as

$$A(\omega) = \sqrt{\left[ \sum_{i=1}^n \frac{g_i^2 (\omega_i^2 - \omega^2)^2 + 4\beta_i^2 \omega_i^2 \omega^2}{(\omega_i^2 - \omega^2)^2 + 4\beta_i^2 \omega_i^2 \omega^2} \right]^2 + \left[ \sum_{i=1}^n \frac{g_i 2\beta_i \omega_i \omega^3}{(\omega_i^2 - \omega^2)^2 + 4\beta_i^2 \omega_i^2 \omega^2} \right]^2}$$

or alternatively

$$A(\omega) = \sqrt{\left[ \sum_{i=1}^n \frac{g_i \omega_i^2 (\omega_i^2 - \omega^2)}{(\omega_i^2 - \omega^2)^2 + 4\beta_i^2 \omega_i^2 \omega^2} + 1 \right]^2 + \left[ \sum_{i=1}^n \frac{g_i 2\beta_i \omega_i \omega^3}{(\omega_i^2 - \omega^2)^2 + 4\beta_i^2 \omega_i^2 \omega^2} \right]^2}$$

If all the modes are considered both formulas give the same results. If only the first few modes are included the results will differ slightly in the high frequency range.

Results obtained with these formulas (taking sufficient number of masses and modes) agree with the amplification curves obtained with the continuous model for the case of rigid rock. Adding to the values of modal damping  $\beta_i$  the equivalent radiation damping previously suggested results for elastic rock are again reproduced.

For all practical purposes it can be considered that the continuous and the discrete model will both be applicable to determine amplification functions and will yield the same results provided modal damping can be specified and an additional radiation damping is added to the lumped system. The continuous model is, however, more flexible since it allows for arbitrary variations of damping from one layer to another. Furthermore, it requires in general less computer time. The discrete model has the advantage that it is easier to visualize since it reduces the problem to a classical case of Structural Dynamics.

### III - TRANSIENT MOTIONS

The amplification function has several important properties:

- a) It gives a clear graphical picture and qualitative information on the effect of the soil. A simple look at the curve is sufficient to determine in what ranges of frequencies the soil can have a serious damaging effect, and in what ranges this effect would not be important or might even be beneficial.
- b) It is independent of any given earthquake and it represents therefore a property or characteristic of the soil itself.
- c) For some of the methods that will be described here, the determination of the amplification curve is a necessary first step to determine accelerograms or response spectra at the top of the soil. For other methods, however, this step may be bypassed.

In spite of these features the amplification curve is by no means the ultimate goal of this type of studies. From the point of view of the structural designer the main objective is to have a set of response spectra which apply to the surface of the soil or less frequently a set of earthquake records which could characterize the motions to be expected. From the point of view of the soils engineer it is important to be able to estimate the magnitude of shear

53

stresses in the soil during an earthquake to determine the factor of safety against liquefaction and to guide in the selection of suitable values for modulus and damping ratios.

In order to obtain these results several methods are still available using either the continuous or the discrete model.

III.1 - Continuous Solution

Given a certain time history of acceleration representing an earthquake record at the outcropping of rock, or at the interface between soil and rock, the corresponding accelerogram at the free surface of the soil can be obtained by:

- a) Obtaining the Fourier transform of the input earthquake.
- b) Multiplying it by the Transfer function of the soil.
- c) Obtaining the inverse Fourier transform of the resulting function.

The Fourier transform of a function of time f(t) can be visualized as a limiting case of a Fourier series expansion. It is given by the formula

$$F(\omega) = \int_0^{\infty} f(t)e^{-i\omega t} dt = \int_{-\infty}^{+\infty} f(t)e^{-i\omega t} dt \text{ (if } f(t) = 0 \text{ for } t < 0)$$

f(t) is then said to be the inverse Fourier transform of F(ω)

$$f(t) = \frac{1}{2\pi} \int_{-\infty}^{+\infty} F(\omega)e^{i\omega t} d\omega$$

It should be noticed that F(ω) is a complex function. writing

it as

$$F(\omega) = C(\omega) - iS(\omega)$$

$$C(\omega) = \int_0^{\infty} f(t) \cos \omega t dt \text{ (is the cosine transform)}$$

$$S(\omega) = \int_0^{\infty} f(t) \sin \omega t dt \text{ (is the sine transform)}$$

If on the other hand it is written as

$$F(\omega) = E(\omega) e^{-i\phi(\omega)t}$$

$$E(\omega) = \sqrt{C(\omega)^2 + S(\omega)^2}$$

$$\phi(\omega) = \tan^{-1} \frac{S(\omega)}{C(\omega)}$$

E(ω) represents the amplitude Fourier spectrum, and φ(ω) the phase spectrum. The amplitude spectrum has an important physical meaning. Given two values of frequency, ω<sub>1</sub>, ω<sub>2</sub>, the area under the curve E(ω) from ω<sub>1</sub> to ω<sub>2</sub> gives the amplitude of the motion in this range of frequencies. A simple look at the Fourier amplitude spectrum (often referred to for short as Fourier spectrum) gives immediately an idea of the range of frequencies where most of the amplitude of the motion is contained. In fact Hudson has shown that this spectrum is a lower bound to the undamped velocity response spectrum and in general a very good approximation to it (they would coincide if the maximum response occurred after the end of the excitation). Arias has also shown that if E(ω) is computed for different durations of the earthquake, the envelope of these spectra is an upper bound to the undamped velocity response spectrum.

The amplitude Fourier spectrum is of course closely related to the spectral density function S(ω)

$$S(\omega) = \frac{1}{T} \frac{E(\omega)^2}{\omega}$$

and

$$S^+(\omega) = \frac{1}{\omega} \frac{E(\omega)^2}{T}$$

where T is the duration of the excitation f(t)

The area under the spectral density function between two frequencies ω<sub>1</sub> and ω<sub>2</sub> gives a measure of the energy of the excitation in that range.

54

The Fourier transform has not been used normally in Structural Dynamics. Its determination is, however, extremely fast and simple with a digital computer. Even if this method of analysis is not going to be used, the Fourier transform will provide significant information on the nature of the excitation and will help to answer such questions as how many modes should be included in a modal analysis.

The transfer function of the soil as determined in II is again a complex function. The product of these two complex functions can be accomplished by

Multiplying the Fourier amplitude spectrum of the input by the amplification function of the soil. The result is the Fourier amplitude spectrum of the earthquake at the free surface of the soil.

Adding to the Fourier phase spectrum the change in phase curve of the soil. The result is the Fourier phase spectrum of the output.

The inverse Fourier transform of this product will be again a real function representing the time history of acceleration on top of the soil. Notice that if the input represents the accelerogram at the interface between rock and soil the transfer function corresponding to rigid rock should be used. If on the other hand the input represents the accelerogram which would be recorded on the rock without any soil on top, the transfer function for elastic rock has to be used. The second approach seems more logical. However, at the present time, there is no clear way to determine what the earthquake records should be at bedrock with soil on top or at the outcropping of rock, since most accelerograms of real earthquakes have been obtained on ground (even if firm ground).

Figures 13 through 17 summarize the procedure as outlined. (The phase spectra are not plotted). Figure 13 shows a record of the Taft earthquake and Figure 14 its amplitude Fourier spectrum. Figure 15

FIG. 13. ACCELEROGRAM OF TAFT EARTHQUAKE

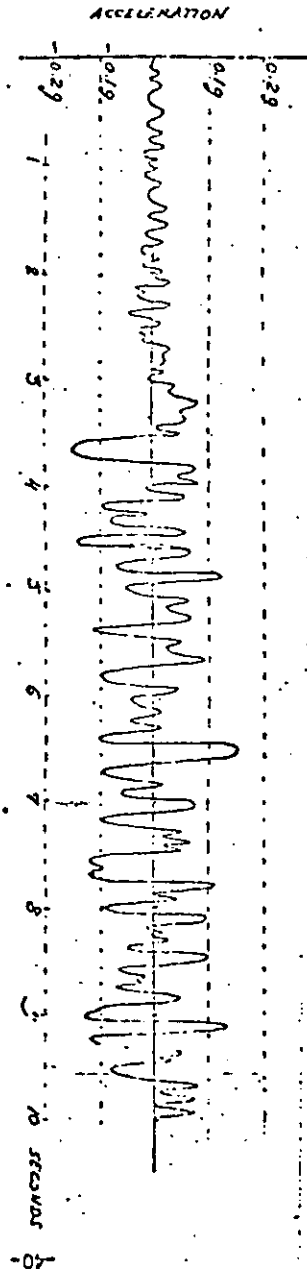
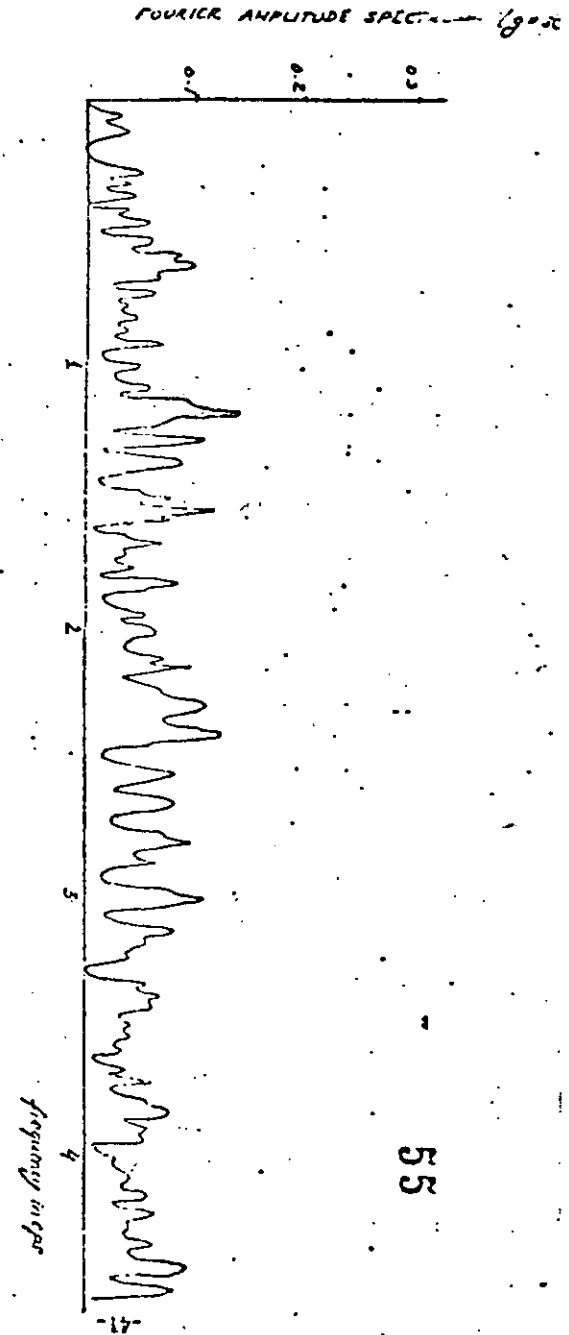


FIG. 14. FOURIER AMPLITUDE SPECTRUM FOR TAFT EARTHQUAKE



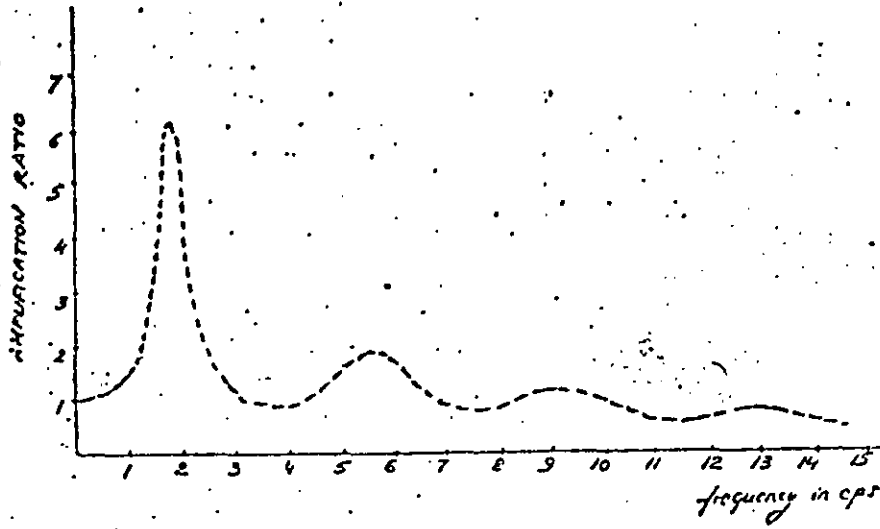


FIGURE 15. AMPLIFICATION FUNCTION OF SOIL

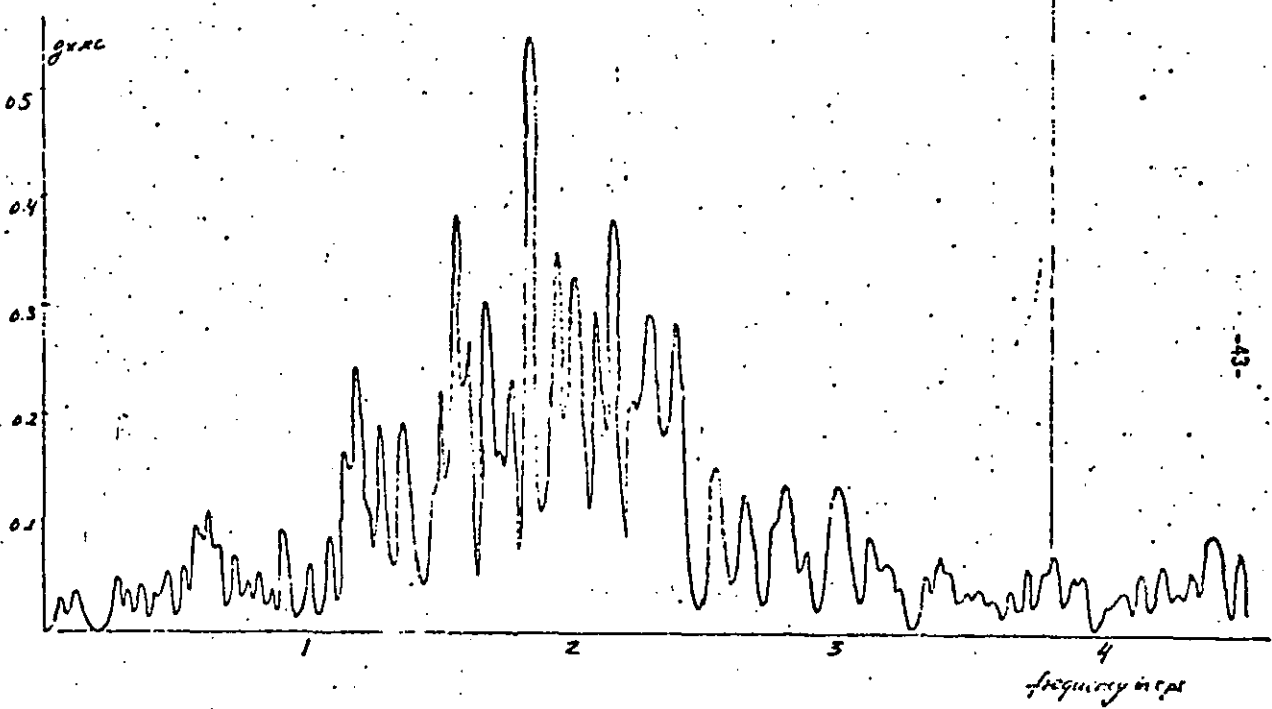


FIGURE 16. FOURIER AMPLITUDE SPECTRUM OF ACCELEROGRAM AT TOP OF SOIL

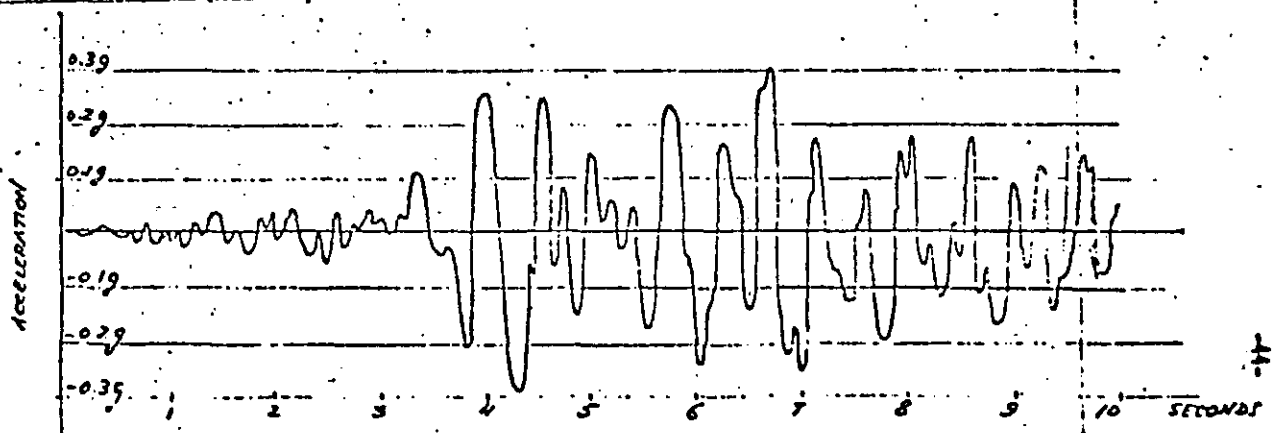


FIGURE 17. ACCELEROGRAM AT TOP OF SOIL

shows the amplification curve for a given soil profile (the uniform layer previously considered with rigid rock). The product of the Fourier spectrum of the input by the amplification function is shown in Figure 17.

Once the earthquake record at the surface of the soil has been obtained, design response spectra can be obtained in two different ways:

a) From the Fourier transform of the output (before inverting it), by multiplying it by the Transfer function of a one-degree-of-freedom linear oscillator, then inverting the result and finding the maximum. The Transfer function of the one-degree-of-freedom system with frequency  $\omega_n$  and damping  $\beta_n$  is

$$H(\omega) = \frac{\omega_n^2 + 2i\beta_n\omega_n\omega}{\omega_n^2 - \omega^2 + 2i\beta_n\omega_n\omega}$$

b) By integrating through a step-by-step procedure, the equation of motion of a one-degree-of-freedom system

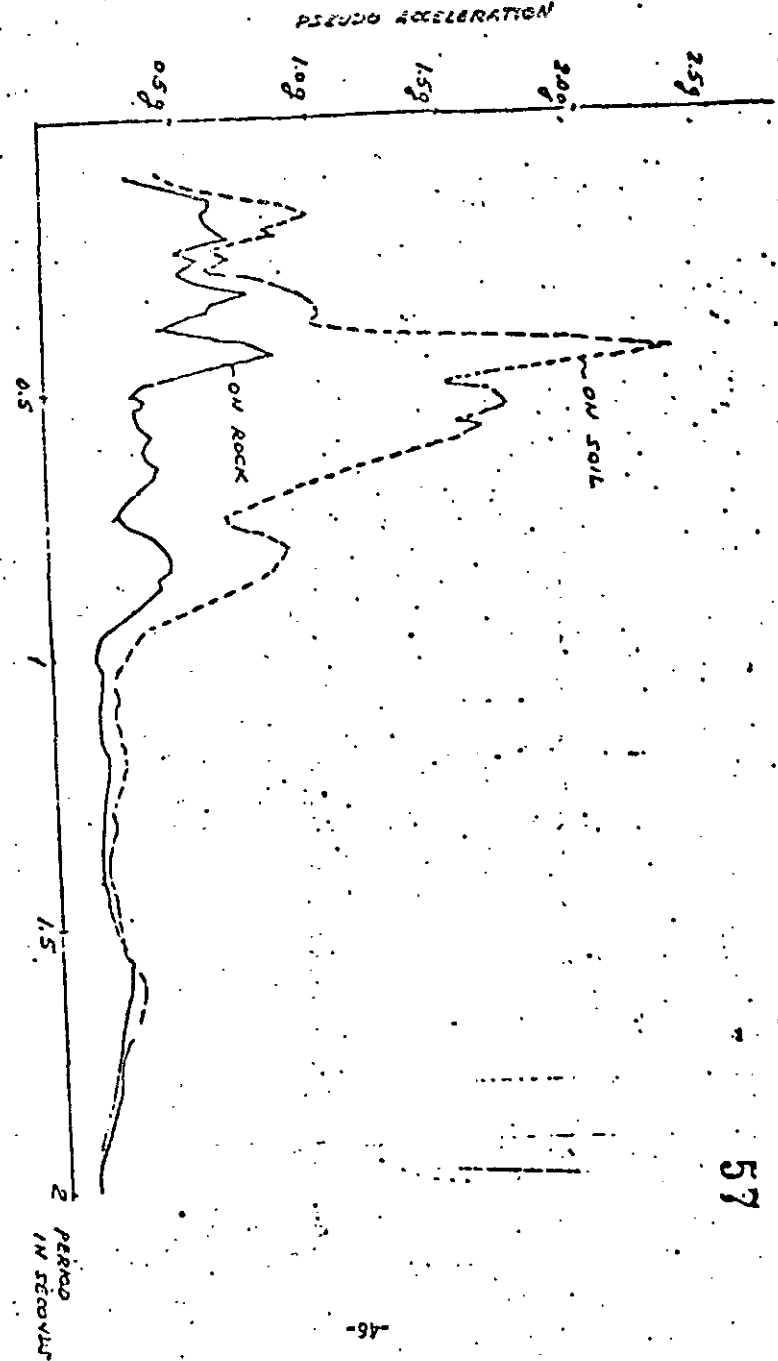
$$\ddot{y} + 2\beta_n\omega_n\dot{y} + \omega_n^2 y = -\ddot{u}_g$$

where  $u_g$  is the acceleration time history on top of soil.

The first procedure is normally referred to as integration in the frequency domain whereas in the second case the solution is said to be carried out in the time domain While the first method would represent a consistent continuation of the procedure followed up to that moment at the present time the second seems more economical as far as computer time is concerned.

Figure 18 shows the pseudo-acceleration response spectrum for the Taft earthquake filtered through the uniform soil deposit. The response spectrum of the input is also shown in the same figure. Figure 19 shows the ratio of both response spectra for 2 and 5%

FIG 18. PSEUDO-ACCELERATION RESPONSE SPECTRA ON ROCK AND ON TOP OF SOIL. (2% STRUCTURAL DAMPING)





Replacing  $\bar{u}_G$  by the accelerogram of the earthquake at bedrock and integrating numerically this set of differential equations, one can obtain the time history of displacements, velocity or acceleration at any of the masses, or what is equivalent at any point in the soil. Once  $\bar{u}$ , absolute acceleration  $= \ddot{y} + \ddot{u}_G$  is obtained at the surface of the soil as a function of time, the procedure to determine response spectra is the same as that described for the continuous model, second approach.

The integration of the set of differential equations as outlined above is normally referred to as physical integration of the equations of motion. This procedure is the only one which can be used if the properties of the soil are considered non-linear. On the other hand, for linear systems if modal damping can be specified it is normally preferred to carry out the solution by modal superposition.

If  $\omega_i$  are the natural circular frequencies of the soil deposit,  $\phi_i$  its modal shapes (eigenvectors), normalized so that  $\phi_i^T M \phi_i = 1$  and  $\Gamma_i$  the participation factor of the  $i$ th mode

$$\Gamma_i = \phi_i^T M 1 = (M_{1+1i} + M_{2+1i} + \dots + M_{n+1i})$$

the solution can be expressed as

$$Y = \sum_i \Gamma_i \phi_i a_i(t)$$

where  $a_i(t)$  is the solution of the one-degree-of-freedom equation

$$\ddot{a}_i + 2\delta_i \omega_i \dot{a}_i + \omega_i^2 a_i = -\bar{u}_G(t)$$

In particular at the surface of the soil

$$\bar{u}_s = \sum_i \Gamma_i \phi_i a_i + \bar{u}_G = \sum_i \Gamma_i a_i + \bar{u}_G$$

The advantage of this type of solution is that it requires only the solution of a one-degree-of-freedom equation for each mode, once the modal shapes, participation factors and natural frequencies are known. Moreover in general only the first few modes contribute significantly to the solution. For the case of the uniform layer, previously considered with the continuous solution the coefficients  $g_i$  are

$$\text{first mode } g_1 = 1.27$$

$$\text{second mode } g_2 = -0.416$$

$$\text{third mode } g_3 = 0.24$$

Only three modes are enough in this case to obtain a good solution. The maximum acceleration in the first mode is of the order of 0.27g, in the second of 0.15g, and in the third of 0.05g.

Response spectra obtained by this method show good agreement with those obtained by the continuous solution, although not as perfect as in the case of the amplification function. The discrepancies are, however, very small and are easy to understand if the large number of computations involved is considered. Each method has its own round-off and truncation errors and they will affect each procedure differently. For all practical purposes the results can, however, be considered equivalent.

Again if the effect of the elastic rock has to be included, it can be done by adding the equivalent radiation damping in each mode.

If the only result desired is the time history of acceleration at the free surface of the soil (or at a small number of points) the continuous solution has an advantage both from the point of view of flexibility (being able to consider different values of damping in each layer) and from the point of view of time of computation. On the other hand, if the time history of acceleration and stresses is desired at many points the modal solution becomes more economical. Damping in the soil does not really come from viscosity but from non-linear

hysteretic dissipation of energy. Correspondingly both shear modulus and damping are functions of strain. If a non-linear analysis is to be performed only the discrete model with physical integration of the equations of motion would be applicable. Often, however, the system is considered linear, assuming values of shear modulus and damping, determining histories of strains, computing new values of modulus and damping and cycling until convergence of the process is obtained. For these preliminary runs the discrete model with modal analysis is convenient and it provides a faster, more economical solution. Once appropriate values of modulus and damping have been obtained, the continuous model can be used for a final series of analyses with different values of damping in each layer. (In the modal solutions the values of damping are averaged and expressed as modal damping, constant in all modes).

#### IV. DERIVATION OF RESPONSE SPECTRA

The methods previously outlined are mainly intended to consider an earthquake at the base of the soil, filter it and obtain the resulting time history of acceleration at the free surface. While it is possible to obtain then design response spectra on top of the soil, the procedure has for this purpose several difficulties:

- a) It requires as an input an actual accelerogram, be it that of a real earthquake, scaled or not, or an artificial earthquake obtained by a simulation process. While the area of Earthquake Simulation has seen a considerable progress in the last years, it is still harder to derive the time history of an earthquake corresponding to a certain magnitude and epicentral distance than it is to derive a response spectrum.
- b) In order to obtain reliable results the analysis cannot be done for just one input earthquake, but should be repeated for several inputs representing samples of earthquakes with the same average characteristics. The resulting response spectra should finally be smoothed by drawing an average or envelope. The process becomes then too long and expensive.

It would be therefore desirable to have simple and approximate ways by which smooth response spectra on top of the soil would be derived from response spectra at bedrock or on firm ground. Figure 19 showed the amplification curve for a given soil profile and the ratio of response spectra for 2 and 5% of structural damping. The similarity of these curves is apparent. In fact, if the Fourier spectrum were exactly the undamped velocity response spectrum, the amplification curve should coincide with the ratio of response spectra for no damping.

There are, however, several important differences between these two curves:

- 1. The amplification curve tends to zero as the frequency increases or as the period becomes very small. The ratio of response spectra on the other hand tends to a finite value which is the ratio of the maximum acceleration on top of the soil to the maximum acceleration of the input. (This ratio can be estimated from the design response spectra at bedrock if the modes of the soil are known). The ratio of response spectra is therefore highly dependent on the input earthquake in the high frequency range (or for very short periods, say T smaller than 0.1 seconds).
- 2. The amplification curve is a function of the soil properties only. The ratio of response spectra on the other hand will depend on the soil properties (periods and damping), the amount of structural damping and the selected earthquake input.
- 3. The ratio of response spectra is in general smoother than the amplification curve with lower peaks and higher valleys and it becomes smoother as the structural damping increases. For damping values of 20 or 25% the ratio of response spectra is practically constant over a long range of periods. On the other hand for very small values of structural damping or for undamped spectra, the ratio of the response spectra should be close to the amplification curve except in the range of very small periods.
- 4. It should also be expected that the agreement between the amplification curve and the ratio of response spectra would be better for

60

high values of damping in the soil since this would tend to eliminate the transients and furnish a motion closer to a periodic one.

In order to determine the applicability of the amplification curve to reproduce the ratio of response spectra, the ratio between both curves  $b$  has been obtained at several points for uniform soils with varying fundamental periods and damping, subject to different earthquake inputs. The earthquake records considered are El Centro, Taft and five artificial earthquakes with a Tajimi type spectral density function.

Figure 20 shows for one of the cases studied the amplification curve and the ratio of response spectra for El Centro and Taft earthquakes. Figure 21 shows the average ratio of response spectra for the five artificial earthquakes, together with the 95% confidence levels (mean  $\pm 2\sigma$ ). Most of the points of the curves for El Centro and Taft fall within this band. It must be therefore realized that even within samples of earthquakes with the same properties (magnitude and epicentral distance) a substantial variation is to be expected in the ratio of response spectra.

Figure 22 shows the effect of the natural period of the soil and the amount of damping in the soil in the value of  $b$  at different points. For  $T = 2T_1$  (1st natural period) the ratio is practically constant, independent of  $T_1$ . For  $T = T_1$  it has again little variation for periods larger than 0.3 seconds. For  $T = 0.5T_1$  the variation is large for periods smaller than 0.5 seconds and for  $T = \frac{1}{3}T_1$  for periods smaller than 0.8 or 0.9 seconds. It should be noticed that in all cases the variation is small for values of  $T$  larger than 0.2 or 0.3 seconds. If it is accepted that in this range (say 0 to 0.2 or 0.3 seconds) the maximum acceleration at top of the soil controls the response spectrum, the values of  $b$  can be considered only slightly depending on the natural period of the soil over the range of application.

FIG. 20. COMPARISON OF AMPLIFICATION CURVE AND RATIO OF RESPONSE SPECTRA  
EL CENTRO AND TAFT EARTHQUAKES

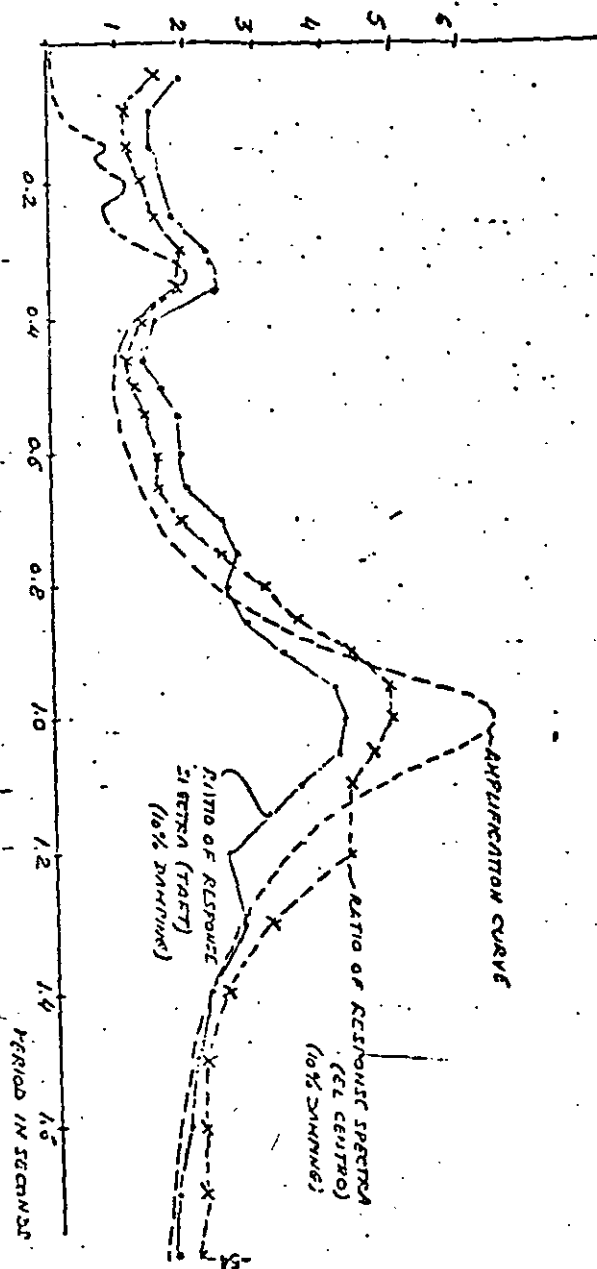
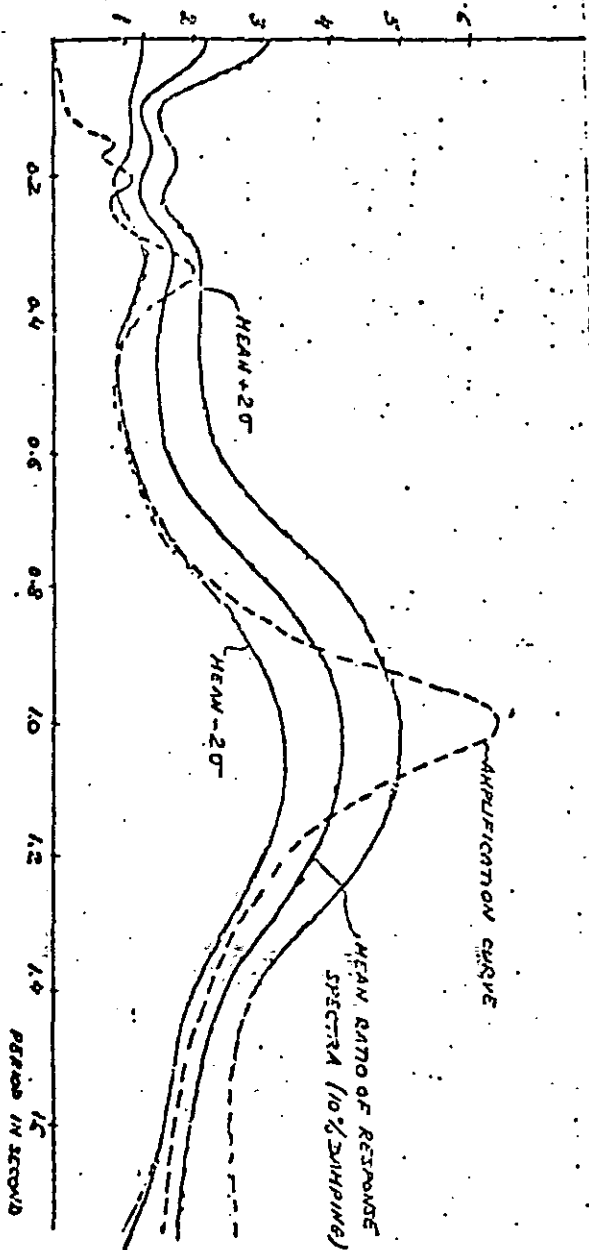
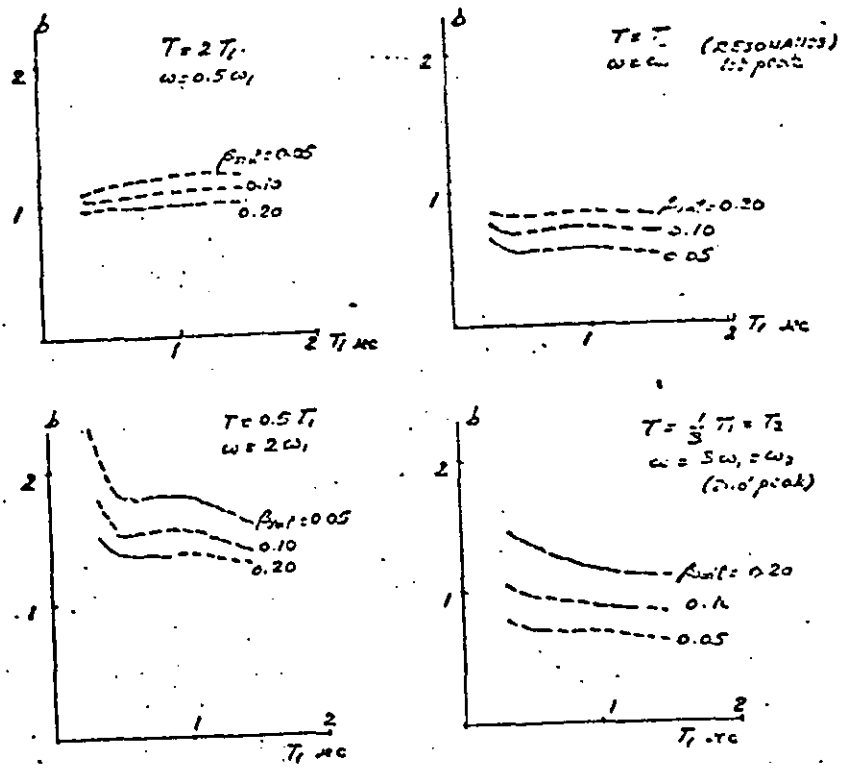


FIG. 21. COMPARISON OF AMPLIFICATION CURVE AND RATIO OF RESPONSE SPECTRA  
 5 ARTIFICIAL TARDIQUAKES.



-55-

-56-



$$b = \frac{\text{ratio of response spectra (5\% DAMPING)}}{\text{amplification ratio}}$$

FIG. 22. RATIO BETWEEN RATIO OF RESPONSE SPECTRA  
 AND AMPLIFICATION CURVE AT DIFFERENT POINTS  
 EFFECT OF NATURAL PERIOD OF SOIL

Figure 23 shows the effect of structural damping in the values of  $b$ . It can be noticed that as it should be expected the value of  $b$  is closer to unity as the damping in the soil increases and the structural damping decreases. While the effect of the structural damping is large in the range 0 to 20% in the normal range of structures (say 0 to 5%) this effect may be considered slight, particularly compared to the variation from one input record to another within a family of earthquakes.

Curves like those shown in Figures 22 and 23 have been obtained for different values of  $T/T_1$ . Using these curves the following procedure is suggested to derive the ratio of response spectra from the amplification curve.

1. At each one of the peaks ( $T = T_1, T = \frac{1}{3} T_1, T = \frac{1}{5} T_1$  etc.) find the value of  $b$  from the curves and obtain the corresponding point (multiplying the amplification by the factor  $b$ ). A horizontal segment is then drawn passing by each one of these points and cutting the peak of the amplification curve if  $b$  is smaller than 1.
2. At each one of the valleys ( $T = \frac{1}{2} T_1, T = \frac{1}{4} T_1$  etc.) the ratio  $b$  is obtained from the curves and a point is drawn. These points are then joined by smooth curves to those resulting from step 1.
3. At  $T = 2T_1$ , the value of  $b$  is again found or can be taken approximately equal to 1. For  $T > 2T_1$  the amplification curve can be used. This point is then joined to the point immediately next to  $T_1$  by a smooth curve if the curve is plotted versus period or a straight line if plotted versus frequency.
4. In the range of small periods or large frequencies the response spectrum has to be controlled by the acceleration on top of the soil. The ratio of this acceleration to the maximum input acceleration can be obtained. At a period of 0.1 seconds (or a frequency of 10 cycles per second) this value may be taken as the ratio of response spectra. Between the value at a period of 0.2 seconds and this value a straight line may be drawn if the curve is plotted versus period or a smooth transition curve if plotted versus frequency.

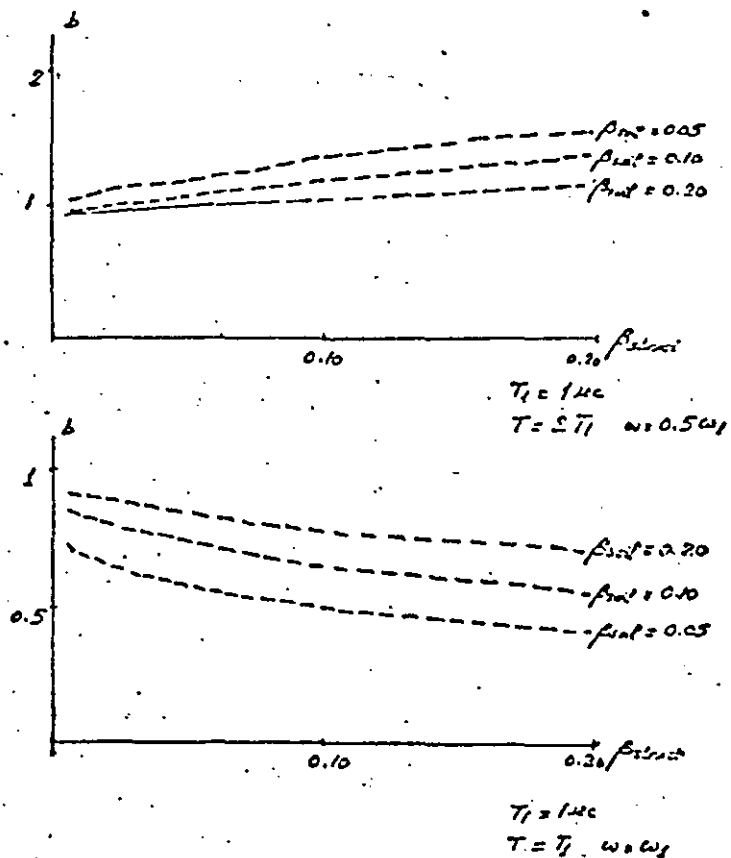
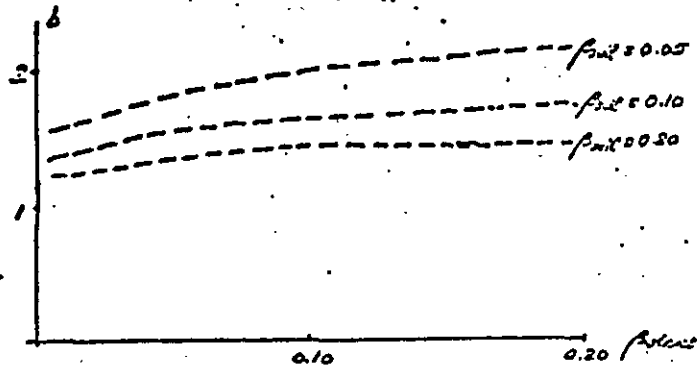
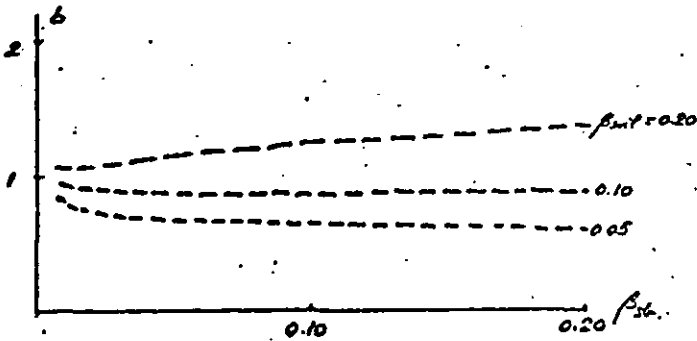


FIG 23. RATIO BETWEEN RATIO OF RESPONSE SPECTRA AND AMPLIFICATION CURVE, AT DIFFERENT POINTS

EFFECT OF STRUCTURAL DAMPING



$T_1 = 1 \text{ sec}$   
 $T = 0.5 T_1$   
 $\omega = 2 \omega_1$



$T_1 = 1 \text{ sec}$   
 $T = \frac{1}{3} T_1$   
 $\omega = 3 \omega_1$

FIG 23 (CONTINUED)

While all the cases considered to derive the curves for the values  $b$  have corresponded to a uniform soil profile and further testing is necessary for multilayer systems, it is believed that such a procedure could also be applied for the latter taking the  $T_1$  as the period at which the maximum amplification occurs rather than the first fundamental period.

Figure 24 shows an example of application of the method. Curves of the standard deviation  $\sigma$  have also been obtained. From these curves it is then possible to draw not only the average ratio of response spectra but also confidence levels.

REFERENCES

1. Seed and Idriss, "Influence of Soil Conditions on Ground Motions during Earthquakes. State of the Art Symposium, Earthquake Engineering of Buildings, San Francisco, California - Feb. 1968 and Journal of Soil Mechanics and Foundations Division ASCE, Jan. 1969.
2. Donovan and Matthesen, "Effects of Site Conditions on Ground Motions During Earthquakes." Same Symposium.
3. Herrera, Rosenblueth and Rascon, "Earthquake Spectrum Prediction for the Valley of Mexico. 3rd World Conference on Earthquake Engineering, 1965.
4. Idriss and Seed, "Seismic Response of Horizontal Soil Layers," Journal of the Soil Mechanics and Foundations Division, ASCE, July 1968.
5. Roesset and Whitman, "Effect of Local Soil Conditions upon Earthquake Damage - Theoretical Background." M.I.T. Dept. of Civil Engineering Report, 1969.
6. "The Use of Amplification Functions to Derive Response Spectra, Including the Effect of Local Soil Conditions," M.I.T. Civil Engineering Dept. Report, 1969.

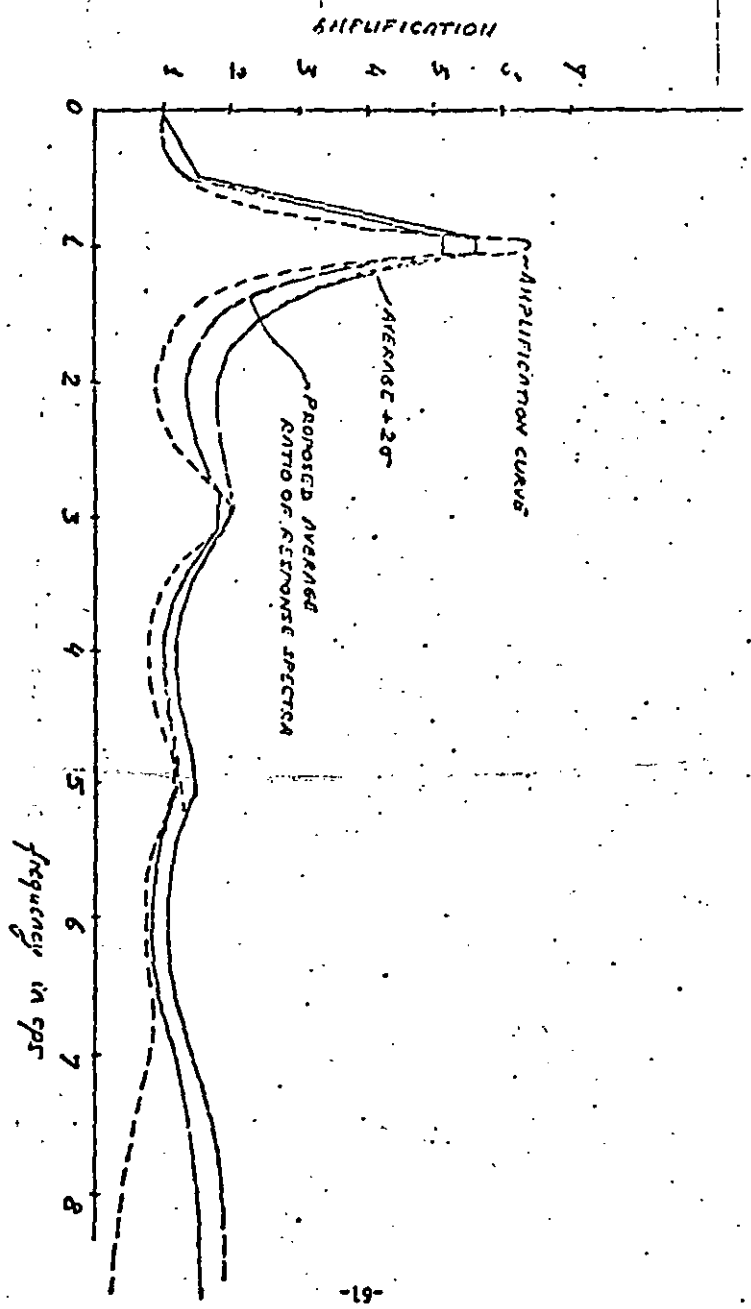


FIGURE 37. SUGGESTED RATIO OF RESPONSE SPECTRA (FOR DRINKING)

DIRECTORIO DE ALUMNOS DEL CURSO "ANALISIS DE RIESGO SISMICO" IMPARTIDO  
EN ESTA DIVISION DEL 30 DE JULIO AL 8 DE AGOSTO DEL PRESENTE AÑO.

- 1.- ABAD MARTINEZ CARLOS  
COMISION FEDERAL DE ELECTRICIDAD  
SUPERVISOR AREA ESTRUCTURAS P.H.  
MISSISSIPPI No. 71 -11o. PISO  
COL. CUAUHEMOC  
DELEGACION CUAUHEMOC  
553-71-33  
CALLE 7 No. 22  
COL. GOMEZ FARIAS  
DELEGACION VENUSTIANO CARRANZA  
15010 MEXICO, D.F.  
784-28-16
- 2.- ACEVEDO VASQUEZ WILFREDO  
RIO TUXPAN No. 5040  
COL. SAN MANUEL  
PUEBLA, PUE.
- 3.- AGUIAR FALCONI ROBERTO  
ESC. POLITECNICO DEL EJERCITO  
PROFESOR  
GENERAL PAZMIÑO Y AV. GRAN COLOMBIA  
QUITO - ECUADOR  
543-500  
SAN IGNACIO No. 1010  
EDIFICIO PATA DE GUAPULO  
DEPTO. 5  
QUITO - ECUADOR  
23-50-16
- 4.- AGUILAR MORALES JOSE ALFREDO  
DIMENSIONAMIENTOS ESTRUCTURALES ,S.C.  
GERENTE GENERAL  
PASEO DEL CANTIL No. 66  
BOSQUES DE TETLAMEYA  
DELEGACION COYOACAN  
559-14-72  
HALCONES No. 175  
LOMA DE GUADALUPE  
DELEGACION ALVARO OBREGON  
680-01-34
- 5.- AMADO ZOGBE JORGE ALEJANDRO  
IMPRES INST. NAC.PREVENCIÓN SISMICA  
PROFESIONAL ESPECIALIZADO  
ROGER BALEL No. 47  
SAN JUAN REP. ARGENTINA  
HOTEL GRECO  
536-77-00 y 563-66-20
- 6.- APARICIO GARDUÑO RODOLFO  
COMISION FEDERAL DE ELECTRICIDAD
- 7.- ARNOLD OJEDA CARLOS  
ESC. DE ING. CIVIL  
UNIV. DE GUANAJUATO  
PROFESOR DE TIEMPO COMPLETO  
AVENIDA JUAREZ No. 77  
GUANAJUATO, GTO.  
2-07-79  
AVENIDA JUAREZ No. 226  
GUANAJUATO, GTO.
- 8.- CALDERON SANTOS HECTOR GUILLERMO  
SEGUROS LA REPUBLICA  
JEFE DE INGENIERO  
PASEO DE LA REFORMA No. 383-5o. PISO  
COL. CUAUHEMOC  
DELEGACION CUAUHEMOC 511-31-33  
06500 MEXICO D F  
GABINO BARREDA No. 3 DEPTO. 32  
COL. SAN RAFAEL  
DELEGACION CUAUHEMOC  
582-19-29

- 9.- CARDENAS ORDOÑEZ HAROLD  
UNIVERSIDAD DEL VALLE  
PROFESOR MATERIALES DE CONSTRUCCION  
CD. UNIVERSITARIA MELENDEZ  
CALI- COLOMBIA  
APARTADO AEREO 2536Q  
39-24-50  
AV. UNIVERSIDAD 1923  
EDIF. F DEPTO. 1001  
COL. COPILCO  
DELEGACION COYOACAN  
04360 MEXICO, D.F.
- 10.- CASTELLANOS PEDRO PABLO  
PETROLEOS MEXICANOS
- 11.- CRUZ CLEMENTE MARIO  
INST. TECNOLOGICO DE OAXACA  
PROFESOR INVESTIGADOR  
CALZ. TECNOLOGICO y CALZ. WILFRIDO MATIEU  
OAXACA, OAX.  
644-13 y 617-22  
ANDADOR DEL VALLE MANZANA D-10  
UNIDAD GUELAGUETZA INFONAVIT  
OAXACA, OAX.
- 12.- CHAVEZ AGUIRRE JOSE MARIA  
COMISION FEDERAL DE ELECTRICIDAD  
JEFE DEL LAB. DE PETROGRAFIA  
SAN RAFAEL SANTA CECILIA No. 211B  
TLALNEPANTLA, EDO. DE MEXICO  
3-90-13-09  
OLMOS No. 10  
JARDINES DE SAN MATEO  
53240 NAUCALPAN EDO. DE MEXICO  
373-12-39
- 13.- CHAVEZ LOPEZ GABRIELA  
INSTITUTO DE INGENIERIA
- 14.- DOMINGUEZ GUILLEN JOSE LUIS
- 15.- DOMINGUEZ HERNANDEZ OSCAR  
INST. DE INGENIERIA  
TECNICO ACADEMICO  
CD. UNIVERSITARIA  
550-52-15 ext. 3642  
CELAYA No. 5=2  
589-98-63
- 16.- ESPINACE ABARZUA RAUL  
U. CATOLICA DE VALPARAISO-CHILE  
ACADEMICO  
AV. BRASIL No. 2157  
VALPARAISO - CHILE  
25-73-33 anexos 408-406  
CAMINO REAL 2080 No. 33  
VIÑA DEL MAR  
CHILE  
21-40-61
- 17.- GARCIA HERNANDEZ ANDRES B.
- 18.- GARCIA ORTIZ GUADALUPE  
INST. TECNOLOGICO DE CD. MADERO  
CATEDRATICO  
AV. 1o. DE MAYO S/N  
CD. MADERO- TAMPS.  
MORELOS 219 NTE -3B  
COL. UNIDAD NACIONAL  
CD. MADERO TAMPS.  
89410  
585-41

19.- GIL ZEPEDA SOTERO ALEJANDRO  
INST. TEC. DE TEHUACAN  
PROFESOR TIEMPO COMPLETO  
KM. 3 CARR. HUAJUAPAN DE LEON  
APARTADO POSTAL 247  
TEHUACAN, PUE.  
2-24-48

AV. INDEPENDENCIA OTE No. 413-A  
TEHUACAN PUE  
2-25-47

20.- GUANI OLALDE JOSE LUIS  
SARH.  
JEFE DE OF. DE PRECIOS DE ALMAC.  
CONSTITUYENTES 33 OTE  
QUERETARO, QRO. 76000  
258-30

FCO. JAVIER ALEGRE No. 13  
FRACC. LOS MOLINOS  
1a. SECCION  
76150 QUERETARO, QRO.

21.- HINOJOSA REBOLLAR SALVADOR  
COMISION FEDERAL DE ELECTRICIDAD

22.- JIMENEZ AQUINO CECILIO  
INST. TEC. DEL ESTADO  
DOCENCIA  
KM. 821 CARRET. PANAMERICANA  
JUCHITAN, OAX. 70000  
200-42

FCO. I. MADERO No. 21  
70000 JUCHITAN, OAX.

33.- LAFUENTE SANGUINETTI MARIANELA  
IMME-MCV  
PROFESOR ASISTENTE  
PLAZA LAS TRES GRACIAS  
LOS CHAGUARAMOS CARACAS VENEZUELA  
662-75-38

C. CUMANA QTA. LOS ALBEMAR U.B.  
EL CAFETAL  
CARACAS, VENEZUELA  
98 78 314

34.- LOPEZ ESQUIVEL MANUEL  
BUFETE INDUSTRIAL  
JEFE DE SECCION  
MORAS No. 850  
COL. DEL VALLE  
DELEGACION BENITO JUAREZ  
03100 MEXICO, D.F.  
658-52-99 ext. 1242

MORELOS 827 EDIF. 16-204  
JARDIN BALBUENA  
658-52-99 ext. 1242

35.- MELGAREJO ARISTIZABAL JUAN  
UNIV. NAC. DE COLOMBIA  
CD. UNIVERSITARIA  
244-28-48

36.- MENDOZA PADILLA MENA GUADALUPE  
COMISION FEDERAL DE ELECTRICIDAD  
INGNEIERO CIVIL  
RIO MISSISSIPPI  
COL. CUAUHTEMOC  
DELEGACION CUAUHTEMOC  
525-78-80 ext. 3295

HUGACEYO No. 340  
COL. INDUSTRIAL  
DELEGACION GUSTAVO A. MADERO  
586-46-68.

- 37.- MILLAN TOLEDQ FELIX  
D. D. F.  
JEFE OFICINA DE INGENIERIA  
SAN ANTONIO ABAD No. 122-6o. PISO  
COL. TRANSITO  
588-33-17 ext. 138
- CALLE 15 No. 542  
COL. STA. CECILIA TLAHUAC  
DELEGACION TLAHUAC  
03110 MEXICO, D.F.  
842-09-64
- 38.- MONTERO HIGAREDA JOSE L.  
COMISION FEDERAL DE ELECTRICIDAD
- 39.- MORALES HERNANDEZ GUILLERMO  
INSTITUTO MEXICANO DEL PETROLEO  
PROFESIONAL "B"  
EJE CENTRAL LAZARO CARDENAS No. 152  
Q7730 MEXICO, D.F.  
567-66-00 567-91-00
- AV. LAS GRANJAS No. 215 "C"  
DEPTO. 301  
02530 MEXICO, D.F.  
355-93-65
- 40.- MORENO GONZALEZ JORGE ARMANDO  
UNIVERSIDAD MOCHOACANA SAN NICOLAS HGO.  
PROFESOR DE CARRERA "B"  
CD. UNIVERSITARIA  
2-09-76 y 2-06-70
- RAYON No. 585  
58000 MORELIA, MICH.  
237-25
- 41.- NIETO FIGUEROA JAIME  
S. A. R. H.  
JEFE DE SECCION  
CONSTITUYENTES No. 33  
QUERETARO, QRO.  
2-58-30
- PIEDRAS NEGRAS No. 118  
COL. VISTA ALEGRE 2a. SECCION  
QUERETARO, QRO.  
2-58-30
- 42.- OÑATE OCAÑA MARIO ANDRES  
INST. DE INGENIERIA  
AYUDANTE DE INVESTIGADOR  
DELEGACION COYOACAN  
Q4510 MEXICO, D.F.  
548-11-35
- SAN FRANCISCO No. 515  
DELEGACION BENITO JUAREZ  
03100 MEXICO, D.F.  
523-48-44
- 43.- PEREZ CABALLERO FRANCISCO J.  
COMISION NACIONAL DE SEGURIDAD NUCLEAR
- 44.- PEREZ VILLAGOMEZ FERNANDO
- 45.- QUIROZ CERVANTES EMMA  
ENEP ARAGON UNAM  
PROFESRO ASIGNATURA "A"  
AV. CENTRAL Y AV. RANCHO SECO  
SAN JUAN DE ARAGON
- 2a. CERRADA DE ALBERTO SALINAS No.26  
COL. AVIACION CIVIL  
DELEGACION VENUSTIANO CARRANZA  
15740 MEXICO, D.F.  
763-37-86

46.- REYES NUÑEZ JUAN  
INSTITUTO MEXICANO DEL PETROLEO  
EJE CENTRAL LAZARO CARDENAS No. 152  
COL. SAN BARTOLO ATEPEHUACAN  
07730 MEXICO, D.F.  
567-66-00 ext. 20298

ANEMONA No. 27 DEPTO. 1  
COL. TLATILCO  
DELEGACION ATZCAPOTZALCO  
02860 MEXICO, D.F.  
355-57-26

47.- RIOS Y LORENZO JOSE LUIS  
FAC. DE ESTUDIOS SUP. CUAUTITLAN

48.- RODRIGUEZ CALLEJA ROGELIO  
COMISION FEDERAL DE ELECTRICIDAD

49.- ROSALES LEON JOSE  
LAB. MATERIALES FAC. ING. UNAM  
TECNICO  
CD. UNIVERSITARIA  
550-52-15 ext. 3733

GUERRERO 330 A 103  
UNIDAD NONOALCO  
DELEGACION CUAUHTEMOC  
06900 MEXICO, D.F.  
583-21-18

50.- SAAVEDRA VASQUEZ WENCESLAO  
INSTITUTO TECNOLOGICO DE OAXACA  
MAESTRO INVESTIGADOR  
CALZ. TECNOLOGICO  
644-13 y 6-17-22

3a. PRIV. DE MACEDONIO ALCALA No. 102  
COL. DIAZ ORDAZ  
OAXACA, OAX.

51.- SOTO DE LA VEGA FRANCISCO  
COMISION FEDERAL DE ELECTRICIDAD

52.- TORRES CAMARGO ADOLFO

53.- VELA TOLEDO PETRA  
INSTITUTO TECNOLOGICO DEL ISTMO  
DOCENTE  
CARRET. PANAMERICANA KM. 821  
JUCHITAN, OAX.  
3-00-42 y 215-55

ALLENDE No. 29  
ESCATEPEC, OAX.  
3-05-50